DSPACE

https://dspace.org/

Aspects of the petrochemistry of the Phalaborwa Complex, northeastern Transvaal, South Africa

Eriksson, Susan Camenisch

1982
http://hdl.handle.net/10539/22073

Downloaded from a DSpace repository. https://dspace.org/

ASPECTS OF THE PETROCHEMISTRY OF THE PHALABORWA COMPLEX, NORTHEASTERN TRANSVAAL, SOUTH AFRICA

Susan Camenisch Eriksson

A Thesis Submitted to the Faculty of Science,
University of the Witwatersrand, Johannesburg
for the Degree of Doctor of Philosophy

Blacksburg, Virginia 1982

RC 692

DECLARATION

The research comprising this doctoral thesis has been my own. Acknowledgements have been made to those individuals who have aided me with various aspects of my work.

No part of this thesis has been submitted in the past or is being submitted for a degree in any other university.

I have been employed by Arco Oil and Gas Company and Virginia Polytechnic Institute and State University during the writing of this thesis but none of the information used in this thesis has been obtained under their auspices.

Susan C. Eriksson

Susan C. Eriksson

ERRATUM

The South African Comm for Stratigraphy recently recommended a change in the name of the carbonatite body at Phalaborwa. This was brought to the attention of the student as the thesis was being completed and too late for some of the references to the Phalaborwa Igneous Complex to be corrected.

Throughout this thesis for Phalaborwa Igneous Complex read Phalaborwa Complex.

ABSTRACT

The Phalaborwa Complex, northeastern Transvaal, South Africa, consists of the main body of clinopyroxenites and subordinate phoscorite, carbonatite and syenite which is surrounded by numerous pipe-like bodies of syenitic compositions and rare clinopyroxenites.

Clinopyroxenites of the main complex are characterized by cumulus textures formed by separation and accumulation of coprecipitating clinopyroxene, apatite and phlogopite. Potassium feldspar is an intercumulus phase in feldspathic pyroxenite. "Inch-scale" layering of clinopyroxene, apatite and phlogopite formed as in situ cumulus layering near the outer contact of the complex early in the cooling of the magma. Breccias of monomineralic assemblages such as glimmerite and massive pyroxenite reflect breaking up of early formed rocks by magmatic currents.

Clinopyroxenes from clinopyroxenites are characterized by Fe/(Fe+Mg) = 0.07-0.29, low TiO_2 (0.00-0.25%), Al_2O_3 (0.00-1.63%), Na_2O (0.00-1.06%), and Cr, and high Wo component and Sr. Micas from pyroxenites have Fe/(Fe+Mg) = 0.12-0.28, low TiO_2 (0.17-1.73%) and have reverse and normal pleochroism and increasing Al with increasing Fe/(Fe+Mg). Mineral compositions among feldspathic, massive and micaceous pyroxenites overlap; no zonation of the complex from outer contact inward is discernible with respect to the Fe and Mg content. However, phlogopites in "inch-scale"

layering have low Fe/(Fe+Mg) of 0.12 and have reverse pleochroism due to Fe^{3+} entry into the Al-deficient tetrahedral site. Micas from phoscorite and carbonatites have reverse pleochroism, Fe/(Fe+Mg) = 0.05-0.58, low TiO_2 (0.00-0.84%) and decreasing Al with increasing Fe/(Fe+Mg).

Olivines range from Fo_{79} to Fo_{91} and have very low Ni content (<0.06% NiO). Olivines interpreted as xenocrysts have Fo_{84} to Fo_{87}. One of the olivine xenocrysts has an NiO content of 0.29%.

Minerals from carbonatites have initial $^{87}Sr/^{86}Sr$ ratios of 0.70393-0.70623 and 0.71022 and minerals from clinopyroxenites have values of 0.71152-0.71242. Small-scale inhomogeneities exist within samples. Post-crystallization processes can account for variations within samples, but cannot account for variations within a rock type or for raising initial $^{87}Sr/^{86}Sr$ ratios of pyroxene from 0.7039 to 0.7115. Magmas forming pyroxenites and some carbonatites were generated in a high Rb/Sr mantle from isotopically distinct sources. Hence, liquid immiscibility and differentiation are not viable mechanisms for relating these rocks to one another. Mixing of magmas and assimilation of crust may account for isotopic variations within a rock type.

U-Pb dating of uranothorianite and baddeleyite from phoscorite and carbonatite yields an age of 2047+11/-8 m.y. Rb-Sr dating of phlogopites gives widely disparate apparent ages. Nine phlogopites yield an isochron of 2012 $\pm$ 19 m.y.

One sample of phlogopite gave ages of 1661-2360 m.y. in nine different determinations. Older micas may be present in the Phalaborwa complex. Based on the two methods, a best age of the Phalaborwa complex is 2030 $\pm$ 18 m.y.

Two of the syenite pipes, Kgopoeloe and Spitskop, show different levels of emplacement. Kgopoeloe is highly brecciated from a fluid derived from the syenite. Spitskop contains minor breccia and represents multiple injection of syenite. At Spitskop, inward crystallization of the second syenite forms a ring syenite and central syenite; both syenites have cumulus enrichment of minerals.

Feldspathic pyroxenite of the Guide Copper Mine is cogenetic with the pyroxenites of the main complex and contains clinopyroxenes with oscillatory zoning. Fluctuations in fO_2 may be attributed to formation of an immiscible sulphide liquid.

Multiple intrusion of the Phalaborwa Complex is proposed. Initial injection of potassic, probably ultrabasic, liquid formed the pyroxenites. A second intrusion of low-silica, carbonate-rich magma formed phoscorite and banded carbonatite. A third intrusion of carbonatite liquid formed the transgressive carbonatite. Magmatic, cumulus processes dominated the formation of the main complex. The syenites of Kgopoeloe and Spitskop are not cogenetic with rocks of the main complex.

ACKNOWLEDGMENTS

The help and co-operation afforded by the following individuals and organizations are gratefully acknowledged:

i) the Palabora Mining Company and its mining and mineralogical staff and FOSKOR, the Phosphate Development Corporation and its geological staff for providing samples, maps, geologic information and hospitality during field work;

ii) the Council for Scientific and Industrial Research and the Council of the University of the Witwatersrand for financial support through post-graduate bursaries;

iii) the Geology Department of the University of the Witwatersrand for laboratory facilities and logistical support;

iv) R. G. Cawthorn for critical supervision during the writing of this thesis and J. B. E. Jacobsen for supervision during the early stages of this study;

v) the Bernard Price Institute of Geophysical Research of the University of the Witwatersrand for use of laboratory facilities;

vi) H. L. Allsopp for non-official supervision of the isotopic study and his patient and persistent instruction;

vii) the Department of Geology of the University of Texas at Dallas and J. Carter, M. Halpern and W. Manton for use of the electron microprobe and mass spectrometer laboratories;

viii) Arco Oil and Gas Company for use of library, secretarial and drafting services;

ix) Department of Geological Sciences of Virginia Polytechnic Institute and State University for computer facilities and use of research time during final writing of this thesis;

x) J. B. E. Jacobsen, S. McCarthy and R. Forester for help in translation of German, Afrikaans and French languages, respectively;

xi) J. Barton, E. Barton, H. Welke and J. Kramers for help in techniques of isotopic analysis;

xii) T. S. McCarthy and P. Richardson for help with x-ray fluorescence analysis;

xiii) S. Chang, M. Eiss, M. Taylor for drafting; M. Hudson for photography; M. Strickler, G. Adian and P. Stout for typing; and R. G. Cawthorn and J. B. E. Jacobsen for some photographs of Spitskop and Kgopoeloe;

xiv) my parents for many years of education; and

xv) my husband Kenneth for help and encouragement through this study.

TABLE OF CONTENTS

ABSTRACT ii
ACKNOWLEDGMENTS v
LIST OF TABLES xii
LIST OF FIGURES xv

Chapter

page

I. INTRODUCTION 1

The Significance of Carbonatite 1
Carbonatite-silicate Association 2
Phalaborwa Igneous Complex: Its Significance 4
Approach and Objectives 5

II. PREVIOUS STUDIES 7

Main Complex 7
General Geology 7
Petrography 14
Pyroxenites 14
Phoscorite 15
Carbonatite 16
Fenite 18
Dating of the Phalaborwa Complex 19
Satellites 20
General Geology 20
Petrography 22

III. GEOLOGY AND FIELD RELATIONS 23

Main Complex 23
Country Rock and Its Fenitization 23
Pyroxenites 25
Feldspathic Pyroxenite 25
Micaceous and Massive Pyroxenites 25
Discussion 27
Satellites 31
Kgopoeloe Hill 32
Granite 32
Breccia 33
Spitskop 39
Discussion 44

IV. PETROGRAPHY 51

Main Complex 51
Fenite 51
Pyroxenites 52
Feldspathic Pyroxenites 52
Massive Pyroxenite 53
Micaceous Pyroxenite 54

Phoscorite 55
Carbonatite 58
Discussion 58
Satellites 68
Kgopoeloe 68
Granitic Breccia Fragments 68
Matrix 70
Spitskop 73
Guide Copper Mine 78
Discussion 80
Kgopoeloe 80
Spitskop 84

V. MINERAL CHEMISTRY 87

Analytical Data 88
Main Complex 89
Clinopyroxenes 89
Crystal Chemistry 89
Mineralogical Characteristics 90
Petrologic Significance 96
Calcium 96
Aluminum 99
Iron and Magnesium 104
Titanium 112
Sodium 114
Zirconium 116
Strontium 118
Chromium 119
Mica 120
Crystal Chemistry 120
Mineralogical Characteristics 121
Petrologic Significance 131
Olivine 143
Crystal Chemistry 143
Mineralogical Characteristics 143
Petrologic Significance 146
Magnetite 149
Mineralogical Characteristics 149
Petrologic Significance 150
Amphibole 150
Crystal Chemistry 150
Mineralogical Characteristics 151
Petrologic Significance 151
Feldspar 153
Mineralogical Characteristics 153
Petrologic Significance 153
Satellites 155
Kgopoeloe and Spitskop 155
Clinopyroxenes 155
Crystal Chemistry 155
Mineralogical Characteristics . . . 155
Amphiboles 157
Crystal Chemistry 157
Mineralogical Characteristics . . . 159

Feldspar 161
Crystal Chemistry 161
Mineralogical Characteristics . . . 161
Petrologic Significance 163
Guide Copper Mine 166
Crystal Chemistry 166
Mineralogical Characteristics 167
Petrologic Significance 170

VI. THERMODYNAMIC CONSIDERATIONS 174

Conditions of Formation at Phalaborwa 176
Pressure 176
Temperature 177
Activity of Components in the Melt 184
Oxygen Fugacity 184
Silica Activity 190
Summary 194

VII. WHOLE ROCK CHEMISTRY 196

Main Complex 197
Major Elements 198
Trace Elements 206
Introduction 206
Trace Element Data 207
Discussion 218
Whole-rock Chemistry of the Satellites . . . 221
Classification of Rock Types 222
Kgopoeloe Hill 223
Chemical Trends 223
Discussion 228
Spitskop 232
Chemical Trends 232
Discussion 245
One-Stage Trace Element Models . . . 246
Two-Stage Trace Element Models . . . 251
Interrelationships of the Satellites . . . 261

VIII. EXPERIMENTAL PETROLOGY AS RELATED TO THE PHALABORWA COMPLEX 263

Ultrapotassic-ultrabasic Magmas 263
Generation of Alkaline Magmas 273

IX. ISOTOPIC STUDIES 276

Samples 277
Quality of Data 281
Rb and Sr 282
Accuracy 282
Precision 284
Sample Heterogeneity 285

Selection of Initial $^{87}Sr/^{86}Sr$ Ratios in Age Determination 286
Blanks 286
Summary of Errors in Rb-Sr Measurements 288
U and Pb 289
Geochronology 291
U-Pb Ages 291
Rb-Sr Ages of Micas 295
Rb-Sr Data 295
Removal of Contaminating Sr-rich Material 295
Compositional Variation 301
Alteration of Micas 301
Presence of Older Micas 303
Presence of Exotic Material 308
Xenoliths in the Phalaborwa Complex 310
Mixing of Minerals to Form Isochrons 312
Unsolved Problems 313
Age of Country Rocks 315
Age of the Phalaborwa Complex 317
$^{87}Sr/^{86}Sr$ Ratios as Tracers 318
Results 318
Carbonatites 318
Pyroxenites 322
Isotopic Inhomogeneity 325
Leaching Experiments on Pyroxenes . . . 328
Oxygen and Carbon Isotopes 330
Country Rocks 330
Vermiculite Composition 334
Significance of Initial $^{87}Sr/^{86}Sr$ Ratios . 334
Effects of Post-crystallization Processes 337
Alteration of Phlogopite to Vermiculite 338
Diffusion from Phlogopite 340
Leaching Experiments 341
Oxygen and Carbon Isotopes 342
Geologic Evidence 346
Conclusions 347
Ratios Inherited from Source Areas . . 348
Aging of Magma 357
Mixing of Magmas 359
Effects of Magma Contamination 362
Bulk Assimilation of Lower Crust by Mantle Material 362
Bulk Assimilation of Upper Crust by Mantle Material 366
Selective Contamination by Crustal Rocks 369
Equilibration of Sr with Crustal Rocks 371
Conclusions 373

X. A PETROGENETIC MODEL 375

Main Complex 375
Origin of Pyroxenites 375
Origin of the Carbonatite 376
Origin of Phoscorite 378
Emplacement History of the Main Complex . 379
Satellites 383
Origin of the Guide Copper Mine 383
A Model for the Syenite Pipes 384
Origin of the Satellites 385
Significance of the Phalaborwa Complex . . . 387
Magmatic versus Metasomatic Processes . . 387
Mantle Inhomogeneity 388
Future Work 389
Conclusions 391

Appendix

page

A. SAMPLE LOCATIONS AND CHEMICAL DATA 393

B. CHEMISTRY - METHODS, TECHNIQUES AND QUALITY OF DATA 431

Analytical Technique for the Electron Microprobe 432
Activity of Components in Minerals 436
X-ray Fluorescence Analytical Procedures . . 437
Wet Chemical Technique 447
Trace Element Model Calculations - Spitskop . 448

C. ISOTOPIC STUDY 450

Sample Descriptions 451
Mass Spectrometry Techniques 455
Notes on Sample Preparation - P29P 465
Alteration of Phlogopite as a Source of Radiogenic Sr 466

REFERENCES 468

LIST OF TABLES

Table		Page
5.1	Microprobe analyses of clinopyroxenes	399
5.2	X-ray fluorescence analyses of clino-pyroxenes	404
5.3	Results of alternate methods of calculating Fe^{3+} in pyroxenes	91
5.4	Microprobe analyses of micas.	405
5.5	X-ray fluorescence analyses of micas.	411
5.6	Microprobe analyses of olivines	412
5.7	Microprobe analyses of amphibole, feldspar and magnetite	414
5.8	Microprobe analyses of minerals from Kgopoeloe and Spitskop.	415
5.9	Microprobe analyses of pyroxenes from the feldspathic pyroxenite, Guide Copper Mine . .	416
5.10	Rim compositions of pyroxenes in sample G8F .	171
6.1	Temperature estimates from the literature for coexisting minerals at Phalaborwa	178
6.2	Temperatures derived from coexisting olivine and clinopyroxene	182
6.3	Activity of silica in melt calculated for phoscorite and carbonatite compared to some other igneous rocks	193
7.1	Whole rock chemistry by x-ray fluorescence, Main Complex and Guide Copper Mine.	418
7.2	Whole rock chemistry by x-ray fluorescence, Kgopoeloe and Spitskop.	424
7.3	Trace elements in carbonatites, Phalaborwa. .	430
7.4	Distribution coefficients for mineral-liquid partitioning.	247

LIST OF TABLES (continued)

Table		Page
7.5	Results of trace element modeling using proportions of minerals observed in the rocks, Spitskop	248
7.6	Results of trace element modeling different proportions of liquid remaining . .	250
7.7	Composition of syenite dykelet in Foskor pit, main complex	260
9.1	Apparent ages of micas using different initial $^{87}/Sr^{86}$ ratios.	287
9.2	U-Pb data for uranothorianite and baddeleyite	292
9.3a	Rb-Sr data for micas.	296
9.3b	Rb-Sr data for various fractions of glimmerite sample P29P.	297
9.4a	Microprobe data for various fractions of glimmerite sample P29P, University of Texas at Dallas	305
9.4b	Microprobe data for various fractions of glimmerite sample P29P, Anglo-American. . . .	306
9.5	Microprobe analyses of trace minerals in sample P29P	309
9.6	Rb-Sr data for country rocks.	316
9.7	Sr-Rb data for carbonatites	319
9.8	Sr-Rb data for clinopyroxenes	321
9.9	Rb, Sr data for apatites.	323
9.10	Rb-Sr data on leached material from clinopyroxenes.	329
9.11	C and O isotopic data for selected carbonatites.	331

LIST OF TABLES (continued)

Table		Page
9.12	Rb and Sr concentrations of country rocks . .	333
9.13	Rb-Sr data for a vermiculite.	335
9.14	Calculated proportions of lower crust required to raise initial $^{87}Sr/^{86}Sr$ ratios at Phalaborwa.	363
9.15	Calculated proportions of upper crust required to raise initial $^{87}Sr/^{86}Sr$ ratios at Phalaborwa	368
A.1	Sample locations, Kgopoeloe	397
A.2	Sample locations, Spitskop.	398
B.1	Replicate analyses of standards, microprobe .	434
B.2	Replicate analyses of unknown, microprobe . .	435
B.3	Replicate analyses of standards, major and minor elements, XRF	438
B.4	Replicate analyses of standards, trace elements, XRF	438
B.5	Replicate analyses of unknown, major and minor elements, XRF	440
B.6	Replicate analyses of unknown, trace elements, XRF	440
B.7	Machine conditions, major and minor elements, XRF	442
B.8	Machine conditions, trace elements, XRF . . .	443
C.1	Rb, Sr, $^{87}Sr/^{86}Sr$ for NBS 607 K-feldspar standard.	461
C.2	$^{87}Sr/^{86}Sr$ values for Eimer and Amend standard	462
C.3	Duplicate $^{87}Sr/^{86}Sr$ data for same dissolutions	463
C.4	Duplicate $^{87}Sr/^{86}Sr$ data for different dissolutions.	464

LIST OF FIGURES

Figure		Page
2.1	Generalized geology of the Phalaborwa Igneous Complex	10
3.1	"Inch-scale" layering in micaceous pyroxenite in the Foskor pit	28
3.2	Fragments of glimmerite in massive pyroxenite from the Foskor pit	28
3.3	Large euhedral clinopyroxenes in mica from the Foskor pit.	29
3.4	Contact of breccia with pink granite at Kgopoeloe	34
3.5	Close-up of microbreccia at Kgopoeloe	34
3.6	Fine-grained trachyte fragment in syenite at Kgopoeloe	35
3.7	Gneissic amphibolite country-rock xenolith in syenite at Kgopoeloe.	35
3.8	Coarse breccia in fine-grained syenite matrix at northeast corner of Kgopoeloe.	37
3.9	Close-up of quartz filling of Figure 3.8, Kgopoeloe	37
3.10	Spalling of granitic fragment into syenite matrix, Kgopoeloe	38
3.11	Gneissic fragment at base of Kgopoeloe syenite with diffuse upper contact with syenite matrix	38
3.12	Schematic representation of the fine-grained syenite layer which occurs on top of some granitic fragments at Kgopoeloe	40
3.13	Outcrop of Spitskop showing the dark, ring syenite at the outer edge of the pipe	41
3.14	Close-up of the ring syenite and its gradational nature with the central syenite, Spitskop	43
3.15	Ring syenite and its contact with the central and outer syenite, Spitskop	43

LIST OF FIGURES (continued)

Figure		Page
3.16	Schematic drawing of a model for emplacement of the syenite pipes surrounding the Phalaborwa complex.	47
4.1	Photomicrograph of fenitized country rock with clinopyroxene lining a crack or dykelet . . .	51
4.2	Photomicrograph of a fenitized country rock containing abundant biotite, feldspar, clinopyroxene and amphibole.	51
4.3	Photomicrograph of olivine crystal with rim of clinopyroxene and phlogopite	56
4.4	Photomicrograph of olivine crystals which have been partially replaced by serpentine enclosed poikilitically in chalcopyrite.	56
4.5	Photomicrograph of zoned phlogopite crystals in carbonatite.	59
4.6	Euhderal grain of clinopyroxene partially intergrown with phlogopite.	63
4.7	Photomicrograph of carbonatite dykelets in feldspathic pyroxenite.	63
4.8	Photomicrograph of microbreccia filling of monomineralic aegirine-augite which is penetrating the fragment and replacing quartz and feldspar, Kgopoeloe	69
4.9	Photomicrograph of microbreccia fragment and aegirine-augite crystals lying parallel to fragment edges, Kgopoeloe	69
4.10	Photomicrograph of microbreccia fragment with aegirine-augite crystals growing perpendicular to edge of the fragment, penetrating the fragment and growing in the interior of the fragment, Kgopoeloe	71
4.11	Photomicrograph of microbreccia at Kgopoeloe showing the close packing of fragments with aegirine-augite filling between fragments . .	72

LIST OF FIGURES (continued)

Figure		Page
4.12	Photomicrograph of fine-grained syenite at Kgopoeloe which contains aegirine-augite and amphibole growing in intimate association . .	72
4.13	Photomicrograph of outer syenite at Spitskop showing granular texture with minor aegirine-augite	74
4.14	Photomicrograph of ring syenite at Spitskop showing granular texture with minor aegirine-augite	74
4.15	Photomicrograph of ring syenite at Spitskop showing aegirine-augite and amphibole poikilitically enclosed in feldspar	76
4.16	Photomicrograph of ring syenite at Spitskop showing a broken aegirine crystal in undeformed, late-stage quartz	76
4.17	Photomicrograph of central syenite at Spitskop showing idiomorphic feldspar with interstitial aegirine-augite and quartz.	77
4.18	Photomicrograph of a cross-cutting dyke at Spitskop with orthoclase and crystals of mixed aegirine-augite and amphibole	77
4.19	Photomicrograph of feldspathic pyroxenite from Guide Copper Mine. Euhedral clinopyroxenes are poikilitically enclosed in microcline.	79
4.20	Photomicrograph of feldspathic pyroxenite from Guide Copper Mine. Zoned pyroxenes laths are poikilitically enclosed in microcline and in chalcopyrite	79
5.1	Clinopyroxene compositions from the Phalaborwa main complex plotted in the pyroxene quadrilateral	93
5.2	Compositions of clinopyroxenes from the main complex plotted in the Mg-(Fe^{2+}+Mn)-Na system	95
5.3	Group I pyroxenes plotted in the pyroxene quadrilateral	97

LIST OF FIGURES (continued)

Figure		Page
5.4	Tetrahedral site occupancies for clinopyroxenes plotted as the number of Al cations against the number of Si cations per formula unit.	100
5.5	Al_2O_3 content of Group I pyroxenes plotted against $Fe^{tot}/(Fe^{tot}+Mg)$.	103
5.6a	Fe/(Fe+Mg) ratios of pyroxenes plotted at their sample locations in the PMC open pit. .	106
5.6b	Fe/(Fe+Mg) of clinopyroxenes plotted at their sample location in the Foskor area. . .	107
5.7	Sketch of the olivine crystal from micaceous pyroxenite with reaction rim of clinopyroxene and mica. The olivine composition and Fe/(Fe+Mg) of clinopyroxenes are shown at the spots measured.	110
5.8	TiO_2 plotted against Fe/(Fe+Mg) for pyroxenes of the main complex	113
5.9	The trends of pyroxenes from Phalaborwa and other igneous occurrences plotted in the system Mg-$(Fe^{2+}$+Mn)-Na.	115
5.10	Compositions of micas plotted as (a) Al versus Fe/(Fe+Mb), (b) tetrahedral iron versus Fe/(Fe+Mg), (c) Al versus total iron, (d) Ti versus Fe/(Fe+Mg), (e) Al versus Ti, (f) Al versus tetrahedral iron, and (g) Si versus tetrahedral iron.	123
5.11	Al contents of phlogopites in sample P120P in which olivine has reacted with liquid to form clinopyroxene and phlogopite.	130
5.12a	Micas from pyroxenites, phoscorite, carbonatite and fenitized country rock shown in the Al-Ti-(Fe+Mg+Mn) system	132
5.12b	Micas from Phalaborwa shown in the system Al-Mg-Fe.	133

LIST OF FIGURES (continued)

Figure		Page
5.13a	Fe/(Fe+Mg) of micas plotted at their sample locations in the Foskor area.	140
5.13b	Fe/(Fe+Mg) ratios for micas from the PMC area at their sample locations	141
5.14	Fe/(Fe+Mg) ratios of olivines plotted at their sample locations in the PMC area. . . .	145
5.15	Compositions of fractionating olivine for sulfide-undersaturated and sulfide-saturated cases and MgO composition of the liquid at saturation.	147
5.16	Composition of the amphibole from fenitized country rock around the main complex plotted in the Mg-Ca-Na system.	152
5.17	Compositions of feldspars from fenitized country rock around the main complex plotted in the orthoclase-albite-anorthite system . .	154
5.18	Compositions of pyroxenes from Kgopoeloe and Spitskop plotted in the Mg-$(Fe^{2+}+Mn)$-Na system.	158
5.19	Amphibole compositions from Kgopoeloe and Spitskop plotted in relation to the end members of the richterite and riebeckite compositional series.	160
5.20	Amphibole compositions from Kgopoeloe and Spitskop plotted in the Mg-Ca-Na system . . .	162
5.21	Feldspar compositions from Kgopoeloe and Spitskop plotted in the orthoclase-anorthite-albite system	164
5.22	Compositions of clinopyroxene G12F plotted in the Mg-$(Fe^{2+}+Mn)$-Na system	168
5.23	Cations per formula unit plotted as distance from core to rim, clinopyroxene G12F.	169
6.1	Lines showing buffer reactions for zircon-baddeleyite and forsterite-enstatite at 5 kb as a function of activity of silica versus temperature	180

LIST OF FIGURES (continued)

Figure		Page
6.2	Calculated temperature curves for the apatite-phlogopite geothermometer of Stormer and Carmichael (1971) with data from Phalaborwa	185
6.3	Lines showing the upper stability of olivines and phlogopites of varying compositions on an oxygen fugacity versus temperature diagram calculated for 5 kb	188
7.1	Compositions of pyroxenites plotted in the FEM-SAL-VOL triangle plot after Dawson (1960)	199
7.2	Variation diagrams for compositions of the pyroxenites, main complex: (a) FeO versus MgO, (b) CaO versus MgO, (c) K_2O versus MgO, (d) Al_2O_3 versus MgO.	200
7.3	CaO versus P_2O_5 for pyroxenites, main complex	203
7.4	CaO versus K_2O for pyroxenites, main complex.	203
7.5	$Fe^{tot}/(Fe^{tot}+Mg)$ ratios for pyroxenites plotted at their sample locations in the Foskor pit.	204
7.6	Sr versus P_2O_5 for pyroxenites, main complex.	208
7.7	Sr versus Ba for pyroxenites, main complex. .	208
7.8	Sr versus Rb for pyroxenites, main complex. .	209
7.9	Rb versus K_2O for pyroxenites, main complex .	209
7.10	Ba versus Rb contents of pyroxenites, main complex	210
7.11	Rare earth elements for carbonatites.	212
7.12	Rare earth elements for pyroxenites, main complex	214
7.13	Major element chemistry plotted to evaluate effects of mixing between syenite and granite at Kgopoeloe.	224
7.14	Trace element chemistry plotted to evaluate mixing at Kgopoeloe	225

LIST OF FIGURES (continued)

Figure		Page
7.15	TiO_2 versus SiO_2 for rocks from Kgopoeloe . .	226
7.16	SiO_2 versus total alkalies, Kgopoeloe	226
7.17	Sr versus P_2O_5, Kgopoeloe	229
7.18	Fe/(Fe+Mg) versus differentiation index, Kgopoeloe	229
7.19	Normative quartz versus normative feldspar, Spitskop.	233
7.20	Differtiation index versus (a) Fe/(Fe+Mg) and (b) $Fe^{3+}/(Fe^{3+}+Fe^{2+})$, Spitskop.	234
7.21	Zr versus differentiation index, Spitskop . .	235
7.22	Nb versus differentiation index, Spitskop . .	235
7.23	Y versus differentiation index, Spitskop. . .	237
7.24	Rb versus differentiation index, Spitskop . .	237
7.25	K_2O versus differentiation index, Spitskop. .	238
7.26	TiO_2 versus differentiation index, Spitskop .	238
7.27	Ba versus differentiation index, Spitskop . .	239
7.28	Sr versus differentiation index, Spitskop . .	240
7.29	Ni versus Fe/(Fe+Mg), Spitskop.	240
7.30	Na_2O versus differentiation index, Spitskop .	241
7.31	Total alkalies versus differentiation index, Spitskop	241
7.32	Sr versus P_2O_5, Spitskop.	242
7.33	Zn versus $Fe^{3+}/(Fe^{3+}+Fe^{2+})$, Spitskop.	242
7.34	Compositions of rocks from Spitskop plotted in the peralkaline residual system.	253
7.35	Differentiation index versus agpaitic index, Spitskop.	254
7.36	Sr versus agpaitic index, Spitskop.	255

Figure		Page
7.37	Ba versus agpaitic index, Spitskop.	255
7.38	Results of trace element chemistry for a two-stage crystallization model for Spitskop.	257
8.1	Diagram showing above-solidus boundaries for appearance of minerals in melting experiments of a highly potassic biotite mafurite with 5% H_2O.	265
8.2	Diagram showing results of water-undersaturated melting experiments on madupite with 2.9% H_2O	266
9.1	Outline of the Phalaborwa complex with sample locations of country rocks, vermiculite, pyroxene from the Guide Copper Mine and index maps for the PMC and Foskor areas . . .	278
9.2	Generalized map of the PMC area with sample locations for uranothorianites, baddeleyites, carbonatites and phlogopites used in the isotopic study.	279
9.3	Generalized map of the Foskor pit with sample locations of phlogopites and clinopyroxenes used in the isotopic study.	293
9.4	Isochron for nine phlogopite samples from Phalaborwa.	298
9.5	Apparent ages for various analyses of glimmerite sample P29P versus (a) ^{87}Rb, (b) total Sr, (c) $^{87}Rb/^{86}Sr$, (d) $^{87}Sr/^{86}Sr$, and (e) radiogenic ^{87}Sr	302
9.6	Summary of initial $^{87}Sr/^{86}Sr$ ratios for rocks and minerals from the Phalaborwa complex measured in this study.	326
9.7	Oxygen and carbon isotopic data for carbonates from Phalaborwa and other alkaline complexes and pipes	344

LIST OF FIGURES (continued)

Figure		Page
9.8	Model for $^{87}Sr/^{86}Sr$ evolution with initial $^{87}Sr/^{86}Sr$ ratios from Phalaborwa and several southern African intrusions	350
9.9	Model for upper mantle growth curve from Moorbath (1976)	351
9.10	Initial $^{87}Sr/^{86}Sr$ ratios of carbonatites from Phalaborwa versus (a) Ba, (b) La, and (c) Y .	360
A.1	Sample locations for mineral and whole rock analyses, PMC area.	395
A.2	Sample locations for minerals and whole rock samples from the Foskor open pit.	396
C.1	Changes in U and Pb spike concentrations through the time of this study.	456

Chapter I
INTRODUCTION

1.1 THE SIGNIFICANCE OF CARBONATITE

Alkaline rocks are estimated to comprise only a few percent of the world's igneous rocks (Daly, 1933; Barker, 1969) and of these, carbonatites are a minor proportion. One may wonder why this group of relatively rare rocks should be studied at all. Although carbonatites pale economically in significance compared to porphyries, layered complexes and volcanic suites, various carbonatites are economically viable deposits of P, REE, V, Cu, Zn, Mo, Pb, Th and U (Deans, 1966).

More importantly, carbonatite petrogenesis directly bears upon some larger geologic problems. It has long been established that H_2O has a dramatic effect on magmatic processes (Yoder and Tilley, 1962). Within the last decade, improvement of experimental techniques has produced innumerable studies to elucidate the influence of CO_2 in production and evolution of magmas. Studies show that CO_2 causes a shift in phase boundaries (Wyllie and Huang, 1975a), alters differentiation paths (Wyllie and Huang, 1976), and lowers the temperature of melting of various mantle assemblages (Wyllie and Huang, 1975b; Eggler and Rosenhauer, 1978).

Tuttle and Gittins (1966) summarized the nature of the problems carbonatites provide: the ultimate origin and evolution of carbonatite magma and nature of their emplacement. The argument for a magmatic origin over assimilation of limestone was strengthened with production of a carbonate melt at geologically reasonable temperatures by Wyllie and Tuttle (1959). The broad relationship in space and time among carbonatites, kimberlites, lamprophyres and other alkaline ultramafic rocks (Tuttle and Gittins, 1966; Verwoerd, 1967; McIver and Ferguson, 1979) along with similarities in mineralogy and chemistry (Dawson, 1967; Bachinski and Scott, 1979) suggest a close genetic link. Current thought is that different degrees of partial melting within the mantle produce ultrabasic magmas with various degrees of undersaturation which in turn evolve into numerous types of rocks through fractional crystallization and formation of immiscible liquids (Koster van Groos and Wyllie, 1966; Koster van Groos and Wyllie, 1973; Eggler and Rosenhauer, 1978; Wyllie, 1978).

1.2 CARBONATITE-SILICATE ASSOCIATION

Carbonatites most commonly are associated with various types and proportions of silicate rocks. In southern Africa alone, Verwoerd (1967) proposed an eight-fold classification of carbonatite complexes based on associated silicate rocks which range from Na-rich volcanic breccias and tuffs, through feldspathoidal lavas and plutonic varieties to K-rich, ultramafic pipes.

Similarly, throughout the world, silicate rocks, intimately associated with carbonatite, show an extreme range in composition. The silicate assemblages are commonly enriched in the same group of elements which are abundant in carbonatite. This is anomalous because the REE, Sr, Ba, Rb, K, and Na are usually associated with crustal rocks, and elements such as Ni, Co, and Cr are known to be abundant in mantle-derived rocks. Although carbonatites are believed to originate in the mantle, it is still unclear as to whether the associated silicate rocks are magmatic products of the mantle or crust or are the results of metasomatic processes.

The important role of volatile species in the genesis of carbonatites and their associated rocks is corroborated by the presence of carbonates, micas, sulphides and sulphates. Fluid inclusion studies (LeBas et al.; 1972, Rankin, 1975; Rankin and LeBas, 1974; Aldous, 1980) are helping to establish the compositions of fluid phases and the differences in those of the silicate- and carbonate-magmas. Metasomatism, the ubiquitous process associated with these complexes, has had a number of functions attributed to it. The three most important questions associated with this process are the source of fluids (Tuttle and Gittins, 1966; Wyllie, 1978), the controls over fenitization of country rock (McKie, 1966) and how gaseous transfer affects both formation of metasomatic minerals (Gittins et al., 1975) and controls partitioning of elements between solids and fluids in the magmatic process (LeBas, 1977).

1.3 PHALABORWA IGNEOUS COMPLEX: ITS SIGNIFICANCE

There are three obvious reasons for studying the Phalaborwa Igneous Complex. Phalaborwa is unique in its being the only carbonatite presently mined for copper (see Palabora Mining Company, 1976, for a review of the economic aspects). Other carbonatites have occurrences of copper, e.g., Bukusu (Bloomfield, 1973), Iron Hill (Nash, 1972), Killala Lake and Port Coldwell (Bell, personal communication, 1978), which indicate that Cu in the Phalaborwa complex is not unique and that metal mineralization is an important process in the petrogenesis of carbonatites. Secondly, Phalaborwa is possibly the world's oldest carbonatite. It has been quoted in the literature as being between 1100 m.y. and 2000 m.y. in age (Heinrich, 1966, 1970) even though a uranothorianite was dated previously which gave a concordant age of 2060 m.y. (Holmes and Cahen, 1956). The emplacement of Phalaborwa at the same time as the Bushveld complex around 2094 $\pm$ 24 m.y. (Hamilton, 1977) has a possible significance both for the tectonic history of the southern African subcontinent and carbonatite magmatism.

Lastly, given the importance of the carbonate-silicate rock association, the Phalaborwa complex presents a unique opportunity for studying a well exposed complex containing ultramafic to salic rocks which appear to have an origin related to the emplacement of carbonatite. Mechanisms for emplacement of carbonatite complexes have been described as injection of liquid (Dawson, 1966; Melcher, 1966), diapiric

flow (Jennings and Mitchell, 1969), and rifting of solid blocks (Lee, 1973). Chemical and mineralogical information can support petrologic and geologic data to interpret emplacement history of these alkaline rocks.

1.4 APPROACH AND OBJECTIVES

Phalaborwa has been the subject of numerous studies since the late 1800's (Hanekom et al., 1965). However, apart from detailed mapping projects in earlier years, most of the recent studies have concentrated on the petrography and chemistry of the carbonatite and phoscorite with isolated measurements of Sr (Powell et al., 1966; Pineau et al., 1973), S (Mitchell and Krouse, 1975; Von Gehlen, 1976), O and C isotopes (Sheppard and Dawson, 1973; Suwa et al., 1975). Frick (1975) studied the plugs surrounding the complex, and Briden (1976) placed the Phalaborwa complex in the palaeomagnetic framework of southern Africa.

Modern petrologic techniques have ample application to the virtually unstudied silicate rocks which constitute about 95 percent of the main complex. The determination of mineral compositions can be used to reflect the compositions of magma from which they formed (Simpkin and Smith, 1970; Arth, 1976) as well as giving information as to pressure, temperature, and composition of fluid phases (Buddington and Lindsley, 1964; Wones and Eugster, 1965; Nicholls, 1976). Minerals found in potassic-ultrabasic rocks have not been studied to the extent of other ultramafic rocks and distribution coefficients of trace elements between solid

and liquid are not well known, but some pertinent information can be gleaned from the chemistry and mineralogy of these rocks. This thesis proposes to study the suite of pyroxenites, the phoscorite, and surrounding syenite plugs with respect to their chemical and isotopic composition and interpret these data in the light of recent petrologic and experimental studies.

The objectives of this study include:

(1) An analysis of the mineral- and whole-rock chemistry for the main complex and an interpretation of the interrelationships of rock types;

(2) An analysis of the time of emplacement of the main complex using uranium-lead and rubidium-strontium dating of minerals;

(3) An evaluation of strontium isotopes as a petrogenetic indicator for the origin of these rocks;

(4) An interpretation of the satellite bodies in terms of their mineralogy and chemistry to determine any relationship with the main complex.

Chapter II
PREVIOUS STUDIES

Many geologists in the late-nineteenth century recognized the "limestone" and copper stainings of Phalaborwa, but Mellor (1906) was the first to postulate a mode of origin involving a modification of granitic magma by pre-existing limestone. Various geologists have since studied the rocks of the Phalaborwa Igneous Complex during exploration and development of mining operations in the complex. Hanekom et al. (1965) summarized the studies done on the Phalaborwa Igneous Complex prior to 1965.

2.1 MAIN COMPLEX

2.1.1 General Geology

The Phalaborwa Igneous Complex is intruded into Archaean rocks which consist of granites, gneisses, quartzites, granulites, amphibolites and talc- and serpentine-schists (Hall, 1912a; Shand, 1931; Brandt, 1948; Hanekom et al., 1965). The main complex is an elongate, irregularly-shaped body covering about 16 sq km. A gravity survey (Hanekom et al., 1965) indicates that it is a pipe-like body, pitching 76-80 degrees to the east and that the pyroxenite has a vertical extent of at least 5 km. Diamond drilling by the Palabora Mining Company indicates a vertical continuity of the carbonatite with respect to lithology, mineralogy, and economic mineralization to at least 1500 m (Palabora Mining Company, pers. comm., 1976).

There has been a great deal of controversy over the contact relations since 1912 when Hall (1912b) postulated the presence of a "Palabora" granite as a distinct rock type surrounding the complex. The nature of the contact lies in the interpretation of feldspathic pyroxenite and its relationship to country rock and to pyroxenite of the complex.

Hall (1912a) described a leucocratic, pink granite which became less siliceous toward the contact with the complex, grading into a feldspar-rich rock containing pyroxene; he attributed these relationships to differentiation of a single magma. Shand (1931) described the feldspathic pyroxenite as a primary rock type, basing his interpretation on the presence of idiomorphic feldspar. Gevers (1948) disregarded Shand's interpretation due to the "schlieren" texture of clinopyroxene in syenite, quartz syenite, and "Palabora" granite and supported Hall's view that feldspathic pyroxenite represents contamination of pure pyroxene rock by mixing with a granitic fraction. Hanekom et al. (1965) reinvestigated the outer boundary of the pyroxenite and concluded that feldspathic pyroxenite occurs on the boundary in most places but is best developed where the pyroxenite is associated with younger syenite intrusions near or on the pyroxenite contact. In the areas where pyroxenite adjoins granite-gneiss, the feldspathic variety is absent or poorly developed, and the intrusive nature of pyroxenite is demonstrated by transgressive pyroxenite dykes

within granite-gneiss. Hanekom and his coworkers interpreted the feldspathic pyroxenite as assimilated Archaean granite by pyroxenite magma, followed by intrusion of syenite.

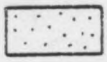
Various types of pyroxenite comprise about 70 percent of the main complex. As can be seen from Figure 2.1, feldspathic pyroxenite occupies a narrow band at the periphery of the complex which varies from zero up to several metres in width. Away from the contact, feldspathic pyroxenite gives way to massive- and micaceous-types of pyroxenite which comprise the main portion of the kidney-shaped body. Hanekom et al. (1965) estimate that micaceous- and massive-pyroxenites are in equal proportions.

Large pegmatoid bodies occur in the northern and southern lobes of the main complex (Figure 2.1), but this rock type is poorly developed in the central part of the complex. The northern pegmatoidal body is zoned with a core consisting of predominant serpentine and phlogopite with minor apatite (Hanekom et al., 1965) and a rim consisting of the same minerals plus clinopyroxene. The southern pegmatoid and the outer portion of the central plug resemble the outer portion of the northern pegmatoid. Diopside crystals reach over 20 cm in length in the outer regions and serpentine is reduced to occasional lenses.

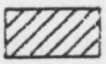
DeJager and Fourie (1978) studied the field relations of the pyroxenites in the Foskor Pit in great detail. They concluded that pyroxenites are the result of multiple

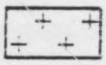
LEGEND


CARBONATITE

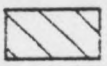

PHOSCORITE

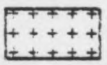

INNER PEGMATOID


OUTER PEGMATOID


PYROXENITE


MICA PEGMATOID


FELDSPATHIC PYROXENITE


FENITE


SYENITE

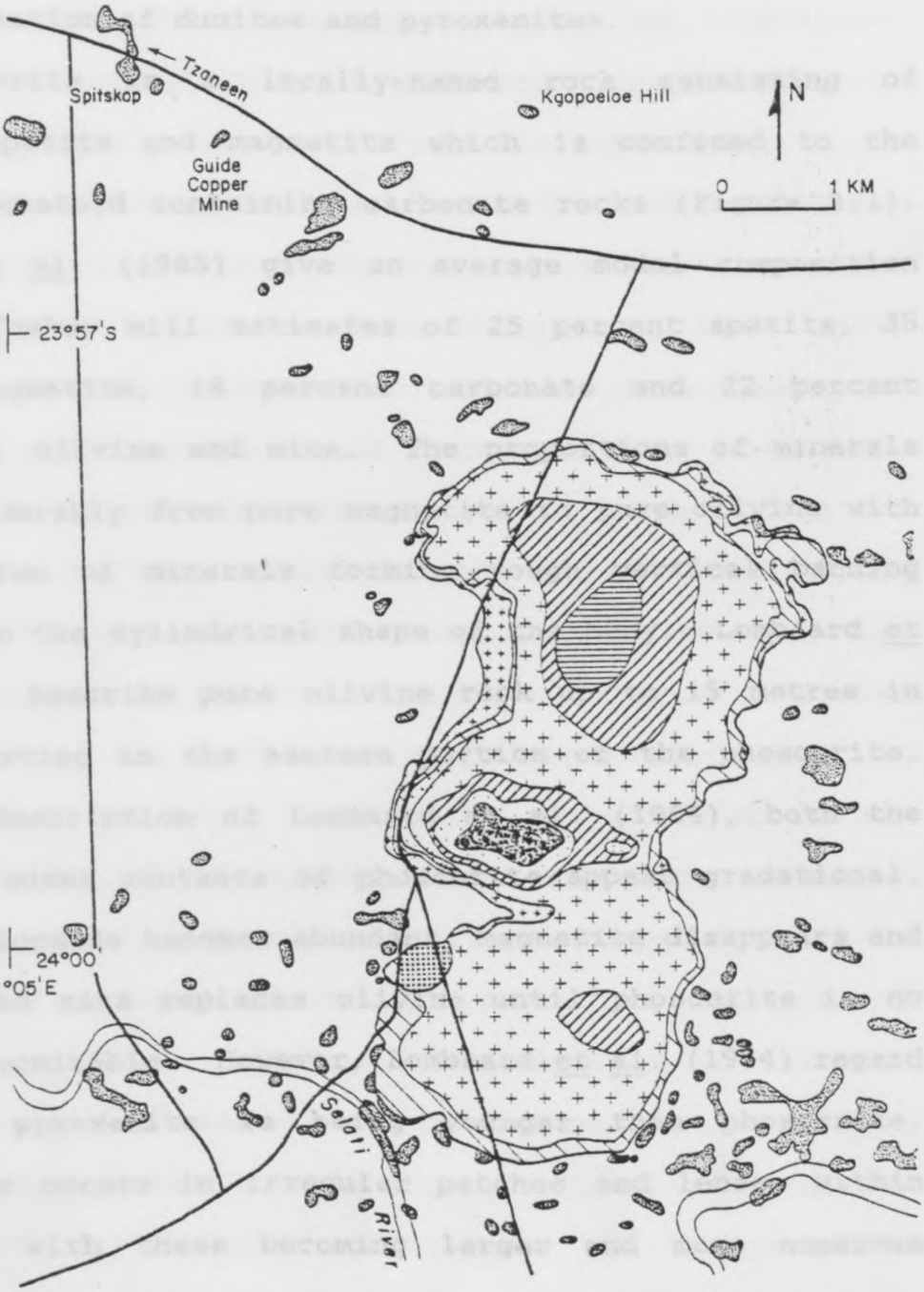


Figure 2.1 The generalized geology of the Phalaborwa Igneous Complex. Late-intruded dolerite dykes have been omitted to clarify the geology of the complex. (after Hanekom et al., 1965).

injections of magma. Phlogopite in the pegmatoidal areas formed from magmatic crystallization but volatile-rich fluids were channeled through fractures to produce phlogopitization of dunites and pyroxenites.

Phoscorite is a locally-named rock consisting of olivine, apatite and magnetite which is confined to the central pegmatoid containing carbonate rocks (Figure 2.1). Hanekom et al. (1965) give an average modal composition based on Foskor mill estimates of 25 percent apatite, 35 percent magnetite, 18 percent carbonate and 22 percent serpentine, olivine and mica. The proportions of minerals vary considerably from pure magnetite to pure olivine with concentration of minerals forming rough vertical banding parallel to the cylindrical shape of the body. Lombaard et al. (1964) describe pure olivine rock up to 15 metres in width occurring in the eastern portion of the phoscorite. From the description of Lombaard et al. (1964), both the inner and outer contacts of phoscorite appear gradational. Outwards diopside becomes abundant, magnetite disappears and fine-grained mica replaces olivine until phoscorite is no longer recognizable. However, Lombaard et al. (1964) regard micaceous pyroxenite as being younger than phoscorite. Carbonatite occurs in irregular patches and lenses within phoscorite with these becoming larger and more numerous inwards, giving way to carbonatite. In a few places, the carbonatite-phoscorite contact is abrupt. DeJager and Fourie (1978) also suggest that the phoscorite (dunite) may

have been the first intruded phase with pyroxenites intruded around it.

The main features of the carbonatite members of the complex have been described repeatedly in the literature, the most recent being the Palabora Mining Company (1976) who recognize two main periods of carbonatite emplacement.

Magnetite-rich carbonatite maintains the elliptical concentric zoning of the phoscorite and is known as banded carbonatite. Early workers (Lombaard et al., 1964) noted several generations of banded carbonatite, each similar in mineralogy and texture, with cross-cutting relations. Relationships between these various phases are not clear and have subsequently been interpreted as remobilization of the banded carbonatite. Current usage classifies all the carbonatites with thickness of magnetite bands on the order of a few millimetres together as banded carbonatite.

A younger, distinct carbonatite member occupies the central portion of the centre plug, radiating primarily along fractures at N70W and N70E (Lombaard et al., 1964). Magnetite and silicate phases are present in disoriented clots and lenses rather than concentric banding. Veining of banded carbonatite, phoscorite, and the massive, micaceous and feldspathic pyroxenites by transgressive carbonatite is common. Two curvilinear intrusions of transgressive carbonatite which persist with depth and contain a larger than normal proportion of mica occur in the eastern portion of the banded carbonatite.

Several dykes of various sizes cut through the entire complex. These have been thought to be dolerites of Karoo age (Hanekom et al., 1965) until Briden (1976) measured paleomagnetic poles on one large dyke which gave an orientation compatible with the Waterberg period of magmatism at around 1900 m.y. More detailed work (Briden, pers. comm., 1977) confirms that most cross-cutting dykes in the Phalaborwa complex are Precambrian in age, although at least one may be Karoo (around 170 m.y.) in age.

Taljaard (1936) documented a medium-grained melilite-augite rock picked up in the Phalaborwa area by E. Cohen in 1895, but there is no documentation on its precise location. Although this rock could have been the product of primitive smelting of copper-bearing rocks, Shand (1931) also sought this rock and "collected a number of dark basaltic-looking rocks but all turned out to be ordinary plagioclase basalts."

Various sized bodies of dark fine-grained rocks described as dolerites and diabases have been mapped in the Foskor pit. New occurrences of similar dark, fine-grained rocks, one with a peculiar arcuate outcrop, have been discovered by mining personnel at the western periphery of the PMC mining area.

2.1.2 Petrography

Petrographic and mineralogic studies up until the mid-1960's concentrated on gross textural descriptions and relied on optical determinations or bulk analyses for mineral compositions. Hanekom et al. (1965) reviewed what had been done but little of the information relates to the petrogenetic implications of the data.

Because of the economic importance of the carbonatite and phoscorite members, most petrographic studies dealt exclusively with these rock types (Lombaard et al., 1964; Van Rensburg, 1965; Hennig-Michaeli, 1968; Palabora Mining Company, 1976). DeJager and Fourie (1978) performed limited petrographic work on the pyroxenites. Details of these studies which pertain to the petrogenesis of the complex are reviewed below.

2.1.2.1 Pyroxenites

Petrographic description of pyroxenite is limited. DeJager and Fourie (1978) note that apatite is both interstitial to diopside or may be partially enclosed by diopside. Microcline and phlogopite are both interstitial to pyroxene. Recrystallization of diopside was noted in cases where phlogopite is present in large amounts (DeJager and Fourie, 1978). They attribute this recrystallization to metasomatism of pyroxene by fluids to form phlogopite.

2.1.2.2 Phoscorite

Olivine grains from 2-3 mm to several centimetres in length are serpentinized to different degrees. There is no decrease in serpentinization with depth (PMC Mining Staff, pers. comm., 1977), and highly serpentinized olivine may exist within a few centimetres of almost fresh olivines. Olivines with rims of phlogopite or chondrodite are sometimes present. Bornite, chalcopyrite, and possibly pentlandite are present within olivines (Van Rensburg, 1965; Aldous, 1980) as minute blebs and in fluid inclusions. These are taken to represent the presence of sulphide liquid prior to crystallization of olivine (Van Rensburg, 1965; Aldous, 1980). Olivine also exists poikilitically enclosed in large sulphide grains.

At least two generations of magnetite exist. Primary magnetite forms anhedral to euhedral grains varying from less than 1 mm to tens of centimetres across. Hennig-Michaeli (1968) noted ilmenite-rich rims on some magnetite grains. Van Rensburg (1965) and Hanekom et al. (1965) observed ulvospinel and ilmenite exsolution in the magnetite. Late magnetite replaces baddeleyite in places (Van Resnburg, 1965) and rims sulphides (Hennig-Michaeli, 1968). Aldous (1980) suggested that magnetite was introduced late as a pneumatolitic/hydrothermal fluid along with apatite and sulphides.

Baddeleyite occurs as black, prismatic crystals up to a few centimetres in length (Hanekom et al., 1965). Apatite

forms short, stubby crystals a few millimetres in length as well as larger, anhedral masses. The {0001} cleavage is pronounced and crystals are sometimes bent and fractured. Phlogopite occurs in anhedral masses around olivine and as euhedral books. Hennig-Michaeli (1968) noted that very often clinohumite is present rather than the commonly-quoted chondrodite, and often replaces olivine.

Fine-grained calcite is present in disseminated grains and in veinlets and can comprise up to several percent of the phoscorite.

Extensive descriptions of the iron- and copper-sulphides are present in the literature (Lombaard et al., 1964; Van Rensburg, 1965; Hennig-Michaeli, 1968; Palabora Mining Company, 1976). Bornite and chalcocite are the dominant sulphides and appear late in the crystallization sequence, with the exception of those enclosed in olivine, as noted earlier (Van Rensburg, 1965).

2.1.2.3 Carbonatite

The division into banded carbonatite and transgressive carbonatite is based primarily on their distinct sulphide mineralogy and gross textural features.

Banded carbonatite contains calcite with up to 7.5 percent $MgCO_3$ (Lombaard et al., 1964) and often contains exsolution lamellae of dolomite (Van Rensburg, 1965). According to Van Rensburg (1965) some of the banded type whose banding is not concordant to the phoscorite-

carbonatite contact contains dolomite as interstitial lenses.

Olivine in the banded carbonatite is rare and is commonly cracked, and partially replaced by phlogopite, monazite, or clinohumite. Serpentinization is minimal.

Magnetite is found as discrete, idiomorphic grains ranging from 1 mm to 1 cm in length. Grains are aligned parallel to the outer contact of the banded carbonatite giving a finely banded appearance. A second stage of magnetite rims the sulphides and lies in phlogopite cleavage planes.

Bornite is the predominant sulphide mineral in the banded carbonatite and occurs as disseminated grains, droplets enclosed within olivine, magnetite and calcite (Van Rensburg, 1965), as massive patches, and lenses occasionally parallel to primary magnetite banding.

The predominant carbonate of the transgressive carbonatite is more Mg-rich than that of banded carbonatite, containing up to 14 percent $MgCO_3$ (Hennig-Michaeli, 1968). Subordinate dolomite occurs as discrete grains.

Apatite is less abundant in the transgressive carbonatite (Hennig-Michaeli, 1968). It occurs as disseminated anhedral grains, as idiomorphic crystals, and, rarely, as extremely elongated crystals with parallel alignment.

Phlogopite is more abundant in the transgressive carbonatite and according to Van Rensburg (1965), strained

biotite is also present. Hennig-Michaeli (1968) described idiomorphic intergrowths of phlogopite and magnetite and carbonate replacing phlogopite along cleavage planes.

The magnetite concentration is about equal in the transgressive- and banded-carbonatites. In transgressive carbonatite, magnetite forms massive blebs and idiomorphic crystals, both varying in size from 1-2 mm to tens of centimetres in diameter. The proportions of magnetite may vary from less than 1 percent of a rock to over 90 percent on the scale of about a metre.

Ilmenite as exsolution lamellae in magnetite has often been reported (Lombaard et al., 1964; Hanekom et al., 1965; Van Rensburg, 1965), and Hennig-Michaeli (1968) has reported isolated grains of ilmenite in association with magnetite in both types of carbonatite.

Chalcopyrite is the major sulphide in the transgressive carbonatite, containing exsolution lamellae of bornite and cubanite. It occurs as disseminated grains and massive blebs along fracture planes.

Olivine is very rare in the transgressive carbonatite but clinohumite or chondrodite appear as large aggregates of crystals varying from less than 1 mm to a few centimetres in diameter.

2.1.2.4 Fenite

Hanekom et al. (1965) did not describe the fenites from Phalaborwa, but concluded from previously reported

descriptions (Brandt, 1948; Gevers, 1948) that metasomatized country rocks graded in texture into syenites and into feldspathic pyroxenites. Frick (1975), however, noted that fenitization around the main complex is less intense than noted by Hanekom et al. (1965). Frick (1975) characterized the fenitization by three stages: (1) small round grains of orthoclase forming at the expense of quartz at orthoclase-quartz and plagioclase-quartz grain boundaries; (2) increase in amount of orthoclase with appearance of alkali-amphibole; and (3) formation of alkali-amphibole at the expense of biotite and chlorite.

2.1.3 Dating of the Phalaborwa Complex

Previous data on the age of the Phalaborwa complex consist of two uranothorianite analyses done in the 1950's (Holmes and Cahen, 1956). There is no information as to what rocks the samples came from and concentration of U and Pb are given in rough percentages. The dating of the uranothorianite by de Villiers (Holmes and Cahen, 1956) gave Phalaborwa the unique distinction of being the oldest known carbonatite (2060 m.y.), one of the rare Precambrian igneous carbonatite complexes (Martineau and Lambert, 1974; Bell, pers. comm., 1978). Data presented by Holmes and Cahen (1956) should have ended the dispute that the Phalaborwa complex is as young as Karoo in age (Brandt, 1948; Truter, 1955). However, many North American and European geologists still question the age (Bell, pers. comm., 1978), and it has

been quoted as possibly Karoo as recently as 1966 (Heinrich, 1966).

2.2 SATELLITES

2.2.1 General Geology

Satellite bodies of syenite and feldspathic pyroxenite are concentrated on the periphery of the main complex but occasional pipe-like intrusions occur throughout the countryside for many kilometres and extend northward to the southern edge of the Soutpansberg Range (Brandt, 1948) and into the northern parts of Kruger Park (Hanekom et al., 1965). Brandt (1948) suggested that passive intrusion of alkali granite preceded explosive brecciation which was a precursor to the main period of syenite emplacement. This resulted in plugs showing various degrees of brecciation from narrow brecciated margins to entire hills of oriented breccia fragments. Brandt (1948) described five types of syenite which are distinguished by differences in grain size and were interpreted by Brandt (1948) as having different origins. Hanekom et al. (1965) gave cursory descriptions of the various types of plugs but discussed the syenites only with respect to relative timing of emplacement of syenite and pyroxenite members of the main complex. Hanekom et al. (1965) interpreted the syenites as being emplaced after the pyroxenites.

Frick (1975) studied the petrography and major element chemistry of the syenites and concluded that, although there

are gross textural differences among syenites of the plugs, they are chemically identical and represent a differentiated end product from an alkali basalt magma which formed the main complex. Briden (pers. comm., 1977) found that palaeomagnetic properties of the syenite satellites suggest that syenite magmatism took place over 200 m.y. beginning with the emplacement of the main complex and occurring in spurts thereafter.

The presence of pyroxenite pipes has long been noted in the area. Two pyroxenite pipes are present on the map of Hanekom et al. (1965) which occur to the east of the main complex; one is at the site of the Palabora Mining Company magnetite dump, and the other is too deeply weathered to yield any petrologic information. The third pyroxenite pipe at the Guide Cooper Mine property is the only one of the three which has been described in any detail (Shand, 1931).

The Guide Copper Mine pyroxenite body is pipe-like in form with a U-shaped outcrop covering approximately 15,000 square metres (Hanekom et al., 1965). The feldspathic pyroxenite which resembles that of the main complex is closely associated with the syenite of the adjoining Kitchener's Kop and carbonatite dykes have been mapped in the area (Shand, 1931). Locally, biotite and bornite form irregular patches and constitute a major proportion of the rock.

2.2.2 Petrography

The syenite plugs surrounding the main complex have been studied petrographically by Frick (1975) in coordination with his chemical study. He divided the syenites into porphyritic, hypidiomorphic, granular and gneissic types. All four textural types contain a similar mineralogy of orthoclase and/or microcline, aegirine-augite, quartz, alkali amphibole, sphene, apatite, calcite, magnetite, and in the case of hypidiomorphic syenite, albite is present. Frick (1975) interpreted the various syenites as being derived from a single magma; various degrees of deformation upon intrusion and cooling caused the different textures.

The Guide Copper Mine was described by Shand (1931) as containing idiomorphic clinopyroxenes poikilitically enclosed in microcline and sulphide. Aldous (1980) thought that the sulphides replace the feldspar although there is no evidence of replacement of pyroxene. Aldous (1980) interpreted the replacement of feldspar as either remobilization of sulphide liquid or hydrothermal emplacement of sulphides. He also cited the lack of replacement of pyroxene as evidence against hydrothermal alteration.

Chapter III

GEOLOGY AND FIELD RELATIONS

The general geologic observations made here relate to the rock types studied in detail chemically and mineralogically. The various textural types of pyroxenites within the main complex have generally been classified together, but when studied in detail, reveal much about the nature of intrusion of the complex. Other features within the main complex, namely the nature of the contact of the main complex to the country rock, were studied when sampling within the open pit areas. Observations on country rock were made while selecting unaltered samples for isotopic analysis. The process of fenitization is not under study here.

The general geology of the satellite bodies has been reviewed in Chapter 2, but two of these, Kgopoeloe and Spitskop, have been studied in detail in order to more clearly understand the relationship of the plugs to each other and to the main episode of igneous activity in the main complex.

3.1 MAIN COMPLEX

3.1.1 Country Rock and Its Fenitization

Two rock types dominate the area surrounding the main complex. To the north and northeast of the complex a pink, equigranular granitic rock occurs and from the central part of the complex to the south, a white, gneissic biotite

granitic rock containing areas of muscovite pegmatite, dominates the geology. These two types of fresh country rock correspond to the two types of metasomatized or fenitized country rocks found near the contact of the complex as exposed in the Foskor and PMC open pits.

The pink, granitic rock is present at the western contact in the Foskor pit and is typical of fenitized rocks by having a distinctly reddish tinge with "schlieren" of dark green pyroxene. Samples taken from diamond borehole cores show progressive desilicification as the contact of the complex is approached with the concomitant replacement of plagioclase by potassium feldspar. Trace amounts of phlogopite have been found in one sample of fenitized country rock.

The second type of metasomatized rock, found at the western and southern edges of the PMC copper pit, retains its gneissic texture but differs from unaltered country rock by its darker appearance caused by the presence of clinopyroxene. Potassium enrichment of feldspar is also present in this fenite as the contact is approached.

The extent of metasomatic effects is difficult to establish. In the northern, equigranular rock type, samples taken up to five km from the contact contain some dark green pyroxenes. Whether these were present prior to the intrusion of the main complex, are related to emplacement of the numerous plugs, or are caused by metasomatism from the main complex is difficult to determine. However, at the

contact with the main complex, both the northern pink type and the southern white type of country rock contain some plagioclase feldspar which has not been completely replaced by the potassium phase; this is indicative that the degree of alteration due to metasomatism is not intense around the Phalaborwa complex.

3.1.2 Pyroxenites

3.1.2.1 Feldspathic Pyroxenite

The most striking feature of the feldspathic pyroxenite is one which has been noted before (Brandt, 1948) but which has generally been ignored, that is the pervasive presence of euhedral pyroxenes set in poikilitic microcline. Not only does this rock type appear in the narrow band shown in Figure 2.1, but the rim thickens noticeably in places and patches occur within the massive- and micaceous-pyroxenites. The feldspathic pyroxenite often grades into massive pyroxenite but in some places there is a sharp contact between the two types of pyroxenites which is interpreted as cross cutting of the feldspathic pyroxenite by intrusion of massive pyroxenite. No chilling of massive pyroxenite at these margins has been observed.

3.1.2.2 Micaceous and Massive Pyroxenites

The micaceous and massive pyroxenites can be conveniently divided into the two types based on modal proportions of phlogopite and clinopyroxene. Pyroxenite with more than 10

percent mica is considered to be micaceous pyroxenite. Geologically, this classification is meaningless for these are gradational rock types believed to result from processes of crystallization and emplacement which together form the various textures. This classification is used, however, for convenience of description.

The massive pyroxenite always contains apatite, from less than one percent up to about 15 percent, and almost always exhibits a flow texture of sub-parallel prisms of clinopyroxene with interstitial apatite. A few areas within the Foskor pit contain friable, granular massive pyroxenite.

Micaceous pyroxenites occur with a wide variety of textures:

(1) almost unimodal rock of mica referred to as glimmerite with minor amount of clinopyroxene and/or apatite;
(2) alternating layers of clinopyroxene-apatite and mica on the scale of a few millimetres;
(3) euhedral clinopyroxene surrounded by varying proportions of mica;
(4) pegmatitic clinopyroxene with mica growing in and around the clinopyroxene; and
(5) angular fragments of glimmerite in a sugary, friable clinopyroxene matrix.

One distinctive texture of micaceous pyroxenite, type 2 from above, is found at the western side of the Foskor pit. Alternating layers of pure phlogopite and clinopyroxene-apatite form outcrops several tens of metres wide. Banding

is parallel to walls of the complex but slumping and folding of these sets of layers have occurred to form complex patterns of phlogopite and pyroxene. Figure 3.1 shows the uniform layering of this rock. The top central portion shows folding of the sets of layers. Each individual layer is remarkable in its constant thickness and lateral continuity. Individual layers can be traced for several metres.

Brecciation of glimmerite which resulted in angular and rounded fragments (Figure 3.2) within massive pyroxenite points to formation of some glimmerite prior to the pyroxene crystallization. Other textures, types 3 and 4 above, show that the two minerals formed contemporaneously, often under pegmatitic conditions (Figure 3.3).

3.1.3 Discussion

From general geological observations, there is no evidence that the feldspathic pyroxenite is a form of fenitized country rock. There is no gradation between the feldspathic pyroxenite and country rock, and feldspathic pyroxenite extends into the interior of the pipe more extensively than is generally noted (DeJager and Fourie, 1978). Whether the feldspathic pyroxenite was formed as a mixing of magma with country rock cannot be determined from field or petrographic evidence. The petrogenesis of the feldspathic pyroxenite will be discussed further with regard to geochemical and isotopic data.



Figure 3.1 "Inch-scale" layering in micaceous pyroxenite in the Foskor pit at Phalaborwa. Slumping off the side of the pipe walls has resulted in folding of sets of banding.



Figure 3.2 Fragments of glimmerite in massive pyroxenite from the Foskor pit at Phalaborwa.



Figure 3.3 Large euhedral clinopyroxenes in mica from the Foskor pit at Phalaborwa.

The "inch-scale" layering (Figure 3.1) found at the outer margin of micaceous pyroxenite is good evidence for magmatic, cumulus processes operating in the main complex. Petrographic evidence for a cumulus origin will be presented in Chapter 4. However, vertical, alternating, often folded layers of phlogopite and clinopyroxene-apatite is a texture similar to some found at the base of several basic intrusions (Hess, 1960; Morse, 1969; Irvine, 1974; Campbell, 1978). Hess (1960) noted regularly alternating layers of plagioclase and pyroxene, each a half inch thick, in the Stillwater intrusion. Similar textures showing layering from millimetre to centimetre dimensions have been described at Kiglapait (Morse, 1969; Irvine, 1974) and most recently by Campbell (1978) at Jimberlana. Campbell suggests that this texture is not a result of minerals being transported great distances as is suggested by the original definition of cumulate but results from crystallization and accumulation in situ, especially along the edge of an intrusion where a magma may be supercooled. All these workers have noted perturbations of the layering resulting from gravity slumping, folding, or magma movement.

The occurrence of "inch-scale" layering at Phalaborwa only near the contact of pyroxenite with the country rock supports a cumulus origin for this rock type. Folding of the sets of layers is consistent with this mechanism of formation because unconsolidated crystals could not be expected to maintain rigid layering parallel to the vertical walls of the complex and slump features would occur.

Flow differentiation (Bhattachari, 1967) may concentrate early formed minerals in the interior of the pipe. Platy minerals such as phlogopite have different behavior from tabular ones and may be concentrated along the pipe wall (Bhattachari, 1967) or may be carried upward in a body (Edgar et al., 1976). Gravity settling must be of some importance due to the specific gravity of many minerals versus the low viscosity of silica under-saturated magmas (Shaw, 1972).

Rifting of early-formed rock fragments by a gently flowing liquid or more probably a crystal mush would produce the broken nature of glimmerite, micaceous pyroxenite and massive pyroxenite blocks and fragments of one type rock included in the others found in the Foskor area. This would account for the sharp and gradational contacts observed between the various types of pyroxenites.

3.2 SATELLITES

Kgopoeloe Hill and Spitskop were chosen for detailed work because they represent two styles of intrusion. The highly brecciated character of Kgopoeloe shows the result of explosive processes whereas Spitskop contains little breccia. The study of these two pipes was intended to give some insight into how the rock types and structures of the various pipes surrounding the Phalaborwa complex relate to one another and to the main complex.

The location of the pipes is shown in Figure 2.1. Kgopoeloe Hill is situated 2 km to the north-northwest of the Phalaborwa township. Spitskop lies 5 km from town to the northwest directly adjacent to the highway to Gravelotte.

3.2.1 Kgopoeloe Hill

Kgopoeloe Hill is a breccia plug about 150 metres in diameter whose top stands about 50 metres above the general landscape. It is comprised of two main parts: a pink, equigranular granite forming a low slope at the base of the pipe and the dominant central portion of the plug composed of spectacular, predominantly horizontally reposing, pink granitic breccia fragments in a darker, syenitic interfragmental matrix.

3.2.1.1 Granite

The granite forms a small hillock which partially encloses the breccia pipe. There is no granite exposed on the southeast and west sides of the pipe. The granite is intruded into the surrounding country rocks which consist predominantly of gneisses, schists, and granites. Some of these country rocks are present in the granite as xenoliths, particularly near the granite-breccia contact. Fractures radiate from the breccia-granite contact out into the granite; metasomatism has occurred along these fractures as indicated by a quartz-poor, 2-3 cm zone along the fracture.

The pink granite and its contact with the breccia are shown in Figure 3.4.

3.2.1.2 Breccia

The breccia is composed predominantly of originally granitic fragments which are small and closely packed on the margin at the breccia-granite contact (Figures 3.4 and 3.5) and which are larger in the centre of the pipe. The fragment size also increases downward. The fragments are primarily tabular in shape with an occasional blocky fragment and range in size from 1-2 mm in thickness and 3-4 mm in length up to about half a metre in thickness by 2-3 m in length and width. The overall horizontal orientation of the tabular fragments and the tabular nature of these rock fragments are distinctive. There are rare fragments of trachyte (Figure 3.6) and amphibolite (Figure 3.7) in the syenite matrix of the pipe. Rarely, fragments contain other rock types, such as gneiss or syenite which were incorporated into the granite before brecciation. Figure 3.5 shows such a breccia-fragment containing a fine-grained syenite.

The matrix of the breccia changes in texture as the proportion of matrix to fragment increases. Figure 3.5 shows two types of matrix. Between the very small, tightly packed fragments the matrix is primarily monomineralic alkali-pyroxene. The lower parts of Figure 3.5 and Figure 3.8 show the fine-grained syenite which fills the interfragmental space where the fragments are further



Figure 3.4 Contact of breccia (dashed line) with pink granite at Kgopoeloe.



Figure 3.5 Close-up of microbreccia at Kgopoeloe. Note the fine-grained rock (upper center) within a granitic fragment which does not extend into matrix.



Figure 3.6 Fine-grained trachyte fragment in syenite at Kgopoeloe.



Figure 3.7 Gneissic amphibolite country-rock xenolith in syenite at Kgopoeloe.

separated. This fine-grained syenite commonly weathers to a smooth, black surface (Figures 3.5 and 3.8). Toward the centre of the pipe and downward, the proportion of matrix increases and it takes on a coarser grained, hypidiomorphic, granular texture. Minor quartz (Figures 3.5, 3.8, 3.9) forms interfragmental matrix in some places, primarily near the granite-breccia contact where the granitic fragments are free of quartz.

The fragments show varying contact relationships with the matrix. Figure 3.5 shows the sharp contact of the small fragments with the matrix. Although there is a sharp contact, the edge of the fragments are "leached"; this leaching of fragments can penetrate the entire fragment. As the fragments get larger, a zone of leaching which rims the fragments is obvious (Figures 3.5 and 3.8).

As the proportion of matrix to fragments increases, the fragment-matrix contact becomes more complicated. Textures which resemble the spalling of weathered granite occur commonly at the ends and rarely within the fragment. Figure 3.10 shows the thin, slightly curved slivers of granite which are separating from the fragment. These slivers are concentrated at the fragment edge and are not dispersed within the matrix. Rare but significant cases of gradational contacts of fragment with matrix occur. Figure 3.11 shows a composite fragment of gneiss with minor granite which has a sharp contact with the breccia matrix on the lower contact but has a wispy, poorly-defined contact on the



Figure 3.8 Coarse breccia in fine-grained syenite matrix at northeast corner of Kgopoeloe breccia contact. Note the interfragmental quartz-filling at lower right of photograph.



Figure 3.9 Close-up of quartz filling of Figure 3.8, Kgopoeloe.



Figure 3.10 Spalling of granitic fragment into syenite matrix, Kgopoeloe. The arrow indicates up.

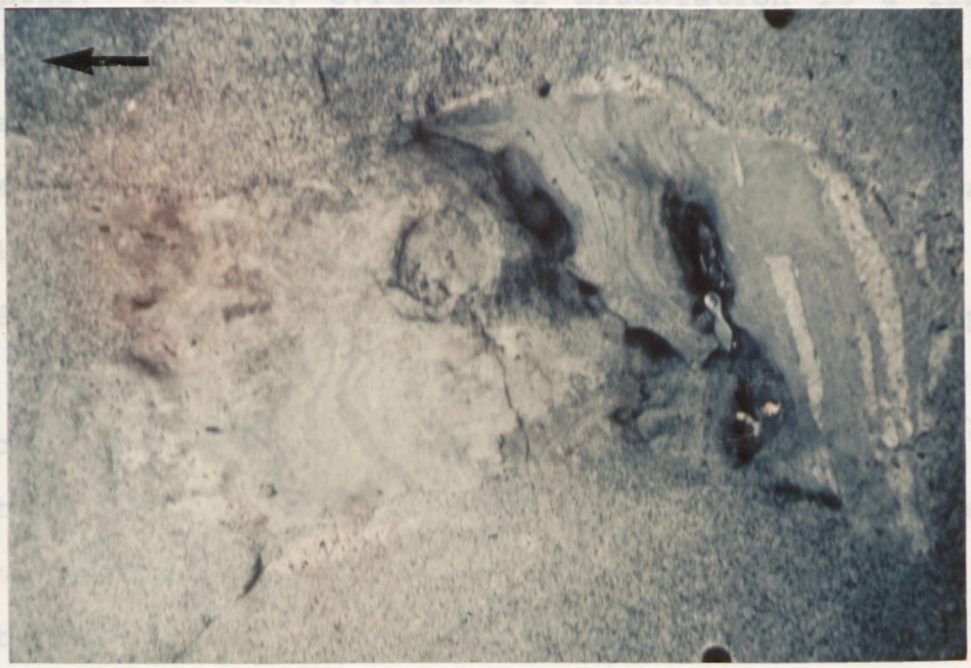


Figure 3.11 Gneissic fragment at base of Kgopoeloe syenite with diffuse upper contact (left of photograph) with syenite matrix. Arrow indicates up.

top. An unusual phenomenon is the occurrence of fine-grained syenite on the upper side of some large fragments. Figure 3.12 is a sketch of one of these fragments. This association of fine-grained syenite at the upper contact with granitic fragment does not occur in the microbreccia or in the lower part of the pipe where there are few fragments in syenite. It mainly occurs in the transitional area where fragments are relatively large and in relatively great abundance.

3.2.2 Spitskop

Spitskop is a larger hill than Kgopoeloe Hill, with a diameter of about 300 metres. From the general erosional level of the countryside, an outcrop of syenite rises to the vertical exposures of the pipe. Breccia is minor around this pipe. The only evidence of brecciation is a limited zone at the contact of the outer syenite with the vertically exposed central syenite where gneissic textured rocks such as the amphibolite found at Kgopoeloe (Figure 3.7) appear as xenoliths within the outer syenite.

From a distance, a black ring of vertically dipping rock is conspicuous at Spitskop. Figure 3.13 shows an outcrop of this rock type, hereafter called the "ring syenite." Where exposed this ring syenite varies in thickness from less than one to about four metres. It cannot be traced in outcrop all the way around the pipe because of the vertical exposure and local pinching out.

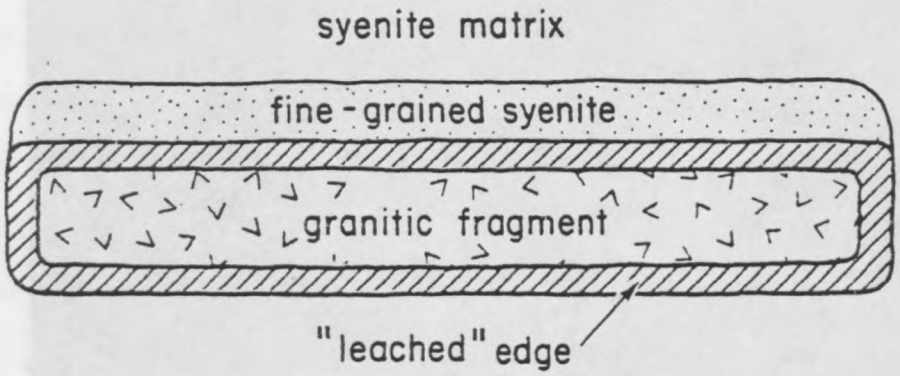


Figure 3.12 Schematic representation of the fine-grained syenite layer which sometimes occurs on top of granitic fragments at Kgopoeloe.



Figure 3.13 Outcrop of Spitskop showing the dark, ring syenite at the outer edge of the pipe.

This ring syenite has a sharp outer contact and, in most places, a gradational contact toward the centre of the pipe. Occasionally the inner contact with the central syenite is abrupt. The ring syenite is black in hand specimen and is comprised of needle-like crystals of clinopyroxene set in poikilitic feldspar. The grain size of the feldspar increases from 1 to 2 cm in length in the outer part of the ring to 2 to 3 cm in length toward the inner edge. Figure 3.14 shows a narrow portion of the inner contact of the ring syenite. The sharp contact at the left of the photograph is parallel to the periphery of the pipe. In this example, the feldspar grain size changes markedly (at the hand lens on Figure 3.14) toward the inside of the ring to a finer-grained rock containing megacrysts, presumably phenocrysts. Figure 3.15 shows a more representative appearance of the ring syenite. The lower part of the photograph shows the sharp outer contact. The upper left corner shows a more gradational contact but the lower right hand corner shows a sharp inner contact. It appears that the ring may be cut by the central syenite giving the sharp inner contact and removing the ring syenite locally.

The rocks of the centre of the plug are predominantly alkali syenite which appear to have a cumulus texture. Rhombs of potassium feldspar with surrounding alkali pyroxene and quartz show flow textures and strong alignment of feldspar grains. These central syenites contain occasional large, 10-15 cm in length, crystals of potassium



Figure 3.14 Close-up of the ring syenite and its gradational nature with the central syenite, Spitskop.



Figure 3.15 Ring syenite and its contact with the central- and outer-syenite, Spitskop.

feldspar. This central syenite retains its texture across the plug but the grain size of the feldspar varies. The centre is coarser-grained overall although dykes of similarly textured but finer-grained syenite occur in the coarser-grained syenite.

Fine-grained, leucocratic trachyte dykes varying from 8-10 cm to 0.5 m in width cut across the pipe. These are vertically dipping and extend across the ring syenite into the syenite surrounding the pipe.

3.2.3 Discussion

Kgopoeloe and Spitskop are enclosed by granite and syenite, respectively, which are slightly more resistant to erosion than the general terrain. At Kgopoeloe it is obvious that the granite was consolidated before the brecciation occurred. Lack of exposure at the base of the granite outcrop precludes discussion on the relationship of the resistive granite to the country rock, but presumably it was an intrusive magmatic event prior to the syenite pipe. The syenite surrounding Spitskop is similar in texture and composition to other syenites at Spitskop, and, therefore,cogenetic magmas may have formed these rocks.

The breccia pipes at Phalaborwa are not unique. The potassium-rich alkaline rocks of southeastern Spain are predominantly breccia-mantled pipes (Borley, 1967) where breccia caps overlie magmatic rocks. Similarly at Phalaborwa, Kgopoeloe may be viewed as the uppermost portion

of a magmatic pipe where rising magma developed a high fluid pressure at the country rock-magma interface. As supersaturation occurred, a fluid phase was generated, possibly with an explosive force which broke the rock at the interface between the country rock and the intruding magma. Close horizontal packing of tabular fragments at Kgopoeloe point to limited amount of movement of breccia fragments in the pipe. However, complex fragments such as the one in Figure 3.5 which contain coarse and fine-grained syenites and quartz fracture-filling attest to the rearrangement of breccia fragments. There are no other fragments on the breccia-face (Figure 3.5) which may have once been attached to this fragment. There may have been some *in situ* brecciation with magma penetrating between fragments to a greater degree as they rifted downward into the magma and the lower viscosity, fluid phase penetrated the upper and outer reaches where breccia fragments remained more closely packed. Spalling (Figure 3.10) may also have been a mechanism of further breaking breccia fragments.

Comparison of densities between granite and syenite liquid show that the breccia fragments should have fallen downward through the magma. Using the data of Bottinga and Weill (1970), syenite magma with a composition of sample K21m (Table 7.2), should have a density of 2.48, 2.39 and 2.30 gm/cm^3 with 1%, 5%, and 10% water content, respectively. These densities are lower than the values for granites which are 2.516-2.809 as given by Daly *et al.* (1966).

The important aspect of the brecciation to the petrochemistry of the syenites surrounding the Phalaborwa complex is the evidence that a volatile-rich phase was important in the emplacement and geochemical development of these syenites. Also important is the fact that the degree of brecciation in a pipe may provide evidence as to how the pipes are related to one another. For example, Kgopoeloe should represent the highest structural level in any pipe. Pipes containing little or no breccia mantle, i.e., Spitskop, may represent a lower level where magmatic intrusion is dominant. Figure 3.16 is a schematic drawing of such a pipe.

The type of intrusive process should influence the composition and textures of the rocks as seen today. The fluid-rich magma at Kgopoeloe reacted with the granite breccia for there is a high surface area of contact between country rock and intruding magma. Evidence supporting this is the metasomatism of breccia fragments as indicated by the silica-poor margins of the fragments. Assimilation may be of importance since spalling of granite edges and wispy, partially melted fragments are present in the syenite at Kgopoeloe.

The texture of fine-grained syenite lining the upper edge of some granitic fragments (Figure 3.12) is interpreted as resulting from the creation of microenvironments on the upper edges of fragments due to their falling through the magma. Factors such as slight variations in fluid pressures

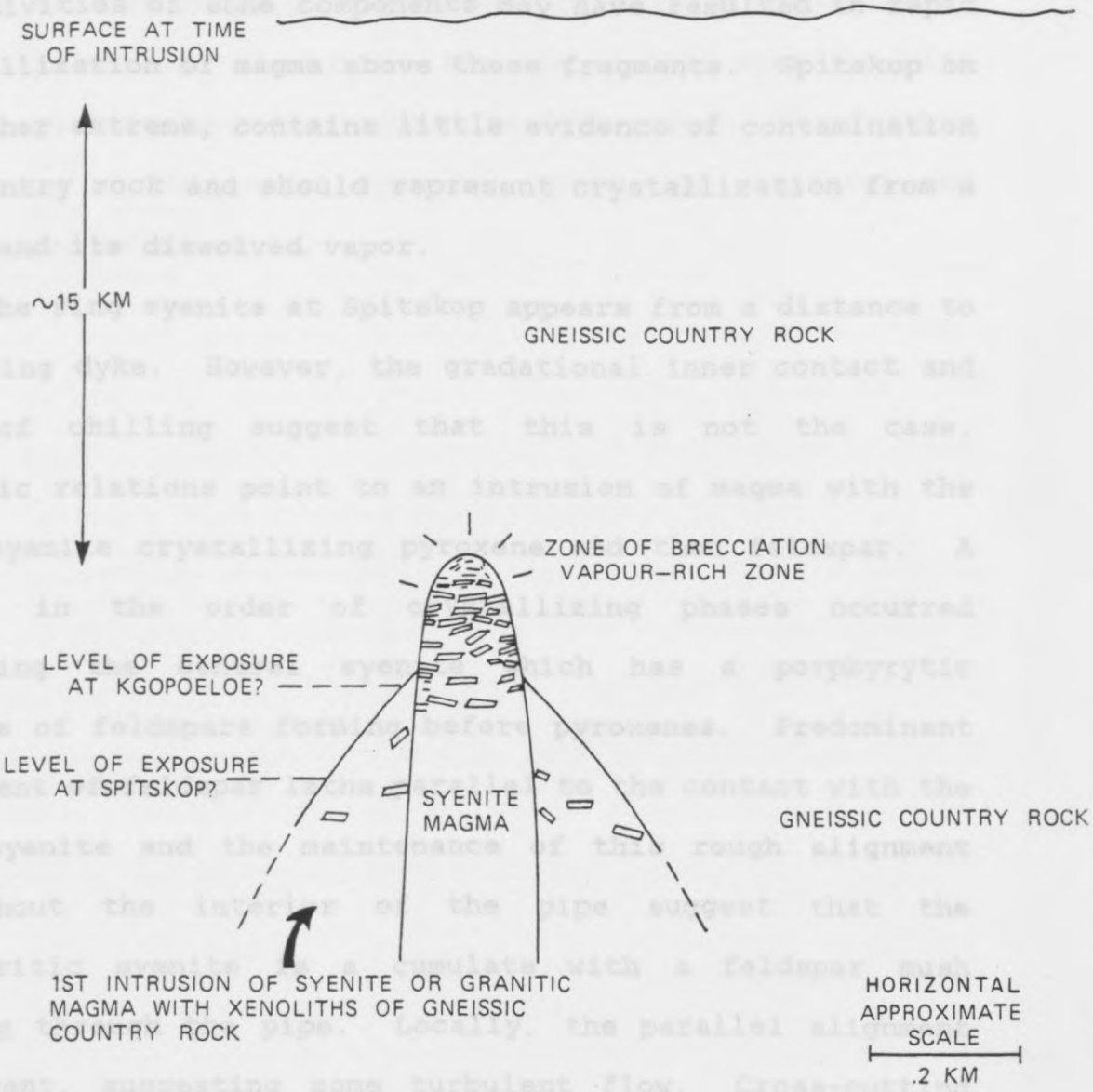


Figure 3.16 Schematic drawing of a model for emplacement of the syenite pipes surrounding the Phalaborwa complex. Kgopoeloe represents the upper portion of the pipe and Spitskop, the lower portion.

or activities of some components may have resulted in rapid crystallization of magma above these fragments. Spitskop on the other extreme, contains little evidence of contamination by country rock and should represent crystallization from a magma and its dissolved vapor.

The ring syenite at Spitskop appears from a distance to be a ring dyke. However, the gradational inner contact and lack of chilling suggest that this is not the case. Geologic relations point to an intrusion of magma with the ring syenite crystallizing pyroxene and then feldspar. A change in the order of crystallizing phases occurred producing the central syenite which has a porphyrytic texture of feldspars forming before pyroxenes. Predominant alignment of feldspar laths parallel to the contact with the ring syenite and the maintenance of this rough alignment throughout the interior of the pipe suggest that the porphyritic syenite is a cumulate with a feldspar mush flowing through the pipe. Locally, the parallel alignment is absent, suggesting some turbulent flow. Cross-cutting dykes may be interpreted as representing intercumulus- or late-stage liquids or multiple injection.

Lack of contact between separate pipes makes any interpretation of the temporal relationship among the pipes around the main Phalaborwa complex conjectural. Guide Copper Mine may represent another part of the same pipe model. However, interpretation of this paleomagnetic data of Briden (pers. comm., 1977) indicates intrusion of syenites

over as much as 200 m.y. Paleomagnetic data on Spitskop are not available and, therefore, the age of this specific pipe with respect to Kgopoeloe cannot be determined. The further discussion of this model must be based on textural and geochemical evidence.

Chapter IV

PETROGRAPHY

4.1 MAIN COMPLEX

The development of a mining industry within the Phalaborwa Igneous Complex provides an excellent opportunity to study a wide variety of non-weathered rock types. Samples were taken from representative textural and compositional rock-types having a wide spatial distribution.

The area of the Foskor open cast mine contains a large range of pyroxenite textures along with contact relations of the complex with the country rocks. Samples of carbonatite, phoscorite, micaceous pyroxenite, and metasomatized country rock were taken from the Palabora Mining Company (PMC) copper mine and their diamond borehole core.

4.1.1 Fenite

Several rocks containing clinopyroxene and feldspar were studied from borehole core around the PMC area. These rocks are a fenitized portion of the white, biotite granitic rock described in Section 3.1.1. Figures 4.1 and 4.2 show two of these rocks, representative of the fenites studied. Clinopyroxene is present but exhibits none of the cumulus textures noted later in the main complex. Pyroxenes are granular and are rarely idiomorphic. Figure 4.1 shows idiomorphic pyroxenes exhibiting colourless to bottle green



Figure 4.1 Photomicrograph of fenitized country rock with clinopyroxene lining a crack or dykelet. Sample P146-610N. Bar represents 3 mm. The rock-type of each sample is coded by the letter following the sample number. See Appendix A.1 for key.

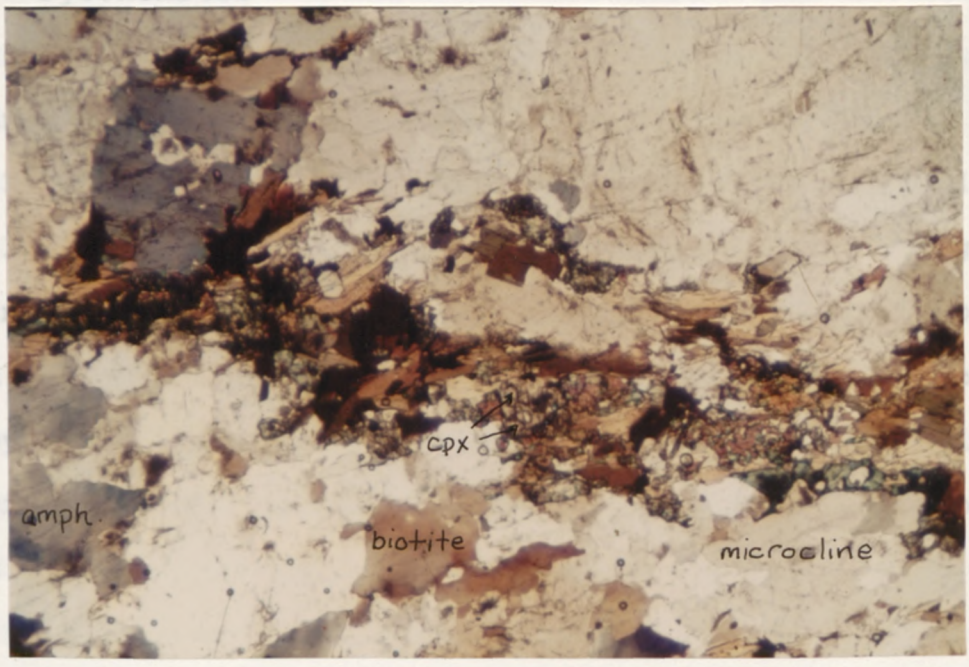


Figure 4.2 Photomicrograph of a fenitized country rock containing abundant biotite, feldspar, clinopyroxene and amphibole. Sample P146-440N. Bar represents 10 mm.

zoning outward; these pyroxenes are aligned perpendicular to the walls of a dykelet or crack. The centre of the filling contains microcline. Dark brown biotite with normal pleochorism is present in the rock but not in the "dykelet." Figure 4.2 shows a granular rock containing abundant biotite, amphibole, and fine-grained clinopyroxene. The microcline exhibits irregular grain boundaries and is highly strained. The amphibole in this sample, P146-440N[1], is the only alkali amphibole seen in or around the main complex. However, as noted in Chapter 2, previous workers have observed amphibole in metasomatized country rocks. Apart from the amphibole, this rock is typical of the fenites around the PMC area.

4.1.2 Pyroxenites

4.1.2.1 Feldspathic Pyroxenites

Subhedral to euhedral clinopyroxenes varying in length from 0.2-0.3 mm to 4-6 mm are poikilitically enclosed in microcline. Pyroxene is generally colourless or pale green in thin section and exhibits no obvious compositional zoning within a grain. However, where feldspar is abundant clinopyroxene rims are often deeper green showing a slight Fe-enrichment. In clinopyroxene-rich patches, clinopyroxene grains exhibit 120° intersections between grains.

---

[1]The rock type of each sample is coded by the letter following each sample number. See Appendix A.1 for the key.

Feldspar commonly exhibits a gridiron pattern of twinning indicating microcline. Grains are commonly anhedral; Shand (1931) reported idiomorphic grains. Nearly equant feldspar grains measure several centimetres across and contain varying proportions of poikilitically enclosed clinopyroxene.

Apatite may be present as a major component or as an accessory mineral. It occurs as small prismatic crystals poikilitically enclosed in both clinopyroxene and feldspar and as interstitial grains.

Phlogopite is rare but occasionally forms irregular patches as small laths interstitial to pyroxene. More rarely, phlogopite forms small, euhedral flakes within the clinopyroxene, and an isolated case of veinlets of calcite with phlogopite rimming the veinlet in feldspathic pyroxenite was found. Phlogopite shows strong absorption and exhibits a normal pleochroism of x = reddish-gold, y = gold-brown.

4.1.2.2 Massive Pyroxenite

The massive pyroxenite consists of 90-100 percent clinopyroxene with varying proportions of minor apatite, phlogopite, and microcline. This pyroxenite is generally well indurated and crystals are well developed, exhibiting flow banding due to parallel alignment of prisms. Massive pyroxenite is gradational into both feldspathic- and micaceous-pyroxenite.

Clinopyroxenes are colourless or pale green and vary from 0.1-0.2 mm to 1 cm in length. They have [110] cleavage and pronounced [001] parting. Grains rarely show compositional zoning and occasionally exhibit two-stage growth by a distinct break in extinction angle.

Apatite occurs as poikilitically enclosed, euhedral crystals within clinopyroxene and as anhedral, interstitial grains.

Rare, colourless amphibole, probably tremolite, occurs as incipient growth along some partings and cleavage planes of the clinopyroxene.

Phlogopite occasionally is found as small flakes within clinopyroxenes but more often is interstitial to it. Both normal and weakly reverse pleochroism may be found in phlogopites of different samples of the massive pyroxenites.

4.1.2.3 Micaceous Pyroxenite

Clinopyroxene occurs as anhedral to euhedral crystals. In varieties (3) and (4) of section 3.1.2.2, grains are always euhedral, often twinned, and show extremely well-defined [001] parting. Clinopyroxenes vary from yellow-green to bottle green among hand specimens but each hand specimen has pyroxenes of the same colour. In thin section, pyroxenes vary from colourless to pale green to grass green. In thin section, pyroxenes are not optically zoned and may enclose or be enclosed in phlogopite. All large crystals contain abundant small flakes of phlogopite.

Mica can comprise from 10 percent to 99 percent of the rock. Laths vary from less than 1 mm to several centimetres in length. DeJager and Fourie (1978) note that in this rock type, phlogopite is always interstitial to diopside and apatite. However, as noted above, many clinopyroxenes poikilitically enclose phlogopite. Pleochroism is strong, varying from yellow-browns to reddish-browns. Occasionally, the pleochroism is reversed but normal and reverse pleochroism are not found in the same specimen. Suwa and Aoki (1975) noted the presence of normal phlogopite with rims exhibiting reverse pleochroism from micaceous pyroxenite at Phalaborwa. However, this feature was not observed in this study.

Olivine crystals from 5-10 cm in length occur rarely in the pyroxenites surrounding the central pegmatoid. Serpentinization is subordinate to oxidation with lamellae and "finger print" dendrites of magnetite occurring along [010] cleavage. Reaction rims are not noticeable in the borehole cores, but one sample taken from the PMC copper pit (Figure 4.3) has a 2 cm wide reaction rim of phlogopite and clinopyroxene.

4.1.3 Phoscorite

The main petrographic feature in phoscorite which has not been described in other works is the reverse pleochroism of phlogopite. The colours of phlogopite from the phoscorite are extreme with X = reddish brown, and Z = colourless to



Figure 4.3 Photomicrograph of olivine crystal with rim of clinopyroxene and phlogopite. Sample P120P, a micaceous pyroxenite. Bar represents 5 mm. The dark rim between the olivine and clinopyroxene-phlogopite is serpentinized olivine.

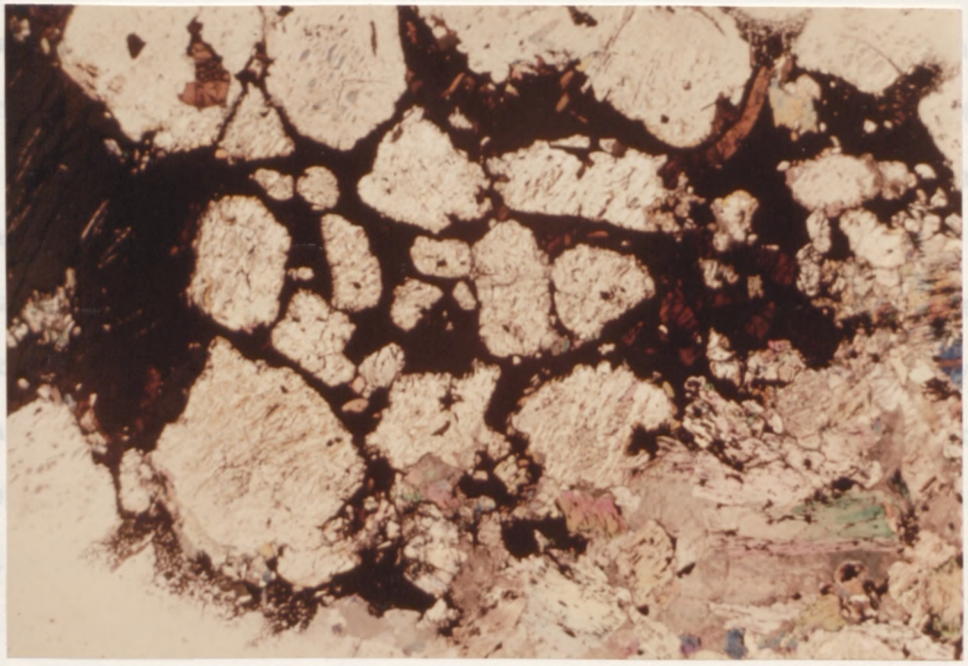


Figure 4.4 Photomicrograph of olivine crystals which have been partially replaced by serpentine enclosed poikilitically in chalcopyrite. Sample P19K. Bar represents 4mm.

pale buff. It occurs as masses around olivine and as euhedral books.

Other workers (Van Rensburg, 1965; Aldous, 1980) have noted sulphides included in olivines. An unusual texture is the reverse of that texture, in which serpentinized olivines are poikilitically enclosed in chalcopyrite with bornite exsolution (Figure 4.4). The discreet olivine grains are not in optical continuity. Although the olivines have been serpentinized, the euhedral nature of the original grain indicates that the serpentinization occurred after the precipitation of the sulphide.

Clinopyroxene is rarely present in phoscorite. In one sample, a centimetre-wide band of granular dark green clinopyroxene is present. The pyroxenes are not of uniform colour, ranging from those which are entirely dark green to others which have dark green cores to colourless rims to colourless pyroxenes containing fine lamellae of magnetite. This sample, P146-1056K, will be discussed further in Chapter 5.

Lastly, although carbonate minerals are not included in the original definition of phoscorite, they invariably are present. Fine-grained calcite occurs as disseminated grains, in veinlets and monomineralic lenses and can comprise up to several percent of the rock.

4.1.4 Carbonatite

Because of previous research on the carbonatite members (section 2.1.2.2), phlogopite and apatite are the only two minerals in which significant new features have been observed in this study. As is the case for the phoscorite, the nature of the phlogopite has generally been overlooked. Phlogopite exclusively exhibits reverse pleochroism in the transgressive and banded carbonatite. Phlogopite is rare in banded carbonatite and much more abundant in transgressive carbonatite. The colours of phlogopite from the carbonatite are similar to those of phlogopite from phoscorite. Phlogopite occasionally shows strain characteristics, and phenocrysts are often zoned (Figure 4.5) and rarely have patchy colouration.

Apatite was found in the PMC copper pit with extremely elongated crystals with parallel alignment, the crystals measuring several centimetres in length with a diameter of 2-3 mm. These are very different in habit from the usual disseminated, anhedral grains and stubby idiomorphic crystals usually observed in the Phalaborwa carbonatite.

4.1.5 Discussion

One of the key factors in unraveling the petrogenesis of the Phalaborwa complex is determining the metasomatic and/or magmatic contribution to the formation of the various rocks and minerals. Some of the criteria for recognizing metasomatic rocks established by Borodin and Pavlenko (1974)



Figure 4.5 Photomicrograph of zoned phlogopite crystals in carbonatite. Sample P134-2056C. Bar represents 10 mm.

may be recognized at Phalaborwa. A tendency for monomineralic assemblages, concentric zoning of ultramafic to more silica-rich rocks, and abundant alkali minerals sometimes replacing magmatic minerals (section 2.1.2.1) can be used as evidence that various pyroxenites, phoscorite, and even some parts of the carbonatites are results of extensive metasomatic processes. However, similar criteria for recognizing magmatic processes, as discussed below, may also explain many textures present in this group of rocks.

The variety of textures in rocks along the contact of the complex has been well exposed due to mining operations. The most problematic relationship is between the fenitized pink, granitic rocks and the feldspathic pyroxenite. As discussed in Chapter 2, controversy regarding the relationhip of the feldspathic pyroxenite to the country rock is resolved because it can be seen today that no one fenite type is present in all parts of the complex. As DeJager and Fourie (1978) point out, in the Foskor area feldspathic pyroxenite does not grade into fenite. In the vicinity of the PMC copper pit, the relatively thin sequence of feldspathic pyroxenite is in contact with a texturally and compositionally distinctively different rock, i.e., micaceous, gneissic white granite.

The origin of the feldspar in the contact rocks of alkali complexes is often attributed to metasomatism. Feldspathization as an extreme product of K-metasomatism has received extensive coverage in the literature (Heinrich and

Moore, 1970; Strauss and Truter, 1950). The feldspar in the feldspathic pyroxenites or the "fenite" at Phalaborwa has none of the features cited by Heinrich and Moore (1970) as being diagnostic of metasomatic feldspar. Turbidity, red staining, lack of gridiron twinning, and coexistence of opal, fluorite, or albite are not characteristic of the feldspar of feldspar-bearing pyroxenites at Phalaborwa. McKie (1966) suggested that microcline is converted to orthoclase during extreme metasomatism, a feature not found at Phalaborwa. While the textural features do not prove that the feldspar of Phalaborwa is magmatic, they do not support a metasomatic origin.

Similarly, the suggestion that phlogopite is a metasomatic mineral in alkalic rocks has an overwhelming support (Borodin and Pavlenko, 1974; Gittins et al., 1975; Borodin, 1965). Advocates of phlogopitization cite the existence of large-scale remnants of dunites and pyroxenites set in phlogopite-rich portions of the same rock types as examples of an incomplete process of phlogopite-replacement of clinopyroxene and olivine. Hanekom et al. (1965) and DeJager and Fourie (1978) use this argument to suggest that glimmerite in Phalaborwa is the result of phlogopitization of pyroxenite by alkali-rich, late-stage fluids. However, as noted in section 3.1.2, large exposures of micaceous pyroxenites in the Foskor pit show angular fragments of glimmerite within unfoliated massive pyroxenite. DeJager and Fourie (1978) explain this as a stage of

phlogopitization followed by glimmerite breakup due to a second injection of pyroxenite magma.

Associated rock types show textures which indicate that at least some of the phlogopite is not secondary but a coprecipitate with clinopyroxene and apatite. Figure 3.1 shows one of these micaceous pyroxenite textures. Infilling of tensional cracks in massive pyroxenite by late-stage fluids (DeJager and Fourie, 1978) does not account for the regular spacing of the bands of constant thickness found in areas tens of metres across. Likewise, the common texture of euhedral crystals of clinopyroxene set in a mass of phlogopite grains (Figure 4.6) points to an equilibrium precipitation relationship between the two minerals rather than a replacement of clinopyroxene by mica. The inclusion of mica in some of these clinopyroxenes suggests that mica was also stable during crystallization of the pyroxene.

On the other hand, rare textural relationships involving phlogopite indicate that it is not always a primary precipitate. Figure 4.7 is an example of phlogopite forming in feldspathic pyroxenite from the introduction of external material in the form of carbonatite veinlets. The lack of parallel alignment of phlogopite crystals suggests a reaction between the carbonate liquid and the vein walls of potassium feldspar and clinopyroxene rather than an accumulation of platy minerals precipitating from through-flowing magma. In this case, the phlogopite may be considered metasomatic because, whether the reaction took

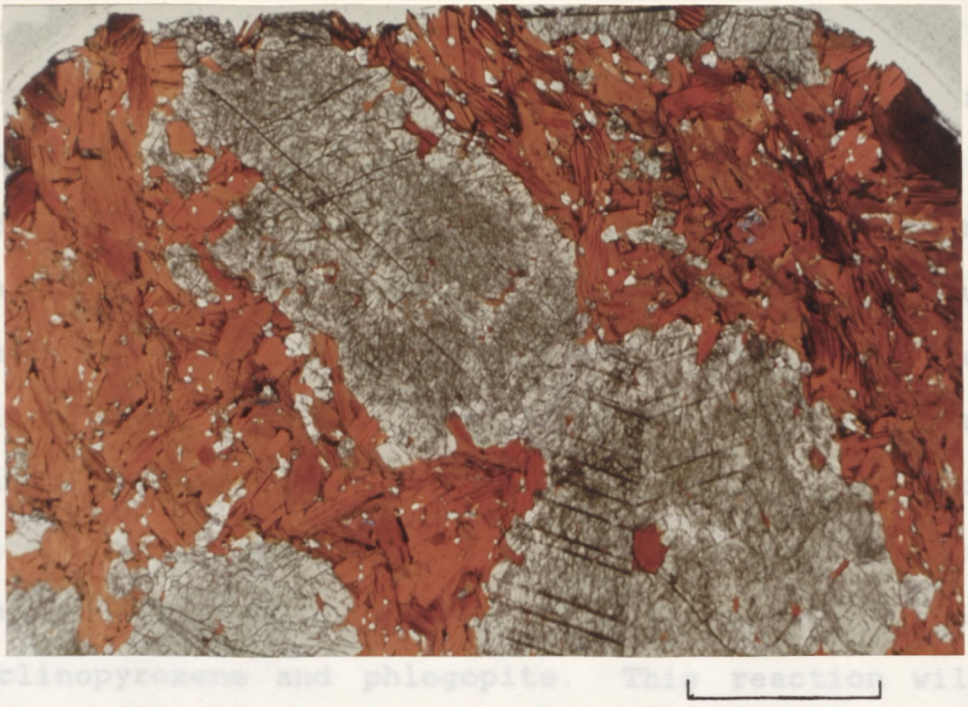


Figure 4.6 Euhedral grain of clinopyroxene partially intergrown with phlogopite. Sample P28P. Bar represents 3 mm.

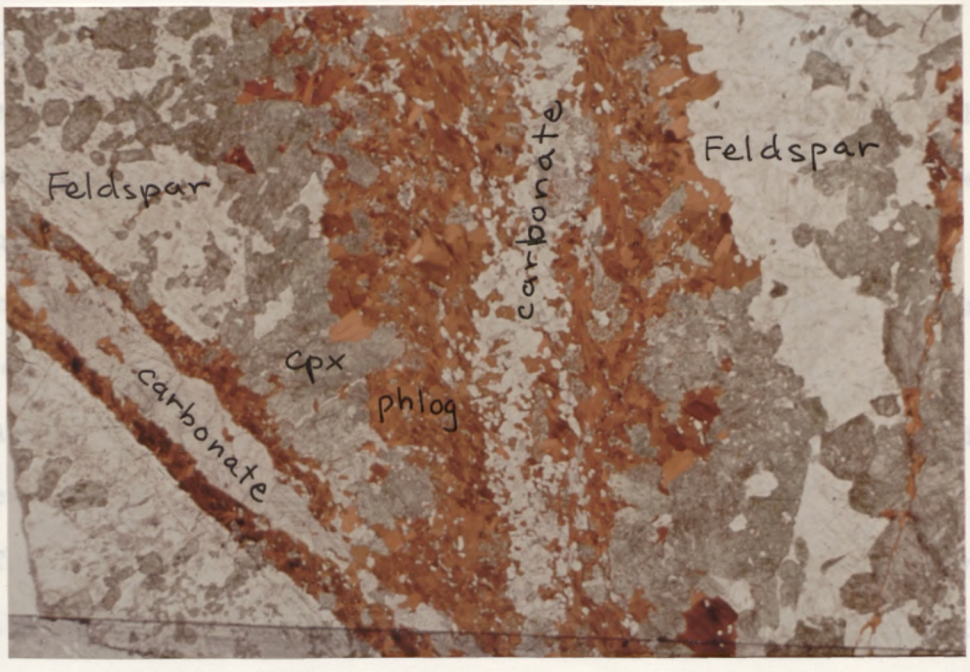


Figure 4.7 Photomicrograph of carbonatite dykelets in feldspathic pyroxenite. Phlogopite is lining the vein showing the reaction of carbonatitic liquid with the feldspathic pyroxenite. Bar represents 2 mm.

place between feldspar and carbonatite magma or feldspar and through-flowing carbonate-rich fluid derived from carbonatite in the centre of the body, fluid was derived externally from the feldspathic pyroxenite.

However, not all such reactions involve externally derived fluids. McKie (1966) cautioned against attributing all features to metasomatism, noting that many are better described as a reaction with liquid rather than a fenitization phenomenon. Figure 4.3 is an example of such a reaction. Figure 4.3 shows an olivine megacryst from a pyroxenite which appears to have reacted with a liquid to form clinopyroxene and phlogopite. This reaction will be discussed further in section 5.2.2.3. The distinction to be made here is that the olivine reacted with a magma, whether the liquid or fluid portion, and that the reacting components are part of the magma and not transported from some external source. The definition of metasomatism (Bates and Jackson, 1980) demands liquid or gases to be present within a body of rock or to be derived externally. This does not pertain to crystal-liquid reaction within a magma. This distinction between metasomatism and reaction of a mineral with a magma is important in the petrogenesis of the Phalaborwa complex.

The samples discussed in section 4.1.1 as fenites contain feldspar and clinopyroxenes but are not considered feldspathic pyroxenites. The micas appear to have been original constituents of the granite although it is possible

that they have been formed metasomatically. Fine-grained, disseminated pyroxenes are present in some rocks but do not have the characteristic colouration of alkali pyroxenes commonly associated with fenitization. The pyroxene in this type of rock is not magmatic but is interpreted as forming from metamorphism related to heat of intrusion of the complex or from a fenitizing fluid which did not contain the high Na normally associated with metasomatism. This fluid must have been rich in Ca and Mg instead. Fenitization is not under study here. The important feature is that these pyroxenes are texturally distinct from the magmatic pyroxenes.

Most of the clinopyroxene in the Phalaborwa complex is a product of crystallization from a magma. The textures of various pyroxenites point to a cumulus origin along with apatite and phlogopite. Similarly-textured rocks have been found as xenoliths in ultrabasic lavas (King and Sutherland, 1966; Dawson et al., 1970), in carbonatites (Erickson and Blade, 1963), and in kimberlites (Dawson and Smith, 1975) and most often are attributed to cumulates formed at depths from magmas congenetic with their host rock (Lloyd and Bailey, 1975). Massive pyroxenite with aligned parallel prisms attest to the presence of a crystal mush in the Phalaborwa pipe.

It has been suggested (DeJager and Fourie, 1978) that the pyroxene in the feldspathic pyroxenite and in many places throughout the complex has been recrystallized as

indicated by triple point junctions. Although this is possible, an equally plausible origin for this texture could result from their cumulate origin. Triple point junctions of 120° are ubiquitous throughout the various pyroxenites, but the feldspathic pyroxenite also shows textural changes over a few millimetres from euhedral, poikilitic pyroxenes to those with granular texture. Wager et al. (1960) show the results of extreme adcumulate growth exhibiting textures in which monomineralic clusters of cumulus crystals are characterized by 120° intersections. Adjustment of grain boundaries to a low-energy configuration at the time of their cooling is common in cumulate rocks (Upton and Thomas, 1973). A crystal mush moving within a large pipe-like body would be as likely to exhibit this texture as those rocks classically used to exhibit cumulate textures; namely, thick sequences of plagioclase at the base of a basic intrusion (Wager et al., 1960).

Furthermore, observations in this study show that of the clinopyroxenes in the complex, those in the feldspathic pyroxenite are the only ones to have some limited optical zoning. A discussion of the complicated kinetics of diffusion must be made in order to determine if primary zoning would be removed during recrystallization, but parameters such as temperature and time are not available. However, the presence of optical zoning in this rock type alone is evidence against extensive recrystallization of the clinopyroxenes.

Clinopyroxene, as noted above, has been observed with phlogopite rimming an olivine megacryst. Clinopyroxene has also been noted by itself as small anhedral grains around large olivine. This, like the phlogopite, is believed to be a reaction of olivine + liquid, but is not volumetrically significant.

Petrographic and geological observations of the carbonate-bearing rocks (Lombaard et al., 1964; Van Rensburg, 1965; Hennig-Micaheli, 1968; Hanekom et al., 1965) described in Chapter 2 indicate that some minerals in each type are cumulus. It has been noted (DeJager and Fourie, 1978) that the average proportion of magnetite to apatite in the phoscorite is identical to that found experimentally (Philpotts, 1967) for a eutectic cooling of a magnetite-apatite liquid. Local accumulations of olivine, magnetite, and apatite account for the large areas of monomineralic rocks and concentric banding within the phoscorite and concordant contact with the carbonatite.

The formation of fine-grained magnetite in vertical concentric bands in the banded carbonatite and local enrichments in the transgressive type suggest that cumulate processes are also operative in this rock type.

4.2 SATELLITES

4.2.1 Kgopoeloe

4.2.1.1 Granitic Breccia Fragments

Fragments in the microbreccia contain granular, fine-grained quartz, albite and microcline. Rarely, a feldspar crystal within a microbreccia fragment is much larger than the quartz grains. These feldspar grains have undulose extinction and are intergrown with quartz at the edge of the feldspar grain. Alkali pyroxene grains, probably aegirine-augite, penetrate the fragment along fractures and feldspar cleavage planes and are rarely enclosed in feldspar and to a lesser degree, in quartz (Figure 4.8), particularly at the fragment edge. The interior of small fragments commonly contains sphene, alkali pyroxene, and amphibole between feldspar grains.

The larger granitic fragments are of similar texture but are enriched in microcline at the outer margin of the fragment. An average composition would be 55 percent microcline, 15 percent albite, 20 percent quartz, and 10 percent aegirine-augite. Feldspar grains are zoned and the rims are recrystallized. The interior of the fragments are recrystallized and equigranular and contain microcline and albite with no zoning, but good twinning, and have sharp edges. An average composition of an unaltered fragment centre would be around 45 percent quartz, 25 percent microcline, 25 percent albite, and 5 percent biotite. Biotite, either a green or brown type, is a common accessory

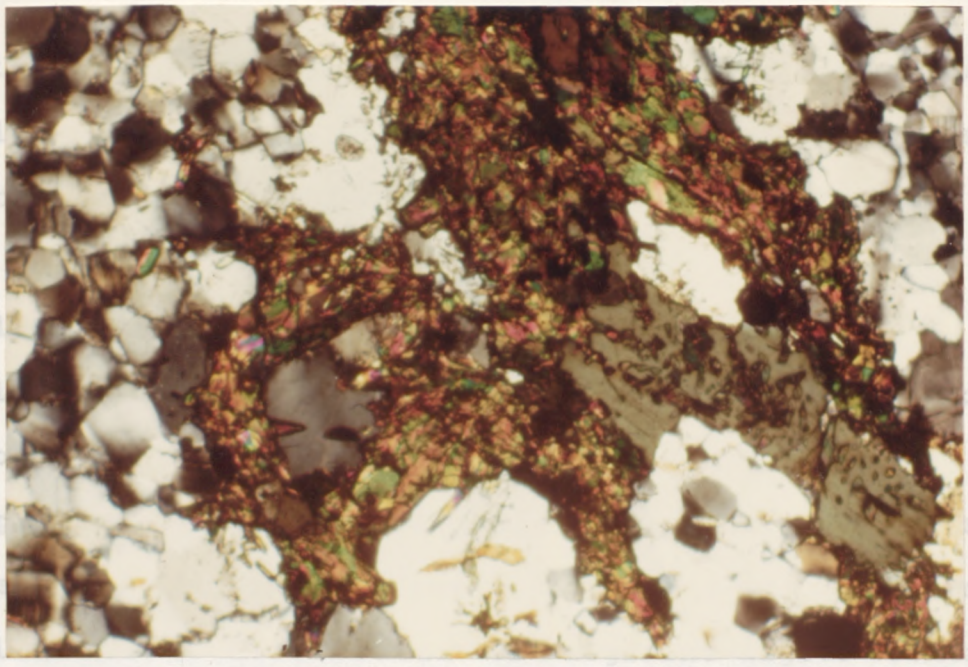


Figure 4.8 Photomicrograph of microbreccia filling of monomineralic aegirine-augite which is penetrating the fragment and replacing quartz and feldspar, Kgopoeloe. Bar represents 0.5 mm.

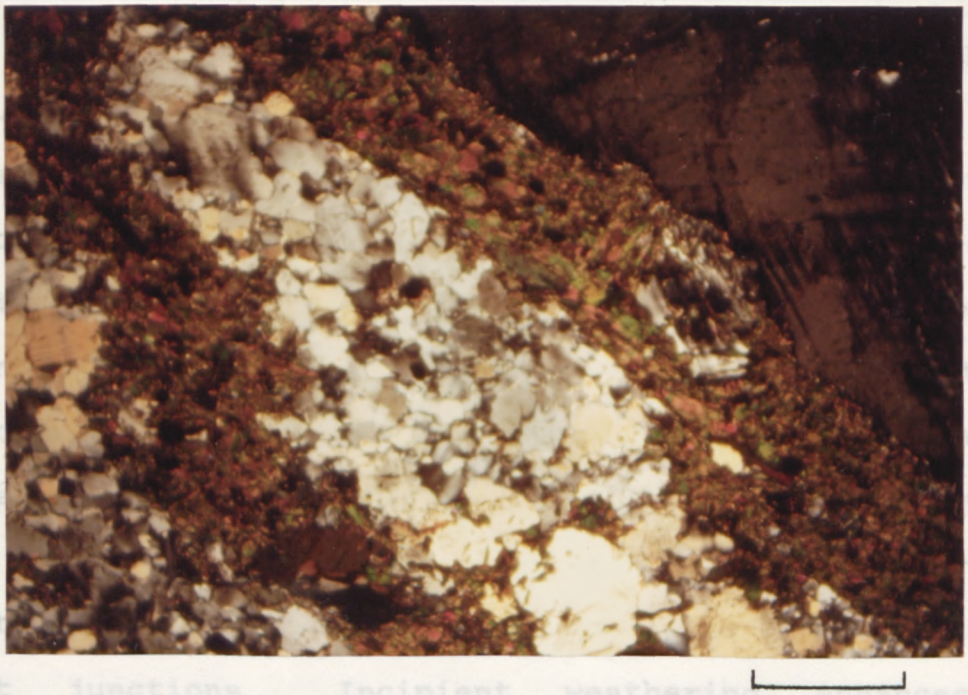


Figure 4.9 Photomicrograph of microbreccia fragment and aegirine-augite crystals lying parallel to fragment edges, Kgopoeloe. Bar represents 3 mm.

in the relatively unaltered granitic fragments. Rarely, alkali amphibole has formed along the boundary between two crystals in the interior of a large fragment.

4.2.1.2 Matrix

Matrix ranges from pure aegirine-augite to syenite from the microbreccia to the base of the pipe, respectively. Where the granitic fragments are small and closely packed and in the spalled corners of large granitic fragments, the matrix consists of a felted mass of aegirine-augite containing minor discrete grains of alkali amphibole (Figures 4.9, 4.10 and 4.11). Pyroxene grains commonly grow perpendicularly to fragment edges indicating growth into interfragmental space. This is seen in outcrop where small cavities in the microbreccia contain a felt of pyroxenes radiating inward.

Two textural types of syenite are found in Kgopoeloe Hill. The fine-grained syenite weathers to a shiny, black surface in outcrop (Figures 3.5 and 3.6). It contains microcline, albite, quartz, aegirine-augite and alkali amphibole with accessory sphene, apatite, and biotite. Sphene can comprise up to one percent of the syenite. A typical modal analysis of the fine-grained syenite would be 60 percent microcline, 15 percent albite, 15 percent quartz, and 10 percent amphibole plus pyroxene. Feldspars and quartz exhibit equigranular texture with uniform triple-point junctions. Incipient weathering enhances the compositional zoning of the feldspars showing them to have



Figure 4.10 Photomicrograph of microbreccia fragment with aegirine-augite crystals growing perpendicular to edge of the fragment, penetrating the fragment and growing in the interior of the fragment, Kgopoeloe. Bar represents 1 mm.

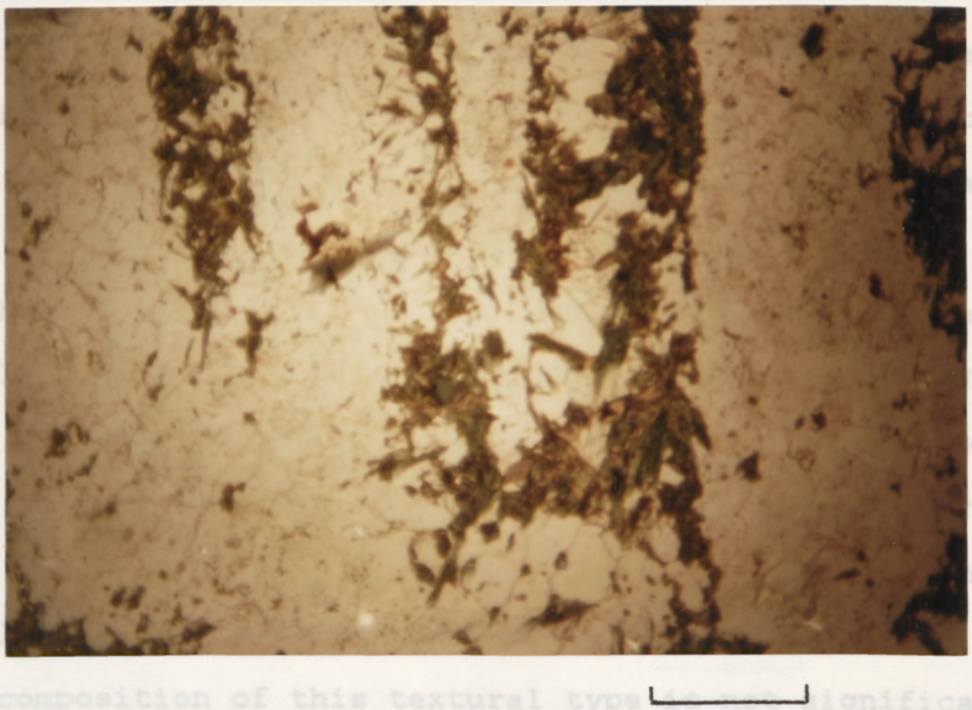


Figure 4.11 Photomicrograph of microbreccia at Kgopoeloe showing the close packing of fragments with aegirine-augite filling between fragments. Bar represents 1 mm.

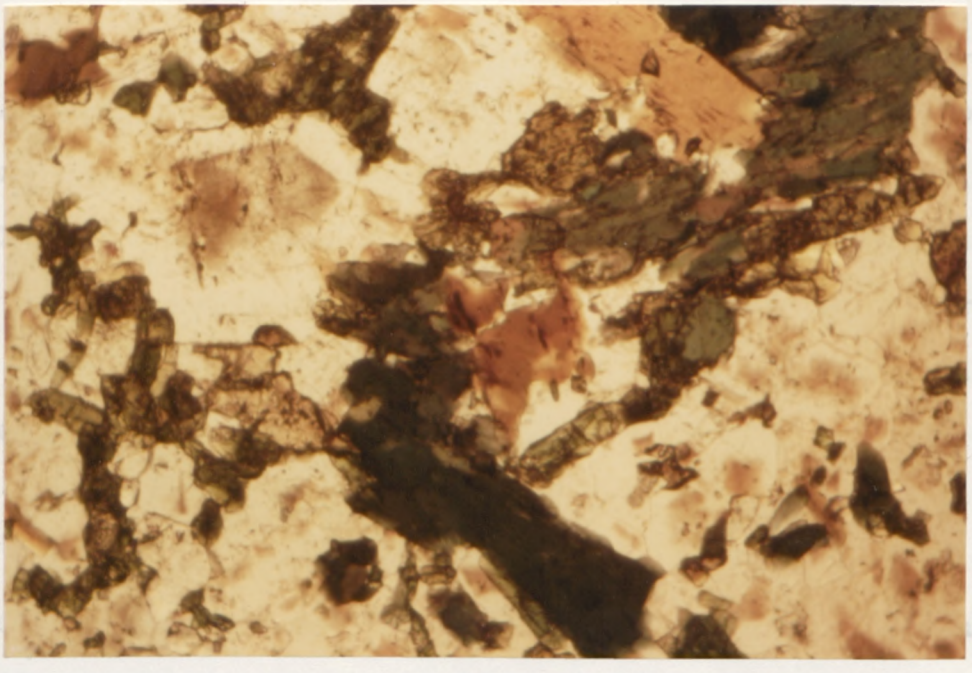


Figure 4.12 Photomicrograph of fine-grained syenite at Kgopoeloe which contains aegirine-augite and amphibole growing in intimate association. Bar represents 0.2 mm.

an albitic core which becomes potassium-rich (microcline) at the edge (Figure 4.12). This type of syenite matrix is found where the proportion of fragment to matrix is about one or more, specifically near the margins of the pipe.

The second textural type and most abundant syenite resembles the hypidiomorphic texture described by Frick (1975). Microcline rather than orthoclase as described by Frick (1975) is the dominant feldspar in this rock, forming large subhedral crystals with smaller, intergranular microcline intergrown with quartz and aegirine-augite. The modal composition of this textural type is not significantly different from the fine-grained syenite.

Throughout the syenite matrix, alkali amphibole and alkali pyroxene exhibit complex textural relations. With the exception of the microbreccia and spalled edge-filling where amphibole and pyroxene form discrete grains, pyroxene and amphibole are commonly intergrown (Figure 4.12). Commonly, the amphibole forms the centre of the grain and has a rim of pyroxene but this occasionally is reversed. These complex intergrowths are a common phenomena in peralkaline rocks (Deer et al., 1978).

4.2.2 Spitskop

Four rock types were sampled at Spitskop; the syenite on the low hill around the pipe, the black rim, the central syenite and the fine-grained, leucocratic dykes cutting across the pipe.

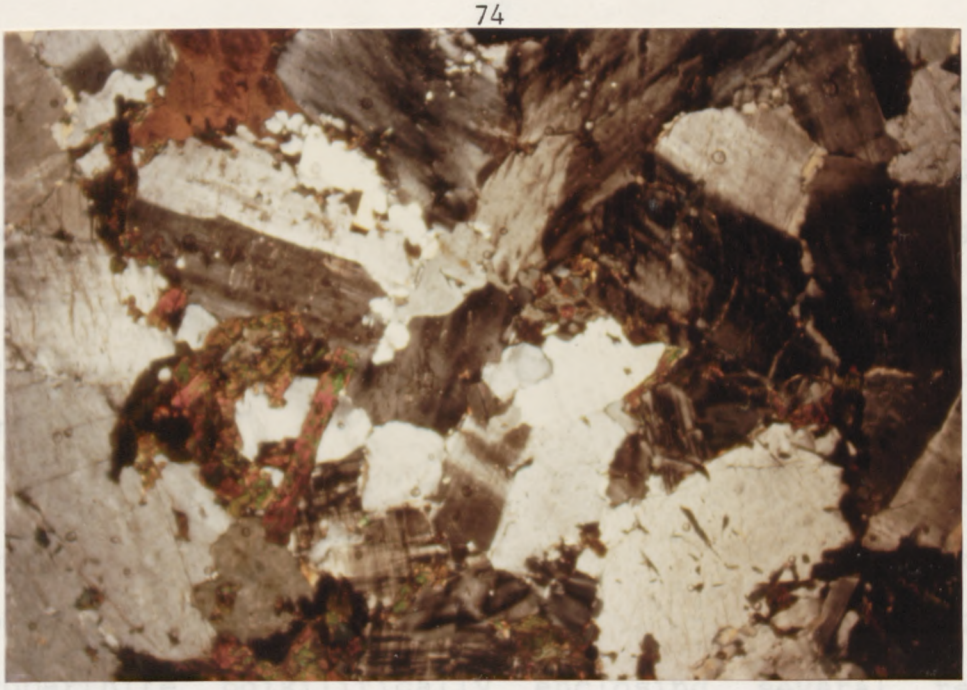


Figure 4.13 Photomicrograph of outer syenite at Spitskop showing granular texture with minor aegirine-augite. Bar represents 1 mm.

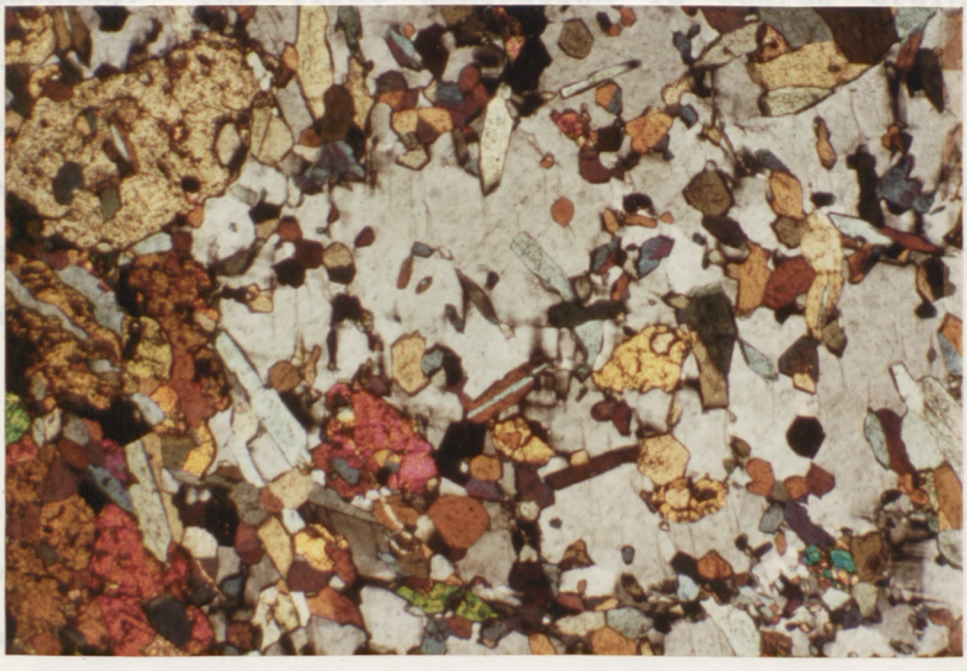


Figure 4.14 Photomicrograph of ring syenite at Spitskop showing aegirine-augite and amphibole poikilitically enclosed in feldspar. Bar represents 0.2 mm.

The syenite surrounding the pipe is similar in texture to the pipe immediately to the north (Figure 2.1); this type of syenite has been described in detail by Frick (1975) as being hypidiomorphic. It is similar in texture and mineralogy to the coarse-grained syenite at Kgopoeloe (Figure 4.13).

The black ring encircling Spitskop consists of dark greenish-black, coarse-grained syenite. The ring syenite is composed primarily of large (4-5 cm diameter) microcline and microperthite poikilitically enclosing several tens of elongate, euhedral alkali-amphibole and aegirine-augite crystals (Figure 4.14). The amphiboles and pyroxenes are aligned sub-parallel to each other within the feldspar grains. There are two generations of microcline and orthoclase. The first generation is coarse grained and encloses the pyroxene and amphibole (Figure 4.14); it is zoned and commonly has undulose extinction. The second generation is not deformed and forms intergranular material along with equigranular quartz and aegirine-augite and alkali-amphibole (Figure 4.15).

Aegirine-augite and alkali amphibole are included in the first generation of feldspar, commonly cutting across grain boundaries. Interstitially, they are randomly orientated. A notable feature is the occurrence of broken laths of the chain silicates within undeformed, granular quartz (Figure 4.16). This indicates some movement of the rock after formation of the pyroxenes and amphiboles prior to crystallization of the quartz.

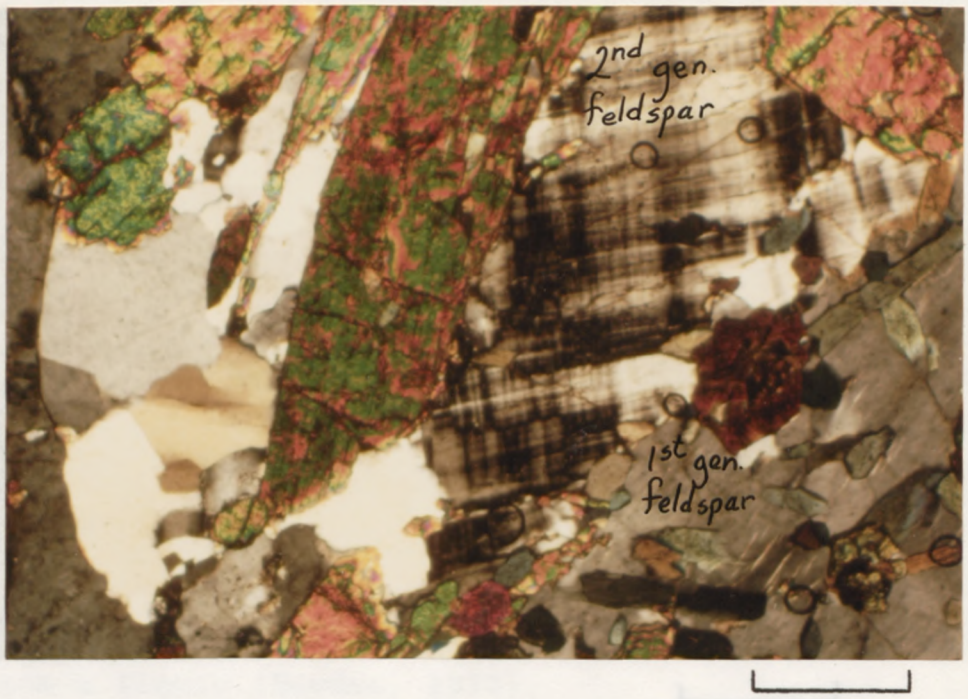


Figure 4.15 Photomicrograph of ring syenite at Spitskop showing microcline, quartz and aegirine-augite between large feldspar grains. Bar represents 0.2 mm.

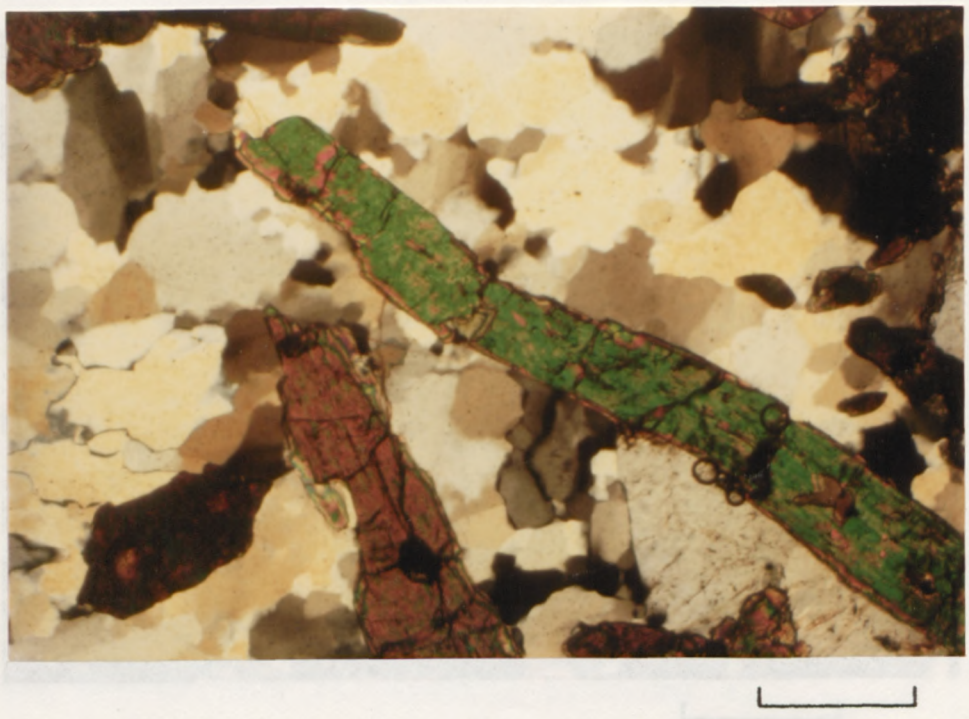


Figure 4.16 Photomicrograph of ring syenite at Spitskop showing a broken aegirine crystal in undeformed, late-stage quartz. Bar represents 0.1 mm.



Figure 4.17 Photomicrograph of central syenite at Spitskop showing idiomorphic feldspar with interstitial aegirine-augite and quartz. Late-stage feldspar has enclosed pyroxene in outer edges of grain (indicated by arrow). Bar represents 2 mm.

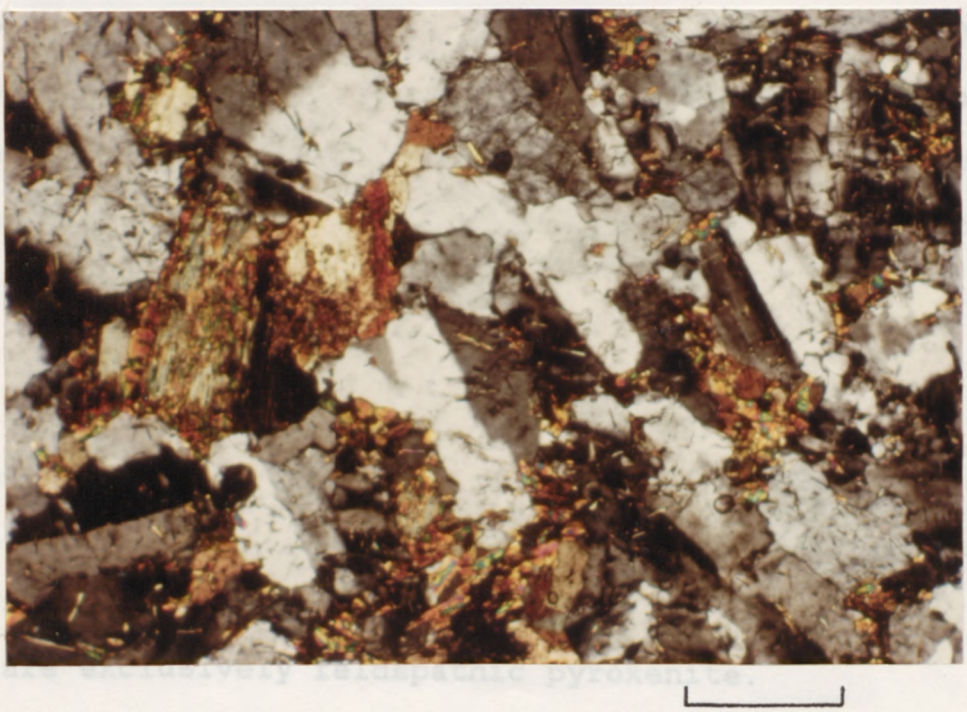


Figure 4.18 Photomicrograph of a cross-cutting dyke at Spitskop with orthoclase and crystals of mixed aegirine-augite and amphibole. Bar represents 2 mm.

The central syenite is that described by Frick (1975) as porphyritic. Figure 4.17 shows a representative sample. One feature not noted in Frick's (1975) description is the presence of pyroxene in the outer rims of some feldspar grains. There is a temptation to describe this rock as a cumulate because of the idiomorphic feldspar, sub-parallel to parallel alignment of tabular feldspar, and the linear arrangement of pyroxene and amphibole around the feldspars. However, similar textures have been described in peralkaline granites which have been interpreted as crystallizing in situ from a liquid (Bowden, 1974).

The fine-grained, leucocratic syenite dykes at Spitskop are comprised of orthoclase, aegirine-augite and alkali amphibole and quartz. The orthoclase grains are orientated subparallel and have triple-joint junctures. Needles of amphibole are commonly included in the feldspars. Minor quartz is present interstitial to the feldspar. Aegirine-augite and alkali amphibole are intergrown with rims of pyroxene on amphibole as the most common occurrence (Figure 4.18).

4.2.3 Guide Copper Mine

Samples studied from the Guide Copper Mine were taken from dumps on the mine property and therefore have no spatial significance with regard to the geometry of the pipe. The rocks are exclusively feldspathic pyroxenite.

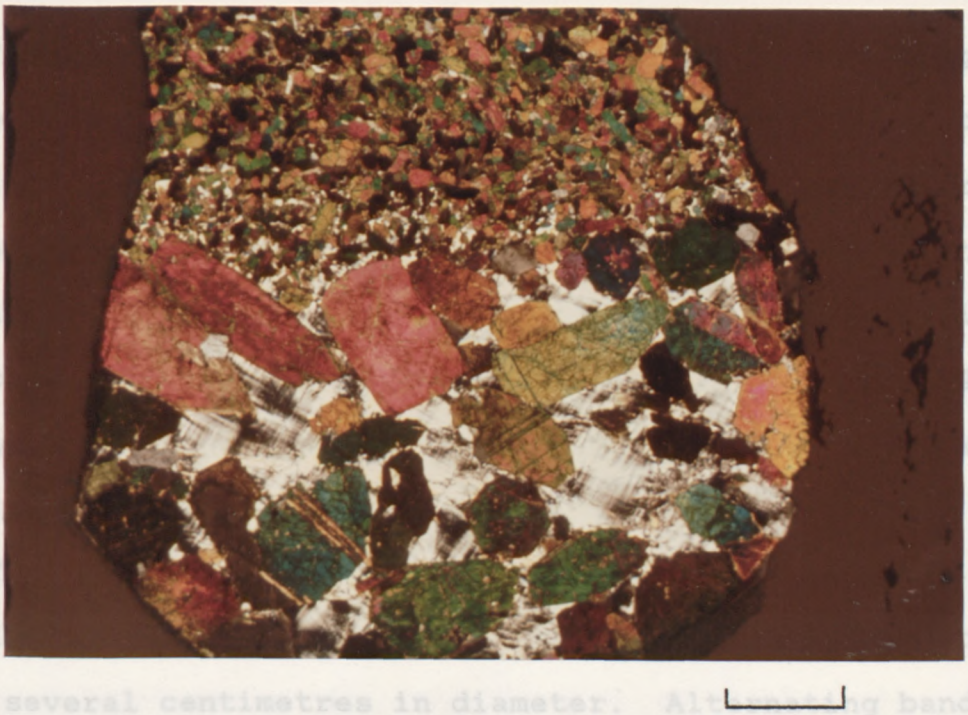


Figure 4.19 Photomicrograph of feldspathic pyroxenite from Guide Copper Mine. Euhedral clinopyroxenes are poikilitically enclosed in microcline. Bar represents 2 cm.

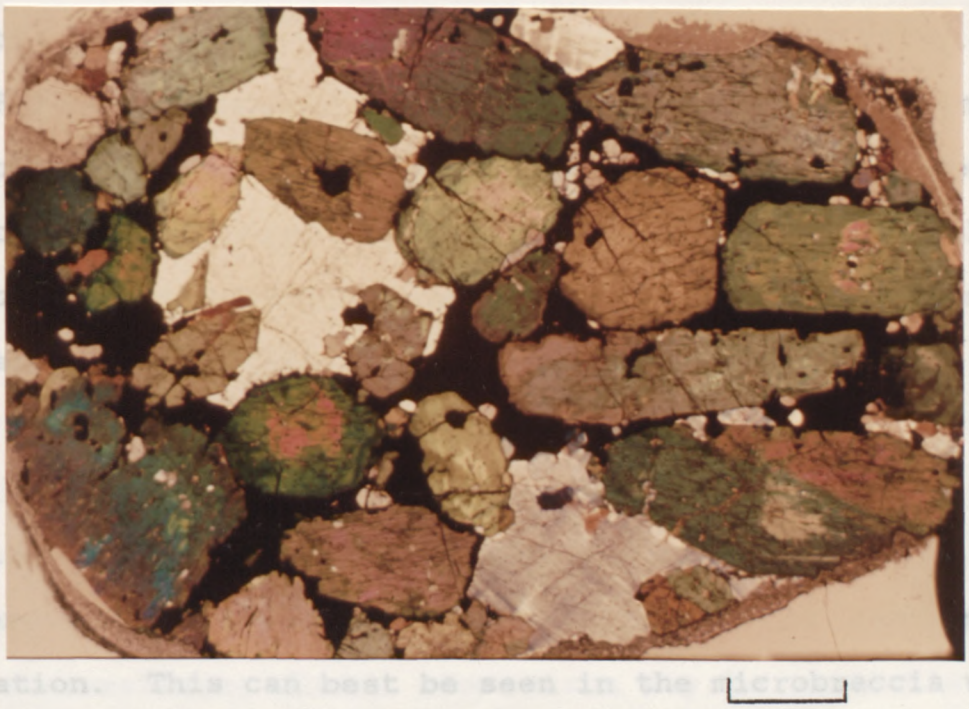


Figure 4.20 Photomicrograph of feldspathic pyroxenite from Guide Copper Mine. Zoned pyroxene laths are poikilitically enclosed in microcline and in chalcopyrite. Bar represents 2 cm.

Figure 4.19 shows the idiomorphic, bottle green clinopyroxene crystals poikilitically enclosed in microcline closely associated with finer-grained, monomineralic clinopyroxenite. Changes in rate of crystal growth and/or accumulation or mechanism of trapping intercumulus liquid may account for rapid changes in texture. In Figure 4.20, the pyroxenes are similarly enclosed in chalcopyrite which contains bornite exsolution.

The most distinctive feature of this rock is the oscillatory banding in the pyroxenes; pyroxenes vary from 1 mm to several centimetres in diameter. Alternating bands of pale green and bottle green clinopyroxene are concentrically arranged. Rarely, pyroxenes are not complete crystals but fragments of crystals. This is suggested by oscillatory banding which abutts perpendicular to the pyroxene-feldspar contact.

Phlogopite forms rare, fine-grained aggregates in the feldspathic pyroxenite. The mica has been subjected to surficial weathering and is associated with cloudy microcline. Apatite occurs as minute accessory, idiomorphic crystals.

4.2.4 Discussion

4.2.4.1 Kgopoeloe

The breccia fragments are classic examples of metasomatic alteration. This can best be seen in the microbreccia where changes in mineralogy across a fragment can be seen within

the area of a thin section. The major features of the metasomatism are the reduction in sodium feldspar and quartz and the formation of potassium feldspar and alkali chain-silicates with progressive metasomatism.

The transformation of plagioclase to potassium feldspar during metasomatism by a potassium-rich fluid is a common occurrence (McKie, 1966; Verwoerd, 1966). The simple exchange of K^+ for Na^+ results in this change in mineralogy (Orville, 1963):

$$NaAlSi_3O_8 + K^+ \rightarrow KAlSi_3O_8 + Na^+ \qquad (4.1)$$

The sodium released by this reaction can unite with quartz and iron from the fluid to form aegirine:

$$Na^+ + Fe^{3+} + 2O^{2-} + 2SiO_2 \rightarrow NaFeSi_2O_6 \qquad (4.2)$$

Similarly, when water is involved, alkali amphibole is formed. Whether riebeckite or arfvedsonite forms is dependent on the oxidation state of the iron. Reaction 4.2 requires one mole of albite for each mole of aegirine formed. Changes in modal albite are significant between the larger granite fragments and the microbreccia fragments and the interiors of large fragments with their rims. Therefore, the sodium for formation of the matrix may have been derived from the granitic fragments. However, the Fe forming the microbreccia matrix must have been present in the metasomatizing fluid. Some iron may be available from the breakdown of biotite, although biotite is found in

accessory amounts in the unaltered granite fragments. This breakdown has been noted in the incipient stages as shown by the alteration of green biotite to a brown variety (McBirney, 1979).

The decrease in quartz at the edge of fragments suggests that, in part, quartz is being utilized for the crystallization of the alkali pyroxenes and amphiboles. The decrease in quartz in the fragment edges may also be a result of simple dissolution by fluids, resulting in its reprecipitation locally in the form of interfragmental quartz filling seen in Figures 3.8 and 3.9. A similar desilicification is found along the fractures radiating outward into the granite surrounding the Kgopoeloe breccia pipe.

Evidence for a vapor-rich phase is also seen in the texture of the microbreccia matrix. The radiating habit of the alkali pyroxene perpendicular to fragment edges and the presence of the mineral in miarolitic cavities suggests that major Fe, and possibly Na, Mg and Al, may have been components of the fluid phase.[2] The fugacity of H_2O in the fluid may have controlled the formation of pyroxene rather than amphibole. A fluid phase is the most likely medium for transporting these elements because a low viscosity phase would be necessary to impregnate the thin spaces in the

---

[2]The phase is being called fluid purposefully, for at the temperatures and pressures in plutonic environments, a gaseous portion of a magma probably is present in one phase which behaves as a fluid.

microbreccia. The textures of the mineral and the rock also preclude a cumulate texture for the monomineralic microbreccia matrix.

The formation of microbreccia matrix is thought to result from forceful intrusion which shattered the edges and top of the pipe. The fragments could have formed a self-supporting framework into which a fluid percolated precipitating the alkali pyroxene. The fluid filling the microbreccia replaced granitic fragments along fractures to form the alkali pyroxene and in-filled spaces between the fragments. The fluid was cogenetic with the syenite liquid and expansion of the fluid, possibly caused by unmixing with the magma, could have acted as the force which caused the brecciation. The formation of microbreccia matrix is distinct from the formation of the macrobreccia in which syenitic magma infilled between rifted breccia fragments.

Metasomatism appears to be the mechanism for the spalling of fragments from edges of large granitic fragments. The penetration of pyroxene and amphibole into fragments along grain boundaries may eventually result in the formation of chain silicates across the fragment and subsequent crystal growth which gives the appearance of slivers fracturing and breaking away into the syenite. However, the reason for the curvature of the granitic slivers formed during this process is not explained by the metasomatic growth of the Fe-rich minerals.

The fine- and coarse-grained syenites contain abundant alkali-pyroxene and -amphibole which are commonly complex intergrowths of the two chain silicates rather than discrete grains. The intimate association of alkali-pyroxene and -amphibole is common in alkaline rocks (Deer et al., 1978), which has been attributed to fluctuating fO_2 conditions (Bailey, 1969; Nash and Wilkinson, 1970) and fluctuating chemical conditions (Jacobson et al., 1958). The difference in mode of occurrence of the pyroxenes and amphiboles between the microbreccia matrix and the syenites may be a function of the cooling of the microbreccia matrix and the syenite. Rapid cooling in the microbreccia provided no opportunity for fluctuating conditions; syenite crystallization was slower with changing conditions, whether fO_2 or chemistry. Feldspars which appear to have crystallized from a sodium-rich core to a potassium-rich rim point to an increase in the activity of potassium in late-stage fluids.

4.2.4.2 Spitskop

The ring syenite of Spitskop shows two generations of crystals. The undulose extinction of the larger feldspar crystals and broken pyroxene grains set in undeformed intergranular material suggests that intrusion of magma with a high proportion of crystals was followed by final cooling in place. The undulose extinction of the large feldspars suggest they were crystallized and deformed before final

cooling of the magma. Van der Molen and Paterson (1979) found that a critical melt fraction exists at which point supension-like behavior of grains changes to one in which granular-framework interaction of grains occurs in a liquid. Although this fraction is dependent on such factors as grain size and grain shape, grain to grain interaction takes place at approximately 30-35 percent melt. With less melt present, differential stress occurs and grains may be deformed. At Spitskop, the undeformed phases are less than 30 percent of the rock. Therefore, this mechanism of deformation is likely to have taken place at Spitskop.

The ring syenite, although very different in macroscopic appearance, is texturally somewhat similar to the surrounding syenite. The major differences are the proportion of amphibole and pyroxene included in the first generation of feldspar of the ring syenite. The texture in the ring syenite implies amphibole crystallizing early. Alkali pyroxenes and amphiboles are generally believed to be late in the cooling history of alkaline rocks (Deer et al., 1978) although as many as three generations of aegirine have been noted (Vlasov et al., 1966), some of which predate potassium feldspar. The sharp outer contact of the ring syenite with the outlying syenite points to an intrusive relationship even though there are petrographic similarities.

The difference in the central syenite and ring syenite lies in the lack of included amphibole in feldspar, the

higher proportion of intergranular material, the proportion of alkali pyroxene and quartz to second generation feldspar, and the flow texture or parallel alignment of interstitial aegirine crystals around feldspar laths in the central syenite. This implies the alkali pyroxene is magmatic. As noted in Figure 4.16, alkali pyroxene of the central syenite is included in some of the feldspar rims indicating that the feldspars crystallized in the presence of a Na- and Fe-rich fluid either during late crystallization of the feldspar laths or upon recrystallization. As Frick (1975) notes, syenites showing a greater degree of recrystallization of feldspars also contain a higher proportion of intergranular quartz and aegirine-augite. It could be that the more quartz-rich rocks are representative of late-stage liquids which would be expected to contain a higher vapor content.

Chapter V

MINERAL CHEMISTRY

Since the widespread use of the electron microprobe has come into being, petrologists can routinely study the distribution of elements between the different phases of a rock. Partition coefficients between coexisting phases and between solids and liquids have been determined both empirically and experimentally for many systems so that chemical changes in minerals can be used to determine the chemistry of the magma from which they have crystallized. This technique has particular application in cumulate rocks in which no "magma" may be sampled. Since petrographic evidence points to accumulative processes at Phalaborwa, this is a most promising method for study on these rocks.

The mineral chemistry previously published from Phalaborwa is limited to a few chemical analyses of phlogopite and vermiculite and one diopside by Gevers (1948), a baddeleyite (Hiemstra, 1955) and a few optical determinations of olivine and feldspar (Shand, 1931; Brandt, 1948; Gevers, 1948; Russell et al., 1954). Suwa and Aoki (1975) give some chemical data for phlogopites but no complete analyses. DeJager and Fourie (1978) give a bulk analysis of apatite from phoscorite. Aldous (1980) lists an olivine and phlogopite analysis from phoscorite and several apatite and magnetite analyses.

The present study has concentrated on the silicate minerals clinopyroxene, mica, and olivine because their crystallization can be used to give some indication of the characteristics of the magma. Limited data on feldspar, magnetite, and amphibole are included.

5.1 ANALYTICAL DATA

Microprobe and XRF analyses of clinopyroxene, mica, olivine, feldspar and magnetite from the main complex are found in Appendix A in Tables 5.1, 5.2, 5.4, 5.5, 5.6 and 5.7. Sample locations are shown in Figures A.1 and A.2 of Appendix A. Mineral analyses from the satellite bodies are listed in Tables 5.8 and 5.9. Analytical information and quality of microprobe data are discussed in Appendix B.

Trace element data measured by XRF for clinopyroxenes and micas are given in Tables 5.2 and 5.5, respectively. Analytical information for these analyses is in Appendix B. Impurities of mica, clinopyroxene and/or apatite could cause values of Ba, Ce, La, Rb and Sr to be incorrect for mineral separates. However, the samples were washed in dilute HCl to remove apatite. Duplicate runs on one clinopyroxene showed that this method was effective.

No effort was made to analyze for F or Cl for all the phlogopites but Gevers (1948) reports 0.62 and 0.92 percent fluorine in unaltered phlogopite from Phalaborwa. Lower concentrations were observed in three phlogopites measured on the microprobe (see Chapter 6) in this study. Because of

the variable water contents of phlogopites which cannot be measured by electron microprobe, it is difficult to assess the accuracy of an analysis. Analyses of phlogopites were considered acceptable if the total oxide weight was in the range 93.5 to 97.0 and providing they yielded a reasonable mineral formula.

5.2 MAIN COMPLEX

5.2.1 Clinopyroxenes

5.2.1.1 Crystal Chemistry

Given the general formula for clinopyroxene $X^{viii}Y^{vi}Z_2{}^{iv}O_4$, the Z position contains from 1.942 to 2.000 cations of Si with Al^{iv} varying from 0.000 to 0.043 cations. Some pyroxenes show a tetrahedral vacancy of about 0.05 cations, but this may reflect the quality of the SiO_2 analysis. For example, if sample F100P, grain 2, with 54.20% SiO_2 and 0.195 cations of Si contained 1.40 percent more silica there would be no deficiency of Si in the tetrahedral position. The important feature of the tetrahedral site occupancy is the low Al content.

The Y position is occupied by Fe and Mg with Al^{vi} of 0.000 to 0.051 cations, a low, constant amount of Mn and little or no Ti. Ca and Na occupy the X site and sometimes exceed one cation per unit formula but only by a small amount, with a maximum of 0.029. There is conflicting experimental work as to whether Ca can occur in the smaller M1 sites of clinopyroxene (Kushiro, 1964; D. H. Lindsley, pers. comm., 1978; Davidson et al., 1979).

Estimation of Fe_2O_3 was calculated by two methods. Cawthorn and Collerson (1974) calculated Fe^{3+} by assuming stoichiometry, i.e., four cations and six oxygens. This method depends on the quality of the analysis and is heavily dependent on the SiO_2 analysis. Alternatively, Fe^{3+} may be equated with Na, assuming that all the Na forms acmite. Tyler and King (1967), Stephenson (1972) and Larsen (1976) show that this is the case in pyroxenes from alkali rocks. In the Phalaborwa samples from the main complex, sodium content is commonly very low and imprecision in Na content will not vary the percentage of acmite content dramatically. The two techniques are compared in Table 5.3. Analyses in Tables 5.1, 5.2, and later in Table 5.8 are calculated by allotting an equal portion of Fe cations to Na, forming Fe_2O_3, with the remaining iron left as FeO.

5.2.1.2 Mineralogical Characteristics

Texturally, the pyroxenes may be divided into two groups: those occurring in rocks with cumulate textures (Group I), and those occurring in rocks with a wide variety of textures (Group II), some of which are considered to be metasomatic. Chemically, the pyroxenes also fall into two distinct groups. Group I pyroxenes generally are chemically homogeneous whereas Group II pyroxenes contain considerable intra- and inter-grain variation. Rocks containing Group I pyroxenes are found in the pyroxenites of the Foskor area and in the PMC area but rocks containing Group II pyroxenes

TABLE 5.3

Results of Alternate Methods of Calculating Fe^{3+} in Pyroxenes

Sample	Fe^{3+} cations per 6 oxygen after Cawthorn and Collerson (1974)	Fe^{3+} as Acmite
P146-218N	0.020	0.021
P146-610N	0.199	0.171
G12F	0.185	0.126
	0.178	0.128

are found in the micaceous pyroxenites, phoscorite and fenitized country rocks exclusively around the carbonatite centre.

Pyroxene microprobe analyses are plotted on the Wo-En-Fs diagram in Figure 5.1. Analyses by XRF method are excluded from this diagram because of inaccuracy of calcium analysis yielding a low cation content for the octahedral sites, as shown in Table 5.2. Analyses for Wo-En-Fs diagrams are commonly plotted two ways, either Ca-Mg-total Fe which is appropriate for rocks of tholeiitic compositions or Ca-Mg-(Fe^{2+}+Mn) in which Fe^{3+} has been removed. This latter method which eliminates the influence of acmite is commonly used for pyroxenes of alkaline rocks; Figure 5.1 is plotted accordingly with the ferrosilite component represented by Fe^{2+} + Mn.

Group I pyroxenes have a range of Fe/(Fe+Mg)[1] of 0.07-0.29. According to Hess (1949) they are termed diopside and salite. Within any one grain or thin section, there is little change in Fe/(Fe+Mg) (Table 5.1) or Wo component (Figure 5.1) but overall there appears to be a fractionation trend, the significance of which will be discussed later in this chapter. Group II pyroxenes vary in Fe^{2+} enrichment with Fe/(Fe+Mg) = 0.12-0.66. There is generally no decrease in Wo component among Group II pyroxenes although two samples, P146-374N and P146-440N show

---

[1]Hereafter, Fe/(Fe+Mg) represents proportion of total iron in the iron/iron + magnesium ratio.

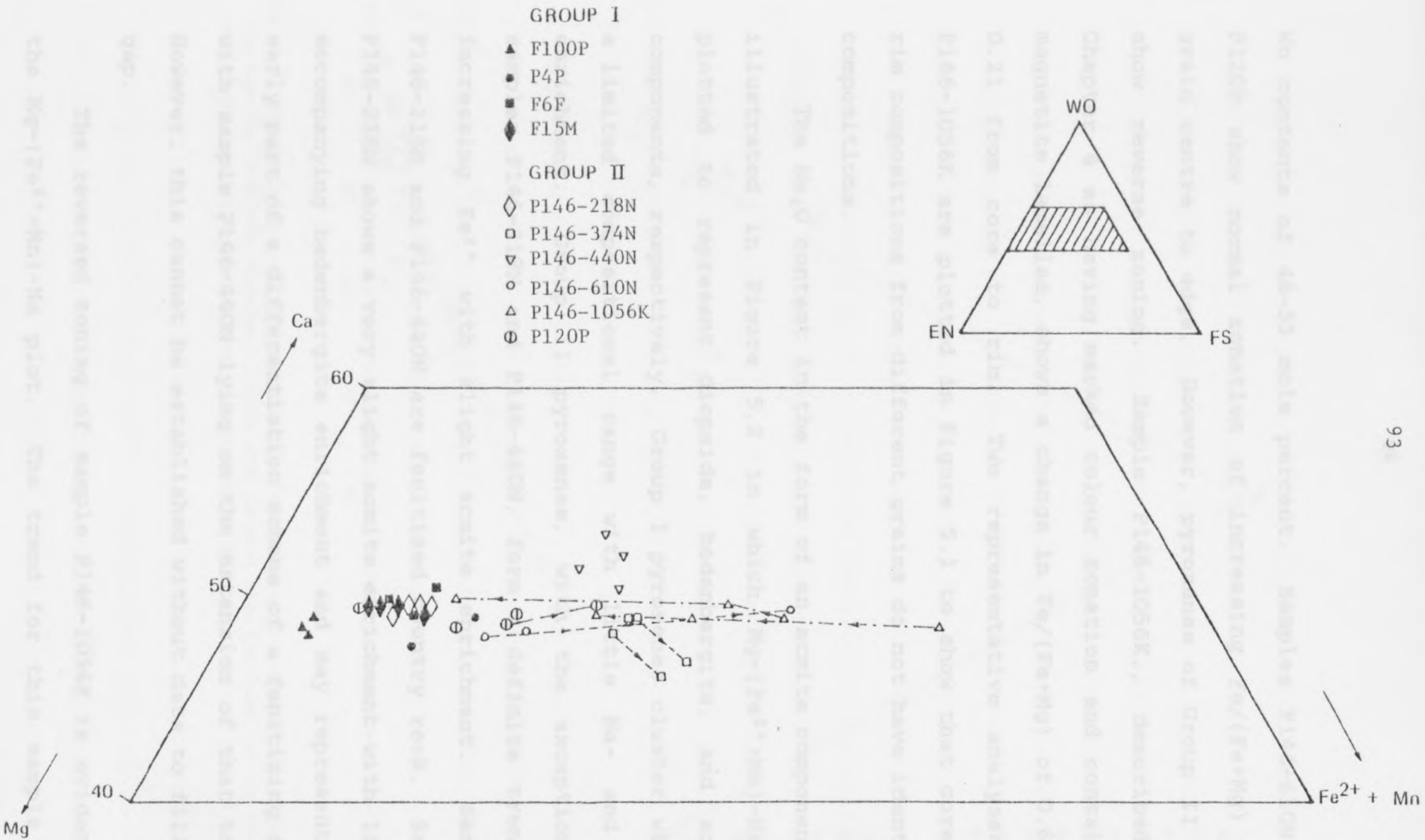


Figure 5.1 Clinopyroxene compositions from the Phalaborwa main complex plotted in the pyroxene quadrilateral. Various lines connect compositions within a zoned crystal; arrows show direction of zoning from core to rim.

Wo contents of 46-53 mole percent. Samples P146-610N and P120P show normal zonation of increasing Fe/(Fe+Mg) from grain centre to edge. However, pyroxenes of Group II also show reverse zoning. Sample P146-1056K,, described in Chapter 4 as having marked colour zonation and containing magnetite lamellae, shows a change in Fe/(Fe+Mg) of 0.66 to 0.21 from core to rim. Two representative analyses of P146-1056K are plotted in Figure 5.1 to show that core and rim compositions from different grains do not have identical compositions.

The Na_2O content in the form of an acmite component is illustrated in Figure 5.2 in which Mg-(Fe^{2+}+Mn)-Na is plotted to represent diopside, hedenbergite, and acmite components, respectively. Group I pyroxenes cluster within a limited compositional range with little Na- and Fe-enrichment. Group II pyroxenes, with the exception of samples P146-218N and P146-440N, form a definite trend of increasing Fe^{2+} with slight acmite enrichment. Samples P146-218N and P146-440N are fenitized country rock. Sample P146-218N shows a very slight acmite enrichment with little accompanying hedenbergite enrichment and may represent the early part of a differentiation scheme of a fenitizing fluid with sample P146-440N lying on the extension of that trend. However, this cannot be established without data to fill the gap.

The reversed zoning of sample P146-1056K is evident in the Mg-(Fe^{2+}+Mn)-Na plot. The trend for this sample lies

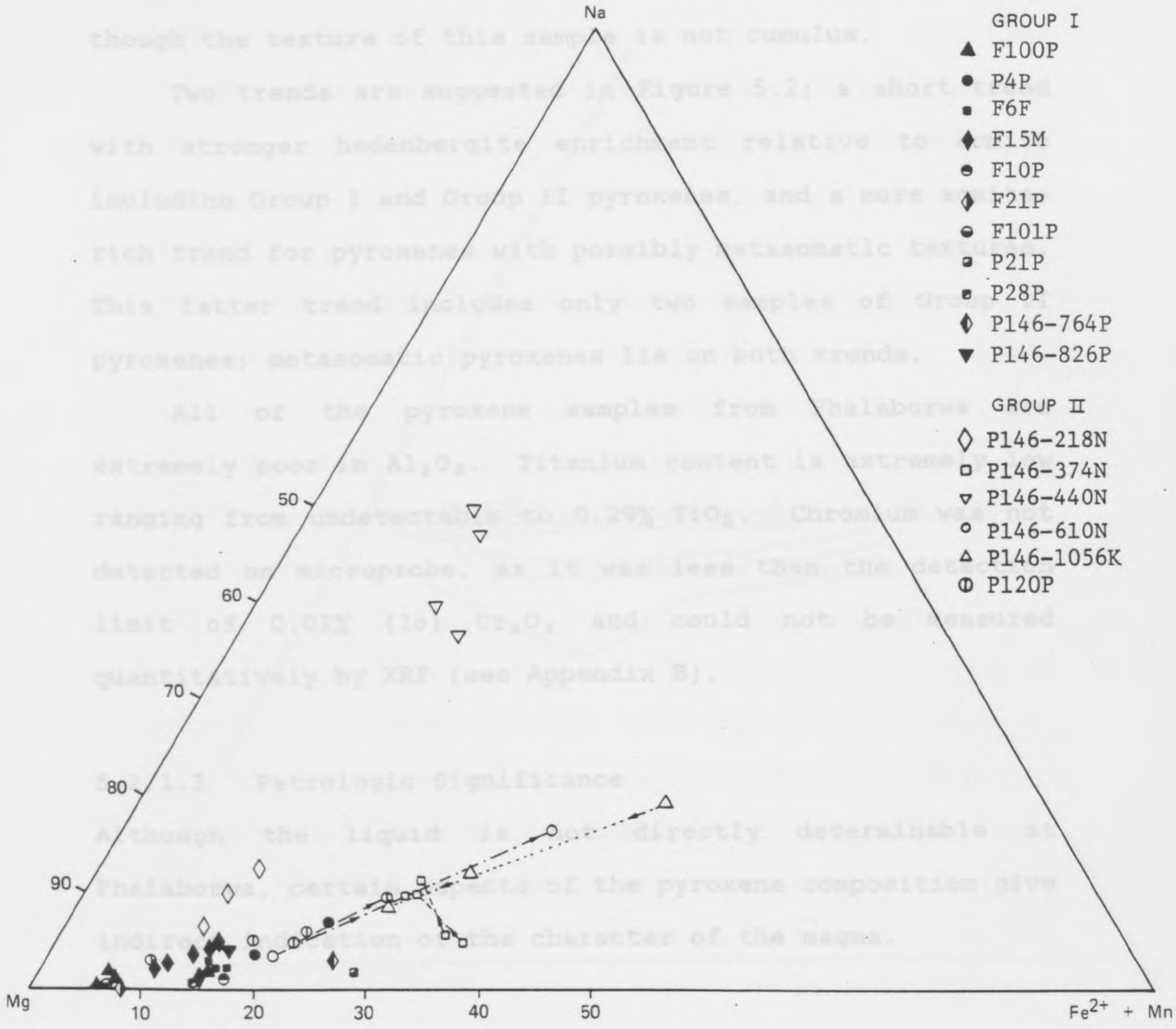


Figure 5.2 Compositions of clinopyroxenes from the main complex are plotted in the Mg-(Fe^{2+}+Mn)-Na system. Lines and arrows are the same as in Figure 5.1. Additional analyses are those performed by XRF.

along the trend established by Group I pyroxenes, even though the texture of this sample is not cumulus.

Two trends are suggested in Figure 5.2; a short trend with stronger hedenbergite enrichment relative to acmite including Group I and Group II pyroxenes, and a more acmite-rich trend for pyroxenes with possibly metasomatic textures. This latter trend includes only two samples of Group II pyroxenes; metasomatic pyroxenes lie on both trends.

All of the pyroxene samples from Phalaborwa are extremely poor in Al_2O_3. Titanium content is extremely low ranging from undetectable to 0.29% TiO_2. Chromium was not detected on microprobe, as it was less than the detection limit of 0.02% (1σ) Cr_2O_3 and could not be measured quantitatively by XRF (see Appendix B).

5.2.1.3 Petrologic Significance

Although the liquid is not directly determinable at Phalaborwa, certain aspects of the pyroxene composition give indirect indication of the character of the magma.

5.2.1.3.1 Calcium

There is little doubt that the Ca content of a clinopyroxene is dependent on the activity of silica ($aSiO_2$) in a magma rather than its alkalinity or calcium content (Smith and Lindsley, 1971; Gibb, 1973; Carmichael *et al.*, 1974). Figure 5.3 shows the position of the Group I clinopyroxenes from Phalaborwa in relation to other pyroxenes from basic

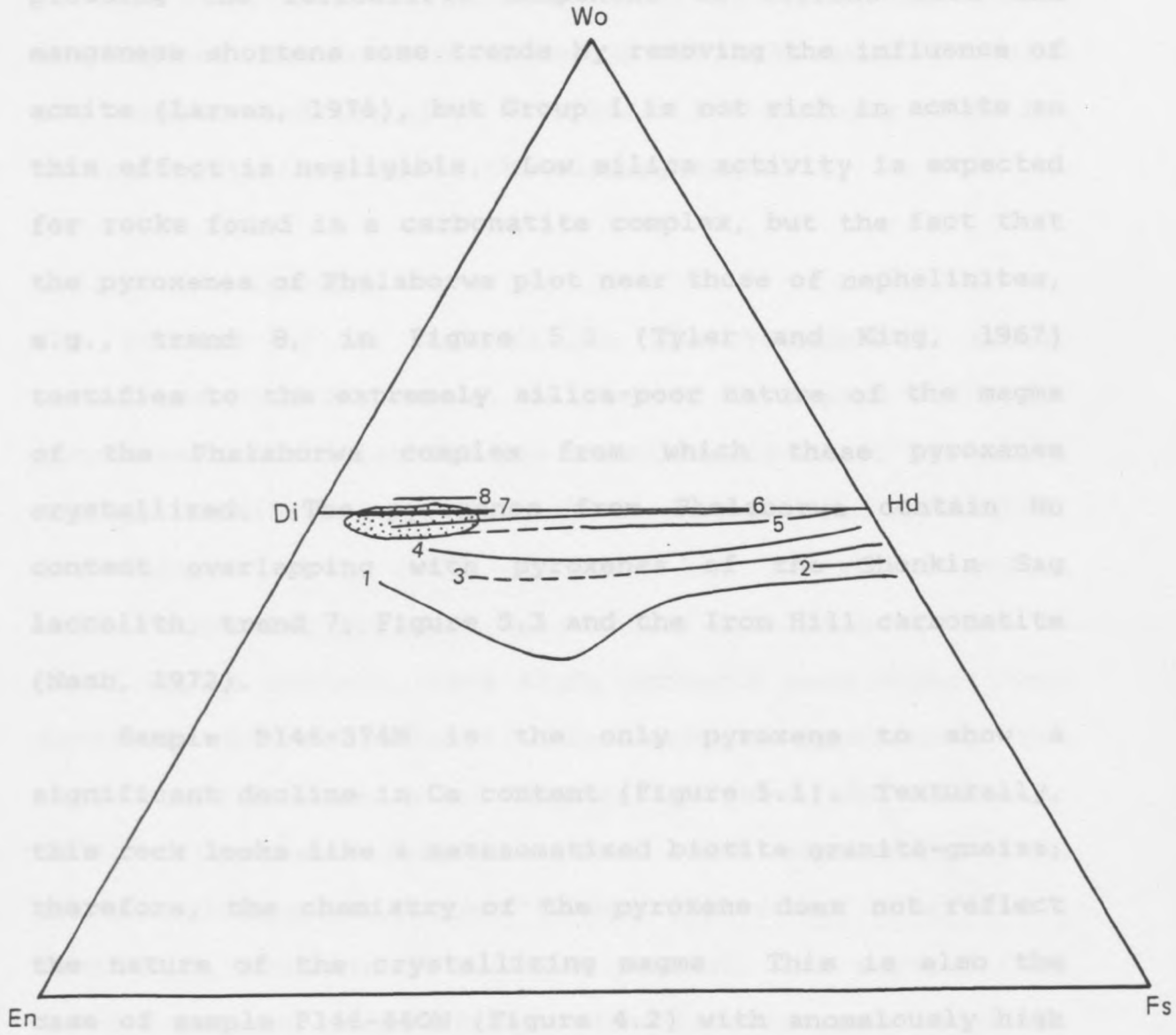


Figure 5.3 Group I pyroxenes (dotted area) plotted in the pyroxene quadrilateral. Compositional trends for various types of rocks are shown: 1) Skaergaard (Brown and Vincent, 1963), 2) pantellerites (Nicholls and Carmichael, 1969), 3) Nandewar volcano (Abbott, 1969) and Kungnat intrusion (Upton, 1960), 4) Shiant Isles sill (Gibb, 1973), 5) Tugtutoq giant dykes (Upton, 1964), 6) Shonkin Sag laccolith main trend (Nash and Wilkinson, 1970), 7) Iron Hill carbonatite (Nash, 1972) and 8) Uganda Nephelinites (Tyler and King, 1967).

and ultrabasic igneous rocks. It should be noted that plotting the ferrosilite component as ferrous iron and manganese shortens some trends by removing the influence of acmite (Larsen, 1976), but Group I is not rich in acmite so this effect is negligible. Low silica activity is expected for rocks found in a carbonatite complex, but the fact that the pyroxenes of Phalaborwa plot near those of nephelinites, e.g., trend 8, in Figure 5.3 (Tyler and King, 1967) testifies to the extremely silica-poor nature of the magma of the Phalaborwa complex from which these pyroxenes crystallized. The pyroxenes from Phalaborwa contain Wo content overlapping with pyroxenes of the Shonkin Sag laccolith, trend 7, Figure 5.3 and the Iron Hill carbonatite (Nash, 1972).

Sample P146-374N is the only pyroxene to show a significant decline in Ca content (Figure 5.1). Texturally, this rock looks like a metasomatized biotite granite-gneiss; therefore, the chemistry of the pyroxene does not reflect the nature of the crystallizing magma. This is also the case of sample P146-440N (Figure 4.2) with anomalously high Wo content. P146-440N also contains alkali amphibole and may represent a metasomatized rock influenced by late-stage Na-rich carbonated fluid.

The presence of anomalously high and low Wo content in clinopyroxenes in fenitized country rocks may reflect the relative importance of the country rock or the metasomatizing fluid in controlling the $aSiO_2$ of the rock. Pyroxenes with high Wo content should reflect low $aSiO_2$.

The presence of amphibole in sample P146-440N with high Wo content of pyroxene may indicate that this rock experienced the highest degree of metasomatism of rocks sampled around the complex, and therefore also had a low activity of silica during crystallization of the clinopyroxene.

5.2.1.3.2 Aluminum

The content of Al and Si in the tetrahedral sites, normalized to 2.0 cations, is plotted in Figure 5.4. The pyroxenes from Phalaborwa are anomalous in their low Al_2O_3 content considering their high Ca content and geological association. Most rocks of basic and ultrabasic origin which, according to their Ca content, come from systems of lower silica content, have Al_2O_3 contents much higher than pyroxenes from Phalaborwa. For example, pyroxenes from large basic plutons, e.g., Shonkin Sag (Nash and Wilkinson, 1970), Ilimaussaq (Larsen, 1976), and some rocks from alkalic plutons of Eastern Uganda (Tyler and King, 1967) have Al_2O_3 contents of 1.3-1.9 percent, 2-5 percent, and 2.9-5.9 percent, respectively. Alkalic pyroxenite xenoliths (Dawson and Smith, 1973) with similar mineralogy and texture to the micaceous- and massive-pyroxenites from Phalaborwa have much higher values of 3.0-4.5% Al_2O_3. Some rocks of kimberlitic affinity which are possibly cogenetic to carbonatites (Dawson et al., 1971) have groundmass diopsides containing 3-6% Al_2O_3. The Shonkin Sag laccolith crystallized at pressures around 0.3 kb (Nash and Wilkinson,

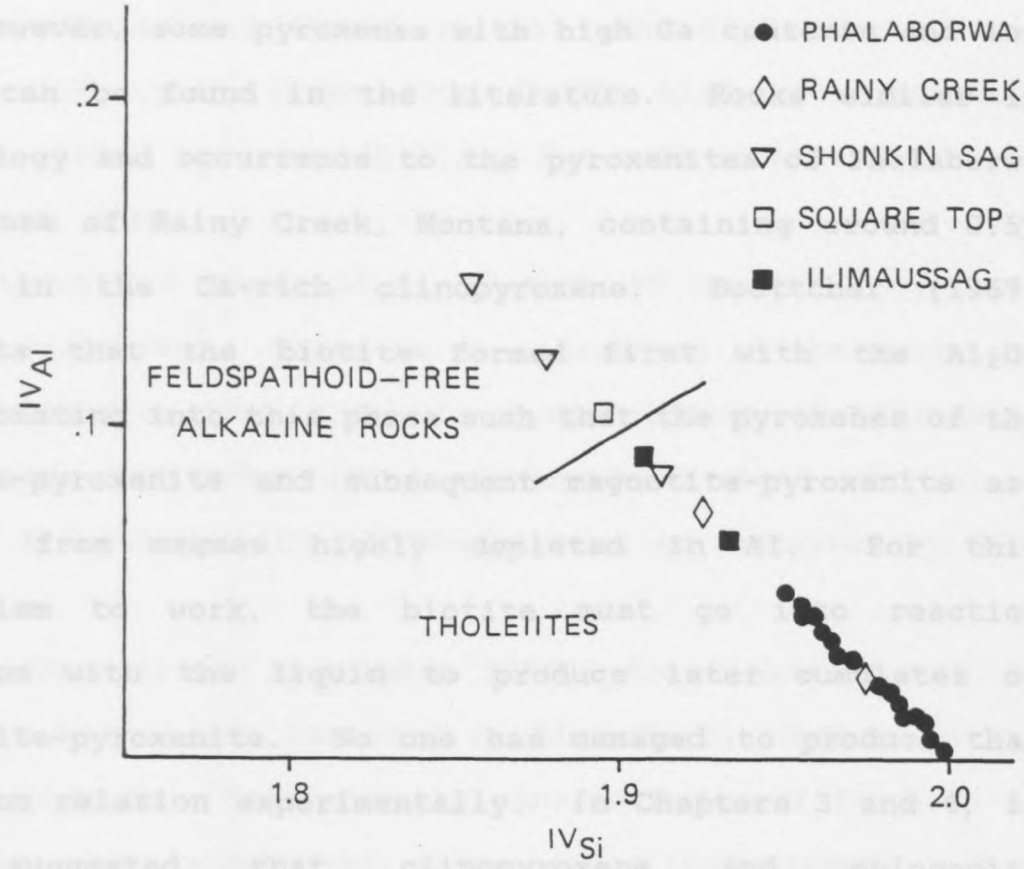


Figure 5.4 Tetrahedral site occupancies for clinopyroxenes from Phalaborwa plotted as the number of Al cations against the number of Si cations per formula unit (after LeBas, 1962). Pyroxenes from Rainy Creek (Boettcher, 1967), Shonkin Sag (Nash and Wilkinson, 1970), Square Top (Wilkinson, 1966) and Ilimaussaq (Larsen, 1976) are shown for comparison.
No distinction has been made as to Groups I and II as the groups cannot be distinquished on the basis of tetrahedral aluminum content.

1970) and Ilimaussaq crystallized at about 1 kb (Sorensen, 1969). The presence of pyroxenes with Al contents much higher than those of Phalaborwa which have crystallized at much lower pressures than those at Phalaborwa (see Chapter 6) argues against a pressure dependence on aluminum in the pyroxenes.

However, some pyroxenes with high Ca contents and low Al_2O_3 can be found in the literature. Rocks similar in mineralogy and occurrence to the pyroxenites of Phalaborwa are those of Rainy Creek, Montana, containing around 0.5% Al_2O_3 in the Ca-rich clinopyroxene. Boettcher (1967) suggests that the biotite formed first with the Al_2O_3 fractionating into this phase such that the pyroxenes of the biotite-pyroxenite and subsequent magnetite-pyroxenite are formed from magmas highly depleted in Al. For this mechanism to work, the biotite must go into reaction relation with the liquid to produce later cumulates of magnetite-pyroxenite. No one has managed to produce that reaction relation experimentally. In Chapters 3 and 4, it was suggested that clinopyroxene and phlogopite coprecipitated and that inclusions of glimmerite in massive pyroxenite were the product of rifting of cumulates in a crystal mush. Hence, there is no evidence of extensive early formation of phlogopite or biotite before clinopyroxene at Phalaborwa. Low Al_2O_3 may be an inherent feature of the original magma. The absence of cumulus feldspar in this level of the complex would support that.

Of the Uganda plutons, only the pyroxenes from the extremely silica-undersaturated melteigites and ijolites (Tyler and King, 1967) have aluminum contents approaching the values reported here. From Leucite Hills, Carmichael (1967) reports several Al-poor pyroxenes with the lowest Al_2O_3 contents occurring in the madupite, the rock with the highest alkalis and lowest silica. The Al_2O_3 contents of these rock types range from 7.32% Al_2O_3 for ugandite (Holmes, 1950) to over 14% Al_2O_3 for some ijolites (Erikson and Blade, 1963).

Figure 5.5 shows Al_2O_3 content of Group I pyroxenes versus Fe/(Fe+Mg). There is no indication in the pyroxenes from Phalaborwa that there is a correlation of increasing Al_2O_3 with Fe/(Fe+Mg) in pyroxenes which would show up as higher Al content with differentiation as suggested by Gibb (1973).

Kushiro (1960) and LeBas (1962) found that low silica activity in a magma resulted in high Al_2O_3 content in Ca-rich pyroxenes. This usually manifests itself by high Al occupancy of tetrahedral sites in clinopyroxenes. From their experimental work on melting relations of Leucite Hill lavas, Edgar et al. (1976) and Barton and Hamilton (1978) suggest that the peralkalinity of a magma influences the entry of Al_2O_3 into the pyroxene structure. Edgar et al. (1976) further suggest that a high concentration of K^+ ions affects the structure of a melt by inhibiting Ca-Al and Ca-Ti bonds. As phlogopite is an abundant early crystallizing

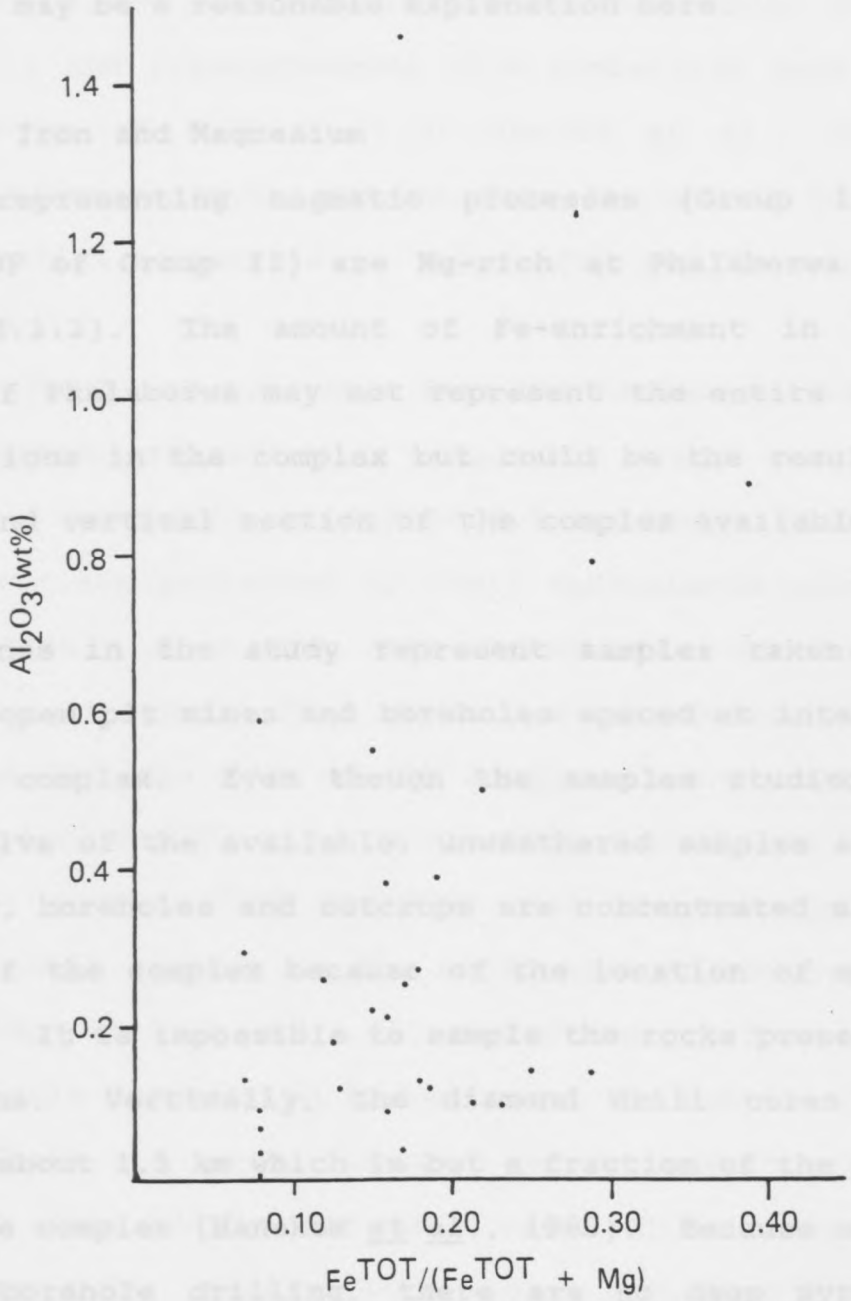


Figure 5.5 Al_2O_3 content of Group I pyroxenes plotted against $Fe^{tot}/(Fe^{tot}+Mg)$. The size of the dots are much less than the precision of the Al_2O_3 analyses,(see Appendix A).

phase together with Mg-rich clinopyroxene at Phalaborwa, the potassium content of the magma probably was quite high. Hence, this may be a reasonable explanation here.

5.2.1.3.3 Iron and Magnesium

Pyroxenes representing magmatic processes (Group I and sample P120P of Group II) are Mg-rich at Phalaborwa (see section 5.2.1.2). The amount of Fe-enrichment in these pyroxenes of Phalaborwa may not represent the entire range in compositions in the complex but could be the result of the areal and vertical section of the complex available for study.

Pyroxenes in the study represent samples taken from outcrop in open pit mines and boreholes spaced at intervals across the complex. Even though the samples studied are representative of the available, unweathered samples across the complex, boreholes and outcrops are concentrated at the periphery of the complex because of the location of mining operations. It is impossible to sample the rocks present at great depths. Vertically, the diamond drill cores have penetrated about 1.5 km which is but a fraction of the known depth of the complex (Hanekom et al., 1965). Because of the angles of borehole drilling, there are no deep pyroxene samples of magmatic origin available for study. However, more differentiated rocks with higher Fe/(Fe+Mg) may have been eroded.

Clinopyroxenes from the mantle commonly have low Fe/(Fe+Mg); groundmass clinopyroxenes from kimberlites have Fe/(Fe+Mg) of 0.05-0.10 (Emeleus and Andrews, 1975; Dawson et al., 1977) and clinopyroxenes from kimberlite xenoliths have Fe/(Fe+Mg) of 0.01 to 0.10 (Dawson et al., 1977). Hence, the clinopyroxenes samples from Phalaborwa possess Fe/(Fe+Mg) ratios comparable to supposedly undifferentiated mantle material.

The Fe/(Fe+Mg) of pyroxenes from the Phalaborwa complex which are interpreted as having a magmatic origin are shown at the sample locations in Figure 5.6. Samples from the borehole cores are projected to their approximate location on the surface. From the area around the carbonatite (Figure 5.6a), it appears that there is no systematic zoning of Fe and Mg from the edge of the complex inward. Samples P146-764P and P146-826P have Fe/(Fe+Mg) of 0.28 and 0.19, respectively; samples P21P and P28P with the same spatial relationship with respect to the outer edge of the complex have Fe/(Fe+Mg) of 0.29 and 0.15, respectively. Thus, both sets of minerals increase in Mg/Fe toward the centre of the complex. There is more intense zoning within single specimen P4P than within the area as a whole. However, despite rock-type designations on published maps, pyroxenites are not well developed around the carbonatite, and it would be unwise to characterize crystallization of the entire complex based on the pyroxenites in the carbonatite centre.

LEGEND


TRANSGRESSIVE CARBONATITE


BANDED CARBONATITE


PHOSCORITE


PYROXENITE PEGMATOID


MICACEOUS PYROXENITE


PREDOMINANTLY MICA ROCK


FELDSPATHIC PYROXENITE


FENITE


GRANITE/GNEISS


DOLERITE

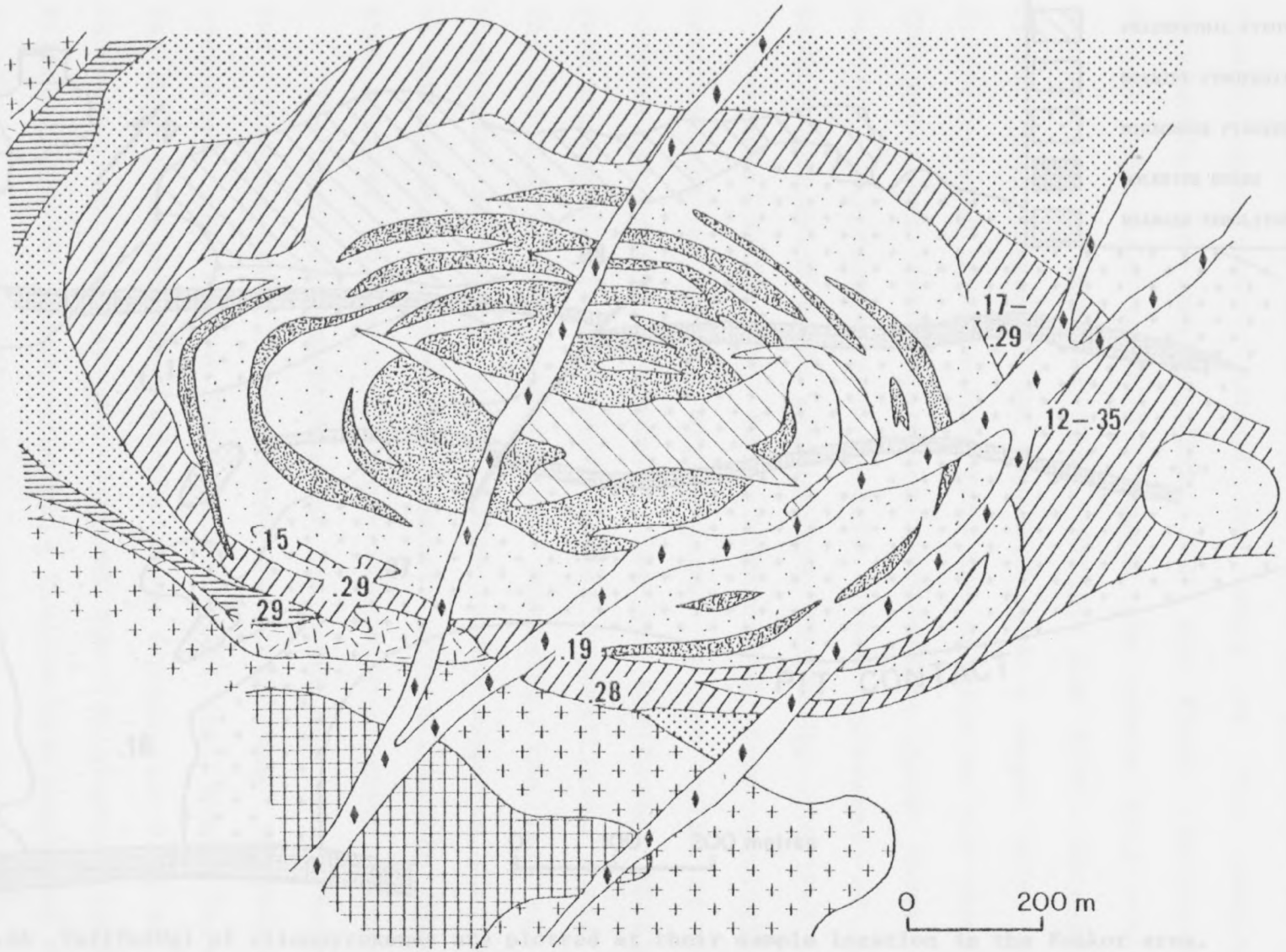


Figure 5.6a Fe/(Fe+Mg) ratios of pyroxenes are plotted at their sample locations in the PMC open pit area. Samples from borehole cores are projected onto the plane of the map. Sample P120P from Group II pyroxenes is plotted here because of the magmatic origin of the pyroxenes.

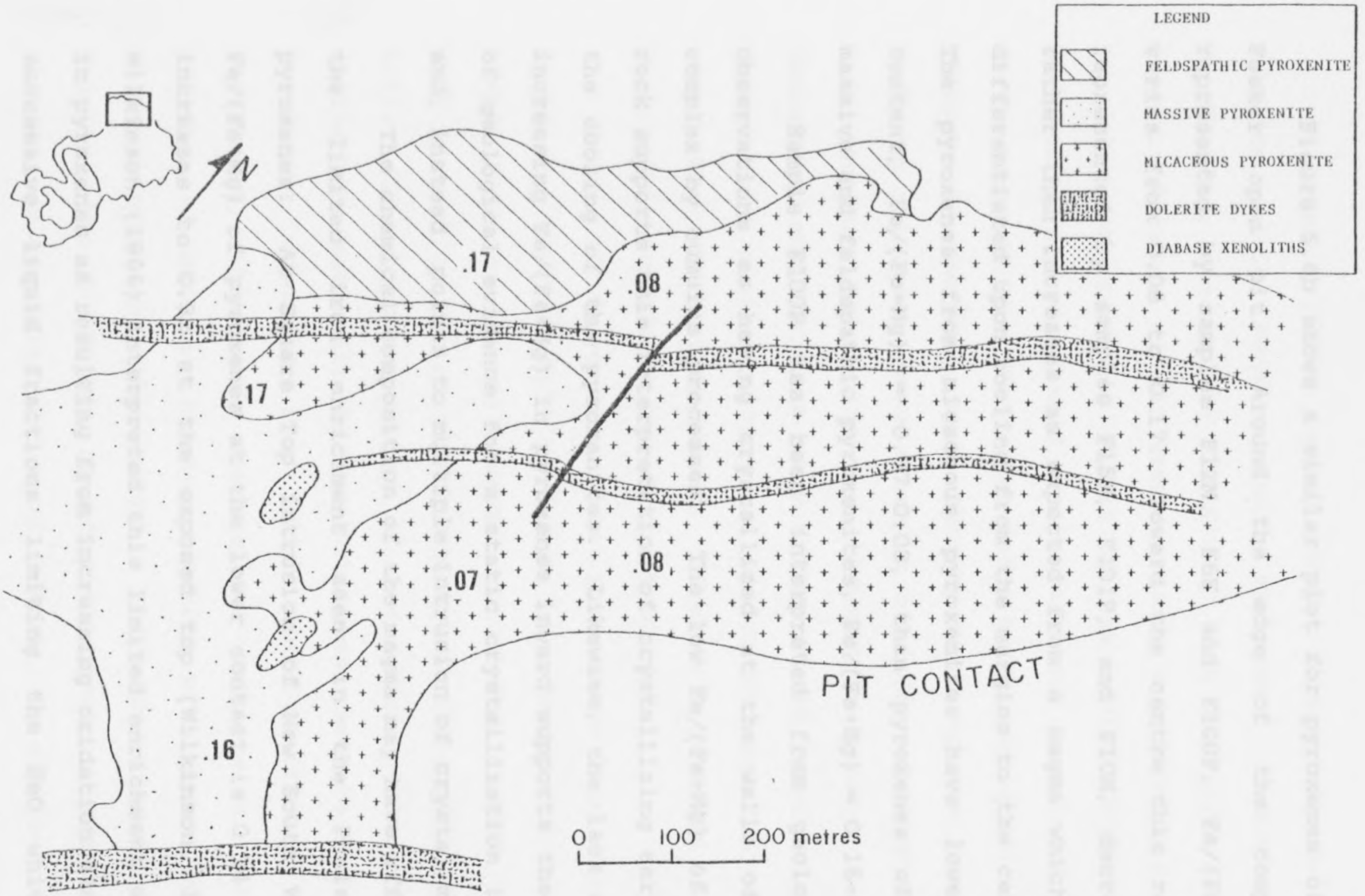


Figure 5.6b Fe/(Fe+Mg) of clinopyroxenes are plotted at their sample location in the Foskor area.

Figure 5.6b shows a similar plot for pyroxenes of the Foskor open pit. Around the edge of the complex, represented by samples F12M, F6F and F100P, Fe/(Fe+Mg) varies from 0.08 to 0.17. Toward the centre this ratio, represented by samples F15M, F101P, and F10M, decreases rather than increases as expected from a magma which has differentiated upon cooling from the margins to the centre. The pyroxenes from micaceous pyroxenites have lower Fe content, Fe/(Fe+Mg) = 0.07-0.08, than pyroxenes of the massive and feldspathic pyroxenites, Fe/(Fe+Mg) = 0.16-0.17.

Sample F100P has been interpreted from geological observations as having crystallized at the walls of the complex by cumulus processes. The low Fe/(Fe+Mg) of this rock supports this interpretation of crystallizing early in the cooling of the pyroxenites. Likewise, the lack of an increasing Fe/(Fe+Mg) in pyroxenes inward supports the lack of geological evidence for a static crystallization inward and, instead, points to multiple intrusion of crystal mush.

The chemical composition of the magma may have affected the limited iron enrichment seen in the Phalaborwa pyroxenes. At Square Top intrusion of New South Wales, Fe/(Fe+Mg) of pyroxenes at the lower contact is 0.24 which increases to 0.32 at the exposed top (Wilkinson, 1966). Wilkinson (1966) interpreted this limited enrichment of FeO in pyroxenes as resulting from increasing oxidation state of successive liquid fractions limiting the FeO which is available to enter the clinopyroxene.

Wilkinson (1966) noted that clinopyroxenes from alkaline basic rocks rarely are more Fe-rich than $Ca_{45}Mg_{25}Fe_{30}$ due to the relatively high Fe_2O_3/FeO in the magmas. Presnall (1966) described such a buffering process for water-rich basaltic magmas in the system CaO-MgO-FeO-Fe_2O_3-SiO_2. He postulated that significant amounts of water in the magma buffer its oxygen fugacity through diffusion of hydrogen to the wall rock, thereby limiting the range of Fe/Mg in silicates among a series of differentiated rocks. With abundant phlogopite and carbonatite present in the Phalaborwa complex, the composition of an abundant vapor phase could similarly have an effect on controlling the composition of silicate phases. However, a possible lack of Na_2O could prevent the formation of acmite.

Group II pyroxenes show pronounced variation in Fe/(Fe+Mg) and in $Fe^{2+}/(Fe^{2+}+Mg)$ (see section 5.2.1.2). Sample P120P is a single sample containing olivine (Fo_{85}) with a reaction rim of clinopyroxene and phlogopite (Figure 4.4). Clinopyroxene grains at the olivine-clinopyroxene contact are extremely Mg-rich but become more Fe-rich with increasing distance from this contact (Figure 5.7). Texturally, this rock appears to indicate a reaction relation of unstable olivine reacting with magma to form clinopyroxene and phlogopite. In nodules and alkali basalts, the Fe/(Fe+Mg) of the clinopyroxene and of the olivine are approximately equal. Hence, an olivine of Fo_{85} would be in equilibrium with a clinopyroxene with a

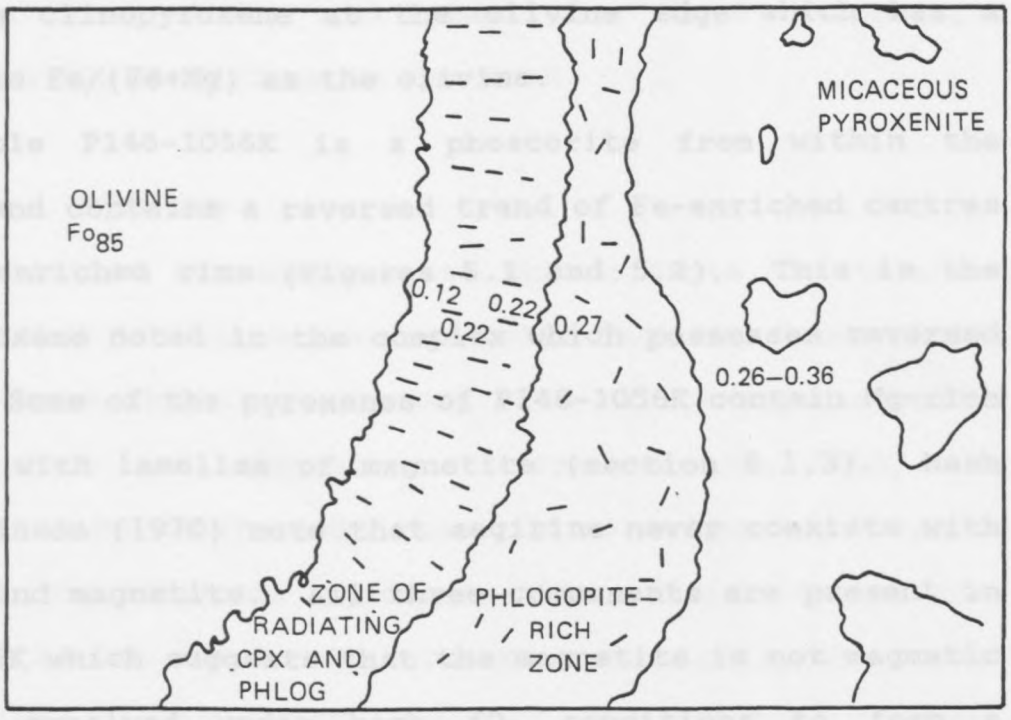


Figure 5.7 Sketch of the olivine crystal from micaceous pyroxenite with reaction rim of clinopyroxene and mica (Figure 4.3). The olivine composition and Fe/(Fe+Mg) of clinopyroxenes are shown at the spots measured. The range of compositions in the micaceous pyroxenite are for a zoned crystal.

comparable Fe/(Fe+Mg) ratio. The clinopyroxene away from the olivine has a Fe/(Fe+Mg) of 0.36 which is crystallizing from the magma; hence, the Fo_{85} olivine and the magma are not in equilibrium and a reaction relation is expected, producing clinopyroxene at the olivine edge which has a comparable Fe/(Fe+Mg) as the olivine.

Sample P146-1056K is a phoscorite from within the complex and contains a reversed trend of Fe-enriched centres with Mg-enriched rims (Figures 5.1 and 5.2). This is the only pyroxene noted in the complex which possesses reversed zoning. Some of the pyroxenes of P146-1056K contain Mg-rich pyroxene with lamellae of magnetite (section 4.1.3). Nash and Wilkinson (1970) note that aegirine never coexists with olivine and magnetite. All three components are present in P146-1056K which suggests that the magnetite is not magmatic but has exsolved under high fO_2 conditions to form a diopsidic pyroxene and magnetite, a process which did not equilibrate in this rock, possible due to a rapid change in oxygen fugacity.

Sample P146-610N (Figure 4.1) shows enrichment of Fe^{2+} and total Fe on grain edges (Table 5.1). Because P146-610N represents fenitized country rock, acmite enrichment represents changes in the fenitizing fluid composition rather than magmatic changes. Along with the iron enrichment in P146-610N, rims of sphene on magnetite give evidence for conditions of high fO_2 or high $aSiO_2$ in the fenites. Haggerty (1976) suggests that in undersaturated

systems, oxygen fugacity plays the more important role. Because the Wo content of P146-610N is comparable to pyroxenes of Group I, there is no indication that $aSiO_2$ was high. This supports Haggerty's suggestion of high fO_2 in the fenitizing fluid and that the fluid composition controlled fO_2 conditions in the rock.

5.2.1.3.4 Titanium

There is little agreement as to what affects the titanium concentration in a pyroxene. Although Yagi and Onuma (1969) found from an experimental study of a silica-undersaturated system that clinopyroxenes increased in TiO_2 as crystallization progressed, there is no evidence of such a trend in the magmatic pyroxenes from Phalaborwa (Figure 5.8). Ti is low and fairly constant. Similarly, the low-Al ferrosalites of Ilimaussaq contain 0.27-0.94% TiO_2 (Larsen, 1976); clinopyroxenes from Iron Hill pyroxenite have 1.50%, from ijolite have 1.30 and from sovite have 0.70% TiO_2 (Nash, 1972). Thermodynamic considerations by Verhoogen (1962) indicate that high temperature and low silica activity enhance the Ti content of pyroxenes and that in undersaturated rocks, temperature has the greatest effect. Gibb (1973) discussed at length the substitution of minor elements in pyroxenes and concludes that Al and Ti contents in pyroxenes are not diagnostic of parental magma but reflect the silica activity and conditions under which they crystallized. From charge balance considerations, he

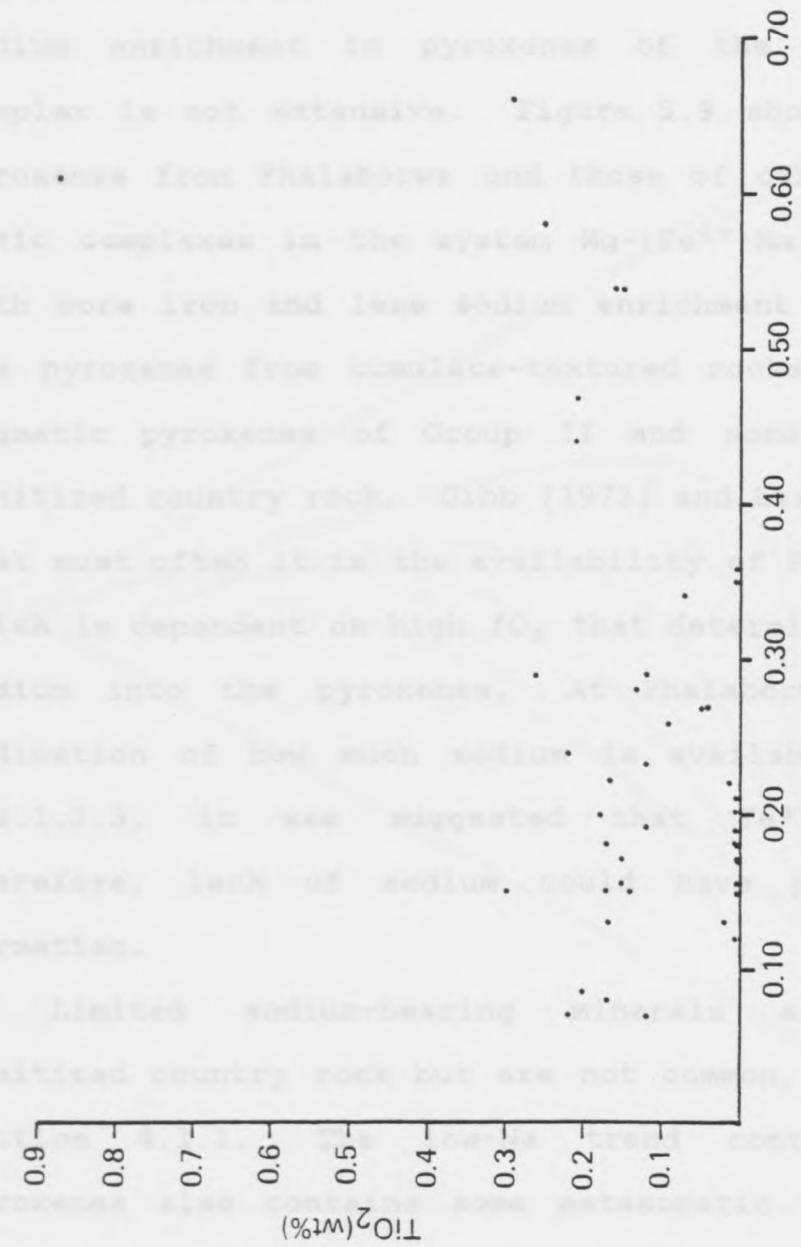


Figure 5.8 TiO_2 plotted against Fe/(Fe+Mg) for pyroxenes of the main complex. Group II pyroxenes are included to determine any Ti enrichment with Fe in the fluid or magma.

pointed out that with low Al in tetrahedral position, it is impossible to add Ti to the pyroxene. Both elements seem deficient in minerals from Phalaborwa.

5.2.1.3.5 Sodium

Sodium enrichment in pyroxenes of the Phalaborwa main complex is not extensive. Figure 5.9 shows the trend of pyroxenes from Phalaborwa and those of other alkaline and basic complexes in the system Mg-(Fe^{2+}+Mn)-Na. The trend with more iron and less sodium enrichment contains all of the pyroxenes from cumulate-textured rocks (Group I), the magmatic pyroxenes of Group II and some pyroxenes from fenitized country rock. Gibb (1973) and Larsen (1976) agree that most often it is the availability of Fe^{3+} in the magma which is dependent on high fO_2 that determines the entry of sodium into the pyroxenes. At Phalaborwa there is no indication of how much sodium is available. In section 5.2.1.3.3, it was suggested that Fe^{3+} was present; therefore, lack of sodium could have precluded acmite formation.

Limited sodium-bearing minerals are present in fenitized country rock but are not common, as described in section 4.1.1. The low-Na trend containing magmatic pyroxenes also contains some metasomatic pyroxenes. This suggests that, for the most part, the fenitizing fluid was also low in sodium and sodium which did go into these pyroxenes may have been derived from breakdown of

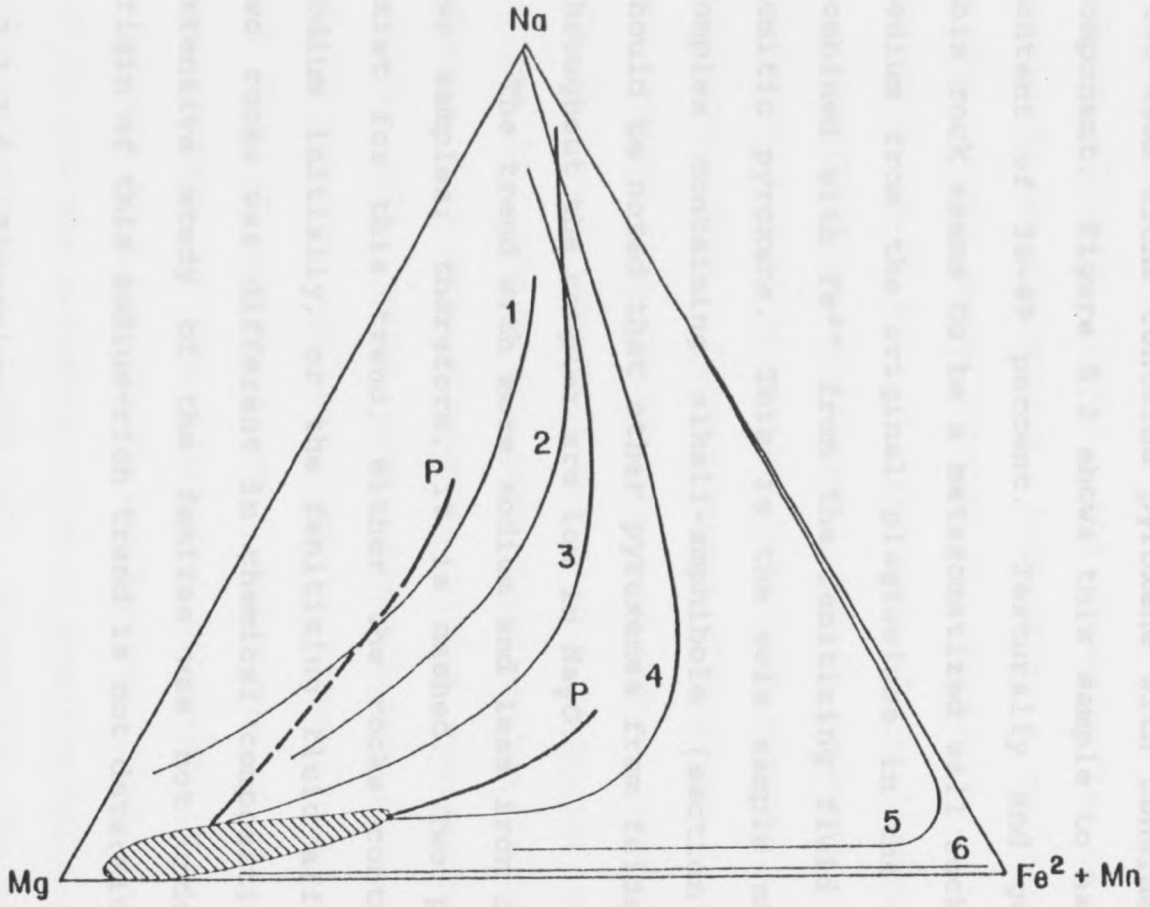


Figure 5.9 The trends of pyroxenes from Phalaborwa (P) and other igneous occurrences are plotted in the system Mg-(Fe^{2+}+Mn)-Na. The cross-marked area represents Group I pyroxenes. Other trends are: 1) Auvergne, France (Varet, 1969),2) Itapirapua, Brazil (Gomes et al., 1970), 3) Uganda (Tyler and King, 1967), 4) South Qoroq, South Greenland (Stephenson, 1972), 5) Ilimaussaq (Larsen, 1976) and 6) Skaergaard (Brown and Vincent, 1963). The dashed line represents a possible trend for Phalaborwa data although there are no data for the compositions on the dashed line.

plagioclase in the granite-gneiss with replacement by K-rich feldspar.

However, there are pyroxenes from fenitized country rocks which are more Na-rich as shown in Figure 5.9. Sample P146-440N alone contains pyroxene with considerable acmite component. Figure 5.2 shows this sample to have an acmite content of 36-49 percent. Texturally and geographically this rock seems to be a metasomatized wall rock. Possibly, sodium from the original plagioclase in the country rock combined with Fe^{3+} from the fenitizing fluid to form the acmitic pyroxene. This is the sole sample near the main complex containing alkali-amphibole (section 5.25). It should be noted that other pyroxenes from feldspathic rocks throughout the complex are low in Na_2O.

The trend with more sodium and less iron contains only two samples; therefore, it is dashed. Two possibilities exist for this trend, either the rocks contained higher sodium initially, or the fenitizing fluid affecting these two rocks was different in chemical composition. Because extensive study of the fenites was not undertaken, the origin of this sodium-rich trend is not determined here.

5.2.1.3.6 Zirconium

Zirconium was not determined directly on mineral separates, but the Zr concentration of the pyroxenes may be inferred from the whole-rock chemistry (Table 7.1). These rocks generally have 2-55 ppm Zr although rarely, concentrations reach 386 ppm (P4P) and 178 ppm (Pir 95-297P). No

baddeleyite or zircon was found in these samples petrographically, but it is possible that inclusions of these minerals may cause the high concentrations in these two samples. Trapped intercumulus liquid may also account for the high Zr. Zr is normally enriched in ultrabasic liquids (Dawson, 1967), and baddeleyite is mined from phoscorite at Phalaborwa, indicating a relatively high Zr content of the magma forming the phoscorite. Larsen (1976) reports 0.4-4.0% ZrO_2 in pyroxenes of the Ilimaussaq pluton.

Distribution coefficient for Zr between clinopyroxene and basic liquid is around 0.10-0.12 (Irving, 1978; Pearce and Norry, 1979). Clinopyroxene with 2 ppm Zr crystallizes from a magma with approximately 16 ppm Zr, and clinopyroxene with 55 ppm Zr crystallizes from a magma of approximately 458 ppm Zr. Using the same distribution coefficient, the pyroxene from the Ilimaussaq pluton containing 4.0% ZrO_2 (Larsen, 1976) would have crystallized from a liquid of 300,000 ppm Zr. As there are no known liquid compositions with this Zr concentration, inclusions of zircon may have been present in the pyroxenes measured from Ilimaussaq. Melteigite from Fen (Barth and Ramberg, 1966) contains up to 0.1% Zr and the potassic lavas of Leucite Hills (Carmichael, 1967) contain up to 0.28% ZrO_2. Therefore, the magma forming the pyroxenites at Phalaborwa is not enriched in Zr. Zr generally behaves as an incompatible element which remains in the liquid until a zircon-rich phase becomes stable. At Phalaborwa, zircon did not form from silicate liquid but

baddleyite crystallized, only in the phoscorite. Deans (1966) notes that Zr is not commonly abundant in carbonatites but reaches its highest concentrations in some nephelinites and rare alkaline rocks. This suggests that the silicate liquid forming the pyroxenites were not highly differentiated.

5.2.1.3.7 Strontium

Strontium contents of the clinopyroxenes from Phalaborwa vary from 200-450 ppm (see Chapter 9 and Table 5.2) which is extremely high, even for such Ca-rich pyroxenes. Shimizu (1975) reported similar concentrations in clinopyroxenes from granular nodules in kimberlites. Shimizu (1975) used his own experimentally determined distribution coefficient of 0.1 to estimate a melt concentration of 3500-9300 ppm Sr which he attributed to a late reequilibration of pyroxenes with a carbonatitic-kimberlitic liquid. Using the same coefficient, a value of 2000-4500 ppm Sr is indicated for the magma producing the clinopyroxene at Phalaborwa. Irving (1978) suggests that Sun et al. (1974) have good data for distribution coefficients of Sr. Their value of D = 0.22 yields a liquid composition of 909-2045 for the Phalaborwa liquid. The chilled lower margin of the Shonkin Sag laccolith has a Sr concentration of 2195 ppm (Nash and Wilkinson, 1970); this is the highest concentration of Sr found in the literature from a rock believed to represent a liquid composition. Using the latter distribution

coefficient, the values for Phalaborwa are comparable to the magma forming the Shonkin Sag laccolith. The values for Phalaborwa are high regardless of which distribution coefficients are used for calculation. Values of 900-4500 ppm Sr are not unrealistic considering the vast amount of Sr-rich apatite (section 7.1.2) and the close association with Sr-rich carbonatite (Table 7.4). Koster van Groos (1975) suggested that Sr fractionated into a silicate melt when in equilibrium with carbonatite. Although he used a granitic silicate liquid, he stated that similar results may be applied to alkaline magmas. Thus, there is ample support for a Sr-rich parental magma for the pyroxenites at Phalaborwa.

5.2.1.3.8 Chromium

Chromium is extremely low in the pyroxenes at Phalaborwa (see section 5.2.1.2). In a primary magma of 200-300 ppm Cr, and D = 4 (Schreiber, 1976), clinopyroxenes should have a concentration of 800-1200 ppm Cr. Thus, some chromium-rich phase must have been removed from the magma at Phalaborwa at an earlier stage. Magnetite is a likely candidate with a distribution coefficient of 10 (Cox et al., 1979). Chromite can only form given around 100 ppm Cr in the liquid, thus removal of chromite cannot reduce the Cr to the observed levels.

5.2.2 Mica

5.2.2.1 Crystal Chemistry

The tetrahedral Z site in micas from the Phalaborwa main complex contains from 7.176 to 8.030 cations of Si, Al and Ti. Ferric iron must be present in tetrahedral coordination to make up the eight cations in some micas. The amount of Fe^{3+} needed to fill the tetrahedral site is shown in parentheses below the Z occupancy in Table 5.4. In subsequent discussions, the deficiency in the tetrahedral site is assumed to equal Fe^{3+}.

The total number of cations in octahedral occupancy is usually over six, indicating the need for iron in the tetrahedral position and the calculation of some iron as Fe^{3+}. The excess Fe in octahedral position is enough to fill the tetrahedral vacancy. An excess of octahedral cations are usually needed to fill the tetrahedral positions. Vacancies may exist in the phlogopite structure. Fe^{3+} was measured on two phlogopites, P28P and P134-577P, by wet chemical techniques (Appendix B) and $Fe^{3+}/(Fe^{3+}+Fe^{2+})$ was 0.10 and 0.16, respectively. In the case of P28P (Table 5.5), the Fe^{3+} should go entirely into the tetrahedral position; sample P134-577P (Table 5.5) indicates that the majority of Fe^{3+} occupies the octahedral site. In many samples, e.g., F100P, Table 5.4, an excess of total cations remains in the octahedral position after removing Fe as Fe^{3+} for the tetrahedral deficiency. Either Fe, Mg or Mn must occupy the large position with potassium, which is highly

unlikely, or the micas are nonstoichiometric. Alternatively, there is some error in the analysis.

Chromium was not detected on microprobe and nickel is extremely low, less than 0.01% NiO. Titanium occupies up to 0.199 cations in the octahedral site and Mn is constant and low, less than 0.024 cations.

The large 12-coordinated position is occupied by K with minor Na. No calcium was detected in microprobe analysis. This position is rarely completely filled by two cations, a feature found in the majority of analyses in the literature. This may be attributed to the difficulty of measuring K and Na, but because both XRF and microprobe give low alkalies, it probably reflects a genuine deficiency in this site. The difference in K content between XRF (1.4-1.6 cations of K) and microprobe analysis (1.7-2.0) reflects the method. There is more error in XRF analysis for mineral separates.

5.2.2.2 Mineralogical Characteristics

Fe/(Fe+Mg) ratios (0.04-0.52) indicate that micas range from Mg-rich phlogopite to Mg-rich biotite. Phlogopite is by far the most abundant mica. Phlogopite in which Fe^{3+} occupies tetrahedral sites is termed tetraferriphlogopite. The micas of Phalaborwa may be divided into two chemical groups which are optically distinct in exhibiting normal and reverse pleochroism.

Reverse pleochroism is a widespread phenomenon in phlogopites from carbonatites (Rimsaite, 1969; Suwa and

Aoki, 1975; Heinrich, 1966) and other ultrabasic rocks (Dawson and Smith, 1977; Emeleus and Andrews, 1975; Smith et al., 1978). Hogarth (1964) suggested that Fe^{3+} in the tetrahedral position accounted for this trait, and Faye and Hogarth (1969) established that it is a charge transfer of $O_2^{-2} \rightarrow Fe^{3+}$ which accounts for the reverse pleochroism. Suwa and Aoki (1975) studied various micas from kimberlites and carbonatites, among them Phalaborwa, to show that a further restriction upon reverse pleochroism is that $Fe^{3+}/(Fe^{3+}+Ti+Cr)$ should be greater than 0.90 and $(Fe^{3+}+Ti+Cr)$ should be greater than 0.30 out of eight tetrahedral cations.

Comparison of optical data and mineral chemistry in micas from Phalaborwa (Table 5.4) show that micas with as little as $Fe^{3+}/(Fe^{3+}+Ti+Cr) = 0.45\pm0.15$ (Sample P120P, grain 6, Table 5.4) and $(Fe^{3+}+Ti+Cr) = 0.058\pm0.80$ (Sample P3C, Table 5.4) exhibit reverse pleochroism. Assuming that microprobe analyses are accurate to one percent (Appendix B), the amount of error in $Fe^{3+}/(Fe^{3+}+Ti+Cr)$ still produces a value lower than the number given by Suwa and Aoki (1975). Inaccuracy of Fe^{3+} places the $(Fe^{3+}+Ti+Cr)$ within their breakoff value of 0.30 for reverse pleochroism.

Figure 5.10 characterizes the two groups of micas with reverse and normal pleochroism through various chemical parameters. Within the reverse pleochroism group, several trends are evident. With the exception of sample P120P, Al decreases and iron in tetrahedral coordination increases as

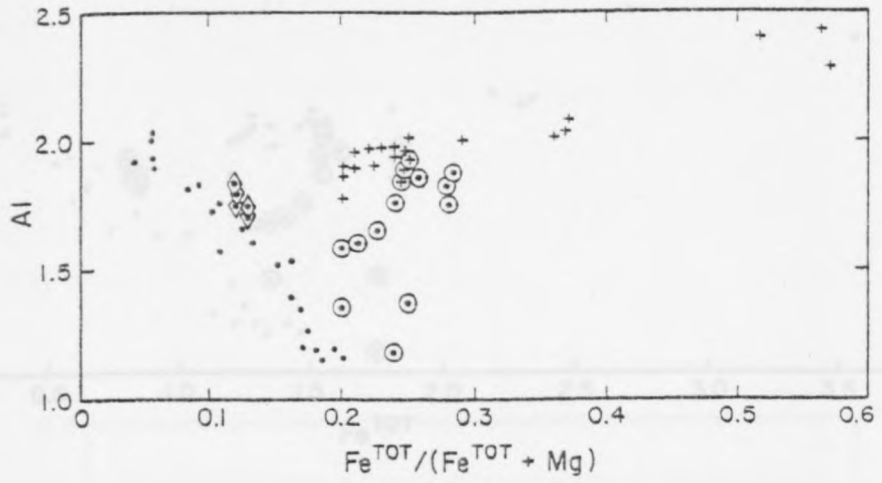


Figure 5.10a Compositions of micas from Phalaborwa plotted as number of Al cations per formula unit versus Fe/(Fe+Mg) ratio. Fe represents total iron. Crosses denote micas with normal pleochroism, dots denote micas with reverse pleochroism, dots with diamonds are sample F100P and symbols with circles are sample P120P.

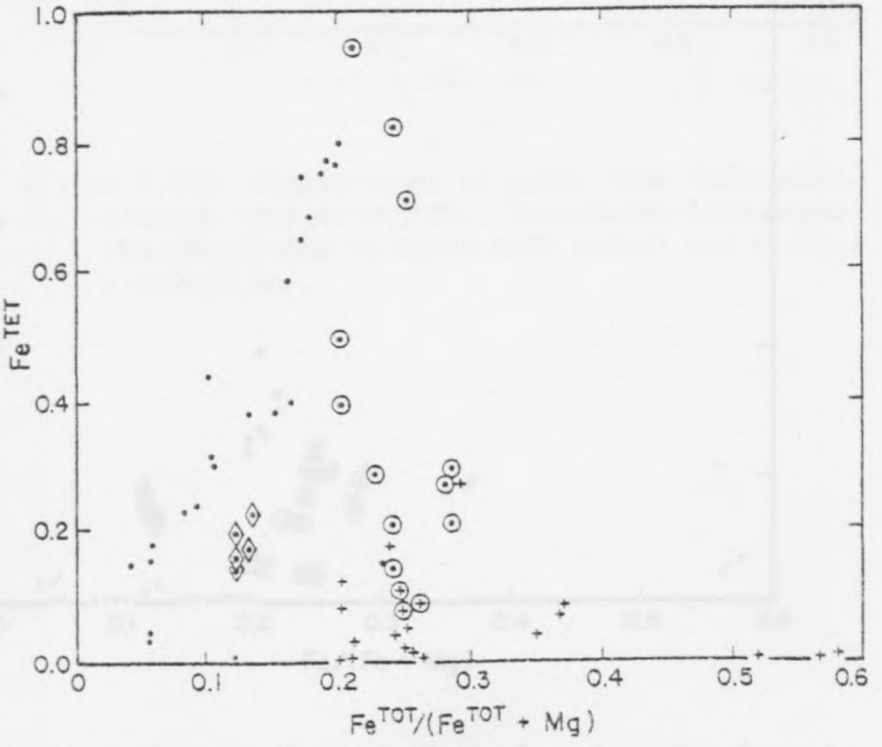


Figure 5.10b Tetrahedral iron in micas plotted against Fe/(Fe+Mg) ratios for micas from Phalaborwa. Symbols are the same as in Figure 5.10a.

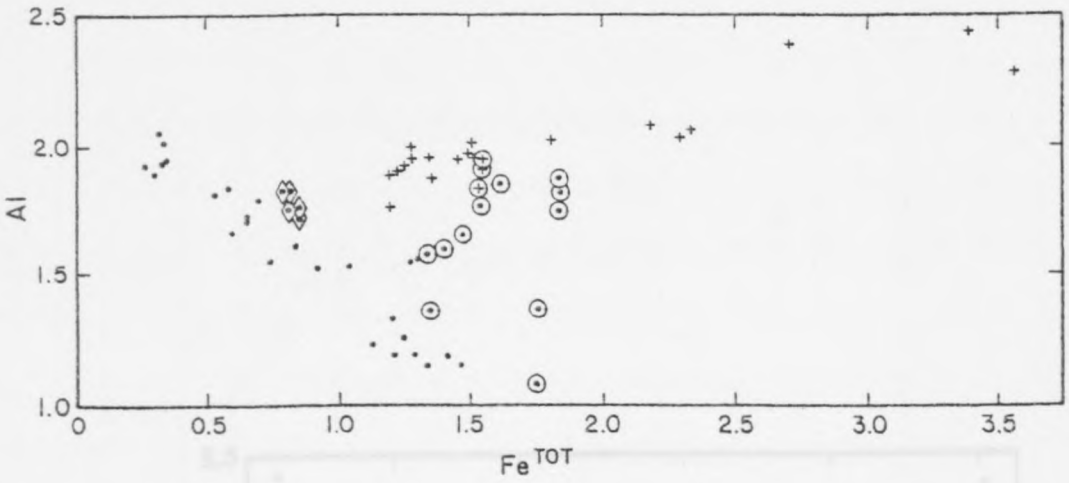


Figure 5.10c Number of Al cations per formula unit plotted against total iron for micas from Phalaborwa. Symbols are the same as in Figure 5.10a.

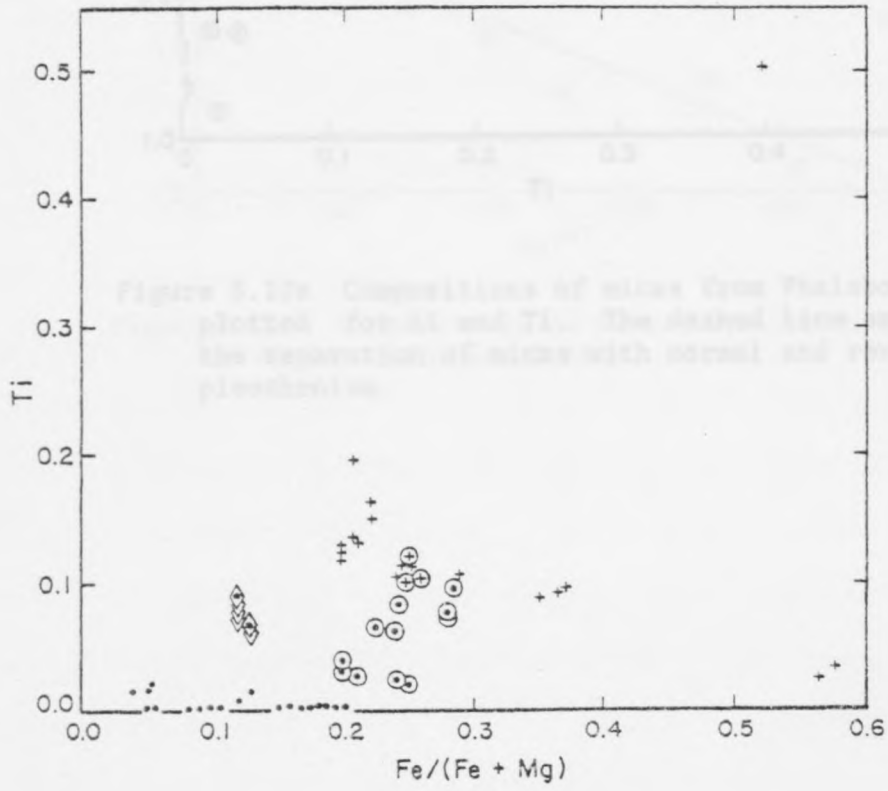


Figure 5.10d Number of Ti cations per formula unit plotted against the Fe/(Fe+Mg) ratio for micas from Phalaborwa.

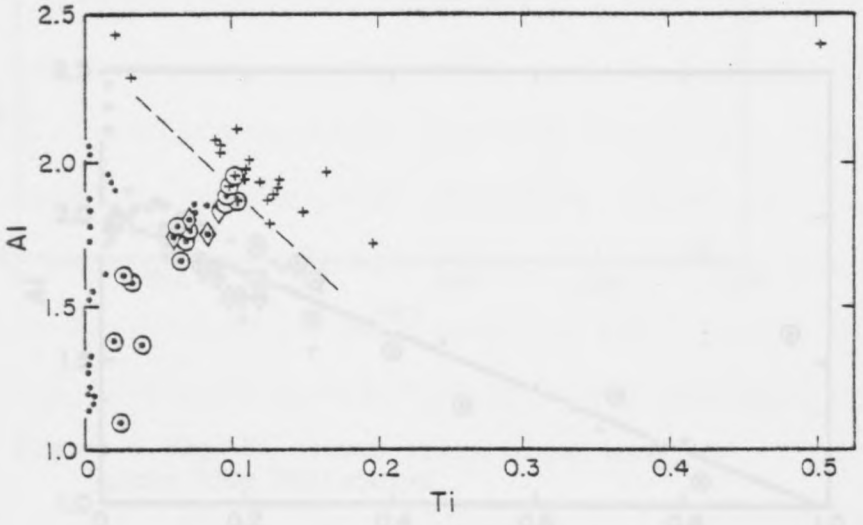


Figure 5.10e Compositions of micas from Phalaborwa plotted for Al and Ti. The dashed line emphasizes the separation of micas with normal and reverse pleochroism.

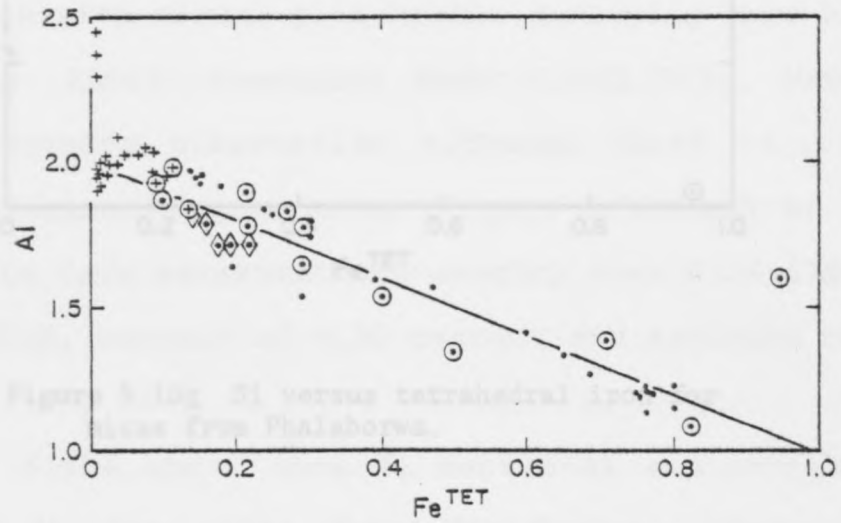


Figure 5.10f Compositions of micas from Phalaborwa for Al and tetrahedral iron.

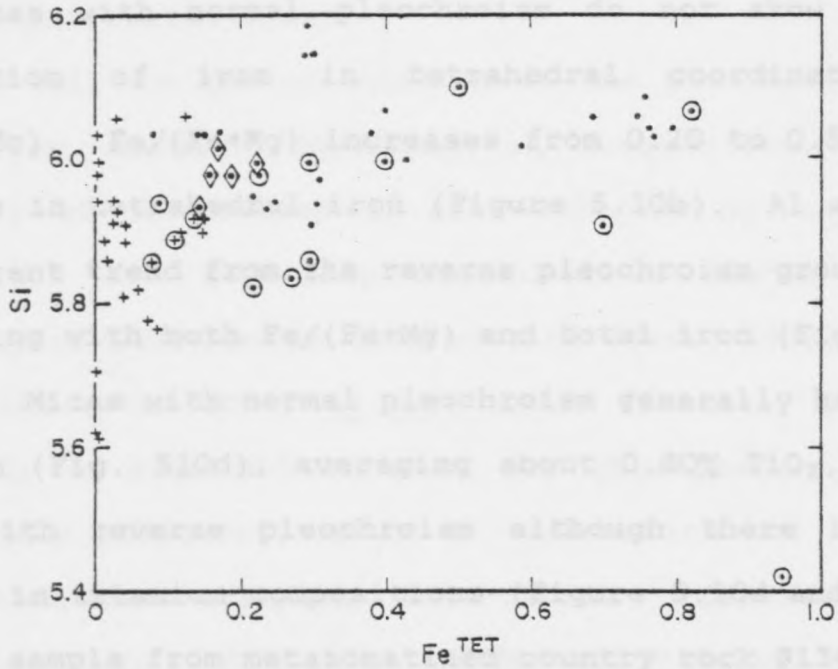


Figure 5.10g Si versus tetrahedral iron for micas from Phalaborwa.

both Fe/(Fe+Mg) (Figure 5.10a and b) and total iron (Figure 5.10c) increase.

Micas with normal pleochroism do not show the same correlation of iron in tetrahedral coordination with Fe/(Fe+Mg). Fe/(Fe+Mg) increases from 0.20 to 0.58 with no increase in tetrahedral iron (Figure 5.10b). Al also shows a different trend from the reverse pleochroism group with Al increasing with both Fe/(Fe+Mg) and total iron (Figure 5.10a and c). Micas with normal pleochroism generally have higher titanium (Fig. 510d), averaging about 0.80% TiO_2, than the micas with reverse pleochroism although there is a wide overlap in titanium compositions (Figure 5.10d and e). The biotite sample from metasomatized country rock P134-474N has a very high TiO_2 content of 4.32 percent and exhibits normal pleochroism.

Figures 5.10e and f show Ti versus Al and tetrahedral iron versus Al for micas from Phalaborwa. There is a definite compositional cutoff in Figure 5.10f at about Fe = 0.1 at the change between normal and reverse pleochroism. Figure 5.10e shows that there is considerable overlap of Ti content and optical properties. However, a sloping line (Figure 5.10e) which is dependent both on Al and Ti content separates the two types of micas. Sample P146-225P (Table 5.4) shows that Al can be as little as 1.88 cations and Ti = 0.125 cations, and pleochroism is normal. Figure 5.10g is a plot of Si cations versus tetrahedral Fe. Micas with normal and reverse pleochroism overlap in Si content. The average

content of micas with normal pleochroism, 5.91 cations, is the same as micas with reverse pleochroism, 5.98 cations, within experimental error.

Not only is the orientation of the pleochroism, i.e., reverse or normal, dependent on composition, but the intensity of pleochroism is also affected by composition. Phlogopites are generally described as having a lower intensity of pleochroism than biotite (Kerr, 1959). It has often been noted (Deer et al., 1962; Rimsaite, 1969) that high TiO_2 or high MnO accounts for this feature, but the very highly pleochroic micas of carbonatite and phoscorite at Phalaborwa (samples P134-2506C, P146-1056K) have negligible TiO_2 (0.00-0.13%) and MnO (0.00-0.11%) but a high Fe^{3+} content (0.238-0.800 cations).

Sample P120P (Figure 4.2), contains micas which change composition and optical properties moving away from the phlogopite + clinopyroxene -- olivine contact described in section 4.1.2.3. Fe/(Fe+Mg) changes from 0.20-0.28 whereas Al increases markedly in the tetrahedral site from 1.085 to 1.934 cations. As the Al content increases (P120P, grains 3-7, Table 5.4 and Figure 5.11), pleochroism becomes less distinct (x = reddish-brown, y = gold-brown). Analyses of sample P120P bridge and merge into both trends (Figure 5.10a,b,c).

Sample F100P shows a low intensity of reverse pleochroism and lies on the junction of trends formed by micas with reverse and normal pleochroism (Figures 5.10 a

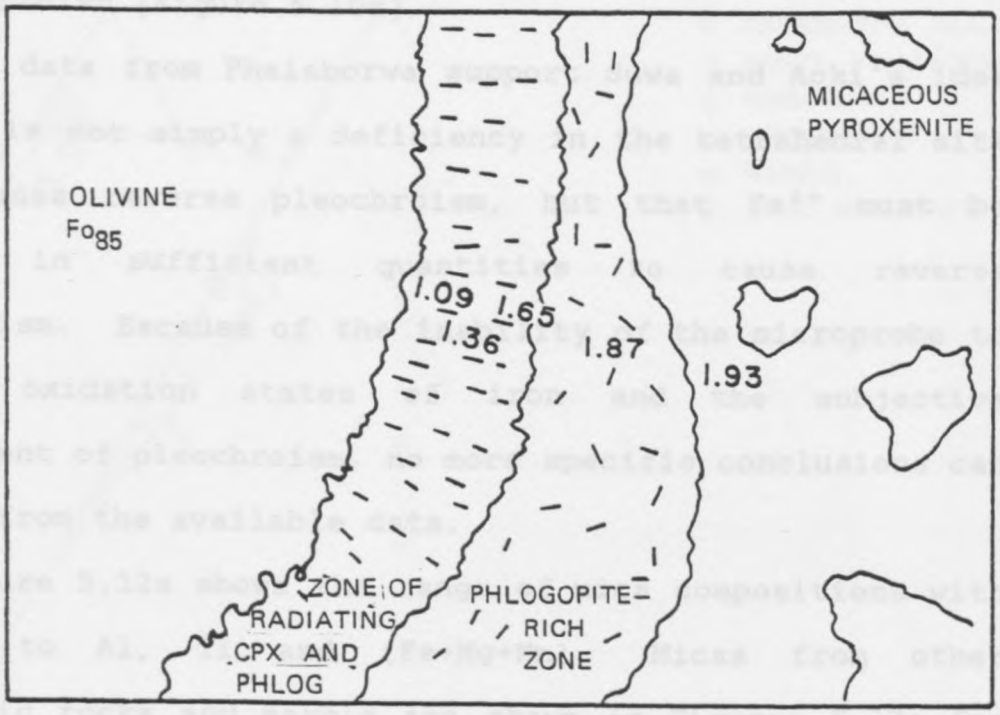


Figure 5.11 Aluminum contents of phlogopites in sample P120P in which olivine has reacted with liquid to form clinopyroxene and phlogopite. The sketch corresponds to the photograph in Figure 4.3.

and c) and clusters (Figure 5.10 b,d,e,f,g). It should be noted that all micas with high intensity of pleochroism also exhibit reverse pleochroism. There is an overlap in Al content and Fe/(Fe+Mg) among micas with reverse, normal, and no pleochroism (Figure 5.10a).

The data from Phalaborwa support Suwa and Aoki's idea that it is not simply a deficiency in the tetrahedral site that causes reverse pleochroism, but that Fe^{3+} must be present in sufficient quantities to cause reverse pleochroism. Because of the inability of the microprobe to measure oxidation states of iron and the subjective measurement of pleochroism, no more specific conclusions can be made from the available data.

Figure 5.12a shows the range of mica compositions with respect to Al, Ti and (Fe+Mg+Mn). Micas from other ultrabasic rocks and marble are shown in Figures 5.12a for comparison. The majority of micas from Phalaborwa are deficient in Al compared to ideal phlogopite and are relatively low in TiO_2. Figure 5.12b shows the phlogopite compositions with respect to Al, Mg and Fe.

5.2.2.3 Petrologic Significance

Reverse pleochroism is a trait particularly found in micas of kimberlites (Suwa and Aoki; 1975; Smith et al., 1978), carbonatites (Rimsaite, 1969; Nash, 1972; Gittins et al., 1975) and occasionally in various ultramafic xenoliths (Boettcher, 1967; Dawson and Smith, 1973).

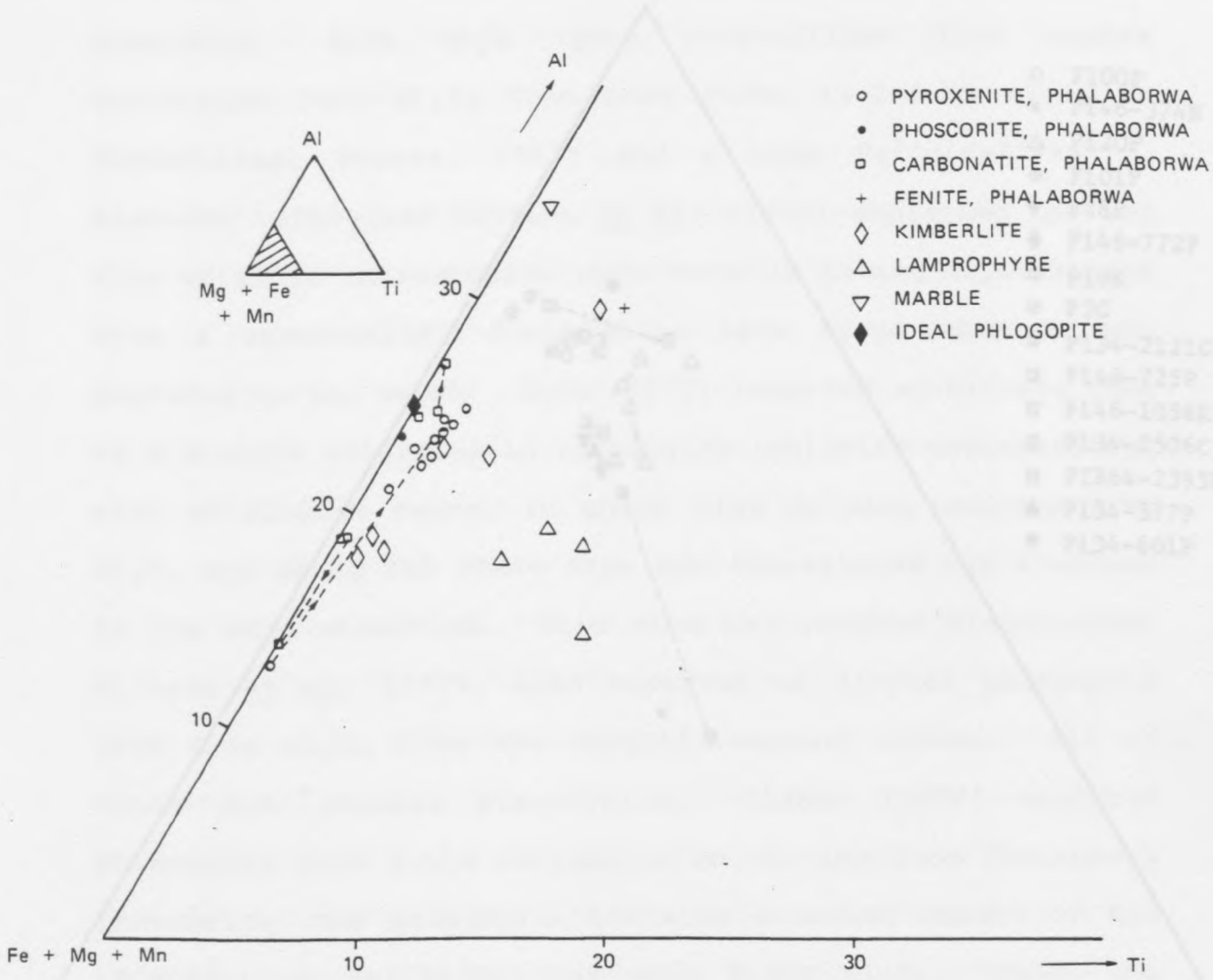


Figure 5.12a Micas of pyroxenites, phoscorite , carbonatite and fenitized country rock are shown in the Al-Ti-(Fe+Mg+Mn) system. Ideal phlogopite, micas from kimberlite (Dawson, 1972), lamprophyre (Scott, 1977), and a marble (Deer et al.,1963) are shown for comparison.

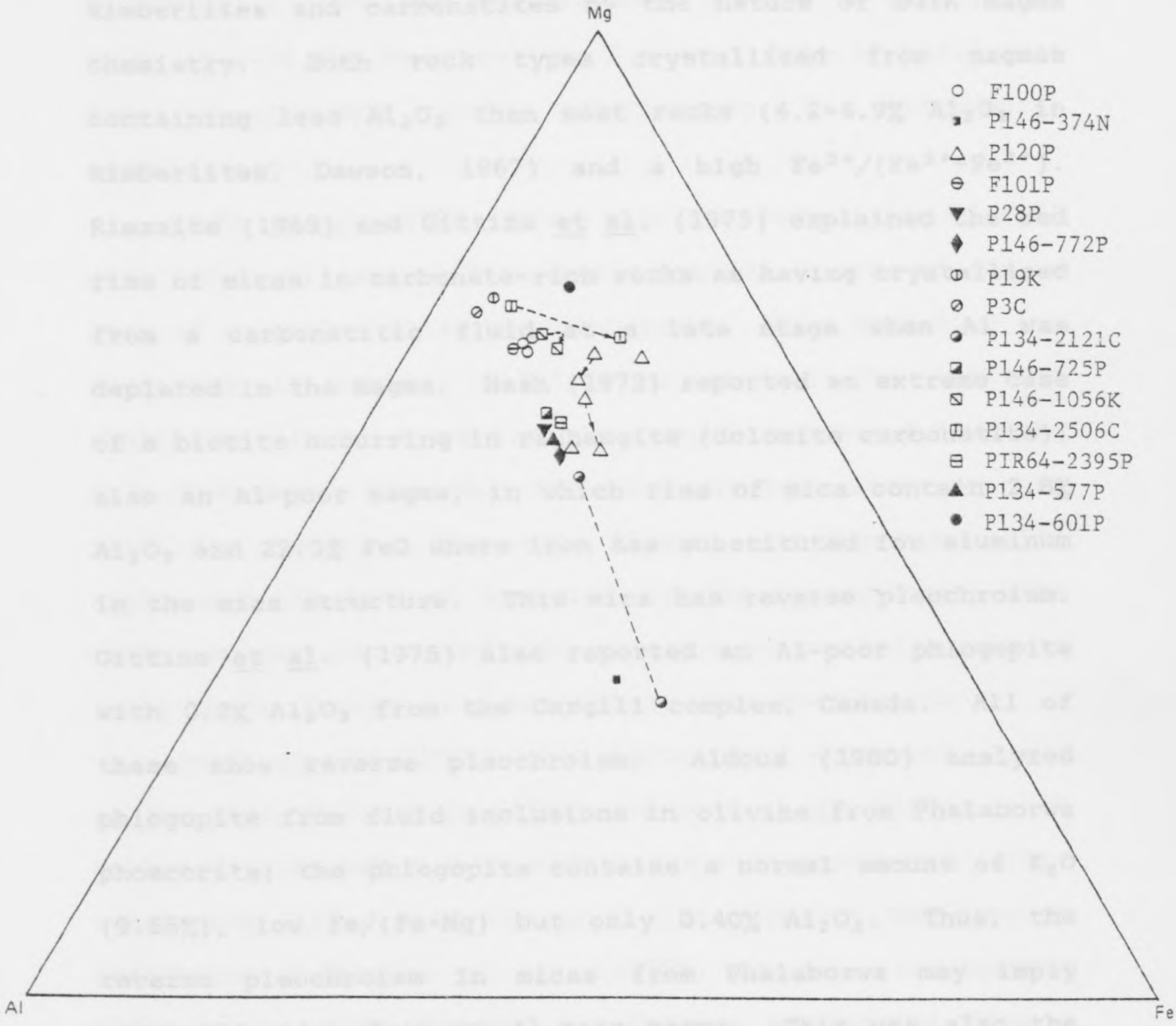


Figure 5.12b Micas from Phalaborwa shown in the system Al-Mg-Fe. The dashed lines connect different compositions in zoned crystals; the arrows show directions of zoning.

Suwa and Aoki (1975) explained the occurrence in kimberlites and carbonatites by the nature of bulk magma chemistry. Both rock types crystallized from magmas containing less Al_2O_3 than most rocks (4.2-4.9% Al_2O_3 in kimberlites, Dawson, 1967) and a high $Fe^{3+}/(Fe^{3+}+Fe^{2+})$. Rimsaite (1969) and Gittins et al. (1975) explained the red rims of micas in carbonate-rich rocks as having crystallized from a carbonatitic fluid at a late stage when Al was depleted in the magma. Nash (1972) reported an extreme case of a biotite occurring in rauhaugite (dolomite carbonatite), also an Al-poor magma, in which rims of mica contain 2.8% Al_2O_3 and 22.3% FeO where iron has substituted for aluminum in the mica structure. This mica has reverse pleochroism. Gittins et al. (1975) also reported an Al-poor phlogopite with 0.2% Al_2O_3 from the Cargill complex, Canada. All of these show reverse pleochroism. Aldous (1980) analyzed phlogopite from fluid inclusions in olivine from Phalaborwa phoscorite; the phlogopite contains a normal amount of K_2O (9.65%), low Fe/(Fe+Mg) but only 0.40% Al_2O_3. Thus, the reverse pleochroism in micas from Phalaborwa may imply crystallization from an Al-poor magma. This was also the conclusion regarding pyroxene compositions (section 5.2.1.3).

Within the group of micas showing reverse pleochroism at Phalaborwa, a positive correlation of tetrahedral Fe and Fe/(Fe+Mg) (Figure 5.10b) exists. This correlation was also noted by Smith et al. (1978) in their Type II micas from

kimberlites. Their Type II micas are characterized by Fe/(Fe+Mg) = 0.07-0.20, and are lower in TiO_2 (0.7-4.0%) and Al_2O_3 (6.8-14.2%) than the Type I micas. Type II micas also have considerable Fe^{3+} substitution in tetrahedral coordination.

Smith et al. (1978) noted that the correlation of Fe^{3+} with Fe/(Fe+Mg) may reflect increasing fO_2 in a magma due to loss of volatiles to surrounding rocks. This mechanism was suggested in section 5.2.1.3 to explain the lack of significant increase of iron in cumulus pyroxenes from the main Phalaborwa complex. High H_2O pressure decreases the stability field of magnetite (Eggler and Burnham, 1973) explaining the lack of magnetite in the pyroxenites. This mechanism may also explain the presence of magnetite only in rocks containing phlogopites with reverse pleochroism.

Smith et al. (1978) also tentatively suggested, based on the data of Rimsaite (1969) and Bass et al. (1974), that carbonatite magmas give rise to micas with tetrahedral sites completely filled with Si and Al; this is not the case at Phalaborwa. Gittins et al. (1975), however, interpreted their micas with reversed pleochroism as forming from a carbonatite magma, a result of either differentiation or immiscibility from a kimberlitic magma.

Phlogopites from Phalabrowa with distinct reverse pleochroism belong primarily to phoscorite and carbonatite but rarely occur in pyroxenites. Samples P19K and P3C as well as about 20 other samples from phoscorite and

carbonatite examined optically show extreme, reverse pleochroism which reflects their extreme undersaturation with respect to Al_2O_3. These micas have the lowest Fe/(Fe+Mg) and may represent very early-formed phlogopites in a magma producing phoscorite and carbonatite.

P120P may provide evidence of the process whereby much of the phoscorite mica formed. Mica at the contact with the olivine is extremely depleted in Al_2O_3, has Fe/(Fe+Mg) = 0.24 and shows reverse pleochroism; mica progressively further from this contact shows enrichment in Al_2O_3 and, to a lesser degree, increases in Fe/(Fe+Mg) and has normal pleochroism. This latter mica reflects the magma producing the pyroxenites. Boettcher (1967) noted a similar texture in the Rainy Creek Igneous Complex where the mica was arrayed in acicular blades perpendicular to the boundary of an altered ultramafic nodule. The reaction

[olivine + liquid 1 → phlogopite + liquid 2]

produces phlogopite with decreasing temperature of an ultrabasic liquid (Edgar et al., 1976). Micas found rimming olivine in phoscorite may represent a reaction of olivine with magma. Clinopyroxene is also present as a reaction product in sample P120P. Whether phlogopite only is formed according to the above reaction or clinopyroxene forms in addition according to the reaction

[forsterite + liquid → phlogopite + diopside + vapor]

(Modreski and Boettcher, 1973) may depend on the type of magma involved.

The group of micas with completely filled tetrahedral sites of (Al+Si) and normal pleochroism occur in pyroxenites with the exception of P134-2121C. An increase in Ti with increasing Fe/(Fe+Mg) might be expected (Suwa and Aoki, 1975; Edgar et al., 1976) because titanium is chemically coherent with Fe, and FeO is generally higher in biotites (Deer et al., 1962). The TiO_2 content is low in phlogopites from Phalaborwa compared to those of other ultrabasic rocks (Figure 5.11) and there is no good correlation between Ti and Fe/(Fe+Mg) (Figure 5.10). Low-temperature phlogopites formed as metasomatic products in kimberlites contain less TiO_2 than high-temperature phlogopites (Gittins et al., 1975) but contain several percent more TiO_2 than phlogopites from Phalaborwa.

The general trend of increasing Al with total Fe (Figures 5.10c and 5.12) and Fe/(Fe+Mg) (Figure 5.10a) in phlogopites from pyroxenites may reflect the increase of Al in silicate magma as Al-deficient phlogopite and Al-poor clinopyroxene crystallize. The only pyroxene analyzed with reverse pleochroism in pyroxenites is sample F100P which occurs in "inch-scale" layering at the edge of the complex. This sample has also among the lowest Fe/(Fe+Mg) of all minerals in the complex. Early crystallization of this rock from silicate magma is postulated on textural and geological evidence. Crystallization of the Al-poor phlogopite provides a mechanism of increasing Al in subsequent liquid so that phlogopites with higher Fe/(Fe+Mg) possess normal

pleochroism. Phlogopite from sample F101P, measured by XRF, has a comparable Fe/(Fe+Mg) ratio to sample F110P but has normal pleochroism. The pleochroism of this sample is very weak, however, and the XRF analyses of mineral separates are considered inferior to those obtained on the electron microprobe. It may be that very small chemical variations may have caused the difference in pleochroism between these two samples with identical Fe/(Fe+Mg). There is no evidence that carbonatitic fluid from which the reverse pleochroic phlogopites crystallized has modified the chemistry of phlogopite from pyroxenites by producing Al-poor rims on these phlogopites. As reported in Chapter 4, rims of reverse pleochroism have been reported by Suwa et al. (1975) but that cannot be widespread as it was not observed in this more detailed study.

The texture and mineralogy of sample P134-2121C may explain why a carbonatite contains mica with high Al and normal pleochroism. Sample P134-2121C is very fine grained, and aside from the dark-brown phlogopite and biotite (Fe/(Fe+Mg) = 0.29-0.58), contains fine-grained, dark green clinopyroxene.[2] Clinopyroxene is extremely rare in carbonatite and is interpreted as being xenolithic. This is discussed further in Chapter 9. The iron-rich nature of the biotite is similar to biotite analyzed from fenite. The mica found in sample P134-2121C most likely formed from a

[2]This clinopyroxene did not yield good microprobe analyses, possibly because of high carbonate content in fractures and grain boundaries.

silica-rich rock being incorporated as a xenolith in the carbonatite magma. Either the clinopyroxene and phlogopite are remnants of the xenolith which were not dissolved in the carbonatite liquid, or the xenolith provided the chemical conditions for forming the anomalous mineralogy found in this rock.

Figure 5.13 shows the Fe/(Fe+Mg) ratios of the phlogopites in relation to sample locations. As with Fe/(Fe+Mg) ratios from clinopyroxenes there is no clear differentiation trend from the rim of the complex inward. Fe/(Fe+Mg) for sample F100P which is interpreted as one of the early-formed pyroxenites is identical to the mica of the coarse pegmatoid in the Foskor pit, sample F101P (Figure 5.13a). Optical properties of 20 other samples suggest that all of the phlogopites in the Foskor area have similar, low Fe/(Fe+Mg) ratios. As with the clinopyroxenes, there is limited iron-enrichment in phlogopites in pyroxenites. Figure 5.13b shows Fe/(Fe+Mg) ratios for phlogopites from fenite, micaceous pyroxenite, phoscorite and carbonatite in the PMC area. Overall, the ratios plotted are lower in carbonatite and phoscorite than in pyroxenites although there is some overlap. Lack of clear-cut Fe enrichment among micas in pyroxenites, phoscorites, and carbonatites supports the conclusion that carbonatites and phoscorite are not formed by differentiation of magma which produced the pyroxenites. There is also significant overlap between Fe/(Fe+Mg) in micas of carbonatite and phoscorite.

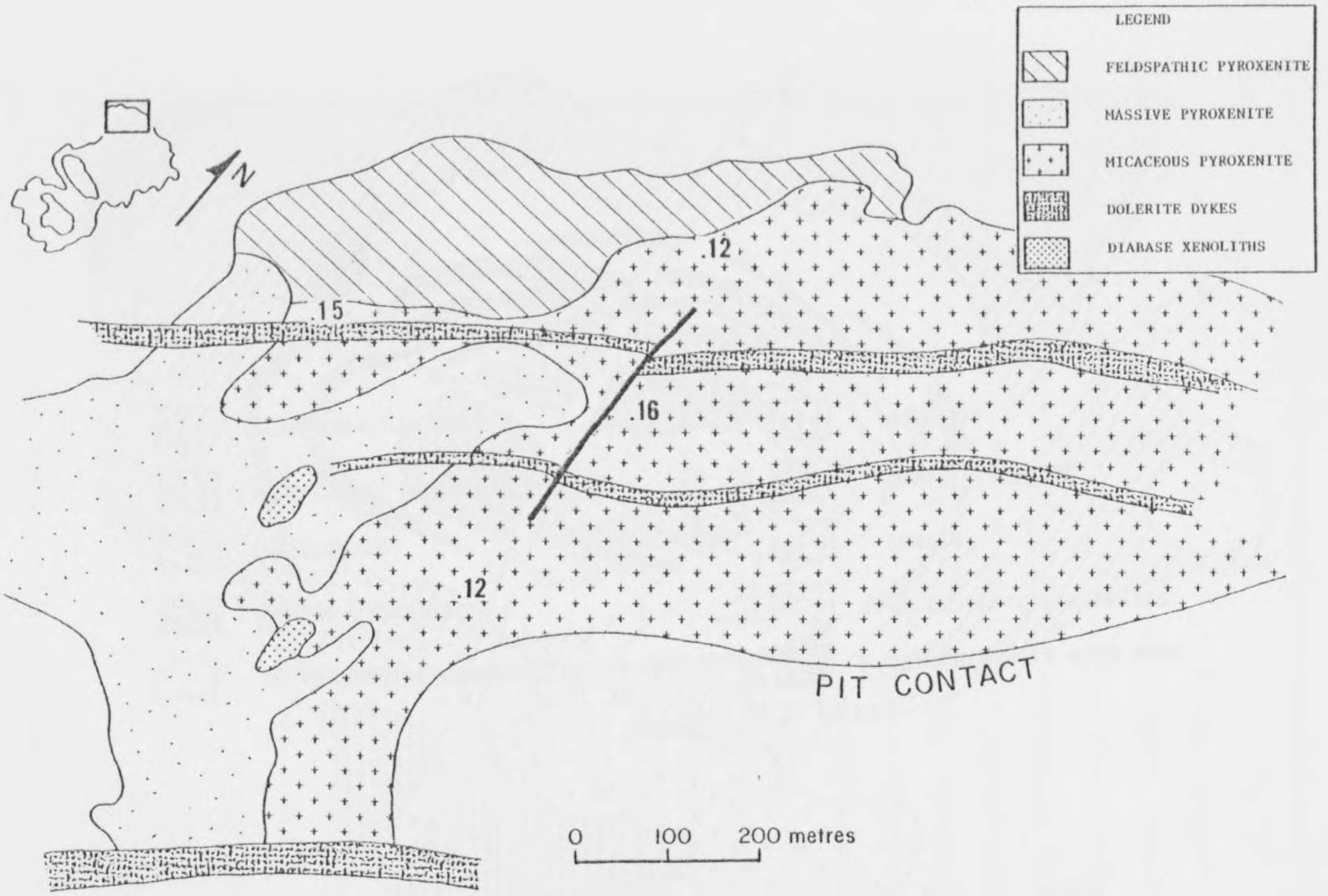


Figure 5.13a Fe/(Fe+Mg) of micas are plotted at their sample locations in the Foskor area.

LEGEND


TRANSGRESSIVE CARBONATITE


BANDED CARBONATITE


PHOSCORITE


PYROXENITE PEGMATOID


MICACEOUS PYROXENITE


PREDOMINANTLY MICA ROCK


FELDSPATHIC PYROXENITE


FENITE


GRANITE/GNEISS


DOLERITE

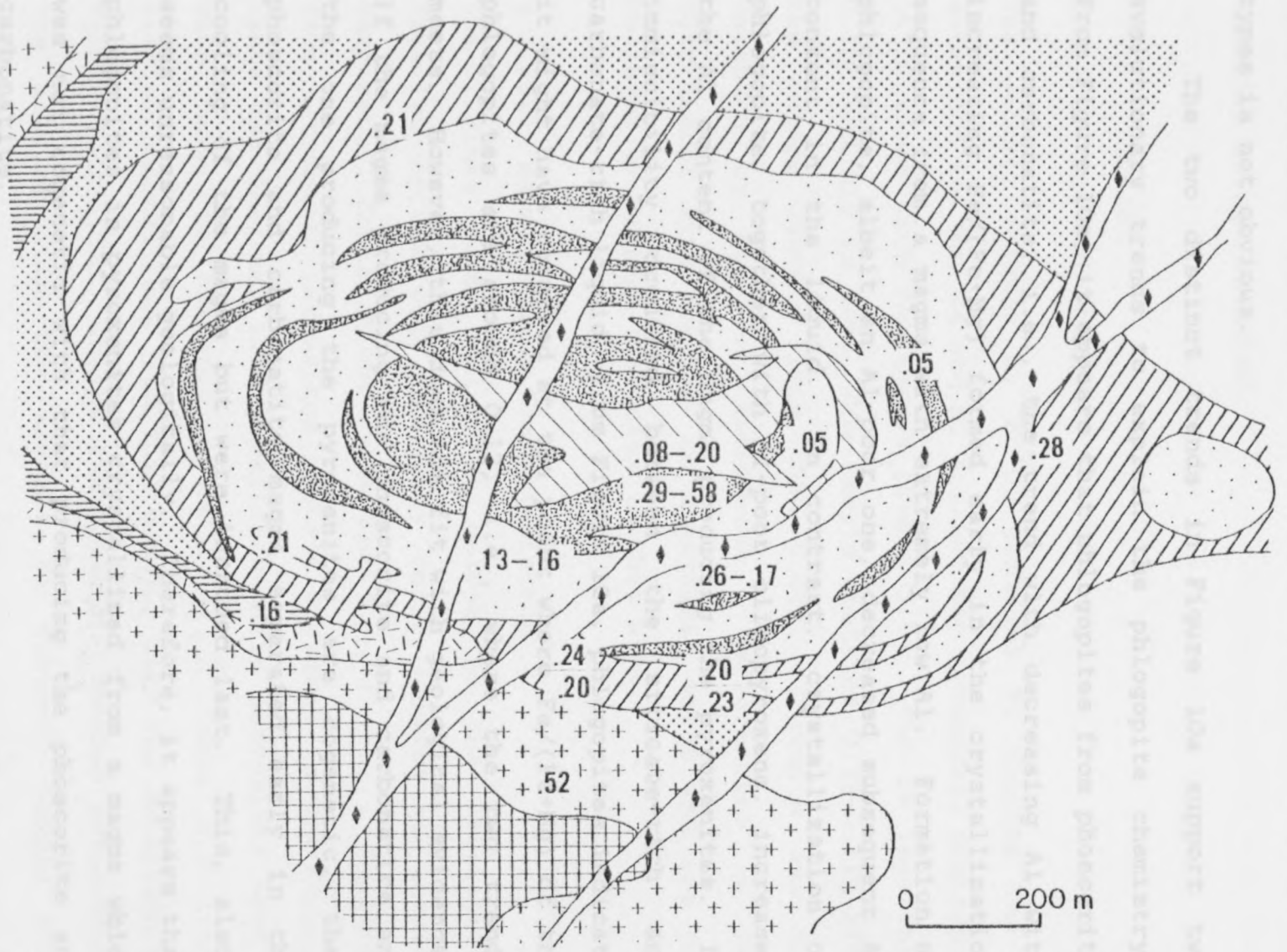


Figure 5.13b Fe/(Fe+Mg) ratios for micas from the PMC area plotted at their sample locations.

Therefore, a differentiation trend between these two rock types is not obvious.

The two distinct trends in Figure 10a support two evolutionary trends to explain the phlogopite chemistry. From Figure 10a, it appears that phlogopites from phoscorite and carbonatite, i.e., the trend with decreasing Al with increasing Fe/(Fe+Mg) formed early in the crystallization sequence from a magma with extremely low Al. Formation of phlogopite, albeit an Al-poor one, decreased subsequent Al content in the liquid. In contrast, crystallization of phlogopite, together with Al-poor clinopyroxene, increased the Al content of the magma producing the pyroxenites. If immiscibility occurred between the silicate-rich and carbonate-rich liquid, from Figure 10a, phlogopites indicate it might have occurred at the point where Fe/(Fe+Mg) of the phlogopites are around 0.12, i.e., where the two trends meets. However, this does not fit with geological evidence. If the magma producing the phoscorite and carbonatite and the one producing the pyroxenites are cogenetic, then phoscorite and carbonatite magma separated early in the cooling of the magma but were intruded last. This, also, seems unreasonable geologically. Therefore, it appears that phlogopites in pyroxenites crystallized from a magma which was not cogenetic with that producing the phoscorite and carbonatite.

Low chromium in the phlogopites is consistent with low Cr content in the clinopyroxenes. Smith et al. (1978) found

that chromium content varies among kimberlite micas and commonly is not detected.

5.2.3 Olivine

5.2.3.1 Crystal Chemistry

The general formula $A_2^{vi}B^{iv}O_4$ contains Si filling the B sites and Fe, Mg, Ca and Ni filling the octahedral positions in olivines from Phalaborwa (Table 5.6). CaO is less than 0.10% and NiO is low. One sample contains 0.28-0.31% NiO; the others contain less than 0.06%. Chromium was not detected by electron microprobe. Deficiencies in the tetrahedral site are due to analytical error and are not believed to reflect vacancies in that site.

5.2.3.2 Mineralogical Characteristics

The olivines from Phalaborwa belong to the forsterite-fayalite series with extremely small amounts of larnite component. Compositions range from Fo_{79} to Fo_{91}. Olivines from ultramafic intrusions contain olivines in the Fo_{85-95} range and olivines from stratiform mafic intrusions have a wide range in composition of Fo_{95-0}. Table 5.6 lists olivine compositions from this study. With the exception of sample P146-1056K, grains are unzoned. Banded carbonatite has olivine with the highest Fo content, sample P3C. Phoscorite contains olivine with the lowest Fo content (P146-1056K) measured here. No olivine was found in transgressive carbonatite (see Chapter 2). P(79a)X is a

coarse-grained, highly serpentinized olivine xenocryst from pyroxenite. Its Fo content is similar to olivines measured from carbonatite and phoscorite but it contains higher Ni, 0.28-0.31% NiO.

Olivine compositions are shown with relation to sample location in Figure 5.14. Sample locations do not give a good cross-section across the phoscorite so no conclusions can be drawn on inward crystallization within the phoscorite. The relatively rare sample of olivine within banded carbonatite shows a decrease of iron in the centre of the pipe but because of the scarcity of data, no crystallization trend should be inferred.

Calcium content of olivines is less than 0.09% CaO, which is compatible with data from rocks of plutonic environment (Simkin and Smith, 1970). NiO is generally low, 0.00-0.06% NiO, in all olivines except the xenocryst which has a NiO content of 0.28±0.03%. This is still relatively low and is within the range of NiO content in terrestrial rocks which generally have less than 0.5% NiO (Brown, 1980). The higher Ni content of sample P(79a)X does not correlate with the Fo content (Table 5.6). Olivines in kimberlites have compositions of Fo_{89-94} with NiO of 0.3-0.5% (Dawson, 1980). NiO decreases with increasing Fo content. If Ni content increases with increasing Fo content as is generally believed (Ribbe, 1980), then sample P3C should contain the highest Ni content. This is not the case.

LEGEND


TRANSGRESSIVE CARBONATITE


BANDED CARBONATITE


PHOSCORITE


PYROXENITE PEGMATOID


MICACEOUS PYROXENITE


PREDOMINANTLY MICA ROCK


FELDSPATHIC PYROXENITE


FENITE


GRANITE/GNEISS


DOLERITE

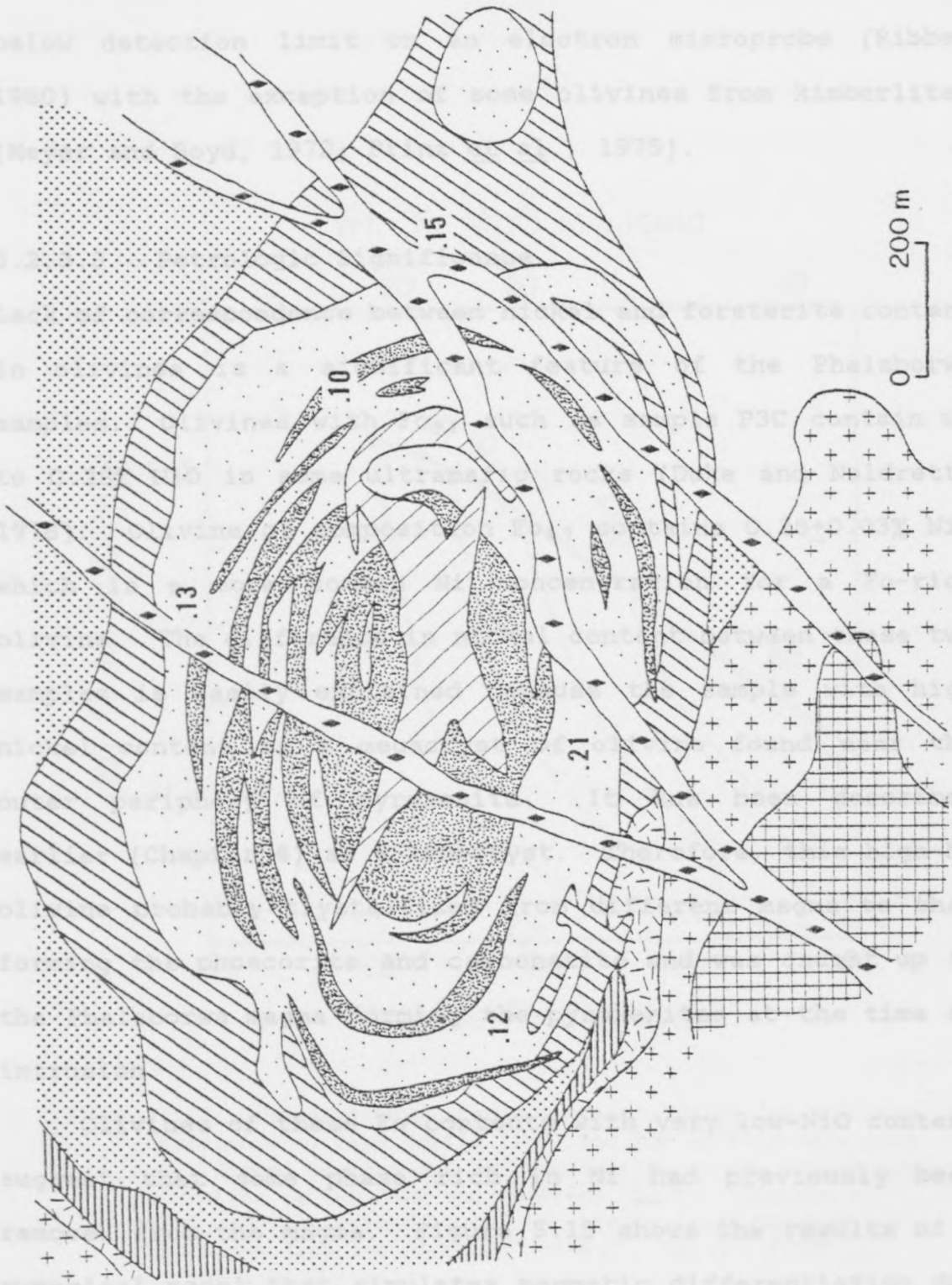


Figure 5.14 Fe/(Fe+Mg) ratios of olivines plotted at their sample locations in the PMC area.

Chromium in olivines of terrestrial rocks is usually below detection limit on an electron microprobe (Ribbe, 1980) with the exception of some olivines from kimberlites (Meyer and Boyd, 1972; Prinz et al., 1975).

5.2.3.3 Petrologic Significance

Lack of correspondence between nickel and forsterite content in olivines is a significant feature of the Phalaborwa samples. Olivines with Fo_{91} such as sample P3C contain up to 0.28% NiO in some ultramafic rocks (Duke and Naldrett, 1978). Olivine of composition Fo_{87} contains 0.28±0.03% NiO which is a more common Ni concentration for a Fo-rich olivine. The difference in nickel content between these two samples is easily explained because the sample with high nickel content is a megacryst of olivine found near the outer periphery of pyroxenite. It has been described earlier (Chapter 4) as a xenocryst. Therefore, this high-Ni olivine probably crystallized from different magma to that forming the phoscorite and carbonatite and was caught up in the Phalaborwa magma forming the pyroxenites at the time of intrusion.

Olivines of these Fo contents with very low-NiO content suggest that some phase rich in Ni had previously been removed from the magma. Figure 5.15 shows the results of a numerical model that simulates magmatic differentiation due to olivine and molten sulphide from mafic and ultramafic liquids (Duke and Naldrett, 1978). Compositions of olivines

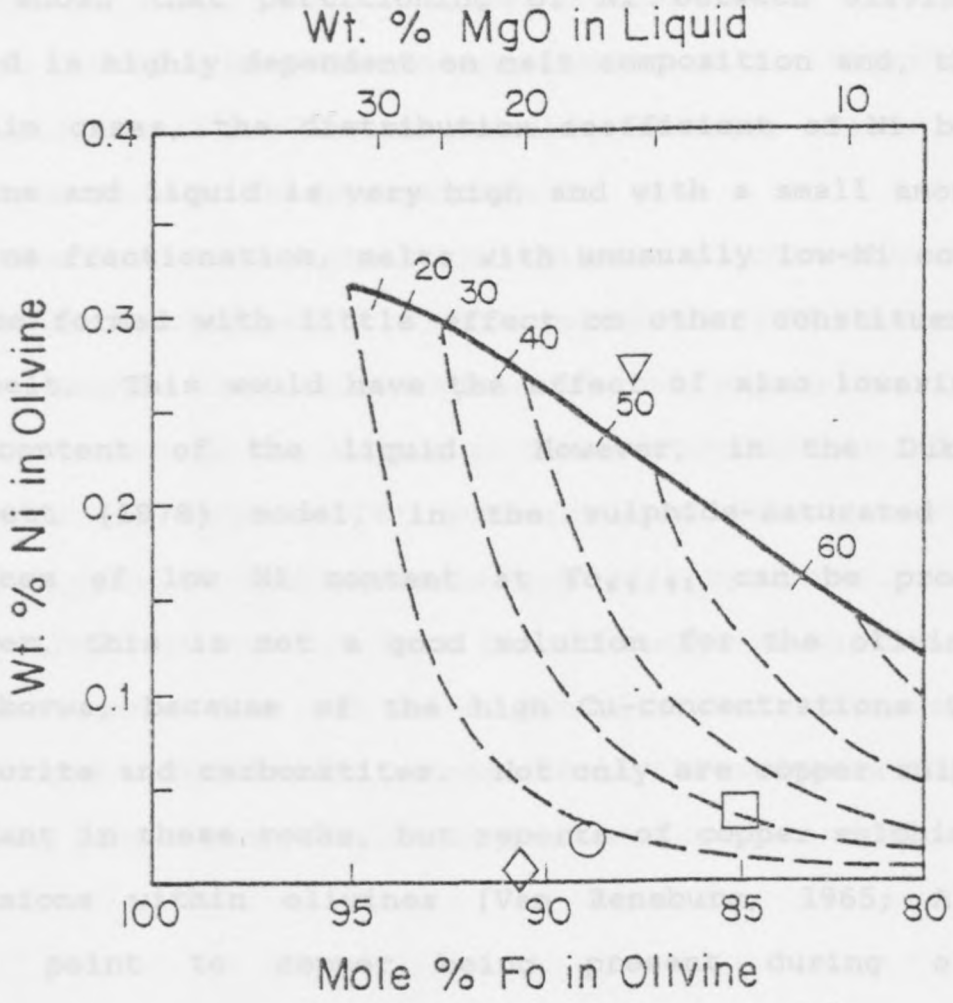


Figure 5.15 Compositions of fractionating olivine for sulfide-undersaturated case (solid line) and for sulfide-saturated case (dashed curves) and MgO composition of the liquid at saturation (after Duke and Naldrett (1978). Numbers on solid curve represents mole% of olivine fractionation. Phalaborwa data are plotted: P42K ○ , P3C ◇ , P120P □ , and P(79a)X ▽ .

from phoscorite and carbonatite from Phalaborwa have been plotted on this diagram (Figure 5.15). Fractionation of olivine alone (solid line) produces later olivines with significant nickel content. However, Hart and Davis (1978) have shown that partitioning of Ni between olivine and liquid is highly dependent on melt composition and, that in certain cases, the distribution coefficient of Ni between olivine and liquid is very high and with a small amount of olivine fractionation, melts with unusually low-Ni contents may be formed with little effect on other constituents of the melt. This would have the effect of also lowering the MgO content of the liquid. However, in the Duke and Naldrett (1978) model, in the sulphide-saturated case, olivines of low Ni content at Fo_{89-91} can be produced. However, this is not a good solution for the olivines at Phalaborwa, because of the high Cu-concentrations in the phoscorite and carbonatites. Not only are copper sulphides abundant in these rocks, but reports of copper sulphides as inclusions within olivines (Van Rensburg, 1965; Aldous, 1980) point to copper being present during olivine crystallization. The partition coefficient of Cu between olivine and sulphide melt, D = 178, is thought to remain of similar magnitude in mafic and ultramafic melts (Rajamani and Naldrett, 1978). This strong partitioning of Cu into sulphide melt precludes significant amounts of sulphide liquid acting as a sink for Ni in Phalaborwa magmatism.

Fractionation of magnetite might produce liquids low in Ni without significantly lowering the MgO content of a magma. D(Ni-mag) can range from 12 to 77 depending on temperature and fO_2 (Lindstrom, 1976). With D(Ni-mag) = 77, removal of small amounts of magnetite from a liquid would reduce the remaining Ni-content dramatically. Magnetite was also postulated earlier as possibly reducing the Cr content in magma forming the pyroxenites.

The low-Ca content of the olivines points to cooling in a plutonic environment. Simkin and Smith (1970) established that pressure and not temperature of crystallization of olivine controls the amount of Ca substitution in olivines. Finnerty and Boyd (1978) substantiated this for olivines coexisting with orthopyroxene and clinopyroxene. However, Brown (1980) points out that the influence of bulk chemistry of the magma has not been established. Obviously, at Phalaborwa, abundant Ca is present in the magma as indicated by the proportion of clinopyroxene, apatite and calcite present.

5.2.4 Magnetite

5.2.4.1 Mineralogical Characteristics

One magnetite was analyzed in this study (Table 5.7). It appears to be pure magnetite with very low Ti and Mn; no chromium was detected. The overall trend in composition of magnetite is known from analyzed concentrates from mining operations (Palabora Mining Company, 1976). Titanium

decreases from 4.0% TiO_2 in magnetite from outer phoscorite to less than 0.10% TiO_2 in magnetite in banded carbonatite. Aldous (1980) gives magnetite analyses for two samples each of phoscorite and banded carbonatite. He shows that magnetite from phoscorite contains more MgO (0.65-1.45% Mg) than magnetites from banded carbonatite (0.35-1.01% MgO).

5.2.4.2 Petrologic Significance

The compositions of primary oxide minerals are dependent on the bulk chemistry of the magma, the depth of emplacement, and the oxygen fugacity of the magma. Haggerty (1976) notes that in highly undersaturated rocks where $aSiO_2$ and fO_2 are dominating parameters, titanium is often depleted in the oxides. The decrease in TiO_2 in magnetite from carbonatite may indicate a decrease in fO_2 from phoscorite to carbonatite or may simply reflect a concentration of Ti in early-formed phases and subsequent depletion in the magma. Haggerty (1976) also notes that composition of the magma rather than pressure, as is commonly believed, determines the Mg content in magnetites. Therefore, the decrease in Mg from phoscorite to carbonatite may represent a direction of crystallization.

5.2.5 Amphibole

5.2.5.1 Crystal Chemistry

Analysis of amphibole from the fenite around main complex is given in Table 5.7. The general formula of amphibole,

$W_{0-1}{}^{x\text{-}xii}X_2{}^{vi\text{-}viii}Y_5{}^{vi}Z_8{}^{iv}O_{22}(OH,F,Cl)_2$ has the tetrahedral position filled with Si + Al; Fe, Mg, Ti, Al and Mn occupy the Y position and the X and W positions are occupied by calcium, sodium, and potassium. The W site is only partially filled as indicated by Ca + Na + K < 3.0 cations. Some of the iron was calculated as Fe^{3+} to fulfill stoichiometric considerations.

5.2.5.2 Mineralogical Characteristics

The amphibole from sample P146-440N is the only one found in the main complex in this study. Its composition indicates that the components richterite ($Na_2CaMg_5Si_8O_{22}(OH)_2$) and magnesioriebeckite ($Na_2Mg_3Fe^{3+}{}_2Si_8O_{22}(OH)_2$) are present. Potassium can substitute for sodium in either series (Ernst, 1968). The composition is plotted in the triangle Mg-Ca-Na (Figure 5.16).

5.2.5.3 Petrologic Significance

Amphibole is one of the few minerals containing significant sodium in the main complex at Phalaborwa. Its coexisting pyroxene is the most sodium-rich of those studied here (Figure 5.2). Figure 5.16 shows the composition of the amphibole from Phalaborwa as well as amphibole compositions from other ultrabasic intrusions. The amphibole from Phalaborwa is relatively Na-poor compared to these amphiboles. Low Ti and Al are chemical characteristics common to the amphibole and pyroxenes of the main complex.

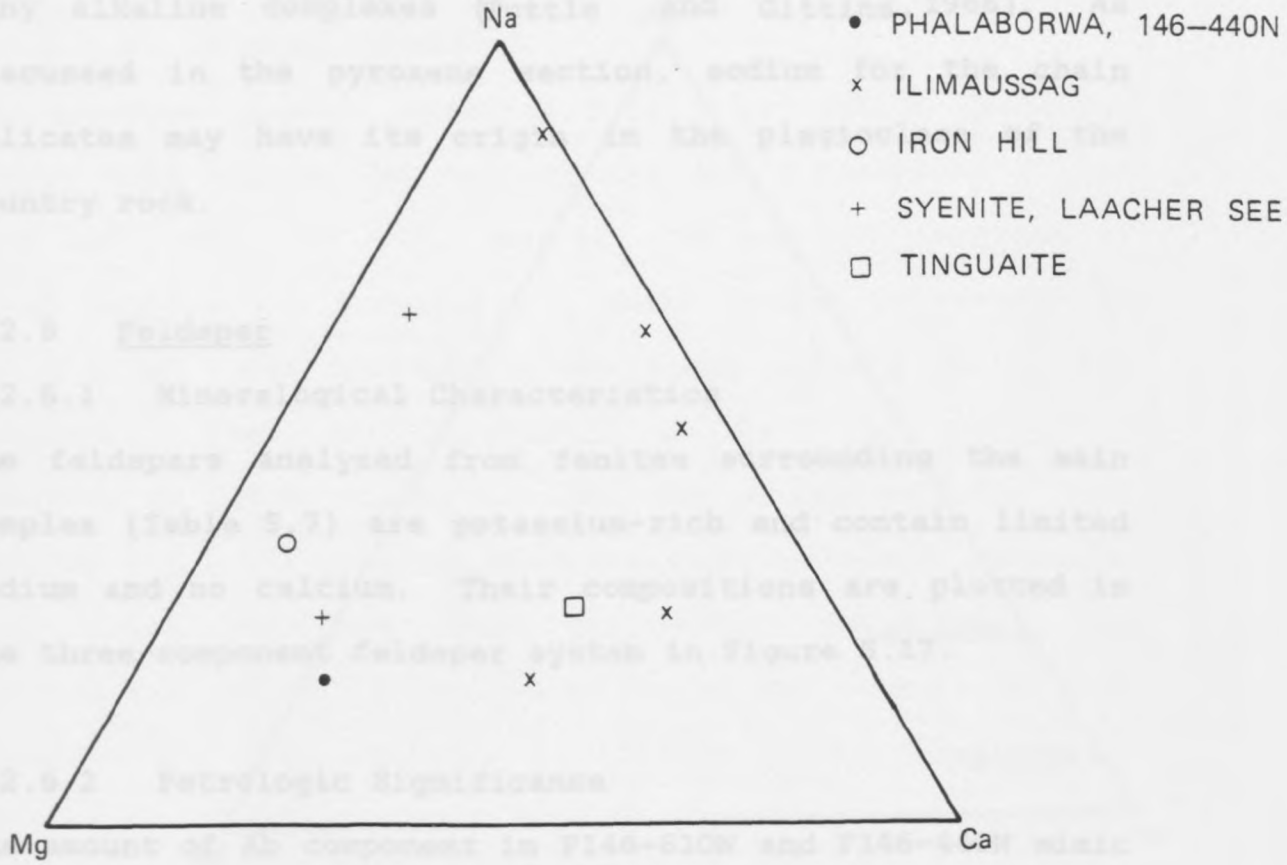


Figure 5.16 The composition of the amphibole from fenitized country rock around the main complex plotted in the Mg-Ca-Na system. Other data are from Ilimaussag(Larsen, 1976), Iron Hill (Nash, 1972), Laacher See (Ferguson, 1978) and a tinguaite (Ferguson, 1978).

The texture of rock P146-440N is suggestive of a fenitized country rock. The fenitizing fluid at Phalaborwa may have contained some sodium but was depleted in sodium compared to many alkaline complexes (Tuttle and Gittins, 1966). As discussed in the pyroxene section, sodium for the chain silicates may have its origin in the plagioclase of the country rock.

5.2.6 Feldspar

5.2.6.1 Mineralogical Characteristics

The feldspars analyzed from fenites surrounding the main complex (Table 5.7) are potassium-rich and contain limited sodium and no calcium. Their compositions are plotted in the three-component feldspar system in Figure 5.17.

5.2.6.2 Petrologic Significance

The amount of Ab component in P146-610N and P146-440N mimic the low amount of sodium in the coexisting pyroxenes. The two fenite samples show that the sample closest to the complex is richer in potassium which suggests a higher degree of metasomatism from a K-rich fluid. The sodium in the feldspar and probably in the pyroxenes may be derived from the plagioclase of the country rock.

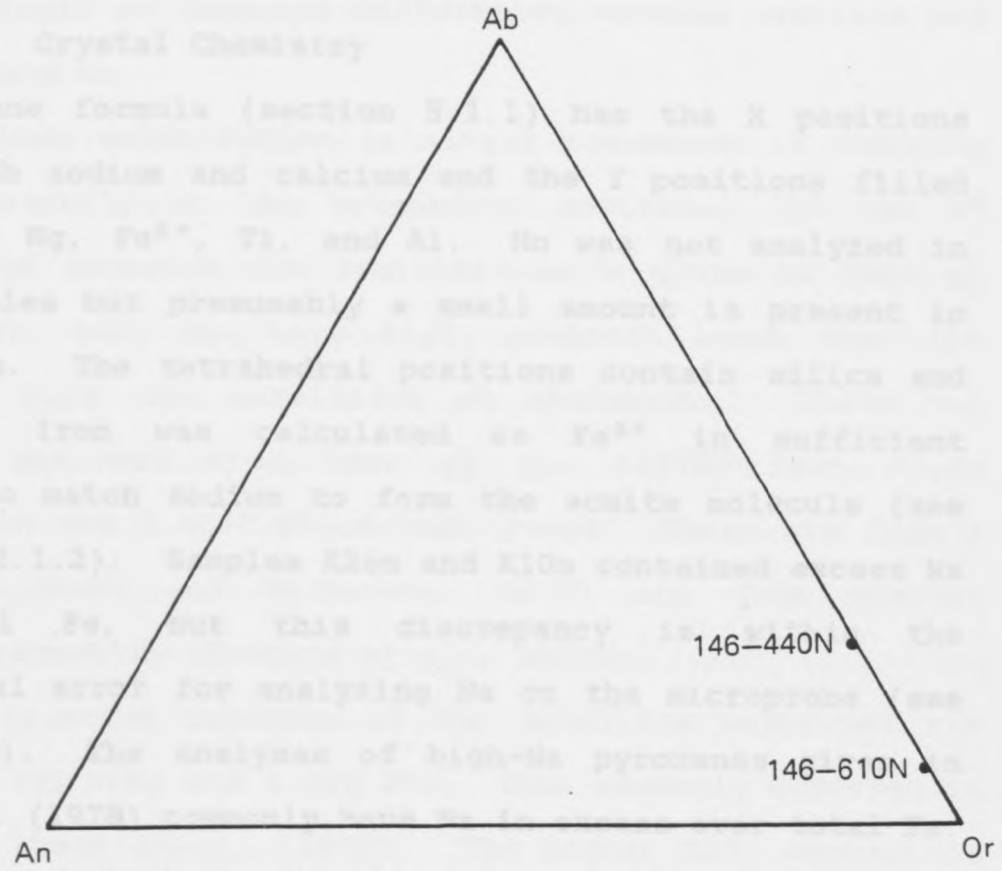


Figure 5.17 Compositions of feldspars from fenitized country rock around the main complex plotted in the orthoclase-albite-anorthite system.

5.3 SATELLITES

5.3.1 Kgopoeloe and Spitskop

5.3.1.1 Clinopyroxenes

5.3.1.1.1 Crystal Chemistry

The pyroxene formula (section 5.1.1) has the X positions filled with sodium and calcium and the Y positions filled with Fe^{3+}, Mg, Fe^{2+}, Ti, and Al. Mn was not analyzed in these samples but presumably a small amount is present in the Y site. The tetrahedral positions contain silica and aluminum. Iron was calculated as Fe^{3+} in sufficient quantity to match sodium to form the acmite molecule (see section 5.2.1.2). Samples K26m and K10m contained excess Na over total Fe, but this discrepancy is within the experimental error for analyzing Na on the microprobe (see Appendix B). The analyses of high-Na pyroxenes given in Deer et al. (1978) commonly have Na in excess over total Fe. The low octahedral totals in Table 5.8 allow for the addition of manganese.

5.3.1.1.2 Mineralogical Characteristics

The separation of pyroxenes into aegirine and aegirine-augite has been defined in many ways (Washington and Merwin, 1927; Sabine, 1950; Troger, 1952). Classification here is based on Deer et al. (1978) who restrict aegirine to compositions containing between $Fe^{3+}_{0.8}$ and $Fe^{3+}_{1.0}$. Therefore, samples K26m and K10m contain aegirine and sample

K8m and K27m contain aegirine-augite. The four samples cluster closely around the defined compositional break of $Fe^{3+}_{0.8}$ and therefore, little emphasis should be placed on the petrologic or chemical differences between aegirine and aegirine-augite.

Aluminum substitution in alkali pyroxenes is commonly low and usually in the octahedral position. Of the 19 analyses of aegirine and aegirine-augite given in Deer et al. (1978), only two have Al_2O_3 contents lower than the pyroxenes from the satellites at Phalaborwa. These two pyroxene analyses from Deer et al. (1978) have Al_2O_3 contents in the 0.40-0.60 percent range. These are from a shonkinite (Nash and Wilkinson, 1970) and from quartz-aegirine pegmatite (Kostyak et al., 1970).

The titanium contents of the satellite aegirines are higher, 1.19% TiO_2 and 1.23% TiO_2, than commonly observed in aegirines (Deer et al., 1978). The higher TiO_2 content in the aegirine-augites from Kgopoeloe is consistent with the general trend of increasing titanium in more ferrous pyroxene (Deer et al., 1978).

The Fe/(Fe+Mg) ratios range from 0.88 to 0.97. The samples with highest ratios occur toward the upper and outer part of the pipe. The microbreccia filling (K26m) has a Fe/(Fe+Mg) ratio of 0.94 as opposed to the base of the pipe exposure which has an Fe/(Fe+Mg) of 0.88. The two samples of matrix which are in areas of high fragments to matrix have an intermediate and a higher Fe/(Fe+Mg) ratio. The

analyses listed in Table 5.8 are averages of four to seven analyses within one hand specimen. No zoning within a grain or compositional differences among grains of one polished thin section were detected with the number of analyses performed.

The sodium-rich character of the pyroxenes is seen in Figure 5.18 where the compositions are plotted on a Mg-(Fe^{2+}+Mn)-Na diagram. (Fe^{2+}+Mn) component was calculated by assuming that manganese makes up the deficiency in the Y position; Mn calculated in this way ranges from 0.047 to 0.067 cations. This was added to the Fe^{2+} as calculated. This calculation will affect the Mg to Fe^{2+}+Mn drastically. However, these pyroxenes are very Na-rich and therefore, any error in these assumptions will not significantly effect any petrogenetic implications derived from Figure 5.18.

5.3.1.2 Amphiboles

5.3.1.2.1 Crystal Chemistry

The general formula for amphiboles may be represented by $W_{0-1}{}^{x\text{-}xii}X_2{}^{vi\text{-}viii}Y_5{}^{vi}Z_8{}^{iv}O_{22}(OH,O,F,Cl)_2$. Analyses 5, 6 and 7 in Table 5.8 give the composition and site-occupancy for the amphiboles measured from the satellites. The W and X positions are occupied by sodium, potassium and calcium; only K26m shows a slight deficiency in the W site as indicated by Na+K+Ca < 3.0 cations. The Y position is filled predominantly with magnesium and ferric iron with a minor amount of ferrous iron, titanium and aluminum. The

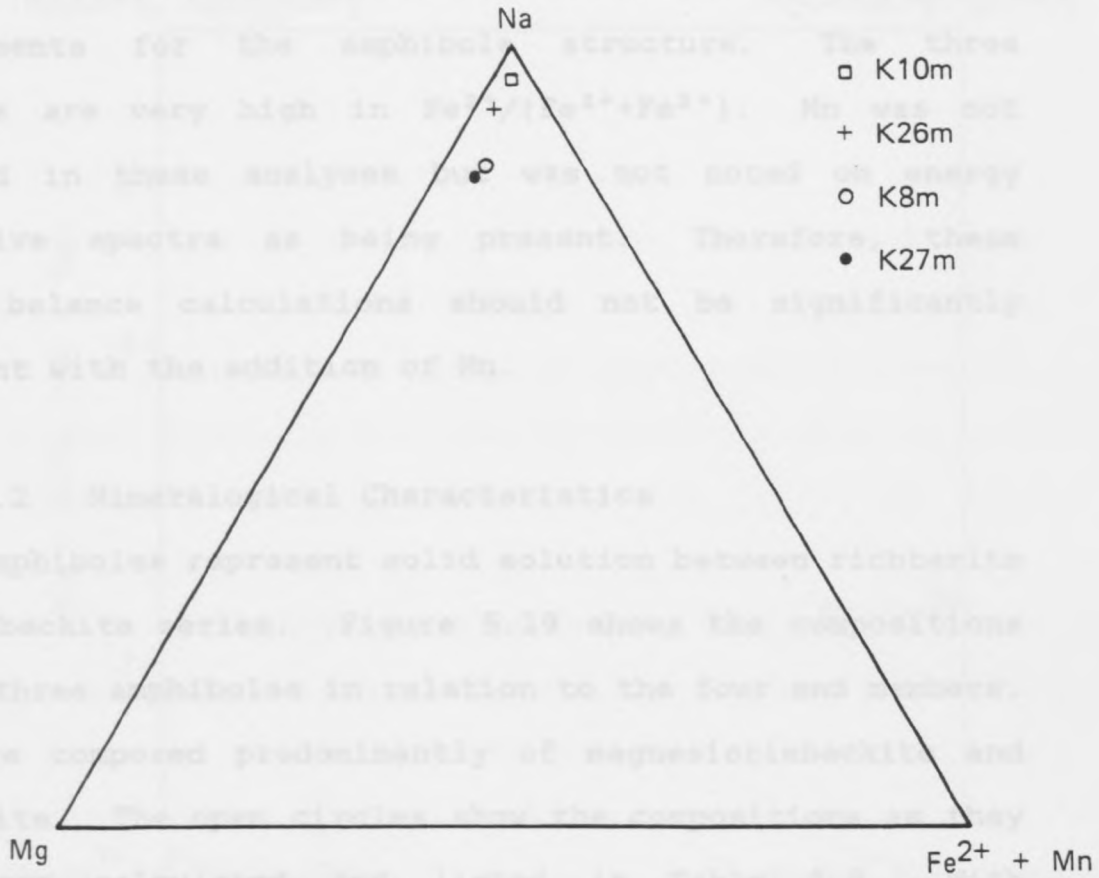


Figure 5.18 Compositions of pyroxenes from Kgopoeloe and Spitskop plotted in the Mg-(Fe^{2+}+Mn)-Na system.

tetrahedral site is comprised predominantly of silica with minor aluminum.

The Fe^{3+} composition was calculated by allocating iron to Fe^{3+} in sufficient quantity to satisfy the charge balance requirements for the amphibole structure. The three analyses are very high in $Fe^{3+}/(Fe^{3+}+Fe^{2+})$. Mn was not included in these analyses but was not noted on energy dispersive spectra as being present. Therefore, these charge balance calculations should not be significantly different with the addition of Mn.

5.3.1.2.2 Mineralogical Characteristics

These amphiboles represent solid solution between richterite and riebeckite series. Figure 5.19 shows the compositions of the three amphiboles in relation to the four end members. They are composed predominantly of magnesioriebeckite and richterite. The open circles show the compositions as they have been calculated and listed in Table 5.8. With complicated chemistry such as amphiboles, the oxidation state of iron is difficult to calculate precisely. If the formula of analysis 5, sample S3r, conforms to the ideal amphibole formula with two cations of Fe^{3+}, then the sample would have a higher percentage of riebeckite component; that alternate composition is also shown in Figure 5.19.

Titanium content is constant and low in the amphiboles (0.15-0.23% TiO_2), alumina is more variable (0.00 to 0.72) and is comparable in Al_2O_3 content to many riebeckites and

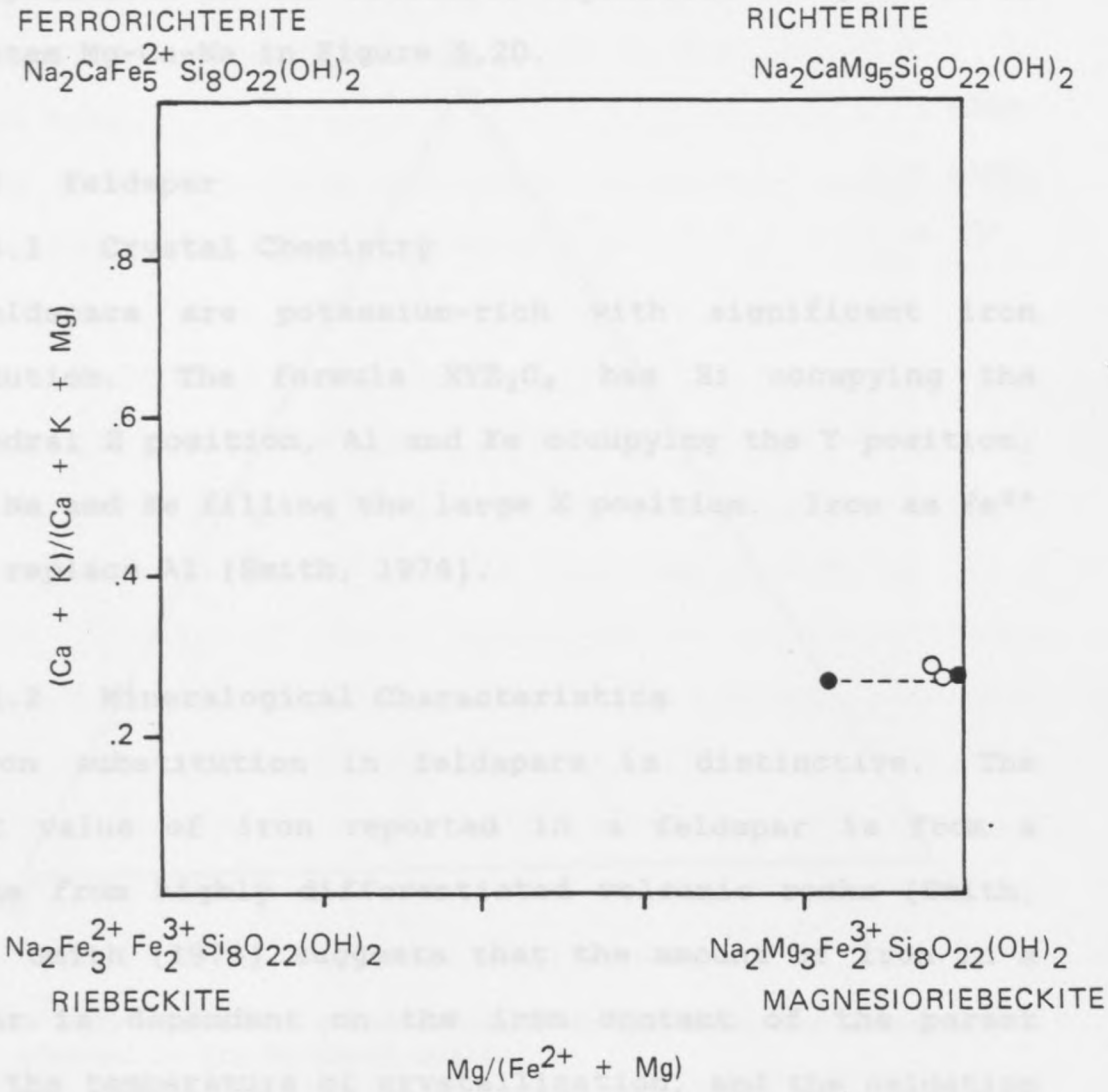


Figure 5.19 Amphibole compositions from Kgopoeloe and Spitskop plotted in relation to the end members of the richterite and riebeckite compositional series. Solid circles represent sample S3r. The right hand circle shows the composition as calculated in Table 5. The left hand circle is the composition if the ideal composition of two cations of Fe^{3+} is used. Open circles represent compositions of samples K26m and K10m.

richterites (Deer et al., 1978; Ferguson, 1978). There is considerable substitution of potassium in these amphiboles. The compositions of the satellite amphiboles are plotted in the system Mg-Ca-Na in Figure 5.20.

5.3.1.3 Feldspar

5.3.1.3.1 Crystal Chemistry

The feldspars are potassium-rich with significant iron substitution. The formula XYZ_3O_8 has Si occupying the tetrahedral Z position, Al and Fe occupying the Y position, and K, Na and Fe filling the large X position. Iron as Fe^{3+} should replace Al (Smith, 1974).

5.3.1.3.2 Mineralogical Characteristics

The iron substitution in feldspars is distinctive. The highest value of iron reported in a feldspar is from a sanidine from highly differentiated volcanic rocks (Smith, 1974). Smith (1974) suggests that the amount of iron in a feldspar is dependent on the iron content of the parent magma, the temperature of crystallization, and the oxidation state of the iron. The deficiency of Al in the three feldspar analyses of Table 5.8 may reflect the amount of Fe^{3+} substitution in the same position. Deer et al. (1963) note that Shand (1931) reported an unusually K_2O-rich feldspar which contained 1.02% Fe_2O_3 from Phalaborwa, but suggest that it is due to inclusion of ferromagnesian material. Microprobe data in this study supports Shand's

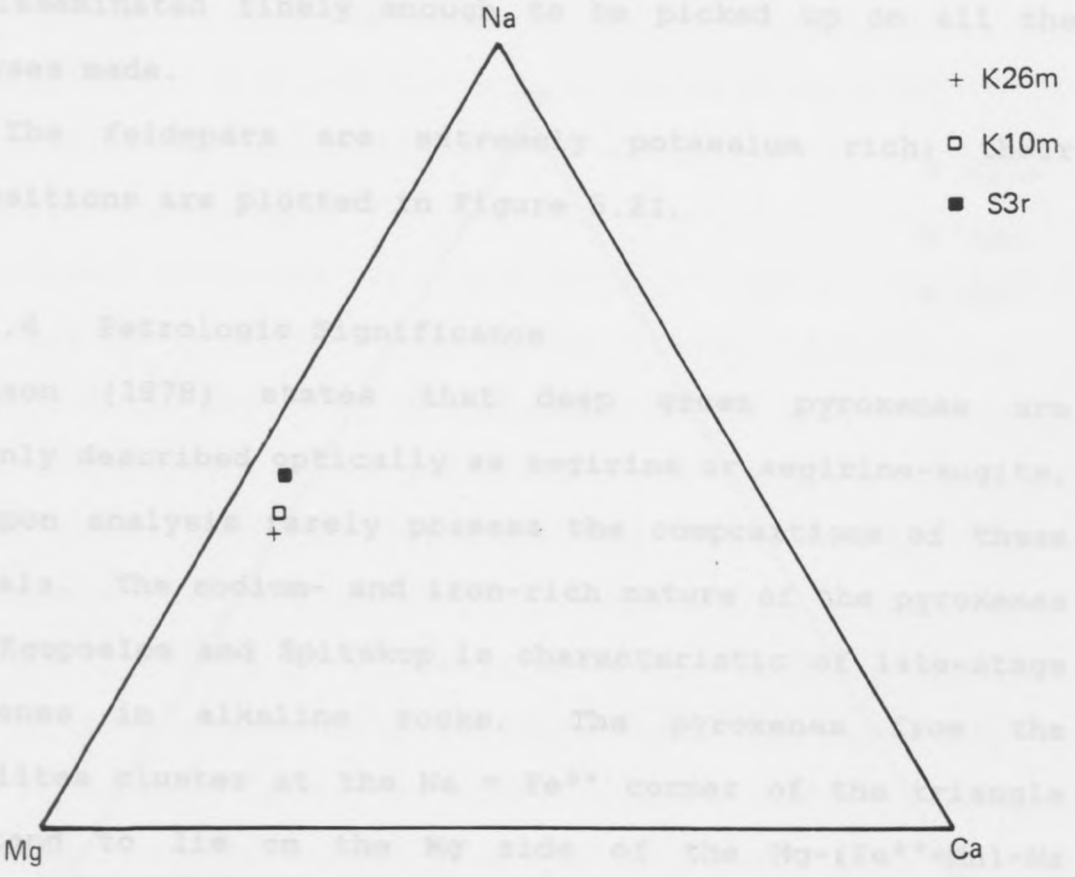


Figure 5.20 Amphibole compositions from Kgopoeloe and Spitskop plotted in the Mg-Ca-Na system.

wet chemical analysis of the iron-rich feldspar. Deer et al. (1963) also suggest that any Fe_2O_3 over 0.50% may be material which has exsolved upon cooling. If this is so, it is disseminated finely enough to be picked up on all the analyses made.

The feldspars are extremely potassium rich; their compositions are plotted in Figure 5.21.

5.3.1.4 Petrologic Significance

Ferguson (1978) states that deep green pyroxenes are commonly described optically as aegirine or aegirine-augite, but upon analysis rarely possess the compositions of these minerals. The sodium- and iron-rich nature of the pyroxenes from Kgopoeloe and Spitskop is characteristic of late-stage pyroxenes in alkaline rocks. The pyroxenes from the satellites cluster at the Na = Fe^{3+} corner of the triangle and tend to lie on the Mg side of the Mg-(Fe^{2+}+Mn)-Na triangle, indicating no strong enrichment of Fe^{2} during the evolution of this magma. End-stage trends of other alkaline rocks are shown in Figure 5.9. If the magma had yielded pyroxenes with a trend similar to Ilimaussaq or South Quoroq, Greenland (Figure 5.9), then end-stage pyroxenes would be closer to the Fe^{2+}+Mn apex of the triangle. The occurrence of aegirine in rocks believed to have formed by vapor, i.e., microbreccia, suggests that Fe^{3+} and Na were enriched in the vapor phase relative to the liquid at Kgopoeloe.

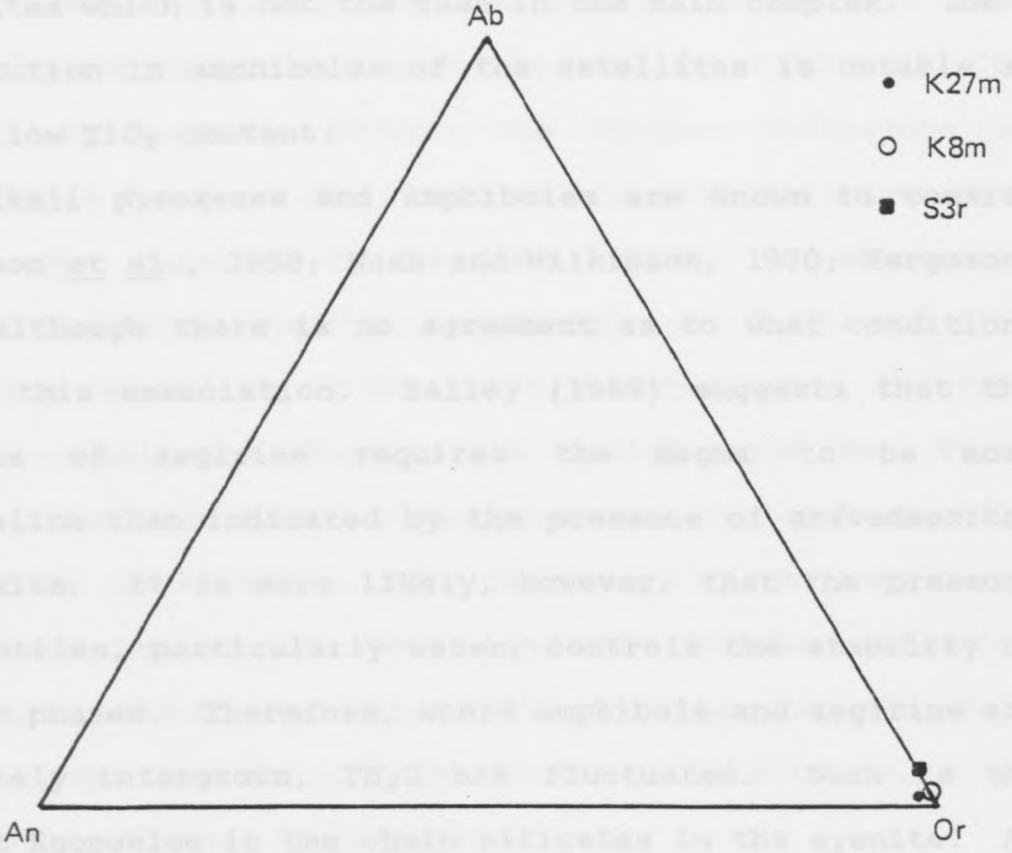


Figure 5.21 Feldspar compositions from Kgopoeloe and Spitskop plotted in the orthoclase-anorthite-albite system.

The amphiboles and pyroxenes show some similar chemical characteristics and some differences. Both are low in Al_2O_3 and have a similar Al_2O_3 composition to pyroxenes of the main complex. TiO_2 is enriched in the pyroxenes of the satellites which is not the case in the main complex. The K substitution in amphiboles of the satellites is notable as is the low TiO_2 content.

Alkali pyroxenes and amphiboles are known to coexist (Jacobson et al., 1958; Nash and Wilkinson, 1970; Ferguson, 1978) although there is no agreement as to what conditions permit this association. Bailey (1969) suggests that the presence of aegirine requires the magma to be more peralkaline than indicated by the presence of arfvedsonite-riebeckite. It is more likely, however, that the pressure of volatiles, particularly water, controls the stability of the two phases. Therefore, where amphibole and aegirine are intimately intergrown, PH_2O has fluctuated. Such is the case at Kgopoeloe in the chain silicates in the syenite. At Spitskop, however, the amphibole and pyroxenes are found in discrete crystals which may be indicative of more stable conditions of volatile content.

A notable feature of the amphiboles and pyroxenes in the satellite bodies is the significant difference in Fe/(Fe+Mg) ratios between coexisting phases (Table 5.8). The Mg content of amphiboles is higher than in the clinopyroxenes. Literature examples of coexisting clinopyroxenes and amphiboles from alkaline rocks in which

the Fe/Mg ratios are similar such as lavas from Leucite Hills are cited by Carmichael (1967). Pyroxenes commonly have Fe/(Fe+Mg) of 0.07-0.08 and coexisting amphiboles have the same ratio of 0.07. Other examples such as Ilimaussaq have pyroxenes of Fe/(Fe+Mg) of 0.50, 1.00, 0.98, with coexisting amphiboles having values of 0.63, 0.95 and 1.00, respectively (Larsen, 1976). The largest difference in Fe/Mg values found in the literature is from a syenite from Laacher See reported by Ferguson (1978) in which the titanian aegirine had a Fe/(Fe+Mg) of 0.93 and the coexisting amphibole, 0.43 to 0.85 from core to rim. Without established distribution coefficients for Fe/Mg between amphibole and clinopyroxenes, no petrogenetic conclusions can be drawn. The importance of the amphiboles and clinopyroxenes at Kgopoeloe and Spitskop lies in contrasting their chemistry with pyroxenes of the main complex, the petrologic significance of which will be discussed in Chapter 10 on petrogenesis.

5.3.2 Guide Copper Mine

5.3.2.1 Crystal Chemistry

The crystallographic site occupancies of the pyroxenes are similar to those of the main complex (see section 5.2.1.1). Microprobe analyses for representative pyroxenes are listed in Table 5.9, Appendix A. Trace elements measured for a clinopyroxene from Guide Copper Mine are listed in Table 5.2, Appendix A.

5.3.2.2 Mineralogical Characteristics

Clinopyroxenes from the Guide Copper Mine range from diopside through Na-rich augite to aegirine-augite (Fe^{3+} > 0.2 cations). The majority of the clinopyroxene compositions are sodian augite. The clinopyroxenes are highly zoned and commonly exhibit the entire compositional range in one crystal. Optical oscillatory zoning described in section 4.2.3 is a result of compositional fluctuations. These are illustrated in Figure 5.22 which shows Mg-(Fe^{2+}+Mn)-Na. Cations per formula unit are plotted against distance from core to rim in Figure 5.23. The plot for sodium is identical to a plot for Fe^{3+} because of the calculation procedure (section 5.2.1.2). Figure 5.23 shows that total iron varies sympathetically with sodium and ferric iron and varies in an opposite manner to ferrous iron, magnesium, and calcium. This implies enrichment of acmite versus diopside components in the dark-green versus light-green bands.

Sodium variation is not constant among various grains. The number of cations of Na in sample G12F increases from 0.037 at the core to 0.223 at the rim, whereas G8F decreases from 0.106 to 0.074. Table 5.9 also shows that rims of various clinopyroxenes are not in equilibrium with one another. For example, the G12F pyroxene contains 0.223 cations of Na at its outer rim and G8F contains only 0.074 cations of Na. This phenomenon is found within one thin section and among different thin sections as recognized by

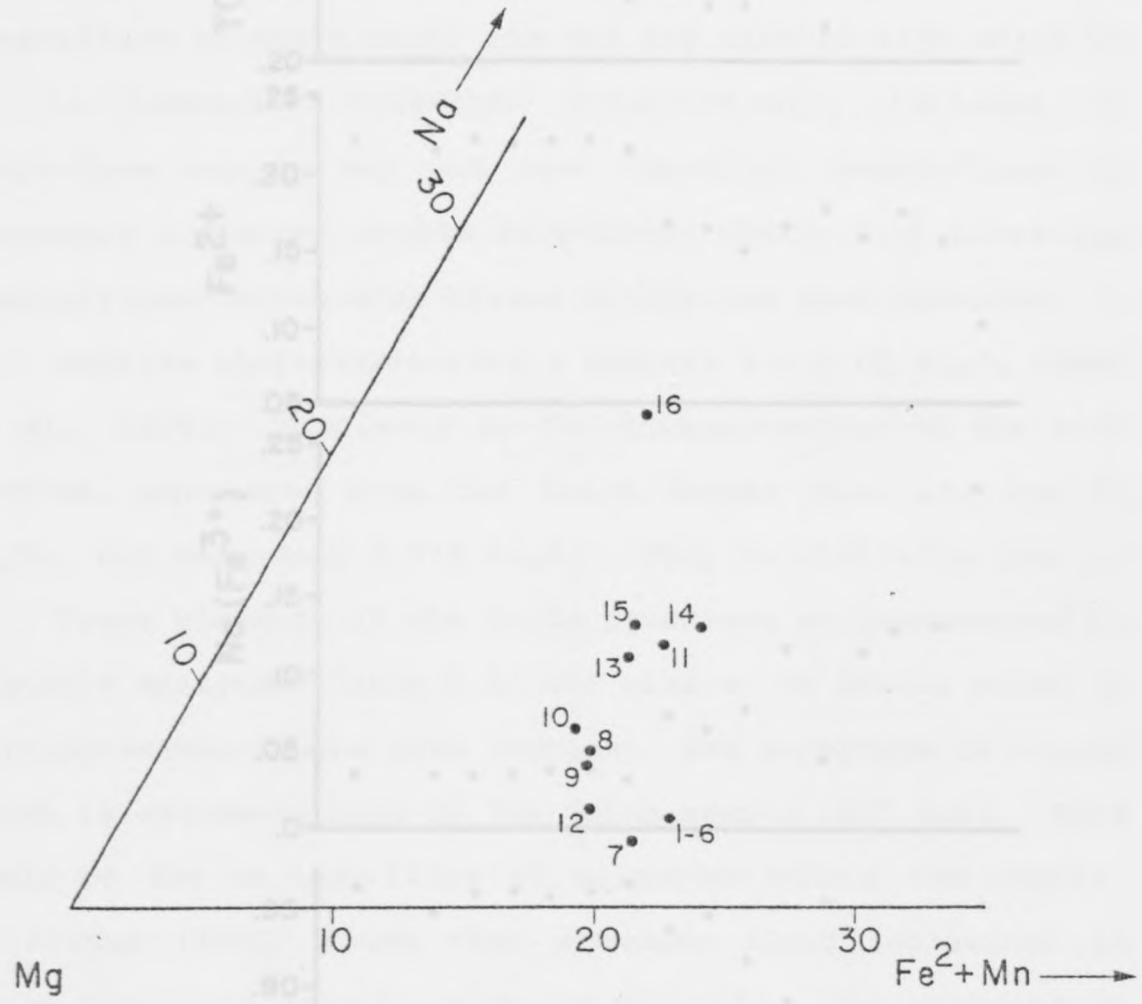


Figure 5.22 Representative analyses of clinopyroxene from Guide Copper Mine, sample G12F, plotted in the system Mg-(Fe^{2+}+Mn)-Na to show oscillatory zoning from core (analysis 1) to rim (analysis 16).

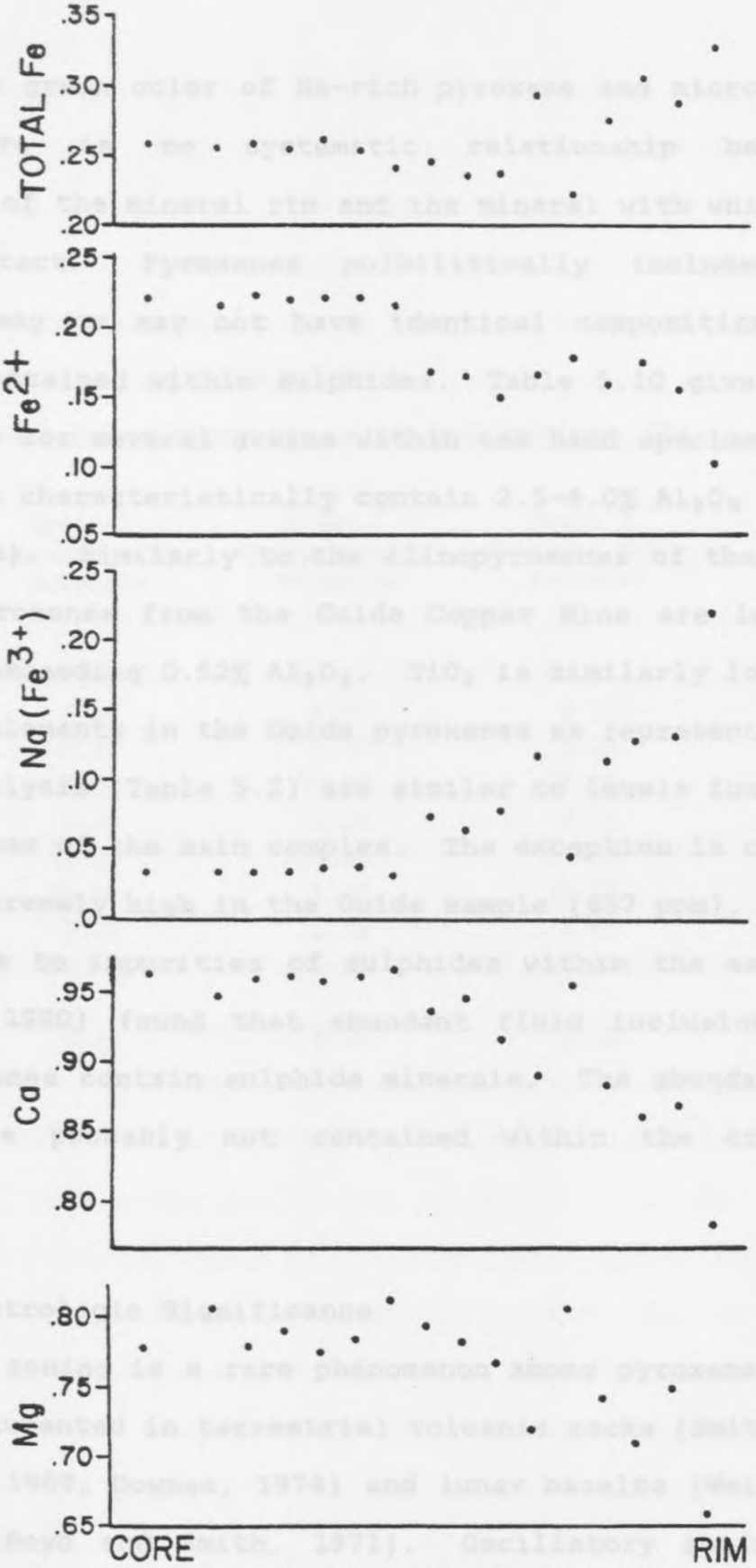


Figure 5.23 Cations per formula unit are plotted as distance from core to rim for analyses from sample G12F. The composition closest to the core represents analysis 1 on Figure 5.22 with successive analyses toward the rim corresponding to numbers through 16 in Figure 5.22.

the distinct green color of Na-rich pyroxene and microprobe data. There is no systematic relationship between composition of the mineral rim and the mineral with which it is in contact. Pyroxenes poikilitically included in microcline may or may not have identical compositions to pyroxenes contained within sulphides. Table 5.10 gives rim compositions for several grains within one hand specimen.

Augites characteristically contain 2.5-4.0% Al_2O_3 (Deer et al., 1978). Similarly to the clinopyroxenes of the main complex, pyroxenes from the Guide Copper Mine are low in Al_2O_3, not exceeding 0.52% Al_2O_3. TiO_2 is similarly low.

Trace elements in the Guide pyroxenes as represented by a single analysis (Table 5.2) are similar to levels found in clinopyroxenes of the main complex. The exception is copper which is extremely high in the Guide sample (457 ppm). This could be due to impurities of sulphides within the sample, as Aldous (1980) found that abundant fluid inclusions in these pyroxenes contain sulphide minerals. The abundant Cu is therefore probably not contained within the crystal lattice.

5.3.2.3 Petrologic Significance

Oscillatory zoning is a rare phenomenon among pyroxenes but has been documented in terrestrial volcanic rocks (Smith and Carmichael, 1969; Downes, 1974) and lunar basalts (Weill et al., 1971; Boyd and Smith, 1971). Oscillatory zoning in clinopyroxenes of the Shonkin Sag laccolith has been noted

TABLE 5.10

Rim Compositions of Pyroxenes in One Hand Specimen, G8F

	Grain 1 Coexists with Sulphide	Grain 2 Coexists with Sulphide	Grain 3 Coexists with Feldspar
SiO_2	52.90	53.17	52.97
TiO_2	0.24	0.00	0.00
Al_2O_3	0.22	0.30	0.28
FeO	8.94	10.88	10.60
MnO	0.20	0.25	0.31
MgO	12.28	10.66	11.18
CaO	23.68	21.42	21.57
Na_2O	0.65	1.83	1.85
Total	99.11	98.51	98.76
Fe/(Fe + Mg)	0.29	0.36	0.35

in passing but with no reference of its origin (Wilkinson and Nash, 1966) or petrogenetic significance. The Mt. Etna calcic augites (Downes, 1974) and the Al- and Ti-rich clinopyroxenes from trachybasalts (Smith and Carmichael, 1969) both exhibit fluctuations in aluminum and titanium contents which are attributed to cooling conditions in which equilibrium growth and normal crystallization cannot be maintained but growth is slow enough to prevent reversed zoning alone. This can happen when supersaturation occurs at the crystal-liquid interface prior to the initiation of growth of each fine band (Downes, 1974). A similar mechanism is invoked to explain the common occurrence of oscillatory zoning in plagioclase (Ribbe, 1979).

The difference in diffusion rates of Ca and Na through magma is another commonly cited mechanism for oscillatory zoning in plagioclase. The lack of correspondence in Na variation between the two samples in Table 5.9 could be due to this phenomenon. An alternate hypothesis is that the equilibrium was not maintained on a larger scale throughout the pipe and that these two grains crystallized at different times or in localized magma with different composition.

The Guide pyroxenes are low in titanium and aluminum and show no evidence of fluctuations in these elements. The fluctuations in acmite component suggest that fO_2 fluctuations may likely influence the crystallization of these pyroxenes.

The presence of copper sulphides in seemingly immiscible blebs within the pyroxenites provides a possible mechanism for fluctuations in oxygen fugacity. Relationships among sulphur, oxygen, and iron in melts of various compositions have been determined experimentally (Haughton et al., 1974; Shima and Naldrett, 1975) which are summarized by Buchanan and Nolan (1978). An immiscible sulphide melt forms when a silicate melt becomes saturated with sulphur. When this happens, the amount of FeO and the fugacity of sulphur decrease in the silicate melt and the oxygen fugacity of the silicate melt rises. The decrease in Fe^{2+} activity and increasing stability of acmite with higher fO_2 produce a pyroxene with lower total FeO and higher Fe^{3+}.

The formation of an immiscible sulphide melt has been suggested by Buchanan (1979) for reversals in Fe/(Fe+Mg) of pyroxenes over very short vertical intervals in the Bushveld complex where sulphide and pyroxene crystallized simultaneously.

Similar trace element abundances of the Guide pyroxenes to those of the main complex (Table 5.2), especially the high Sr, Ce and La, point to a similar origin for the pyroxenes of both intrusions. Similarly, the low Al and Ti contents of the pyroxenes of the Guide Copper Mine and the main complex suggest that the temperature and composition of the two magmas may have been similar.

Chapter VI

THERMODYNAMIC CONSIDERATIONS

A modern petrological-thermodynamic approach to the study of rocks utilizing theory, experimental work, and mineral chemical data now allows the petrologist to place more accurate constraints on the various factors influencing the cooling history of a magma. This approach is most often used to determine either the pressure or temperature at which minerals equilibrated or to determine the activity or effective concentrations of components in a melt.

Equation 6.1 involves the exchange of Fe and Mg between coexisting phases which may be used to determine a temperature of equilibration:

$$\underset{\text{clinopyroxene}}{2CaMgSi_2O_6} + \underset{\text{olivine}}{Fe_2SiO_4} \rightarrow \underset{\text{clinopyroxene}}{2CaFeSi_2O_6} + \underset{\text{olivine}}{Mg_2SiO_4} \qquad (6.1)$$

The Gibbs free energy for this reaction may be written:

$$\Delta G = \Delta G^\circ + 2.303RT \log K \qquad (6.2)$$

where ΔG is the change in the Gibbs free energy for the reaction at some P and T (°K), G° is the free energy of the reactants in their standard states, R is the gas constant, and K is the equilibrium constant for the reaction.

For reaction 6.1, K may be written

$$K = \frac{\left[a^{oliv}_{Mg_2SiO_4}\right]\left[a^{cpx}_{CaFeSi_2O_6}\right]^2}{\left[a^{cpx}_{CaMgSi_2O_6}\right]^2\left[a^{oliv}_{Fe_2SiO_4}\right]} \qquad (6.3)$$

where a^m_x is the activity of the component x in the mineral m. At equilibrium, $\Delta G = 0$ and the reaction may be written

$$\Delta G^\circ = -2.303RT \log K \tag{6.4}$$

For reactions in which ΔG° has been determined experimentally, knowing the compositions of the phases involved will enable equation 6.4 to be solved for T.

In the case of solving for the activity of some component in a melt, for example,

$$\underset{\text{magnetite}}{2/3\ Fe_3O_4} + \underset{\text{melt}}{SiO_2} \rightarrow \underset{\text{olivine}}{Fe_2SiO_4} + \underset{\text{fluid}}{1/3\ O_2} \tag{6.5}$$

$$\Delta G^\circ = -2.303\ RT \log \frac{\left[a^{oliv}_{Fe_2SiO_4}\right]\left[f_{O_2}\right]^{1/3}}{\left[a^{melt}_{SiO_2}\right]\left[a^{mag}_{Fe_3O_4}\right]} \tag{6.6}$$

one must have an idea of T and the fugacity of oxygen (fO_2) to solve for the activity of silica in the melt. Data for many petrologically significant reactions have been published in recent years (Nicholls et al., 1971; Nicholls and Carmichael, 1972, Bacon and Carmichael, 1973; Carmichael et al., 1977).

As sophisticated as this technique is, it is liable to several uncertainties. The thermodynamic equations are approximations of what occurs in nature but are assumed in petrologic calculations to adequately describe the reactions measured. The problem of relating compositions to activities has received wide attention (Carmichael et al., 1977), and activities of components in a mineral are

calculated differently depending on what solution model is thought to best fit the mineral. Activity of a component in a melt is more difficult to predict and its formulation is in an early stage of development. The most important source of error in current use of thermodynamic data is the measurement of compositions of mineral phases. Microprobe measurements commonly give variable results for different elements and are less precise at low concentrations. The inability to distinguish between Fe^{3+} and Fe^{2+} on this instrument is a source of error for some calculations.

6.1 CONDITIONS OF FORMATION AT PHALABORWA

6.1.1 Pressure

Geological evidence provides the only method for estimating the pressure of equilibration for the rocks studied from Phalaborwa. The configuration of sediments in the Transvaal Basin shows that there was a maximum of 12 kilometres of stratigraphic overburden in the Phalaborwa area around 2100-2000 million years ago (Button, 1976), consisting of sandstone, dolomite with chert, shale and mafic volcanics in the proportion of about 1:1:1.2:1. Using the rock densities of Daly et al. (1966) and adding about 3 km of granite-gneiss, as estimated by extending the dip of the Transvaal Supergroup sediments to the location of Phalaborwa, this overburden gives a lithostatic pressure of 4.9 kilobars. A value of 5 kb will be used in subsequent calculations.

6.1.2 Temperature

Former workers at Phalaborwa have used various mineral assemblages and mineral compositions to estimate temperatures of formation. These are listed in Table 6.1. Subsequent studies have shown that these temperature estimates are of varying effectiveness in measuring magmatic temperatures.

Use of calcite-dolomite pairs as geothermometers gives minimum temperatures which are usually much lower than the magmatic temperature because of the migration of Mg from calcite into dolomite at subsolidus temperatures. Gittins (1979) criticizes almost all published temperature data on calcite-dolomite pairs on this basis, emphasizing that temperatures in the range of 300-500°C are much too low for temperature of crystallization. However, Gittins (1979) accepts that, in rare instances, temperatures derived from calcite-dolomite pairs may approach magmatic temperatures which should be on the order of 900°C. The temperatures reported for Phalaborwa carbonates (Table 6.1) are lower than the 900°C but much higher than commonly quoted in the literature (Gittins, 1979). On the basis of the above argument, Van Rensburg's (1965) temperature estimate is most likely the closest to the actual solvus temperature. Pressure affects on the solvus are small (Goldsmith and Newton, 1969) so temperatures are unaffected by uncertainties in pressure estimates.

TABLE 6.1 - Temperature Estimates for Coexisting Minerals from the Literature

Temperature (°C)	Assemblage	Rock Type	Method Used for T. estimation	Reference
675	calcite-dolomite	carbonatite	solvus	Verwoerd (1966)
750-800 minimum	calcite-dolomite	transgressive carbonatite	solvus	Van Rensburg (1965)
600 minimum	calcite-dolomite	phoscorite	solvus	Hennig-Michaeli (1968)
600-1000	baddeleyite	phoscorite	stability of mineral	Hennig-Michaeli (1968)
1000	olivine	phoscorite	composition	Hennig-Michaeli (1968)
600	ilmenite-magnetite ulvospinel	transgressive carbonatite	assemblage	Van Rensburg (1965)
500	magnetite-ilmenite	phoscorite	compositions of phases	Hennig-Michaeli (1968)
500-600	chondrodite	phoscorite	stability of phase	Henning-Michaeli (1968)
500	sulphides	transgressive carbonatite	assemblage	Van Rensburg (1965)
600	sulphides	carbonatite	assemblage	Hanekom et al. (1965)
450-600	sulphides	phoscorite	assemblage	Henning-Michaeli (1968)
400-550	magnetite-ilmenite	phoscorite	composition of phases	Aldous (1980)
400-475	magnetite-ilmenite	carbonatite	composition of phases	Aldous (1980)

The temperatures derived from stability of baddeleyite and chondrodite (Hennig-Michaeli, 1968) should be considered rough estimates at best because of the wide range of conditions which can govern the stability of these minerals. For instance, $aSiO_2$ governs the stability of baddeleyite (Figure 6.1), and the partial pressure of water can affect the stability of chondrodite (Butler, 1972).

The Buddington and Lindsley (1964) iron-oxide geothermometer is widely used today although temperatures derived from it are often subsolidus rather than magmatic temperatures. Ilmenite coexisting with magnetite has been reported in a number of previous studies on Phalaborwa (Van Rensburg, 1965; Hanekom et al., 1965; Hennig-Michaeli, 1968; Aldous, 1980). Many descriptions of the textures indicate that ilmenite has exsolved from more Ti-rich magnetite, a situation yielding the exsolution-equilibration temperature. Aldous (1980) described the textures which he used as being coarse grains of ilmenite at the edge of magnetite grains which are thought to represent a higher temperature process than fine exsolution (Rollinson, 1979). Temperatures of 400-600°C have been derived from magnetite-ilmenite pairs of phoscorite (Van Rensburg, 1965; Hennig-Michaeli, 1968; Aldous, 1980) and a lower temperature range, 400-475°C, for banded carbonatite (Aldous, 1980). These temperatures are in the range estimated for the equilibration of sulphides in the phoscorite and carbonatite (Table 6.1).

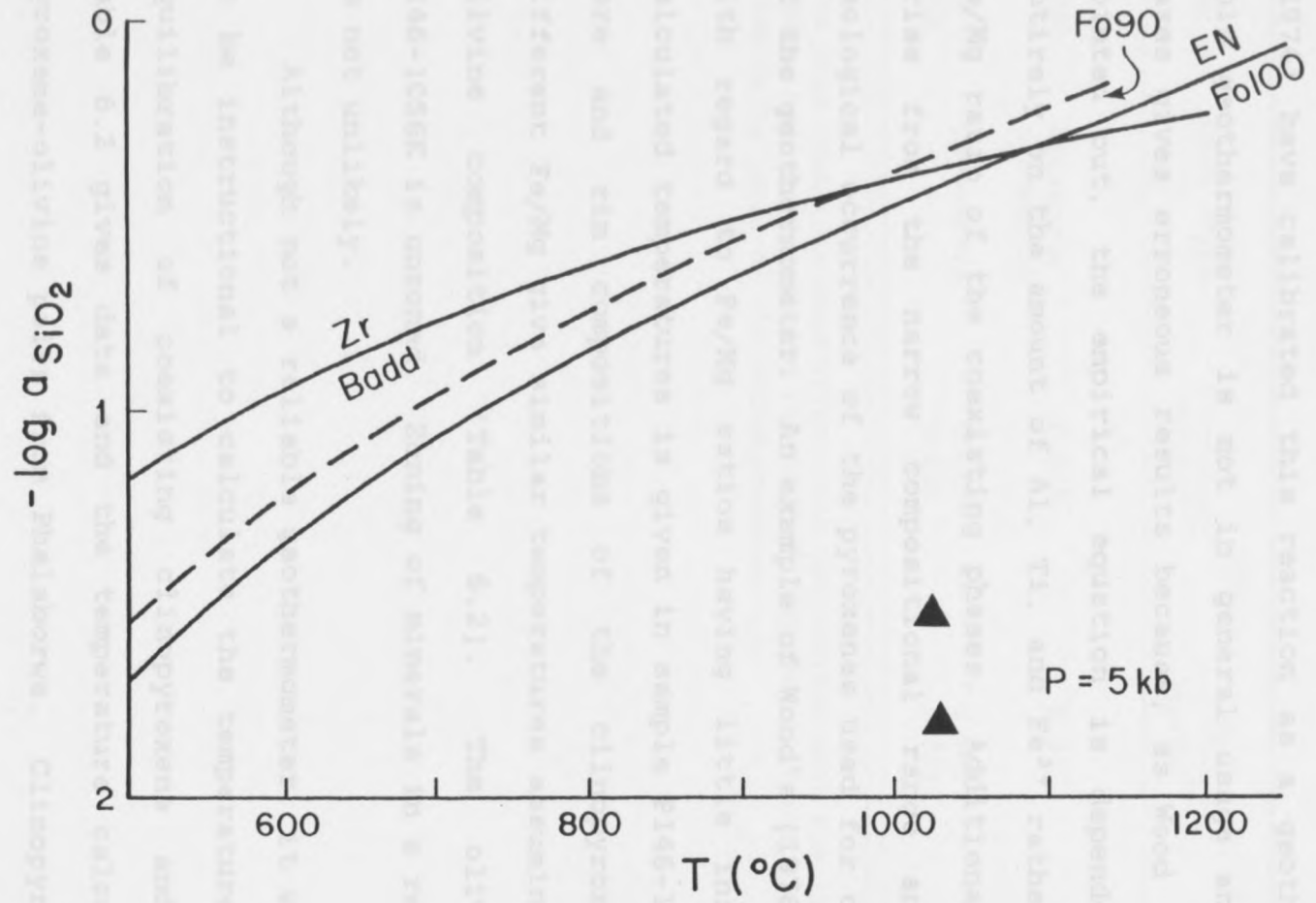


Figure 6.1 Lines showing buffer reactions for zircon-baddeleyite and forsterite-enstatite at 5 kb as a function of activity of silica versus temperature. The dashed line represents the stability of olivine with a composition of Fo_{90} coexisting with enstatite. The data points represent the calculations in section 6.1.3.2 for olivine-magnetite pairs from phoscorite and carbonatite from Phalaborwa. Calculated silica activity for carbonatite at 1200° C plots off this diagram.

The exchange of Fe and Mg between Ca-rich pyroxene and olivine is expressed in equation 6.1. Powell and Powell (1974) have calibrated this reaction as a geothermometer. This geothermometer is not in general usage and in many cases gives erroneous results because, as Wood (1976) has pointed out, the empirical equation is dependent almost entirely on the amount of Al, Ti, and Fe^{3+} rather than the Fe/Mg ratio of the coexisting phases. Additional problems arise from the narrow compositional range and limited geological occurrence of the pyroxenes used for calibration of the geothermometer. An example of Wood's (1976) argument with regard to Fe/Mg ratios having little influence on calculated temperatures is given in sample P146-1056K where core and rim compositions of the clinopyroxenes with different Fe/Mg give similar temperatures assuming the same olivine composition (Table 6.2). The olivine from P146-1056K is unzoned. Zoning of minerals in a reaction rim is not unlikely.

Although not a reliable geothermometer, it was thought to be instructional to calculate the temperatures for the equilibration of coexisting clinopyroxene and olivine. Table 6.2 gives data and the temperature calculated for pyroxene-olivine pairs from Phalaborwa. Clinopyroxene used for P120P is in direct contact with olivine and, because of this petrographic relationship and similar Fe/Mg between the two minerals, is assumed to be in equilibrium with the olivine (see section 5.2.1.3.3).

Table 6.2. Temperatures derived from coexisting olivine and clinopyroxene.

Sample	Rock Type	$(\frac{Mg}{Mg+Fe^{2+}})^{cpx}$	$(\frac{Mg}{Mg+Fe^{2+}})^{oliv}$	T°C
P120P	micaceous pyroxenite	0.878	0.841	1024
P146-1056K	phoscorite	0.425*	0.785	1046
		0.828	0.785	1040

* The more iron-rich composition does not coexist with the olivine but is given here to illustrate the lack of dependency of the geothermometer on the Fe/Mg ratio of the clinopyroxenes.

The temperature calculated from sample P146-1056K (1040-1046°C) is close to that derived from sample P120C (1024°C). It was shown in the geologic and petrographic descriptions in Chapters 3 and 4 that olivine and clinopyroxene do not commonly coexist in the Phalaborwa complex. Therefore, the temperature derived from this mineral pair at Phalaborwa is the temperature at which the two minerals have equilibrated. It is not necessarily the temperature at which they crystallized initially for one or both may have been xenocrysts.

The exchange of fluorine and hydroxyl anions between phlogopite and apatite has been established as a geothermometer by Stormer and Carmichael (1971), equation 6.7, but is not thought to be reliable for plutonic rocks because of extensive post-crystalline exchange of OH^- and F^- between late-stage fluids and phlogopite.

$$\underset{\text{fluorphlogopite}}{[KMg_3AlSi_3O_{10}]_{1/2}F} + \underset{\text{hydroxyapatite}}{Ca_5(PO_4)_3OH}$$

$$\underset{\text{fluoroapatite}}{Ca_5(PO_4)F} + \underset{\text{hydroxyphlogopite}}{[KMg_3AlSi_3O_{10}]_{1/2}OH} \qquad (6.7)$$

Phlogopites and apatites from phoscorite and micaceous pyroxenite were analyzed in this study, but microprobe conditions which prevent extensive fluorescence of fluorine cannot detect the low levels of F^- present in the phlogopite from Phalaborwa. Although not quantitative and, therefore, not reported here, the microprobe data did indicate that F/(F+OH) in the phlogopites measured would be around 0.1 or

less. This is used to plot the upper limit of F/(F+OH) in phlogopite of the box in Figure 6.2.

Data from Hanekom et al. (1965) and De Jager and Fourie (1978) for F^- and OH^- from minerals which come from the same rock type but from different samples and therefore cannot be considered to coexist have been plotted in Figure 6.2. These data have been used here because the low values of F^- in phlogopite have been shown above to be representative of phlogopites in several samples from Phalaborwa.

Temperatures of 150-600°C are inferred which supports Stormer and Carmichael's (1971) idea that extensive low temperature re-equilibration of volatiles with phlogopite occurs in plutonic settings. The metasomatic formation of phlogopite would also be compatible with these data. However, from arguments presented previously, the low temperature equilibration is preferred here.

6.1.3 Activity of Components in the Melt

6.1.3.1 Oxygen Fugacity

An assemblage containing magnetite-sanidine-biotite has been calibrated by Wones and Eugster (1965) to determine the fugacity of gaseous species. Knowing the compositions of the phases and the temperature of equilibration and assuming the vapor is made up solely of H_2O and O_2, one can calculate the fugacities of both these vapor species. Unfortunately, at Phalaborwa this assemblage is unknown. Feldspar and phlogopite coexist in the feldspathic pyroxenite, and

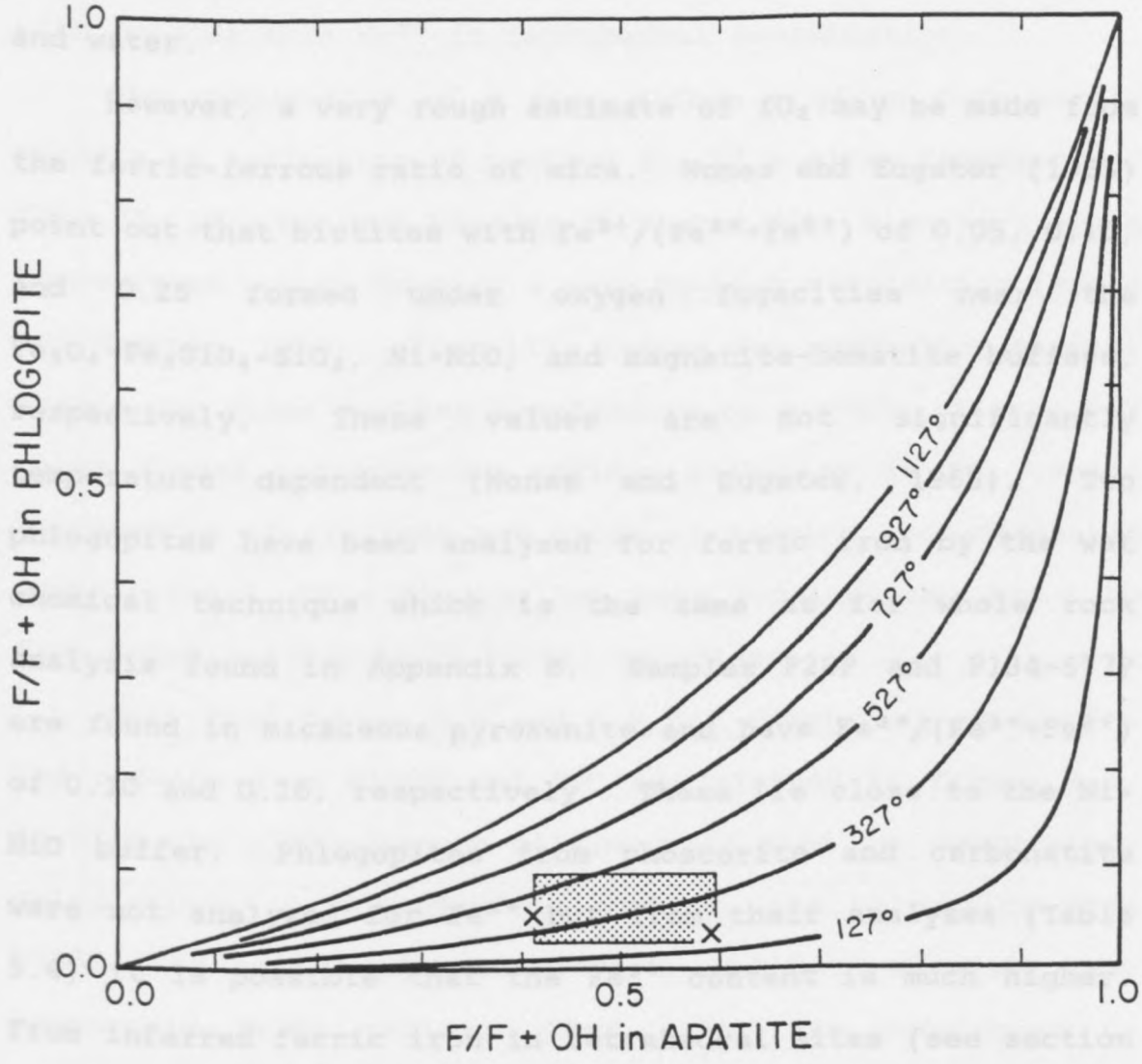


Figure 6.2 Calculated temperature curves for the apatite-phlogopite geothermometer of Stormer and Carmichael (1971) are shown with data from Phalaborwa (X) calculated from published data (Hanekom et al., 1965; DeJager and Fourie, 1978). The box encompasses the area covered by phlogopite compositions measured on the microprobe which have low F contents.

phoscorite contains both magnetite and phlogopite but no rocks contain all three minerals. Secondly, the vapor phase at Phalaborwa would contain carbon dioxide as well as oxygen and water.

However, a very rough estimate of fO_2 may be made from the ferric-ferrous ratio of mica. Wones and Eugster (1965) point out that biotites with $Fe^{3+}/(Fe^{3+}+Fe^{2+})$ of 0.05, 0.10, and 0.25 formed under oxygen fugacities near the Fe_3O_4-Fe_2SiO_4-SiO_2, Ni-NiO, and magnetite-hematite buffers, respectively. These values are not significantly temperature dependent (Wones and Eugster, 1965). Two phlogopites have been analyzed for ferric iron by the wet chemical technique which is the same as for whole rock analysis found in Appendix B. Samples P28P and P134-577P are found in micaceous pyroxenite and have $Fe^{3+}/(Fe^{3+}+Fe^{2+})$ of 0.10 and 0.16, respectively. These lie close to the Ni-NiO buffer. Phlogopites from phoscorite and carbonatite were not analyzed for Fe^{3+} but from their analyses (Table 5.4) it is possible that the Fe^{3+} content is much higher. From inferred ferric iron in tetrahedral sites (see section 5.2.2.1), one obtains $Fe^{3+}/(Fe^{3+}+Fe^{2+})$ of 0.38 for sample P146-1056K. Comparing this value to the compositional ranges given above for the various buffers (Wones and Eugster, 1965) suggests that the fO_2 of phoscorite P146-1056K lies above that of the magnetite-hematite buffer. This is impossible since carbonatite and phoscorite contain abundant magnetite and no hematite. This means that either

the stoichiometric inferences concerning Fe^{3+} in tetrahedral position are incorrect or the values given by Wones and Eugster (1965) are not valid for phlogopite compositions with considerable Fe^{3+} in tetrahedral coordination.

The composition of a mica within a given rock merely permits an estimation of maximum fO_2 at a given temperature. This fO_2 is a maximum because at higher fO_2, mica of a given composition breaks down to a more Mg-rich composition (Wones and Eugster, 1965). Stability ranges for coexisting mineral phases can place further constraints on a rock. Figure 6.3 shows curves representing maximum stability in fO_2 versus temperature of olivines and micas of varying iron-magnesium compositions. This diagram has been recalculated for 5 kb from Wones and Eugster's (1965) equations.

Data from Tables 5.4 and 5.6 for coexisting phlogopite and olivine from P120P and P3C are plotted in Figure 6.3. As with the clinopyroxene-olivine pair used for temperature calculations in the previous section, the phlogopite from P120P lies at the olivine contact, and both minerals have comparable Fe/Mg ratios. Thus, they are considered to represent conditions of equilibration of the two minerals.

Both of the samples plotted in Figure 6.3 lie on or near the Ni-NiO buffer curve as plotted in Figure 6.3; this agrees with the results using the $Fe^{3+}/(Fe^{3+}+Fe^{2+})$ of mica for pyroxenites. The mica from P120P lies approximately 60° below the temperature calculated for the olivine-clinopyroxene pair from the same sample. Phlogopite could

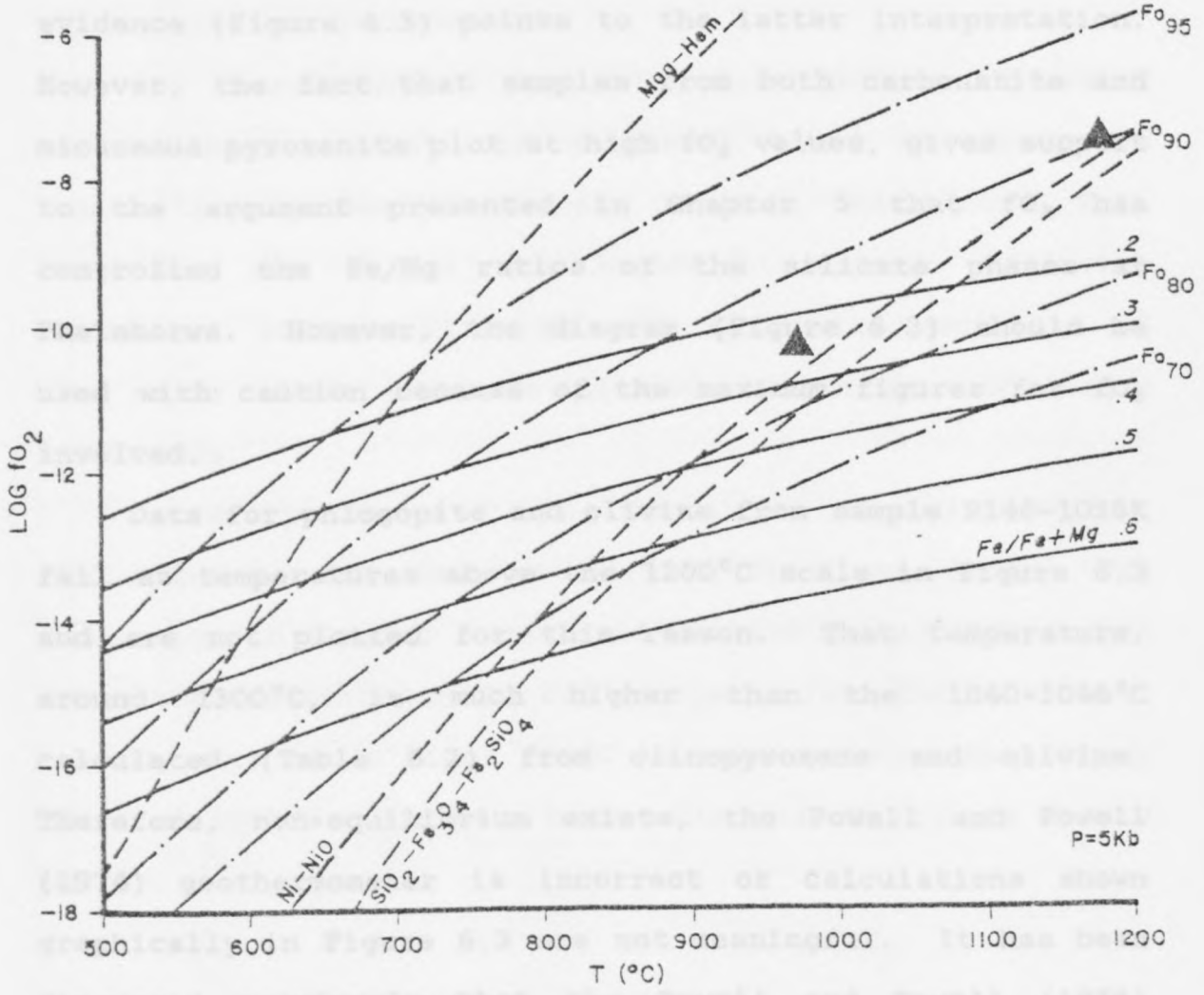


Figure 6.3 Lines showing the upper stability of olivines and phlogopites of varying compositions on an oxygen fugacity versus temperature diagram calculated for 5 kb (after Wones and Eugster, 1965). Fe/(Fe+Mg) represents the ratio of total iron to iron and magnesium for the micas. Buffer curves for magnetite-hematite, Ni-NiO, and quartz-magnetite-fayalite assemblages are plotted in dashed lines.

have formed at a lower temperature than the clinopyroxene or could have re-equilibrated to a lower temperature. Textural evidence (Figure 4.3) points to the latter interpretation. However, the fact that samples from both carbonatite and micaceous pyroxenite plot at high fO_2 values, gives support to the argument presented in Chapter 5 that fO_2 has controlled the Fe/Mg ratios of the silicate phases at Phalaborwa. However, the diagram (Figure 6.3) should be used with caution because of the maximum figures for fO_2 involved.

Data for phlogopite and olivine from sample P146-1056K fall at temperatures above the 1200°C scale in Figure 6.3 and are not plotted for this reason. That temperature, around 1300°C, is much higher than the 1040-1046°C calculated (Table 6.2) from clinopyroxene and olivine. Therefore, non-equilibrium exists, the Powell and Powell (1974) geothermometer is incorrect or calculations shown graphically in Figure 6.3 are not meaningful. It has been discussed previously that the Powell and Powell (1974) geothermometer does not give accurate numbers in all cases. The textures in P146-1056K are not considered equilibrium textures as discusssed in Chapter 5.

The oxygen fugacity for carbonatites at Phalaborwa suggested by Mitchell and Krouse (1975) based on the sulphide assemblage, i.e., at T = 700°C, $fO_2 = 10^{-16}$ lies on the curve of the Ni-NiO buffer. However, the magnetite-ilmenite work of Aldous (1980) yields fO_2 values of the QFM

buffer. The data of Mitchell and Krouse imply that similar buffering conditions prevailed during the formation of the pyroxenites and carbonatites.

Any discrepancy of fO_2 data among methods is easily reconcilable in that the estimates based on phlogopite compositions probably represent magmatic conditions. Both sulphides and oxides are known to undergo extensive subsolidus recrystallization, and therefore, estimates of fO_2 using these minerals probably represent subsolidus conditions.

Certainly, the available tools for measuring fO_2 at Phalaborwa are not well established for these rocks. The discussion in Chapter 5 centered on high versus low oxygen fugacities controlling the Fe^{2+} entrance into the silicates. Low fO_2 such as 10^{-16} at 700°C is a lower value than fO_2 = 10^{-10} at 1000°C. However, both values of fO_2 lie on Ni-NiO buffer.

6.1.3.2 Silica Activity

Silica activity or effective concentration of silica in a melt may be calculated from the reaction 6.5 based on the composition of olivine and magnetite and using previously estimated values of fO_2. In cases where magnetite and ilmenite have exsolved, as in samples measured by Aldous (1980), calculations of fO_2 yield conditions of subsolidus equilibration and not magmatic conditions. Buchanan (1976) found this was the case in the Bushveld Complex where

calculated fO_2 and crystallization temperatures were unreasonably low; therefore, they could not be used in calculating $aSiO_2$.

However, as mentioned in Chapter 3 and earlier in this chapter, the majority of magnetite occurring in the Phalaborwa complex does not contain exsolved ilmenite and, therefore, its composition may be used in calculating $aSiO_2$.

Equation 6.8 was used in calculating $aSiO_2$ for phoscorite in which fO_2 may be estimated using Figure 6.3 from coexisting olivine and phlogopite. These minerals commonly coexist with magnetite in phoscorite; rarely, these three minerals are present in carbonatite. Formulae used for calculating activities of components in minerals are listed in Appendix B.

$$\log a^{melt}_{SiO_2} = \Delta G°/2.303\ RT + \log a^{div}_{Fe_2SiO_4} + 1/3 \log fO_2 - 2/3 \log a^{mag}_{Fe_3O_4} \qquad (6.8)$$

Using compositions of olivine P42K (Fo_{87}) and a common magnetite composition for phoscorite of ulvospinel content of 5.5 mole percent (Aldous, 1980), with $fO_2 = 10^{-10}$:

$$\log aSiO_2 = -1.52 \quad \text{at } 1025°C, 5 \text{ kb.}$$

Calculations for carbonatite may be made using olivine sample P3C (Fo_{90}) with a more Fe-rich magnetite (Usp = 0.035) (Aldous, 1980) giving:

$$\log aSiO_2 = -2.51 \quad \text{at } 1200°C, 5 \text{ kb}$$

and

$$\log aSiO_2 = -1.75 \qquad \text{at } 1025^{\circ}C, \text{ 5 kb.}$$

Calculation of $aSiO_2$ at a given pressure is highly dependent on T, fO_2 and olivine composition. Small changes in magnetite composition do not affect $aSiO_2$ significantly.

Comparison of silica activity of the carbonatite and phoscorite from Phalaborwa with those calculated for the Bushveld Complex (Buchanan et al., 1980), kimberlite and ugandite lava (Nicholls et al., 1971) are listed in Table 6.3. As expected from the mineralogy, ultrabasic kimberlite and ugandite show $aSiO_2$ less than that of the basic Bushveld rocks of harzburgite and diorite. Silica activities calculated for the phoscorite and carbonatite from Phalaborwa lie close to the values for kimberlite and ugandite with silica activity for the carbonatite being the lowest. This is not surprising considering there are fewer silicate minerals present in carbonatite.

Reactions defining silica activity for zircon-baddeleyite and enstatite-forsterite from Nicholls et al. (1971) have been recalculated for P = 5 kb (Figure 6.1) and for olivine (Fo_{90}) coexisting with orthopyroxene. The curves for these two buffer reactions at 5 kb change in relationship to the one bar configuration in which the Fo-En curve lies above the zircon-baddeleyite curve (Nicholls et al., 1971). Because forsterite (Fo_{90}) and baddeleyite occur together in phoscorite, silica activity must be below the curve delineated by dashes. The values of $aSiO_2$ calculated

Table 6.3. Activity of silica in the melt calculated for phoscorite and carbonatite from the Phalaborwa complex and for some other igneous rocks.

Rock Type	Assemblage Used	log a_{SiO_2}	T	P	Reference
kimberlite	baddeleyite-zircon	-1.70	1327°C,	56 kb	Nicholls et al. (1971)
harzburgite Basal zone, Bushv.	forsterite-enstatite	-0.119	1114°C,	3.65	Buchanan et al. (1980)
diorite Upper zone, Bushv.	fayalite-ferrosilite	-0.0108	904°C,	3.26	Buchanan et al. (1980)
phoscorite	magnetite-olivine	-1.52	1025°C,	5 kb	this study
carbonatite	magnetite-olivine	-1.75	1025°C,	5 kb	this study
		-2.51	1200 C,	5 kb	" "
ugandite	kaliophilite-leucite	-1.46	990°C,	1 b	Nicholls et al. (1971)

above for carbonatite and phoscorite lie in the correct field. It should be noted that $aSiO_2$ calculated with fO_2 from the magnetite-hematite buffer lies above the zircon-baddeleyite curve (Figure 6.1).

6.2 SUMMARY

The level of the Phalaborwa complex exposed today crystallized at pressure of approximately 5 kb based on estimates of overburden at the time of intrusion. No well-established geothermometers exist for the assemblages present in the Phalaborwa complex. Best estimates are 800°C for calcite-dolomite pairs (Van Rensburg, 1965) and 1175° for olivine-phlogopite pairs in carbonatites, 1024°C and 975°C for pyroxenites based on an olivine-pyroxene pairs, respectively. Temperatures are those of equilibration and not crystallization.

Estimates of oxygen fugacity based on Fe^{3+} content of phlogopite agrees with estimates of fO_2 based on coexisting phlogopite and olivine. The agreement in values of fO_2 based on silicate and sulphide assemblages (Mitchell and Krouse, 1975) suggest constant buffering during formation of the main complex. Subsolidus equilibration of oxides is thought to account for the discrepancy in fO_2 values based on the oxide assemblage (Aldous, 1980). Implications of constant buffering of fO_2 for the petrogenesis of the complex will be discussed in Chapter 10.

Estimates of low silica activity for phoscorite and carbonatite based on fO_2 estimates in this study and compositions of magnetite and olivine are reasonable and fall in predicted ranges of silica activity when compared to published data for basic and ultrabasic rocks.

Chapter VII

WHOLE ROCK CHEMISTRY

Published chemical data for the rocks of the Phalaborwa complex are rare and are restricted to major and minor elements of the carbonatites (Lombaard et al., 1967; Van Rensburg, 1965; Hennig-Michaeli, 1967), syenite satellites (Frick, 1975) and a few feldspathic pyroxenites (Hanekom et al., 1965).

Whole rock chemistry in the main complex is largely restricted in this study to the various clinopyroxenites because they comprise a large portion of the complex, have a wide spatial distribution, and appear to be rocks least affected by late-stage fluids. The phoscorite, for example, has been altered by late-stage magmatic fluids as evidenced by the widespread serpentinization of the olivine.

Certain minor and trace elements have been measured on carbonatites for comparison to the clinopyroxenites, and one syenite dykelet from the Foskor pit was analyzed for comparison with the syenites of the satellite pipes.

The whole-rock chemistry of the satellite pipes are represented by 37 samples from Kgopoeloe and Spitskop and one sample from the Guide Copper Mine covering the range in textures and composition including Kgopoeloe granite outcrop, breccia-fragments and matrix and the various types of syenite found at Spitskop.

Chemical analyses and CIPW norms are listed in Appendix A in Tables 7.1 and 7.2.

Sample locations of whole rocks are listed in Appendix A; analytical methods and descriptions of the quality of data are found in Appendix B.

7.1 MAIN COMPLEX

In a complex such as Phalaborwa which has experienced widespread surface alteration and which contains rocks formed with an abundant gaseous phase in an alkali-rich environment, it is instructive to note what information may be gained from whole rock analyses.

Metasomatism is a frequently postulated mechanism for the formation of alkali-rich minerals in alkaline complexes (Borodin and Pavlenko, 1974; Gittins et al., 1975). Workers at Phalaborwa have unanimously regarded phlogopite as a metasomatized pyroxene or olivine (Hanekom et al., 1965; DeJager and Fourie, 1978). If this is so, then whole rock, or any chemistry, will not reflect the product of crystallization from a magma. However, as indicated in Chapter 4, phlogopite displays textures best described as cumulus and, as such, phlogopite-bearing rocks should reflect a magmatic rather than metasomatic origin. Similarly, the chemistry of other cumulus pyroxenites should be compatible with this origin.

Both magmatic and late-stage hydrothermal fluids must have played a part in the formation of the Phalaborwa

complex. Serpentinization extending to depths of over 1-1/2 km in the phoscorite suggests that serpentinization of the phoscorite took place at somewhat elevated temperatures as an intrinsic part of the cooling of the complex rather than by surface weathering. However, there is no evidence that the pyroxenites were affected by this process.

Lastly, nearly-monomineralic rocks will reflect the chemistry of the dominant minerals thus providing an additional method of studying trace element abundances.

7.1.1 Major Elements

The pyroxenite compositions are plotted in the system FEM-SAL-VOL after Dawson (1960) in Figure 7.1. They show their ultrabasic nature by covering portions of the triangle occupied by kimberlites, lamprophyres and certain ultra-potassic volcanic rocks. Phoscorites would plot within the triangle defined by olivine-magnetite-apatite/calcite. Dawson (1960) showed that the kimberlite field is continuous with that of carbonatite, but that there is a density minimum between them. Based on the modal proportion of minerals, some of the more silicate-rich carbonatites in the Phalaborwa complex would lie in the area connecting these two fields.

Variation diagrams in Figure 7.2 show that most pyroxenite compositions lie near to the composition of clinopyroxene (sample F6F, Table 5.1) and scatter from there toward compositions for phlogopite (sample F100P, Table

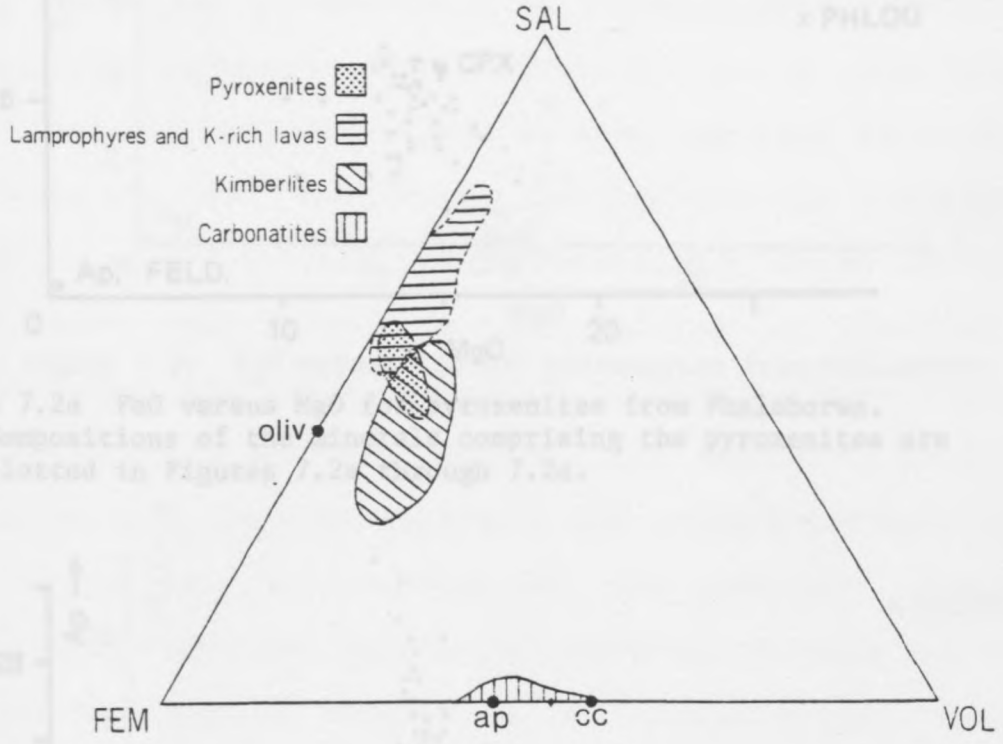


Figure 7.1 Compositions of pyroxenites from Phalaborwa plotted in the FEM-SAL-VOL triangle after Dawson (1960). Compositions of other ultrabasic rocks are shown for comparison. Data for lamprophyres and potassium-rich lavas are from Scott(1977); data for kimberlites and carbonatites are from Dawson (1960). The dashed lines represent the compositional transition between kimberlites and carbonatites. This area covers rock types such as carbonated kimberlites and silicate-rich carbonatites.

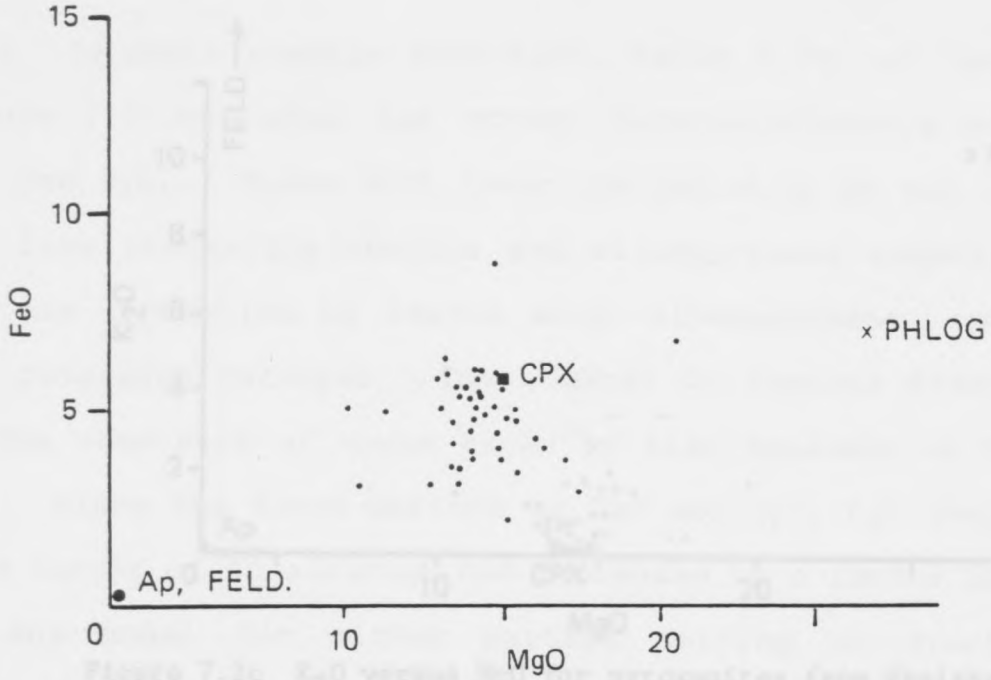


Figure 7.2a FeO versus MgO for pyroxenites from Phalaborwa. Compositions of the minerals comprising the pyroxenites are plotted in Figures 7.2a through 7.2d.

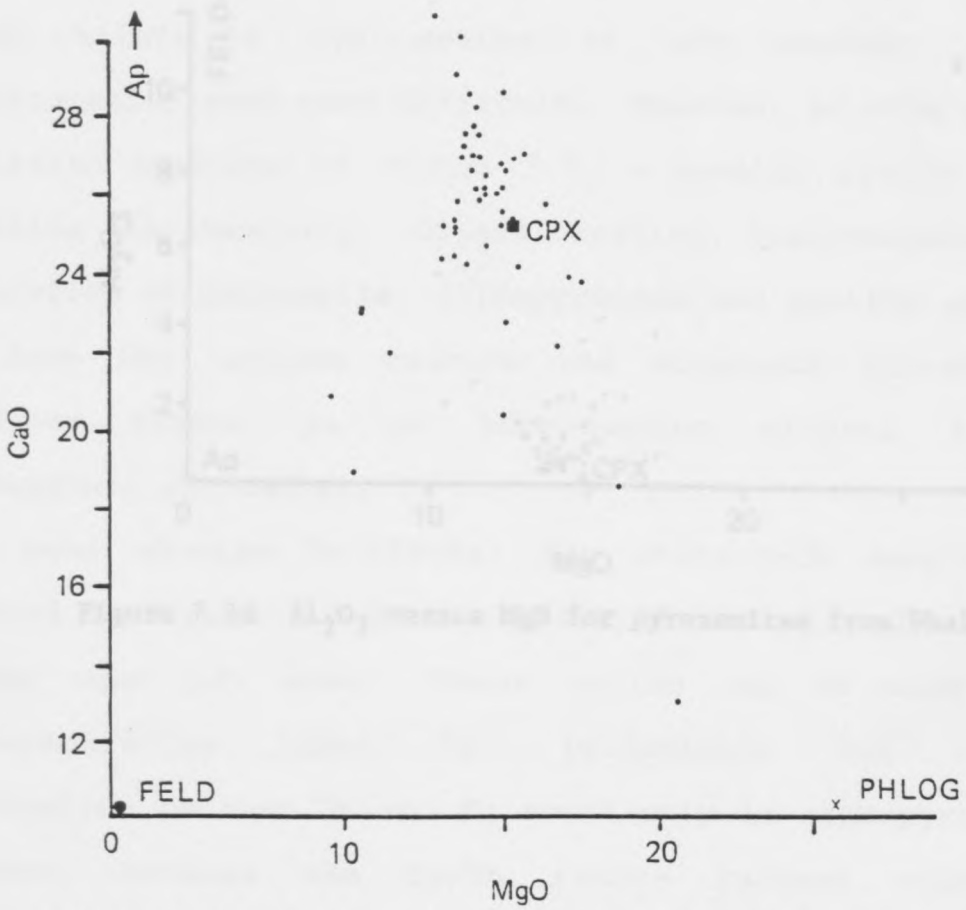


Figure 7.2b CaO versus MgO for pyroxenites from Phalaborwa.

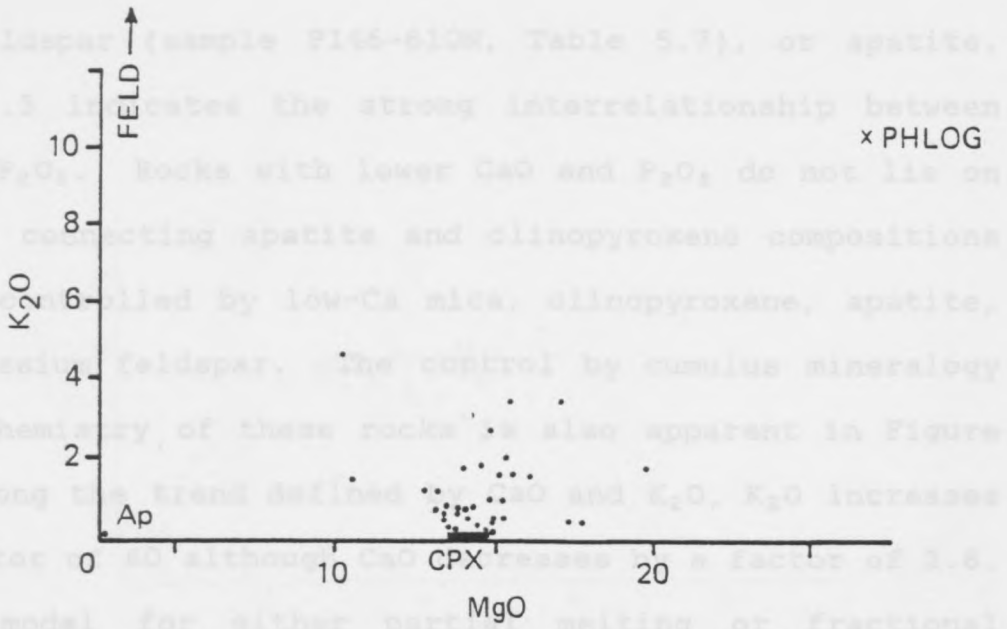


Figure 7.2c K_2O versus MgO for pyroxenites from Phalaborwa.

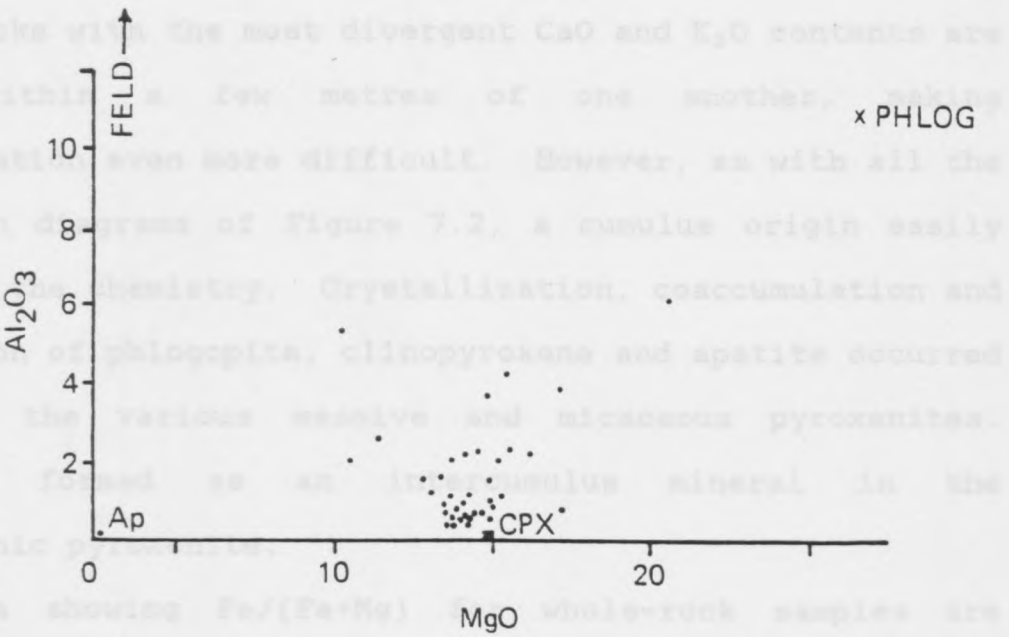


Figure 7.2d Al_2O_3 versus MgO for pyroxenites from Phalaborwa.

5.3), feldspar (sample P146-610N, Table 5.7), or apatite. Figure 7.3 indicates the strong interrelationship between CaO and P_2O_5. Rocks with lower CaO and P_2O_5 do not lie on the line connecting apatite and clinopyroxene compositions but are controlled by low-Ca mica, clinopyroxene, apatite, and potassium feldspar. The control by cumulus mineralogy on the chemistry of these rocks is also apparent in Figure 7.4. Along the trend defined by CaO and K_2O, K_2O increases by a factor of 60 although CaO decreases by a factor of 2.6. In any model for either partial melting or fractional crystallization involving a Ca-rich or K-rich phase such a relationship would be very unlikely for liquids. Some of these rocks with the most divergent CaO and K_2O contents are found within a few metres of one another, making fractionation even more difficult. However, as with all the variation diagrams of Figure 7.2, a cumulus origin easily explains the chemistry. Crystallization, coaccumulation and separation of phlogopite, clinopyroxene and apatite occurred to form the various massive and micaceous pyroxenites. Feldspar formed as an intercumulus mineral in the feldspathic pyroxenite.

Data showing Fe/(Fe+Mg) for whole-rock samples are plotted in Figure 7.5 on a simplified geologic plan of the Foskor open pit area. These ratios can be used as a differentiation index for feldspathic and massive pyroxenites because Fe and Mg occur only in clinopyroxenes. However, because the Fe/Mg ratios between coexisting

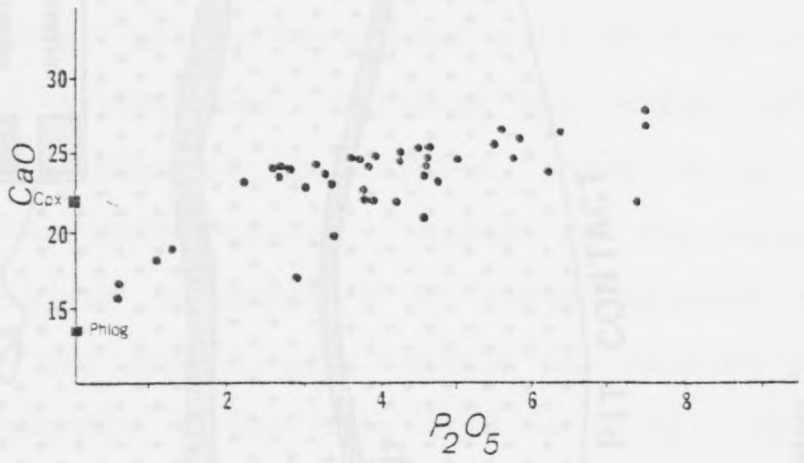


Figure 7.3 CaO versus P_2O_5 for pyroxenites from Phalaborwa. Data are plotted in weight percent.

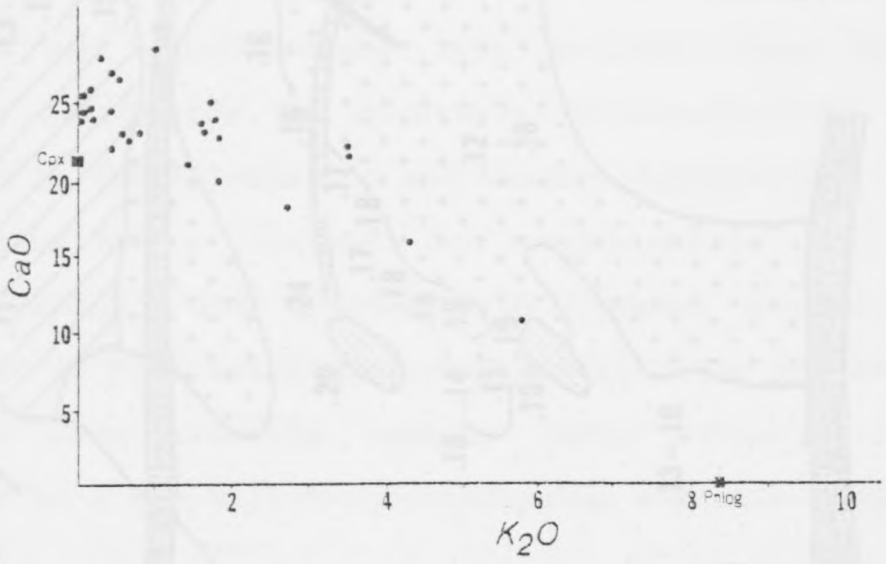


Figure 7.4 CaO versus K_2O for pyroxenites from Phalaborwa. Data are plotted in weight percent.

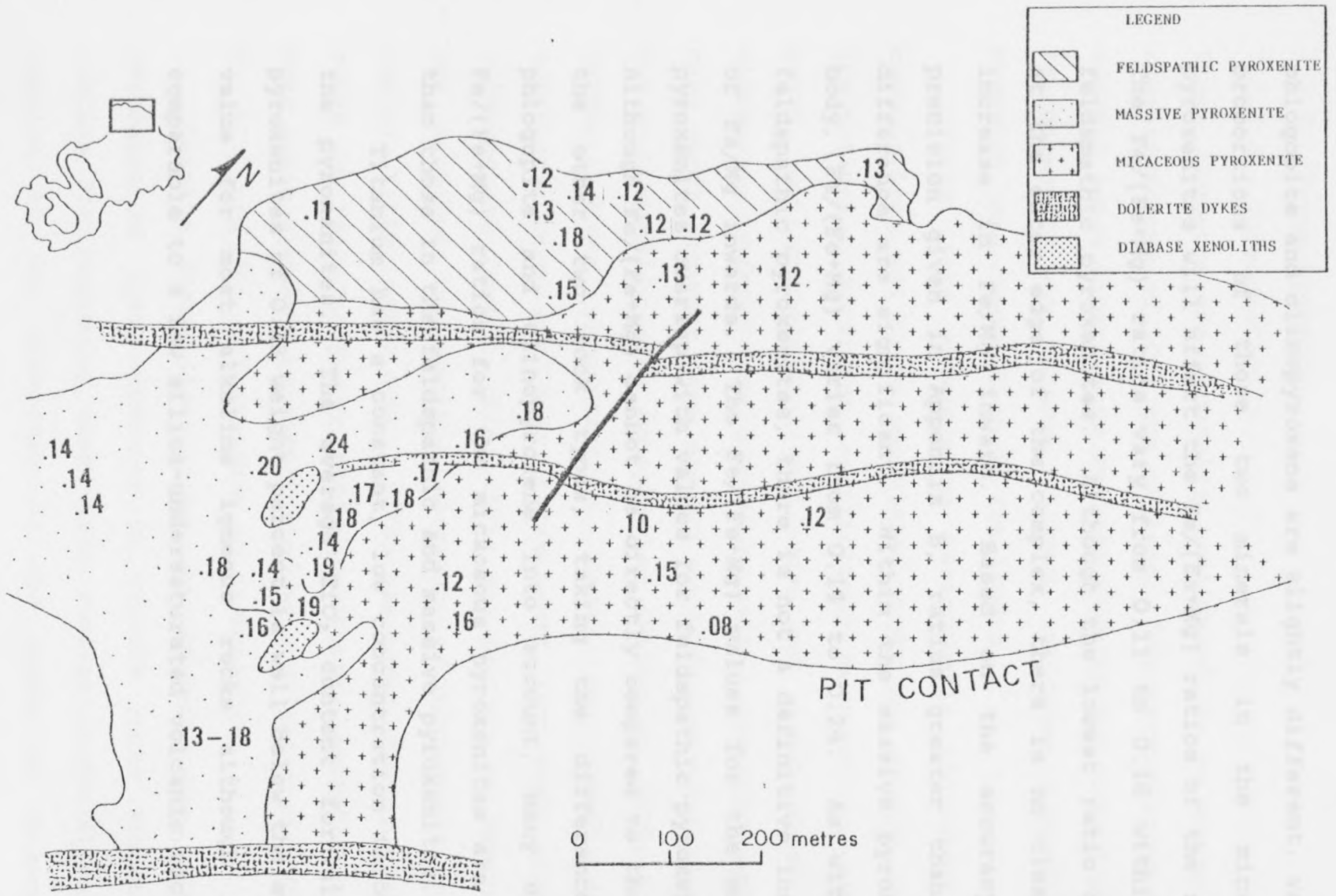


Figure 7.5 $Fe^{tot}/(Fe^{tot}+Mg)$ ratios for pyroxenites plotted at their sample locations in the Foskor pit. The locality map at the upper left hand corner is an outline of the Phalaborwa complex showing the central and lower pegmatoids in outline.

phlogopite and clinopyroxene are slightly different, varying proportions of those two minerals in the micaceous pyroxenites will affect the Fe/(Fe+Mg) ratios of the rocks. The Fe/(Fe+Mg) ratios vary from 0.11 to 0.18 within the feldspathic pyroxenites. Although the lowest ratio occurs at the outer edge of the complex, there is no clear cut increase in Fe/Mg inward. Based on the accuracy and precision given in Appendix B, ratios greater than 0.01 difference are significant. Within the massive pyroxenite body, Fe/(Fe+Mg) varies from 0.14 to 0.24. As with the feldspathic pyroxenites, there is not a definitive increase of Fe/Mg inwards. The Fe/(Fe+Mg) values for the massive pyroxenites overlap with values for feldspathic pyroxenites. Although Fe/(Fe+Mg) cannot be directly compared to those of the other two rock types, taking the differences in phlogopite and clinopyroxene into account, many of the Fe/(Fe+Mg) ratios for the micaceous pyroxenites are lower than those in the feldspathic and massive pyroxenites.

Titanium has a constant, low concentration throughout the pyroxenites. The average TiO_2 content for all the pyroxenites of 0.23 weight percent is well below the average value for most alkaline igneous rocks although it is comparable to a few silica-undersaturated volcanic rocks.

7.1.2 Trace Elements

7.1.2.1 Introduction

Trace elements are generally considered to be those with concentrations of 1000 ppm or less. The partitioning of an element among minerals or between mineral and liquid phases is dependent on various factors including temperature, pressure, and composition of the liquid.

Using trace elements as petrogenetic indicators for carbonatites and their associated rocks has several severe limitations. Partition coefficients measured on mineral pairs and phenocryst-liquid are not well known for ultrabasic rocks. Some elements, mainly strontium and the rare earth elements, are present in high concentrations and may not strictly obey Henry's law (Nicholls, 1976; Mysen, 1978). Since concentration limits for ideal dilute solutions have not been established for most elements (O'Nions and Powell, 1976), this may pertain to several of the enriched incompatible elements of ultrabasic rocks. Lastly, Kable (pers. comm., 1978) has noted that in plutonic rocks of relatively low pressure regime, partitioning of many trace elements is complicated by complexing with CO_2^{2-}, F^-, Cl^-, and OH^-, all abundant in carbonatites.

Despite these limitations, by studying the relative abundance of trace elements in various rocks within the complex and comparing these with similar rocks elsewhere, aspects of the chemistry of the magma or magmas at Phalaborwa may be ascertained.

7.1.2.2 Trace Element Data

Strontium content in the measured pyroxenites averages 1032 ppm. Feldspathic pyroxenites have the highest content (1175 ppm) and micaceous pyroxenites the lowest (150 ppm), with massive pyroxenites averaging around 1040 ppm. Figure 7.6 shows the strong correlation of Sr concentration with P_2O_5 content reflecting the high Sr content of apatite (see Table 9.10).

Figures 7.7 and 7.8 show that the cumulus apatite content strongly influences the trace element concentration of Sr in the pyroxenites; no increase or decrease of Sr with mica, pyroxene, or feldspar content can be discerned.

Table 7.3 contains strontium abundances for 20 whole-rock carbonatites. Values are high as expected for carbonatites. Apatite-rich carbonatites are richer in Sr. There is no obvious difference in Sr content between the transgressive and banded carbontatites.

Rubidium content varies sympathetically with K_2O and with Ba (Figures 7.9 and 7.10). Figure 7.9 shows a very good correlation between Rb and K_2O. Concentration of Rb in the mica gives the micaceous pyroxenites the highest values with an average of 300 ppm Rb.

Barium attains the highest concentration in the feldspathic pyroxenite (up to 1103 ppm). Barium is generally enriched in micaceous pyroxenites (average = 438) but is often below detection limit in the massive pyroxenites. Barium contents of the feldspathic and

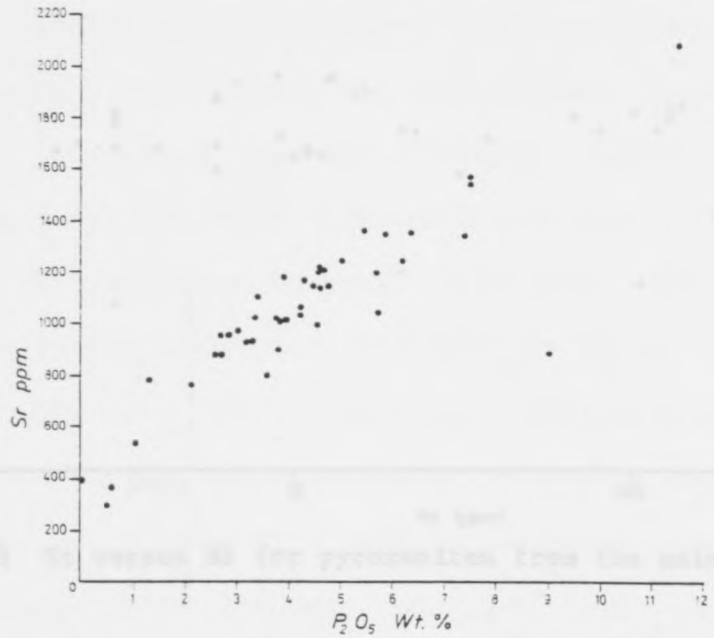


Figure 7.6 Sr versus P_2O_5 for the pyroxenites from the main complex.

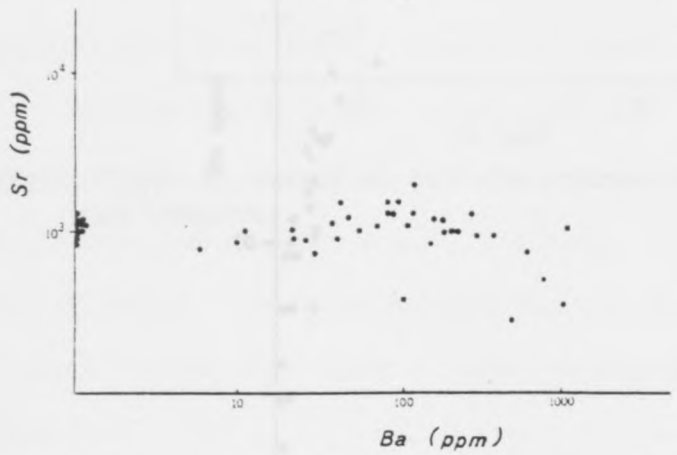


Figure 7.7 Sr versus Ba for the pyroxenites from the main complex.

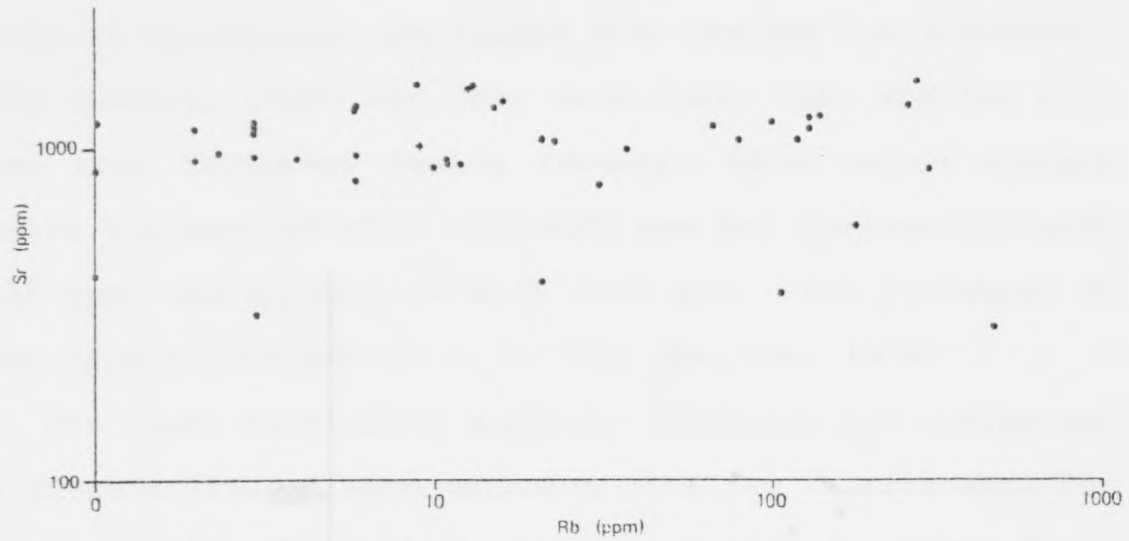


Figure 7.8 Sr versus Rb for pyroxenites from the main complex.

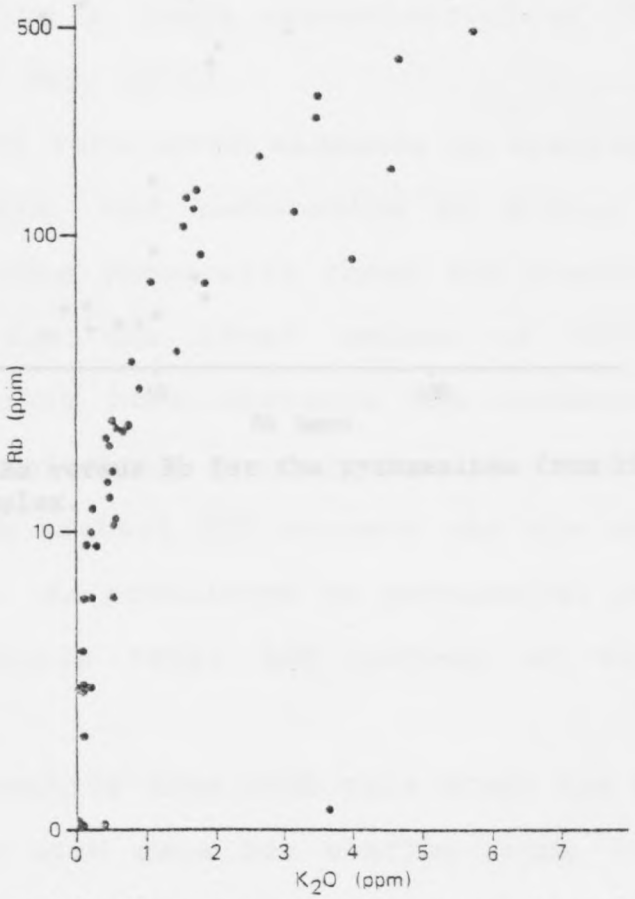


Figure 7.9 Rb versus K_2O for pyroxenites from the main complex.

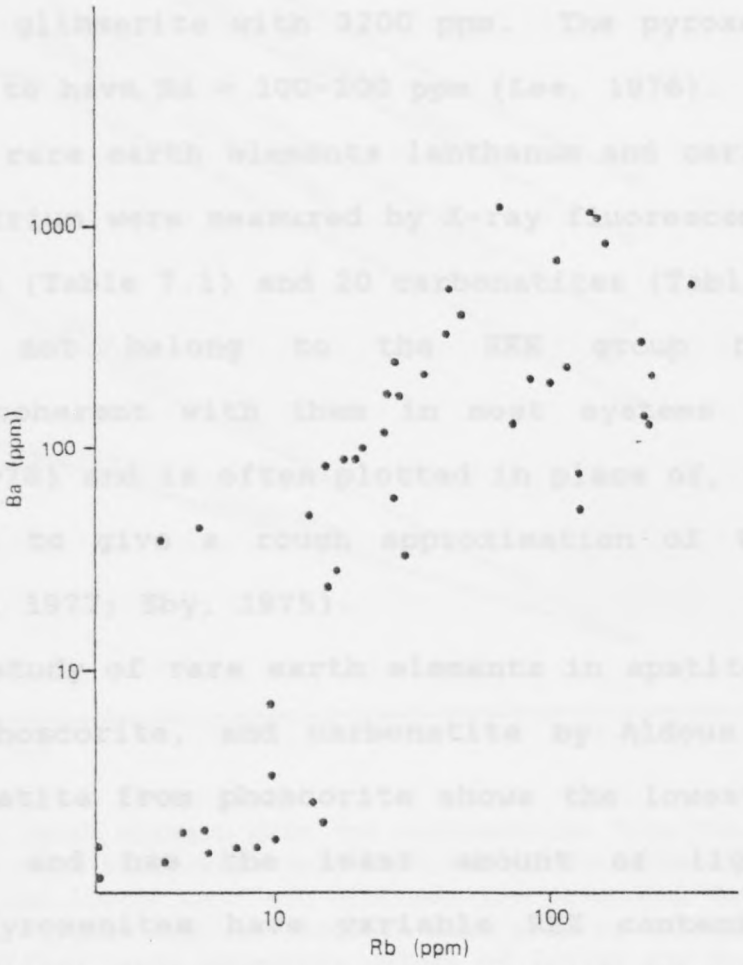


Figure 7.10 Ba versus Rb for the pyroxenites from the main complex.

micaceous pyroxenites are higher than average for ultrabasic rocks (Dawson, 1966) but very much lower than similar rock types from Southwest Uganda (Higazy, 1954) which contain biotite pyroxenites with 1200-2000 ppm Ba, pyroxenites with 15-50 ppm, and glimmerite with 3200 ppm. The pyroxenes of Shawa carbonatite have Ba = 100-200 ppm (Lee, 1976).

The light rare earth elements lanthanum and cerium and the element yttrium were measured by X-ray fluorescence for the pyroxenites (Table 7.1) and 20 carbonatites (Table 7.3). Yttrium does not belong to the REE group but is geochemically coherent with them in most systems (Kable, pers. comm., 1978) and is often plotted in place of, or next to, dysprosium to give a rough approximation of the REE pattern (Scott, 1977; Eby, 1975).

Detailed study of rare earth elements in apatites from pyroxenites, phoscorite, and carbonatite by Aldous (1980) showed that apatite from phoscorite shows the lowest total REE abundance and has the least amount of light REE enrichment. Pyroxenites have variable REE contents with light REE enrichment slightly greater than phoscorite, and carbonatites have the highest REE content and the greatest light REE enrichment. As postulated on geochemical grounds, apatite content controls total REE content of the rock (Aldous, 1980).

Normalized carbonatite data from this study are plotted in Figure 7.11 along with data for similar rocks from Oka (Eby, 1975), Lashaine carbonatite and calcite from

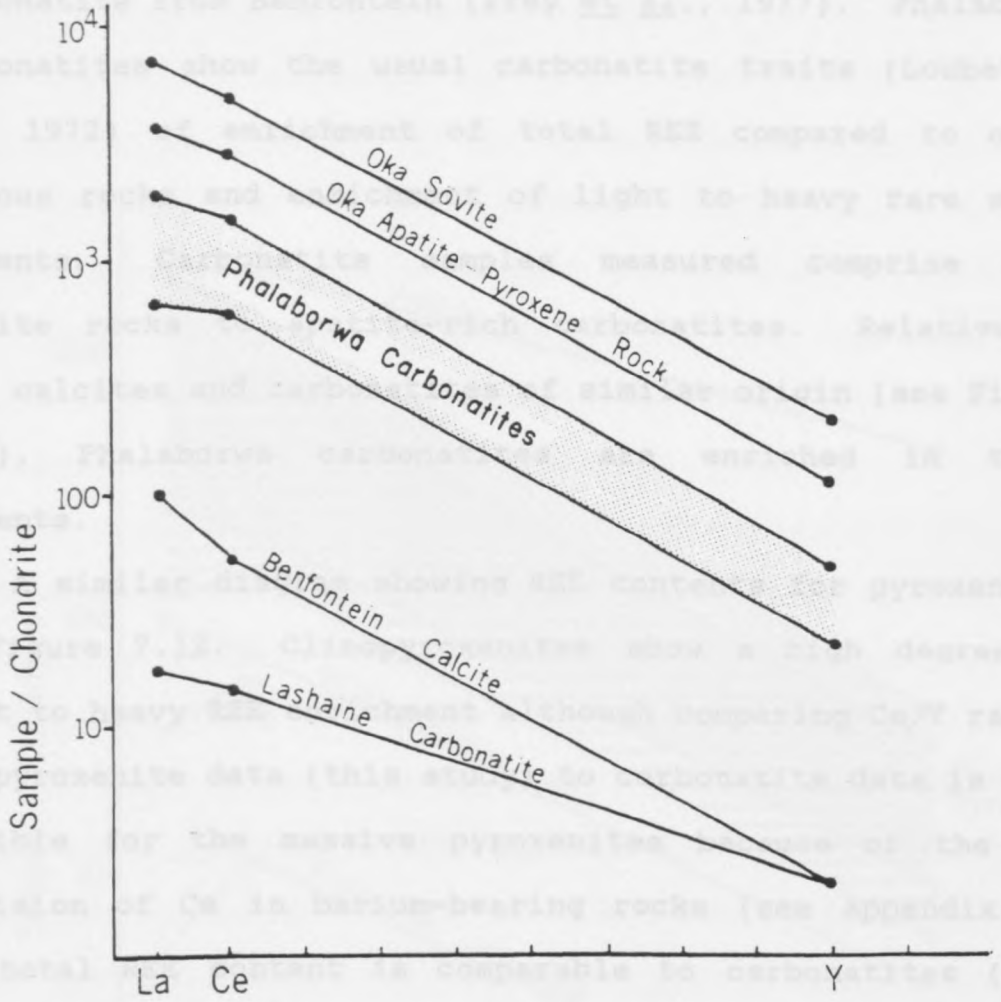


Figure 7.11 Rare earth element data for carbonatites from Phalaborwa. The stippled area represents data from twenty analyses of carbonatites; the highest and lowest data are plotted; the remaining data completely fill in the stippled area.. Chondrite data used to normalize the data are modified Leedy chondrite values of Taylor and Gorton (1977). Other data plotted for comparative purposes are from Lashaine (Ridley and Dawson, 1975), Benfontein kimberlite sill and the Oka carbonatite complex (Frey et al., 1977).

carbonatite from Benfontein (Frey et al., 1977). Phalaborwa carbonatites show the usual carbonatite traits (Loubet et al., 1972) of enrichment of total REE compared to other igneous rocks and enrichment of light to heavy rare earth elements. Carbonatite samples measured comprise pure calcite rocks to apatite-rich carbonatites. Relative to some calcites and carbonatites of similar origin (see Figure 7.11), Phalaborwa carbonatites are enriched in these elements.

A similar diagram showing REE contents for pyroxenites is Figure 7.12. Clinopyroxenites show a high degree of light to heavy REE enrichment although comparing Ce/Y ratios for pyroxenite data (this study) to carbonatite data is only possible for the massive pyroxenites because of the low precision of Ce in barium-bearing rocks (see Appendix B). The total REE content is comparable to carbonatites (Eby, 1975; Mitchell and Brunfelt, 1975; Aldous, 1980) as well as to kimberlites (Fesq et al., 1975), potassic volcanic rocks (Mitchell and Bell, 1976) and lamprophyres (Bachinski and Scott, 1979).

The pyroxenite data fall into two overlapping groups, one of lower average total REE with La/Ce less than one and the other with higher average total REE and La/Ce greater than one. Phlogopite, apatite and a massive pyroxenite containing less than five percent phlogopite from Phalaborwa are plotted in Figure 7.12 along with phlogopite from kimberlite (Fesq et al., 1975). Comparing modal mineralogy

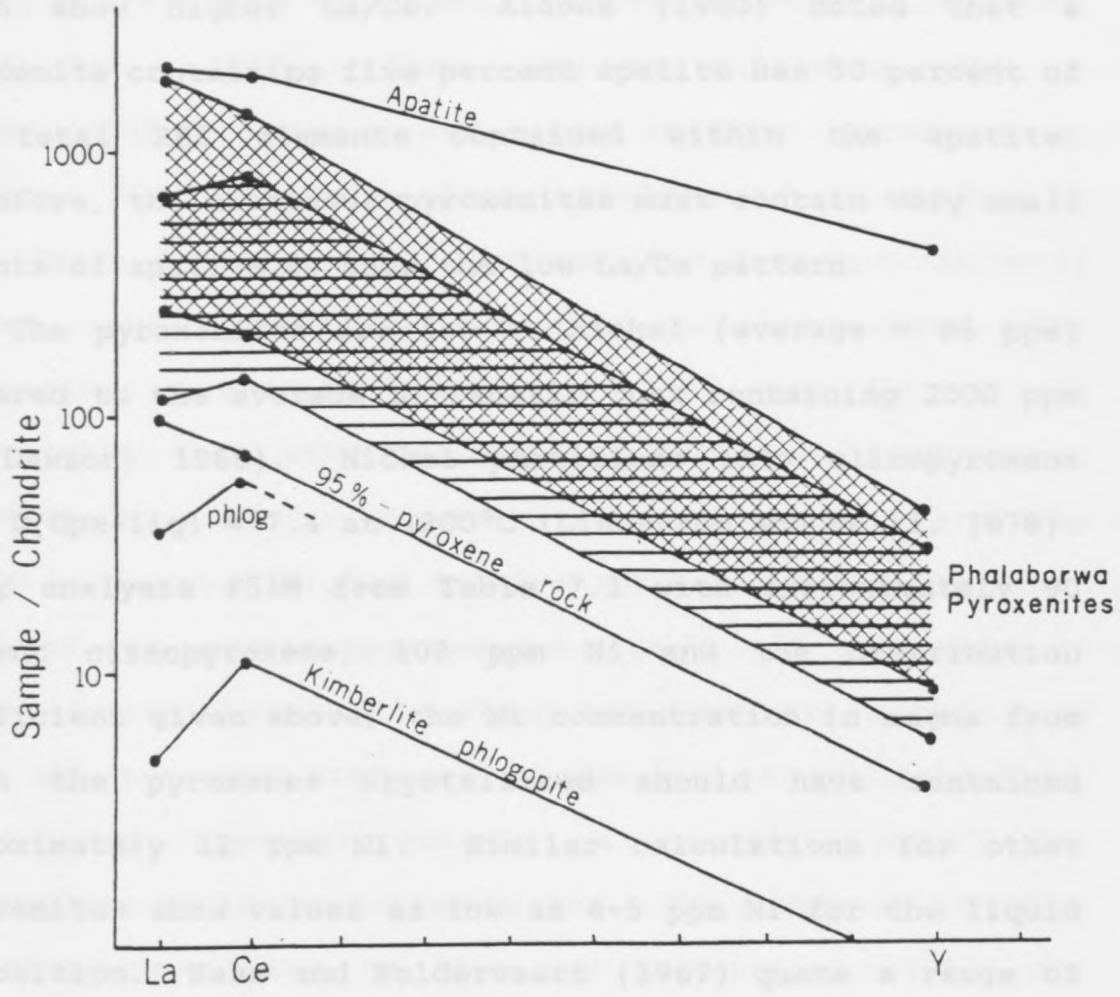


Figure 7.12 Rare earth element data for forty-three pyroxenites from Phalaborwa. The normalizing data are the same as for Figure 7.11. The cross-hatched area represents the field of pyroxenites with La > Ce. The horizontally-lined area represents pyroxenites with La < Ce. The phlogopite with La and Ce only recorded is from Phalaborwa, Table 5.5. The apatite is from Phalaborwa (DeJager and Fourie, 1978) and the kimberlite phlogopite is from Fesq et al.,1975).

for the two groups of pyroxenites, it can be seen that the lower La/Ce is produced by high mica content of the pyroxenites as opposed to the apatite-bearing pyroxenites which show higher La/Ce. Aldous (1980) noted that a pyroxenite containing five percent apatite has 50 percent of the total REE elements contained within the apatite. Therefore, the micaceous pyroxenites must contain very small amounts of apatite to show the low La/Ce pattern.

The pyroxenites are low in nickel (average = 86 ppm) compared to the average ultrabasic rock containing 2000 ppm Ni (Dawson, 1966). Nickel partitions into clinopyroxene with D(Cpx-liq) = 7.4 at 1200°C (Lindstrom and Weill, 1978). Using analysis F51M from Table 7.1 with approximately 90 percent clinopyroxene, 102 ppm Ni and the distribution coefficient given above, the Ni concentration in magma from which the pyroxenes crystallized should have contained approximately 12 ppm Ni. Similar calculations for other pyroxenites show values as low as 4-5 ppm Ni for the liquid composition. Hess and Poldervaart (1967) quote a range of 0-350 ppm Ni for alkali basalts although the mean value for alkali basalts is 98 ppm Ni. Such low values for liquid composition imply that some early crystallized, Ni-rich phase has removed Ni from the magma forming the pyroxenites. In Chapter 5, it was suggested that magnetite might be a likely early-crystallizing phase.

Vanadium has an average concentration of 27 ppm for the pyroxenites which is slightly lower than the average for

ultrabasic rocks (Dawson, 1966). Vanadium concentrations in the clinopyroxenes at Phalaborwa are very low (2-3 ppm) as measured by XRF (Table 5.2). Partition coefficients for vanadium are highly dependent on oxygen fugacity (Lindstrom, 1976; Duke, 1976). There are no published data on partitioning of vanadium into alkali feldspar, phlogopite or apatite. However, trace element analysis of phlogopites by XRF (Table 5.5) shows that phlogopites have significantly higher concentrations of V than clinopyroxenes. The phlogopites measured range from 3-15 ppm V. It is conceivable that other phlogopites may have much higher concentrations of V. However, higher V contents are also found in feldspathic and massive pyroxenes indicating that feldspar and apatite may contain some V. At conditions of lowest oxygen fugacity in which vanadium more easily goes into the pyroxene structure, D(Cpx-liq) = 10 (Lindstrom, 1976), the vanadium content of parental liquid for pyroxenites would be extremely low. The range of vanadium concentrations given by Hess and Poldervaart (1967) for alkalic basalts is 37-500 ppm.

In the case of oxidizing conditions, or 8-10 times higher than the iron-wustite buffer, however, V is excluded from clinopyroxene, D(Cpx-liq) = 0.03 (Lindstrom, 1976) and the vanadium content of liquid could be as high as 100 ppm. The calculated content of vanadium in the magma at high fO_2 conditions implies some V may have been present in the magma.

Deans (1966) reported that the magnetite from Phalaborwa contains about 0.1 percent V_2O_5 which is considerable compared to magnetite from other carbonatites. D(Mag-liq) for V established by Lindstrom (1976) for magnetite in an alkali basalt varies from 0 to 60 under conditions of high and low oxygen fugacity, respectively. If conditions of high oxygen fugacity were operative as implied from phlogopite compositions in Chapter 6, then vanadium content of the carbonatite magma could be several percent V_2O_5. This is very different from the implied concentrations of V in the magma forming the pyroxenites.

Copper concentrations range from an average of 15 ppm for the feldspathic pyroxenites to 166 ppm average for the massive type. A few pyroxenites have Cu abundances of 300-500 ppm with the Guide Copper Mine satellite pyroxenite containing 1804 ppm. These pyroxenite values from the main complex are higher than the average ultrabasic rock (20 ppm) and lie around the value for kimberlites of Yakutia (60 ppm) and Basutoland (100 ppm) (Dawson, 1967). Copper is highly concentrated as a sulphide phase in the phoscorite and carbonatites.

Zinc concentrations in pyroxenites average 34 ppm. There are little data with which to compare the Phalaborwa data and, therefore, zinc values are not definitive in describing petrogenetic conditions.

Niobium often attains economic abundances in carbonatites (Tuttle and Gittins, 1966), but at Phalaborwa

it is extremely depleted. Not only are niobium minerals absent but pyroxenites average 5 ppm and niobium in the carbonatite is below the detection limit of 8-9 ppm for that rock type.

Zirconium in the Phalaborwa pyroxenites (average = 36 ppm) is similar to the average for ultrabasic (30 ppm) rocks given by Dawson (1966). The feldspathic pyroxenites are slightly higher (37 ppm) than micaceous (15 ppm) or massive types (11 ppm). The Guide Copper Mine feldspathic pyroxenite has considerably higher (162 ppm) zirconium. Pyroxenes in ijolites at Shawa (Lee, 1976) have 8-70 ppm Zr.

Chromium is generally low in the entire complex. Values for pyroxenites are not given here due to problems with analytical equipment but are in the range of 0-10 ppm. Chromium was not found in clinopyroxene, phlogopites or olivines using the energy and wave length dispersive units of an electron microprobe. The significance of low Cr was discussed in Chapter 5.

7.1.3 Discussion

The chemistry of the various pyroxenites points to a cumulus origin. The use of partition coefficients between minerals and liquid has permitted some estimates of magma composition to be made from mineral chemistry (Chapter 5) for elements which can be measured on an electron microprobe or deduced from analysis by XRF. Whole-rock chemistry allows us to make some estimates of magma compositions for elements which

are more easily measured in whole-rock samples, namely the REE and to compare mineral analyses with whole-rock compositions.

There is little agreement in the literature as to how light and heavy rare earths behave in a volatile-rich environment (Mysen, 1977). Cullers and Medaris (1977) found that some sovites showed higher values and a more fractionated pattern than those of cogenetic ijolites. Eby (1975) was the first to find that, although pyroxenes showed slightly different fractionation patterns between rock types, apatites in silicate and carbonate rocks had similar values and patterns.

The variation in pyroxenite values with the higher values dominated by apatite suggests that Phalaborwa data mimic the Oka data (Eby, 1975). However, data for apatites (Aldous, 1980) shows a fractionation between apatites of the different rock types with the total REE being fractionated into the carbonatite and light REE fractionated from phoscorite to pyroxenite to carbonatite.

Early workers (Eby, 1975; Cullers and Medaris, 1977) believed that the difference in patterns and abundances between rock types indicated a path of differentiation. More recently (Wendlandt and Harrison, 1979), experimental data have indicated that coexisting carbonate and silicate liquid have a light REE and total REE partitioning into the carbonate phase. Experimental work by Watson and Green (1981) on REE partitioning between apatite and liquid shows a high dependence on temperature and melt composition.

Therefore, nothing can be deduced from the whole rock data of pyroxenites and carbonatites from Phalaborwa as to whether the carbonatite separated early as an immiscible liquid or was derived through fractionation. However, the fact that the pyroxenites contain REE patterns similar to those of carbonatites points to similarities in their geological history.

Pecora (1956) explained the presence or absence of Nb in carbonatites by the miascitic or agpaitic nature of the rocks, but his association of low Nb with agpaitic nature of a rock and numerous Ti-species does not fit Phalaborwa or numerous other carbonatites (Heinrich, 1966). Pecora (1956) did not distinguish between cumulates and liquids. Deans (1966) notes that niobium is minor or absent in complexes where carbonatite is subordinate to syenites, pyroxenites, and dunites and is minimal in late-stage, rare earth-strontium-barium carbonatites. It may be that at Phalaborwa niobium has partitioned into a fluid phase or into liquid and has reached upper levels of the intrusion which have subsequently been eroded. Nb substitutes readily for Ca and has been shown to be an intrinsic part of carbonatite magmatism (Watkinson, 1970) so its absence at Phalaborwa is problematic.

As mentioned in sections 7.1.1 and 7.1.2, the major- and trace-element chemistry of the pyroxenites, phoscorites, and carbonatites of Phalaborwa is similar to kimberlites and ultrapotassic lavas (Dawson, 1967; Carmichael, 1967). The

significance of chemistry of Phalaborwa in relationship to the phase relations and the mineralogy of these other rocks will be discussed in Chapters 8 and 10.

7.2 WHOLE-ROCK CHEMISTRY OF THE SATELLITES

The chemistry of the pipes surrounding the main Phalaborwa complex is important in determining if there was a common parental magma to the main complex and the pipes and, if so, how such a magma evolved to give the various rock types found in the main complex and the pipes. The chemistry can elucidate the relationships between Kgopoeloe and Spitskop which have been established by field and petrographic methods.

The following sections explore the following questions:

(1) How do the various rock types in Kgopoeloe, Spitskop, and Guide Copper Mine relate to each other chemically;
(2) what roles do assimilation and metasomatism play in determining the chemistry of the rocks in the satellites; and
(3) are the various rock types in the pipes part of a differentiation trend related to crystallization of the main complex?

7.2.1 Classification of Rock Types

Nomenclature of the rock types in Kgopoeloe and Spitskop in the preceding chapters has been based on hand specimen descriptions. Here, a more formal classification is made based on the chemistry of the rocks. A classification is based on the system of Streckeisen (1967) using normative mineralogy as found in Table 7.2. Descriptive terms such as mela- referring to colour index is used to indicate high content of mafic minerals instead of obscure rock names such as lusitanite and ordosite.

Kgopoeloe contains breccia matrix with compositions of mela-alkali syenite, alkali quartz syenite and granite. Matrix from the lower part of the pipe, where there is a high proportion of matrix to fragment, generally contains normative acmite and has between 5 and 20 percent normative quartz; these rocks are termed alkali quartz syenites and mela-alkali quartz syenites. One sample of matrix has greater than 20 percent quartz and must be termed granite.

The chemistry of the granitic rocks surrounding the Kgopoeloe pipe show the effects of metasomatism described in Chapters 3 and 4. Most granites from outcrop are true granite (>20% quartz) but one of those (K17g) and one breccia fragment (K11f) are syenites. None of the analyzed granites or fragments contain normative acmite. Fragments of quartzo-feldspathic gneiss need not be considered in terms of igneous nomenclature because of their metamorphic origin.

At Spitskop, the ring syenite and most of the central syenites have the composition of alkali quartz syenite (5-20% quartz) with the ring syenites being higher in mafic phases. One sample (S8c) is considered an alkali granite. The sample from the surrounding syenite (S16s) is slightly silica-oversaturated and is an alkali syenite bordering on a syenite. The leucocratic dykes are trachytes and alkali trachytes.

7.2.2 Kgopoeloe Hill

The close association of granitic fragments dispersed throughout syenite matrix demands that the effects of contamination on the syenite be established before the chemistry of an uncontaminated syenite is compared to the Spitskop and Guide Copper Mine pipes or to the main complex. Two mechanisms, metasomatism and assimilation, must be addressed in this section.

7.2.2.1 Chemical Trends

The major and trace element chemistry of the various rocks from Kgopoeloe has been plotted in Figures 7.13 and 7.14 according to their SiO_2 contents. Silica content increases from left to right from the most silica-poor matrix sample to the most silica-rich granitic rock. TiO_2 has been plotted separately in Figure 7.15 because of the low concentration of the oxide. The granitic rocks, both granite outcrop and granitic breccia fragments, lie along

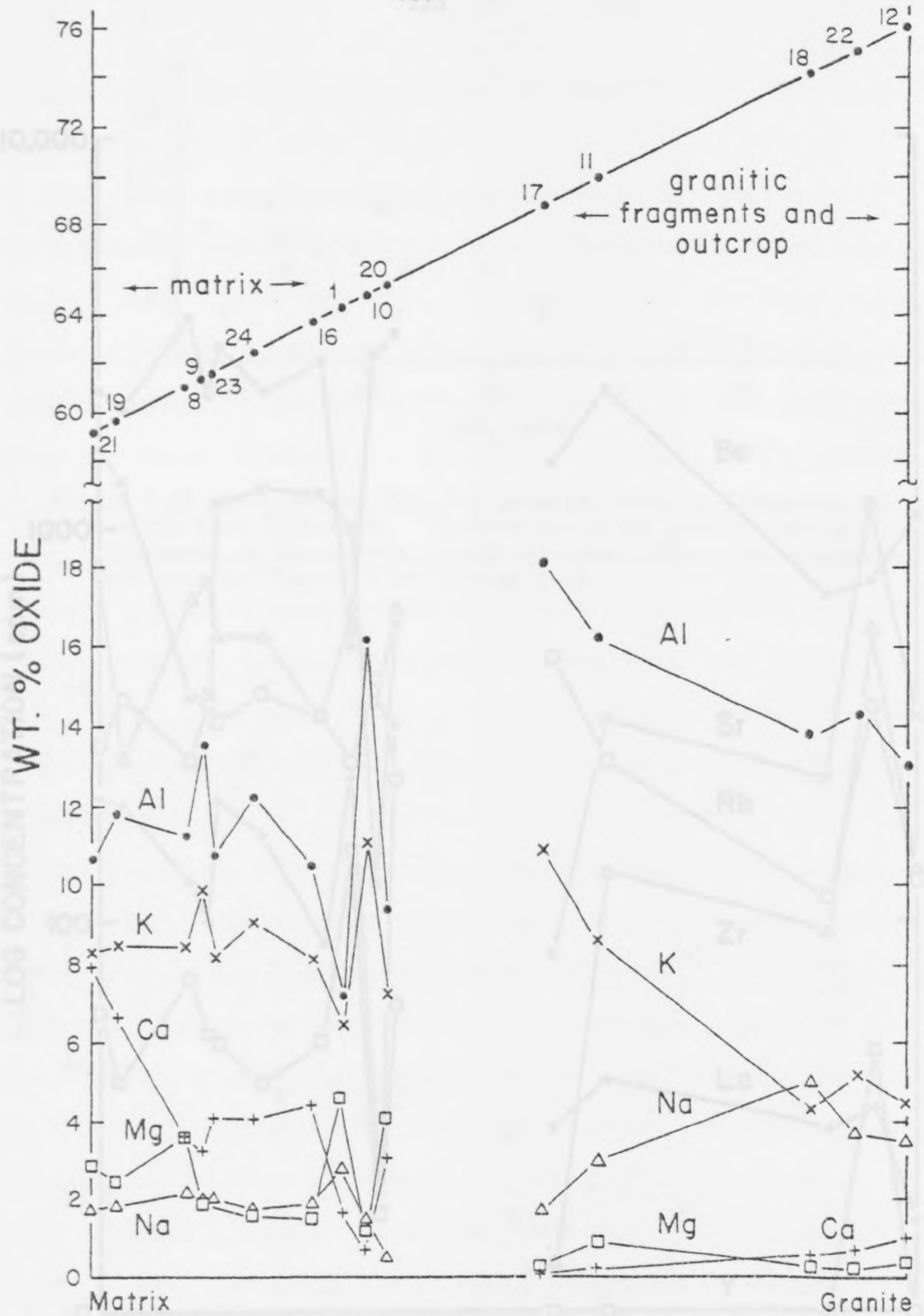


Figure 7.13 Major element chemistry plotted to evaluate effects of mixing between granite and syenite at Kgopoeloe. The top line represents SiO_2 content of the rocks. Numbers on the SiO_2 line refer to sample numbers prefixed by K in Table 7.2. The left hand side of the diagram is taken to be the least contaminated syenite and the right side the least altered granite.

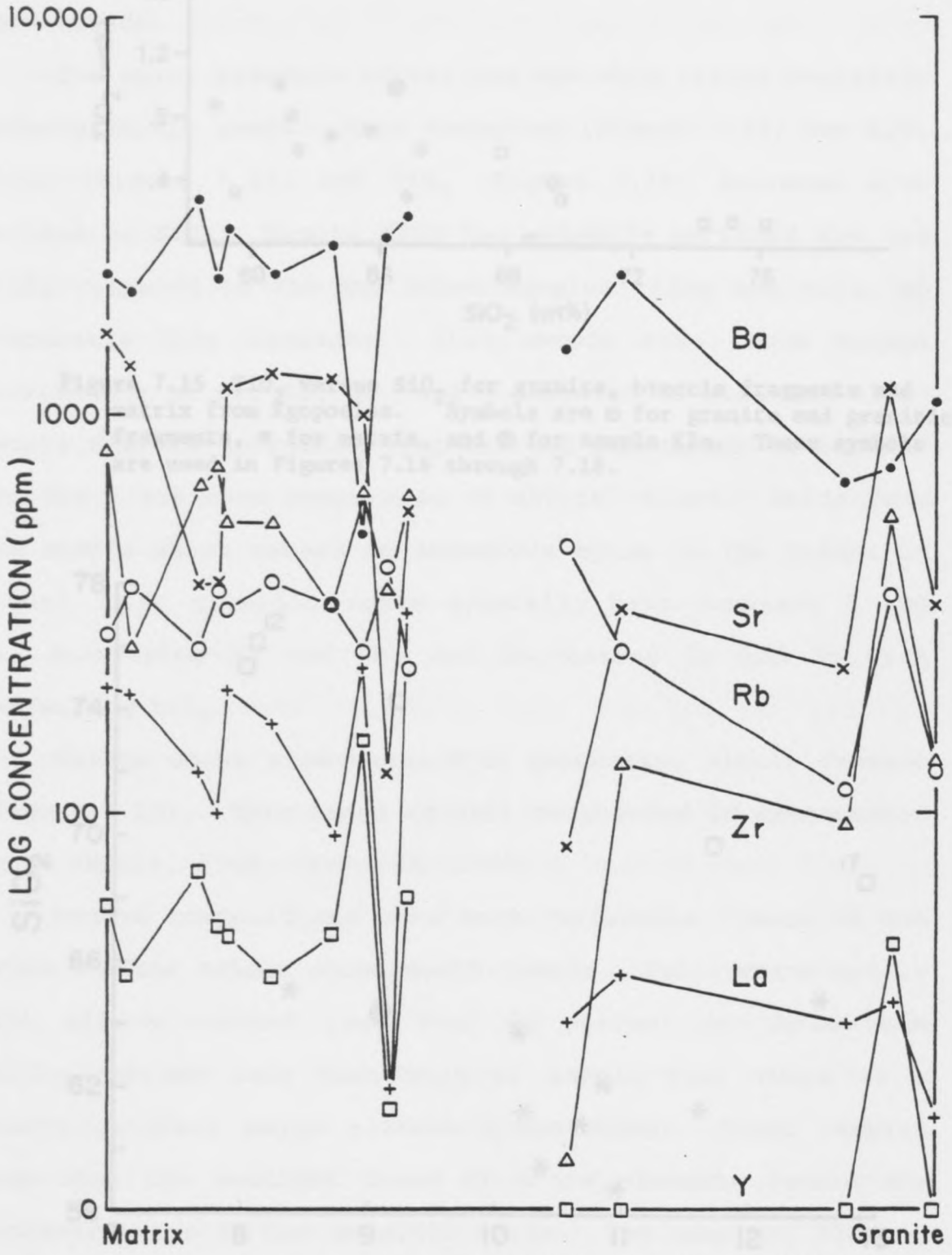


Figure 7.14 Trace element chemistry plotted in a similar manner to Figure 7.13. Sample distribution on matrix-granite scale is the same as in the previous figure.

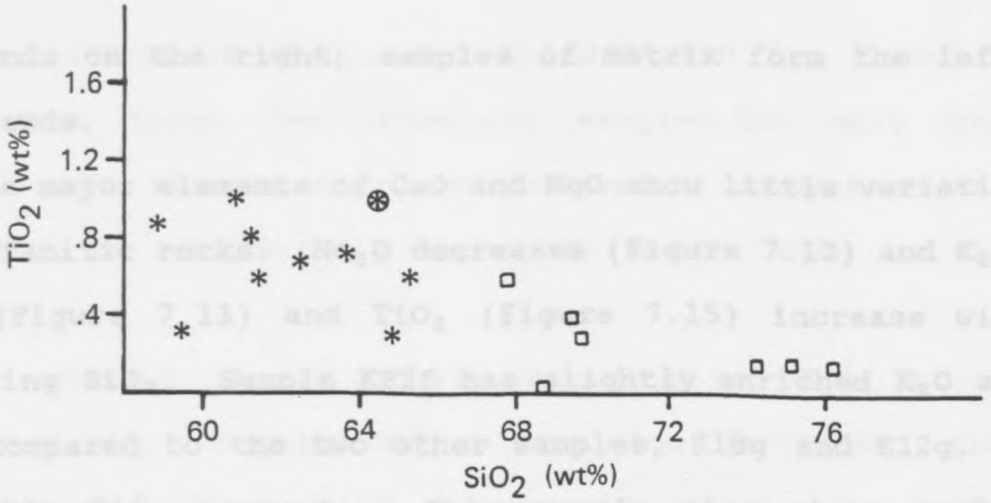


Figure 7.15 TiO_2 versus SiO_2 for granite, breccia fragments and matrix from Kgopoeloe. Symbols are □ for granite and granitic fragments, * for matrix, and ⊛ for sample Klm. These symbols are used in Figures 7.16 through 7.18.

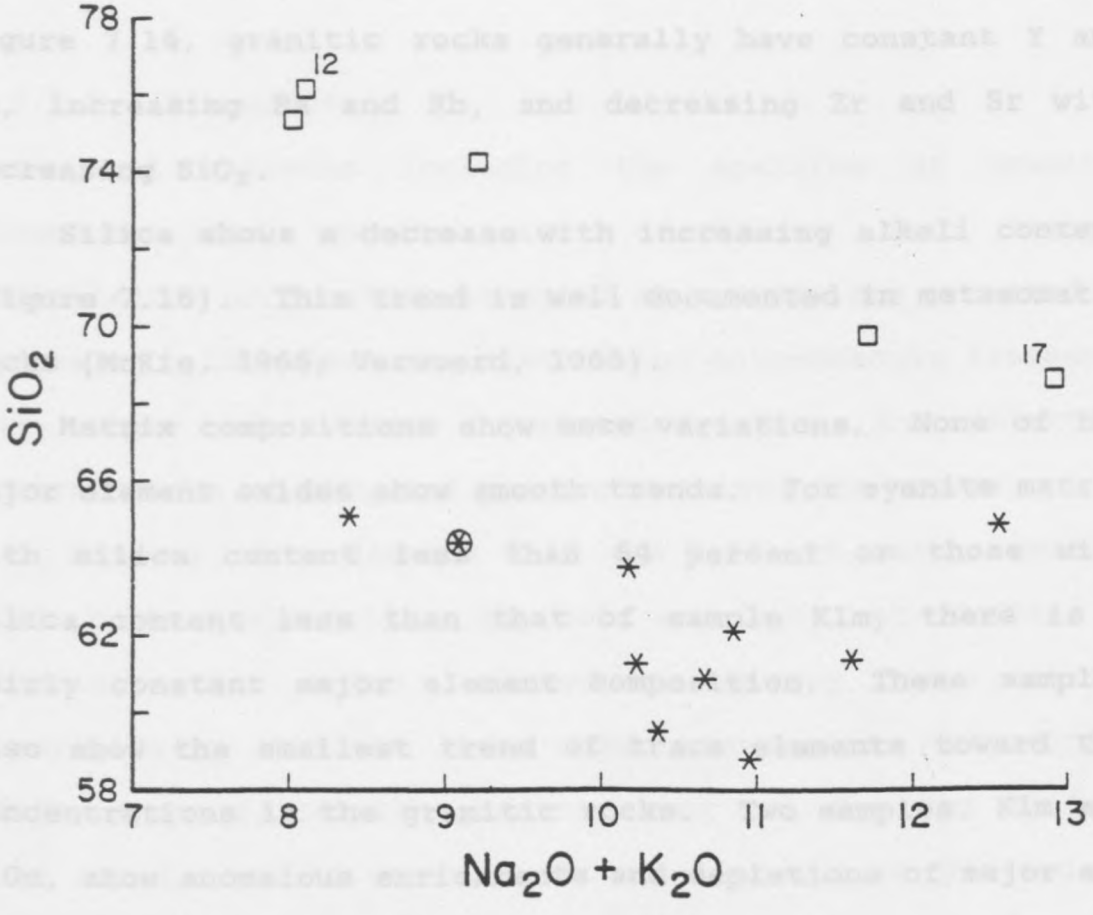


Figure 7.16 SiO_2 versus total alkalies ($Na_2O + K_2O$) for rocks from Kgopoeloe.

the trends on the right; samples of matrix form the left-hand trends.

The major elements of CaO and MgO show little variation among granitic rocks. Na_2O decreases (Figure 7.13) and K_2O, Al_2O_3 (Figure 7.13) and TiO_2 (Figure 7.15) increase with decreasing SiO_2. Sample K22f has slightly enriched K_2O and Al_2O_3 compared to the two other samples, K18g and K12g, of comparable SiO_2 contents. This sample also shows marked enrichments of Sr, Rb, Zr, and Y compared to K18g and K12g. Sample K22f is a breccia fragment and abundances of Sr, Rb, Zr, and Y are more comparable to matrix values. Aside from the sample which causes an anomalous spike in the trends in Figure 7.14, granitic rocks generally have constant Y and La, increasing Ba and Rb, and decreasing Zr and Sr with decreasing SiO_2.

Silica shows a decrease with increasing alkali content (Figure 7.16). This trend is well documented in metasomatic rocks (McKie, 1966; Verwoerd, 1966).

Matrix compositions show more variations. None of the major element oxides show smooth trends. For syenite matrix with silica content less than 64 percent or those with silica content less than that of sample K1m, there is a fairly constant major element composition. These samples also show the smallest trend of trace elements toward the concentrations in the granitic rocks. Two samples, K1m and K10m, show anomalous enrichments and depletions of major and trace elements compared to the other samples.

Sample K1m shows depletion of Al_2O_3, K_2O and Ba and enrichment in MgO, and Y; K10m

shows enrichment of Al_2O_2, K_2O and depleted Sr, Y and La. Aside from these two anomalous samples,the only major element oxide showing a dramatic change in concentration is CaO which is considerably higher in matrix with low SiO_2 content.

Sr content is not solely dependent on P_2O_5 content (Figure 7.17). Within the matrix, the Fe/(Fe+Mg) ratio varies from 0.45 to 0.70. There is no clearly defined linear trend of increasing Fe/(Fe+Mg) in matrix with increasing values of the Thornton and Tuttle (1960) differentiation index (Figure 7.18) which is based on the feldspar and quartz content of the rock.

7.2.2.2 Discussion

Geological evidence including the spalling of granitic fragments into syenite matrix indicates that limited assimilation of granitic material by syenite has operated at Kgopoeloe. Likewise, the leaching of microbreccia fragments and edges of larger fragments point to selective incorporation of SiO_2 and plagioclase into the matrix.

However, from Figures 7.13 and 7.14, it can be deduced that bulk assimilation is not an important factor in altering the major element chemistry of matrix. Theoretically straight lines drawn between the composition of the most silica-rich granitic rock and the most silica-poor matrix should correspond to compositions plotted in Figures 7.13 and 7.14. There is no geochemical evidence for

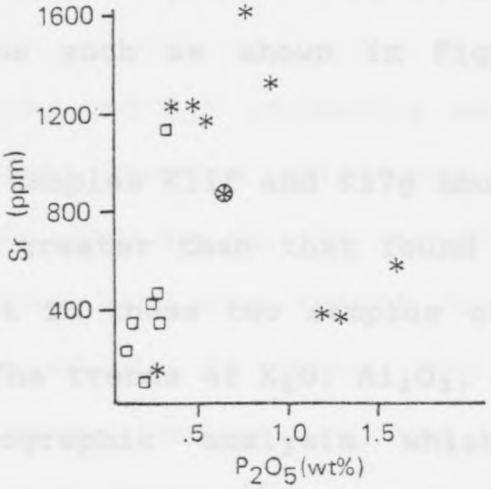


Figure 7.17 Sr versus P_2O_5 for rocks from Kgopoeloe.

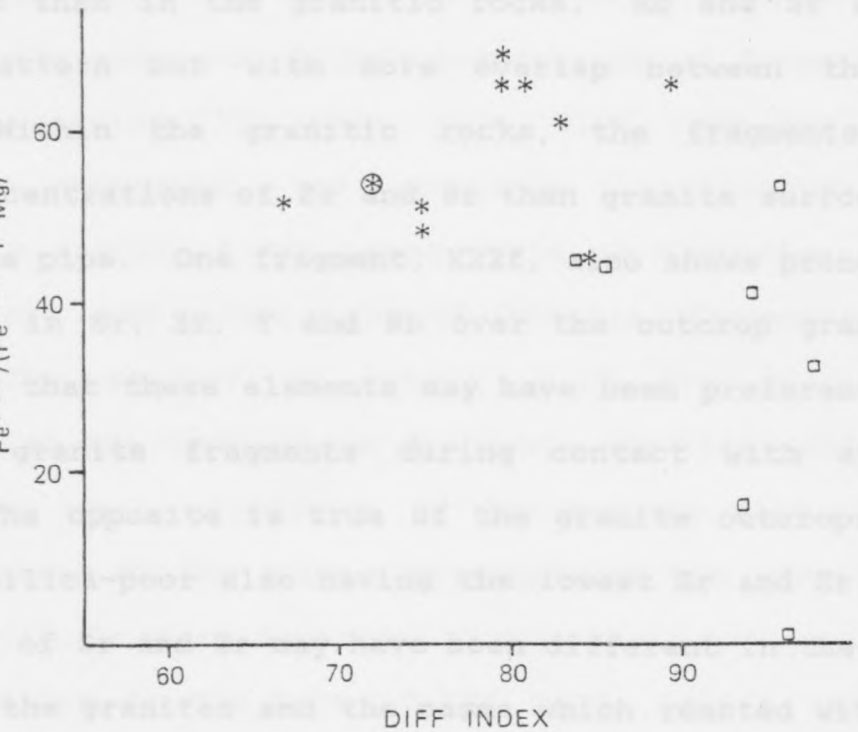


Figure 7.18 Fe/(Fe+Mg) versus the Differentiation Index for rocks from Kgopoeloe.

large-scale assimilation of granitic material as suggested by geologic relations such as shown in Figures 3.10 and 3.11.

In Figure 7.13, samples K11f and K17g show aluminum and potassium abundances greater than that found in either end member. Na is lowest in these two samples of granite with the lowest silica. The trends of K_2O, Al_2O_3, Na_2O, and TiO_2 correspond to petrographic analysis which noted that potassium feldspar and to a limited extent alkali pyroxene was formed at the expenses of sodium plagioclase in granitic outcrop and breccia fragments.

Overall, Ba, La, Y, and Zr have higher concentration in the matrix than in the granitic rocks. Rb and Sr show a similar pattern but with more overlap between the two groups. Within the granitic rocks, the fragments show higher concentrations of Zr and Sr than granite surrounding the breccia pipe. One fragment, K22f, also shows pronounced enrichment in Sr, Zr, Y and Rb over the outcrop granites. It appears that these elements may have been preferentially added to granite fragments during contact with syenite matrix. The opposite is true of the granite outcrops with the most silica-poor also having the lowest Sr and Zr. The activities of Sr and Zr may have been different in the fluid affecting the granites and the magma which reacted with the fragments. If the fluid was derived from the magma, then activity of a component in fluid should be equal to activity of that component in the magma. However, if both fluid and

liquid evolve separately, then activities in each phase may be different.

Enrichment of Al_2O_3 and K_2O in matrix samples K9m and K10m may indicate slight cumulus enrichment of potassium feldspar. However, Rb and Ba do not increase in these samples. A cumulus mineral of mica rather than feldspar is indicated. Depletion of Sr in these two samples may indicate a higher mica content because Sr is also concentrated in alkali feldspar (Pearce and Norry, 1979). Sample K1m, on the other hand, may be enriched in aegirine, based on the higher Na_2O, MgO, Y and La content.

The microbreccia matrix of nearly pure aegirine has not been analyzed for trace elements. However, samples K1m, K10m, K8m, K9m represent higher proportions of fragment to matrix than samples K16m, K21m, K23m, K19m, K20m and K24m. Metasomatic enrichment and selective assimilation are operative in matrix of the upper parts of Kgopoeloe where fluid content and proportion of breccia fragments are highest. The samples of matrix which are relatively uncontaminated are those where fragments are large and form a relatively small proportion of the breccia pipe, i.e., toward the base of the pipe. In comparing the syenite at Kgopoeloe with those at Spitskop, compositions corresponding to the syenites at the base of the pipe, namely, samples K21, K23, K24 and K16, will be used.

7.2.3 Spitskop

The whole-rock chemistry of Spitskop covers four rock types: the ring syenite, the central syenite, the fine-grained dykes, and the syenite surrounding the pipe. The main purpose in selecting samples was to determine the origin of the black, ring syenite and the central syenite, and their relationship to each other. Samples were taken radially from the ring and the central syenite.

7.2.3.1 Chemical Trends

Spitskop rocks are peralkaline as indicated by the normative acmite and the agpaitic index greater than 100 (Table 7.2). The only exception is a dyke rock, sample S22d, which contains more feldspar than the other rocks and has no normative acmite.

Figures 7.20-7.28 and 7.30-7.31 are variation diagrams for the rocks from Spitskop using the differentiation index of Thornton and Tuttle (1960) as a common plotting parameter. Increasing differentiation index for the ring syenite and central syenite corresponds to samples taken progressively inward. Figure 7.19 shows the amounts of normative quartz and feldspar indicating that the differentiation index depends more on the quartz content than the feldspar content.

Increasing differentiation within the ring syenite corresponds to increasing Fe/(Fe+Mg) and $Fe^{3+}/(Fe^{3+}+Fe^{2+})$ (Figure 7.20a and b), Zr (Figure 7.21), Nb (Figure 7.22),

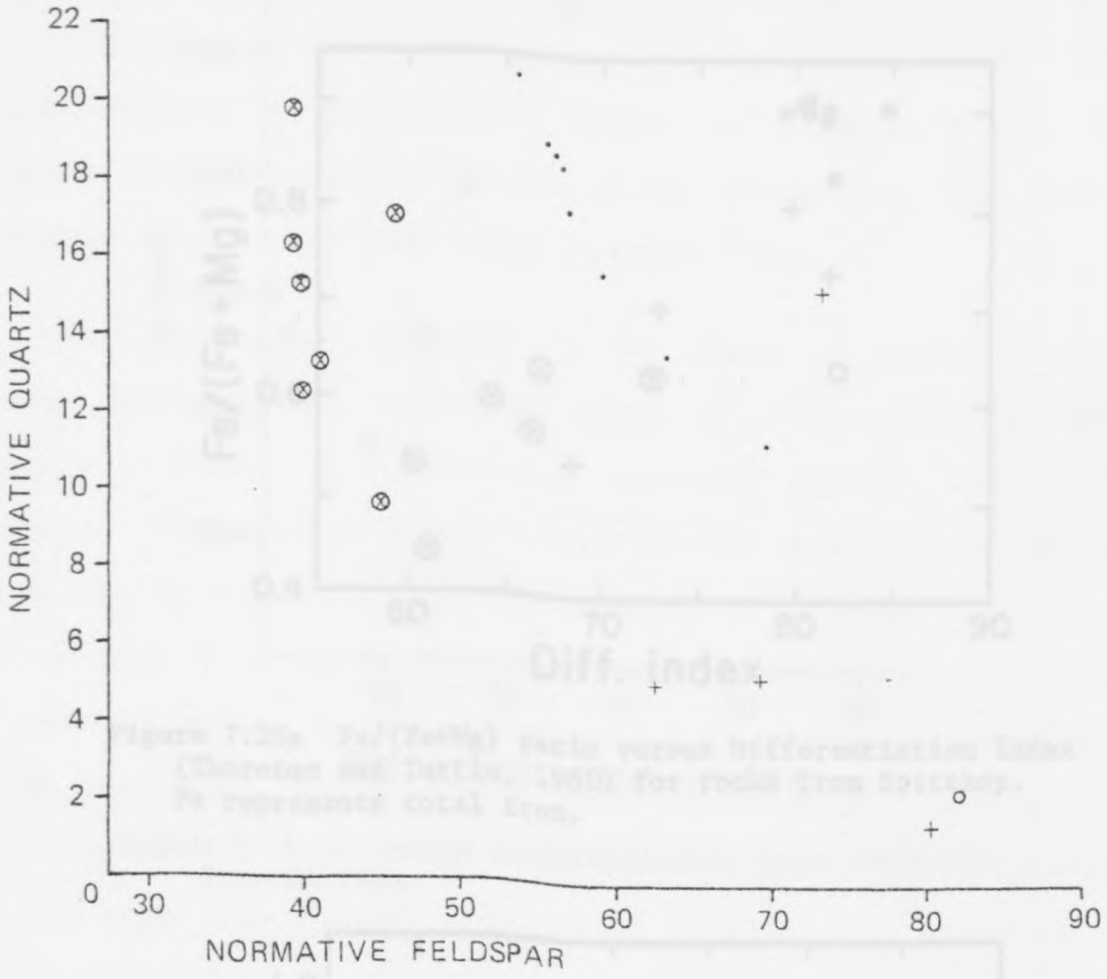


Figure 7.19 Normative quartz versus normative feldspar for rocks from Spitskop. The ring syenite is represented by circled x's, the central syenite by closed circles, the outer syenite by open circle and the cross-cutting, fine-grained dykes by crosses. These symbols are used in the remaining figures in chapter 7.

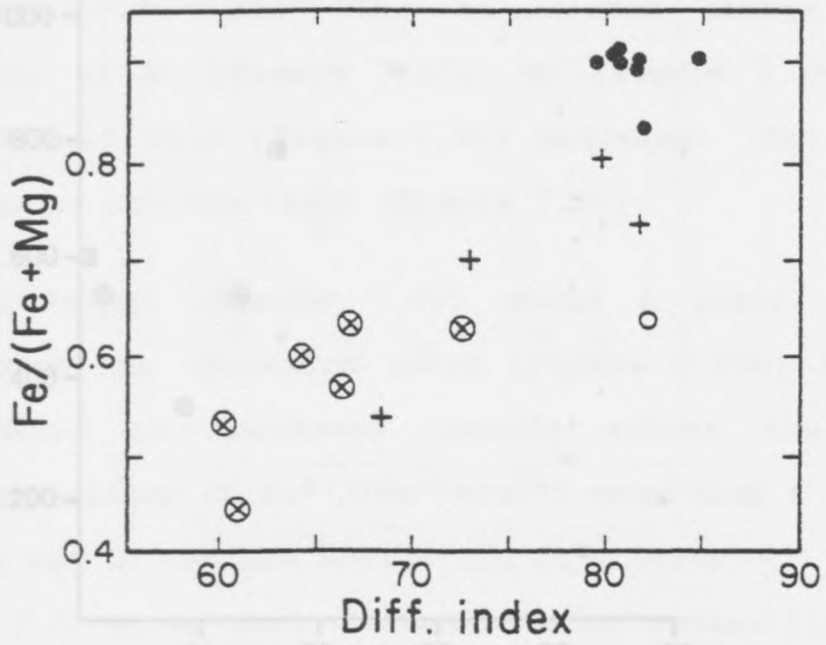


Figure 7.20a Fe/(Fe+Mg) ratio versus Differentiation Index (Thornton and Tuttle, 1960) for rocks from Spitskop. Fe represents total iron.

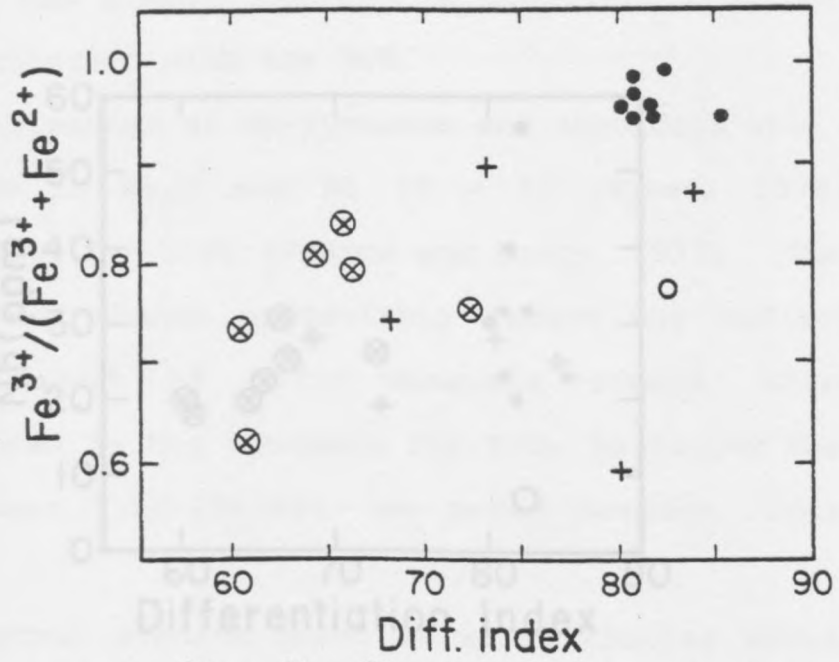


Figure 7.20b $Fe^{3+}/(Fe^{3+}+Fe^{2+})$ versus Differentiation Index for rocks from Spitskop.

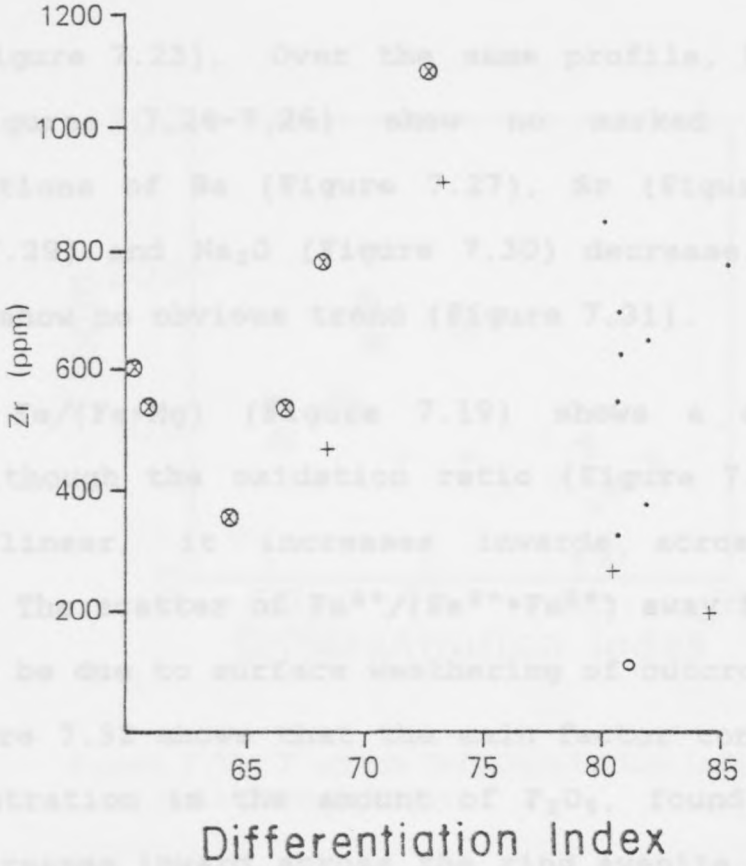


Figure 7.21 Zr versus Differentiation Index for rocks from Spitskop.

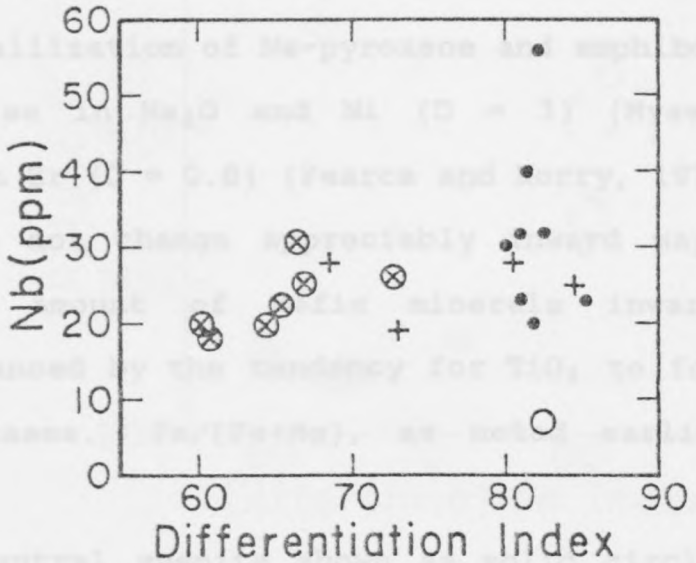


Figure 7.22 Nb versus Differentiation Index for rocks from Spitskop.

and Y (Figure 7.23). Over the same profile, Rb, K_2O, and TiO_2 (Figures 7.24-7.26) show no marked change, and concentrations of Ba (Figure 7.27), Sr (Figure 7.28), Ni (Figure 7.29) and Na_2O (Figure 7.30) decrease. The total alkalies show no obvious trend (Figure 7.31).

The Fe/(Fe+Mg) (Figure 7.19) shows a clear linear trend; although the oxidation ratio (Figure 7.20b) is not clearly linear, it increases inwards across the ring syenite. The scatter of $Fe^{3+}/(Fe^{3+}+Fe^{2+})$ away from a linear trend may be due to surface weathering of outcrop.

Figure 7.32 shows that the main factor controlling the Sr concentration is the amount of P_2O_5, found as apatite, which decreases inward across the ring syenite. This makes the increase in Y over the same profile problematic because of the high REE element content in apatite. Y is normally chemically coherent with the REE.

Crystallization of Na-pyroxene and amphibole will cause the decrease in Na_2O and Ni (D = 3) (Mysen, 1978) and increase in Zr (D = 0.8) (Pearce and Norry, 1979). The TiO_2 which does not change appreciably inward may reflect the decreasing amount of mafic minerals inward, which is counterbalanced by the tendency for TiO_2 to follow the more Fe-rich phases. Fe/(Fe+Mg), as noted earlier, increases inward.

The central syenite shown as solid circles shows much less variation in chemistry across the pipe. The

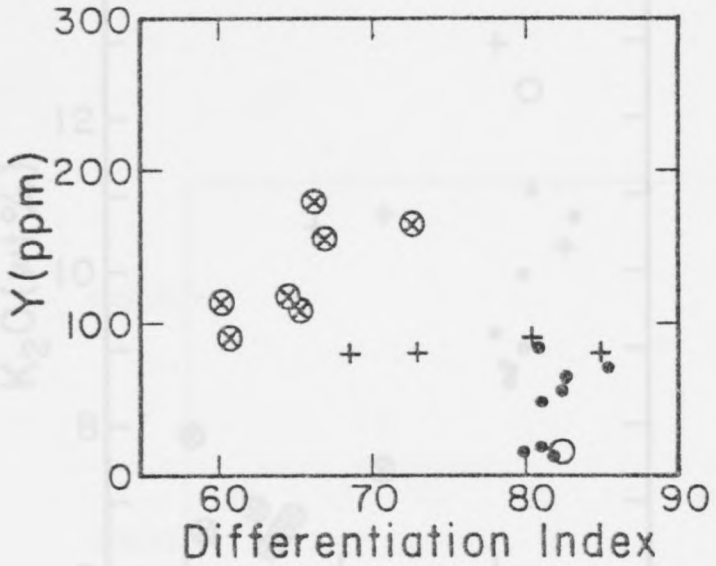


Figure 7.23 Y versus Differentiation Index for rocks from Spitskop.

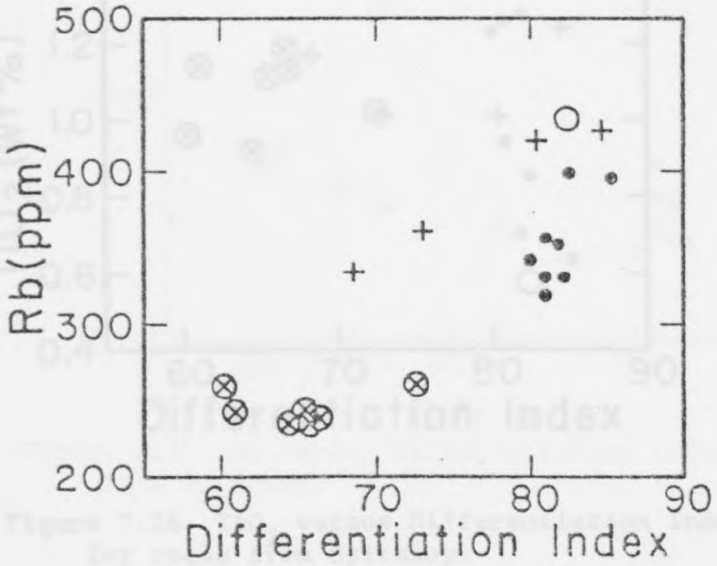


Figure 7.24 Rb versus Differentiation Index for rocks from Spitskop.

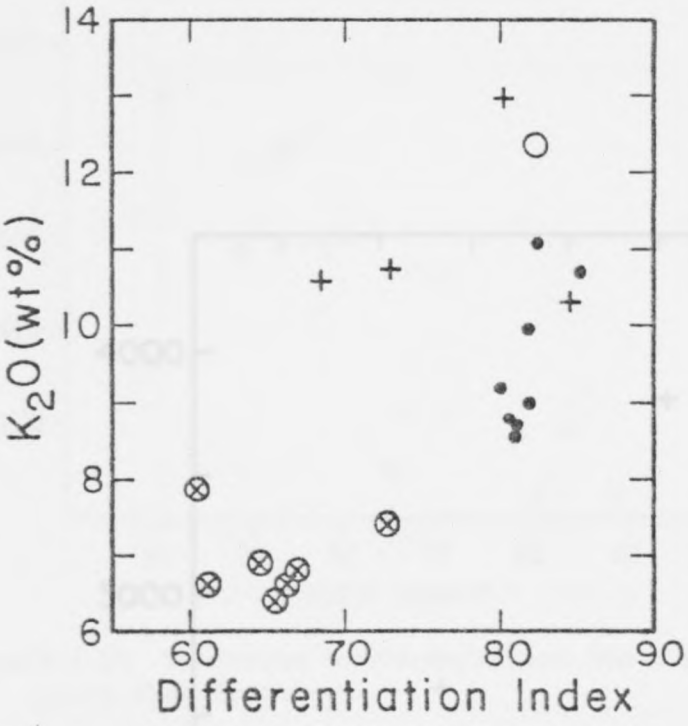


Figure 7.25 K_2O versus Differentiation Index for rocks from Spitskop.

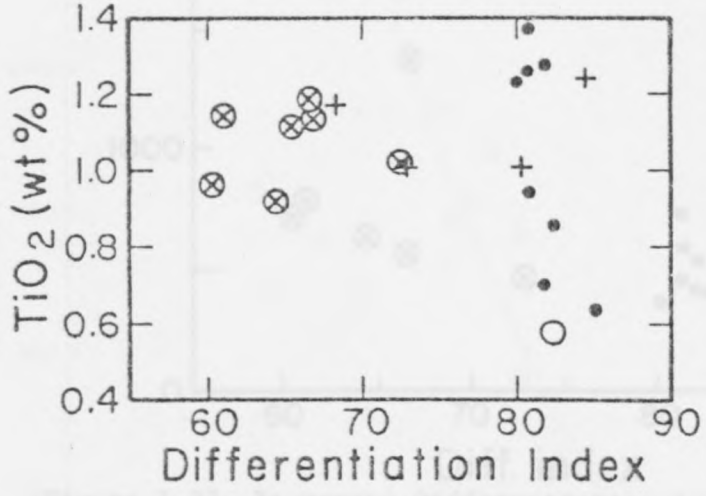


Figure 7.26 TiO_2 versus Differentiation Index for rocks from Spitskop.

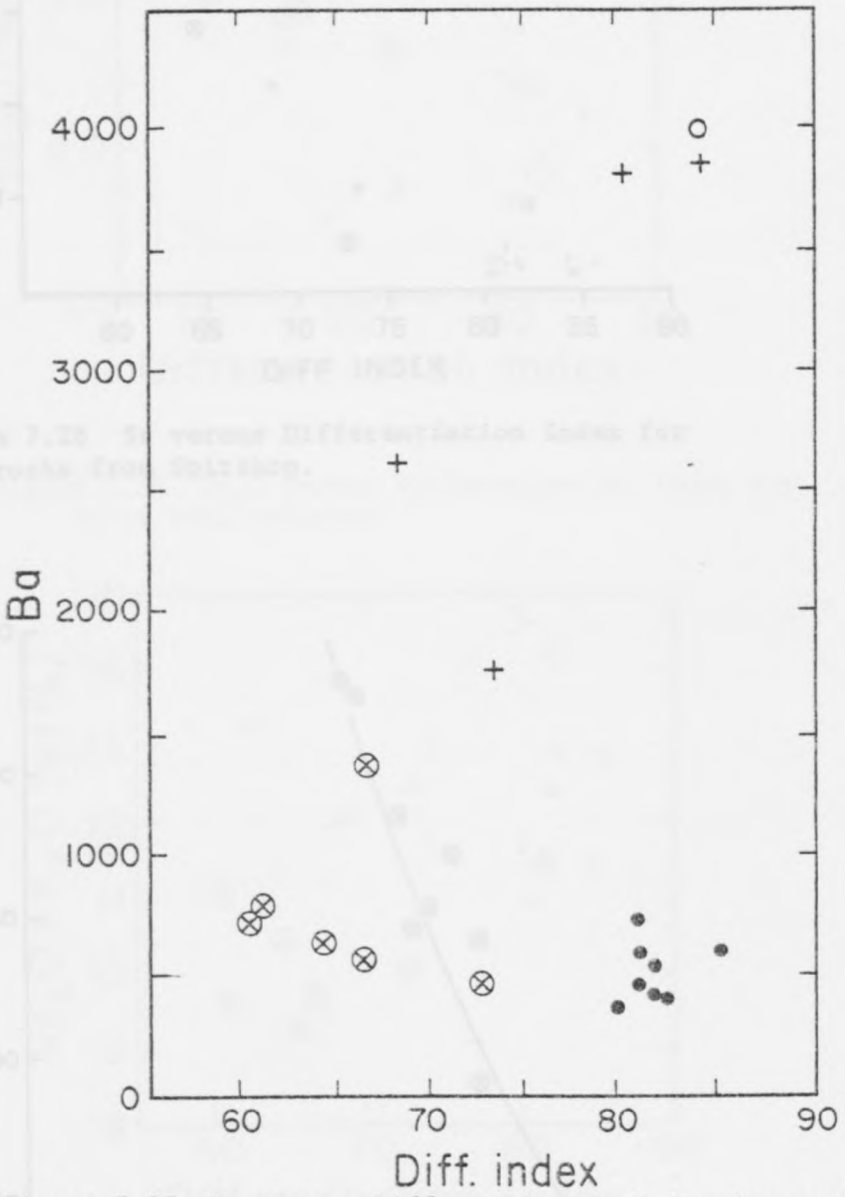


Figure 7.27 Ba versus Differentiation Index for rocks from Spitskop.

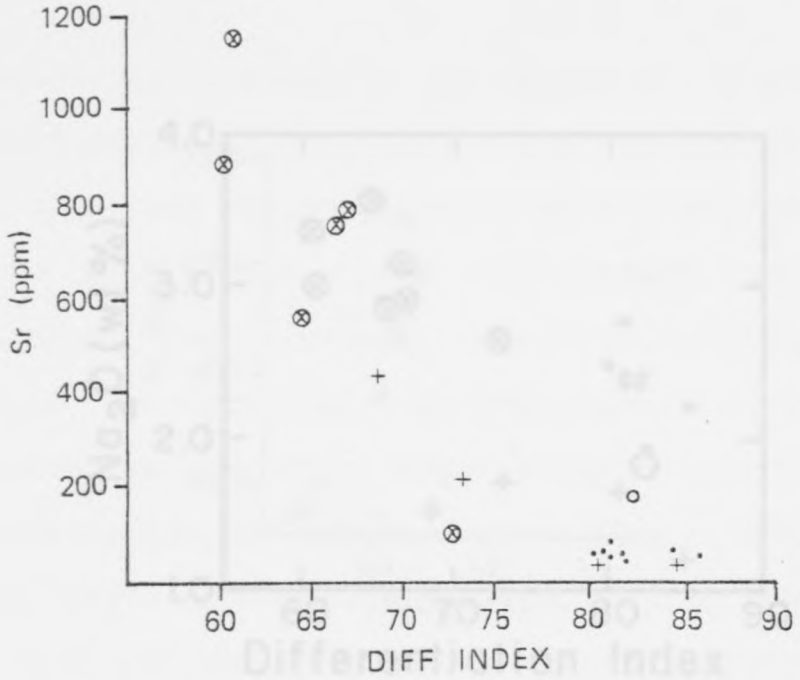


Figure 7.28 Sr versus Differentiation Index for rocks from Spitskop.

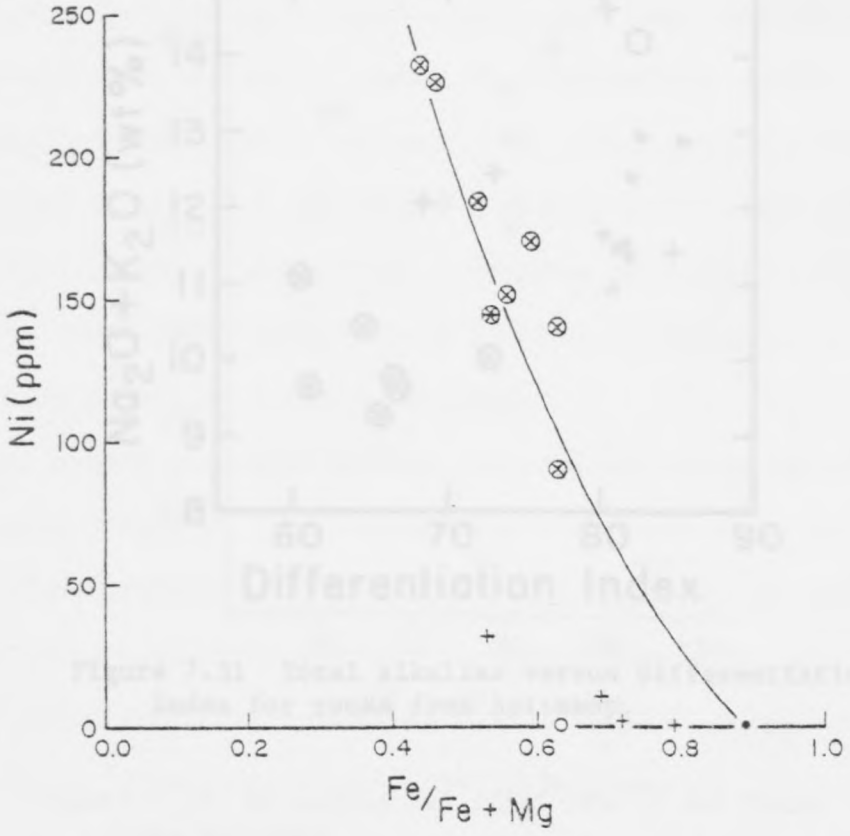


Figure 7.29 Ni versus Fe/(Fe+Mg) ratios for rocks from Spitskop.

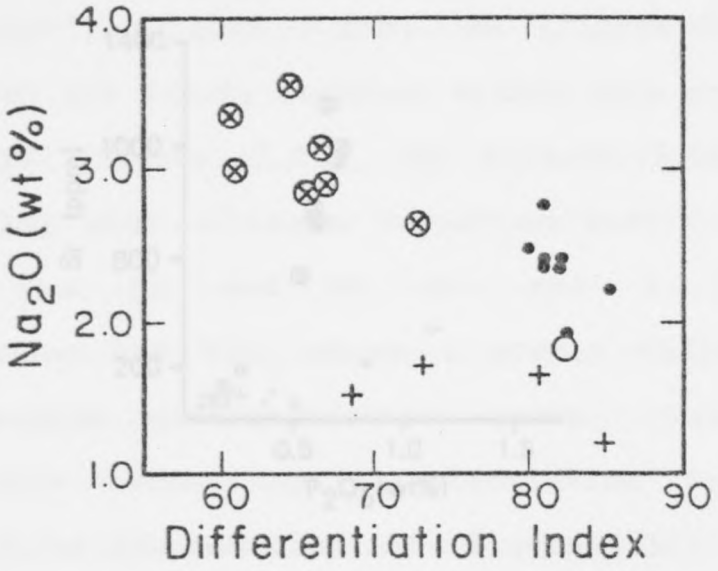


Figure 7.30 Na_2O versus Differentiation Index for rocks from Spitskop.

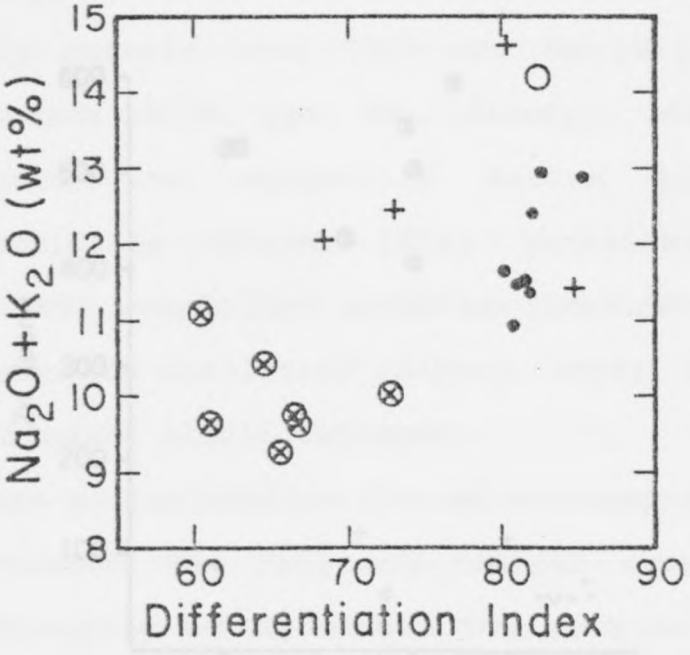


Figure 7.31 Total alkalies versus Differentiation Index for rocks from Spitskop.

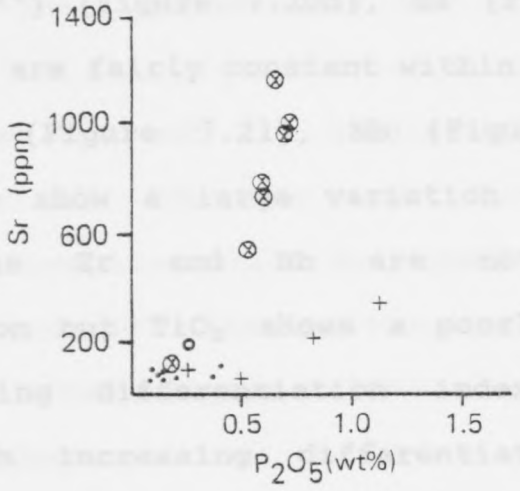


Figure 7.32 Sr versus P_2O_5 for rocks from Spitskop.

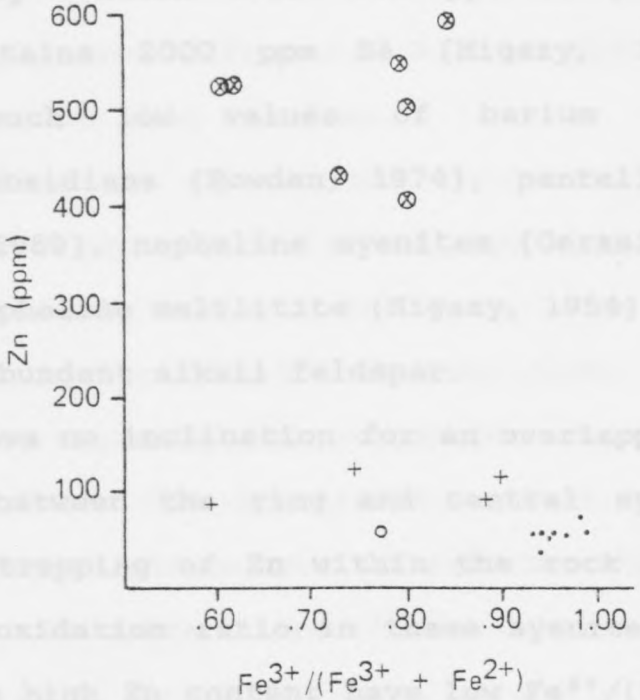


Figure 7.33 Zn versus $Fe^{3+}/(Fe^{3+}+Fe^{2+})$ for rocks from Spitskop.

differentiation index, Fe/(Fe+Mg) (Figure 7.20a), $Fe^{3+}/(Fe^{3+}+Fe^{2+})$ (Figure 7.20b), Ba (Figure 7.27) and Sr (Figure 7.28) are fairly constant within this rock type. In contrast, Zr (Figure 7.21), Nb (Figure 7.22) and TiO_2 (Figure 7.26) show a large variation within the central syenite. The Zr and Nb are not a function of differentiation but TiO_2 shows a poorly defined decrease with increasing differentiation index. Total alkalies increase with increasing differentiation index (Figure 7.31). P_2O_5 is low and constant (Figure 7.32). Rb and K_2O increase over the same profile (Figures 7.24 and 7.25).

Barium in the central syenites is anomalously low for a rock rich in potassium feldspar. Lavas from the Leucite Hills commonly contain over 7000 ppm Ba (Higazy, 1954); ugandite contains 2000 ppm Ba (Higazy, 1954). Rocks containing such low values of barium include some peralkaline obsidians (Bowden, 1974), pantellerites (Noble and Haffty, 1969), nepheline syenites (Gerasimovsky, 1963) and potash nepheline melilitite (Higazy, 1954), but these do not contain abundant alkali feldspar.

Zinc shows no inclination for an overlapping of values or a trend between the ring and central syenite (Figure 7.33). The trapping of Zn within the rock is probably a function of oxidation ratio in these syenites as the ring syenites with high Zn content have low $Fe^{3+}/(Fe^{3+}+Fe^{2+})$ and the central syenites have $Fe^{3+}/(Fe^{3+}+Fe^{2+})$ greater than 0.90. Zinc preferentially resides in rocks richer in Fe^{2+}.

Ni content was measured on only one sample of the central syenites. It has 2 ppm which is just at the detection limit for Ni.

The dykes are not all highly differentiated liquids according to the Thornton and Tuttle index. Their Fe/(Fe+Mg) ratios lie within the trend defined by the ring and central syenites. The low value of $Fe^{3+}/(Fe^{3+}+Fe^{2+})$ of one dyke rock (S2d, Figure 7.20b) cannot be attributed to surficial weathering.

The dykes are enriched in Ba (Figures 7.27) and K_2O (Figure 7.25) compared to the other rock types but contain low Sr (Figure 7.28), Na_2O (Figure 7.30), Ni (Figure 7.29) and Zn (Figure 7.33). The low Sr is particularly notable because the dykes contain appreciable amounts of P_2O_5; the Sr versus P_2O_5 trend (Figure 7.32) is different for the dykes than for the ring syenites.

The Zn in the dykes does not correlate with the oxidation trend seen in the alkali syenites (Figure 7.33). Zirconium is highly variable and Y is lower than the ring syenites, but higher than the central rocks. Rb is higher than the ring syenite but comparable to values of the central syenites. The dyke rocks contain lower normative quartz and higher potassium feldspar than the other rocks (Table 7.2). Nb content lies close to the other rocks of the pipe.

Sample S16s is from the syenite slopes outside the Spitskop pipe. It has a differentiation index comparable to

the central syenites but contains much higher Ba, Rb, similar Zn and Sr content and low Zr, Nb, La compared to the central syenite. Ba contents are comparable to the dykes.

7.2.3.2 Discussion

Chemical trends such as increasing Fe/(Fe+Mg), Rb and Zr and decreasing Sr and Ba with increasing values of differentiation index inward across the syenite suggest that Spitskop crystallized from the edge toward the centre. An inward decrease in Sr and Ba concentrations could be accounted for by the fractional crystallization of apatite and/or microcline or by cumulus enrichment of these minerals in the outer portions of the pipe, i.e., in the ring syenite. Modeling of the partitioning of trace elements can help distinguish among possible mechanisms of crystallization.

The bulk partition coefficient for an element in a rock is calculated by combining mineral-liquid partition coefficients for individual minerals in the proportions in which they crystallize in a rock. Phases crystallizing in the ring syenite at Spitskop are microcline, riebeckite and aegirine-augite, quartz, apatite, and magnetite. They are present in approximate proportions of 40 percent feldspar, 40 percent amphibole and pyroxene, 16 percent quartz, 2.5 percent magnetite, and 1.5 percent apatite, but these are not necessarily the proportions in which they crystallize if there has been cumulus enrichment of one or more phases.

Values of D(Min-liq) for the various minerals are listed in Table 7.4. Few partition coefficients have been determined for alkali-amphibole and alkali-pyroxene; values for hornblende are used in these calculations because the chemistry of hornblende is closer to the phases found in these rocks than is Ca-rich clinopyroxene for which coefficients have been determined. This is an approximation at best. Choosing values for Sr, Ba and Rb is an important factor in these calculations because of the strong dependence of the partition coefficients of these elements in alkali feldspar on the bulk composition of the magma (Pierozynski and Henderson, 1978).

Various calculations have been made to estimate the proportions of various minerals crystallizing to produce the chemical trends observed at Spitskop. Three methods have been used; first, using the chemistry of two compositions to calculate the proportion of liquid remaining for selected trace elements and second, calculating proportions of minerals crystallizing by assuming a certain amount of crystallization. Third, a two-stage model has been proposed. The results of these methods are discussed below.

7.2.3.2.1 One-Stage Trace Element Models

Assuming perfect fractional crystallization and using the bulk partition coefficients for Ba, Rb, Sr, Zr and Nb (Table 7.5) from the proportions of minerals present in the outer part of the ring syenite, calculations of liquid

Table 7.4. Distribution Coefficients for Mineral-Liquid Partitioning

Element	K-feldspar	Hornblende	Apatite
Ba	6.12 (3,4)	0.044 (1)	-
Rb	0.34	0.014 (1)	-
Sr	4.5 (4)	0.022 (1)	15(?)
Zr	-	0.80 (2)	-
Nb	-	1.4 (2)	-
Ni	-	2.9 (5)	-

Source of distribution coefficients (references in parentheses above):

1. Nagasawa and Schnetzler (1971)
2. Pearce and Norry (1979)
3. Pierozynski and Henderson (1978)
4. Long (1978)
5. Mysen (1978)

Table 7.5. Calculated Bulk Distribution Coefficients for Spitskop with Concentrations of Elements for Initial and Final Liquids, and Degree of Liquid Remaining

Element	Bulk Distribution Coefficients	Concentration in remaining liquid (ppm)	Concentration in initial liquid (ppm)	Proportion of liquid remaining
Ba	2.46	598	777	0.84
Rb	0.142	395	244	0.56
Sr	2.034	58	1156	0.06
Zr	0.56	792	559	0.44
Nb	0.32	23	18	0.72

remaining after crystallization from the outer edge of the ring syenite to the most central syenites have been made (Table 7.5). In this first model, the initial liquid composition was taken to be approximately the composition of sample S23r which was taken from the outer part of the ring. Sample S10c is considered to be the sample nearest the centre of the pipe and is taken here as the composition of the remaining liquid. As mentioned earlier, these compositions may not represent liquid compositions but may be enriched in one or more cumulus phases. However, the calculations should show whether these are reasonable liquid compositions.

Table 7.5 shows the proportions of liquid remaining using the bulk distribution coefficients based on rock compositions. The proportion of liquid remaining varies from 6 percent to 84 percent. Clearly, fractional crystallization of phases in the modal amount in the rock cannot account for crystallization of Spitskop.

The results of the second method of assuming a certain amount of residual liquid and calculating the proportion of minerals needed to produce the observed chemistry are listed in Table 7.6. Several degrees of crystallization have been used (F = 0.4 to 0.9) but none of the sets of proportions of minerals fit with crystallization of nearly equal proportions of feldspar and chain silicate. With half of the liquid remaining, all of the coefficients are positive indicating that crystallization and removal of the phases

Table 7.6. Results of calculations for modeling of trace elements assuming the proportion of liquid remaining.

Concentration of initial liquid:	Ba = 777 ppm Sr = 1156 ppm Rb = 244 ppm
Concentration of remaining liquid:	Ba = 598 ppm Sr = 58 ppm Rb = 395 ppm

Assumed Proportion of Liquid Remaining	Calculated Bulk Distribution Coefficients			Calculated Proportion of Minerals Crystallizing		
	Ba	Rb	Sr	Feldspar	Aegirine-augite & amphibole	Apatite
0.4	1.29	0.475	4.27	-0.040	34.9	0.246
0.5	1.38	0.305	5.32	0.083	19.8	0.301
0.6	1.51	6.85	0.058	0.262	-2.12	0.386
0.9	1.19	0.653	3.16	-0.170	50.8	2.80

explain the chemical trends. However, for the other residual liquids, i.e., F = 0.4, 0.6, 0.7, and 0.9, one coefficient is negative indicating that that phase must be resorbed by the liquid. The most reasonable solution is for F = 0.6 where amphibole is resorbed and minor amounts of feldspar are removed. However, for this solution, more apatite is being removed than feldspar. This does not correspond to any of the modal compositions in the pipes and, therefore, is not considered a viable explanation.

Neither of these calculations can reasonably explain the chemical trends. Errors in distribution coefficients may be one of the reasons, although the solutions are so extreme, e.g., 20 parts amphibole for 0.1 part feldspar crystallization, that small changes in D's would not bring the solutions into line with observed mineralogy. A more likely explanation is that either the ring syenite, the central syenite, or both, are enriched in cumulus phases and, therefore, do not represent reasonable liquid compositions.

7.2.3.2.2 Two-Stage Trace Element Models

Liquids of peralkaline composition may be plotted on a modified version of "Petrogeny's Residua System" termed the peralkaline residua system (Bailey and Schairer, 1966). Lavas from the Roman Province (Cundari, 1979) show differentiation trends with increasing peralkalinity due to the removal of feldspar.

The various types of syenites and trachytes from Spitskop are plotted in a similar manner in Figure 7.34. However, the trend postulated for the evolution of trachytic magma to oversaturated equivalents is not consistent with the geologic relations of Spitskop.

According to such a model involving liquid compositions, the rocks which are the most differentiated should lie furthest away from the feldspar composition; these are the first to crystallize at Spitskop. On the other extreme, the dykes which are rich in feldspar and barium lie at the non-differentiated end of the trend toward the feldspar.

Peralkalinity also should increase with fractionation of feldspar. Figure 7.35 shows that the ring syenite has higher agpaitic index or degree of peralkalinity than the central syenite. LeMaitre (1962) found that Sr and Ba decreased with peralkalinity in the volcanic rocks of Gough Island. The opposite trends occur at Spitskop (Figures 7.36 and 7.37).

The ring syenites and central syenites form two distinct trends as plotted in Figure 7.34. The ring dyke trend may be extrapolated to a point between the feldspar and aegirine compositions. The trend formed by the central syenites, the outer syenite and the dykes may be extrapolated toward the feldspar composition. A two-stage model for crystallization of Spitskop with changes in accumulating phases may best describe the chemistry. If an

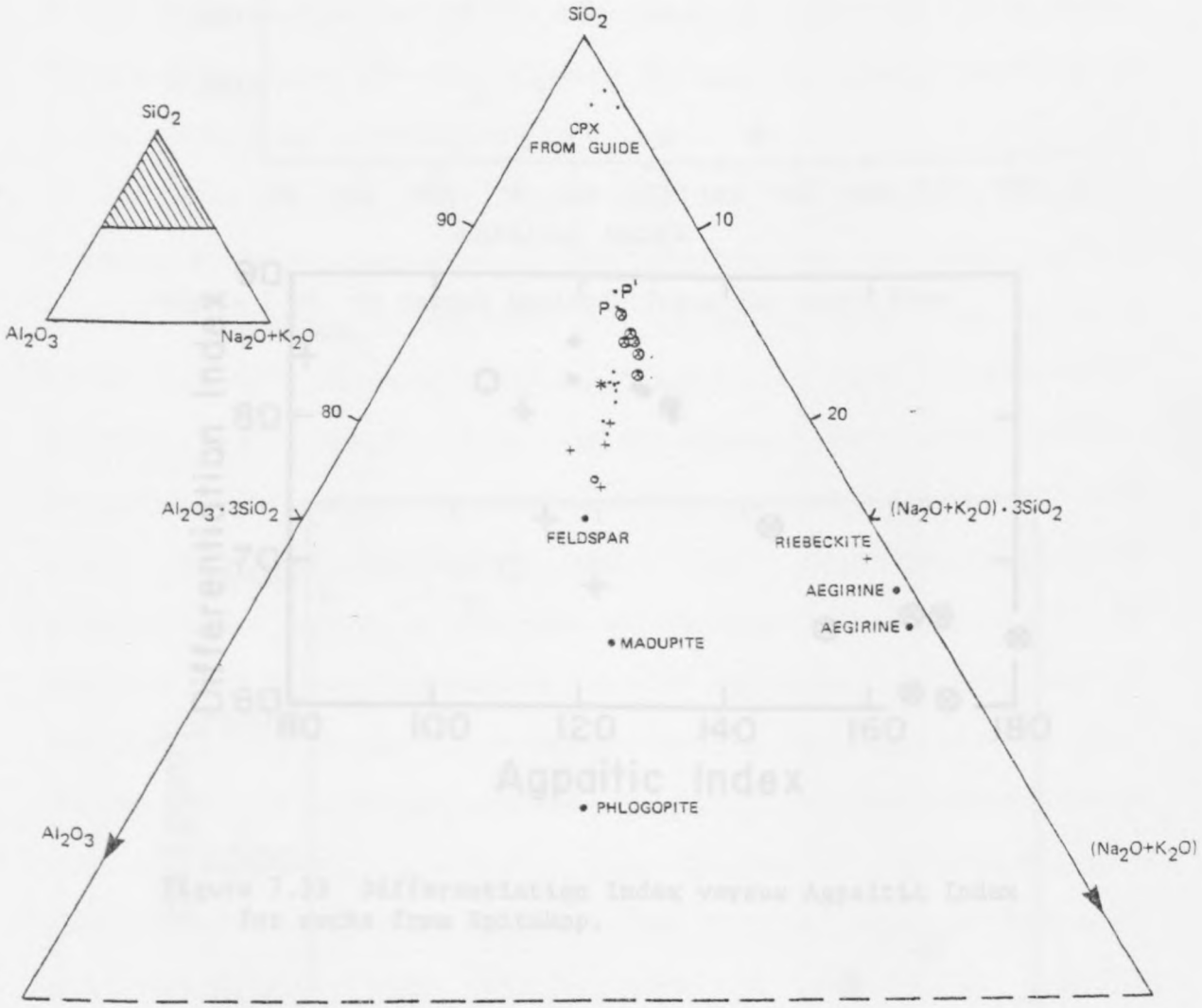


Figure 7.34 Rock compositions from Spitskop plotted in the peralkaline residual system (Al_2O_3-SiO_2-Na_2O+K_2O). P and P' represent liquid compositions as discussed in the text. A syenite from Kgopoeloe is plotted as an asterisk. Clinopyroxenes from Kgopoeloe, Guide Copper Mine, amphibole from Kgopoeloe, and phlogopite from the main complex are plotted on the diagram. A madupite (Edgar, 1979) is plotted for comparison.

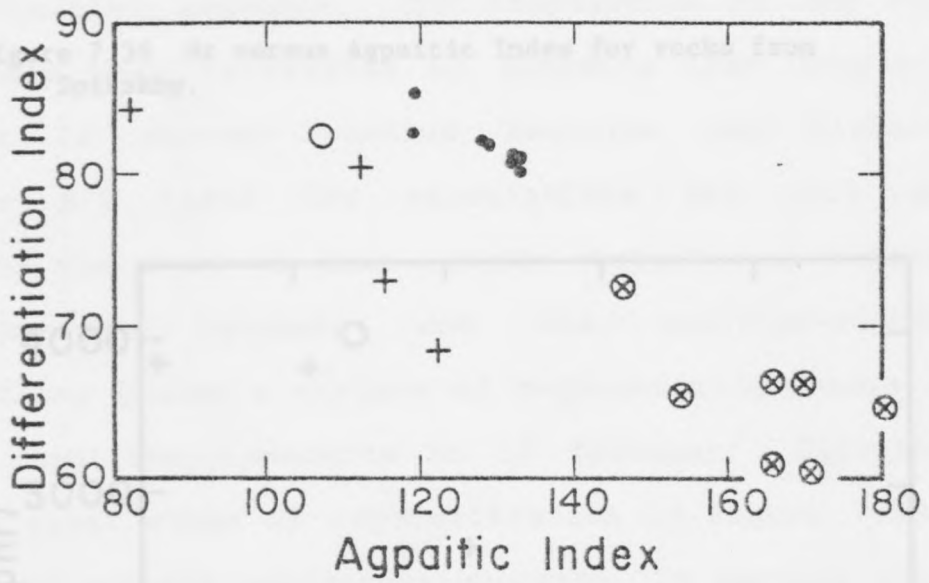


Figure 7.35 Differentiation Index versus Agpaitic Index for rocks from Spitskop.

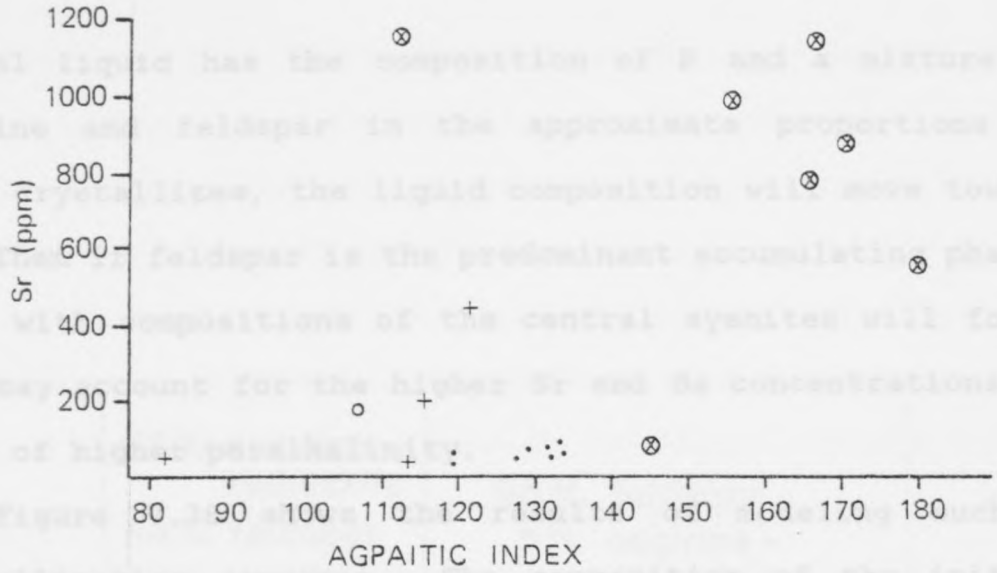


Figure 7.36 Sr versus Agpaitic Index for rocks from Spitskop.

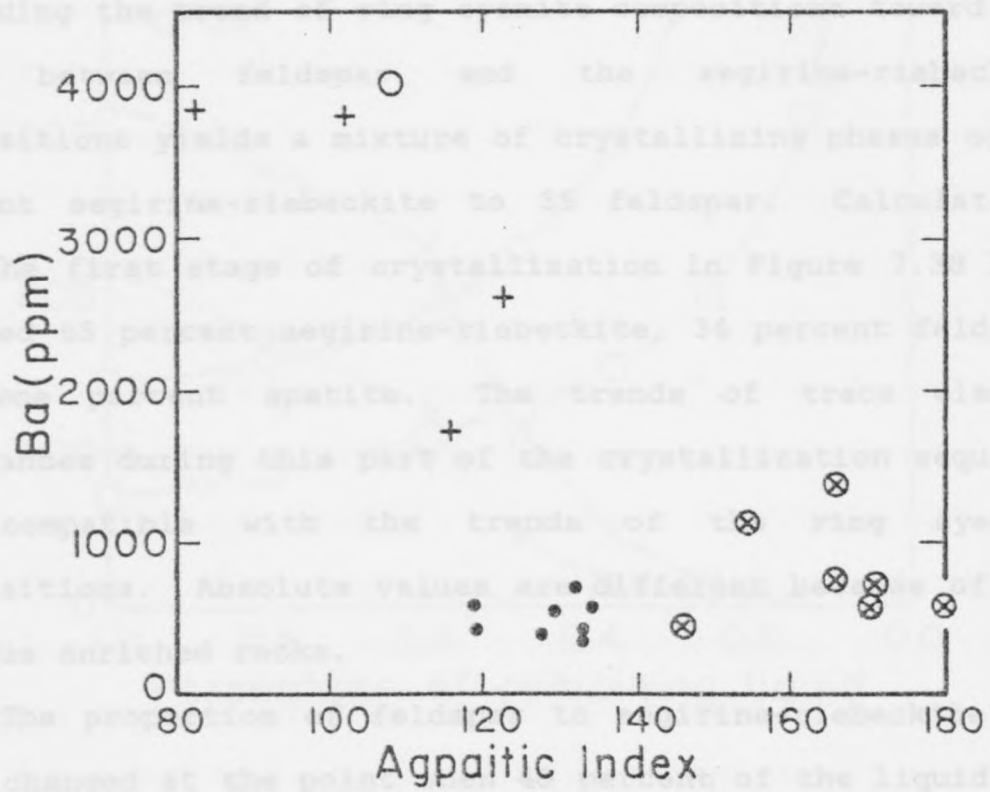


Figure 7.37 Ba versus Agpaitic Index for rocks from Spitskop.

initial liquid has the composition of P and a mixture of aegirine and feldspar in the approximate proportions of 65:35 crystallizes, the liquid composition will move toward P'. Then if feldspar is the predominant accumulating phase, rocks with compositions of the central syenites will form. This may account for the higher Sr and Ba concentrations in rocks of higher peralkalinity.

Figure 7.38 shows the results of modeling such a crystallization sequence. The composition of the initial liquid has been calculated by assuming that sample S23r contains 10 percent cumulus aegirine and riebeckite. Appendix B.5 lists the calculations for this model. Extending the trend of ring syenite compositions toward the join between feldspar and the aegirine-riebeckite compositions yields a mixture of crystallizing phases of 65 percent aegirine-riebeckite to 35 feldspar. Calculations for the first stage of crystallization in Figure 7.38 have assumed 65 percent aegirine-riebeckite, 34 percent feldspar and one percent apatite. The trends of trace element abundances during this part of the crystallization sequence are compatible with the trends of the ring syenite compositions. Absolute values are different because of the cumulus enriched rocks.

The proportion of feldspar to aegirine-riebeckite has been changed at the point when 40 percent of the liquid has crystallized. This has been chosen because abundances of Sr and Ba have been significantly reduced at this point which

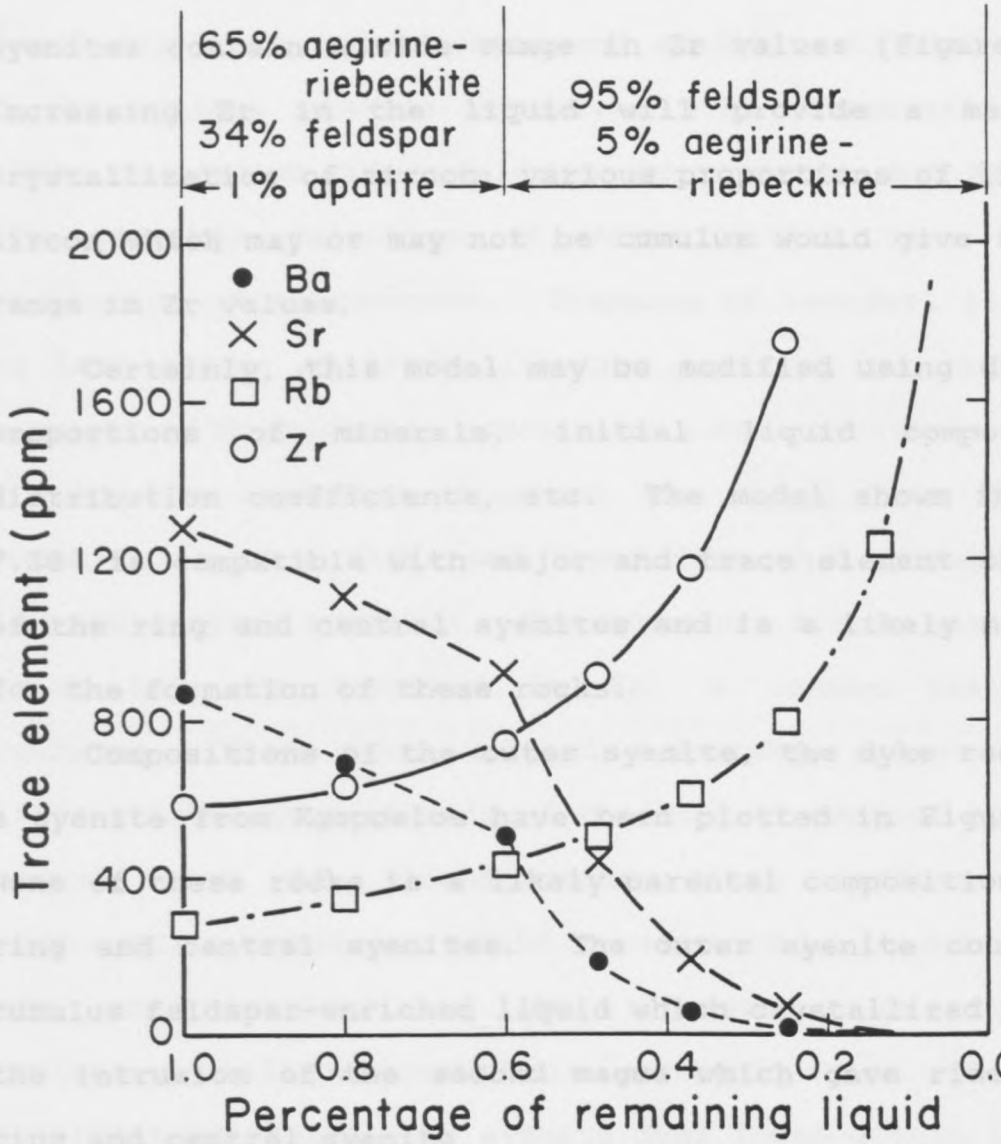


Figure 7.38 Trace element model for crystallization of Spitskop involving a two-stage sequence of different mineral assemblages crystallizing.

is compatible with the compositions of the ring syenites. Further crystallization of the liquid proceeds with 95 percent feldspar and five percent riebeckite-aegirine. The trend of increasing Rb and Zr and rapidly decreasing Sr and Ba fits with the compositions of the central syenites. Zr does not show an increasing trend as such but the central syenites contain a wide range in Zr values (Figure 7.21). Increasing Zr in the liquid will provide a means for crystallization of zircon; various proportions of liquid to zircon which may or may not be cumulus would give the wide range in Zr values.

Certainly, this model may be modified using different proportions of minerals, initial liquid compositions, distribution coefficients, etc. The model shown in Figure 7.38 is compatible with major and trace element chemistry of the ring and central syenites and is a likely mechanism for the formation of these rocks.

Compositions of the outer syenite, the dyke rocks, and a syenite from Kgopoeloe have been plotted in Figure 7.34. None of these rocks is a likely parental composition to the ring and central syenites. The outer syenite could be a cumulus feldspar-enriched liquid which crystallized prior to the intrusion of the second magma which gave rise to the ring and central syenite.

The model most compatible with the chemistry, textures and geological relationships of Spitskop is a two-stage intrusion starting with the outer syenite which comprises

the lower slope of Spitskop and the adjacent connected hill to the northwest. After consolidation, a second liquid intruded causing the brecciation of the narrow band around Spitskop. Crystallization inward produced the ring syenite which was rapidly decreasing in Ba and Sr due to crystallization and accumulation of alkali feldspar and alkali amphibole and pyroxene and apatite. Crystallization of the central syenite continued with accumulation of a higher proportion alkali feldspar to pyroxene and amphibole with possible pulsation of magma giving rise to the orientation of phenocrysts. Trapping of residual liquid at the last stages of crystallization produced the rocks high in quartz with feldspars containing alkali pyroxenes.

In the variation diagrams the dykes from Spitskop commonly lie on a different trend from that formed by the ring and central syenites. The dykes are highly enriched in barium but are depleted in Sr, a common feature of trachytes. These dykes intruding Spitskop cannot be late differentiates from liquids of the ring or central syenites, because even if clinopyroxene alone influenced the fractionation trend, it would be impossible to attain such high concentrations of Ba. However, as discussed previously, clinopyroxene is probably not the sole fractionating phase. The syenite dyke found within the main complex (F20s, Table 7.7) has a similar concentration of Ba although Sr is higher. The fact that the Sr content of the syenite from the main complex is 465 ppm for a rock

Table 7.7. Syenite dykelet in Foskor Pit.

F20S		Normative Mineralogy	
SiO_2	60.30	qtz	9.63
TiO_2	0.89	orth	58.23
Al_2O_3	16.45	ab	8.84
Fe_2O_3	2.97	an	12.18
FeO	1.20	di	3.63
MnO	0.05	hy	1.80
MgO	1.36	mag	1.49
CaO	3.57	ilm	1.73
Na_2O	1.02	hem	2.02
K_2O	9.62	ap	0.48
P_2O_5	0.15		
H_2O^-	0.65		
LOI	1.60		
Total	100.18		
Sr	465	Diff index	79.92
Rb	402		
Ba	4372	Fe/(Fe+Mg)	0.62
Ce	(116)		
La	32	Agpaitic	
V	37	Index	73.4
Cu	52		
Ni	1		
Zn	34		
Nb	22		
Zr	525		
Y	(7)		

containing 0.15 percent P_2O_5 compared to a dyke of Spitskop, sample S2d, which has a comparable differentiation index of 80.39, P_2O_5 = 0.26 and 46 ppm Sr makes a crystallization from the same liquid untenable.

7.2.4 Interrelationships of the Satellites

The geology, petrography and whole-rock chemistry have indicated an extremely complex history for the intrusion and crystallization of the satellite pipes. The major- and trace-element chemistry does not follow a simple crystallization path because of the partitioning of elements between liquid and vapor phases and variation in cumulus phases.

The syenites at Kgopoeloe and Spitskop may have crystallized from a similar parental liquid. Syenites at Kgopoeloe are influenced by accumulation of feldspar while those at Spitskop are influenced by aegirine-augite and riebeckite as well, at least in the ring syenite. Thus, the model proposed in Chapter 3 holds up to geochemical evidence.

Chemically, it is difficult to compare Kgopoeloe and Spitskop with the feldspathic pyroxenite pipes like the Guide Copper Mine. The moderate values of barium, rubidium and strontium (Table 7.1) in a rock with cumulus clinopyroxene and intercumulus feldspar suggests crystallization at the Guide pyroxenite from a liquid which is highly differentiated. The low concentrations of REE and

high Cu and Zr values relative to the main complex suggest that rocks from Guide Copper Mine could be differentiates from a common magma to the main complex.

The relationship of the syenites from Kgopoeloe and Spitskop to the main complex is not clear-cut. However, nickel concentrations in the ring syenites are comparable or higher than those of pyroxenites in the main complex. Because Ni is strongly partitioned into olivine, it is unlikely that syenites would have such high concentrations of Ni with large amounts of olivine fractionation. Therefore, a cogenetic relationship with the phoscorites is unlikely.

The syenites of the satellites share many chemical characteristics with pyroxenites of the main complex, namely high K_2O/Na_2O and high REE. Other characteristics such as higher Fe/Mg and Zr and lower Sr and Ba in the satellites relative the main complex may have resulted through differentiation. These features are suggestive of a cogenetic relationship but are not conclusive. Chapters 8 and 10 further explore chemical and mineralogical relationships between the satellites and the main complex.

Chapter VIII

EXPERIMENTAL PETROLOGY AS RELATED TO THE PHALABORWA COMPLEX

During the past 20 years, experimental studies have provided additional clues as to the origin and crystallization of alkaline rocks. The wide variations in composition of this group of rocks makes it impossible for every natural system to be studied, but basic principles and general trends have been established to help interpret the complex suites of alkaline rocks. This chapter reviews experimental work on the origin of alkaline magmas in general and more specifically reviews experimental studies which may pertain to the crystallization of the main complex and how a magma producing such a suite of rocks might evolve to form the rocks comprising the surrounding satellites.

8.1 ULTRAPOTASSIC-ULTRABASIC MAGMAS

Experimental studies on the melting relationships of highly potassic and ultrabasic rocks similar to the classic examples of Leucite Hills (Carmichael, 1967) and East Africa (Holmes, 1950; Cundari and Le Maitre, 1970), provide the closest analogue available to magma producing the main Phalaborwa complex. Low SiO_2 and high K_2O, MgO, CaO, and incompatible elements are characteristics of potassic lavas and rocks from Phalaborwa, but certain elements such as Ti and Nb are not as enriched in the Phalaborwa complex as they

are in potassic lavas. Melting experiments on these lavas (Edgar et al., 1976; Barton and Hamilton, 1978, 1979) have bearing on the proportions and order of crystallization of phases and on the mineral chemistry of precipitating phases.

Experimental work on melting of potassic lavas has utilized various natural compositions including the least siliceous mafurite through madupite and wyomingite compositions to the most silica-rich orendite under dry conditions through various degrees of water content to water saturation at pressures up to 30 kb. Liquidus relations, proportions of the crystallizing minerals and order of crystallization vary under different experimental conditions (Edgar et al., 1976; Barton and Hamilton, 1978, 1979), but major phases are ubiquitously olivine, clinopyroxene, and phlogopite. Figure 8.1 shows the order of crystallization of a biotite mafurite with 5% H_2O (Edgar et al., 1976). Olivine crystallization is followed by crystallization of phlogopite and clinopyroxene; the order of the last two minerals is determined by pressure. Clinopyroxene and phlogopite appear within a short temperature interval. Figure 8.2 shows crystallization behavior of madupite under water-undersaturated conditions (Barton and Hamilton, 1979). At pressures above 7 kb, clinopyroxene is the primary liquidus phase. Below that pressure, clinopyroxene and olivine are the first precipitates. In all of the experiments performed by Barton, Hamilton, Edgar and coworkers, olivine appears to react with liquid to form

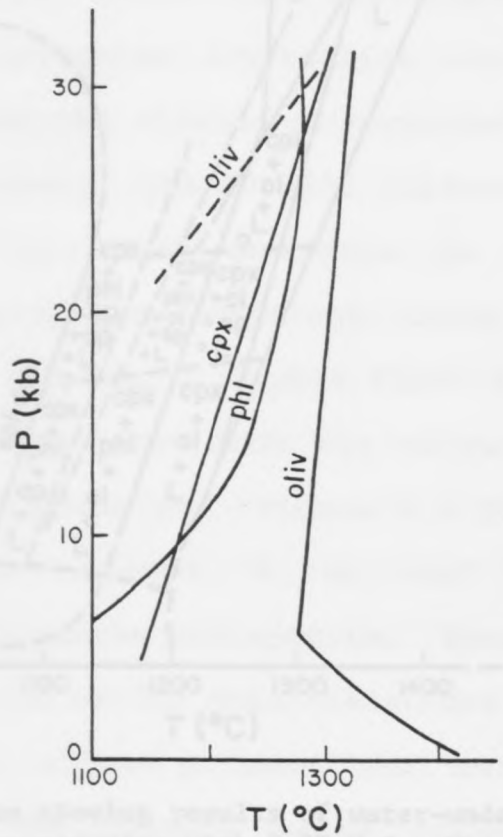


Figure 8.1 Diagram showing above-solidus boundaries for appearance of minerals in melting experiments of a highly potassic biotite mafurite with 5% H_2O. The olivine-out boundary at high pressure is shown as a dashed boundary (after Edgar et al., 1976).

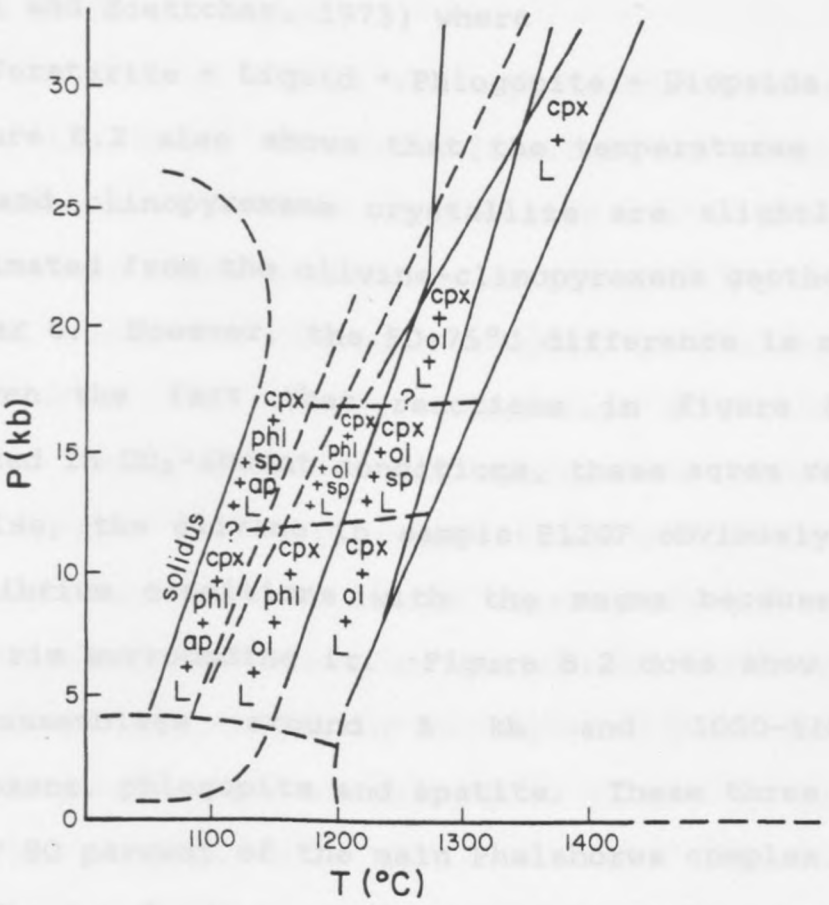


Figure 8.2 Diagram showing results of water-undersaturated melting experiments on madupite with 2.9% H_2O. The boundaries which are not well determined are shown in dashed lines (after Barton and Hamilton, 1979).

clinopyroxene and phlogopite. This reaction has also been found in the synthetic system of K_2O-CaO-MgO-Al_2O_3-SiO_2-H_2O (Modreski and Boettcher, 1973) where

Forsterite + Liquid → Phlogopite + Diopside.

Figure 8.2 also shows that the temperatures at which olivine and clinopyroxene crystallize are slightly higher than estimated from the olivine-clinopyroxene geothermometer in Chapter 6. However, the 50-75°C difference is not great and, given the fact that reactions in Figure 8.2 were synthesized in CO_2-absent conditions, these agree remarkably well. Also, the olivine in sample P120P obviously was not in equilibrium conditions with the magma because of the reaction rim surrounding it. Figure 8.2 does show that the stable assemblage around 5 kb and 1050-1100°C is clinopyroxene, phlogopite and apatite. These three minerals form over 90 percent of the main Phalaborwa complex.

In Chapter 5, it was proposed that early crystallizing phases depleted the primary magma in Ni and Cr. Two possible phases were magnetite and olivine. Although clinopyroxene is a liquidus phase at all T and P in Figure 8.2, spinel crystallizes at all T between 12 and 17 kbar and may act as a sink for Ni and Cr. Olivine crystallizes from the liquid at higher T and P than the clinopyroxene-phlogopite-apatite assemblage and may act as the sink for Ni. Likewise, earlier crystallizing clinopyroxene may help deplete the liquid in Cr. However, olivine and clinopyroxene crystallization could not be extensive or the

Mg/Fe ratio of the minerals at Phalaborwa would be lower. Hence, spinel is a more likely candidate for early depletion of Cr and Ni in the magma.

The addition of CO_2 to the experiments discussed above may alter the order of crystallization and proportion of various minerals. However, two points are in favour of a highly potassic magma similar to the Leucite Hills lavas as a parental magma for the main complex at Phalaborwa. As mentioned above, the mineral assemblage at Phalaborwa is similar to those produced at appropriate pressures for potassic lavas. Secondly, compositions of the phlogopites and clinopyroxenes formed in the experiments are strikingly similar to minerals formed at Phalaborwa, most noticably, the low Al and Ti content of Ca, Mg-rich diopsides and the Al- and Ti-poor nature of phlogopite (Edgar et al., 1976; Barton and Hamilton, 1979). The lavas studied experimentally contain up to 4.9% TiO_2 and 11.39% Al_2O_3 so are by no means depleted in these elements. This is an extremely important point because, as shown in Chapter 5, there are few analyses in the literature of clinopyroxenes with similar compositions to those at Phalaborwa. This is also the case with the phlogopites, although to a lesser degree.

Up to this point in this thesis, the relationship between the satellite pipes and the main complex has been discussed only in comparative terms, avoiding discussion of a genetic relationship. At this point, it is useful to look

at experimental evidence to establish if the various syenites, alkali granites and pyroxenites of the satellites can be derived by differentiation or some other mechanism from magma producing rocks of the main complex.

The bulk composition of crystal aggregates precipitated from liquid will determine the differentiation path a magma will take upon cooling. If silica-undersaturated minerals are removed from a liquid, it will become more silica rich. Barton and Hamilton (1978) note that peralkaline liquid, represented by madupite, produces minerals in which Al does not appreciably substitute for Si. Therefore, progressive liquids are silica deficient. Clinopyroxenes and phlogopites at Phalaborwa have similar characteristics, with clinopyroxene in particular being silica rich with approximately 54% SiO_2. The micaceous pyroxenites from Phalaborwa have 43-51% SiO_2 and massive pyroxenites a range of 48-52% SiO_2 (Table 7.1). Apatite-rich pyroxenites have as little as 39% SiO_2. It would be difficult to derive silica-rich liquids such as the syenites of Kgopoeloe and Spitskop (Table 7.2) by crystallization of pyroxenites at Phalaborwa from a composition similar to Leucite Hills madupite with 43% SiO_2 (Carmichael, 1967). However, if a peralkaline equivalent of wyomingite or orendite (with 55% SiO_2) were the parental magma, such a trend towards silica enrichment may be more plausible.

Experimental work on alkaline systems presents a myriad of mechanisms for the evolution of alkaline liquids. Edgar

(1979) reviews these with an emphasis on application to naturally occurring assemblages. Because of uncertainty in the parental magma composition, it is difficult to relate the evolution of liquid from the main complex at Phalaborwa to crystallization of satellite pipes within such an experimental framework. However, using certain assumptions, a few important points from experimental work suggest ways to produce both the main complex and satellites.

It is necessary to find a way to produce:

(1) peralkaline, basic liquid as discussed above to produce the main complex. The SiO_2 content of this magma is not known,

(2) trachytes (Spitskop),

(3) syenite, alkali syenite, alkali granite (Kgopoeloe and Spitskop),

(4) liquid which will produce the cumulus feldspathic pyroxenite (Guide Copper Mine).

The liquid must be capable of producing diopside and phlogopite which later precipitates aegirine, riebeckite, microcline and quartz. The undersaturated (glimmerite) versus oversaturated assemblage suggests that the liquids producing these assemblages may be under- and oversaturated, respectively. In some cases, however, such as the system quartz-nepheline-kalsilite, quartz normative liquid can produce undersaturated minerals, in this case, leucite (Hamilton and MacKenzie, 1965). Precipitation of leucite further enriches the liquid in SiO_2. Early experimental

work based on that of Bowen (1937) found a thermal barrier which prevents an undersaturated liquid evolving to an oversaturated liquid. However, later work (Carmichael and MacKenzie, 1963; Bailey and Schairer, 1964; Edgar and Nolan, 1966; Nolan, 1966) found mechanisms by which the thermal barrier could be "bridged."

The "plagioclase effect" whereby removal of $CaAl_2Si_2O_8$ component enriches residual liquids in sodium and silica, is not operable as such at Phalaborwa because plagioclase is not found in rocks of the main complex (Chapter 4) and anorthite component is nonexistent in plagioclase in syenites of the satellites (Chapter 5). However, a similar effect has been found involving diopside (Nolan, 1966) and alkali feldspar (Bailey and Schairer, 1964). Diopside, $CaMgSi_2O_6$, will have the effect of increasing alkalis in the liquid from which it crystallizes while alkali feldspar, particularly $KAlSi_3O_8$, will have the effect of increasing the acmite and silica components of a liquid, thus producing aegirine and quartz in late-stage rocks. Diopside and alkali feldspar are the primary phases in the three pyroxenite pipes surrounding the main complex, as well as in the feldspathic pyroxenites of the main complex. If liquid forming the cumulus rocks of Guide Copper Mine is close to liquid producing pyroxenites of the main complex, not an unreasonable assumption given the mineral assemblage and trace element content, then residual liquids will be driven toward a more peralkaline silica-rich composition.

Although not mentioned in experimental work on synthetic systems, the precipitation of phlogopite would have a similar effect. Phlogopite at Phalaborwa (Tables 5.4 and 5.5) contains approximately equal molecular proportions of Al and K. Removal of this phase will produce a liquid enriched in Na, thereby increasing (Na+K)/Al. Because phlogopite is an undersaturated phase, i.e., leucite-normative, SiO_2 will also be increased in liquid with removal of phlogopite. Addition of forsterite component to the residual system involves the precipitation of forsterite and phlogopite (Luth, 1967) which would enhance silica enrichment with crystallization.

In summary, it has been shown in experimental systems that there are ample opportunities for liquids to evolve in a manner compatible with the assemblages seen at Phalaborwa. Removal of an immiscible carbonate liquid to form the carbonatite would further enrich a liquid in silica and sodium, thereby enhancing the previously discussed mechanisms.

Alternatively, can the liquids producing the satellites be unrelated to the liquids producing the main complex? A likely alternative source for the liquids producing the satellite bodies might be a partial melt of crustal rocks. The strongest evidence against this is the work of Bailey and Schairer (1966) who showed that eutectic compositions of peralkaline, oversaturated rocks, corresponding to some syenites of Kgopoeloe and Spitskop, do not correspond to

granitic eutectic compositions which would be expected in partial melting of granite. Experimental work in part of the basalt tetrahedron (Sood and Edgar, 1972; Platt and Edgar, 1972) shows that silica-saturated, peralkaline magmas may evolve from alkali olivine basalts and that predominantly K-rich magmas are produced by fractionation of liquid originating in or near the leucite volume in the system SiO_2-$KAlSiO_4$-$NaAlSiO_4$. It is not the purpose of this chapter to explore experimental work related to syenite generation. However, a mantle origin for these syenites is reasonable.

8.2 GENERATION OF ALKALINE MAGMAS

The general consensus today is that kimberlites, carbonatites, and other volatile-rich alkaline magmas are derived from the mantle, either directly by partial melting (Dawson, 1971; Mitchell and Crockett, 1972, Mysen and Boettcher, 1975) or through fractional crystallization of a mantle-derived liquid (O'Hara and Yoder, 1967; MacGregor, 1970). Extensive experimental work during the 1970's coupled with more sophisticated geochemical measurements on natural assemblages have derived models for the evolution of these rocks.

Most workers agree that the major constituents of the mantle acting as a source for the kimberlite and related rocks is a four-phase peridotite consisting of olivine-orthopyroxene-clinopyroxene with either a spinel or a

garnet. There is strong evidence that minerals and magmas derived from the mantle contain CO_2 and H_2O (Wyllie, 1971; Eggler, 1978) which has led to extensive experimental work on the effects of these two volatile phases on the melting and phase relationships of systems modeling peridotite compositions. Many workers (Eggler, 1975, 1978; Wyllie and Huang, 1975a,b, 1976; Mysen and Boettcher, 1975) have demonstrated that the presence of CO_2 produces liquids strongly depleted in SiO_2 and, that by varying the partial pressures of these volatile phases, liquids with various compositions containing different proportions of carbonatitic component can be formed.

Pressure differences (Modreski and Boettcher, 1973) could produce from the same starting material, magmas ranging from a quartz-normative composition at 15 kb to leucite-normative at depths of 35 kb under vapor-absent conditions. Wendlandt (1977) used a constant vapor composition and produced carbonatitic to kimberlitic compositions with increasing depth. Eggler (1978) formed nephelinites from a similar composition at shallow depths.

Under a constant CO_2-rich vapor composition, the mineral assemblage is important in controlling magma composition (Wyllie, 1979). Small degrees of partial melting of phlogopite peridotite produces a high K_2O liquid with high Mg/Ca resembling leucite-normative magmas and kimberlites. With phlogopite absent, melilitic compositions are formed. The presence of dolomite ensures that the silica content of all these liquids is low.

Another approach to the origin of alkaline magmas involves studies of fractional crystallization. O'Hara (1965) and O'Hara and Yoder (1967), found that removal of an eclogite fraction from a picritic magma could produce kimberlitic compositions, and Green and Ringwood (1967) produced nephelinite from picrite.

Barton and Hamilton (1979), however, found no evidence that the highly potassic lavas they studied could originate as primary magmas in the upper mantle. At no pressures up to 30 kb was orthopyroxene in equilibrium with liquids. They do state that other experimental work (Eggler, 1975; Kushiro, 1975; Brey and Green, 1977) shows that the addition of CO_2 to a system has the effect of stabilizing orthopyroxene at high pressures. Wendlandt and Eggler (1980a) modeled the generation of potassic lavas by studying a potassic peridotite containing forsterite, enstatite, pyrope, phlogopite and magnesite. In melting experiments, Wendlandt and Eggler (1980b) found that in vapor-absent conditions, small degrees of partial melting at pressures of 20-30 kb produced potassic, silica-undersaturated magmas. Therefore, regardless of the specific composition of the liquid producing the Phalaborwa complex, a mantle origin is probable.

Chapter IX
ISOTOPIC STUDIES

The objectives of the isotopic study were two-fold: to obtain a reliable age for the carbonatite and pyroxenites of the complex and to obtain accurate strontium isotopic data to aid in establishing the petrogenesis of the complex. Plans to fulfill these objectives included: (1) obtaining initial strontium isotopic ratios to provide constraints on the origin of the magma, and (2) determining the age relationships of the carbonatites, phoscorite and pyroxenite by dating of mica using the Rb-Sr method, corroboration of earlier U-Pb data on uranorthorianite and dating of another uranium-bearing phase, baddeleyite.

This study proposed to date a previously undated U- and Pb-bearing phase, baddeleyite (ZrO_2), and to redate uranothorianite from known rock types. In addition, modern equipment allows for greater precision in measuring isotopic compositions than was available in 1956 (see section 2.1.3). Uranothorianite and baddeleyite occur exclusively in the carbonatite and phoscorite rock types of the Phalaborwa complex and, thus, give no information about age of the pyroxenites. Phlogopite, an abundant constituent in both silicate and carbonate rocks of the complex, was dated by the Rb-Sr method to provide data on pyroxenites as well as carbonatite and phoscorite.

Initial $^{87}Sr/^{86}Sr$ ratios on the carbonatite from Phalaborwa have been reported by Powell et al. (1966) and Pineau et al. (1973). The 0.7051 ± 0.0012 ratio of Powell et al. (1966) may be slightly inaccurate because of an arbitrary correction factor applied to the data. However, Pineau et al. (1973) confirmed the work of Powell et al. (1966) by reporting a $^{87}Sr/^{87}Sr$ ratio of 0.7053 ± 0.0005 for the carbonatite. These values are considerably higher than expected for uncontaminated material derived from the mantle around 2000 m.y. ago. These data prompted further work on the $^{87}Sr/^{86}Sr$ ratios of the carbonatite. Clinopyroxenes and apatite from pyroxenites were also measured for $^{87}Sr/^{86}Sr$ ratios in this study to place constraints on the origin of the pyroxenites. For the carbonatites, $^{87}Sr/^{86}Sr$ ratios for apatite and clinopyroxene were measured to establish whether homogeneity in the initial $^{87}Sr/^{86}Sr$ ratios existed among minerals of the carbonatite and between the pyroxenite and carbonatite phases.

9.1 SAMPLES

Sample locations are shown in Figures 9.1 and 9.2. Carbonatite samples include transgressive and banded types. Clinopyroxenes come from the PMC and Foskor areas, and one sample G12F is from the Guide Copper Mine pyroxenite pipe. Apatite samples also come from both the PMC and Foskor areas. Samples of mica representing various textures, derived from different rock types and from different



Figure 9.1 Outline of the Phalaborwa complex with sample locations of country rocks, vermiculite, pyroxene from the Guide Copper Mine and index maps for the PMC and Foskor areas of Figure 9.2.

LEGEND


TRANSGRESSIVE CARBONATITE


BANDED CARBONATITE


PHOSCORITE


PYROXENITE PEGMATOID


MICACEOUS PYROXENITE


PREDOMINANTLY MICA ROCK


FELDSPATHIC PYROXENITE


FENITE


GRANITE/GNEISS


DOLERITE

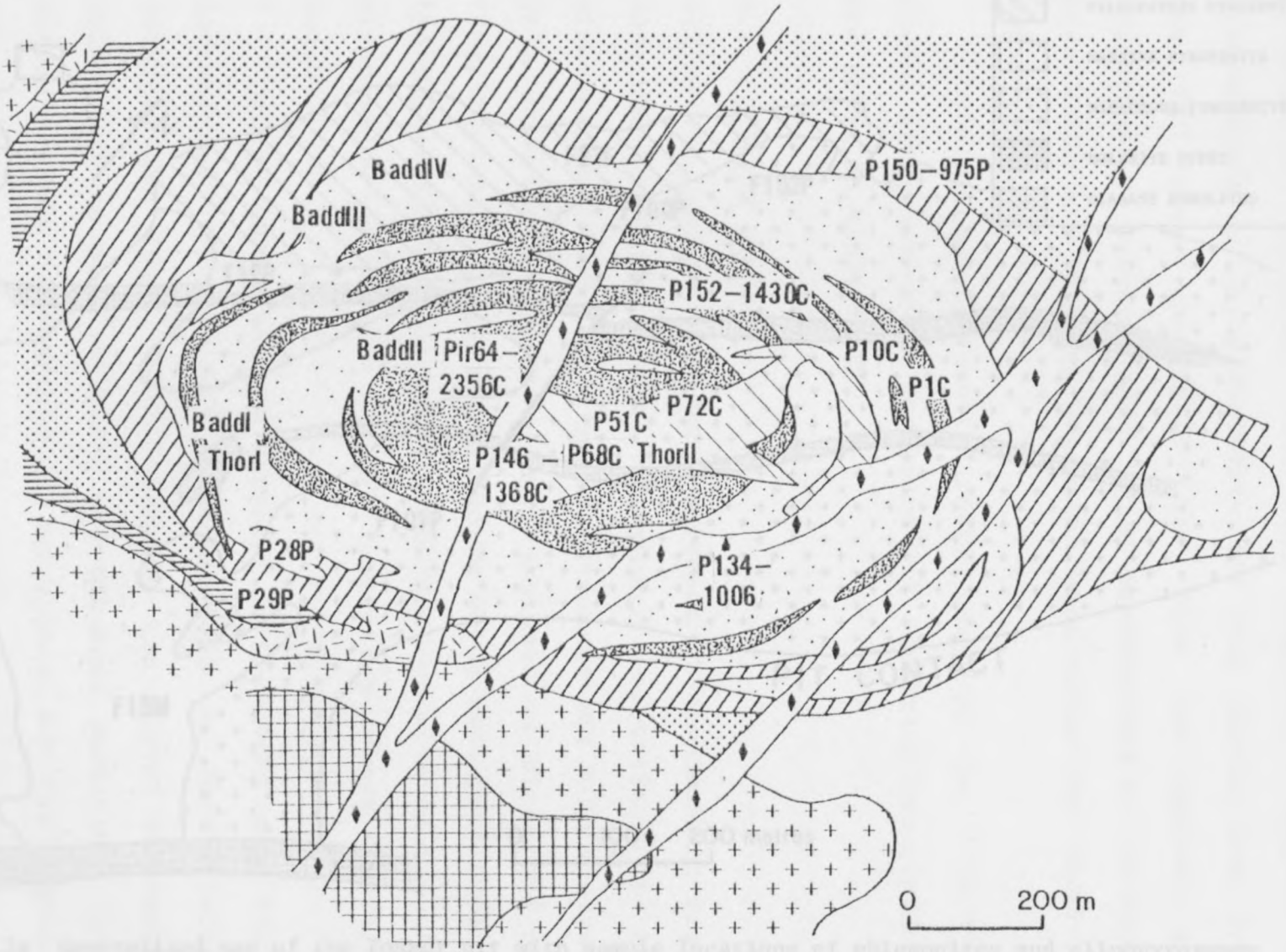


Figure 9.2 Generalized map of the PMC area with sample locations for uranothorianites, baddeleyites, carbonatites and phlogopites used in the isotopic study.

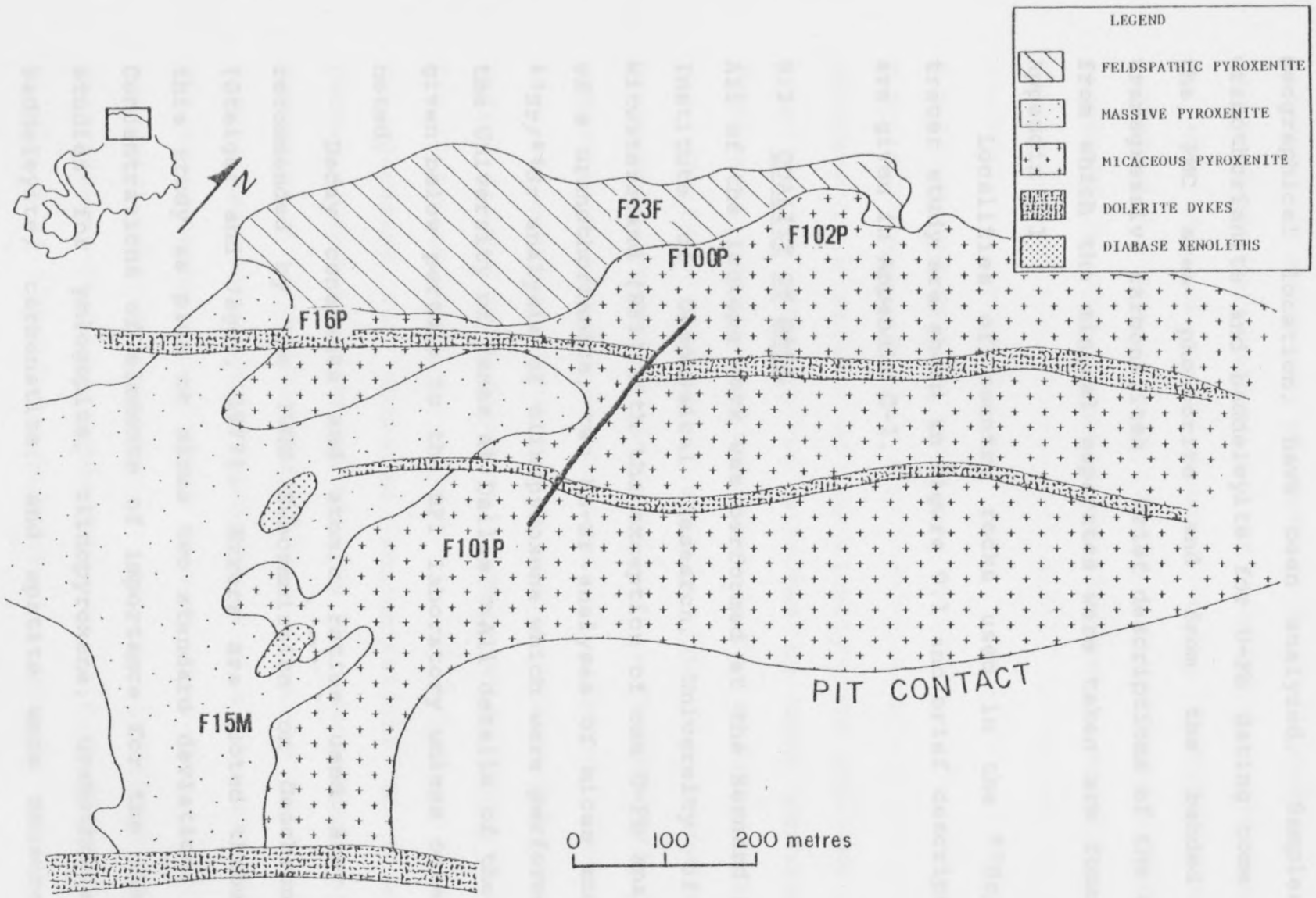


Figure 9.2a Generalized map of the Foskor pit with sample locations of phlogopites and clinopyroxenes used in the isotopic study.

geographical location, have been analyzed. Samples of uranothorianite and baddeleyite for U-Pb dating come from the PMC area phoscorite and from the banded and transgressive carbonatites. Brief descriptions of the rocks from which the mineral separates were taken are found in Appendix C-1.

Localities of country rocks used in the $^{87}Sr/^{86}Sr$ tracer study are shown in Figure 9.1 and brief descriptions are given in Appendix C-1.

9.2 QUALITY OF DATA

All of the isotope work was performed at the Bernard Price Institute of Geophysical Research, University of the Witwatersrand (BPI) with the exception of one U-Pb analysis of a uranothorianite, two Rb-Sr analyses of micas and one $^{87}Sr/^{86}Sr$ analysis of clinopyroxene which were performed at the University of Texas at Dallas. All details of the data given below pertain to the BPI laboratory unless otherwise noted.

Decay constants and atomic ratios used are those recommended by the IUGS Subcommission on Geochronology (Steiger and Jäger, 1977). Errors are quoted throughout this study as plus or minus two standard deviations (2σ). Concentrations of elements of importance for the isotopic studies for phlogopite, clinopyroxene, uranothorianite, baddeleyite, carbonatite, and apatite were measured by isotope dilution with the exception of Sr and Rb contents of

carbonatites which were measured by x-ray fluorescence using as standards carbonatite samples in which concentrations of Sr and Rb had been measured using isotope dilution technique. Details of sample preparation, chemical procedures and instrument conditions are given in Appendix C-2.

9.2.1 Rb and Sr

9.2.1.1 Accuracy

Accuracy is a measure of how closely data approach their true value. Accuracy is affected by such experimental factors as sampling and weighing errors, spike calibration, and chemical procedures and is commonly measured by performing replicate analyses of a sample of known composition, usually an international standard. Details of accuracy obtained for Rb and Sr concentrations and $^{87}Sr/^{86}Sr$ ratios in the BPI laboratory are listed in Tables C-1 and C-2 in Appendix C-2.

Accuracy for elemental concentrations in micas is better than 0.5% based on the NBS feldspar standard. The accuracy of $^{87}Sr/^{86}Sr$ ratios for micas is difficult to assess because no fully homogeneous mica standard exists. The Sr concentration of micas is much lower than that in the commonly used NBS standard, and the precision of the measurements is lower. Therefore, in this study the in-run precision of $^{87}Sr/^{86}Sr$ ratios of mica runs is taken as the accuracy of the BPI data because the in-run precision is

larger (0.57%) than accuracy measured from the NBS feldspar standard (0.05%) as listed in Table C-1 in Appendix C-2.

Accuracy of elemental concentrations determined by isotope dilution for carbonatites, pyroxenes and apatites is taken to be the same as for the micas, i.e., 0.5% as determined by the NBS standard data. In samples in which elemental concentrations were measured by x-ray fluorescence, accuracy is taken as 1.0%. The details of this method are listed in Appendix B. Accuracy of $^{87}Sr/^{86}Sr$ ratios of carbonatite, pyroxene, and apatite was determined by replicate analysis of the Eimer and Amend $SrCO_3$ sample which gave an average value of 0.70799 ± 0.00002 (2σ) with an accuracy of better than 0.01%. The accepted value for the Eimer and Amend standard given by the manufacturers of this standard is 0.7080 ± 0.0001 (2σ). The accuracy of the $^{87}Sr/^{86}Sr$ ratio of pyroxene measured at UTD by M. Halpern is inferior to that of the data obtained at the BPI. The in-run precision of sample F23F is ± 0.0012 (2σ) which may be up to 0.34% uncertainty in the measured $^{87}Sr/^{86}Sr$ ratio. This is taken as both the accuracy and precision of the UTD data on the clinopyroxene. As the upper and lower limits of these data fall within the variation in $^{87}Sr/^{86}Sr$ ratios of clinopyroxenes measured at BPI, this larger degree of inaccuracy does not affect the results of this study. All $^{87}Sr/^{86}Sr$ ratios are normalized to a $^{86}Sr/^{88}Sr$ ratio of 0.1194.

9.2.1.2 Precision

Precision of data describes how well measurements agree with one another. The best measurement of precision is the variation in machine readings, i.e., in-run precision of a single run. In-run precision is better than 0.00072 or 0.2% for $^{87}Sr/^{86}Sr$ ratios of natural strontium runs of carbonatite, pyroxene and apatite. Almost all of these analyses have an in-run precision of better than 0.1%. As mentioned earlier, one run of natural strontium at UTD has an in-run precision of 0.34%. Spiked strontium runs on pyroxene-leach material give in-run precision of $^{87}Sr/^{86}Sr$ ratios at better than 0.00008 or 0.02%.

In-run precision of spiked strontium ratios in micas is better than 0.005 or 0.57%. The lesser degree of precision in micas is due to the small concentration of strontium in the samples and the presence of an interfering Rb beam. Because of the high Rb concentration with respect to Sr, the degree of imprecision in this measurement does not affect the calculated ages significantly.

Duplicate runs of the same dissolutions are listed in Table C-3 in Appendix C-2; the results overlap. Apart from giving information on the instrument blank, found to be negligible in these two cases, such data augment the assessment of in-run precision.

9.2.1.3 Sample Heterogeneity

Reproducibility of data on a fully homogeneous sample involves the accuracy of the investigator, and has been considered above. However, duplicates of geological samples are normally separately prepared from the bulk rock and are not identical with one another in terms of mineralogical purity.

Accordingly, duplicate measurements of separate dissolutions of a sample show greater variation (Table C-4, Appendix C-2). The additional factor of possible sample heterogeneity is added to the data when different splits of the same sample are analyzed.

Duplicate mica samples (Table C-4, Appendix C-2) show that although $^{87}Sr/^{86}Sr$ ratios may vary by as much as 16.5% and elemental concentrations by as much as 22.3% (Table 9.3), calculated ages are in agreement by 0.10% and 0.25% for P134-1006K and P28P, respectively. This indicates significant sample heterogeneity in micas from Phalaborwa which is extremely common in micas (H. Allsopp, pers. comm., 1981).

Natural strontium measurements on separate dissolutions of carbonatite (Table C-4, Appendix C-2) show that while some samples give identical results within the precision of the analysis, others have greater variation. Two runs of sample P72C differ by 0.00001 but are within the 0.01% accuracy and thus have the same $^{87}Sr/^{86}Sr$ measured ratios. Carbonatite sample Pir64-2356C varies in $^{87}Sr/^{86}Sr$ by 0.015%

which is slightly greater than the 0.01% quoted accuracy. Apatite F16M has measured $^{87}Sr/^{86}Sr$ ratios which are different by 0.1%. Clinopyroxene sample F101P varies in $^{87}Sr/^{86}Sr$ by 0.03%. Sample inhomogeneity is indicated in the latter two samples.

9.2.1.4 Selection of Initial $^{87}Sr/^{86}Sr$ Ratios in Age Determination

Imprecision in mica ages also arises from arbitrary selection of the initial $^{87}Sr/^{86}Sr$ ratio used in calculating the apparent age. However, because the $^{87}Sr/^{86}Sr$ ratios in the micas are high, small differences in initial ratio make little difference in the calculated age. The exception to this is sample P29P which has a low $^{87}Sr/^{86}Sr$ ratio. Listed in Table 9.1 are apparent ages for mica samples P1C and P29P to illustrate the effects of using different initial $^{87}Sr/^{86}Sr$ ratios.

9.2.1.5 Blanks

Blank concentrations could be significant for samples with low levels of the element of interest; namely, K and Rb in clinopyroxene and Rb in carbonatite and apatite and Sr for mica. Blanks for Rb did not change over the time interval of the study as the value of 0.1 µg Rb reported for carbonatites is the same as that reported for clinopyroxenes although these were measured at least one year apart.

Table 9.1. Apparent Ages of Micas Using Different Initial $^{87}Sr/^{86}Sr$ Ratios

Sample	($^{87}Sr/^{86}Sr$) Initial	Apparent Age (m.y.)*
P1C	0.700	1991 ± 3
(measured $^{87}Sr/^{86}Sr$		
3.304±4)	0.705	1988 ± 3
	0.710	1984 ± 3
P29P	0.700	2086 ± 60
(measured $^{87}Sr/^{86}Sr$		
0.8708±50)	0.705	2026 ± 60
	0.710	1966 ± 60

*In-run precision used to calculate error in age.

Corrections for blanks of 0.1 µg Rb do not affect the calculated $^{87}Sr/^{86}Sr$ initial ratios for any of the minerals reported because of the very high Sr/Rb ratios of all the minerals. Sr blanks were not run because these are only applicable to micas; mica ages are insensitive to blanks where samples with high $^{87}Sr/^{86}Sr$ ratios are involved as in almost all of the Phalaborwa samples.

9.2.1.6 Summary of Errors in Rb-Sr Measurements

The largest contribution to error in age determination is the measurement of the concentrations of elements. Although a figure of 0.5% was quoted earlier in this section as the accuracy of data obtained by isotope dilution for BPI measurements, a more conservative estimate of 1% will be used in this study. This value of 1% reflects the difference in experience between the analysts listed in Table C-1 of Appendix C-2 and the primary investigator in this study. In addition, work for this study was done over a span of five years; lack of practice may also contribute error to the data. The quoted 1% error in age determinations includes reproducibility, standard calibration, weighing and sampling.

Errors used in calculation of isochrons for micas are taken as 1% for elemental concentrations, as discussed above, and as the in-run precision for $^{86}Sr/^{86}Sr$ ratios because the error in in-run precision is greater than any measured error in $^{87}Sr/^{86}Sr$ of standards.

Total error in determination of elemental concentrations and $^{86}Sr/^{86}Sr$ ratios for the two micas measured at the University of Texas at Dallas is given as 2% by M. Halpern (pers. comm., 1981).

Error in $^{87}Sr/^{86}Sr$ ratios of carbonatites, clinopyroxenes and apatites is taken to be the square root of the sum of squares of the accuracy and precision of each analysis. In most cases the accuracy of 0.01% is much larger than in-run precision.

9.2.2 U and Pb

Accuracy of U and Pb analyses is much more difficult to assess than the Rb-Sr method because there is no internationally accepted isotopic standard for U and Pb, particularly for U-rich samples. Error in the U-Pb ages include errors in U and Pb concentrations, in isotopic ratios of natural Pb runs, and in the initial lead isotopic composition used in the calculation of an age. Initial ratios for Pb isotopic compositions at 2050 m.y. are taken as 15.15 for $^{207}Pb/^{204}Pb$ and 15.10 for $^{206}Pb/^{204}Pb$ (Zartman and Wasserburg, 1969). The highly radiogenic nature of the samples measured in this study makes errors in initial lead composition negligible compared to other sources of error.

Estimates of error at the BPI laboratory have been obtained through discussion with Dr. Hans Welke of the BPI (pers. comm., 1981). Separate gravimetric analyses of standards over the years have shown very little variation,

on the order of less than 0.5%. However, Welke quotes an error of 1% for BPI which is based on his experience of replicate analyses of samples. This includes errors in concentrations of elements, isotopic ratios in natural runs, spike calibration and operator errors. The value of 1% error was used in this study in calculating the age of minerals from the concordia diagram.

The 1% error quoted above does not, however, include any systematic error in laboratory measurements. This systematic error, normally assessed by measurement of an international standard such as NBS-607 feldspar for Rb and Sr, may add an additional 1% error in age determination (H. Welke, pers. comm., 1981). Welke points out that this systematic error is not commonly quoted in U and Pb isotopic studies because there is no way of measuring it.

Spike calibrations were performed by BPI personnel at the beginning and at the end of the course of this study. Concentrations of U and Pb were found to increase with time according to the curves shown in Figure C.1 of Appendix C.2. Data listed in Table 9.2 were recalculated to coincide with concentrations of spike at the time of sample spiking.

Measurement of reproducibility by this investigator was through duplicate runs of one sample, uranothorianite I (Table 9.2). Samples were taken from a single dissolution and were spiked separately. These data show a 0.05% difference in Pb concentration, 0.92% difference in U concentration, and 0.32% difference in $^{207}Pb/^{206}Pb$ ratio. These are within the 1% error quoted by Welke.

The discordia was calculated by linear regression according to the method of York (1966). This straight line fit is acceptable because only small degrees of discordance are involved.

It is not possible to distinguish between episodic loss of Pb, time-dependent diffusion (Wasserburg, 1963) and continuous diffusion (Wetherill, 1963), in cases where data lie on the upper 25% of the discordia array. This is the case for the data from Phalaborwa. The intersection of the discordia with the concordia was calculated by a reiteration technique. Error in the intersection was calculated by rotating the fitted line with its associated errors in slope around the centroid of the data and recalculating the intersection of discordia and concordia of these new discordia.

9.3 GEOCHRONOLOGY

9.3.1 U-Pb Ages

Pb isotopic data and U and Pb elemental concentrations for two uranothorianites and four baddeleyites are listed in Table 9.2 along with the calculated ages. The data are plotted on a concordia diagram in Figure 9.3. All samples show some discordance; a maximum of 7% discordance is found in uranothorianite I from banded carbonatite. There is no correlation in degree of discordance with mineral or rock type (Table 9.2, Figure 9.3).

TABLE 9.2 U-Pb Data for Uranothorianite and Baddeleyite

Sample			Concentrations (ppm)		Pb Isotopic Ratios			Concordia Ratios		Calculated Ages (my)		
Type	Rock Type	Sample #°	U	Pb	$\frac{^{206}Pb}{^{204}Pb}$	$\frac{^{207}Pb}{^{204}Pb}$	$\frac{^{208}Pb}{^{204}Pb}$	$\frac{^{207}Pb}{^{235}U}$	$\frac{^{206}Pb}{^{238}U}$	$\frac{^{207}Pb}{^{206}Pb}$	$\frac{^{207}Pb}{^{235}U}$	$\frac{^{206}Pb}{^{238}U}$
U-thorianite	BC	Ia*	118900	88360	10000	1260	1403	5.869	0.3429	2018	1956	1885
U-thorianite	BC	Ib*	120000	88400	10000	1256	1400	5.843	0.3374	2011	1946	1881
U-thorianite	TC	II	137700	86950	9825	1258	8713	6.339	0.3631	2053	2023	1994
Baddeleyite	PH	I	420.9	150.4	3383	431.8	40.63	6.312	0.3649	2017	1989	1997
Baddeleyite	TC	II	2052	5939	13000	1660	48.19	6.203	0.3552	2053	2003	1957
Baddeleyite	PH	III	1790	468.3	666.6	97.79	7511	6.107	0.3493	2055	1985	1920
Baddeleyite	PH	IV	164.5	451.7	3158	409.6	36.16	6.432	0.3718	2037	2031	2026
Thorianite†	C		115400	455300	4951	612	2843	-	-	2060	2020	2000

° Sample numbers and locations listed in Appendix C.1

† Holmes and Cahen (1956)

BC Banded Carbonatite

TC Transgressive Carbonatite

PH Phoscorite

C Undesignated Carbonatite

* Thorianite duplicates from same dissolution

a) run at Bernard Price Institute

b) run at University of Texas at Dallas

$\lambda^{238}U = 1.55125 \times 10^{-10}$ yr.

$\lambda^{235}U = 9.8485 \times 10^{-10}$ yr.

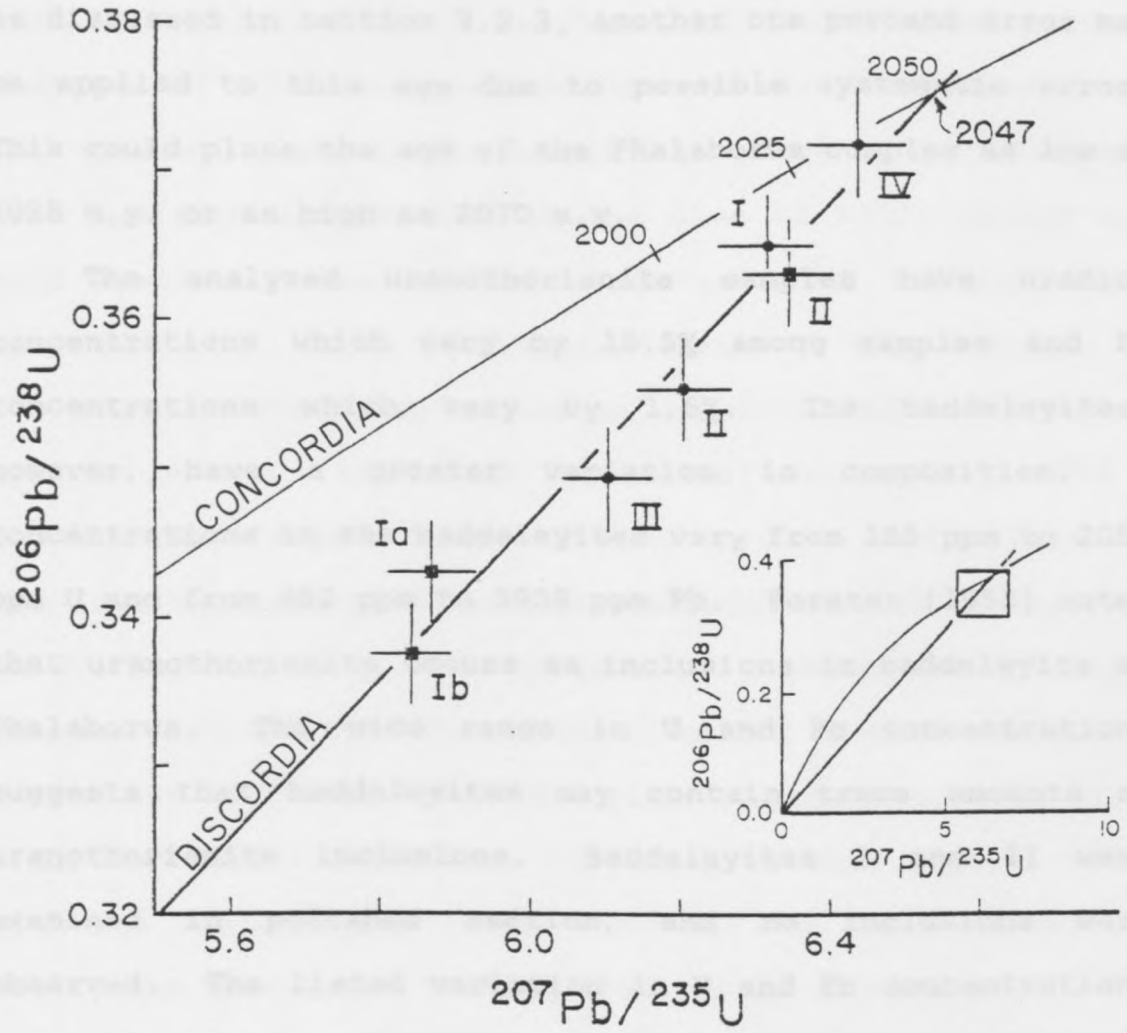


Figure 9.3 Concordia diagram showing compositions of uranothorianites (squares) and baddeleyites (circles) from Phalaborwa. Intersection of the isochron with the concordia curve is at 2047 +11/-8 m.y.

The data define an isochron (MSUM = 0.307) which intersects the concordia curve at 2047 + 11/-8 m.y. This error takes into account only scatter in the data. However, as discussed in section 9.2.3, another one percent error may be applied to this age due to possible systematic error. This could place the age of the Phalaborwa complex as low as 2025 m.y. or as high as 2070 m.y.

The analyzed uranothorianite samples have uranium concentrations which vary by 15.5% among samples and Pb concentrations which vary by 1.6%. The baddeleyites, however, have a greater variation in composition. U concentrations in the baddeleyites vary from 165 ppm to 2052 ppm U and from 452 ppm to 5939 ppm Pb. Forster (1958) noted that uranothorianite occurs as inclusions in baddeleyite at Phalaborwa. The wide range in U and Pb concentrations suggests that baddeleyites may contain trace amounts of uranothorianite inclusions. Baddeleyites I and II were examined in polished section, and no inclusions were observed. The listed variation in U and Pb concentrations may therefore represent variation in baddeleyite compositions. Baddeleyite samples with lower concentrations of U and Pb show smaller degrees of discordance. The implications of the variation in composition are not explored in this study.

9.3.2 Rb-Sr Ages of Micas

9.3.2.1 Rb-Sr Data

Tables 9.3a and b list Rb and Sr data from eight hand specimens taken from carbonatite, phoscorite and various textures of micaceous pyroxenite. Gross discrepancies in the apparent ages of the micas are present, both between hand specimen samples and in the case of P29P, within one hand specimen. Ten of the micas are from the same hand specimen, P29P, which is discussed later in this chapter.

Nine of the micas define an isochron (MSUM = 1.36) of 2012 ± 19 m.y. (2σ) with an initial ratio of 0.70558 ± 0.00724 (2σ) (Figure 9.4). Several points on the isochron are from the same hand specimen but are counted as separate points because of the heterogeneity in composition within samples (Table 9.3). The isochron method does not provide a definitive initial $^{87}Sr/^{86}Sr$ ratio because of the high $^{87}Rb/^{87}Sr$ ratios. However, the value of this initial ratio with its accompanying large error will be used in section 9.4 in the discussion of $^{87}Sr/^{86}Sr$ ratios as tracers.

Micas which do not belong on the isochron defining the age of 2012 m.y. are generally older in apparent age. Two samples yield younger apparent ages. Most of these data are from sample P29P.

9.3.2.2 Removal of Contaminating Sr-rich Material

Total Sr in the micas analyzed from Phalaborwa ranges from 13 to 295 ppm Sr. The large percentage of variation in

Table 9.3a Isotopic Data for Micas

	^{86}Sr	$^{87}Sr/^{86}Sr$	Sr^{total}	^{87}Rb	Rb^{total}	$^{87}Rb/^{86}Sr$ atomic	$^{87}Sr^{*}$	$\frac{Age^{+}}{R_o=.705}$	Rock Type
P1C*	2.189	3.304±4	27.88	201.0	723.6	90.77	5.755	1988±3	Transgressive carbonatite
F16P	0.6318	11.1774±6	13.02	217.7	783.7	340.7	6.694	2132±1	Micaceous pyroxenite
PIR64-2395P	0.4294	16.761±4	11.25	224.5	808.2	516.7	6.974	2155±1	Glimmerite fragment in pyroxenite
P28P	1.953	3.1987±7	24.67	170.9	615.2	86.65	4.927	2001±1	Micaceous pyroxenite
P28P	1.821	3.342±5	23.26	168.9	608.0	90.76	4.858	1996±13	Micaceous pyroxenite
P134-1006K	2.402	3.157±3	30.78	207.6	747.4	85.41	5.958	1994±4	Phoscorite
P134-1006K	2.987	2.709±1	36.27	211.0	759.6	69.84	6.055	1992±2	Phoscorite
P29P(a)*	28.59	0.8708±50	294.6	164.3	591.5	5.681	4.795	2026±60	Glimmerite
F100P°	5.186	1.908±4	58.81	217.5	783.0	41.46	6.311	2014±6	Micaceous pyroxenite
F102X°	1.299	5.912±12	19.93	230.2	828.7	175.2	6.842	2062±5	Micaceous pyroxenite xenolith

*Samples not washed in ultrasonic bath.
Errors are two standard deviations.
$^{+}\lambda = 1.42 \times 10^{-11}$ (Steiger and Jäger, 1977); error calculated using in-run precision of $^{87}Sr/^{86}Sr$.
°Run at UTD by M. Halpern.

Table 9.3b. Isotopic data of sample P29P.

	^{86}Sr	$^{87}Sr/^{86}Sr$	Total Sr	^{87}Rb	$^{87}Rb/^{86}Sr$ atomic	$^{87}Sr^*$	Apparent Age (m.y.) R_o=.705
a(1) SCE	28.59	0.8708±50	294.6	164.3	5.681	4.802	2026±60
a(2) SCE	3.7990	1.8601±5	42.90	173.8	45.22	4.438	1776±1
a(3) HLA	4.557	1.8961±8	51.62	175.3	38.03	5.489	2171±1
b(1) SCE	18.12	0.9442±11	188.0	183.8	10.03	4.383	1661±7
b(2) SCE	1.276	4.630±4	17.94	173.3	134.26	5.065	2029±2
b(3) HLA	2.391	3.1429±8	30.07	181.3	74.96	5.895	2254±1
c(1) SCE	0.14	41.98±60	7.197	171.5	1211	5.844	2360±33
c(2) SCE	0.3795	14.063±60	8.917	151.8	390.9	5.125	2340±11
c(3) HLA	47.71	0.7983±2	488.1	144.2	2.988	4.502	2165±4
c(4) HLA	1.54	4.0486±3	20.761	173.7	111.5	5.207	2081±1

Analysts: SCE = S. C. Eriksson
HLA = H. L. Allsopp

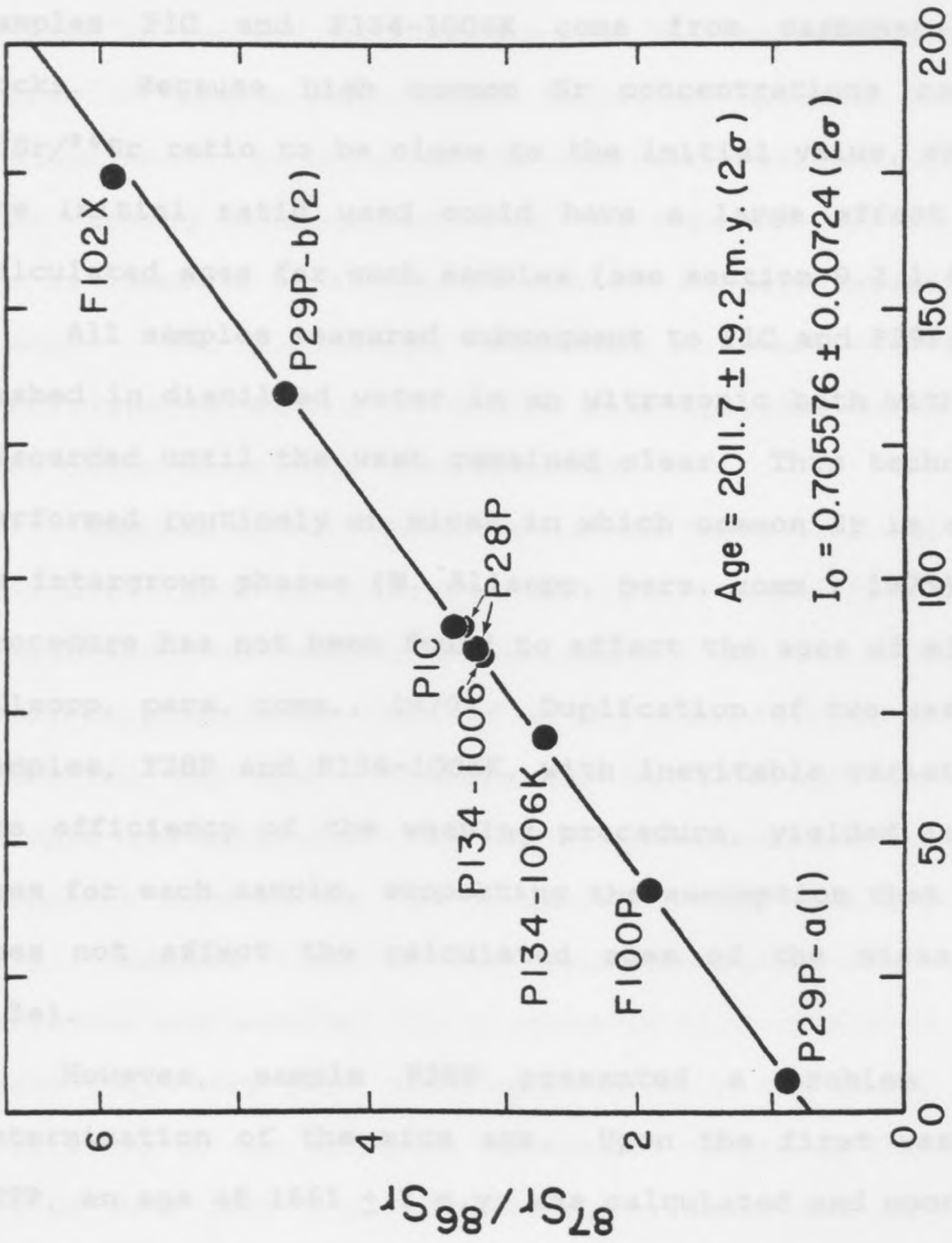


Figure 9.4 Isochron for nine phlogopite samples from Phalaborwa.

total Sr suggests that a Sr-rich phase may be present in the micas. The rocks at Phalaborwa are commonly apatite-rich and many rocks contain cross-cutting carbonatite dykelets. Samples P1C and P134-1006K come from carbonate-bearing rocks. Because high common Sr concentrations cause the $^{87}Sr/^{86}Sr$ ratio to be close to the initial value, choice of the initial ratio used could have a large effect on the calculated ages for such samples (see section 9.2.1.4).

All samples measured subsequent to P1C and P29P(a) were washed in distilled water in an ultrasonic bath with washes discarded until the wash remained clear. This technique is performed routinely on micas in which common Sr is enriched as intergrown phases (H. Allsopp, pers. comm., 1975). This procedure has not been found to affect the ages of micas (H. Allsopp, pers. comm., 1979). Duplication of two washed samples, P28P and P134-1006K, with inevitable variations in the efficiency of the washing procedure, yielded identical ages for each sample, supporting the assumption that washing does not affect the calculated ages of the micas (Table 9.3a).

However, sample P29P presented a problem in the determination of the mica age. Upon the first washing of P29P, an age of 1661 $\pm$ 7 m.y. was calculated and upon dating of a different portion of the P29P sample, an age of 2360 $\pm$ 33 m.y. was obtained (Table 9.3b). The dating of P29P was repeated several times, as discussed below, by this investigator and by H. Allsopp to determine the cause of

this discrepancy in ages. Descriptions of sample preparation for the various samples of P29P are given in Appendix C-3; results of the isotopic measurements are listed in Table 9.3b. The purpose in performing the various types of sample preparation listed in Appendix C-3 was to determine if, in spite of the conclusion reached previously, the washing technique affected the apparent age of the mica or if minerals of different ages are actually present in the sample. Dr. H. Allsopp performed at least one dating of each type of sample to ensure that operator error was not the cause of the age discrepancies.

Samples of P29P labelled (a) in Table 9.3b and Appendix C-3 are flakes of P29P with no visible impurities but which experienced no washing or grinding. Ages from this group vary significantly from 1776 m.y. to 2171 m.y. Samples labelled (b) are characterized by a slight grinding of sample and extensive cleaning in an ultrasonic bath of H_2O. Apparent ages of the (b) group range from 1661 m.y. to 2254 m.y. Samples labelled (c) have undergone both extensive grinding and washing, the purpose of this treatment being to date only very pure mica, particularly any which might be resistive to the grinding treatment. Micas of the (c) group range from 2081 m.y. to 2421 m.y. There are no "younger" ages in this latter group.

Because no obvious cause and effect of washing is evident from Table 9.3, a more detailed study of sample P29P was required and is discussed below.

9.3.2.3 Compositional Variation

Figures 9.5a through 9.5e show apparent ages of the various P29P fractions plotted against (a) ^{87}Rb, (b) total Sr, (c) $^{87}Rb/^{86}Sr$, (d) $^{87}Sr/^{86}Sr$, and (e) radiogenic ^{87}Sr.

The scatter of points and the overlap of unwashed, washed, and finely-ground samples suggest that the washing procedure does not preferentially remove any component to give the variation in ages. Figures 9.5a through 9.5d show no correlation and so preferential removal or addition of these components has not occurred during processing. Figure 9.5e shows a broad correlation in amount of radiogenic Sr with age. This correlation does not reflect washing technique as washed samples lie at the lowest and highest values of radiogenic Sr. However, with one exception, the samples labelled (c) which were finely ground and washed show the same pattern as fractions (a) and (b), but are offset to higher ages. This pattern may reflect the gain or loss of radiogenic Sr through natural causes or may be explained by mixing of a highly radiogenic, older component with micas of younger ages. These two possibilities will be explored in the next two sections.

9.3.2.3.1 Alteration of Micas

There is experimental evidence that, under various conditions, ^{87}Rb, ^{87}Sr radiogenic, and common Sr may be added to or removed from a mica lattice. From experiments under various pressure and temperature conditions and

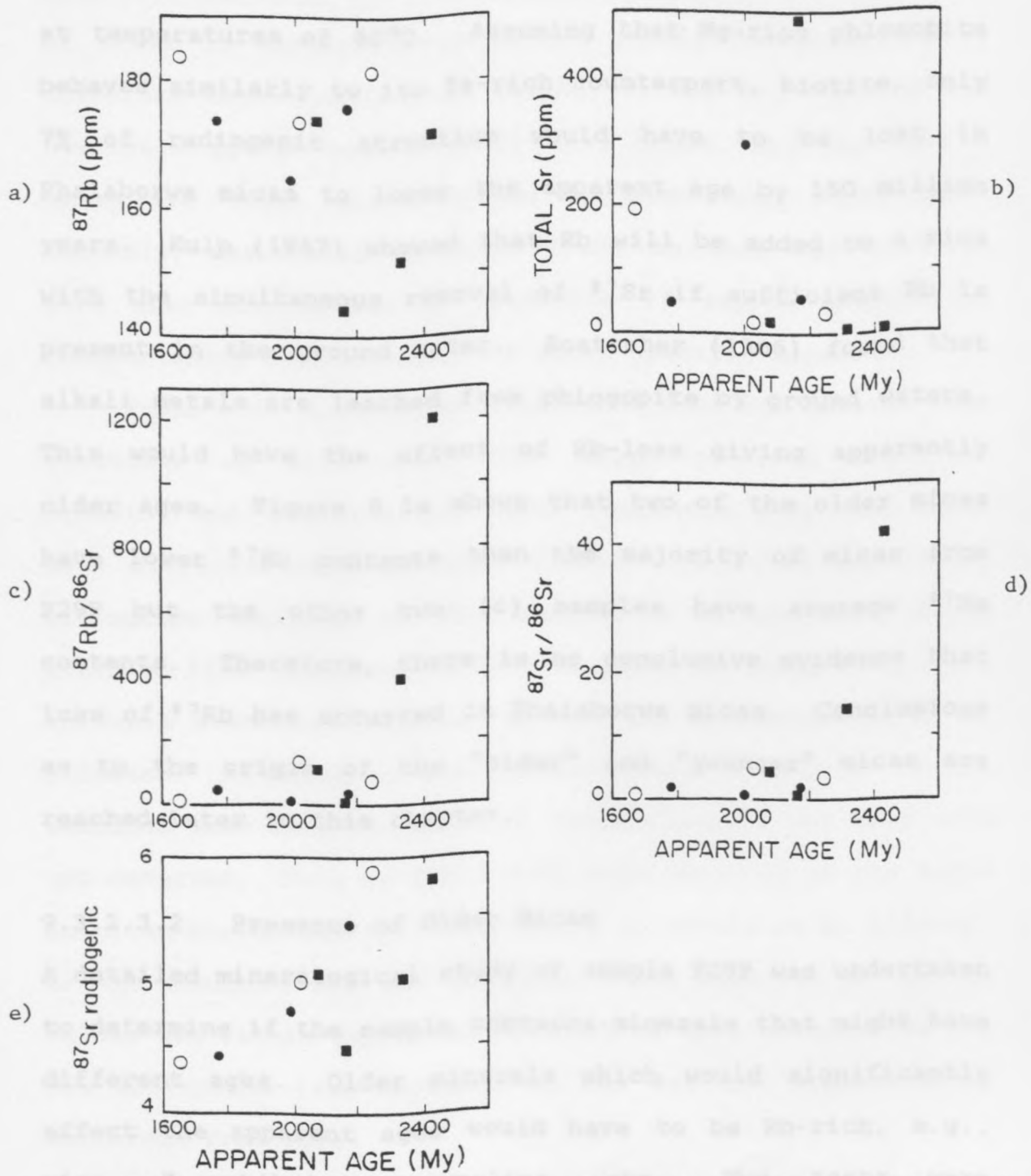


Figure 9.5 Apparent ages for various analyses of sample P29P (Table 9.3b) versus a) ^{87}Rb, b) total Sr, c) ^{87}Rb/^{86}Sr, d) ^{87}Sr/^{86}Sr and e) ^{87}Sr radiogenic. Samples labelled a in Table 9.3b and text are denoted by closed circles, those labelled b by open circles and those labelled c by squares.

various aqueous fluid compositions, McNutt (1964) calculated from diffusion equations that Precambrian biotites should lose 50% of their radiogenic strontium in 1000 million years at temperatures of 60°C. Assuming that Mg-rich phlogopite behaves similarly to its Fe-rich counterpart, biotite, only 7% of radiogenic strontium would have to be lost in Phalaborwa micas to lower the apparent age by 150 million years. Kulp (1967) showed that Rb will be added to a mica with the simultaneous removal of ^{87}Sr if sufficient Rb is present in the ground water. Boettcher (1966) found that alkali metals are leached from phlogopite by ground waters. This would have the effect of Rb-loss giving apparently older ages. Figure 9.5a shows that two of the older micas have lower ^{87}Rb contents than the majority of micas from P29P but the other two (c) samples have average ^{87}Rb contents. Therefore, there is no conclusive evidence that loss of ^{87}Rb has occurred in Phalaborwa micas. Conclusions as to the origin of the "older" and "younger" micas are reached later in this chapter.

9.3.2.3.2 Presence of Older Micas

A detailed mineralogical study of sample P29P was undertaken to determine if the sample contains minerals that might have different ages. Older minerals which would significantly affect the apparent ages would have to be Rb-rich, e.g., mica, K-amphibole, tourmaline, etc. Two tests were performed. In the first, numerous grains of the highly ground and washed fractions labelled (c) were analyzed by

electron microprobe to determine if mica with a distinct chemical character (representing older material) might be present. Smith et al. (1978) found two compositional types of micas in kimberlite which are partly characterized by different concentrations of Fe, Mg, Ti and Cr. Allsopp and coworkers (pers. comm., 1982) have found that the Type I micas are often characterized by anomalously high ages. Secondly, associated minerals found in this (c) fraction were also microprobed to determine if sample preparation inadvertently concentrated any other specific minerals.

Table 9.4a and b lists microprobe data for several fine fractions of mica from P29P which received different cleaning and grinding treatment (Appendix C-3) and which gave different apparent ages (Table 9.3b). An additional microprobe analysis of this sample on an unwashed, large grain of P29P (labelled P29H/A) is given in Table 5.4. Data in Table 9.4a were obtained on the UTD microprobe by S. C. Eriksson. Although no analyses are reported for Cr or Ni, searches were made for both of these elements but they were not detected. Data in Table 9.4b were obtained on the Anglo American microprobe in Johannesburg on behalf of H. Allsopp. Cr was analyzed but not detected. The measured Ni and Na values are within experimental error of data obtained on the UTD microprobe (see Appendix B) and are not significantly different from zero.

An average of four analyses of P29H/a (Table 5.4) gives an Fe/(Fe+Mg) = 0.16. Large, washed grains labelled b(3) in

Table 9.4a. Microprobe data for various fractions of glimmerite sample P29P, by S. Eriksson University of Texas at Dallas microprobe.

	b(3)			c(3)	c(4)
	1(2)	2(3)	3(2)	(2)	(3)
SiO_2	42.02	42.14	41.84	41.80	42.35
TiO_2	1.55	1.60	1.64	1.57	1.18
Al_2O_3	11.16	10.67	10.62	11.17	10.29
FeO	8.27	8.15	8.37	6.80	7.93
MgO	23.22	22.92	22.97	23.66	23.75
K_2O	10.18	10.38	10.14	10.20	10.10
Total	96.40	95.84	95.58	95.20	95.42
Number of cations based on 22 oxygens.					
Si	6.017	6.054	6.031	6.003	6.089
Al	1.872	1.807	1.803	1.890	1.743
Ti	0.160	0.172	0.178	0.169	0.127
Fe	0.984	0.979	1.009	0.816	0.953
Mg	4.928	4.905	4.938	5.068	5.051
K	1.860	1.902	1.863	1.869	1.853
Site Occupancy					
Z	7.889	7.861	7.834	7.893	7.832
	(0.111)	(0.139)	(0.166)	(0.107)	(0.168)
Y	6.072	6.056	6.125	6.053	6.131
X	1.860	1.902	1.863	1.869	1.853
Fe/(Fe+Mg)	.17	.17	.17	.14	.16

Table 9.4b. Microprobe data for various fractions of glimmerite sample, P29P, Anglo American microprobe.

	29/Ha	Pal 29/H a Av. of 3	Pal 29/H b Av. of 3	Pal 29/H c(3) Av. of 3	c(4) Av. of 3
SiO_2	40.36	40.60	40.06	40.74	40.56
TiO_2	1.35	1.31	1.40	1.28	1.37
Al_2O_3	10.77	10.64	10.48	10.36	11.08
Cr_2O_3	0.00	0.00	0.00	0.00	0.00
FeO	7.79	7.86	7.98	7.61	6.99
MnO	0.04	0.05	0.04	0.05	0.02
NiO	0.02	0.01	0.01	0.02	0.00
MgO	23.61	23.39	23.44	23.44	23.40
CaO	0.00	0.00	0.00	0.01	0.00
Na_2O	0.11	0.09	0.10	0.11	0.10
K_2O	10.29	10.03	10.34	10.10	10.18
Total	94.34	93.98	93.85	93.72	93.70

Table 9.3 show similar Fe/(Fe+Mg) ratios. Two fine fractions, c(3) and c(4) which were ground extensively and sieved, show Fe/(Fe+Mg) ratios of 0.14 and 0.16, respectively; these values are significantly different and may indicate the presence of mica of slightly lower FeO content (Sample c(3)). The data in Table 9.4b show slightly lower Fe/(Fe+Mg) ratios of 0.15 and 0.14 for samples c(3) and c(4), respectively. Comparison of standard data between the two laboratories shows the data to be the same (Table B.1, Appendix B). Although slight compositional zoning may be present in sample P29P, this is characteristic of phlogopites throughout the complex. Other micas studied from Phalaborwa (Chapter 5) exhibit compositional zoning of Fe and Mg which are as great or larger than that shown among various fractions analyzed from sample P29P. Sample P134-1006K (Table 5.4) shows more extreme zoning from Fe/(Fe+Mg) = 0.17-0.26 and has an apparent age of 1993 $\pm$ 4 m.y. Other elements, such as Ti, Ni, Cr and Na, show no differences among analyses of P29P. Therefore, there is nothing inherent in the composition of the micas of P29P to indicate the presence of micas of different ages. The two other samples in Table 9.3a which gave older apparent ages, F16P and Pir64-2395P were also probed to detect possible compositional differences in older micas. The data (Table 5.4) show the micas to be similar to other phlogopites of the Phalaborwa complex.

The possibility of older micas cannot be excluded, however, because older micas may not have possessed or maintained a different chemistry. Whether micas can maintain their isotopic character at elevated temperatures is a controversial topic. Xenolithic mica in kimberlites may retain older ages (H. Allsopp, pers. comm., 1981); they also exhibit a chemical distinction.

9.3.2.3.3 Presence of Exotic Material

Descriptions of various fractions analyzed isotopically (Appendix C-3) show that long grinding and washing did not yield a completely pure phlogopite sample for dating. These minerals found in trace amounts and taken from samples c(3) and c(4) were analyzed by microprobe; their compositions are listed in Table 9.5. The majority of minerals analyzed were apatite with fewer grains of diopside. However, the minerals amphibole, olivine, orthopyroxene, and magnetite, not normally associated with micaceous pyroxenites or glimmerite, were found in this sample. The magnetite has concentrations of TiO_2, Al_2O_3 and Cr_2O_3 which are below detection limit. This may be a breakdown product of olivine or phlogopite rather than an igneous magnetite.

The olivine has higher forsterite content (Fo_{93}) than any other olivine analyzed from the Phalaborwa complex and is comparable in forsterite content to olivines from mantle-derived, ultramafic nodules found in kimberlites (Boyd, 1975; Danchin, 1979). Similarly, orthopyroxene from P29P is

Table 9.5

Microprobe Analyses of Minerals
in Trace Amounts in Sample P29P-c(3) and c(4)

	Amphibole (3)	Diopside (3)	Olivine (3)	Opx (3)	Magnetite (2)
SiO_2	56.34	55.17	42.15	59.34	1.00
TiO_2	0.13	0.39	0.00	0.00	0.00
Al_2O_3	0.49	0.00	0.00	0.75	0.00
Cr_2O_3	0.00	0.00	0.00	0.39	0.00
FeO	6.35	3.22	7.34	3.87	96.52
MgO	19.36	17.05	51.53	36.16	0.42
CaO	6.55	25.54	0.00	0.47	-
Na_2O	5.12	0.00	-	-	-
K_2O	2.16	-	-	-	-
Total	96.50	101.34	101.02	100.98	97.94
Number of cations on the basis of:					
	24 0	6 0	4 0	6 0	
Si	7.691	1.988	1.006	1.992	
Al	0.080	0.000	0.000	0.000	
Cr	0.000	0.000	0.000	0.038	
Ti	0.013	0.011	0.000	0.000	
Fe	0.718	0.097	0.147	0.111	
Mg	3.939	0.916	1.837	1.814	
Ca	0.957	0.986	0.000	0.014	
Na	1.339	0.000	-	-	
K	0.375	-	-	-	
Fe/Fe+Mg	.15	.10	.07	.06	

extremely Mg-rich and contains appreciable Al_2O_3 and Cr_2O_3, suggesting crystallization from a different magma or under different P,T conditions than the majority of pyroxenes at Phalaborwa.

The amphibole from P29P contains Ca, Na, and K. The magnesioriebeckite composition is somewhat similar to the amphibole found in fenitized country rock at Phalaborwa (P146-440N) (Table 5.7) but the amphibole from P29P is much lower in Fe/(Fe+Mg) with a ratio of 0.15 versus 0.35 in P146-440N; K and Na are also higher in the glimmerite sample. The magnesioriebeckite contains 2.16% K_2O and, therefore, would contain substantial amounts of Rb. However, if the amphibole is the cause for the older apparent ages, it would have been present in sufficient quantity to have been observed optically in thin section as its green color and crystal habit are distinctive. Therefore, although K-amphibole is present, it is not present in sufficient quantities to have mixed with phlogopite to give the ages found in Table 9.3.

9.3.2.3.4 Xenoliths in the Phalaborwa Complex

Although chemically and texturally sample P29P resembles the majority of glimmerites in the main Phalaborwa complex, the presence of a wide suite of accessory minerals in a hand sample of a few hundred grams suggests a complex history for this sample. It should be noted that a thin section was examined carefully to detect these minerals. Small

inclusions appear but are too small to be identified optically. They have only been identified after separation and probing. The presence of high-Mg orthopyroxene and olivine suggests that these minerals did not form at conditions of the overall complex at the level studied. A xenolithic component, whether a precipitate from a Phalaborwa magma at depth or as a non-cognate xenolith from mantle or crust, may account for micas of older age in sample P29P. Such micas appear not to have had a unique chemical composition but retained, at least in part, their isotopic characteristics. The majority of mica in sample P29P could have crystallized with the rest of the main complex, thus possessing the mineral-chemistry characteristics of other micas in the complex; the trace amounts of diopside, apatite and possibly magnetite crystallized at this time.

There is supporting evidence for xenolithic components at Phalaborwa. High concentration of Ni is present in olivine found in a sample very near the outer contact of the complex [Sample P(79a)X, Table 5.6]. No other olivines from phoscorite and carbonatite approach this sample in Ni content. Brandt (1948) reported the presence of orthopyroxene in phoscorite but this has generally been disregarded by subsequent workers at Phalaborwa as a misidentification because of the petrologic association. However, on the basis of Brandt's work and the presence of other xenoliths found in this study, more xenocrysts of orthopyroxene may be present in the complex.

Although there is no unequivocal evidence for the presence of older minerals in the Phalaborwa complex, the presence of exotic phases suggests that older micas may account for the ages obtained in sample P29P. The wide range in apparent ages are then a result of mixing different proportions of younger and older phases. The lengthy grinding of samples labelled (c) appear to have concentrated the older mica which was resistant to the grinding technique.

9.3.2.3.5 Mixing of Minerals to Form Isochrons

There is a possibility that the isochron for the nine micas is a mixing line rather than a true isochron in which minerals of different composition crystallized at the same time. Two possibilities exist for mixing of mica with extraneous material. Mica with high Rb/Sr ratios coprecipitated with low-Rb apatite. In this case the apatite and mica would be in isotopic equilibrium and the apatite would maintain an $^{87}Sr/^{86}Sr$ very close to the initial $^{87}Sr/^{86}Sr$ ratio. The "isochron" or mixing line would then represent very nearly the true age of the micas.

In the second case, mica which may or may not be older than later carbonatite could have been permeated by carbonate-rich fluids derived from intrusion of the carbonatite. Carbonate fluid could penetrate grain boundaries and may not easily be removed by grinding and washing. Because of the intimate association of these

fluids with micas, they may be a more significant contaminant than apatite described above.

The carbonatites generally have lower initial $^{87}Sr/^{86}Sr$ than clinopyroxenites, as discussed later in this chapter, but as Table 9.1 illustrates, apparent ages of micas with high Rb/Sr ratios will be relatively unaffected by mixing of mica with a component having a slightly different initial $^{87}Sr/^{86}Sr$ ratio. The differences in initial $^{87}Sr/^{86}Sr$ ratios of concern here are between 0.704 and 0.710. Therefore, consideration of the scatter in mica ages resulting from mixing of two or more components does not affect the apparent ages significantly nor does it account for the discrepancies in apparent ages of micas.

9.3.2.4 Unsolved Problems

The two younger apparent ages obtained on sample P29P have not been explained. Although groundwater alteration can cause lowering of apparent ages in micas at Phalaborwa (see vermiculite analysis, Table 9.14), it would be unjustifiable to invoke this mechanism for these two specific samples because of the intimate association with very old micas. The possibility of experimental error cannot be ruled out, specifically weighing errors of sample or spike. One purpose in performing experiments, labelled (c) in Table 9.4 which were performed in cooperation with Dr. H. L. Allsopp, was to take extreme care throughout the procedure to exclude such errors. No younger ages were found in this group.

Therefore, taking the above considerations and the overall purpose of this thesis into account, the younger ages are interpreted as being due to experimental error.

The isotopic data do not exclude the possibility that intrusion of pyroxenite occurred around 2150 m.y. or earlier. There is a suggestion of an isochron (MSUM = 0.846) of four phlogopites with an age of 2152 ± 24 m.y. (2σ) but two of these points are from sample P29P which yielded a range of apparent ages. Because this same sample also yielded older ages of 2360 m.y. and 2340 m.y., the ages around 2150 m.y. could be geologically meaningless artifacts of mixing micas of 2360 m.y. and 2011 m.y.

The problem of older micas remains unsolved although steps were taken to find the source of apparent age differences. The possibility exists that multiple intrusion of magma forming pyroxenite occurred or that intrusion producing the pyroxenites occurred at around 2350 m.y. and that some mica ages were reset by intrusion of carbonatite at around 2012 m.y. However, given the agreement in ages of numerous samples with cumulus textures and the span of time of approximately 300 m.y. between possible intrusive events, based on Rb-Sr dating, the intrusion of the Phalaborwa complex is considered as taking place as one intrusive event around 2012 ± 19 m.y. Although widely disparate ages have been obtained on different events in kimberlite pipes (Allsopp, pers. comm., 1981), most workers on kimberlites do not accept that a single conduit is operative over wide time intervals.

More detailed study of mica ages is needed. The main purpose in dating the Phalaborwa complex was to define an age to use in calculating initial $^{87}Sr/^{86}Sr$ ratios to aid in the determination of the petrogenesis. The U-Pb data and the bulk of the Rb-Sr data define an age, as discussed below, which is sufficient for this purpose.

9.3.3 Age of Country Rocks

Three country rocks were also dated by Rb-Sr method utilizing muscovite and one whole-rock sample with very high Rb/Sr ratio. Data for these rocks are given in Table 9.6. Sample locations are noted in Figure 9.1. The significance of these rocks in this study will be discussed in section 9.4.2.3.2 on mixing of magma with upper crust.

The ages were calculated using the measured $^{87}Sr/^{86}Rb$ assuming an initial $^{87}Sr/^{86}Sr$ ratio of 0.705 and represent minimum ages for the country rocks. Muscovite pegmatoids yielded ages of 2647 ± 4 and 2725 ± 1 m.y. and pink granite gave an apparent age of 2707 ± 9 m.y. The maximum age of 2725 m.y. was used as the minimum age of country rocks in later calculations.

Biotite from the suite of country rocks collected in this study was measured by J. Barton (pers. comm., 1979) who obtained an age of 2811 m.y. for the biotite from granite. From other unpublished data which yields an errorchron (MSUM = 2.14) of 3266 ± 113 m.y. (2σ), Barton suggested that country rocks of the Phalaborwa area may be much older.

Table 9.6. Sr-Rb Data for Country Rocks

Sample		^{87}Rb (ppm)	^{86}Sr (ppm)	$^{87}Sr/^{86}Sr_{measured}$	$^{87}Rb/^{86}Sr$	Apparent Age*
C8V	muscovite	245.8	0.3410	28.82 ±1	68.01	2725±1 m.y.
C12V	muscovite	120.2	1.0967	4.856±7	27.16	2647±4 m.y.
C(27a)B	granite	50.12	1.328	2.167±5	11.50	2707±9 m.y.
C13B+	biotite	183.93	2.545	3.611	71.43	2811 m.y.

*$^{87}Sr/^{86}Sr$ initial ratio of 0.705 used for calculation of age.

+J. Barton, personal communication, December 1979, error in $^{87}Sr/^{86}Sr$ not available.

Error calculated using in-run precision of $^{87}Sr/^{86}Sr$ analyses.

9.3.4 Age of the Phalaborwa Complex

The age of 2012 ± 19 m.y. obtained by the Rb-Sr method on micas and the age of 2047 ± 23 m.y. based on the U-Pb method dating of uranothorianite and baddeleyite agree within experimental error.

Inherent differences in the U-Pb and Rb-Sr methods exist and may bring the ages obtained by the two methods into closer agreement. The half-lifes of ^{238}U and ^{235}U are amenable to accurate determination and are well established. However, as discussed earlier, the error in determination of elemental concentrations is less well known in this method. On the other hand, from use of international standards, we have a very good knowledge of error in elemental determination in Rb and Sr. However, the decay constant for ^{87}Rb is not well known and the internationally accepted value changes every few years. BPI uses the accepted value of $\lambda = 1.42 \times 10^{-11}$; however, many laboratories use $\lambda = 1.41 \times 10^{-11}$ at the present time and, as recently as 1975, a value of $\lambda = 1.39 \times 10^{-11}$ was accepted. The lower values of the ^{87}Rb half-life have the effect of raising the calculated ages of the micas which would place them in closer agreement with the U-Pb ages.

A "best age" for the Phalaborwa complex is taken as an average of the ages obtained by the two methods, i.e., the age of the Phalaborwa complex is 2030 ± 18 m.y. The age obtained from the Rb-Sr method will be used in correction of $^{87}Sr/^{86}Sr$ ratios in a later section because of internal consistency of the system.

9.4 $^{87}SR/^{86}SR$ RATIOS AS TRACERS

9.4.1 Results

9.4.1.1 Carbonatites

Strontium isotopic ratios and Sr and Rb concentrations for nine carbonatite samples are listed in Table 9.7. Of these nine, two samples are listed in duplicate because the analyses are of separate dissolutions. Initial $^{87}Sr/^{86}Sr$ ratios have been calculated for an age of 2012 m.y. (section 9.3.4). Rb contents are very low and, even for the sample with detectable Rb content, the calculated initial ratio is within the 0.01% accuracy of the measured $^{87}Sr/^{86}Sr$ ratio.

Initial $^{87}Sr/^{86}Sr$ ratios range from 0.70393 $\pm$ 6 to 0.71022 $\pm$ 6. The bulk of initial $^{87}Sr/^{86}Sr$ ratios lie in the range of 0.704-0.706 with sample Pir64-2356C possessing an anomalously high ratio of 0.710. Within the group of lower ratios, $^{87}Sr/^{86}Sr$ ratios vary. As discussed in section 9.2, some of these variations are within experimental error, e.g., sample P72C, while other variations, e.g., Pir64-2356C, are slightly greater than experimental error of isotopic analyses. Sample inhomogeneity is indicated by the two analyses of Pir64-2356C; differing Rb contents of the two samples might cause these slightly different values between samples. However, Rb is not detectable in other samples and cannot account for variation among samples within the 0.704-0.706 range or between that group and sample Pir64-2356C with the higher $^{87}Sr/^{86}Sr$ ratio.

TABLE 9.7 Sr-Rb Data for Carbonatites

Sample	$^{87}Sr/^{86}Sr)_{measured}$	Total Sr† (ppm)	Rb† (ppm)	$^{87}Sr/^{86}Sr)_{inital}$	Carbonatite Type
P152-1430C	0.70393 ± 6	4957	ND	0.70393 ± 6	B
P72C#	0.70425 ± 4	4365	ND	0.70425 ± 4	T
P72C§	0.70448 ± 18	4365	ND	0.70448 ± 18	T
P68C	0.70458 ± 72	200[x]	ND	0.70458 ± 72	T
P146-1368C	0.70542 ± 38	4817 (ID)	0.27*(ID)	0.70542 ± 38	T
P51C	0.70569 ± 8	4585	ND	0.70569 ± 8	T
P10C	0.70623 ± 42	4250	ND	0.70623 ± 42	B
PIR64-2356C	0.71006 ± 4	4312 (ID)	2-3	0.71000 ± 4	T
PIR64-2356C§	0.71027 ± 6	4312	2-3	0.71022 ± 6	T

Initial ratios calculated for an age of 2012 m.y.
x Low value caused by high magnetite content of whole rock sample
* 2 Rb blanks average 0.075 µg Rb
† Determined by X-ray fluorescence unless noted by (ID) for isotope dilution
B Banded carbonatite
T Transgressive carbonatite
ND Not detected by XRF, detection limit 2ppm
Precisions quoted are ± 2σ
§ Duplicates are separate dissolutions
# Portion of sample P72C with abundant mica(removed); duplicate analysis from magnetite-rich area.

The two samples of banded carbonatite (Table 9.7) have different initial $^{87}Sr/^{86}Sr$ ratios. Sample P152-1430C possesses the lowest initial $^{87}Sr/^{86}Sr$ ratio obtained in this study. The five samples of transgressive carbonatite overlap the values from banded carbonatite; the highest $^{87}Sr/^{86}Sr$ ratio measured belongs to a sample of transgressive carbonatite. Variation in initial $^{87}Sr/^{86}Sr$ ratios between samples P72C and P68C is within experimental error as is the difference in samples P146-1368C and P51C. However, these two groups of samples are different from one another and from samples of banded carbonatite with initial $^{87}Sr/^{86}Sr$ ratio of 0.70393 $\pm$ 6 in sample P152-1430C and of 0.70623 $\pm$ 42 in sample P10C, and from the higher initial ratios of 0.71006 $\pm$ 4 and 0.71027 $\pm$ 6 in sample Pir64-2356C.

The mineralogy of the carbonatites varies considerably. Descriptions of the samples are listed in Appendix C-2. Carbonatite samples represent whole rock samples with the exception of visible magnetite and phlogopite which were removed from each sample. The two dissolutions of sample P72C represent two portions of a large specimen about 400 cm^3. The magnetite-rich area of this sample possesses the same $^{87}Sr/^{86}Sr$ ratio as the portion of sample which contained a considerable amount of phlogopite.

Clinopyroxene from sample P72C has a measured $^{87}Sr/^{86}Sr$ ratio (Table 9.8) of 0.70529 $\pm$ 10. This value is slightly higher than the coexisting carbonate fraction of the rock which has an initial $^{87}Sr/^{87}Sr$ ratio of 0.70448 $\pm$ 18. Elemental concentrations were not measured in this pyroxene.

TABLE 9.8 Sr, K, Rb Data for Clinopyroxenes

Sample	$^{87}Sr/^{86}Sr$ measured	Sr(ppm)†	K(ppm)*	Rb(ppm)*	K/Rb	$^{87}Sr/^{86}Sr$ initial
F15M	0.71246 ± 14	553 (ID)	78	0.35	224	0.71240 ± 14
F101P	0.71282 ± 24	318	585	3.01	194	0.71204 ± 24
F101P	0.71229 ± 6	318	585	3.01	195	0.71151 ± 6
P150-975P	0.71210 ± 14	403 (ID)	530	2.19	242	0.71165 ± 14
P72C	0.70529 ± 10	-	-	-	-	-
G12F	0.71178 ± 6	419	223	0.96	232	0.71159 ± 6
F23F[X]	0.7114 ± 12	-	-	-	-	-

† Determined by X-ray fluorescence unless noted by (ID) for isotope dilution
X Measured at UTD by M. Halpern
* Samples corrected for K blank = 2.7 μg/g; Rb blank = 0.1 μg/g ; K and Rb measured by isotope dilution.
Initial ratios calculated for an age of 2012 m.y.
Duplicate runs are of separate dissolutions
Precision reported as ± 2σ

However, clinopyroxene is extremely rare in carbonatite and is considered a xenocryst, possibly derived from the pyroxenite body. It is significant that the initial $^{87}Sr/^{86}Sr$ ratio of the pyroxene would be equal to or very close to the initial ratio of the carbonatite. The difference between measured and initial $^{87}Sr/^{86}Sr$ ratios required for pyroxene and carbonatite from P72C to be equal is in the same range as that between measured and initial ratios of the other samples. As discussed in the next section, the $^{87}Sr/^{86}Sr$ ratio of this pyroxene is very different from pyroxenes of the pyroxenites. Because of its non-cognate nature, it is not crucial whether the initial $^{87}Sr/^{86}Sr$ ratios of pyroxene and host rock are identical.

Apatite from sample Pir64-2356C (Table 9.9) has an initial $^{87}Sr/^{86}Sr$ ratio of 0.71008 $\pm$ 8 which is the same as both dissolutions of carbonatite whole rock of that sample.

Previously measured values of $^{87}Sr/^{86}Sr$ by Powell *et al*. (1966) and Pineau *et al*. (1973) are identical to each other and, although lying in the range of $^{87}Sr/^{86}Sr$ ratios measured in this study, they do not represent the wide range in values revealed in the Phalaborwa complex by this study.

9.4.1.2 Pyroxenites

$^{87}Sr/^{86}Sr$ ratios were measured on clinopyroxenes from five different rocks: micaceous pyroxenites (F101P and P150-975P), massive pyroxenite (F15M), feldspathic pyroxenite (F23F) and carbonatite (P72C) from the main

Table 9.9. Rb, Sr data for apatites.

Sample	$^{87}Sr/^{86}Sr$ measured	Sr^{total} #	Rb^{total} #	$^{87}Sr/^{86}Sr$ initial
F16M	0.71236±16°* 0.71125±10 0.71039±4	14113	3.22	0.71234±16
PIR64-2356C	0.71003±6 0.71010±8°*	2904	0.65	0.71008±8
F15M	0.71202±10°*	2609	1.23 1.24	0.71198±10

Initial ratios calculated for an age of 2012 m.y.
Duplicate runs are of separate dissolutions.
Precision reported as ±2σ.
°Not leached in dilute HCl.
*Spiked runs, all others natural Sr runs; analysis by H. Allsopp.
measured by isotope dilution.

complex and feldspathic pyroxenite (G12F) from the Guide Copper Mine. Details of their preparation are given in Appendix C-2. Sr, Rb and K contents were measured by isotope dilution; initial $^{87}Sr/^{86}Sr$ ratios are calculated for samples in which elemental abundances were measured. These are listed in Table 9.8.

Pyroxenes from pyroxenites have initial $^{87}Sr/^{86}Sr$ ratios ranging from 0.71152 $\pm$ 6 to 0.71241 $\pm$ 14. In addition, F23F has a measured $^{87}Sr/^{86}Sr$ ratio of 0.7114 $\pm$ 12; the initial ratio has not been measured. Even though it could have the lowest $^{87}Sr/^{86}Sr$ ratio of the pyroxenes from pyroxenites, because of the large error associated with this analysis, it also overlaps in $^{87}Sr/^{86}Sr$ with the highest value measured, i.e., sample F15M.

Sample F101P exhibits slight differences in initial $^{87}Sr/^{86}Sr$ ratios between separate dissolutions. Taking the accuracy and precision into account, the two analyses differ by 0.0002. Concentrations of elements were measured on different dissolutions; thus, slight differences in Sr and/or Rb concentrations between the two dissolutions may bring the initial ratios into agreement. These differences must be larger than the 1% accuracy quoted for measurement of elemental abundances.

Initial $^{87}Sr/^{86}Sr$ ratios fall into two groups. Sample F15M is the same as one dissolution of F101P. The second dissolution of F101P overlaps the initial $^{87}Sr/^{86}Sr$ ratio of P150-975P and G12F.

As mentioned in the previous section, pyroxene from carbonatite P72C has a measured $^{87}Sr/^{86}Sr$ ratio of 0.70529 ± 10. This value falls in the range of ratios for carbonatites but is much lower than any value of $^{87}Sr/^{86}Sr$ measured on pyroxene from a pyroxenite.

Clinopyroxene from the satellite body, the Guide Copper Mine, has an initial $^{87}Sr/^{86}Sr$ ratio identical to two clinopyroxenes of the main complex. The significance of this analysis will be discussed in Chapter 10.

9.4.1.3 Isotopic Inhomogeneity

Initial $^{87}Sr/^{86}Sr$ ratios for the rocks and minerals measured in this study are shown in Figure 9.6. Analyses fall into two groups which are distinctive in initial $^{87}Sr/^{86}Sr$ ratios and in rock type. The one exception is carbonatite sample Pir64-2356C in which both carbonatite and apatite lie in the high $^{87}Sr/^{86}Sr$ group with minerals from pyroxenites.

Within the cluster of lower $^{87}Sr/^{86}Sr$ ratios, values range from 0.70393 ± 6 to 0.70623 ±42. As discussed in section 9.4.1.1, some of these values overlap, but the variation between the upper and lower values of the group is significant. A clinopyroxene megacryst, probably of xenocrystal origin, has an initial $^{87}Sr/^{86}Sr$ equal to or very close to host carbonatite.

The cluster of higher initial $^{87}Sr/^{86}Sr$ ratios contains values ranging from 0.71008 ± 8 to 0.71241 ± 14. Isotopic inhomogeneity exists within samples and between samples.

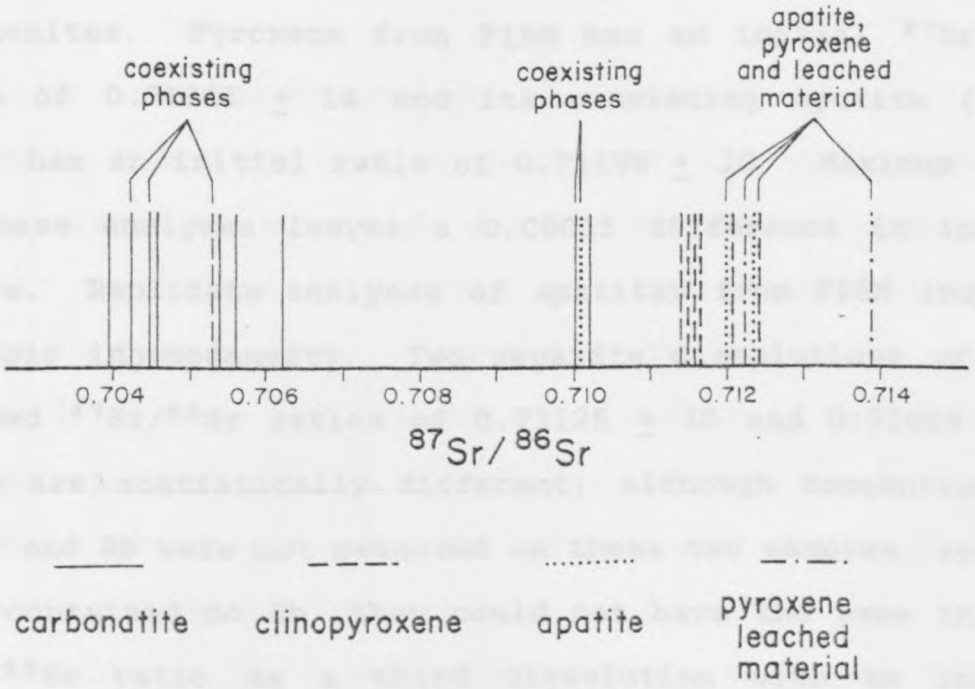


Figure 9.6 Summary of initial $^{87}Sr/^{86}Sr$ ratios for rocks and minerals from the Phalaborwa complex measured in this study. Measured $^{87}Sr/^{86}Sr$ ratios are shown for those minerals in which element concentrations were not measured. Coexisting phases are denoted above the histogram.

Carbonatite sample Pir64-2356C has slightly different ratios between dissolutions, a minimum of 0.00005 difference taking into account accuracy and precision of the analyses. Apatite, on the other hand, is in agreement with both dissolutions of this sample.

Isotopic inhomogeneity is also indicated for pyroxenites. Pyroxene from F15M has an initial $^{87}Sr/^{86}Sr$ ratio of 0.71241 $\pm$ 14 and its coexisting apatite (Table 9.10) has an initial ratio of 0.71198 $\pm$ 10. Maximum error on these analyses leaves a 0.00015 difference in initial ratios. Replicate analyses of apatites from F16M indicate isotopic inhomogeneity. Two separate dissolutions of F16M yielded $^{87}Sr/^{86}Sr$ ratios of 0.71125 $\pm$ 10 and 0.71039 $\pm$ 4. These are statistically different; although concentrations of Sr and Rb were not measured on these two samples, even if they contained no Rb, they could not have the same initial $^{87}Sr/^{86}Sr$ ratio as a third dissolution with an initial $^{87}Sr/^{86}Sr$ ratio of 0.71234 $\pm$ 10. Concentrations of elements were measured on the same aliquot of sample as the $^{87}Sr/^{86}Sr$ measurement, and, therefore, sample inhomogeneity has no effect on the calculation of this initial ratio. A minimum amount of difference between the upper and lower values obtained for F16M is 0.00169.

Two magnitudes of variation in initial $^{87}Sr/^{86}Sr$ ratios must be accounted for geologically, the larger differences between the two groups of ratios and the smaller variations within a single sample and among samples within a group.

The larger variation is on the order of 0.005; the smaller variations are on the order of 0.0025 or less. The subsequent four sections describe additional analyses obtained to help explain the variations in initial $^{87}Sr/^{86}Sr$ ratios in the Phalaborwa complex. The implications of these data are then discussed in section 9.4.2.

9.4.1.4 Leaching Experiments on Pyroxenes

Leaching experiments were performed on one sample of clinopyroxene to establish whether contaminating material, rich in radiogenic Sr derived from hydrothermal fluids or groundwater may have contributed to the high initial $^{87}Sr/^{86}Sr$ ratios of pyroxenes. Material deposited by contaminating fluid is thought to reside along cleavage planes, partings and in pits and other surface irrregularities in a mineral.

Results of the leaching experiments on sample F15M are listed in Table 9.10. Material for these analyses was prepared by placing a known amount of clinopyroxene, comparable in purity to that reported in Table 9.8, in 6N HCl and leaching to remove material which may be adhering to surfaces and cracks within the crystal. The pyroxene of Leach B experiment was leached cold for one hour, the identical treatment to all other pyroxenes measured. Pyroxene of Leach A experiment was subjected to ultrasonic treatment in the cold HCl; the purpose of the ultrasonic treatment was to detect any additional contaminant which might be released under more drastic conditions.

Table 9.10. Rb, Sr Data for Leached Material from Clinopyroxene F15M

	$^{87}Sr/^{86}Sr_{measured}$	^{86}Sr (ppm)	^{87}Rb (ppm)	$^{87}Sr/^{86}Sr_{initial}$
Unleached pyroxene (from Table 9.3)	0.71246±14	553	0.350	0.71240±14
A (ultrasonic leach)	0.71227± 8	55.5	0.0756	0.71223± 8
B (non-ultrasonic leach)	0.71390± 5	59.0	0.0133	0.71387± 5

Chemistry for these samples, spiked Sr runs, by S. C. Eriksson, December 1979; run on mass spectrometer by H. L. Allsopp, May 1980.

$^{87}Sr/^{86}Sr_{initial}$ calculated for 2012 m.y.

Analyses reported in Table 9.10 represent the leachate or liquid portion of the leaching experiments. This portion contains whatever contaminant has been removed from crystal cracks and surfaces. Leach B material has the highest initial $^{87}Sr/^{86}Sr$ ratio measured in this study (0.713388 $\pm$ 5); Leach A, which was expected to remove more contaminant from the pyroxene, has the same initial $^{87}Sr/^{86}Sr$ ratio (0.71224 $\pm$ 8) as the pyroxene (Table 9.8). The Rb content of the leached material is very low compared to the Sr content; this is compatible with either carbonate or apatite contaminant.

9.4.1.5 Oxygen and Carbon Isotopes

Table 9.11 lists oxygen and carbon isotopic data for carbonatites from Phalaborwa performed for this study. The error in the measurements from this study are $\pm$0.1% as given by R. Forester of Arco Oil and Gas Co. who supervised the analyses. Analyses are compared to standard mean ocean water for oxygen and limestone standard PDB for carbon. Variations in $\delta^{18}O$ and $\delta^{13}C$ values, in excess of the associated experimental error, were observed.

9.4.1.6 Country Rocks

In order to test the extent to which magma from the Phalaborwa complex may have mixed with upper crust, composition of a "bulk country rock" was established by study of 30 samples of country rock. These were collected

Table 9.11. C and O isotopic data for selected carbonatites.

Sample	Initial $^{87}Sr/^{86}Sr$ Ratio	$\delta^{18}O$ (SMOW)	$\delta^{13}C$ (PDB)
P51C	0.70569±8	7.6±.1 o/oo	-4.3±.1 o/oo
P152-1430C	0.70393±6	7.1±.1 o/oo	-4.5±.1 o/oo
PIR64-2356C	0.71000+4 0.71022±6	8.1±.1 o/oo	-3.9±.1 o/oo

from a 2-3 km radius surrounding the Phalaborwa complex. To the north and west of the complex, pink equigranular granitic rock is prominent which occasionally contains irregular schlieren of dark-green pyroxene. South and southeast of the complex, the dominant rock is gneissic biotite granite containing numerous areas of muscovite pegmatite. To the southwest, pink granitic and gneissic rocks are interbanded in approximately equal proportions. The Kruger National Park bounds the complex to the east; it was not logistically practical to sample in the park.

A petrographic study was undertaken and Rb-Sr concentrations (Table 9.12) were measured by XRF to determine the effects of surface weathering and/or metasomatism from the complex. J. Barton (pers. comm., 1979) found that three samples of gneissic biotite granite, C9B, C25B and C28B, did not lie on the errorchron established for country rocks, and he surmised that they had been affected by metasomatism from the main complex. From Rb and Sr compositions, petrography and Barton's work, 18 samples were judged to be free from metasomatism and weathering; rock powders were mixed in proportions estimated from sample collecting, i.e., pink granite : biotite gneiss; muscovite pegmatite are present in a ratio of 5:4:1. Isotopic measurement on this mixture yielded an $^{87}Sr/^{86}Sr$ ratio of 0.7527 $\pm$ 8 with a Sr concentration of 261 ppm and a Rb concentration of 119 ppm.

TABLE 9.12

Rb and Sr Concentrations of Country Rocks

Sample	Sr(ppm)	Rb(ppm)
Gneissic Biotite Granite		
C13B	435	75
C14B	611	35
C(27A)B	15	186
C(24A)B	470	60
C9B	330	91
C25B	342	58
C28B	302	143
C(27B)G	237	182
C(21)B		
Gneissic Fenite		
P75N	642	203
P78N	394	100
P79N	690	126
P81N	344	96
P86N	563	177
P87N	658	140
Muscovite Pegmatite		
C7V	98	224
C8V	42	143
Pink Fenite		
F73N	241	213
F(79A)N	406	377
P76N	114	194
F81N	369	268
Pink Granite		
C1G	197	155
C(10A)G	60	127
C16G	103	130
C20G	151	186
C22G	269	113
C29G	327	131
C30G	346	271
C(20A)G	547	32
C3G	155	150
C2G	256	124

9.4.1.7 Vermiculite Composition

Table 9.13 contains Rb and Sr concentrations and isotopic compositions for a vermiculite sample from Phalaborwa. The sample was taken from the open pit on PMC property where mining for vermiculite takes place. The location of the sample is shown in Figure 9.1. The total Rb content of the vermiculite is 332 ppm compared to 615 ppm to 829 ppm Rb for phlogopites listed in Table 9.3a.

9.4.2 Significance of Initial $^{87}Sr/^{86}Sr$ Ratios

The concept of using $^{87}Sr/^{86}Sr$ ratios as petrogenetic tracers (Gast, 1960; Faure and Hurley, 1963; Hedge and Walthall, 1963) is based on the tenet that a rock has the same initial $^{87}Sr/^{86}Sr$ ratio as the magma from which it formed and that the magma is derived from a homogeneous source area with a unique initial $^{87}Sr/^{86}Sr$ ratio. With subsequent study, it soon became apparent from differences in $^{87}Sr/^{86}Sr$ ratios of basalts from oceanic floor and islands that the mantle is inhomogeneous laterally and vertically (Gast et al., 1964; Hofmann and Hart, 1978).

The assumption that erupted material is isotopically representative of the source material has also been questioned. Some workers postulated that, although derived from a homogeneous source, disequilibrium melting (O'Nions and Pankhurst, 1974; Gast et al., 1964; Peterman et al., 1970; Harris et al., 1972) or changes within the magma during its ascent (O'Hara, 1973, 1975) account for variations of isotopic ratios within a given rock type.

Table 9.13. Sr and Rb data for vermiculite.

	$^{87}Sr/^{86}Sr$	^{86}Sr	Sr^{total}	^{87}Rb	Rb^{total}	$^{87}Rb/^{86}Sr$ atomic	$\frac{^{87}Sr^{*}}{R_o=.705}$	Age^{+} m.y.	Rock Type
Vermiculite	3.782±1	0.7975	10.54	91.34	332.5	114.5	2.482	1887±2	Pegmatoid

Study of oceanic rocks essentially should overcome the problem of contamination by crustal rocks. However, continental suites possess the additional problem of possible contamination by crustal rocks during ascent through a thicker, chemically different crust. Studies of ultrapotassic lavas of Africa, North America, and Australia provide extreme cases of possible crustal influence on strontium isotopes. Initial $^{87}Sr/^{86}Sr$ ratios of East African ultrapotassic lavas range from 0.7035 to 0.708 with a strong correlation of $^{87}Sr/^{86}Sr$ with Rb/Sr (Bell and Powell, 1969, 1970), a feature compatible with crustal contamination. However, other lavas of similar composition, such as those of Australia and Spain (Powell and Bell, 1970) have negative correlation between these two ratios.

A corollary of the basic theory that initial strontium ratios of rocks reflect their source is that comagmatic rocks should have identical initial strontium ratios. This has been used to test whether certain rocks in intimate spatial association are in fact cogenetic (Allsopp and Ferguson, 1970; Powell et al., 1966; Foland and Friedman, 1977).

Changes in strontium ratios by post-crystallization processes can mask the petrogenetic character of a rock. Characteristics not related to the isotopic system are necessary to determine if such processes have taken place. For instance, oxygen and carbon isotopes have been used to determine if rocks have experienced deuteric alteration by ground water (Taylor, 1968).

The strontium isotopic data from the Phalaborwa complex represent a wide range in initial $^{87}Sr/^{86}Sr$ ratios. As discussed in section 9.4.1.3, these variations are small within single samples, are somewhat larger within each rock type studied, and are generally very large between carbonatites and pyroxenites. The following sections explore different possibilities as to the origin of this range in initial $^{87}Sr/^{86}Sr$ ratios. The initial $^{87}Sr/^{86}Sr$ ratios in the Phalaborwa complex represent their source region or regions or must have been altered either during ascent and cooling or by post-crystallization processes.

9.4.2.1 Effects of Post-crystallization Processes

An obvious possibility for the cause of a wide range of $^{87}Sr/^{86}Sr$ values with small-scale inhomogeneities within a rock is groundwater contamination. The geographical location of the Phalaborwa complex in flat-lying terrain of semi-tropical climate suggests that groundwater interaction could play a large role in altering isotopic compositions. The erosional pattern of South Africa (Brink, 1979) shows that the Phalaborwa complex could have interacted with ground water for the last 20 m.y. The overlying Malmani Dolomite of the Transvaal Supergroup had retreated to the escarpment and caves had formed which are similar to the famous archaeological sites dated at 20 m.y. (Partridge, 1973). This estimate is probably a minimum age for groundwater interaction.

9.4.2.1.1 Alteration of Phlogopite to Vermiculite

The Phalaborwa complex contains vast quantities of phlogopite which have been altered in places to vermiculite and hydrobiotite (Hanekom et al., 1965; Gevers, 1948).

Table 9.13 contains an analysis of vermiculite taken from the northern pegmatoid body which is mined for commercial vermiculite. This vermiculite has lost about 110 ppm ^{87}Rb and 3.4 ppm radiogenic ^{87}Sr compared to the average phlogopite. Probably all the mica within a few metres of the surface has been transformed to vermiculite, and large bodies in the northern and southern pegmatoid bodies extend to depths of 50 metres below the present erosional surface (Hanekom et al., 1965). Hydrobiotite is confined to a small body on the western contact and small, scattered outcrops within the complex. It is volumetrically insignificant compared to the vermiculite. X-ray diffraction on phlogopites listed in Table 9.3a from the Foskor and PMC pits showed the phlogopite to be unaltered. These analyses included K-saturation of the mineral to measure expansibility.

Calculations may be made to determine whether the radiogenic strontium derived from mica during alteration of phlogopite to vermiculite could account for the variations in $^{87}Sr/^{86}Sr$ ratios in the complex. Appendix C-4 contains estimates of vermiculite tonnage in the Phalaborwa complex;

these are slightly higher than the amounts given by Hanekom et al. (1965) in order to allow a generous source of radiogenic strontium for contamination. The amount of ^{87}Sr generated from ^{87}Rb in 20 m.y. and ^{87}Sr lost from the phlogopite structure during alteration is added to clinopyroxenes of the complex to a half kilometre depth and to carbonatite to a similar depth. These calculations, listed in Appendix C-4, assume that clinopyroxenites and carbonatites are cogenetic and possessed an initial $^{87}Sr/^{86}Sr$ ratio of 0.704 upon intrusion.

Clearly, vast tonnages of ^{87}Sr percolating through the complex will raise the initial strontium ratios. The magnitude of the change estimated from the data in Appendix C-4 is of the order of 0.0003. Changes of this magnitude may account for many of the smaller variations in initial $^{87}Sr/^{86}Sr$ ratios found within single samples. Differences in initial strontium ratios between clinopyroxene and carbonatite in sample P72C, apatite and pyroxene in F15M, and the two dissolutions of clinopyroxene in sample F101P and of carbonatite in sample Pir64-2356C may be accounted for by this mechanism.

Changes of the order calculated in Appendix C-4 are about eight to 10 times too small to account for the variations in $^{87}Sr/^{86}Sr$ ratios found among pyroxenes and among carbonatites and are about 20 times too small to account for variations between the majority of carbonatites and the pyroxenites.

Based on these calculations, radiogenic strontium derived from alteration of phlogopite to vermiculite can account for much of the isotopic inhomogeneity found within coexisting minerals and duplicate samples of the same rock. However, this mechanism cannot account for variations among samples within a rock type or for variations between the two groups of initial $^{87}Sr/^{86}Sr$ ratios.

9.4.2.1.2 Diffusion from Phlogopite

A distinct but similar source for ^{87}Sr is from diffusion of ^{87}Sr from phlogopite. This may occur as a continuous process not associated with vermiculitization. In this case, solid state diffusion would transport the ^{87}Sr to the grain boundaries and some other mechanism, such as movement of ground water, would have to transport the ^{87}Sr out of the mica into the rock. Carbonatite samples from P72C were measured with this in mind. However, the mica-rich portion of the rock has the same initial $^{87}Sr/^{86}Sr$ ratio (0.70425 $\pm$ 4) as an area free of mica (0.70448 $\pm$ 18) within experimental error. Clinopyroxenes from micaceous pyroxenites generally have lower $^{87}Sr/^{86}Sr$ ratios than pyroxene from massive pyroxenite (Table 9.8). Therefore, diffusion of ^{87}Sr out of phlogopite is not considered a viable mechanism for raising initial $^{87}Sr/^{87}Sr$ ratios even the small amounts observed within samples.

9.4.2.1.3 Leaching Experiments

Leaching experiments were carried out on one pyroxene to determine if contaminating material with high $^{87}Sr/^{86}Sr$ is present along cracks, cleavages and imperfections in clinopyroxene and if isotopic measurements reflect these mixtures. Results listed in Table 9.10 show that the leach material from one sample is comparable in $^{87}Sr/^{86}Sr$ to the leached pyroxene (Table 9.8) and does not approach the $^{87}Sr/^{86}Sr$ ratios of the present-day country rock (section 9.4.1.6). This leach which included ultrasonic treatment may have leached intergrown apatite or calcite as well as surface contaminant. Leach B has a slightly higher $^{87}Sr/^{86}Sr$ ratio than the clinopyroxene and contains 58 ppm total Sr. Using the mixing equation of Ewart and Stipp (1968)*, an initial ratio of 0.704 for the clinopyroxene (550 ppm Sr), 0.714 for contaminant (58 ppm Sr) and 0.712 for hybrid gives 37.9 units of contaminant per unit of clinopyroxene needed to raise the initial ratio to 0.712.

Similar calculations for raising initial $^{87}Sr/^{86}Sr$ ratios from the lowest to highest within the group of ratios in the 0.710-0.712 range show a high proportion of contaminant is needed. Using data from Table 9.8, raising a $^{87}Sr/^{86}Sr$ ratio of 0.71152 with 318 ppm Sr in the

---

$$*\left[\frac{Sr_p}{Sr_p + X\ Sr_c}\right]\left[\frac{^{87}Sr}{^{86}Sr}\right]_p + \left[\frac{X\ Sr_c}{Sr_p + X\ Sr_c}\right]\left[\frac{^{87}Sr}{^{86}Sr}\right]_c = \left[\frac{^{87}Sr}{^{86}Sr}\right]_h$$

p = parent; c = contaminant; h = hybrid; x = proportion of contaminant needed.

clinopyroxene to a ratio of 0.7124 (F15M), requires three units of contaminant for every unit of clinopyroxene. Similar calculations for apatites show proportions of contaminant required are of the order of several hundred units contaminant.

The initial $^{87}Sr/^{86}Sr$ ratio of contaminant is very near the values of the minerals and the relatively low Sr contents precludes contaminant transported by groundwater having made any significant changes in initial $^{87}Sr/^{86}Sr$ ratios. Contaminant could not have raised the initial $^{87}Sr/^{86}Sr$ ratios from the carbonatite values to those of the pyroxenites and could not have caused the range in values observed among rocks of similar type. The contaminating material probably does represent material precipitated from ground waters percolating through the complex. These experiments do not address the problem of exchange in Sr within the pyroxene structure with Sr in the ground water. However, the $^{87}Sr/^{86}Sr$ composition of the leached material is only slightly different from the composition of the pyroxene so that, at best, actual alteration of pyroxene by ground water is only capable of explaining the small scale variation in initial $^{87}Sr/^{86}Sr$ ratios within the pyroxenes.

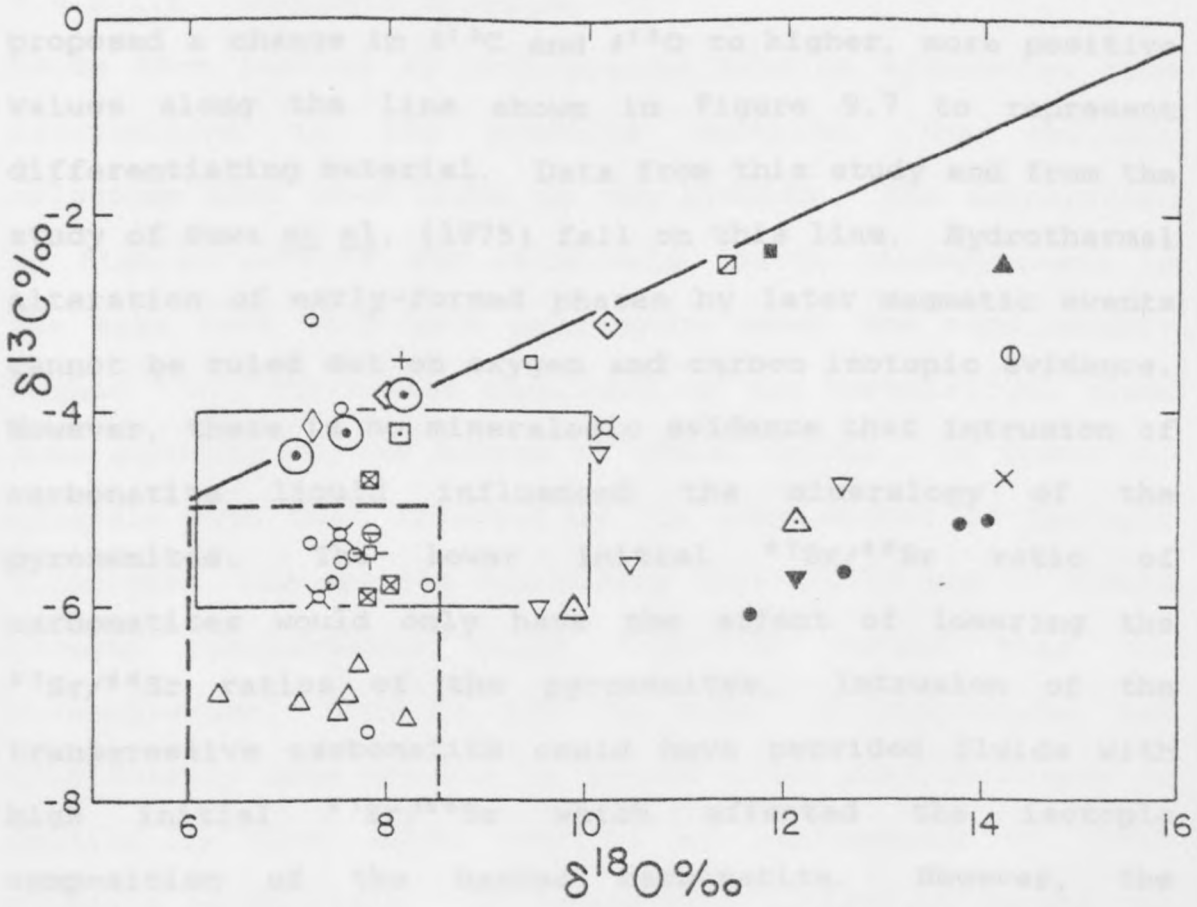
9.4.2.1.4 Oxygen and Carbon Isotopes

A final estimate of degree of groundwater alteration of the complex was made by measuring oxygen and carbon isotopes for carbonatite members. Three samples of carbonatite

representing lowest to highest $^{87}Sr/^{86}Sr$ ratios measured were submitted to the Geological Research facilities of ARCO Oil and Gas, Dallas, Texas, for stable isotope analysis. The results along with errors are listed in Table 9.11 and plotted in Figure 9.7 with data from other carbonatites, including previously reported data for the Phalaborwa complex (Pineau and Javoy, 1969; Sheppard and Dawson, 1973; Suwa et al., 1975).

None of the data from Phalaborwa lie in the box which Taylor et al. (1967) interpreted as primary, unaltered igneous carbonatites (Figure 9.7). However, there is considerable disagreement as to what represents unaltered carbonatite material. Deines (1970) established a wider range of values for the Oka complex which he and others (Suwa et al., 1975) interpret as unaltered carbonatite (Figure 9.7). Sheppard and Dawson (1973) advocated a range of $\delta^{13}C$ of -2 to -9 per mil for "primary" igneous carbonatite; Dawson and Fuge (1980) extended the "primary" box to enclose $\delta^{13}C$ values up to -2 per mil and accept that data from Phalaborwa lie in this primary carbonatite field. Thus, from the more recent studies, data from Phalaborwa may be considered as primary, igneous values.

In addition, because meteoric water compositions have negative $\delta^{18}O$ values, alteration of carbonates by groundwater interaction should have the effect of creating lower $\delta^{18}O$ values in altered carbonatites. This is not the case at Phalaborwa. Higher values of $\delta^{18}O$ are commonly



- ⊙ Phalaborwa, this study
- △ Phalaborwa (Sheppard and Dawson, 1973)
- ⊡ Phalaborwa, banded carbonatite (Suwa et al., 1975)
- ◇ Phalaborwa, transgressive carbonatite (Suwa et al., 1975)
- × Oldoinya Lengai (Fontes)*
- □ Busumbu (Pineau)*
- ◊ Sukulu Hill (Pineau)*
- ■ Lime Kiln Hill, Tororo (Pineau)*
- \+ Tororo Hill (Pineau)*
- ● Kirumba (Pineau, Fontes)*
- ⊠ Lueshe (Pineau, Fontes)*
- ▲ Napak (Pineau)*
- ▽ Bachelor Lake (Sheppard and Epstein, 1970)
- ▼ Kimberlite calcite vein (Baertschi, 1957)
- ⊖ Spitzkop (Baertschi, 1957)
- ⊕ Tundula (Baertschi, 1957)
- ⊠ Chilwa Island (Baertschi, 1957)
- ⊗ Iron Hill (Taylor et al., 1967)
- ⊹ Cripple Creek (Taylor et al., 1967)
- o Alno (Taylor et al., 1967)
- △ Laacher See (Taylor et al., 1967)

*Pineau and Fontes data as quoted in Denauyer (1970).

Figure 9.7 Oxygen and carbon isotopic data for carbonates from Phalaborwa and other alkaline complexes and pipes. The box denoted by dashed lines refers to values considered as primary igneous values of mantle-derived rocks by Taylor et al. (1967); the solid box covers 'primary' mantle-derived rocks by Deines (1970). The line represents a differentiation path suggested by Denauyer (1970).

attributed to hydrothermal alteration or differentiation (Taylor et al., 1967; Denauyer, 1970). Denauyer (1970) proposed a change in $\delta^{13}C$ and $\delta^{18}O$ to higher, more positive values along the line shown in Figure 9.7 to represent differentiating material. Data from this study and from the study of Suwa et al. (1975) fall on this line. Hydrothermal alteration of early-formed phases by later magmatic events cannot be ruled out on oxygen and carbon isotopic evidence. However, there is no mineralogic evidence that intrusion of carbonatite liquid influenced the mineralogy of the pyroxenites. The lower initial $^{87}Sr/^{86}Sr$ ratio of carbonatites would only have the effect of lowering the $^{87}Sr/^{86}Sr$ ratios of the pyroxenites. Intrusion of the transgressive carbonatite could have provided fluids with high initial $^{87}Sr/^{86}Sr$ which affected the isotopic composition of the banded carbonatite. However, the transgressive carbonatite also contains samples with low $^{87}Sr/^{86}Sr$ ratios, thereby making hydrothermal alteration an unlikely process to explain the observed range in initial $^{87}Sr/^{86}Sr$ ratios.

There is also a correlation among initial $^{87}Sr/^{86}Sr$ ratios, $\delta^{18}O$ and $\delta^{13}C$ (Table 9.11). The significance of this relationship is not clear cut, but, along with the absolute values of $\delta^{18}O$ and $\delta^{13}C$ being regarded as primary igneous values, groundwater alteration as a mechanism for raising the $^{87}Sr/^{86}Sr$ ratio may be ruled out. The ramifications of the oxygen and carbon isotopic compositions with regard to magma mixing are discussed later.

9.4.2.1.5 Geologic Evidence

Aside from looking at post-crystallization alteration from calculations in the previous sections, the geologic relations also shed light on the problem. The association of high-Sr apatite and relatively low-Sr clinopyroxene in the same rock with both possessing equal and considerably higher $^{87}Sr/^{86}Sr$ ratios than most of the carbonatites sheds some evidence on the nature of these ratios. If these two minerals have been affected by the same amount of isotopic alteration, the apatite containing over 10,000 ppm Sr should possess considerably lower $^{87}Sr/^{86}Sr$ ratios than the clinopyroxene. This is not the case. Clinopyroxenes are considerably less soluble in ground water than carbonate or apatite so that equal amounts of replacement of these minerals is unlikely. If groundwater alteration caused the variation in Sr ratios, then it also might be expected that samples from diamond-drill core would have lower Sr ratios than samples taken from open pit areas. However, Tables 9.8, 9.9 and 9.11 show that there is no correlation between depth and $^{87}Sr/^{86}Sr$ for pyroxenites or for carbonatites. Certainly, fractures within the complex and the relatively porous nature of the rocks provide conduits for groundwater migration which can obliterate depth variation; this is not substantial evidence against groundwater alteration, but it is one piece of negative evidence. In addition, studies

which do invoke groundwater alteration as a mechanism for raising $^{87}Sr/^{86}Sr$ initial ratios (Kramers, 1977; Bolivar and Brookins, 1979) generally have substantial mineralogical alteration as proof of this process.

9.4.2.1.6 Conclusions

It has been shown that there is no evidence to support post-crystallization alteration of $^{87}Sr/^{86}Sr$ ratios to such an extent that all measured rocks and minerals possessed a common initial strontium ratio and were altered to their present values. ^{87}Sr derived from alteration of phlogopite to vermiculite and transported by ground water will account for the minor variations within samples. No mechanism discussed, however, will account for pyroxenites and carbonatites having a common initial $^{87}Sr/^{86}Sr$ ratio with later alteration of pyroxenites yielding the present-day high values. Neither can these mechanisms account for the high $^{87}Sr/^{86}Sr$ value of carbonatite Pir64-2356C which has an initial strontium ratio comparable to pyroxenites. Hydrothermal fluids from intrusion of a second carbonatite liquid could account for recrystallization of the earlier carbonatite but not for the lower initial $^{87}Sr/^{86}Sr$ ratios of some of the samples of transgressive carbonatite. Lastly, variations within rock types are too great to be explained by post-crystallization processes.

9.4.2.2 Ratios Inherited from Source Areas

It is generally accepted that carbonatites are derived from the mantle. Geological evidence (Ferguson and Currie, 1972; Tuttle and Gittins, 1966), radiogenic and stable isotope studies (Powell et al., 1966; Deines and Gold, 1973; Lancelot and Allegre, 1974; Mitchell and Krouse, 1975) and experimental work (Huang and Wyllie, 1974; Wyllie and Huang, 1976, Wyllie, 1977a, Eggler, 1978) point to the upper asthenosphere as a probable source for CO_2-rich rocks. Powell et al. (1966) reported low values of $^{87}Sr/^{86}Sr$ ratios for carbonatites which have been cited extensively in the last decade as representing uncontaminated mantle ratios.

All types of mantle-derived rocks occasionally show perturbations in $^{87}Sr/^{86}Sr$ ratios from what was once considered uncontaminated mantle source material. Ocean-floor basalts show the least amount of variation ($^{87}Sr/^{86}Sr$ = 0.7025-0.7035) and oceanic island basalts show a slightly greater variation ($^{87}Sr/^{86}Sr$ = 0.7025-0.7065) (Hofmann and Hart, 1978). Likewise, rocks intruded through continental crust such as continental basalts (Brooks et al., 1976b; Brooks and Hart, 1978; Carter et al., 1978), alkalic lavas (Bell and Powell, 1969; Peterman et al., 1970; Paul, 1971), carbonatites (Deans and Powell, 1968; Rock, 1976), and ultramafic nodules (Kudo et al., 1972; Allsopp and Barrett, 1975; Burwell, 1975) show variations in initial strontium ratios within minerals, nodules and coexisting magmas.

The most simple explanation for variation in initial $^{87}Sr/^{86}Sr$ ratios is contamination by crustal rocks, discussed in the next section. In many cases, however, this can be ruled out on the basis of geochemical and Pb-isotopic data. A more fundamental question is whether the isotopic composition of uncontaminated magmas is truly representative of the source region or is unrelated to the source region through the process of disequilibrium melting. Several workers in isotope systems (Gast et al., 1964; Peterman et al., 1970; Harris et al., 1972; O'Nions and Pankhurst, 1974; Flower et al., 1975) invoked disequilibrium melting rather than heterogeneous mantle to account for variations in $^{87}Sr/^{86}Sr$ in cogenetic rocks. Most of these workers now accept that heterogeneities in isotopic composition are present in the mantle.

There is considerable evidence that the Precambrian mantle was isotopically heterogeneous. The simplest models for upper mantle isotopic evolution are based on one-stage (Faure and Hurley, 1963) or two-stage (Birch, 1965; Steuber and Murthy, 1966) development. Figures 9.8 and 9.9 show two models. The first (Figure 9.8) from Davies et al. (1970), shows an evolution curve (AB) based on the Rb/Sr ratio of oceanic basalts with an early separation of mantle and crust; also shown is curve (AC) based on a higher Rb/Sr ratio of 0.10 invoking a model where crustal material separates later, around 3500 m.y., leaving a mantle depleted in alkalis (CD) relative to crust (CG). Data from some

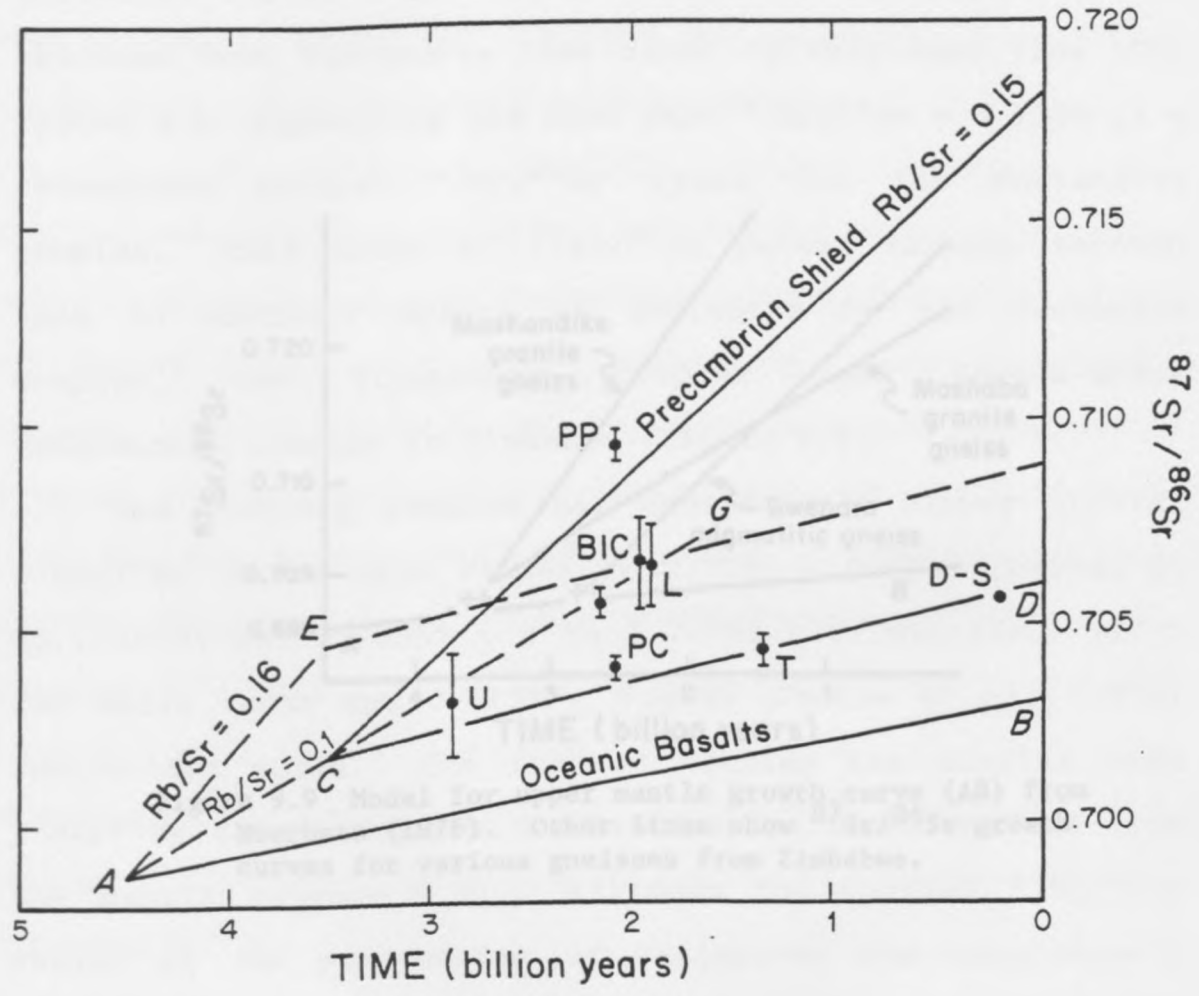


Figure 9.8 Model for $^{87}Sr/^{86}Sr$ evolution (from Davies et al., 1970) with initial $^{87}Sr/^{86}Sr$ ratios from Phalaborwa (this study) and several southern African intrusions. PC=the lower values for Phalaborwa carbonatites, PP= Phalaborwa pyroxenites, D-S= Dorowa-Shawa, BIC= Bushveld Igneous Complex, U=Ushushwana, T=Trompsburg and L=Losberg.

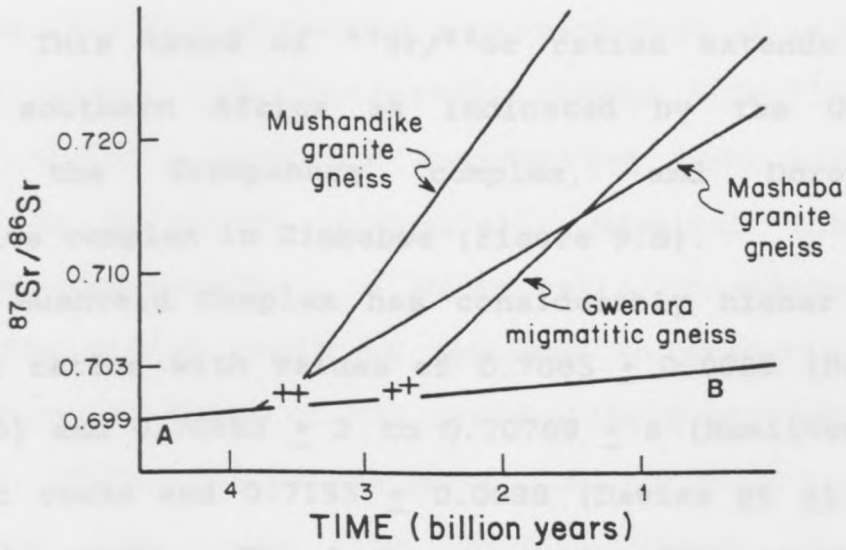


Figure 9.9 Model for upper mantle growth curve (AB) from Moorbath (1976). Other lines show $^{87}Sr/^{86}Sr$ growth curves for various gneisses from Zimbabwe.

southern African layered complexes lie along the line (CD) indicating higher $^{87}Sr/^{86}Sr$ ratios were present in sub-continental mantle than estimated from the oceanic basalt evolution curve. The lowest value of initial $^{87}Sr/^{86}Sr$ obtained from Phalaborwa lies close to this same line (CD, Figure 9.8) supporting the fact that $^{87}Sr/^{86}Sr = 0.7039$ is a reasonable initial $^{87}Sr/^{86}Sr$ ratio for the Phalaborwa complex. This trend of $^{87}Sr/^{86}Sr$ ratios extends through time in southern Africa as indicated by the Usushwana complex, the Trompsburg complex, and Dorowa-Shawa carbonatite complex in Zimbabwe (Figure 9.8).

The Bushveld Complex has considerably higher initial $^{87}Sr/^{86}Sr$ ratios with values of 0.7065 ± 0.0020 (Davies *et al.*, 1970) and 0.70563 ± 2 to 0.70769 ± 6 (Hamilton, 1977) for mafic rocks and 0.7153 ± 0.0088 (Davies *et al.*, 1970) for acidic rocks. The Losberg complex has similar high $^{87}Sr/^{86}Sr$ initial ratios for Precambrian rocks derived from the mantle (Figure 9.8). Although the initial $^{87}Sr/^{86}Sr$ ratios of the pyroxenites of Phalaborwa are considerably higher than these other complexes, from the data on Figure 9.8 it is easy to envisage a heterogeneous mantle which produces rocks with a wide range in isotopic compositions.

If one considers the majority of carbonatites to have an initial $^{87}Sr/^{86}Sr$ of around 0.7039 with the variation among them resulting from some modification on their path toward final emplacement and cooling, then those data fall well within values of $^{87}Sr/^{86}Sr$ ratios for subcontinental

mantle in southern Africa; i.e., Phalaborwa data fall very near line CD in Figure 9.8 and fall well below line CG. Thus, the lowest value of initial $^{87}Sr/^{86}Sr$ for the Phalaborwa complex fits well with other data supporting a subcontinental mantle in southern Africa which is enriched in Rb/Sr relative to normal oceanic basalts.

If the initial $^{87}Sr/^{86}Sr$ ratios measured for pyroxenites from Phalaborwa are representative of relatively unmodified values, i.e., possessed a common $^{87}Sr/^{86}Sr$ ratio of around 0.7100, then the pyroxenites must have been derived from a source isotopically distinct from that forming the carbonatites. A Rb/Sr ratio of approximately 0.15 for the mantle would be required to produce initial ratios similar to those of the pyroxenites from Phalaborwa. This value (Rb/Sr = 0.15) is more compatible with crustal compositions than with the mantle unless there is significant Rb enrichment of the mantle locally. The presence of phlogopite in the mantle would provide a source for high Rb/Sr.

The presence of phlogopite in the mantle has long been postulated on experimental (Yoder and Kushiro, 1969) and geochemical (Carmichael et al., 1974) grounds. More recently (Aoki, 1974; Dawson and Smith, 1977), nodules labelled the MARID-suite containing phlogopite as a main constituent have been identified as being derived from the mantle. Some of these nodules are sufficiently mica-rich to be termed glimmerites. Megacrysts of phlogopite thought to

have crystallized from kimberlitic magma (Dawson and Smith, 1975) also provide evidence of a Rb-rich mantle.

This model postulating a distinct source for pyroxenites and most of the carbonatites requires an inhomogeneous mantle which has maintained isotopic disequilibrium for some time in order for the source of the pyroxenites to attain such a high $^{87}Sr/^{86}Sr$ ratio. It also requires that phlogopite be present in the mantle for a substantial amount of time before generation of the pyroxenite magma. The amount of time and the proportion of mica required cannot be discussed quantitatively because the degree of partial melting of the source rock is not known. However, there is a suggestion that older micas may be present in the Phalaborwa complex (section 9.2) which may represent mantle-derived cognate or non-cognate xenoliths transported into the crust by the magma. The $^{87}Sr/^{86}Sr$ of the source must have been at least 0.7100. The isochron based on micas around 2000 m.y. has an initial $^{87}Sr/^{86}Sr$ of 0.70558 ± 0.00724 (2σ). The error associated with the initial ratio is quite large but allows the calculated ratio to have an upper limit of 0.71282. This is higher than all of the initial $^{87}Sr/^{86}Sr$ ratios measured for apatites and pyroxenes of the pyroxenites.

Ramifications of a phlogopite-bearing mantle for isotopic data have been discussed at length (Beswick, 1976; Hofmann and Hart, 1978); these workers conclude that low K/Rb phlogopite can produce local isotopic heterogeneities

in a completely crystalline upper mantle. Mineral disequilibria have been observed in nodules (Dasch and Green, 1975; Basu and Murthy, 1977) and long-term heterogeneities have been present over long time periods of 1.5-2.0 b.y. as indicated by Pb (Gast et al., 1964; Tatsumoto, 1966) and Nd isotopes (DePaolo and Wasserburg, 1976).

It is significant that rocks varying in age from the Archaean Messina Layered Intrusion (Barton et al., 1979) to Cretaceous kimberlite nodules (Kramers, 1977) have high initial $^{87}Sr/^{86}Sr$ ratios which are interpreted as being derived from a heterogeneous subcontinental mantle. Both longevity of heterogeneous mantle and extremely high initial $^{87}Sr/^{86}Sr$ ratios have been indicated. Barton et al. (1979) suggested that the inhomogeneity must have been present from around 3570 m.y. to the time of intrusion of the Messina Layered Intrusion at 3157 m.y. Initial $^{87}Sr/^{86}Sr$ ratios of micas in kimberlite nodules can be as high as 0.71282 (Kramers, unpublished data).

Differences in initial $^{87}Sr/^{86}Sr$ ratios between the pyroxenites and carbonatites at Phalaborwa could also be a result of how much phlogopite was involved in the melting of magmas giving rise to these two rock types. This implies disequilibrium melting. Phlogopite would contribute high $^{87}Sr/^{86}Sr$ to a melt; $^{87}Sr/^{86}Sr$ could increase or decrease in melt fractions depending on the amount of partial melting involving phlogopite. This mechanism could also account for

the smaller variations in $^{87}Sr/^{86}Sr$ ratios found within carbonatite and within pyroxenites. The melt would have to maintain isotopic disequilibrium during intrusion and cooling. However, because of the order of intrusion of the pyroxenites and carbonatites, i.e., pyroxenites before carbonatite, disequilibrium melting cannot account for differences in these two types of magmas. Small degrees of partial melting would form carbonatite first; larger degrees of partial melting would produce silicate melts (Wyllie, 1978).

The carbonatite with an initial $^{87}Sr/^{86}Sr$ ratio of 0.71000 falls in the same group as the pyroxenites and cannot be raised from 0.7039 to its present value by post-crystallization processes. It is conceivable that this carbonatite was derived from a phlogopite-rich source similar to that acting as source for the pyroxenites. Texturally or mineralogically there is nothing to distinguish Pir64-2356C from the other carbonatites.

Discussion of the initial $^{87}Sr/^{86}Sr$ ratios being inherited from the source rocks has established that an initial $^{87}Sr/^{86}Sr$ ratio of 0.7039 is a reasonable value for carbonatites derived from subcontinental mantle in southern Africa. A phlogopite-rich source area for pyroxenites which is not in isotopic equilibrium with the source of carbonatites is feasible but requires a Rb/Sr ratio of the mantle that is locally higher than any reported to date. The possible presence of older micas at Phalaborwa and the

recognized existence of phlogopite-rich rocks in the mantle support such a hypothesis.

Because small variations within a sample may be explained by post-crystallization alteration, these small-scale inhomogeneities do not argue against separate source areas. However, variations in $^{87}Sr/^{86}Sr$ within rock types suggest an almost continuous variation in degree of partial melting with each fraction possessing and maintaining a different $^{87}Sr/^{86}Sr$ ratio. This manifestation of disequilibrium melting cannot be ruled out. However, other possibilities will be explored. Changing of isotopic composition during cooling, mixing of magmas and contamination of magma by crustal rocks are possibilities discussed further below.

9.4.2.3 Aging of Magma

It has been suggested (McCarthy and Cawthorn, 1980) that decay of ^{87}Rb to ^{87}Sr over the cooling life time of a differentiating magma may significantly change $^{87}Sr/^{86}Sr$ ratios so that the measured initial $^{87}Sr/^{86}Sr$ ratio of a rock is significantly higher than that of its source region. For this to happen, two conditions must be met: (1) the cooling time must be very long, and (2) at some point, Rb/Sr must be quite high.

As discussed in section 9.2, both the pyroxenites and carbonatites are considered to have an age of 2030 m.y. Micas with apparent ages greater than 2100 m.y. are present

at Phalaborwa, but because of the problem in age differences due to sample preparation, it has not been determined if the older micas represent multiple intrusion, are xenolithic, or are altered by sample washing to give older apparent ages. It is unlikely that the range in mica ages documents the cooling time of the complex.

The second condition for raising the initial $^{87}Sr/^{86}Sr$ ratios of a magma, i.e., a high Rb/Sr ratio is present, is more easily studied. Even though certain rocks such as glimmerites have extremely high Rb/Sr ratios of 17-35, these rocks are cumulates which crystallized from a magma with extremely high Sr concentrations. In Chapter 5, it was estimated that the magma producing the micas and pyroxenes would have a Sr concentration of 2000-4500 ppm Sr. Rb is concentrated in phlogopite, but using the Rb composition of phlogopite as an upper limit of Rb concentration in melt (808 ppm Rb), the Rb/Sr ratio could not exceed 0.4. A magma with an initial ratio of 0.704, Sr = 2000 ppm and Rb = 800 ppm would take about 500 m.y. to raise the initial $^{87}Sr/^{86}Sr$ ratio from 0.704 to 0.712. Variation in initial $^{87}Sr/^{86}Sr$ within the pyroxenites, i.e., 0.00232, would take about 146 m.y. Four micas define an isochron of 2152 $\pm$ 24 m.y. (2σ) which is very close to 146 + 2012 = 2158 m.y. Thus, the magma forming the pyroxenites either cooled over 146 m.y. at the level of study or may have been aging in a lower magma chamber and spurts of magma were emplaced at the present level of erosion to give the diversity of initial $^{87}Sr/^{86}Sr$

ratios present today. The latter possibility is more probable on the basis of thermal behavior of cooling magmas.

It is very difficult to estimate Rb and Sr contents of the carbonatite magma. The transgressive carbonatite locally contains abundant phlogopite. However, from U-Pb data, there is no indication of an extended cooling period of the carbonatites.

Aging of magma cannot account for differences in initial strontium ratios between carbonatites and pyroxenites or the two values of carbonatites. This mechanism might account for the variation in initial $^{87}Sr/^{86}Sr$ ratios within pyroxenites if cooling within the pyroxenites took place over about 150 m.y. However, aging of magma is rejected on the basis of the very long cooling time required.

9.4.2.4 Mixing of Magmas

Although there is no correlation of mineralogy with $^{87}Sr/^{86}Sr$ composition in carbonatites, there is an indication of chemical characterization. The anomalous sample Pir64-2356C has the highest Ba content and lowest Y and La contents of any of the carbonatites studied. Figure 9.10a is a plot of initial $^{87}Sr/^{86}Sr$ ratios versus Ba content of the carbonatites; Figures 9.10b and c are similar plots for initial $^{87}Sr/^{86}Sr$ versus La and Y. These trace elements were measured by XRF method; because of matrix effect differences between carbonatite and silicate rock

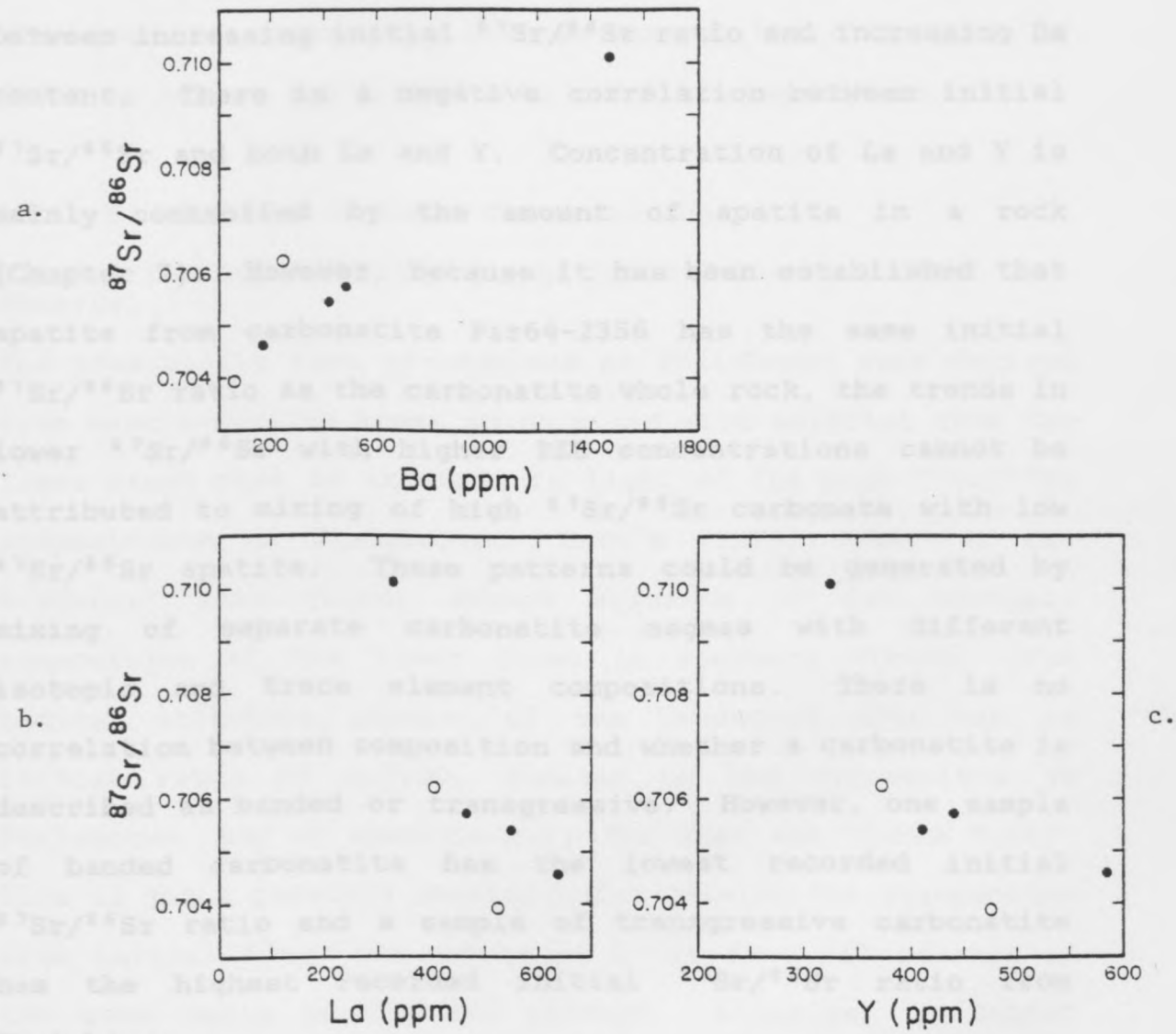


Figure 9.10 Initial $^{87}Sr/^{86}Sr$ ratios of carbonatites from Phalaborwa versus a) Ba, b) La and c) Y. Transgressive and banded types of carbonatites are denoted by closed and open circles respectively.

standards, these concentrations do not have the same accuracy as trace elements for silicate rocks and minerals. There is no estimate of error for these analyses. However, even with a large error there is a definite correlation between increasing initial $^{87}Sr/^{86}Sr$ ratio and increasing Ba content. There is a negative correlation between initial $^{87}Sr/^{86}Sr$ and both La and Y. Concentration of La and Y is mainly controlled by the amount of apatite in a rock (Chapter 7). However, because it has been established that apatite from carbonatite Pir64-2356 has the same initial $^{87}Sr/^{86}Sr$ ratio as the carbonatite whole rock, the trends in lower $^{87}Sr/^{86}Sr$ with higher REE concentrations cannot be attributed to mixing of high $^{87}Sr/^{86}Sr$ carbonate with low $^{87}Sr/^{86}Sr$ apatite. These patterns could be generated by mixing of separate carbonatite magmas with different isotopic and trace element compositions. There is no correlation between composition and whether a carbonatite is described as banded or transgressive. However, one sample of banded carbonatite has the lowest recorded initial $^{87}Sr/^{86}Sr$ ratio and a sample of transgressive carbonatite has the highest recorded initial $^{87}Sr/^{86}Sr$ ratio from Phalaborwa.

The linear array of oxygen and carbon isotopic compositions as discussed in section 9.4.2.1.4 is compatible with magma mixing.

Mixing of carbonatite magmas must be considered a possibility for explaining the variation in $^{87}Sr/^{86}Sr$ within

carbonatites. Such a mechanism requires at least two carbonatitic liquids from isotopically distinct sources. The first would be the banded carbonatite with a lower initial $^{87}Sr/^{86}Sr$ and $\delta^{18}O$ and $\delta^{13}C$ values followed by the transgressive carbonatite with an initial $^{87}Sr/^{86}Sr$ ratio of 0.710 or higher and higher $\delta^{18}O$ and $\delta^{13}C$ composition.

9.4.2.5 Effects of Magma Contamination

9.4.2.5.1 Bulk Assimilation of Lower Crust by Mantle Material

The possibility that pyroxenites of Phalaborwa were derived from mantle-derived magma which mixed with material from the lower crust must be examined in light of the high $^{87}Sr/^{86}Sr$ compositions at Phalaborwa. Hart's (1978) study of the Vredefort dome yields direct evidence of the isotopic composition of the lower crust in southern Africa. The central intrusive granite of the Vredefort dome has an initial ratio of 0.7100, similar to the pyroxenites at Phalaborwa, and of approximately the same age (Table 9.14). This is not a possible candidate for raising the pyroxenites from initial $^{87}Sr/^{86}Sr$ ratios of 0.704 to 0.710 because of the same ratio as the end product. Likewise, it cannot account for raising pyroxenite initial strontium ratios above 0.710. The three other rocks reported by Hart (1978) are better prospects for raising the pyroxenite values above 0.710. Using the mixing equation of Ewart and Stipp (1968), only 1.5 units of Inlandsee leucogranofels are required to

Table 9.14. Isotopic compositions of possible lower crust contaminants and proportions needed to raise magmas at Phalaborwa to present levels.

Rock Unit	Location	Age	Reference	^{87}Rb	^{86}Sr	Initial $^{87}Sr/^{86}Sr$	$^{87}Sr/^{86}Sr$ at 2012	Proportion needed to raise: pyroxenites (2000 ppm Sr) .704-.710	pyroxenites (2000 ppm Sr) .710-.7125	carbonatites (4500 ppm Sr) .704-.706
Central Intrusive Granite	Vredefort	1950 ±60	Hart (1978)	49.2 (Av. of 4)	30.4 (Av. of 4)	.7100±4	.7100	-	-	7.2
Outer Granite Gneiss	"	3001 ±27	"	31.38	22.69	.7019±2	.7212	4.7	2.5	2.6
Steynskraal metasediments and metabasites	"	3656 ±320	"	17.79	21.04	.7009±4	.7206	5.3	2.9	2.9
Inlandsee Leucogranofels	"	2828 ±32	"	40.88	16.30	.7044±4	.7333	3.1	1.5	2.0
Diabase	Messina	1749 ±104	Barton (1979)	1.63	20.79	.7108±15	.7108	49	-	8.8
Leucogabbro	Messina Layered Intrusion	3153 ±47	Barton et al. (1979)	5.47	21.20	.70331±6	.7038	-	-	-

one unit of pyroxenite magma to raise the initial $^{87}Sr/^{86}Sr$ ratios from 0.710 to 0.7125 (Table 9.14). It is unlikely that these rocks have raised the pyroxenite initial strontium ratios from 0.704 to 0.710.

Moorbath (1975, 1976) has plotted isotopic compositions of Archaean gneisses of Zimbabwe showing the hypothetical growth curve of $^{87}Sr/^{86}Sr$ with time for appropriate Rb/Sr ratios in each area (Figure 9.9). Similarly to rocks of the Vredefort area, compositions of the Mushandike granite gneiss, Mashaba granite gneiss and the Gwenoro migmatitic gneiss have low initial $^{87}Sr/^{86}Sr$ ratios but could have generated very high $^{87}Sr/^{86}Sr$ ratios (Figure 9.9) by the time of the Phalaborwa intrusion. The Mushandike granite gneiss in particular possesses a high $^{87}Sr/^{86}Sr$ ratio at around 2000 m.y. Calculations of proportions of these rocks needed to raise the Phalaborwa initial $^{87}Sr/^{86}Sr$ would yield similar results to those for the more Rb-rich rocks from Vredefort. The work of Barton (1979) and Barton *et al.* (1979) on rocks of the Limpopo mobile belt also shows that rocks which may represent lower crustal components in the southern Africa region have a wide range in $^{87}Sr/^{86}Sr$ compositions. Two of these are listed in Table 9.14. Although the initial ratios are considerably higher than mantle forming oceanic basalts, the leucogabbro (Barton *et al.*, 1979) is not a candidate and the diabase (Barton, 1979) must be mixed in very high proportions to have the required effect. Spooner and Fairbairn (1970) report isotopic data

on numerous pyroxene granulites throughout the world. None of these are prospective candidates for a contaminant.

There is no geochemical evidence that large proportions of rocks with high percentages of Ca-, Al-rich plagioclase contributed to the magma producing the Phalaborwa pyroxenites. On the contrary, lower crustal material is generally depleted in alkali elements and REE, all of which are extremely high in the rocks of the Phalaborwa complex. Using the mixing model of Ewart and Stipp (1968), calculations for raising carbonatites to account for variation within the majority of them (0.704-0.706) show 2.0-8.8 units of lower crustal material required for each unit of carbonatite magma. It is doubtful whether a carbonatite would maintain its identity as a carbonate rock if mixed with such proportions of silicates. These calculations suggest that at least 1.5 units of lower crust is required to mix with magma to account for variation within the pyroxenites at Phalaborwa. Much larger amounts of lower crust, from 3 to 49 units of crust per unit of magma, are required to raise the magma forming pyroxenites from around 0.704 to their present values. This is highly unlikely, supporting the existence of pyroxenite magma being derived from a Rb-rich heterogeneous mantle. Likewise, raising carbonatites to values of 0.710 would be extremely unlikely and raising carbonatites from 0.704 to 0.706 is improbable.

9.4.2.5.2 Bulk Assimilation of Upper Crust by Mantle Material

Many of the early workers at Phalaborwa (Mellor, 1906; Hall, 1912b; Shand, 1931) attributed the carbonatite member to metamorphism of limestone. Brandt (1948) recognized that the carbonate was intruded, but it was believed that true magmatic carbonate could not exist. Therefore, the substratum must include sedimentary carbonate. Powell et al. (1966) measured one sample of Transvaal Dolomite with an initial $^{87}Sr/^{86}Sr$ ratio of 0.7099. Its low Rb/Sr ratio means that there would have been little change in the $^{87}Sr/^{86}Sr$ of the rocks in 2000 m.y. Clearly, the majority of carbonatites with values in the 0.704-0.706 range were not derived from the Transvaal Dolomite. Sample Pir64-2356C has an initial $^{87}Sr/^{86}Sr$ very close to the value for the sedimentary carbonate. However, the high Sr and REE content of carbonatites including sample Pir64-2356C preclude a sedimentary origin.

It has been suggested (DuToit, 1931; Shand, 1931) that the Phalaborwa complex was generated from a sialic crust. Hanekom et al. (1965) proposed a mixing of magma with Archaean granite to form the Phalaborwa complex. Although geochemical evidence refutes this model, strong correlation of $^{87}Sr/^{86}Sr$ with Rb/Sr ratios and SiO_2 content in other continental rocks has led to models of bulk assimilation of crustal material (Holmes, 1950; Heier and Adams, 1965; Compston and Lovering, 1969; Bell and Powell, 1969).

A bulk country rock was synthesized from samples around the Phalaborwa complex. Details are given in section 9.4.1.6. The $^{87}Sr/^{86}Sr$ ratio today of 0.7527 $\pm$ 8 was recalculated for the time of intrusion of the Phalaborwa complex around 2012 m.y. ago. The $^{87}Sr/^{86}Sr$ of the total country rock around the Phalaborwa complex was 0.7157 $\pm$ 8 at that time. Although the measurement of $^{87}Sr/^{86}Sr$ is very precise, the initial ratio calculated for the country rock is very imprecise primarily because of the estimation of mixing proportions used and the assumption that the measured concentrations are representative of the area sampled. However, the calculated initial ratio is a good indicator of the range of initial $^{87}Sr/^{86}Sr$ ratios which may have influenced the magma if extensive bulk assimilation did occur.

Similarly to previous sections, several mixing calculations were made using the equation of Ewart and Stipp (1968); values of $^{87}Sr/^{86}Sr$ of contaminant of 0.716 and a Sr concentration of contaminant of 260 ppm Sr. $^{87}Sr/^{86}Sr$ of 0.716 was used instead of 0.7157 in order to allow for errors in its estimation and to enhance calculations of mixing by using conservative estimates of mixing parameters.

Table 9.15 summarizes the calculations using the same magma compositions as in the previous section for magmas forming pyroxenite and carbonatites. The number of units (3.5) of country rock required to raise carbonatites within the range of 0.704-0.706 is quite high; to raise

Table 9.15. Calculated proportions of upper crust required to raise initial $^{87}Sr/^{86}Sr$ ratios at Phalaborwa complex.

Rock	Magma Composition	Proportion needed to raise initial ratios: .704-.706	.704-.710	.710-.7125
Pyroxenite	2000 ppm Sr	-	7.7	5.5
Carbonatite	4500 ppm Sr	3.5	17.3	-

Pir64-2356C to its present value requires 17.3 units of country rock to each unit of magma. Likewise, the number of units of country rock needed to raise a pyroxenite magma from 0.704 to 0.710 is 7.7; the amount required just to cause variation within the pyroxenites is 5.5, a very high proportion of country rock to magma. Bulk assimilation of these proportions is generally considered on heat considerations to be improbable (Ewart and Stipp, 1968).

The mineralogy of some of the rocks with high ratios is sufficient to rule out bulk assimilation of higher-level crustal rocks. Most simply, the carbonatite Pir64-2356C is pure calcium carbonate with minor apatite. It is clearly unlikely that four or five parts of country rock would mix with anything, vapor or liquid of any known geological material, to produce such a rock. In all the cases described above, excessive amounts of country rock seem to be necessary to raise initial ratios. The model for bulk assimilation of upper crust is thus rejected on the basis of the large amounts required. Bulk assimilation of upper crust cannot account for raising $^{87}Sr/^{86}Sr$ values of pyroxenites to 0.710 nor can it account for variation within each rock type.

9.4.2.5.3 Selective Contamination by Crustal Rocks

Mitchell and Crockett (1972) explained the anomalous ratios of the Fen complex by contamination of primary magma by mixing with a partial melt of crustal rocks. Average

crustal compositions with one percent pore fluids start melting at around 700°C under crustal pressures (Wyllie, 1977b) with biotite completely absent at around 900°C. Jaeger (1957) has calculated temperatures of country rock which have been intruded by magma. These temperatures are highly dependent on the range in cooling temperature and the latent heat of the magma. Temperatures of country rock at the contact of an intrusive body range from 586°C-728°C for magma intruding from 1000°C to 1200°C into rocks at 0°C. At 15 km (Chapter 6), the country rocks would have been considerably warmer than 0°C, thus raising the calculated temperatures some tens of degrees, depending on the geothermal gradient and surface temperature. Thus, depending on the composition of the country rock and the temperature of the magma, partial melting could have taken place around the Phalaborwa pipe.

The breakdown of potassium feldspar and mica occurs early in partial melting. These minerals would add much more Rb than ^{87}Sr. To raise values of $^{87}Sr/^{86}Sr$ to the extreme that Phalaborwa rocks have been raised necessitates addition of significant ^{87}Sr without ^{86}Sr. Green and Ringwood (1967) noted that strontium which primarily resides in plagioclase would be one of the last elements to enter a melt. Therefore, high degrees of partial melting would have to take place around Phalaborwa so that plagioclase would contribute natural strontium.

Blaxland et al. (1976) rejected this type of contamination in Ilimaussaq on grounds that considerable partial melting involving plagioclase would probably eliminate the peralkaline nature of the magma. As stated in Chapters 5, 7 and 8, the magma forming the pyroxenites was probably peralkaline; therefore, the same reasoning is also applicable at Phalaborwa.

Calculations involved in partial melting of crustal material with intruding magmas would be based on so many assumptions as to composition, and degree of partial melting that they are not appropriate. However, they would probably be on the order of magnitude of bulk assimilation and, therefore, may account for variations of initial $^{87}Sr/^{86}Sr$ ratios but would not account for raising initial ratios around 0.704 to 0.710 or higher. Therefore, the initial $^{87}Sr/^{86}Sr$ of the pyroxenites and sample Pir64-2356C must be considered as not being modified by partial melting of crustal material.

9.4.2.5.4 Equilibration of Sr with Crustal Rocks

Equilibration of Sr between a magma and crustal rock has been postulated by Heier (1964) and Pankhurst (1969). Little is known about how such a mechanism might work and it is usually called upon when all other theories fail to explain the data. It is particularly attractive for Phalaborwa rocks, because, unlike volcanic rocks and some carbonatites, these rocks are coarse grained, sometimes

pegmatitic, indicative of slow cooling in a crustal environment, which would be an ideal setting in which this process could operate.

Experimental work on transfer and diffusion of Sr under different conditions yields supportive information. Baadsgaard and Van Breemen (1970) heated adamellite in air and found that apatite gained considerable ^{87}Sr but little Rb while biotite gained common Sr and lost ^{87}Sr. Base exchange experiments by Kulp (1967) showed that ^{87}Sr and common Sr are readily movable in biotite and plagioclase.

The flexibility of this mechanism is that it could have taken place anywhere within the crust both at lower levels where the magma may have undergone fractionation or near the present emplacement level where there is indication of limited fluid interaction with wall rock in the form of narrow fenites. Clinopyroxene from feldspathic pyroxenite, found at the periphery of the main complex, does not have a higher initial $^{87}Sr/^{86}Sr$ ratio than clinopyroxenes toward the interior; this indicates that equilibration of Sr with crustal rocks at the present emplacement level did not occur. In addition, because of the lack of information on this process of equilibration with no melting, it is only conjectural to postulate this mechanism to explain the range in initial $^{87}Sr/^{86}Sr$ ratios at Phalaborwa.

9.4.3 Conclusions

Some of the mechanisms discussed in this chapter may account for variations in initial $^{87}Sr/^{86}Sr$ within single samples of a rock and within the pyroxenites as a group. None of the processes explored here can account for the range in carbonatites in the 0.704-0.706 range or for the high initial $^{87}Sr/^{86}Sr$ ratio of carbonatite and pyroxenites by methods of contamination of magma.

Post-crystallization process of diffusion of ^{87}Sr from phlogopite does not account for any of the variations. ^{87}Sr generated from formation of vermiculite may account for variations of initial $^{87}Sr/^{86}Sr$ ratios within single samples of handspecimens but cannot account for the larger variations observed here. Leaching experiments on clinopyroxenes and oxygen and carbon isotopic data confirm that groundwater alteration, by providing contaminant or altering the pyroxene composition, was not effective in altering the initial $^{87}Sr/^{86}Sr$ ratios to the values measured.

Processes operating prior to crystallization such as aging magma or assimilation of lower or upper crust may account for variations of initial $^{87}Sr/^{86}Sr$ within the pyroxenites as a rock type. These pre-crystallization processes do not account for variations within carbonatites in the 0.704-0.706 range, the high value of 0.710 found in one carbonatite, or for raising the pyroxenites from values of 0.704 to 0.710.

Disequilibrium melting cannot be ruled out. However, the sequence of events described below is preferred over disequilibrium melting, based on the sequence of intrusion of silicate liquid before carbonatite magma and the general lack of evidence that disequilibrium melting occurs.

Therefore, it is proposed here that the magmas forming the pyroxenites and the carbonatites are not cogenetic but were derived from an isotopically inhomogeneous mantle. The carbonatites were formed by at least two magmas, one with an initial $^{87}Sr/^{86}Sr$ of around 0.7039 which was typical of the southern African subcontinental mantle at 2030 m.y. The second carbonatite magma was characterized by very high $^{87}Sr/^{86}Sr$, around 0.7100, and was derived from a Rb-rich portion of the mantle. Mixing of these two carbonatite magmas created the range in initial $^{87}Sr/^{86}Sr$ ratios observed in the carbonatites. The magma forming pyroxenites originated in a Rb-rich mantle containing abundant phlogopite. This magma was modified during intrusion by interaction with wall rock or aging in the crust to form the observed variation in initial $^{87}Sr/^{86}Sr$ ratios.

However, because carbonatite magma is unlikely to be produced from mantle having undergone a previous melting episode, the carbonatite with high initial $^{87}Sr/^{86}Sr$ was produced from a different part of the mantle from that producing the magma forming the pyroxenites. Because of the sequential intrusion of distinct magmas in one place, this implies a mantle which is vertically inhomogeneous.

Chapter X

A PETROGENETIC MODEL

10.1 MAIN COMPLEX

10.1.1 Origin of Pyroxenites

The various types of pyroxenites in the main Phalaborwa complex formed by cumulus processes which included *in situ* accumulation of clinopyroxene, phlogopite and apatite to form the "inch-scale" layering at the outer contact of the complex, flow differentiation to form glimmerite and some flow-banded massive pyroxenites, and gravity separation. The magma from which the pyroxene, phlogopite, feldspar and apatite crystallized had a peralkaline composition as recorded by the low Al in clinopyroxene and phlogopite. The low silica activity, denoted by the high wollastonite content of clinopyroxene, may be a function of the peralkalinity of the liquid or the liquid may have been ultrabasic as well. Chemistry of the minerals at Phalaborwa are very similar to those produced experimentally in ultrabasic, peralkaline liquids such as the ultrapotassic lavas of Uganda and Wyoming (Barton and Hamilton, 1978).

The high Mg/Fe ratios and low Zr content of the pyroxenites suggest that the magma forming the pyroxenites was not highly differentiated. Low concentrations of Cr in the rocks point to earlier crystallization and removal of magnetite from the magma. The low concentrations of Na in

minerals within the complex suggest that the K/Na ratio in the magma was very high. The abundance of Fe^{3+} in phlogopites suggests that fO_2 was relatively high; this supports a low abundance of Na because Fe^{3+} was available for formation of acmite in pyroxenes.

Apatite was an inherent part of the magmatic crystallization of the pyroxenites as evidenced by its textural relations with pyroxene and phlogopite and its isotopic equilibrium with coexisting pyroxene. These features do not support a hydrothermal origin for apatite as suggested by Hanekom et al. (1965), DeJager and Fourie (1978), and Aldous (1980).

Feldspathic pyroxenites did not result from mixing of pyroxenite magma with country rock or as metasomatic replacement of country rock but crystallized as a cumulate. Pyroxene from feldspathic pyroxenite has the same initial $^{87}Sr/^{86}Sr$ ratio as pyroxenes from massive and micaceous pyroxenites, textures of pyroxenites and feldspar are indicative of magmatic minerals, and trace element chemistry of the rocks are similar to the other pyroxenites.

10.1.2 Origin of the Carbonatite

The carbonatites of the Phalaborwa complex have chemical characteristics such as high REE, Sr and Ba which preclude the theory of limestone assimilation for their origin. The initial $^{87}Sr/^{86}Sr$ ratios for the majority of carbonatite samples studied are characteristic of a mantle origin. The

initial $^{87}Sr/^{86}Sr$ ratios of the carbonatites are much lower than those for the pyroxenites which points to separate magmas for the carbonatite and pyroxenite rock types. The large range in $^{87}Sr/^{86}Sr$ ratios in the carbonatites may be accounted for by mechanisms occurring prior to emplacement and crystallization. The most likely mechanism is mixing of magmas of different initial $^{87}Sr/^{86}Sr$ ratios during ascent into the crust. The anomalously high initial $^{87}Sr/^{86}Sr$ ratio of 0.7100 for one carbonatite suggests that local heterogeneities are present in the mantle and that very high Rb/Sr is present in some pockets of the mantle, probably due to the presence of phlogopite. The lowest initial $^{87}Sr/^{86}Sr$ ratio of 0.7039 for the carbonatite measured is characteristic of continental mantle under the southern African subcontinent and points to a mantle enriched in Rb relative to suboceanic mantle.

Evidence such as Fe/(Fe+Mg) ratios and chemical trends in mineral chemistry of phlogopites and forsterite contents of olivine support the suggestion from isotopic data that the carbonatites are not cogenetic with the pyroxenites either by differentiation or immiscibility.

Isotopic equilibrium between apatite and its host carbonatite suggests that apatite results from magmatic crystallization with carbonates and was not a later, unrelated mineralization event. Textures such as extremely elongate apatites also point to magmatic crystallization.

The age of the carbonatite magmatism is well established as 2030 ± 18 m.y. based on U-Pb dating of uranothorianite and baddeleyite and Rb-Sr dating of phlogopite. Baddeleyite proved to be a reliable indicator of age for the Phalaborwa complex.

10.1.3 Origin of Phoscorite

Several lines of evidence point to a cogenetic origin for phoscorite with carbonatite magmatism. The age of the phoscorite, based on both U-Pb and Rb-Sr methods, is the same as the carbonatite. The mineral chemistry of the phlogopites is very similar to those in carbonatites in having relatively low Al, high Fe^{3+} and similar chemical trends. Likewise, olivine compositions are similar to those found in the banded carbonatite. Based on the low Ni content of olivine from phoscorite it was suggested earlier that magnetite may have been an early fractionating phase to deplete the magma in Ni. This was also the case with regard to depleting the magma forming the pyroxenites in Cr. If these two magmas are indeed not related genetically, it is surprising that magnetite crystallizes early in both magmas. Compositions of coexisting phases point to a low silica activity in magma forming the phoscorite.

Because most of the effort in the $^{87}Sr/^{86}Sr$ study was concentrated on explaining the wide range in initial $^{87}Sr/^{86}Sr$ ratios and the high values in both carbonatites and pyroxenites, there are no data concerning the initial $^{87}Sr/^{86}Sr$ of phases of the phoscorite.

The geologic relationship between the pyroxenite and phoscorite has been described as gradational by Lombaard et al. (1964) although this has not been observed in this study or by staff of PMC after extensive open pit mining operations (PMC staff, pers. comm., 1977). Therefore, it is considered here that phoscorite intruded into the pyroxenite forming sharp contacts and interleaved rocks due to intrusion along fractures parallel to the contact. Chill margins are absent due to the short time between intrusive events. There is no textural evidence that olivine formed metasomatically from pyroxene as postulated by Hanekom et al. (1965).

10.1.4 Emplacement History of the Main Complex

Intrusion of the main Phalaborwa complex commenced with a peralkaline, possibly ultrabasic liquid derived as a partial melt from a mantle highly enriched in phlogopite. At the edge of the complex, liquid crystallized to form inch-scale layering of phlogopite, apatite and clinopyroxene. Feldspathic pyroxenite formed as a cumulate with pyroxene as a cumulus phase and trapped intercumulus liquid forming intercumulus feldspar and minor apatite. Isotopic evidence suggests that assimilation of country rock was not operative in forming the feldspathic pyroxenite. Crystallization of phlogopite, pyroxene and apatite along with internal flow within the pipe promoted separation of phlogopite from clinopyroxene and apatite to form glimmerites and massive

pyroxenites. Micaceous pyroxenites formed in those places where separation was minimal. Undisturbed cooling of the complex from the edge inward did not occur, but multiple pulses of magma created internal currents within the magma and provided new magma. These pulses were not in isotopic equilibrium indicating that, in the upper mantle or more probably the crust, different amounts of contamination occurred prior to emplacement.

Quiescent spots within the pipe occurred as testified by pegmatoidal textures within micaceous pyroxenite. These are not the result of late stage crystallization because of the high Mg/Fe content of the pegmatoidal clinopyroxene and phlogopite.

Previously published maps of the Phalaborwa complex suggest that at least three centers of intrusion were operative with a coalescing of pyroxenite rock types.

Subsequent to intrusion of magma forming the pyroxenites, a silica-poor, carbonate-rich magma was intruded. This magma was derived from a part of the mantle which was isotopically distinct from the first magma. The timing of this magmatic event is well established at 2030 $\pm$ 18 m.y. Olivine, magnetite, apatite, and carbonate crystallized from this silica-poor magma forming the phoscorite. Mineral compositions indicate that conditions of oxygen fugacity were much the same as in the crystallizing pyroxenes. Constant buffering in two non-related magmas is not unrealistic, particularly if the

magmas have similar vapor compositions. As with the pyroxenites, cumulus processes were dominant giving rise to monomineralic assemblages such as dunite observed in previously published work (Lombaard et al., 1964; Hanekom et al., 1965).

Although not conclusively established, banded carbonatite probably formed from the second intrusion. The similar character of olivine and phlogopite between phoscorite and carbonatite, the same age, and the geologic relations point to these being cogenetic rocks.

However, the relationship of the phoscorite to carbonatite is not well established from the data presented here. There is no clear-cut indication of differentiation from phoscorite to carbonatite although it cannot be ruled out. Immiscibility of the magma to form a carbonate versus silicate-rich rock is also a possibility.

Lastly, intrusion of the transgressive carbonatite completed the magmatic activity of the main complex. This was limited to the previously formed carbonatite plug and cut across banding of earlier carbonatite as well as through phoscorite and pyroxenite; a few dykes of transgressive carbonatite extend into the country rock. The transgressive carbonatite is richer in phlogopite than the banded carbonatite. This may reflect higher silica composition than magma forming the banded carbonatite. The phoscorite contains some phlogopite but it is not as abundant as in the transgressive carbonatite.

One sample of transgressive carbonatite has a very high $^{87}Sr/^{86}Sr$ ratio. The transgressive carbonatite as defined may consist of multiple intrusions of magma not in isotopic equilibrium. These could result from various amounts of partial melting in a locally inhomogeneous mantle. The wide spread in initial $^{87}Sr/^{86}Sr$ ratios within the 0.704-0.706 range may reflect mixing with magmas of different initial $^{87}Sr/^{86}Sr$ during ascent and emplacement. Contamination by crustal rocks is difficult to envisage, but contamination by a phlogopite bearing rock, such as micaceous pyroxenite at depth, could account for the high ratios of the carbonatites.

Mineralization of the complex has not been under study here. However, no petrogenetic model of the Phalaborwa complex would be complete without some statement concerning the economic minerals of the complex. It has been suggested previously that apatite is an inherent part of the magmas forming Phalaborwa and is not a result of a late-stage hydrothermal fluid. This is based on textural, isotopic and chemical data. A strong piece of evidence for other minerals such as uranothorianite, baddeleyite, magnetite and sulphides being part of the magmatic process and not an unrelated, later hydrothermal event is the geologic relations. These minerals are strictly confined to phoscorite and carbonatite in the main complex. Late-stage fluids would surely permeate radial fractures in pyroxenite similarly to the intrusion of transgressive carbonatite.

There is no indication of such a process. Texturally, uranothorianite and baddeleyite have been placed early in the petrogenetic sequence (Van Rensburg, 1965). Likewise, copper sulphides have been found as inclusions in olivine (Aldous, 1980; Van Rensburg, 1965) indicating the presence of sulphide liquid during olivine crystallization. It is proposed here that sulphides may have separated from silicate-carbonate liquid at any point, but because of their low crystallization temperature relative to other phases, were mobilized late into fractures and around grain boundaries.

10.2 SATELLITES

10.2.1 Origin of the Guide Copper Mine

Several lines of evidence point to a cogenetic relationship of the feldspathic pyroxenite of the Guide Copper Mine with pyroxenites of the main complex. The rare, low-Al composition of Ca-rich pyroxenes and cumulus textures have analogues in the main complex. Isotopically, pyroxene from the Guide Copper Mine is indistinguishable from those of the main complex, and trace element chemistry is similar to feldspathic pyroxenites in the main complex.

The presence of abundant copper sulphides is suggestive of a link to the main complex although it is interpreted here that the pyroxenite magma of the main complex was not derived from the same magma as the copper-bearing rocks.

The oscillatory zoning of the pyroxenes in the Guide Copper Mine resulted from internal crystallization processes within the confines of the pipe.

10.2.2 A Model for the Syenite Pipes

The model of intrusion presented in Figure 3.16 for the relationships of satellite pipes to each other was based on field relations. It holds up with the addition of petrographic and chemical data. Vapor exsolving from a magma upon movement into the crust expanded rapidly to create the brecciation at the magma front. Release of pressure caused rapid infilling of brecciated space by minerals, namely alkali pyroxene from a vapor. Slightly lower in the pipe, magma also crystallized fairly rapidly with no opportunity for extensive separation although minor accumulation of feldspar occurred. Syenite at the base of Kgopoeloe represents this portion of the idealized model.

Still further away from the magma front, little brecciation occurred but cooling against country rock or previously intruded syenite or granite formed abrupt outer margins of syenites. Cooling inward accompanied by accumulation of various proportions of alkali-amphibole, -pyroxene, -feldspar and apatite falling through a low-viscosity liquid caused the textures and chemical characteristics exemplified at Spitskop.

Fine-grained dykes did not form from late-stage, highly differentiated liquid from these syenites or from liquids

forming the syenite dykes in the main complex. Heat from the intrusions may have caused partial melting of country rocks to produce these volumetrically insignificant rocks.

The magma forming these rocks of the satellite pipes was peralkaline but only slightly silica-undersaturated as indicated by the rocks overlapping syenitic to granitic compositions.

10.2.3 Origin of the Satellites

Evidence for a direct relationship between the syenites and pyroxenites of the satellites and the main complex consists of certain chemical characteristics. The mineral chemistry of chain silicates in the satellites and main complex is distinctive in the low Al_2O_3 content pointing to a peralkaline parental magma. Similarly, enriched total REE and high K/Na ratios are characteristics of both satellites and the main complex. The increased SiO_2, Zr, Fe/(Fe+Mg), Na/(Na+K) and reduced Ba and Sr concentrations point to increased differentiation from main complex to satellites.

However, other features put doubt on a cogenetic relationship. Certain aegirines in the satellites are high in Ti, a characteristic not compatible with pyroxenes of the main complex. High Wo components in clinopyroxenes of the main complex point to crystallization from a relatively silica-undersaturated liquid. In Chapter 8, it was pointed out that for liquid compositions from the main complex to be driven to the more silica-rich compositions of the

satellites, then a liquid must have at least 54-55% SiO_2. It is doubtful whether the clinopyroxenes of the main complex crystallized from such a liquid. In addition, the occurrence of differentiated pipes very close to the main complex places doubt on extensive fractionation over short distances.

Geological evidence from other workers also questions a direct relationship between these various intrusions. As discussed in Chapter 2, Brandt (1948) pointed out that similar syenites to the ones immediately surrounding the Phalaborwa main complex occur hundreds of kilometres from Phalaborwa. Briden (pers. comm., 1978) has paleomagnetic evidence that syenite magmatism may have taken place over a time span of some 150 m.y. or longer.

In view of the available data, it is suggested here that the syenites were not derived directly from the main complex at or near the level presently exposed. They may have been intruded as liquids from a much more deeply seated magma chamber. Evidence of multiple intrusion within the main complex argues for such a deep-seated chamber. The syenites may also be derived through a separate line of differentiation of a mantle-derived liquid originating at a different level or with higher degrees of partial melting than liquid forming the main complex. Wendlandt and Eggler (1980b) suggest depth of melting may control the Na/K ratio of a magma due to the relative stabilities of amphibole and phlogopite. More K-rich liquids corresponding to liquids of the main complex would originate at the greater depth.

10.3 SIGNIFICANCE OF THE PHALABORWA COMPLEX

10.3.1 Magmatic versus Metasomatic Processes

It has been emphasized throughout this thesis that solely metasomatic processes do not explain the petrogenesis of the Phalaborwa complex. Unquestionably, metasomatism has played a strong role in modifying country rocks but the main features in the rocks of Phalaborwa resulted from magmatic processes.

There is little study to date on the complex relationship of fluid interaction with rock during crystallization. Reaction relations such as olivine reacting with liquid to form clinopyroxene and phlogopite is commonly cited as phlogopitization, a form of metasomatism (Borodin and Pavlenko, 1974; Gittins et al., 1975). Certainly, water must be involved to form a hydrous mineral, but such a reaction is better described as strictly igneous.

Previous interpretations of metasomatic alteration of pyroxene to olivine (Hanekom et al., 1965; Palabora Mining Company, 1976) has no geologic basis other than the spatial arrangement of more silica-rich minerals such as clinopyroxene through olivine to carbonates. Again, based on current geologic knowledge, these may be ascribed to cumulus processes.

Thus, it must be stated that petrologists should use caution in describing alkaline rocks as generally being due to metasomatism. The petrogenesis of alkaline rocks may involve magmatic processes to a greater degree than has generally been accepted.

10.3.2 Mantle Inhomogeneity

The pyroxenites and carbonatites at Phalaborwa are characterized by significantly different, high initial $^{87}Sr/^{86}Sr$ ratios. These features lend strong support to a subcontinental mantle in southern Africa which is enriched in Rb/Sr relative to suboceanic mantle. The arguments for such a subcontinental mantle in southern Africa were presented in detail in section 9.4.2.2.

The presence of various types of igneous bodies with elevated initial $^{87}Sr/^{86}Sr$ ratios intruded over a time span of over three billion years in a geographical area of thousands of square kilometers points to large scale heterogeneities in the mantle. Within the Phalaborwa complex, magma possessing different initial $^{87}Sr/^{86}Sr$ ratios intruding through the same conduit suggest that local inhomogeneities also exist. These inhomogeneities may be on a grain-to-grain scale if pyroxenites and carbonatites originated by different amounts of partial melting from the same source. More likely, vertical inhomogeneities exist on a larger scale with different rock types originating from different depths. Vertical inhomogeneities as well as lateral variations probably exist in the mantle.

Data from Phalaborwa, namely the high Rb/Sr for the source region of magma producing the pyroxenites, suggest that mantle inhomogeneities would have occurred well before production of magma and that inhomogeneities must have been maintained for a significant period of time. Other workers

in southern Africa have come to the same conclusion (Barton et al., 1979, 1980).

Two main theories for isotopic and chemical inhomogeneities in the mantle are currently in vogue. One is that mixing of crustal material with the mantle at their interface has occurred through convective processes. Secondly, alkali metasomatism within the mantle has resulted in phlogopite enrichment and CO_2-rich phases. Metasomatism is preferred here because of the extreme isotopic compositions, REE and alkali enrichment.

10.4 FUTURE WORK

This study raises numerous questions with regard to Phalaborwa and to alkaline magmatism on a broader scale.

Phoscorite appears to be closely related to carbonatite magmatism, but any relationship with the pyroxenites of the main complex may be obscured by modification by carbonatite liquid. More extensive mineral chemistry on olivines and phlogopite may provide additional data as to the relationship between phoscorite and carbonatite. Initial $^{87}Sr/^{86}Sr$ ratios of olivines should be examined. Pb isotopes of sulphide inclusions in olivines and their comparison with later sulphide mineralization would also shed light on the origin of these minerals. Similar study on sulphides of the Guide Copper Mine would be useful in deciphering any genetic relationship between copper deposits.

Pleochroism in micas and its cause is receiving widespread attention due to the recognition of phlogopites with reverse pleochroism as megacrysts and in nodules in a variety of mantle-derived rocks. The dependency of pleochroism on composition of magma and fO_2 conditions should be studied experimentally and empirically.

The initial $^{87}Sr/^{86}Sr$ ratios of pyroxenites and some carbonatites from Phalaborwa are extremely high for mantle-derived rocks. Oxygen and carbon isotopic data suggest that there may be some correlation in $\delta^{18}O$, $\delta^{13}C$, and $^{87}Sr/^{86}Sr$ in carbonatites. More work is needed in this field, both at Phalaborwa and in general. O and C isotopic analyses of silicate phases will reinforce similar data on carbonate minerals. Nd isotopic study of the minerals of Phalaborwa will shed light the role of contamination in modifying $^{87}Sr/^{86}Sr$ ratios and provide information on the nature of subcontinental mantle with high $^{87}Sr/^{86}Sr$ values.

Dating of phlogopite resulted in unexpected difficulities. Washing of micas is generally considered a viable tool in dating such minerals. It was not proven to be detrimental or helpful here. The relationship between mica composition, rock type and age should be explored further to clarify the ages of pyroxenites. This has direct bearing on the petrogenesis of Phalaborwa and all mica-bearing rocks from the mantle.

Dating and obtaining initial $^{87}Sr/^{86}Sr$ ratios on the syenites will be a large step in clarifying the relationship

of the satellites to the main complex of Phalaborwa. More detailed work on additional satellites with different intrusive mechanisms and rock types will also fill in gaps in the model presented here.

10.5 CONCLUSIONS

(1) Magmatic processes dominate the formation of the main Phalaborwa complex. Pyroxenites, phoscorite and carbonatites are primarily cumulates with phlogopite, pyroxene, apatite, olivine, magnetite and calcite of these rocks crystallizing from magma.

(2) Metasomatism in the main complex is limited to fenitization of country rocks and minor amounts of phlogopite in carbonatite and phoscorite.

(3) Feldspathic pyroxenite crystallized as a cumulate and not from metasomatism of country rock or extensive mixing of magma with granite.

(4) The feldspathic pyroxenites of the Guide Copper Mine are cogenetic with pyroxenites of the main complex.

(5) Pyroxenites and carbonatites of the main complex are not cogenetic but crystallized from at least three magmas derived from different sources.

(6) Variation in initial $^{87}Sr/^{86}Sr$ ratios in carbonatites resulted from mixing of two carbonatite magmas.

(7) Pyroxenites crystallized from a peralkaline, ultrabasic liquid with high K, Sr, P_2O_5, REE. The magma had been modified prior to crystallization of pyroxenites by

removal of Cr, probably through crystallization of magnetite.

(7) Phoscorites are not cogenetic with pyroxenites but are most likely cogenetic with carbonatite.

(8) Reverse pleochroism in micas is due to the presence of Fe^{3+} greater than 0.1 cation per formula unit. This is due to an Al deficient magma as well as high fO_2 conditions.

(9) The syenite satellites are not cogenetic with pyroxenites of the main complex.

(10) The age of the Phalaborwa complex is 2030 $\pm$ 18 m.y. based on U-Pb dating of uranothorianite and baddeleyite and Rb-Sr dating of phlogopite. The ages of uranothorianite and baddeleyite are well established, but apparent ages of phlogopites are not in agreement; older micas may be present in the Phalaborwa complex.

(11) The main complex crystallized from magmas derived from subcontinental mantle which is isotopically heterogeneous, both on a local and regional scale. Phlogopite was present in the source regions of both carbonatites and pyroxenites.

Appendix A

SAMPLE LOCATIONS AND CHEMICAL DATA

A.1 Sample Numbering System

Figure A.1 Sample locations, PMC Area

Figure A.2 Sample locations, Foskor Area

Table A.1 Sample locations, Kgopoeloe

Table A.2 Sample locations, Spitskop

Table 5.1 Clinopyroxenes, microprobe data

Table 5.2 Clinopyroxenes, XRF data

Table 5.4 Micas, microprobe data

Table 5.5 Micas, XRF data

Table 5.6 Olivines, microprobe data

Table 5.7 Amphibole, feldspar, magnetite, main complex, microprobe data

Table 5.8 Clinopyroxene, amphibole, feldspar, satellites, microprobe data

Table 5.9 Clinopyroxenes, Guide Copper Mine, microprobe data

Table 7.1 Whole rock analyses, main complex, XRF

Table 7.2 Whole rock analyses, satellites, XRF

Table 7.3 Trace element data, carbonatites, XRF

SAMPLE NUMBERING SYSTEM

Prefix: Location

P Main Complex, PMC area
F Main Complex, Foskor area
K Kgopoeloe Hill
S Spitskop
C Country rock
G Guide Copper Mine

Samples with hyphenated numbers are from borehole cores - first letters refer to borehole designation - digits after hyphen refer to depth (m). For example, LK153-400K is a phoscorite sample from borehole LK153 at 400 m.

Suffix: Rock Type

F feldspathic pyroxenite
P micaceous pyroxenite
M massive pyroxenite
C carbonatite
K phoscorite
N fenitized country rock
X xenolith
S syenite, undesignated variety
m breccia matrix, Kgopoeloe
f breccia fragment, Kgopoeloe
g granite outcrop, Kgopoeloe
n gneissic fragment, Kgopoeloe
d dyke, Spitskop
r ring syenite, Spitskop
c central syenite, Spitskop
B gneissic biotite granite, country rock
V muscovite pegmatite, country rock
G pink granite, country rock

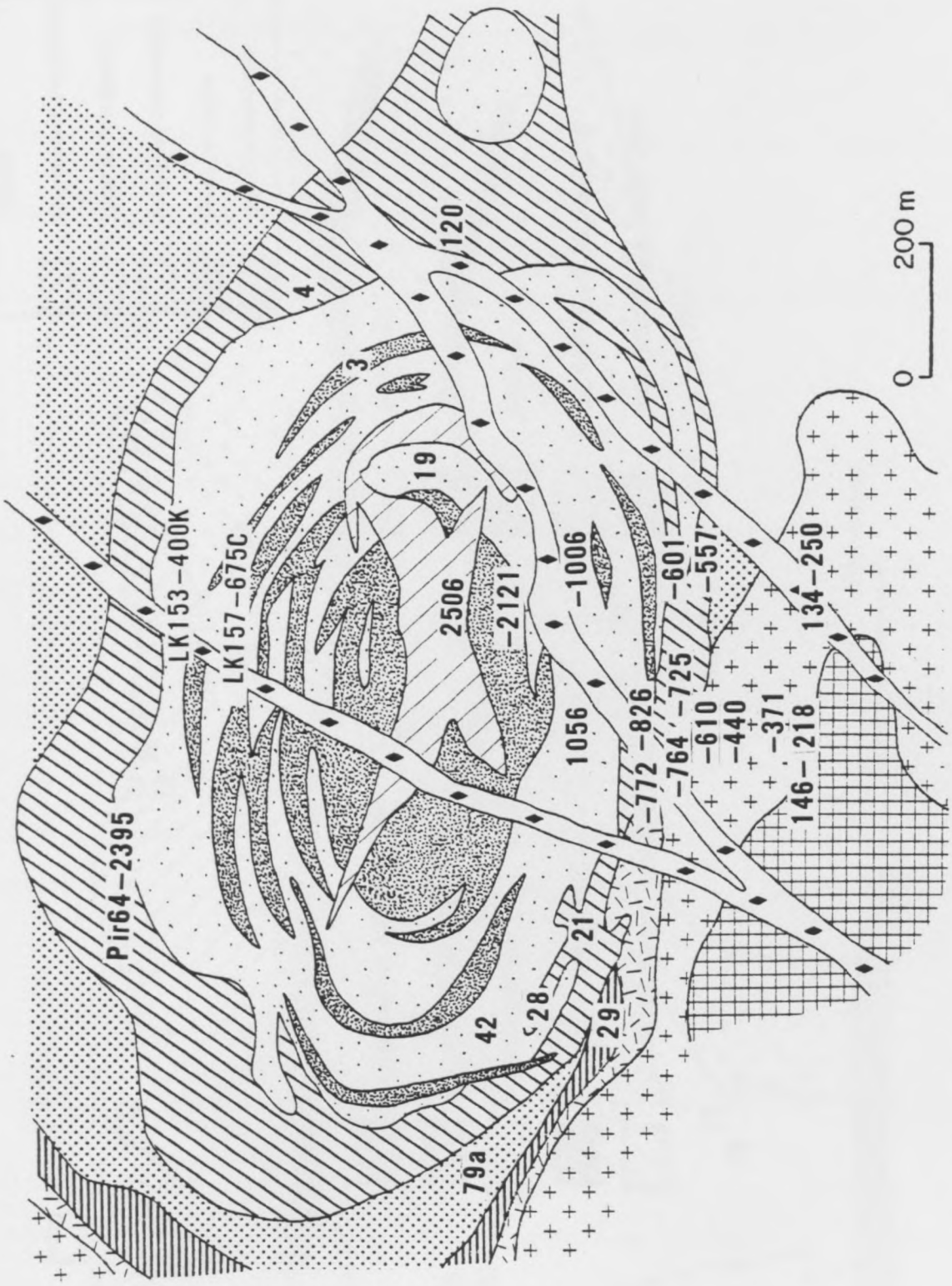


Figure A.1 Sample locations for mineral and whole rock analyses, PMC area.

LEGEND


TRANSGRESSIVE CARBONATITE


BANDED CARBONATITE


PHOSCORITE


PYROXENITE PEGMATOID


MICACEOUS PYROXENITE


PREDOMINANTLY MICA ROCK


FELDSPATHIC PYROXENITE


FENITE


GRANITE/GNEISS


DOLERITE

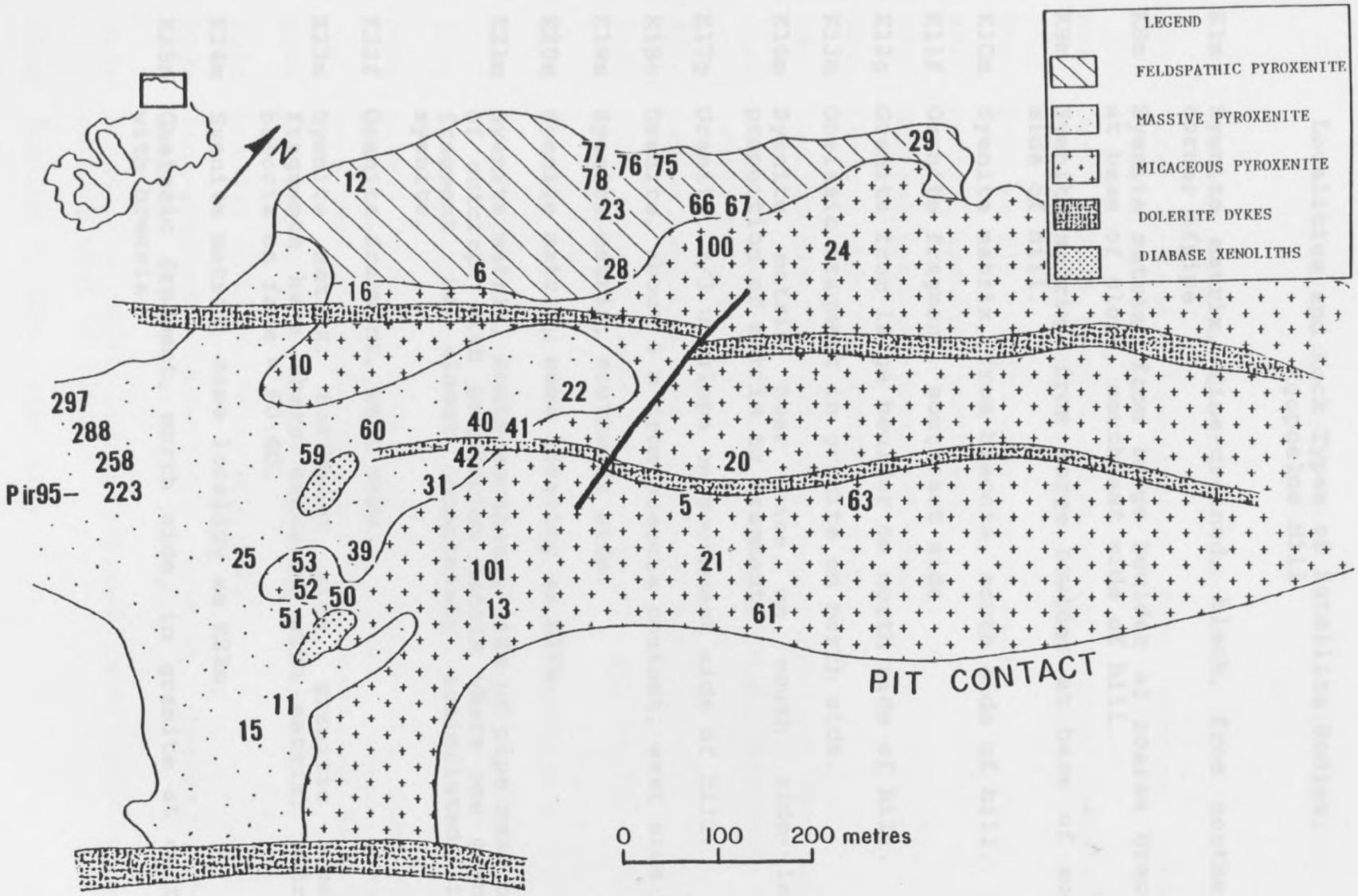


Figure A.2 Sample locations for minerals and whole rock samples from the Foskor open pit. These samples are prefixed by the letter F in the text with the exception of core samples from well Pir95.

Table A-1

Localities and Rock Types of Satellite Bodies, Kgopoeloe Hill

K1m Syenite matrix, fine-grained, black, from northeast corner ofpipe.

K8m Syenite matrix, from large boulder of coarse breccia at base of slope, southeast side of hill.

K9m Syenite matrix, from large boulder at base of south side of hill.

K10m Syenite matrix, from breccia, south side of hill.

K11f Granite fragment, southeast side.

K12g Granite from large boulder on north side of hill.

K13n Gneissic fragment in granite on north side.

K16m Syenite matrix near base on south side--large proportion of matrix to fragment.

K17g Granite, 2/3 up slope on southwest side of hill.

K18g Granite, about 4 m from breccia contact, west side.

K19m Syenite matrix, southwest side.

K20m Syenite matrix, same locality as K19g.

K21m Syenite matrix, south-southeast side of pipe near base of outcrop, high proportion matrix where one granite fragment is almost completely assimilated into syenite.

K22f Granite fragment, west side.

K23m Syenite matrix, northeast side, granitic breccia fragments have sharp contacts with matrix; matrix: breccia on face = 60:40.

K24m Syenite matrix, same locality as K23m.

K25n Gneissic fragment, north side, in granite at contact with breccia.

Table A-2

Localities and Rock Types of Satellite Bodies, Spitskop

S1c	Central syenite, northeast side.
S2d	Fine grained, leucocratic dyke cutting central syenite, north side.
S3r	Dark, alkali syenite, ring around central syenite--at contact with central syenite, north side.
S4r	Same as S3r - 2 ft. away, north side.
S5c	Central syenite, north side.
S7c	Central syenite, northwest side.
S8c	Central syenite, northwest side.
S9c	Central syenite, extremely coarse-grained, west side.
S10c	Central syenite, north side near top, probably near centre of pipe.
S11c	Central syenite, east side near top.
S12d	Fine grained leucocratic dykelet, strike 80°, top of pipe near S11c.
S13c	Central syenite, very fine grained, south side.
S16s	Syenite from low hillock on east side of Spitskop.
S17c	Syenite, south side of Spitskop.
S19r	Alkali syenite, fine grained, needle-like dark green pyroxenes in poikilitic microcline, coarse grained rock west of large outcrop at northeast side of hill.
S20r	Similar to S19r, outer edge of outcrop.
S21r	Similar to S20r, finer grained.
S22r	Fine-grained, leucocratic dykelet, inside central syenite, near outcrop of S19r-S21r.
S23r	Similar to S20r, coarse grained, near outer edge of outcrop west of S20r.
S24r	Similar to S21r, near S23r.

TABLE 5.1
Microprobe Analyses of Clinopyroxenes

	P146-218N				P146-374N					P146-440N			
	1(2)	2(2)	2(3)	3(2)	1(1)	2(2)	2(2)	3(2)	3(2)	1(2)	2(2)	3(2)	3(2)
SiO_2	53.87	53.50	53.58	53.53	52.02	52.32	51.89	52.21	50.82	51.12	52.38	52.20	51.59
TiO_2	0.15	0.21	0.00	0.14	0.00	0.00	0.00	0.00	0.00	0.05	0.05	0.06	0.00
Al_2O_3	0.20	0.38	0.28	0.24	2.02	1.83	2.11	0.89	1.04	0.11	0.15	0.14	0.12
FeO	5.08	6.07	7.26	8.35	12.05	12.32	12.76	12.64	12.84	20.38	17.52	17.72	19.94
MnO	0.18	0.14	0.09	0.22	0.49	0.53	0.44	0.49	0.50	0.33	0.34	0.33	0.32
MgO	15.27	15.01	13.95	13.26	11.12	10.73	11.25	10.74	10.79	6.06	7.74	7.65	6.21
CaO	24.47	23.18	22.20	21.56	21.01	21.32	20.99	21.43	21.26	13.44	15.81	15.49	13.62
Na_2O	0.26	0.96	1.38	1.76	1.35	1.51	0.73	1.46	0.63	6.40	5.00	5.25	6.19
Total	99.51	99.61	98.73	99.09	100.06	100.36	100.16	99.68	98.03	97.86	99.01	98.85	98.00
No. of cations based on 6 oxygens													
Si	1.992	1.978	1.996	1.993	1.957	1.957	1.957	1.979	1.972	1.962	1.986	1.978	1.977
Al	0.008	0.017	0.004	0.007	0.043	0.043	0.043	0.021	0.028	0.005	0.007	0.006	0.005
Tet. Total	2.000	1.995	2.000	2.000	2.000	2.000	2.000	2.000	2.000	1.967	1.993	1.984	1.983
Al	0.000	0.000	0.008	0.003	0.046	0.038	0.051	0.019	0.020	0.000	0.000	0.000	0.000
Ti	0.005	0.004	0.000	0.004	0.000	0.000	0.000	0.000	0.000	0.000	0.001	0.002	0.000
Fe^{3+}	0.020	0.069	0.100	0.127	0.099	0.110	0.053	0.107	0.047	0.476	0.369	0.387	0.463
Fe^{2+}	0.138	0.119	0.126	0.134	0.270	0.276	0.343	0.282	0.364	0.137	0.187	0.150	0.153
Mn	0.006	0.004	0.003	0.007	0.016	0.017	0.014	0.016	0.016	0.011	0.011	0.011	0.010
Mg	0.842	0.825	0.775	0.736	0.623	0.598	0.632	0.607	0.624	0.347	0.437	0.432	0.355
Ca	0.970	0.916	0.887	0.860	0.847	0.855	0.848	0.863	0.884	0.553	0.642	0.629	0.559
Na	0.021	0.068	0.100	0.127	0.098	0.110	0.053	0.107	0.047	0.476	0.367	0.386	0.460
Oct. Total	2.000	2.003	2.000	2.004	1.999	2.002	1.996	2.001	2.004	2.000	2.016	2.001	2.000
Fe/(Fe + Mg)	0.16	0.18	0.23	0.26	0.37	0.39	0.39	0.39	0.40	0.65	0.56	0.57	0.64

The numbers beneath sample numbers represent the grains analyzed and, in parentheses, the number of analyses averaged. For example, 2(3) represents grain two with three analyses averaged for that spot.

TABLE 5.1 (Continued)
Microprobe Analyses of Clinopyroxenes

	P146-610N			F6F			F15M						
	1(2)	2(2)	2(2)	1(2)	1(2)	2(2)	1(2)	1(2)	2(2)	2(3)	3(2)	3(2)	4(2)
SiO_2	51.27	52.51	51.33	54.28	54.38	54.82	53.44	53.22	53.93	52.27	53.35	53.72	54.09
TiO_2	0.19	0.35	0.16	0.17	0.00	0.00	0.00	0.17	0.17	0.00	0.00	0.00	0.00
Al_2O_3	0.41	0.04	0.41	0.27	0.25	0.18	0.09	0.22	0.12	0.12	0.21	0.13	0.26
FeO	16.99	7.66	16.86	5.78	5.57	4.69	5.10	4.94	4.48	6.20	5.29	6.01	4.02
MnO	0.45	0.23	0.36	0.18	0.21	0.00	0.29	0.00	0.13	0.18	0.16	0.17	0.00
MgO	8.01	14.23	7.97	15.10	14.99	15.52	15.46	15.69	16.13	15.15	15.36	15.08	16.20
CaO	19.80	23.23	19.88	24.96	25.14	24.35	24.44	24.55	24.87	24.02	24.65	23.94	24.77
Na_2O	2.30	0.51	2.22	0.42	0.37	0.38	0.49	0.37	0.41	0.63	0.33	0.62	0.28
Total	99.44	98.77	99.24	101.18	100.91	99.98	99.30	99.16	100.24	98.57	99.39	99.68	99.63
No. of cations based on 6 oxygens													
Si	1.970	1.972	1.978	1.982	1.989	2.007	1.983	1.976	1.977	1.965	1.981	1.987	1.988
Al	0.019	0.002	0.019	0.012	0.011	0.000	0.004	0.010	0.005	0.005	0.009	0.006	0.011
Tet. Total	1.989	1.974	1.996	1.993	2.000	2.007	1.987	1.986	1.982	1.970	1.990	1.993	1.999
Ti	0.005	0.010	0.005	0.005	0.000	0.000	0.000	0.005	0.005	0.000	0.000	0.000	0.000
Fe^{3+}	0.171	0.037	0.166	0.030	0.026	0.027	0.035	0.027	0.029	0.046	0.024	0.045	0.020
Fe^{2+}	0.364	0.204	0.376	0.147	0.144	0.117	0.123	0.127	0.108	0.149	0.140	0.141	0.104
Mn	0.015	0.007	0.012	0.006	0.007	0.000	0.009	0.000	0.004	0.006	0.005	0.005	0.000
Mg	0.459	0.796	0.458	0.882	0.817	0.847	0.855	0.868	0.881	0.849	0.852	0.832	0.888
Ca	0.815	0.935	0.821	0.997	0.985	0.956	0.972	0.977	0.977	0.968	0.981	0.949	0.976
Na	0.171	0.037	0.166	0.030	0.026	0.027	0.035	0.027	0.029	0.046	0.024	0.044	0.020
Oct. Total	2.000	2.027	2.004	2.014	2.006	1.996	2.029	2.029	2.034	2.063	2.025	2.017	2.007
Fe/(Fe + Mg)	0.54	0.23	0.54	0.18	0.17	0.15	0.16	0.15	0.13	0.19	0.16	0.18	0.12

TABLE 5.1 (Continued)
Microprobe Analyses of Clinopyroxenes

	F100P						P4P			
	1(2)	1(2)	2(2)	2(3)	3(2)	3(2)	1(2)	1(2)	2(2)	2(2)
SiO_2	55.28	54.65	54.20	53.67	53.22	53.56	53.14	53.82	53.7	54.02
TiO_2	0.12	0.20	0.15	0.16	0.23	0.22	0.12	0.08	0.08	0.12
Al_2O_3	0.13	0.09	0.00	0.00	0.07	0.04	0.10	0.04	0.14	0.14
FeO	2.26	2.61	2.72	2.64	2.61	2.49	7.60	5.82	8.27	9.63
MnO	0.04	0.05	0.04	0.06	0.05	0.04	0.23	0.23	0.25	0.29
MgO	17.50	17.24	17.16	17.15	17.47	17.72	14.67	15.81	14.09	13.25
CaO	24.39	23.84	24.75	24.66	25.15	25.22	23.68	23.46	23.41	22.70
Na_2O	0.12	0.21	0.00	0.00	0.17	0.14	0.70	0.39	0.58	0.93
Total	99.84	98.89	99.02	98.34	98.97	99.43	100.24	99.65	100.52	101.08
No. of cations based on 6 oxygens										
Si	2.006	2.004	1.995	1.990	1.966	1.967	1.974	1.989	1.987	1.993
Al	0.000	0.000	0.000	0.000	0.003	0.002	0.004	0.002	0.006	0.006
Tet. Total	2.006	2.004	1.995	1.990	1.969	1.969	1.978	1.991	1.993	1.999
Al	0.012	0.008	0.000	0.000	0.000	0.000	0.000	0.000	0.000	0.000
Ti	0.003	0.006	0.004	0.004	0.006	0.006	0.003	0.002	0.002	0.003
Fe^{3+}	0.008	0.015	0.000	0.000	0.012	0.010	0.051	0.028	0.042	0.067
Fe^{2+}	0.060	0.065	0.084	0.082	0.068	0.067	0.185	0.152	0.215	0.230
Mn	0.001	0.002	0.001	0.002	0.002	0.001	0.811	0.871	0.777	0.729
Mg	0.947	0.942	0.941	0.948	0.962	0.970	0.007	0.007	0.008	0.009
Ca	0.948	0.932	0.976	0.980	0.995	0.993	0.941	0.929	0.928	0.897
Na	0.008	0.015	0.000	0.000	0.012	0.010	0.050	0.028	0.042	0.067
Oct. Total	1.988	1.989	2.007	2.016	2.058	2.057	2.049	2.017	2.014	2.002
Fe/(Fe + Mg)	0.07	0.08	0.08	0.08	0.08	0.07	0.23	0.17	0.25	0.29

TABLE 5.1 (Continued)
Microprobe Analyses of Clinopyroxenes

	P120P								
	1(2)	1(2)	2(2)	2(2)	3(2)	3(2)	5(2)	6(2)	6(2)
SiO_2	54.50	54.50	54.29	53.07	53.28	53.52	51.82	52.39	52.96
TiO_2	0.00	0.02	0.01	0.01	0.04	0.05	0.07	0.09	0.00
Al_2O_3	0.00	0.00	0.00	0.00	0.17	0.07	0.42	0.03	0.02
FeO	4.04	4.63	7.32	7.17	8.84	8.78	11.05	8.43	11.33
MnO	0.13	0.15	0.17	0.17	0.18	0.17	0.23	0.18	0.18
MgO	16.29	16.79	14.41	14.21	13.17	13.20	11.72	13.61	11.37
CaO	24.51	23.60	23.20	23.65	23.04	23.21	22.32	23.32	21.98
Na_2O	0.43	0.42	0.73	0.72	0.83	0.91	1.06	0.65	1.24
Total	99.90	100.11	100.13	98.97	99.55	99.91	98.69	98.70	99.08
No. of cations based on 6 oxygens									
Si	1.995	1.995	2.003	1.987	1.993	1.994	1.976	1.981	2.005
Al	0.000	0.000	0.000	0.000	0.007	0.003	0.019	0.001	0.000
Tet. Total	1.995	1.995	2.003	1.987	2.000	1.997	1.995	1.982	2.005
Al	0.000	0.000	0.003	0.000	0.001	0.000	0.000	0.000	0.006
Ti	0.000	0.001	0.000	0.000	0.001	0.001	0.002	0.003	0.000
Fe^{3+}	0.031	0.013	0.052	0.052	0.060	0.066	0.079	0.048	0.091
Fe^{2+}	0.093	0.129	0.174	0.172	0.216	0.208	0.274	0.219	0.268
Mn	0.004	0.005	0.005	0.005	0.006	0.005	0.007	0.006	0.006
Mg	0.889	0.916	0.793	0.793	0.734	0.733	0.666	0.767	0.642
Ca	0.962	0.926	0.917	0.949	0.924	0.927	0.912	0.945	0.892
Na	0.031	0.030	0.052	0.052	0.060	0.066	0.078	0.048	0.091
Oct. Total	2.009	2.019	1.996	2.023	2.002	2.006	2.018	2.034	1.995
Fe/(Fe + Mg)	0.12	0.13	0.22	0.22	0.27	0.27	0.34	0.26	0.36

TABLE 5.1 (Continued)
Microprobe Analyses of Clinopyroxenes

	P146-1056K													
	1(2)c	2(2)c	2(2)	2(3)r	3(2)c	3(2)	3(2)r	4(1)c	4(2)	4(2)	4(2)r	5(2)c	5(2)	5(2)c
SiO_2	50.53	51.78	49.94	53.51	51.36	52.07	52.90	53.52	54.11	53.72	52.04	49.92	50.18	53.50
TiO_2	0.25	0.15	0.87	0.26	0.29	0.21	0.00	0.17	0.18	0.18	0.16	0.16	0.21	0.00
Al_2O_3	0.55	0.34	0.31	0.36	0.45	0.60	0.48	0.19	0.18	0.20	0.20	0.63	0.63	0.18
FeO	18.83	17.38	20.08	9.51	21.50	14.60	11.60	7.48	6.86	6.85	7.05	16.79	15.22	7.24
MnO	0.39	0.45	0.37	0.31	0.51	0.35	0.51	0.18	0.19	0.31	0.28	0.16	0.00	0.28
MgO	7.39	8.01	7.03	13.44	6.02	10.09	11.94	14.74	14.86	14.91	14.42	8.58	9.50	14.53
CaO	21.21	21.48	19.32	22.71	18.83	21.47	22.69	23.41	23.80	23.63	23.58	21.07	21.44	24.37
Na_2O	1.69	1.66	2.44	1.30	2.72	1.69	1.20	0.87	0.71	0.91	1.04	1.85	1.66	0.72
Total	100.83	101.25	100.33	101.40	101.66	101.07	101.13	100.56	100.89	100.71	98.81	99.46	98.85	100.85
No. of cations based on 6 oxygens														
Si	1.954	1.977	1.942	1.971	1.973	1.965	1.972	1.975	1.985	1.976	1.959	1.946	1.946	1.974
Al	0.025	0.015	0.014	0.016	0.020	0.027	0.021	0.008	0.008	0.009	0.009	0.029	0.029	0.008
Tet. Total	1.979	1.993	1.957	1.987	1.993	1.992	1.993	1.983	1.992	1.984	1.968	1.975	1.977	1.982
Ti	0.007	0.004	0.025	0.007	0.008	0.006	0.000	0.005	0.005	0.005	0.005	0.005	0.006	0.000
Fe^{3+}	0.127	0.123	0.184	0.095	0.203	0.124	0.087	0.062	0.051	0.065	0.076	0.140	0.125	0.052
Fe^{2+}	0.468	0.418	0.449	0.187	0.466	0.323	0.265	0.162	0.154	0.139	0.138	0.392	0.355	0.166
Mn	0.013	0.015	0.012	0.010	0.017	0.011	0.016	0.006	0.006	0.010	0.009	0.005	0.000	0.009
Mg	0.426	0.456	0.408	0.738	0.345	0.568	0.663	0.811	0.812	0.817	0.809	0.498	0.550	0.799
Ca	0.879	0.879	0.806	0.896	0.775	0.868	0.906	0.926	0.935	0.930	0.951	0.880	0.892	0.964
Na	0.127	0.123	0.184	0.093	0.203	0.124	0.087	0.062	0.050	0.065	0.076	0.140	0.125	0.052
Oct. Total	2.047	2.018	2.068	2.026	2.016	2.024	2.025	2.033	2.014	2.031	2.064	2.060	2.054	2.041
Fe/(Fe + Mg)	0.58	0.54	0.61	0.28	0.66	0.44	0.35	0.22	0.20	0.20	0.21	0.52	0.47	0.21

c=core
r=rim

TABLE 5.2

X-ray Fluorescence Analyses of Clinopyroxenes

	F10P	F15M	F21P	F101P	P21P	P28P	P146-764P	P146-826P	G12F
SiO_2	53.48	54.10	55.17	55.46	53.26	54.38	53.90	53.41	53.05
TiO_2	0.15	0.15	0.17	0.21	0.26	0.30	0.13	0.12	0.22
Al_2O_3	1.46	0.38	0.59	0.29	0.79	0.55	1.23	0.39	0.50
FeO	6.00	5.54	2.99	2.49	10.52	5.17	9.69	6.68	9.54
MnO	0.13	0.13	0.05	0.06	0.22	0.10	0.21	0.22	0.20
MgO	16.74	16.26	19.79	19.11	14.17	16.92	13.76	15.66	14.17
CaO	22.44	23.02	21.92	22.29	20.94	21.71	19.74	22.49	20.92
Na_2O	0.15	0.22	0.00	0.00	0.24	0.02	0.44	0.61	0.41
K_2O	0.06	0.02	0.08	0.10	0.20	0.14	0.49	0.09	0.03
P_2O_5	0.42	0.22	0.06	0.05	0.06	0.21	0.08	0.00	0.00
LOI	0.06	0.01	0.16	0.57	0.30	0.55	0.76	0.43	1.38
Total	100.93	100.03	100.99	100.65	100.95	100.05	100.13	100.14	100.44
No. Cations based on 6 oxygens									
Si	1.960	1.988	1.980	2.002	1.981	2.000	2.019	1.977	1.969
Al	0.040	0.012	0.020	0.000	0.019	0.000	0.000	0.017	0.022
Tet. Total	2.000	2.000	2.000	2.002	2.000	2.000	2.019	1.994	1.991
Al	0.023	0.005	0.005	0.014	0.016	0.024	0.074	0.000	0.000
Ti	0.004	0.004	0.005	0.006	0.007	0.008	0.004	0.003	0.006
Fe^{3+}	0.011	0.016	0.000	0.000	0.017	0.001	0.032	0.044	0.030
Fe^{2+}	0.173	0.155	0.090	0.075	0.310	0.158	0.232	0.163	0.272
Mn	0.004	0.004	0.002	0.002	0.007	0.003	0.007	0.007	0.006
Mg	0.914	0.892	1.059	1.028	0.786	0.928	0.773	0.864	0.829
Ca	0.865	0.908	0.843	0.862	0.835	0.856	0.797	0.892	0.848
Na	0.011	0.016	0.000	0.000	0.017	0.001	0.032	0.044	0.030
Oct. Total	2.005	1.999	2.003	1.986	1.994	1.979	1.950	2.017	2.022
Trace Elements									
Sr	532	533	369	318	296	360	449	382	419
Rb	6	2	5	BDL	7	BDL	26	6	11
Ba	BDL	BDL	30	67	378	46	319	164	BDL
Ce	71	69	24	30	35	76	68	55	33
La	33	41	9	15	21	39	32	12	16
V	2	2	3	BDL	2	BDL	3	1	2
Ca	8	6	10	16	21	5	24	6	457
Ni	72	70	197	56	53	40	28	89	30
Zn	44	40	21	21	69	39	68	45	67
Fe/(Fe+Mg)	0.17	0.16	0.08	0.07	0.29	0.15	0.28	0.19	0.24

TABLE 5.4
Microprobe Analyses of Micas

	F100P					P146-374N	P146-772P			
	1(2)	2(2)	3(2)	4(2)	5(2)	(5)	1(3)	2(2)	3(2)	4(3)
SiO_2	43.55	42.52	42.44	41.85	42.70	36.13	40.51	40.84	40.71	40.65
TiO_2	0.64	0.58	0.79	0.88	0.68	4.32	1.03	0.96	1.03	1.03
Al_2O_3	10.50	10.44	10.60	11.02	10.85	13.09	11.79	11.43	11.47	11.58
FeO	7.16	7.07	6.62	6.39	6.47	20.84	12.44	12.07	12.48	12.24
MnO	0.07	0.07	0.07	0.08	0.08	0.18	0.10	0.10	0.11	0.11
MgO	26.46	26.46	26.37	26.09	26.42	10.75	21.25	21.62	21.38	21.27
K_2O	10.15	10.22	10.22	10.25	10.31	9.29	10.11	9.95	9.96	9.86
Na_2O	0.05	0.06	0.07	0.06	0.06	0.07	0.08	0.08	0.08	0.08
Total	98.58	97.42	97.19	96.62	97.57	94.67	97.31	97.05	97.22	96.82
No. of cations based on 22 oxygens										
Si	6.040	5.982	5.974	5.925	5.979	5.616	5.859	5.905	5.890	5.894
Al	1.719	1.732	1.749	1.839	1.791	2.399	2.009	1.948	1.956	1.979
Fe	0.830	0.832	0.779	0.758	0.758	2.711	1.505	1.459	1.510	1.485
Ti	0.067	0.061	0.083	0.094	0.072	0.505	0.113	0.104	0.112	0.113
Mn	0.009	0.008	0.009	0.009	0.009	0.024	0.012	0.012	0.014	0.014
Mg	5.469	5.550	5.533	5.505	5.516	2.491	4.582	4.659	4.610	4.596
K	1.796	1.834	1.836	1.852	1.843	1.843	1.865	1.835	1.839	1.824
Na	0.014	0.017	0.019	0.015	0.016	0.021	0.023	0.021	0.022	0.023
Site Occupancy										
Z	7.826	7.775	7.806	7.858	7.842	8.009	7.981	7.957	7.958	7.986
	(.174)	(.225)	(.194)	(.142)	(.158)	-(.009)	(.019)	(.043)	(.042)	(.014)
Y	6.308	6.390	6.321	6.272	6.283	5.731	6.099	6.13	6.134	6.095
X	1.810	1.851	1.855	1.867	1.859	1.864	1.888	1.856	1.861	1.847
Fe/(Fe + Mg)	0.13	0.13	0.12	0.12	0.12	0.52	0.25	0.24	0.25	0.24
Pleochroism	R	R	R	R	R	N	N	N	N	N

R = Reverse; N = Normal
Numbers in parentheses represent the deficiency in the tetrahedral site.

TABLE 5.4 (Continued)
Microprobe Analyses of Micas

	P120P													
	1(1)	2(1)	3(1)	3(1)	3(1)	4(1)	4(1)	4(1)	4(1)	6(1)	6(1)	7(1)	7(1)	7(1)
SiO_2	41.29	39.74	41.77	42.51	41.48	41.54	41.90	40.23	40.75	40.10	41.27	39.95	40.48	40.93
TiO_2	0.21	0.17	0.34	0.28	0.24	0.59	0.60	0.68	0.65	0.88	0.96	1.09	0.90	0.75
Al_2O_3	6.27	7.81	7.92	9.49	9.52	9.71	10.59	10.65	10.39	10.93	10.99	11.18	11.17	10.82
FeO	14.22	14.14	11.10	11.33	11.92	12.18	13.03	15.19	15.20	15.00	13.45	12.65	12.75	12.63
MnO	0.06	0.06	0.07	0.05	0.12	0.07	0.08	0.07	0.09	0.09	0.08	0.07	0.10	0.07
MgO	25.24	24.36	24.87	25.26	25.32	23.46	23.01	21.80	22.06	21.28	21.38	21.17	21.61	21.95
K_2O	9.62	9.77	9.73	10.08	9.70	9.57	9.82	9.56	9.79	9.95	9.80	9.96	9.94	10.06
Na_2O	0.02	0.02	0.01	0.01	0.02	0.02	0.01	0.03	0.01	0.02	0.01	0.02	0.03	0.01
Total	96.93	96.07	95.81	99.13	98.32	97.18	99.05	98.22	98.95	98.24	97.95	96.09	96.98	97.21
No. of cations based on 22 oxygens														
Si	6.068	5.908	6.099	5.997	5.425	5.991	5.948	5.835	5.868	5.821	5.940	5.864	5.882	5.929
Al	1.085	1.369	1.363	1.578	1.601	1.650	1.773	1.821	1.764	1.870	1.864	1.934	1.913	1.847
Fe	1.748	1.757	1.355	1.337	1.423	1.470	1.547	1.842	1.830	1.821	1.620	1.553	1.550	1.530
Ti	0.023	0.019	0.038	0.030	0.026	0.064	0.062	0.074	0.070	0.095	0.104	0.120	0.099	0.082
Mn	0.007	0.007	0.008	0.006	0.015	0.008	0.010	0.009	0.010	0.011	0.010	0.009	0.012	0.009
Mg	5.529	5.398	5.413	5.310	5.386	5.044	4.869	4.712	4.736	4.604	4.586	4.633	4.681	4.741
K	1.804	1.853	1.813	1.814	1.766	1.762	1.778	1.766	1.799	1.843	1.799	1.865	1.843	1.859
Na	0.000	0.007	0.002	0.002	0.002	0.006	0.002	0.007	0.003	0.005	0.004	0.007	0.009	0.003
Site Occupancy														
Z	7.176	7.296	7.500	7.605	7.052	7.705	7.783	7.730	7.702	7.786	7.908	7.918	7.894	7.858
	(.824)	(.704)	(.500)	(.395)	(.948)	(.295)	(.217)	(.270)	(.298)	(.214)	(.092)	(.082)	(.106)	(.142)
Y	7.278	7.162	6.776	6.653	6.824	6.522	6.426	6.563	6.576	6.436	6.216	6.195	6.243	6.280
X	1.804	1.860	1.815	1.816	1.768	1.768	1.780	1.773	1.802	1.848	1.803	1.872	1.852	1.862
Fe/(Fe + Mg)	0.24	0.25	0.20	0.20	0.21	0.23	0.24	0.28	0.28	0.28	0.26	0.25	0.25	0.24
Pleochroism	R	R	R	R	R	R	R	R	R	R	R	R+	R+	R+

TABLE 5.4 (continued)
Microprobe Analyses of Micas

	P146-725P				P146-1056K		
	1(2)	2(2)	2(2)	3(2)	1(2)	1(2)	2(2)
SiO_2	42.21	41.81	42.04	42.44	40.04	42.00	42.05
TiO_2	1.20	1.23	1.25	1.17	0.00	0.00	0.13
Al_2O_3	11.33	11.45	11.72	11.29	8.55	8.73	9.25
FeO	10.19	10.45	10.66	10.28	8.22	7.47	6.69
MnO	0.04	0.03	0.05	0.03	0.11	0.00	0.00
MgO	22.85	22.66	22.51	22.90	24.31	24.72	24.47
K_2O	9.86	9.98	9.97	9.82	10.44	10.56	10.59
Na_2O	0.08	0.08	0.10	0.09	0.00	0.00	0.00
Total	97.75	97.68	98.30	98.02	91.67	93.48	93.18
No. of cations based on 22 oxygens							
Si	5.982	5.946	5.942	5.997	6.072	6.190	6.189
Al	1.892	1.920	1.953	1.880	1.529	1.517	1.605
Fe	1.208	1.243	1.260	1.215	1.043	0.921	0.824
Ti	0.128	0.132	0.134	0.125	0.000	0.000	0.014
Mn	0.005	0.004	0.005	0.004	0.014	0.000	0.000
Mg	4.827	4.802	4.741	4.824	5.495	5.430	5.368
K	1.783	1.810	1.799	1.770	2.020	1.986	1.989
Na	0.022	0.021	0.028	0.024	0.000	0.000	0.000
Site Occupancy							
Z	8.002	7.998	8.029	8.002	7.601	7.707	7.808
	(+.002)	(.002)	(+.029)	(+.002)	(.399)	(.293)	(.192)
Y	6.040	6.049	6.006	6.043	6.552	6.351	6.192
X	1.805	1.831	1.827	1.794	2.020	1.986	1.989
Fe/(Fe + Mg)	0.20	0.21	0.21	0.20	0.16	0.15	0.13
Pleochroism	N	N	N	N	R	R	R

TABLE 5.4 (Continued)
Microprobe Analyses of Micas

	P134-2121C						P19K			P3C	
	1(3)	2(3)	3(2)	3(2)	3(2)	3(2)	1(2)	2(2)	2(3)	1(2)	2(2)
SiO_2	39.24	39.58	38.91	39.83	35.97	36.66	42.46	42.48	42.62	41.36	40.86
TiO_2	0.84	0.79	0.82	0.95	0.20	0.27	0.18	0.14	0.17	0.23	0.28
Al_2O_3	11.85	11.97	11.58	11.68	13.27	12.49	11.55	11.65	11.84	11.89	11.87
FeO	19.00	17.75	18.40	14.74	26.77	27.19	3.01	2.19	2.96	2.73	2.66
MnO	0.09	0.09	0.07	0.07	0.16	0.16	0.01	0.01	0.01	0.00	0.01
MgO	18.05	18.45	17.73	20.28	11.48	11.25	29.01	29.25	29.05	26.95	26.75
K_2O	9.30	9.32	9.42	9.34	8.72	8.91	10.49	10.23	10.38	10.72	10.49
Na_2O	0.14	0.16	0.19	0.21	0.22	0.23	0.08	0.07	0.08	0.02	0.01
Total	98.52	98.10	97.15	97.11	96.79	97.16	96.80	96.02	97.10	93.65	92.93
No. of cations based on 22 oxygens											
Si	5.769	5.803	5.799	5.822	5.608	5.705	5.906	5.922	5.900	5.931	5.916
Al	2.053	2.070	2.034	2.012	2.438	2.290	1.895	1.915	1.932	2.011	2.026
Fe	2.336	2.177	2.294	1.802	3.491	3.540	0.350	0.255	0.343	0.327	0.322
Ti	0.094	0.089	0.093	0.105	0.024	0.032	0.019	0.015	0.017	0.025	0.030
Mn	0.012	0.011	0.009	0.008	0.021	0.021	0.001	0.001	0.001	0.000	0.001
Mg	3.955	4.032	3.939	4.419	2.668	2.610	6.015	6.078	5.996	5.761	5.773
K	1.744	1.744	1.791	1.742	1.734	1.768	1.861	1.820	1.833	1.962	1.938
Na	0.039	0.044	0.056	0.061	0.066	0.069	0.023	0.020	0.020	0.000	0.003
Site Occupancy											
Z	7.916	7.962	7.926	7.939	8.070	8.027	7.820	7.852	7.849	7.967	7.972
	(.084)	(.038)	(.074)	(.061)	(+.070)	(+.027)	(.180)	(.148)	(.151)	(.033)	(.028)
Y	6.303	6.220	6.242	6.229	6.180	6.170	6.366	6.334	6.340	6.088	6.096
X	1.783	1.788	1.847	1.803	1.800	1.837	1.884	1.840	1.853	1.962	1.941
Fe/(Fe + Mg)	0.37	0.35	0.37	0.29	0.57	0.58	0.06	0.04	0.05	0.05	0.05
Pleochroism	N	N	N	N	N	N	R	R	R	R	R

TABLE 5.4 (Continued)
Microprobe Analyses of Micas

	P134-2506C											
	1(2)	1(2)	1(2)	1(1)	1(2)	1(1)	2(2)	2(2)	2(2)	2(2)	2(2)	2(1)
SiO_2	41.82	42.16	41.23	41.40	41.80	41.47	41.82	41.62	41.83	41.69	41.56	41.99
TiO_2	0.01	0.01	0.01	0.01	0.01	0.02	0.01	0.02	0.01	0.01	0.01	0.01
Al_2O_3	9.21	10.32	6.91	6.90	8.16	6.74	10.82	10.46	10.96	7.32	6.98	6.73
FeO	5.99	5.52	10.37	9.82	9.30	11.88	4.41	5.82	4.88	10.19	11.58	10.88
MnO	0.08	0.07	0.08	0.07	0.09	0.09	0.05	0.06	0.06	0.08	0.08	0.08
MgO	27.72	27.70	26.93	27.03	26.91	26.46	27.98	27.45	27.78	26.85	26.64	27.02
K_2O	10.67	10.65	10.41	10.43	10.49	10.43	10.34	10.28	10.23	9.94	10.04	9.87
Na_2O	0.06	0.07	0.07	0.09	0.06	0.05	0.09	0.08	0.08	0.08	0.07	0.06
Total	95.56	96.50	96.00	95.75	96.81	97.13	95.52	95.78	95.84	96.16	96.96	96.64
No. of cations based on 22 oxygens												
Si	6.006	5.968	6.035	6.060	6.020	6.041	5.939	5.936	5.929	6.059	6.038	6.090
Al	1.558	1.722	1.192	1.191	1.385	1.157	1.812	1.759	1.831	1.254	1.195	1.151
Fe	0.720	0.654	1.270	1.202	1.120	1.447	0.523	0.694	0.578	1.238	1.408	1.324
Ti	0.001	0.002	0.002	0.001	0.001	0.002	0.001	0.002	0.002	0.001	0.002	0.001
Mn	0.009	0.008	0.009	0.009	0.011	0.010	0.006	0.007	0.006	0.010	0.010	0.010
Mg	5.934	5.846	5.877	5.896	5.778	5.745	5.923	5.837	5.869	5.817	5.769	5.841
K	1.955	1.923	1.945	1.948	1.927	1.939	1.874	1.871	1.849	1.843	1.862	1.826
Na	0.017	0.019	0.020	0.025	0.017	0.016	0.026	0.023	0.023	0.022	0.019	0.016
Site Occupancy												
Z	7.565	7.692	7.229	7.252	7.406	7.200	7.752	7.697	7.762	7.314	7.235	7.242
	(.435)	(.308)	(.771)	(.748)	(.594)	(.800)	(.248)	(.303)	(.238)	(.685)	(.765)	(.758)
Y	6.663	6.508	7.156	7.107	6.909	7.202	6.452	6.538	6.453	7.065	7.187	7.175
X	1.972	1.942	1.965	1.973	1.944	1.955	1.900	1.894	1.872	1.872	1.881	1.842
Fe/(Fe + Mg)	0.11	0.10	0.18	0.17	0.16	0.20	0.08	0.10	0.09	0.18	0.20	0.18
Pleochroism	R	R	R	R	R	R	R	R	R	R	R	R

Table 5.4 (Continued)
Microprobe Analyses of Micas

	PIR64-2395P			P134-1006K			F16P		Pal29H/A
	1,core(3)	1,rim(2)	2(2)	1,core(2)	1,rim(2)	2(2)	1(2)	2(2)	(4)
SiO_2	41.70	42.13	42.10	42.75	42.92	41.85	41.92	42.32	41.81
TiO_2	1.73	1.10	1.59	0.43	0.38	0.80	1.29	1.36	1.50
Al_2O_3	10.76	11.22	10.50	9.17	9.29	9.37	11.70	11.67	10.83
FeO	10.66	10.16	10.37	9.22	9.21	10.63	7.28	6.99	8.06
MgO	21.55	22.15	21.59	24.37	24.58	23.91	22.80	22.74	23.11
K_2O	10.23	10.18	10.34	10.34	10.08	9.94	10.26	10.29	10.11
Total	96.63	96.95	96.34	96.28	96.46	96.50	95.25	95.37	95.42
No. of cations based on 22 oxygens									
Si	6.029	6.028	6.072	6.145	6.145	6.039	6.025	6.061	6.025
Al	1.820	1.891	1.783	1.553	1.567	1.581	1.981	1.969	1.839
Ti	0.180	0.119	0.172	0.047	0.041	0.091	0.139	0.146	0.162
Fe	1.268	1.216	1.263	1.608	1.102	1.333	0.874	0.837	0.971
Mg	4.632	4.725	4.642	5.222	5.246	5.094	4.885	4.855	4.916
K	1.859	1.858	1.902	1.896	1.841	1.798	1.880	1.880	1.857
Site Occupancy									
Z	7.849	7.919	7.855	7.698	7.712	7.620	8.006	8.030	7.864
	(0.151)	(0.081)	(0.145)	(0.302)	(0.288)	(0.380)	(+0.006)	(+0.030)	(0.136)
Y	6.080	6.060	6.077	6.877	6.389	6.518	5.898	5.838	6.049
X	1.859	1.858	1.902	1.896	1.841	1.798	1.880	1.880	1.857
Fe/(Fe+Mg)									
	0.21	0.20	0.21	0.26	0.17	0.21	0.15	0.15	0.16
Pleochroism									
	N	N	N	R	R	R	N	N	N

TABLE 5.5

	X-ray Fluorescence Analyses of Phlogopites				
	F101P	P28P	PIR 64-2395P	P134-577P	P134-601P
SiO_2	47.35	42.34	42.83	42.59	42.56
TiO_2	0.72	1.90	1.45	1.57	1.14
Al_2O_3	10.33	12.18	11.28	11.62	10.56
FeO	5.57	10.86	11.92	11.60	10.27
MnO	0.05	0.07	0.08	0.15	0.09
MgO	23.91	21.54	23.09	21.61	20.82
K_2O	8.52	8.63	9.01	7.97	8.13
Na_2O	0.39	0.00	0.00	0.00	0.00
Total	96.84	97.52	91.76	97.11	96.25
No. of cations based on 22 oxygens					
Si	6.493	5.884	5.955	5.985	5.996
Al	1.670	1.996	1.849	1.925	1.754
Fe	0.639	1.262	1.386	1.363	1.210
Ti	0.074	0.199	0.152	0.166	0.121
Mn	0.006	0.008	0.009	0.018	0.011
Mg	4.887	4.625	4.786	4.526	4.777
K	1.491	1.530	1.599	1.429	1.461
Na	0.104	0.00	0.00	0.00	0.00
Site Occupancy					
Z	8.163	7.880	7.804	8.076	7.871
Y	5.606	6.094	6.333	5.907	5.998
X	1.595	1.530	1.599	1.429	1.461
Trace Elements					
Sr	9.5	56(8.2)*	21(8.0)*	35	203
Rb	844.3	552(616)*	725(808)*	617	508
Ba	970	1939	879	3252	2418
Ce	BDL	(169)	(35)	(69)	(83)
La	3	88	BDL	18	34
V	3	10	14	15	8
Cu	0	6	6	1	4
Ni	273	146	113	106	105
Zn	67	126	132	162	119
Fe/Fe+Mg	0.12	0.21	0.22	0.23	0.20
Pleochroism	N	N	N	N	N

*Numbers in parenthesis are values obtained by isotope dilution.

TABLE 5.6
Microprobe Analyses of Olivines

	P3C						P146-1056K	P42K		
	1(2)	2(2)	3(3)	4(2)	5(2)	5(1)	1(3)	1(2)	1(1)	2(2)
SiO_2	40.78	40.81	40.75	40.92	40.36	40.07	40.16	39.84	39.38	41.04
FeO	8.67	9.07	9.81	10.59	8.57	8.70	17.91	12.16	12.16	11.54
MgO	50.77	50.46	49.64	49.73	50.62	50.66	39.21	47.64	47.70	47.81
CaO	0.01	0.06	0.04	0.01	0.01	0.03	0.07	0.02	0.03	0.04
NiO	0.00	0.01	0.02	0.00	0.00	0.00	0.00	0.00	0.02	0.00
Total	100.23	100.41	100.27	101.24	99.58	99.46	97.94	99.67	99.29	100.44
No. of cations based on 4 oxygens										
Si	0.992	0.992	0.995	0.993	0.987	0.982	1.041	0.991	0.984	1.007
Fe	0.176	0.185	0.200	0.215	0.175	0.178	0.388	0.253	0.254	0.237
Mg	1.840	1.829	1.810	1.799	1.846	1.851	1.515	1.766	1.777	1.748
Ca	0.001	0.002	0.001	0.000	0.000	0.001	0.002	0.001	0.001	0.001
Ni	0.000	0.000	0.000	0.000	0.000	0.000	0.000	0.000	0.000	0.000
Total	2.017	2.016	2.011	2.014	2.021	2.030	1.905	3.001	3.016	2.993
Mg/(Fe + Mg)	0.91	0.91	0.90	0.89	0.91	0.91	0.79	0.87	0.87	0.88

TABLE 5.6 (Continued)
Microprobe Analyses of Olivines

	LK153-400K			P(79a)X			P120P				
	1(2)	2(2)	2(2)	1(2)	2(2)	3(2)	1(1)	1(1)	1(1)	1(1)	1(1)
SiO_2	40.00	39.03	39.42	40.11	39.52	39.83	39.65	39.71	39.33	39.51	39.52
FeO	12.59	15.03	16.96	12.50	12.37	12.53	13.85	13.79	14.52	14.54	15.26
MgO	47.85	46.04	44.79	47.60	47.77	47.81	46.45	46.62	46.18	46.04	45.29
CaO	0.00	0.01	0.00	0.04	0.01	0.05	0.08	0.06	0.09	0.09	0.08
NiO	0.00	0.00	0.00	0.26	0.31	0.28	0.03	0.01	0.03	0.04	0.06
Total	100.44	100.12	101.18	100.52	99.97	100.51	100.06	100.19	100.14	100.21	100.21
No. of cations based on 4 oxygens											
Si	0.989	0.980	0.987	0.991	0.983	0.985	0.990	0.990	0.985	0.988	0.991
Fe	0.260	0.316	0.355	0.258	0.257	0.259	0.289	0.287	0.304	0.304	0.320
Mg	1.763	1.724	1.671	1.753	1.771	1.763	1.729	1.732	1.724	1.716	1.694
Ca	0.000	0.000	0.000	0.001	0.000	0.001	0.002	0.002	0.002	0.002	0.002
Ni	0.000	0.000	0.000	0.005	0.006	0.006	0.001	0.001	0.001	0.001	0.001
Total	3.012	3.020	3.013	3.008	3.017	3.014	2.021	2.022	2.031	2.023	2.017
Mg/(Fe + Mg)	0.87	0.84	0.82	0.87	0.87	0.87	0.86	0.86	0.85	0.85	0.84

Table 5.7

	Amphibole P146-440N		Feldspar P146-440N		Feldspar P146-610N		Magnetite LK157-675C
SiO_2	54.07		64.60		64.72		0.07
TiO_2	0.07		-		-		0.00
Al_2O_3	0.33		17.90		18.21		0.00
FeO	14.52		0.52		0.14		93.90
MnO	0.27		-		-		0.16
MgO	14.96		-		-		0.00
CaO	7.35		0.00		0.00		-
Na_2O	3.53		2.61		0.76		-
K_2O	1.69		13.81		15.38		-
Total	96.79		98.81		99.21		93.97
	Number of cations on the basis of						
	24 O				32 O		
Si	8.104		12.002		12.046		
Al	0.164		3.921		4.006		
Ti	0.008		-		-		
Fe^{3+}	1.640	5.192	0.081	4.002	0.022	4.028	
Mn	0.036		-		-		
Mg	3.344		-		-		
Ca	1.180		0.000		0.000		
Na	1.024	2.528	0.940	4.065	0.274	3.926	
K	0.324		3.125		3.652		
Fe/(Fe+Mg)	0.35	An	0.00		0.00		
		Or	0.77		0.92		
		Ab	0.23		0.07		

TABLE 5.8

Microprobe analyses for minerals from Kgopoeloe and Spitskop

	Clinopyroxene				Amphiboles			Feldspars		
	K26M(3)	K10m(5)	K8m(5)	K27m(4)	S3r	K26m	K10m	K8m	K27m	S3r
SiO_2	53.03	52.32	52.54	52.41	54.21	54.16	54.84	64.64	64.42	65.01
TiO_2	1.19	1.23	1.58	1.32	0.23	0.15	0.19	–	–	–
Al_2O_3	0.69	0.40	0.54	0.49	0.72	0.00	0.11	18.22	17.71	16.20
FeO	26.70	27.59	25.67	25.71	16.36	16.17	15.24	0.52	1.10	0.58
MgO	0.96	0.40	1.68	1.88	11.76	12.54	13.34	–	–	–
CaO	4.40	3.34	6.00	6.00	1.30	2.17	1.73	0.00	0.00	0.00
Na_2O	11.84	12.69	10.81	10.73	8.06	6.50	7.62	0.17	0.12	0.39
K_2O	–	–	–	–	2.88	2.79	2.95	16.01	15.89	16.27
Total	98.81	97.97	98.82	98.53	95.52	94.48	96.02	99.56	99.25	98.45
	No. of cations based on:									
	6 oxygens				24 oxygens			8 oxygens		
Si	1.988	1.983	1.973	1.975	7.932 } 8.000	8.256 } 8.256	8.212 } 8.212	2.996	3.008	3.059
Al	0.012	0.017	0.024	0.022	0.068	–	–	0.996	0.974	0.899
Tet. Total	2.000	2.000	1.997	1.997				3.992	3.982	3.958
Al	0.015	0.001	0.000	0.000	0.056	0.256	0.232	–	–	–
Ti	0.034	0.035	0.045	0.037	0.024	0.016	0.200	–	–	–
Fe^{3+}	0.837	0.874	0.789	0.786	2.456 } 5.136	1.920 } 5.176	1.908 } 5.136	–	–	–
Fe^{2+}	0.000	0.000	0.017	0.024	0.036	0.136	0.000	0.200*	0.043*	0.023*
Mg	0.054	0.023	0.094	0.106	2.564	2.848	2.976	–	–	–
Ca	0.177	0.136	0.241	0.242	0.204	0.356	0.276	0.000	0.000	0.000
Na	0.861	0.933	0.787	0.784	2.288 } 3.028	1.920 } 2.820	2.212 } 3.052	0.015	0.011	0.035
K					0.536	0.544	0.564	0.947	0.947	0.976
Oct. Total	1.978	2.002	1.973	1.979				1.162	1.001	1.034
Fe/(Fe + Mg)	0.94	0.97	0.90	0.88	0.44	0.42	0.39	–	–	–

TABLE 5.9
Pyroxenes - Guide Copper Mine

	G12F															
	core	(2)	(2)	(2)	(2)	(2)	(2)	(2)	(2)	(2)	(2)	(2)	(2)	(2)	(2)	rim
SiO_2	52.21	53.39	52.82	52.24	52.82	52.32	51.40	52.87	52.85	53.72	52.35	52.81	52.96	53.53	52.40	51.96
TiO_2	0.30	0.19	0.28	0.61	0.30	0.37	0.26	0.10	0.00	0.23	0.26	0.12	0.26	0.35	0.29	0.22
Al_2O_3	0.26	0.31	0.33	0.34	0.35	0.31	0.31	0.23	0.36	0.52	0.34	0.27	0.44	0.29	0.47	0.33
FeO	8.34	8.36	8.40	8.27	8.47	8.20	7.70	8.02	7.58	7.76	9.44	7.45	9.28	10.30	9.67	11.30
MnO	0.19	0.20	0.21	0.17	0.15	0.16	0.15	0.17	0.19	0.16	0.24	0.19	0.18	0.29	0.20	0.18
MgO	14.04	14.33	14.19	14.28	14.17	14.24	14.51	14.50	14.16	14.10	12.94	14.64	13.53	12.96	13.45	11.85
CaO	23.93	23.93	24.11	24.06	24.09	24.04	23.72	23.53	23.57	23.23	22.04	23.89	22.28	21.81	21.72	19.29
Na_2O	0.51	0.54	0.49	0.50	0.56	0.55	0.43	1.04	0.91	1.15	1.63	0.63	1.62	1.80	1.82	3.03
Total	99.78	101.25	100.83	100.47	100.91	100.19	99.48	100.46	99.62	100.87	99.24	100.00	100.55	100.97	100.02	98.16
No. of cations based on 6 oxygens																
Si	1.959	1.969	1.960	1.947	1.958	1.954	1.951	1.961	1.972	1.975	1.969	1.967	1.963	1.973	1.955	1.976
Al	0.012	0.013	0.014	0.015	0.015	0.014	0.014	0.010	0.016	0.023	0.015	0.012	0.019	0.013	0.021	0.015
Fe	1.970	1.982	1.975	1.962	1.974	1.967	1.965	1.971	1.988	1.997	1.984	1.979	1.983	1.986	1.976	1.991
Al	0.000	0.000	0.000	0.000	0.000	0.000	0.000	0.000	0.000	0.000	0.000	0.000	0.000	0.000	0.000	0.000
Ti	0.008	0.005	0.008	0.017	0.008	0.010	0.007	0.003	0.000	0.006	0.007	0.003	0.007	0.010	0.008	0.006
Fe^3	0.037	0.039	0.035	0.036	0.040	0.040	0.032	0.075	0.066	0.082	0.119	0.045	0.116	0.129	0.132	0.224
Fe^2	0.220	0.215	0.222	0.218	0.218	0.212	0.209	0.166	0.164	0.148	0.165	0.179	0.158	0.175	0.155	0.102
Mn	0.006	0.006	0.007	0.005	0.005	0.005	0.005	0.005	0.006	0.005	0.008	0.006	0.006	0.009	0.006	0.006
Mg	0.785	0.788	0.785	0.793	0.783	0.793	0.821	0.802	0.788	0.773	0.726	0.813	0.748	0.712	0.748	0.672
Ca	0.962	0.946	0.959	0.961	0.957	0.962	0.965	0.935	0.943	0.915	0.888	0.954	0.885	0.862	0.869	0.786
Na	0.037	0.039	0.035	0.036	0.040	0.040	0.032	0.075	0.066	0.082	0.119	0.046	0.116	0.129	0.132	0.223
Oct. Total	2.056	2.037	2.050	2.067	2.052	2.062	2.070	2.060	2.032	2.010	2.032	2.045	2.037	2.025	2.050	2.019
Fe/(Fe + Mg)	0.25	0.24	0.25	0.24	0.25	0.24	0.23	0.23	0.23	0.23	0.28	0.22	0.27	0.30	0.28	0.33

TABLE 5.9 Continued
Pyroxenes - Guide Copper Mine

	G8F								
	core	(2)	(2)	(2)	(2)	(2)	(2)	(2)	rim
SiO_2	51.82	52.11	51.64	52.84	52.59	52.65	52.01	52.57	51.89
TiO_2	0.24	0.32	0.23	0.21	0.29	0.23	0.15	0.00	0.00
Al_2O_3	0.46	0.45	0.39	0.25	0.29	0.25	0.29	0.11	0.12
FeO	9.48	9.52	9.39	8.01	7.68	8.48	8.43	9.69	10.15
MnO	0.24	0.26	0.25	0.22	0.13	0.35	0.23	0.19	0.18
MgO	11.57	11.72	11.94	13.11	13.11	12.32	12.15	11.94	11.57
CaO	22.06	22.20	22.25	22.84	22.69	23.33	22.54	22.63	22.69
Na_2O	1.42	1.42	1.37	1.18	1.21	0.76	1.18	1.14	0.99
Total	97.29	98.00	97.46	98.66	97.99	98.37	96.98	98.27	97.59
No. of cations based on 6 oxygens									
Si	1.987	1.984	1.978	1.986	1.987	1.995	1.995	1.990	1.994
Al	0.013	0.016	0.018	0.011	0.013	0.005	0.005	0.005	0.005
Tet. Total	2.000	2.000	1.995	1.997	2.000	2.000	2.000	1.995	1.999
Al	0.008	0.004	0.000	0.000	0.000	0.007	0.008	0.000	0.000
Ti	0.007	0.009	0.007	0.006	0.008	0.007	0.004	0.000	0.000
Fe^{3+}	0.106	0.105	0.102	0.086	0.089	0.056	0.088	0.084	0.074
Fe^{2+}	0.198	0.198	0.199	0.165	0.154	0.213	0.182	0.226	0.252
Mn	0.008	0.008	0.008	0.007	0.004	0.011	0.007	0.006	0.006
Mg	0.661	0.665	0.680	0.734	0.738	0.697	0.695	0.677	0.663
Ca	0.907	0.906	0.912	0.919	0.919	0.949	0.927	0.922	0.934
Na	0.106	0.105	0.102	0.085	0.089	0.056	0.088	0.084	0.074
Oct. Total	2.000	2.000	2.009	2.004	2.000	2.000	2.000	2.000	2.002
Fe/(Fe + Mg)	0.31	0.31	0.31	0.26	0.25	0.28	0.28	0.31	0.33

TABLE 7.1 Whole Rock Chemistry - Main Complex

	F6F	F12F	F23F	F29F	F66F	F67F	F75F	F76F	F77F	F78F	PIR95-288F	G1F	P4P
SiO_2	49.08	54.41	54.15	50.14	49.86	39.89	45.96	45.01	47.16	48.00	50.15	53.18	44.37
TiO_2	0.27	0.14	0.13	0.17	0.16	0.21	0.15	0.17	0.16	0.15	0.16	0.19	0.21
Al_2O_3	2.18	1.00	5.28	1.16	0.82	1.55	0.79	0.66	1.02	0.89	0.94	3.61	6.66
Fe_2O_3	2.06	0.38	2.32	1.33	1.14	0.81	0.96	1.79	0.57	1.27	0.81	3.33	1.90
FeO	2.77	2.82	2.70	2.41	2.51	2.31	2.43	2.27	2.90	2.56	3.59	4.88	4.41
MnO	0.14	0.05	0.09	0.24	0.28	0.29	0.30	0.28	0.35	0.25	0.23	0.15	0.24
MgO	14.50	13.72	10.16	14.15	14.95	12.76	13.43	13.58	13.68	14.03	14.92	9.56	9.62
CaO	22.53	22.04	16.76	24.69	24.42	28.41	26.90	27.85	26.36	25.98	24.53	18.70	19.21
Na_2O	0.66	0.61	0.81	0.08	0.68	0.58	0.60	0.53	0.61	0.58	0.07	1.06	0.02
K_2O	1.83	0.65	4.62	0.74	0.46	1.14	0.48	0.32	0.57	0.46	0.53	3.24	5.81
P_2O_5	3.73	4.18	0.61	4.99	4.58	11.44	7.45	7.46	6.33	5.84	3.72	1.29	5.85
H_2O^-	0.02	0.06	0.17	0.04	0.04	0.04	0.17	0.21	0.11	0.13	0.26	0.00	0.14
LOI	0.87	0.65	1.44	0.47	0.57	0.72	0.47	0.62	0.51	0.45	0.57	0.86	1.88
Total	100.64	100.65	99.22	100.61	100.48	100.16	100.09	100.74	100.32	100.59	100.49	100.11	100.32
Trace Elements (ppm)													
Sr	1015	1039	361	1243	1138	2084	1546	1571	1359	1354	1027	781	1612
Rb	86	22	168	23	20	71	13	9	16	15	11	120	282
Ba	194	57	1040	166	115	126	85	43	94	86	80	641	720
Ce	383	373	113	476	590	1213	926	828	827	720	372	189	366
La	135	132	36	167	295	627	479	412	401	362	124	62	131
Cu	6	BDL	35	BDL	2	BDL	3	8	7	10	22	1804	2051
Ni	52	44	36	64	47	36	41	49	48	49	58	43	18
Zn	37	30	34	32	18	16	18	13	9	15	37	66	54
Nb	3	4	3	4	4	3	4	4	4	4	3	3	5
Zr	40	55	42	33	31	6	23	30	30	14	30	162	386
Y	42	44	11	56	42	93	69	67	60	58	42	25	53
V	1	23	47	25	-	-	-	-	-	-	37	8	-

	F6F	F12F	F23F	F29F	F66F	F67F	F75F	F76F	F77F	F78F	PIR95-288F	G1F	P4P
qtz	0.00	9.56	0.00	4.54	0.94	0.00	1.06	0.04	0.16	0.84	1.48	0.29	0.00
orth	8.80	3.84	25.27	4.36	2.72	6.76	2.85	1.89	3.37	2.71	3.14	19.30	9.94
ab	0.00	1.52	0.00	0.68	1.66	1.63	1.40	1.61	2.08	2.01	0.59	0.53	0.00
an	0.00	0.00	0.00	0.62	0.00	0.00	0.00	0.00	0.00	0.00	0.69	0.00	0.94
neph	0.56	0.00	0.80	0.00	0.00	0.00	0.00	0.00	0.00	0.00	0.00	0.00	0.09
lc	1.60	0.00	2.11	0.00	0.00	0.00	0.00	0.00	0.00	0.00	0.00	0.00	19.59
di	69.18	64.99	64.21	70.31	72.22	53.05	67.59	70.72	71.19	71.78	76.90	67.48	45.85
hy	0.00	8.56	0.00	5.67	8.13	3.15	6.52	4.24	6.22	5.70	7.05	0.00	0.00
ac	4.02	0.95	4.89	0.00	3.30	2.35	2.79	2.53	1.65	2.54	0.00	7.49	0.00
ol	5.67	0.00	0.02	0.00	0.00	5.83	0.00	0.00	0.00	0.00	0.00	0.00	6.60
mag	0.98	0.00	1.00	1.92	0.00	0.00	0.00	1.33	0.00	0.56	1.18	1.11	2.80
ilm	0.51	0.27	0.25	0.32	0.30	0.40	0.29	0.32	0.30	0.28	0.30	0.36	0.41
ap	8.68	9.71	0.45	11.57	10.65	26.69	17.38	17.32	14.73	13.55	8.67	3.02	13.81
Fe/(Fe + Mg) x100													
	15.18	11.31	14.40	12.51	11.72	11.79	12.10	13.82	12.28	12.90	13.97	31.62	19.58

	F5P	F13P	F24P	F28P	F42F	F50F	F52P	F53P	F60P	F61P	F63P	PIR95-297P	PIR95-223P	PIR95-258M	F11M
SiO_2	39.24	54.09	46.35	45.86	44.41	50.73	40.28	46.99	49.17	55.27	43.66	52.44	49.59	48.20	49.93
TiO_2	0.40	0.14	0.32	0.36	0.36	0.21	0.56	0.33	0.80	0.22	0.33	0.19	0.20	0.16	0.17
Al_2O_3	3.78	0.52	2.12	6.02	2.25	1.54	4.16	1.95	3.63	0.62	2.22	1.47	1.02	0.52	0.50
Fe_2O_3	1.89	0.89	1.24	2.73	1.44	1.62	1.00	1.57	2.21	0.56	1.14	1.02	1.10	1.33	1.05
FeO	1.78	3.78	2.97	4.02	3.77	4.25	3.89	3.15	6.45	2.22	2.80	3.41	3.30	2.72	4.63
MnO	0.14	0.10	0.19	0.20	0.35	0.36	0.32	0.32	0.24	0.21	0.22	0.20	0.18	0.17	0.22
MgO	17.08	13.44	16.14	20.57	14.12	13.30	15.32	15.17	14.77	17.32	15.54	14.92	15.27	14.98	14.14
CaO	21.69	22.22	23.52	10.83	23.77	22.94	21.97	23.26	18.07	21.62	24.84	23.08	24.71	26.42	24.81
Na_2O	0.00	0.48	0.00	0.00	0.51	0.73	0.75	0.57	0.69	0.86	0.67	0.20	0.05	0.01	0.45
K_2O	3.53	0.21	1.60	5.82	1.81	0.79	3.53	1.64	2.71	0.42	1.71	0.91	0.57	0.18	0.05
P_2O_5	8.97	3.77	4.56	0.48	6.19	3.02	7.35	4.72	1.04	0.01	5.74	2.11	4.21	5.69	3.92
H_2O^-	0.09	0.05	0.24	0.09	0.05	0.08	0.08	0.10	0.06	0.04	0.06	0.05	0.16	0.16	0.05
LOI	1.81	0.73	0.99	2.37	1.04	0.72	0.95	0.69	1.08	1.59	1.27	0.58	0.56	0.43	0.87
Total	100.40	100.41	100.24	99.36	100.06	100.29	100.16	100.45	100.93	100.96	100.17	100.58	100.90	100.95	100.78

Trace Elements (ppm)															
Sr	870	898	1199	289	1230	982	1345	1148	537	397	1044	762	1065	1189	1013
Rb	302	12	106	485	145	38	265	134	185	21	124	31	24	-	-
Ba	161	27	190	500	49	305	285	76	802	107	219	203	31	-	-
Ce	646	301	454	21	753	511	182	580	167	57	657	450	388	605	479
La	208	125	153	20	374	261	391	297	91	30	322	171	166	201	173
Cu	-	25	-	114	29	3	6	7	296	4	5	-	-	-	27
Ni	87	120	159	48	51	57	58	55	137	103	71	57	69	61	50
Zn	32	40	39	97	42	40	50	29	74	4	18	38	39	31	41
Nb	-	5	3	8	5	5	3	3	5	4	4	5	3	4	4
Zr	21	17	18	12	24	37	3	9	25	39	2	178	32	27	19
Y	62	39	46	12	56	37	62	44	18	8	44	30	48	55	47
V	10	1	2	68	-	-	-	-	-	-	-	17	38	29	46

	F5P	F13P	F24P	F28P	F42P	F50P	F52P	F53P	F60P	F61P	F63P	PIR95-297P	PIR95-223P	PIR95-258M	F11M
qtz	0.00	9.45	0.00	0.00	0.00	0.49	0.00	0.00	0.00	0.88	0.00	1.19	1.22	2.79	1.58
orth	3.94	1.24	4.25	0.00	10.71	4.69	0.00	3.46	1.48	2.50	0.00	5.38	3.36	1.06	0.30
ab	0.00	1.41	0.00	0.00	0.26	3.54	0.00	0.00	0.00	0.86	0.00	1.69	0.42	0.08	2.29
an	0.00	0.00	1.07	0.00	0.00	0.00	0.00	0.00	0.00	0.00	0.00	0.43	0.87	0.78	0.00
neph	0.00	0.00	0.00	0.00	0.00	0.00	0.98	0.49	1.95	0.00	0.00	0.00	0.00	0.00	0.00
lc	13.34	0.00	4.15	26.86	0.00	0.00	16.92	4.91	11.42	0.00	3.52	0.00	0.00	0.00	0.00
di	40.24	68.35	68.39	36.39	58.12	75.29	36.47	67.18	66.25	84.83	68.80	79.33	74.34	73.21	77.77
hy	0.00	8.03	0.00	0.00	0.00	5.01	0.00	0.00	0.00	7.78	0.00	5.24	8.06	6.69	6.43
ac	0.00	2.35	0.00	0.00	2.49	2.35	2.99	3.46	1.99	1.63	3.41	0.00	0.00	0.00	1.33
ol	18.12	0.00	9.02	30.30	10.13	0.00	23.55	8.33	10.75	0.00	9.36	0.00	0.00	0.00	0.00
mag	2.78	0.12	1.81	4.13	0.84	1.18	0.00	0.55	2.21	0.00	0.00	1.48	1.59	1.92	0.85
ilm	0.77	0.27	0.61	0.71	0.68	0.40	1.10	0.63	1.52	0.42	0.65	0.36	0.38	0.30	0.32
ap	20.74	8.79	10.69	1.16	16.08	7.05	17.67	10.99	2.42	0.02	13.79	4.90	9.76	13.16	9.11
Fe/(Fe + Mg) x100	10.26	16.06	12.44	15.01	16.76	19.41	14.93	14.44	24.28	8.11	12.14	14.00	13.62		

	F22M	F25M	F32M	F31M	F38M	F39M	F41M	F51M	F59M	F33M	F34M	F35M	F36M	F37M
SiO_2	48.88	50.50	49.73	50.20	48.11	48.25	50.05	51.23	50.79	50.40	51.07	49.49	52.22	48.68
TiO_2	0.19	0.18	0.16	0.16	0.15	0.15	0.19	0.14	0.19	0.17	0.21	0.14	0.15	0.14
Al_2O_3	0.66	0.70	0.74	0.36	0.45	0.40	1.16	0.46	0.61	0.43	0.43	0.39	0.57	0.36
Fe_2O_3	1.86	1.91	1.51	1.24	1.02	1.88	1.45	1.31	1.65	1.31	1.01	1.27	1.51	1.77
FeO	4.07	4.05	4.03	4.30	3.35	4.22	4.30	3.78	4.63	4.55	4.94	4.04	3.84	3.25
MnO	0.18	0.22	0.28	0.35	0.35	0.16	0.31	0.29	0.44	0.34	0.32	0.38	0.34	0.31
MgO	14.49	14.77	13.94	13.65	14.04	13.74	13.02	14.78	13.43	14.29	14.18	13.67	14.28	14.18
CaO	24.87	23.88	24.37	25.02	25.54	25.43	23.03	23.99	23.70	24.28	23.90	24.78	23.85	25.49
Na_2O	0.04	0.17	0.69	0.67	0.69	0.76	0.78	0.76	0.71	0.68	0.71	0.69	0.65	0.52
K_2O	0.28	0.18	0.14	0.06	0.12	0.09	0.59	0.18	0.31	0.08	0.08	0.07	0.19	0.07
P_2O_5	3.57	2.72	3.80	4.26	5.44	4.47	3.35	2.81	3.28	3.15	2.58	4.60	2.67	4.65
H_2O^-	0.09	0.17	0.09	0.09	0.04	0.07	0.07	0.07	0.07	0.06	0.03	0.09	0.07	0.14
LOI	0.66	0.56	0.66	0.67	0.81	0.76	0.78	0.62	0.91	0.87	0.80	0.68	0.56	0.66
Total	100.82	100.01	100.14	101.02	99.99	100.39	99.06	100.92	100.71	100.61	100.26	100.29	99.90	100.22

Trace Elements (ppm)														
Sr	800	874	1010	1173	1362	1147	1026	958	934	930	873	1211	937	1203
Rb	6	10	9	3	6	3	23	6	11	4	1	3	3	1
Ba	7	2	BDL	BDL	BDL	BDL	228	BDL	23	BDL	BDL	BDL	43	BDL
Ce	435	356	827	706	760	620	653	418	530	562	456	729	419	691
La	151	127	401	364	378	322	354	202	271	285	231	388	208	353
Cu	43	94	6	18	81	483	115	48	582	311	32	287	15	11
Ni	50	110	45	48	50	55	44	102	53	53	24	56	47	49
Zn	43	43	30	31	16	29	33	34	28	43	43	22	32	24
Nb	3	3	3	3	5	3	5	4	5	4	5	3	3	4
Zr	19	19	11	10	18	12	34	20	13	11	19	11	10	2
Y	45	35	39	48	54	46	41	30	37	34	33	46	32	51
V	41	47	-	-	-	-	-	-	-	-	-	-	-	-

	F22M	F25M	F32M	F31M	F38M	F39M	F41M	F51M	F59M	F33M	F34M	F35M	F36M	F37M
qtz	2.43	2.18	1.01	2.27	1.22	0.00	0.00	0.93	1.69	0.19	0.54	2.11	2.19	1.57
orth	1.65	1.07	0.83	0.35	0.71	0.53	3.44	1.06	1.84	0.47	0.48	0.42	1.12	0.42
ab	0.34	1.45	3.04	1.51	1.66	1.56	2.65	1.36	1.41	1.93	1.78	1.62	1.87	1.47
an	0.79	0.62	0.00	0.00	0.00	0.00	0.00	0.00	0.00	0.00	0.00	0.00	0.00	0.00
neph	0.00	0.00	0.00	0.00	0.00	0.00	0.00	0.00	0.00	0.00	0.00	0.00	0.00	0.00
lc	0.00	0.00	0.00	0.00	0.00	0.00	0.00	0.00	0.00	0.00	0.00	0.00	0.00	0.00
di	78.58	79.83	76.86	76.61	73.00	77.55	72.51	79.76	76.98	79.85	81.66	74.41	79.91	76.57
hy	4.87	5.35	5.62	5.69	7.24	4.05	1.41	6.15	5.66	6.31	5.96	6.75	4.67	4.97
ac	0.00	0.00	2.49	3.57	2.97	4.31	3.41	3.78	4.06	3.38	2.94	3.69	3.18	2.60
ol	0.00	0.00	0.00	0.00	0.00	0.71	8.17	0.00	0.00	0.00	0.00	0.00	0.00	0.00
mag	2.69	2.79	0.95	0.00	0.00	0.58	0.37	0.00	0.36	0.21	0.00	0.00	0.59	1.28
ilm	0.36	0.34	0.31	0.30	0.29	0.29	0.36	0.27	0.36	0.32	0.40	0.27	0.28	0.27
ap	8.28	6.36	8.80	9.86	12.72	10.43	7.69	6.51	7.64	7.34	6.03	10.73	6.18	10.86

Fe/(Fe + Mg) x100

18.20	17.98	17.83	18.21	14.57	19.45	16.41	15.84	20.35	18.37	18.80	17.54	16.96	16.08

Kgopoeloe and Spitskop

	K1m	K8m	K9m	K10m	K16m	K19m	K20m	K21m	K23m	K24m	K11f	K12g	K13n	K17g	K18g
SiO_2	64.32	60.94	61.40	64.90	63.76	59.44	65.14	58.84	61.27	62.16	69.81	76.19	69.48	68.74	74.33
TiO_2	1.03	0.90	0.59	0.29	0.76	0.31	0.57	0.84	0.83	0.66	0.31	0.16	0.40	0.02	0.17
Al_2O_3	7.23	11.21	13.56	16.28	10.50	11.78	9.43	10.65	10.85	12.21	16.17	13.15	13.81	18.12	13.83
Fe_2O_3	7.47	5.32	5.05	3.58	6.50	3.35	3.83	4.70	5.02	5.44	0.19	0.94	3.67	0.09	0.24
FeO	2.97	1.91	0.94	0.51	0.68	1.17	2.55	1.50	1.57	0.83	1.00	0.00	–	–	–
MnO	0.40	0.20	0.07	0.03	0.11	0.15	0.30	0.32	0.25	0.47	0.04	0.00	0.06	0.45	0.03
MgO	4.65	3.68	1.92	1.09	1.58	2.50	4.09	3.06	1.81	1.65	0.92	0.41	2.37	0.23	0.25
CaO	1.69	3.36	3.22	0.73	4.37	6.66	3.05	7.93	4.09	4.07	0.25	1.06	3.28	0.08	0.60
Na_2O	2.60	2.17	1.72	1.47	1.92	1.85	0.58	1.79	2.08	1.82	3.12	3.60	3.38	1.84	4.89
K_2O	6.48	8.51	9.90	11.10	8.21	8.52	7.80	8.19	8.16	9.02	8.58	4.50	2.63	10.96	4.31
P_2O_5	0.71	1.09	1.14	0.18	0.31	0.78	1.45	0.69	0.46	0.40	0.17	0.11	0.20	0.15	0.09
H_2O^-	0.13	0.08	0.11	0.00	0.77	0.03	0.16	0.47	0.05	0.08	0.00	0.07	0.07	0.06	0.11
LOI	1.02	1.56	0.66	0.39	2.23	3.73	1.64	1.97	4.32	2.07	0.43	0.26	0.80	0.17	0.16
Total	100.71	100.93	100.47	100.55	101.14	100.60	100.58	100.53	100.77	100.86	101.01	100.43	100.16	100.50	99.00

Trace Elements (ppm)

Sr	981	377	374	131	1216	1314	567	1644	1167	1226	321	352	434	81	228
Rb	250	259	363	409	327	370	232	284	324	383	249	133	162	463	114
Ba	524	3427	2240	2772	2613	2026	3059	2254	2964	2260	2226	1086	1554	1468	685
Ce	618	262	269	53	233	366	570	365	355	305	99	46	39	39	46
La	233	125	99	20	87	200	326	208	203	167	39	17	71	29	29
V	–	–	–	–	–	–	–	–	–	–	–	–	–	–	–
Cu	25	86	165	31	61	221	65	24	12	21	BDL	BDL	3	5	3
Ni	144	30	103	BDL	9	16	25	45	18	13	3	BDL	54	5	BDL
Zn	488	186	81	77	122	125	136	201	137	118	34	20	71	BDL	BDL
Nb	21	17	11	7	25	6	9	19	15	12	5	6	8	3	5
Zr	650	660	751	369	337	262	625	815	535	533	130	130	134	13	93
Y	152	70	52	18	50	39	62	59	47	39	9	8	16	3	2

	K1m	K8m	K9m	K10m	K16m	K19m	K20m	K21m	K23m	K24m	K11f	K12g	K13n	K17g	K18g
qtz	19.89	10.09	8.82	11.16	16.60	7.12	24.32	6.45	13.65	11.58	16.73	35.41	30.02	15.55	28.34
orth	38.46	50.64	58.78	65.42	49.15	52.16	46.65	49.12	50.02	53.98	50.42	26.56	15.65	64.32	25.80
ab	1.12	10.35	14.62	12.42	8.41	13.63	4.97	9.32	10.77	12.75	26.25	30.43	28.81	14.89	41.91
an	0.00	0.00	0.04	2.45	0.00	0.00	0.09	0.00	0.00	0.00	0.14	4.54	14.85	0.00	2.43
di	3.05	7.54	6.69	0.95	8.60	13.91	4.51	16.68	10.09	8.98	1.69	0.00	0.00	0.00	0.00
hy	13.77	5.76	1.70	2.71	0.00	0.00	9.34	0.00	0.00	0.00	3.51	1.02	5.94	1.29	0.63
ac	18.48	7.17	0.00	0.00	7.09	2.28	0.00	5.33	6.60	2.51	0.00	0.00	0.00	0.00	0.00
mag	1.62	4.18	1.56	0.90	0.35	3.48	5.62	3.50	3.60	2.33	0.27	0.00	0.00	0.13	0.00
ilm	1.96	1.72	1.13	0.55	1.46	0.61	1.10	1.62	1.64	1.27	0.59	0.00	0.13	0.04	0.06
hem	0.00	0.00	4.00	2.95	3.89	0.28	0.00	0.52	0.44	3.04	0.00	0.94	3.70	0.00	0.24
rut	0.00	0.00	0.00	0.00	0.00	0.00	0.00	0.00	0.00	0.00	0.00	0.16	0.27	0.00	0.14
sph	0.00	0.00	0.00	0.00	0.00	0.00	0.00	0.00	0.00	0.00	0.00	0.00	0.17	0.00	0.00
ap	1.66	2.55	2.66	0.42	0.73	1.88	3.41	1.63	1.11	0.94	0.39	0.26	0.47	0.35	0.21

Differentiation Index (mole percent)

72.08	74.73	82.66	88.84	79.62	74.79	84.54	66.74	79.35	80.73	93.43	95.60	85.53	93.38	97.50

Fe/(Fe+Mg)

0.54	0.51	0.62	0.66	0.70	0.48	0.45	0.51	0.65	0.66	0.42	0.54	0.44	0.16	0.33

$Fe^{3+}/(Fe^{3+}+Fe\ )$

0.69	0.71	0.82	0.86	0.89	0.72	0.57	0.74	0.74	0.85	0.15	1.00	-	-	-

Agpaitic index (mole percent)

156.1	114.0	99.9	88.6	114.7	104.1	99.6	110.9	112.9	104.4	89.2	82.1	60.8	82.2	91.9

	K22f	K25n	S2d	S5d	S12d	S22d	S19r	S20r	S21r	S23r	S24r	S1c	S3r	S4r	S7c
SiO_2	75.26	67.90	61.19	58.75	58.01	61.97	61.66	62.06	62.47	61.54	61.22	65.55	61.01	61.75	64.43
TiO_2	0.16	0.50	1.04	1.17	1.00	1.24	1.18	1.12	1.10	1.14	1.14	0.70	0.97	0.92	1.23
Al_2O_3	14.38	15.12	14.96	11.39	12.50	15.87	7.25	7.29	8.42	7.26	7.31	11.39	8.16	7.41	10.54
Fe_2O_3	0.00	0.17	3.87	5.20	7.77	4.91	9.47	6.27	9.96	6.35	12.57	8.44	7.82	9.99	10.29
FeO	-	3.09	2.45	1.57	0.83	0.65	2.24	3.67	2.28	3.45	2.20	0.48	2.65	2.06	0.33
MnO	0.02	0.04	0.06	0.15	0.12	0.06	0.64	0.62	0.56	0.52	0.67	0.08	0.41	0.42	0.10
MgO	0.19	2.21	0.88	3.09	1.95	1.06	4.67	6.11	3.74	6.47	4.46	0.57	4.95	4.23	0.65
CaO	0.70	3.16	0.55	3.98	2.29	0.34	1.50	2.24	0.92	2.40	1.63	0.73	1.93	1.36	0.77
Na_2O	3.83	3.92	1.66	1.53	1.73	1.20	3.16	2.86	2.65	3.01	2.91	2.41	3.36	3.57	2.48
K_2O	5.23	3.23	12.99	10.58	10.74	10.26	6.61	6.40	7.38	6.60	6.79	9.99	7.80	6.91	9.19
P_2O_5	0.31	0.21	0.26	1.13	0.85	0.57	0.60	0.70	0.23	0.65	0.60	0.09	0.58	0.53	0.21
H_2O^-	0.13	0.37	-	0.11	0.31	0.40	0.12	0.21	0.16	0.06	0.07	0.06	0.05	0.11	0.10
LOI	0.33	0.78	0.78	0.83	1.01	1.89	1.01	1.37	1.12	1.39	0.68	0.19	0.71	0.79	0.30
Total	100.54	100.35	100.69	100.47	99.11	100.06	100.12	100.93	100.99	100.83	100.04	100.69	100.39	100.06	100.60

Trace Elements (ppm)

Sr	1167	448	46	423	208	56	754	961	96	1156	782	63	878	566	58
Rb	324	185	420	336	361	432	238	244	262	244	239	361	262	235	342
Ba	723	1268	3822	2618	1746	3856	572	1137	460	777	1371	542	720	629	357
Ce	50	62	340	400	309	490	886	442	438	611	1057	226	355	418	145
La	33	52	138	131	145	339	481	241	293	375	651	95	128	164	82
V	-	-	22	32	46	-	-	-	-	-	-	12	13	16	9
Cu	12	9	18	121	31	12	5	6	12	1	2	5	3	11	6
Ni	18	47	BDL	32	10	2	152	226	90	231	140	-	184	158	-
Zn	137	67	86	122	119	94	547	523	405	523	590	62	454	504	63
Nb	15	10	28	28	19	25	31	23	26	18	25	20	20	20	31
Zr	535	121	270	473	918	204	795	666	1167	559	550	381	603	356	850
Y	47	15	88	78	79	79	182	109	164	91	156	56	113	117	17

	K22f	K25n	S2d	S5d	S12d	S22d	S19r	S20r	S21r	S23r	S24r	S1c	S3r	S4r	S7c
qtz	32.02	21.22	1.50	5.20	5.10	15.28	15.45	16.30	17.13	12.15	16.26	15.71	9.47	13.67	17.40
orth	30.88	19.17	76.83	63.09	64.89	63.80	39.46	37.81	43.74	39.24	39.37	58.78	45.14	40.91	54.19
ab	32.38	33.32	4.63	0.00	4.60	10.34	0.50	0.78	2.23	1.54	0.00	2.96	0.64	0.00	3.04
an	1.47	14.19	0.00	0.00	0.00	0.00	0.00	0.00	0.00	0.00	0.00	0.00	0.00	0.00	0.00
di	0.00	0.16	0.87	9.85	4.67	0.00	2.85	2.67	2.41	6.21	3.23	2.15	4.68	2.66	0.00
hy	0.47	10.25	3.83	3.42	2.80	2.69	12.56	13.20	8.48	18.68	9.45	0.42	14.17	11.77	1.62
ac	0.00	0.00	8.30	11.57	9.13	0.00	23.36	22.17	17.85	18.48	21.37	15.28	22.70	26.84	15.76
mag	0.00	0.25	1.45	1.85	0.17	0.00	2.16	4.52	5.54	0.00	5.88	0.00	0.00	1.16	0.00
ilm	0.04	0.95	1.98	2.25	1.94	1.53	2.26	1.06	2.10	2.18	2.13	1.18	1.85	1.76	0.91
hem	0.00	0.00	0.00	0.00	4.67	5.00	0.00	0.00	0.00	0.00	0.94	3.12	0.00	0.00	4.82
rut	0.14	0.00	0.00	0.00	0.00	0.46	0.00	0.00	0.00	0.00	0.00	0.00	0.00	0.00	0.04
sph	0.00	0.00	0.00	0.00	0.00	0.00	0.00	0.00	0.00	0.00	0.00	0.19	0.00	0.00	1.73
ap	0.72	0.49	0.60	2.66	2.02	1.35	0.41	1.49	0.54	1.52	1.37	0.21	1.35	1.24	0.49
Differentiation Index (mole percent)															
	96.21	83.83	80.39	68.52	73.03	84.79	66.40	65.45	72.65	60.88	66.84	81.89	60.24	64.56	80.09
Fe/(Fe+Mg)															
	0.00	0.45	0.79	0.53	0.69	0.72	0.56	0.46	0.63	0.44	0.63	0.89	0.52	0.59	0.89
$Fe^{3+}/(Fe^{3+}+Fe^{2+})$															
	0.47	0.05	0.59	0.74	0.89	0.87	0.79	0.61	0.80	0.62	0.84	0.94	0.73	0.81	0.96
Agpaitic index (mole percent)															
	83.2	65.7	112.2	122.6	115.7	82.4	170.3	154.6	146.6	166.7	166.0	129.7	171.1	180.2	133.1

	S8c	S9c	S10c	S11c	S13c	S16s	S17c
SiO_2	64.69	64.82	65.51	65.18	64.55	62.15	63.00
TiO_2	1.37	1.25	0.64	0.94	1.27	0.58	0.85
Al_2O_3	9.92	10.55	12.74	10.45	10.61	15.19	12.72
Fe_2O_3	10.59	9.98	6.88	9.92	9.43	3.19	7.33
FeO	0.32	0.22	0.39	0.55	0.45	1.04	0.03
MnO	0.11	0.12	0.03	0.10	0.09	0.06	0.10
MgO	0.64	0.56	0.43	0.55	0.57	1.50	0.77
CaO	0.73	0.61	0.46	0.73	0.63	1.27	0.44
Na_2O	2.39	2.76	2.20	2.82	2.34	1.83	1.92
K_2O	8.55	8.72	10.68	8.64	8.99	12.35	11.07
P_2O_5	0.36	0.14	0.11	0.11	0.14	0.25	0.34
H_2O^-	0.20	0.15	0.07	0.08	0.21	0.13	0.16
LOI	0.47	0.09	0.17	0.19	0.47	0.32	0.39
Total	100.33	99.96	100.31	100.26	99.59	100.59	99.11

Trace Elements (ppm)							
Sr	59	70	58	82	50	178	58
Rb	319	357	395	329	329	433	406
Ba	458	718	598	589	401	4044	440
Ce	277	275	254	281	215	80	591
La	125	141	102	150	111	35	308
V	15	4	8	9	9	16	7
Cu	16	25	5	8	7	74	9
Ni	-	-	-	-	2	3	-
Zn	62	76	43	63	59	58	74
Nb	40	23	23	32	56	7	32
Zr	531	709	792	339	658	107	626
Y	49	16	71	85	11	17	63

	S8c	S9c	S10c	S11c	S13c	S16s	S17e
qtz	20.75	18.19	13.72	18.43	18.84	2.39	11.34
orth	50.69	51.67	63.07	51.06	53.52	72.89	66.36
ab	3.44	5.73	6.07	5.65	4.56	9.36	3.85
an	0.00	0.00	0.00	0.00	0.00	0.00	0.00
di	0.00	0.00	0.75	1.68	0.00	3.64	0.00
hy	1.60	1.40	0.72	0.59	1.43	2.04	1.95
ac	14.85	15.58	11.04	16.05	13.56	5.37	11.13
mag	0.00	0.00	0.00	0.00	0.00	1.86	0.00
ilm	0.91	0.72	0.89	1.38	1.15	1.10	0.28
hem	5.49	4.62	3.06	4.37	4.81	0.76	3.59
rut	0.52	0.26	0.00	0.00	0.23	0.00	0.71
sph	0.91	1.50	0.42	0.53	1.58	0.00	0.00
ap	0.84	0.33	0.26	0.26	0.33	0.58	0.80

Differentiation Index (mole percent)

81.05	80.96	85.24	80.99	81.92	82.39	82.52

Fe/(Fe+Mg)

0.90	0.90	0.90	0.91	0.90	0.63	0.83

$Fe^{3+}/(Fe^{3+}+Fe^{2+})$

0.97	0.98	0.94	0.94	0.95	0.77	0.99

Agpaitic index (mole percent)

132.9	132.4	119.1	133.9	128.0	107.8	119.0

TABLE 7.3

TRACE ELEMENTS IN CARBONATITES

	Sr	Ba	Ce	La	Y
P1B	953	346	1059	581	519
P10B	4250	256	832	406	374
P51T	4585	489	863	463	439
P59B	5678	543	1158	603	443
P63T	-	-	-	-	292
P68T	-	170	1202	636	585
P69T	5307	231	846	422	397
P(69a)T	5565	205	898	470	474
P73T	4275	696	651	341	305
P99B	3672	431	464	219	165
P100B	4416	1174	821	428	418
P102T	5275	1391	887	505	439
P104B	4306	1126	734	412	349
P110B	6301	523	746	382	348
PIR64-2356T*	4312	1475	625	332	324
P146-1128B	-	624	873	469	424
P146-1368T*	4817	418	982	546	413
P146-1391T	5620	741	748	393	434
P152-1430B	4957	60	1034	523	474
P153-1301B	4269	616	464	228	215

*Sr measured by isotope dilution or mass spectrometer and used for XRF Sr standard.

Appendix B

CHEMISTRY - METHODS, TECHNIQUES AND QUALITY OF DATA

B.1 Electron Microprobe

Table B.1 Replicate analyses of standards, microprobe

Table B.2 Replicate analyses of unknown, microprobe

B.2 Activities of Components in Minerals

B.3 X-ray Fluorescence

Table B.3 Replicate analyses of standards, major and minor elements, XRF

Table B.4 Replicate analyses of standards, trace elements, XRF

Table B.5 Replicate analyses of unknown, major and minor elements, XRF

Table B.6 Replicate analyses of unknown, trace elements, XRF

Table B.7 Machine conditions, major and minor elements, XRF

Table B.8 Machine conditions, trace elements, XRF

B.4 Wet Chemistry Determination of FeO

B.5 Trace Element Model Calculations - Spitskop

B.1 ANALYTICAL TECHNIQUE FOR THE ELECTRON MICROPROBE

Equipment

Three microprobes were used to collect the data presented in this study: an ARL probe (model SEMQ) at Angle American Research facilities in Johannesburg, the ARL probe (model SEMQ) at the University of the Witwatersrand and an ARL (model EMX-SM) at the University of Texas at Dallas. The majority of data were obtained on the latter two probes.

Method

Standard procedures for slide preparation were used.

Analytical conditions included: 15 kv accelerating potential, 150 μ amp emission current, and beam current of 0.10-0.15 μ amp for pyroxenes, olivines, feldspars, magnetite and apatite, and 0.05 μ amp for micas and amphiboles.

Counting time varied among probes and minerals to ensure adequate counting statistics with minimum damage to specimen.

Beam size varied among minerals from finely focused (1-2 microns) for anhydrous minerals such as pyroxene to a more dispersed beam (up to 4-5 microns) for micas.

Pulse height analyzers on the amplifiers were controlled to insure highest peak/background ratio.

Standards varied among laboratories but standards of clinopyroxene and feldspars were most commonly used. Mn was measured on pyrope with 0.33 percent MnO, Cr on chromite and

Ni on NiS_2 standards. Calibration was checked when instability beam current occurred or at a maximum of one hour intervals.

Data reduction on all three microprobes used the Bence-Albee method to correct for absorption and matrix effects.

Mineral Formulas

Calculations of proportions of cations in a formula unit were performed using the program of R. G. Cawthorn, developed at Newfoundland University. The exception to this was calculation of Fe^{3+} which was calculated by alloting an equal molar proportion of Fe to the Na content. This is discussed in Chapter 5.

Quality of Data

Accuracy of microprobe data is measured by performing replicate analyses of minerals with known composition. Listed below (Table B.1) are results of replicate analyses of standards performed on the Anglo American and UTD microprobes. Data from WITS is of comparable accuracy.

Interlaboratory consistency was measured by utilization of a working standard. Clinopyroxene F100P was used. Table B.2 lists results of replicate analyses from the WITS and UTD probes. Comparable results were obtained on the Anglo American microprobe.

Precision of analyses is measured by replicate analyses. Data in Table B.2 are a reflection of the precision obtained in this study.

Table B.1. Replicate analyses of standards.

	Clinopyroxene M1 (Anglo American)		Clinopyroxene Cpx-K (UTD)	
	Accepted Value	Value Obtained in the Study	Accepted Value	Value Obtained in the Study
SiO_2	51.40	51.23±.31	50.72	50.95±.27
TiO_2	0.53	0.49±.01	0.73	0.71±.05
Al_2O_3	5.51	5.19±.20	7.85	7.79±.30
FeO	3.80	3.92±.03	6.77	6.57±.23
MgO	16.07	16.01±.04	16.64	16.44±.09
MnO	0.08	0.07±.02	0.12	0.10±.02
CaO	21.06	20.93±.06	15.82	15.99±.12
Na_2O	0.95	0.92±.02	1.26	1.04±.36
Total	99.40	98.76	99.91	99.59

Table B.2
Replicate analysis of unknown, electron microprobe
F100P (Average of five analyses)

	WITS	UTD
SiO_2	53.59±.15	53.69±.48
TiO_2	0.21±.02	0.18±.04
Al_2O_3	0.09±.02	0.07±.02
FeO	2.48±.33	2.65±.03
MnO	0.05±.01	0.05±.01
MgO	17.41±.26	17.28±.21
CaO	24.81±.04	24.58±.23
Na_2O	0.08±.01	0.07±.03
Total	98.72	98.57

Appendix B.2

ACTIVITY OF COMPONENTS IN MINERALS

Clinopyroxene ($CaMgSi_2O_6$)

$$a^{cpx}_{CaMgSi_2O_3} = X^{M_2}_{Ca} (X^{Ml}_{Mg})(X^{t}_{Si})^2$$ Carmichael et al. (1977)

where X_{Ca} = Ca/Ca + Mn + Na + Mg + Fe in cation proportions

X_{Mg} = Mg/Mg + Fe + Al + Ti + Cr

X_{Si} = Si/Si + Al

Olivine ($(Mg,Fe)_2SiO_4$)

$$a^{oliv}_{Fe_2SiO_4} = (X^{oliv}_{Fe_2SiO_4})^2$$ Nicholls et al. (1971)

where $X^{oliv}_{FeSiO_4}$ = Fe/Fe + Mg in cation proportions

Magnetite (Fe_3O_4)

$$a^{mag}_{Fe_3O_4} = 1 - X_{usp}$$ Carmichael (1967)

where X_{usp} = Ti/Ti + Fe

APPENDIX B.3

X-ray Fluorescence Analytical Procedures

QUALITY OF DATA

The values quoted below for analytical accuracy and precision are taken from McCarthy (1977, personal communication). They are the accepted values for the facilities in the Department of Geology, University of the Witwatersrand. During this study at least one standard or duplicate sample was run with each group of samples, and values not agreeing with the accepted laboratory values were rerun. The values presented here were obtained on sample powder treated as separate samples and thus reflect the entire analytical procedure.

Accuracy

Table B.3 lists values for major and minor elements obtained on National Institute of Metallurgy standards in the Department of Geology X-ray facilities along the recommended values of the National Institute of Metallurgy.

P_2O_5 accuracy mainly reflects the correction for Ca interference as noted in Table B.3. Since international standards do not cover the range of values in the rocks measured in this study, standards for high P_2O_5 values were prepared using analytical grade CaO and $Ca_2P_2O_7$. Values obtained from these standards did not differ from those using international standards so were subsequently discarded. Thus the accuracy at high P_2O_5 values is believed to be comparable to that at low values.

Table B.4 presents values for international trace element standards obtained in this study combined with those for the lab (McCarthy),

TABLE B.3
Accuracy - Major and Minor Elements

	NIM P		NIM S		NIM G		NIM D	
	WITS	REC	WITS	REC	WITS	REC	WITS	REC
SiO_2	51.52	50.88	64.02	63.72	75.69	75.59	38.25	38.86
TiO_2	0.20	0.20	0.06	0.05	.11	.09	.03	.04
Al_2O_3	4.45	4.38	17.81	17.33	12.42	12.08	.44	.44
Fe_2O_3	12.91	12.29	1.44	1.40	1.98	2.02	17.07	16.97
MnO	0.23	0.18	0.02	0.01	0.03	0.02	0.22	0.20
MgO	26.41	25.19	0.57	0.48	0.08	0.10	44.42	43.30
CaO	2.69	2.68	0.69	0.70	.79	.80	.27	.31
Na_2O	0.76	0.37	0.49	0.43	3.76	3.32	.34	.10
K_2O	0.10	0.10	14.93	15.34	4.99	4.98	0.02	0.04
P_2O_5	0.02	0.04	0.12	0.13	0.02	0.03	.01	.03

TABLE B.4
Accuracy - Trace Elements

	Sr		Rb		Nb		Zr		Y		Cu	
	WITS	REC	WITS	REC	WITS	REC	WITS	REC	WITS	REC	WITS	REC
AGV	657.0	667.7	67.0	66.4	15.0	12.7	225.0	226.6	21.7	21.7	59.7	63.4
GSP	233.0	229.6	254.0	254.2	29.0	30.4	562.0	563.8	30.4	31.6	-	-
W-1	-	-	-	-	9.5	8.5	105.0	95.4	25.0	23.2	110.0	107.6
BCR	330.	329.8	47.0	47.6	-	-	-	-	-	-	18.4	17.5
PCC-1	-	-	-	-	-	-	-	-	-	-	-	-
GR	-	-	-	-	-	-	-	-	-	-	345.0	355.5

TABLE B.4 (continued)
Accuracy - Trace Elements

	Zn		Ni		V		Ba		Ce		La	
	WITS	REC	WITS	REC	WITS	REC	WITS	REC	WITS	REC	WITS	REC
AGV	84.0	91.3	18.5	18.2	-	-	1208	1213	-	-	-	-
GSP	-	-	-	-	-	-	1300	1287	394.0	394.0	191.0	191.0
W-1	86.0	77.1	76.0	79.8	264.0	259.0	160	154	-	-	-	-
BCR	120.0	115.9	15.8	14.1	399	402	675	708	-	-	-	-
PCC-1	-	-	-	-	30.0	28.0	-	-	-	-	-	-
GR	60.0	64.8	55.0	61.2	-	-	-	-	-	-	-	-

1977, personal communication) and the recommended values published by Flanagan (1973).

Precision

Table B.5 lists values of replicate analyses for internal laboratory standards along with their standard deviations.

Table B.6 lists similar values for trace elements. Precision for each element decreases as the abundance approaches the detection limit, and MnO precision reflects its low, measured intensity due to instrumental conditions. Loss on ignition figures are determined by mass loss and are not as good at low levels.

SAMPLE PREPARATION

Whole rock samples ranged in size from a few grams to about 7-8 kilograms depending on grain size and the amount of fresh material available. Weathered surfaces were removed by cutting with a diamond saw and were broken into blocks of a few centimetres by sawing or breaking by sledge hammer. There were further crushed by a jaw crusher, split, and finally pulverized in a tungsten steel Siebteknik mill to minus 120 mesh.

Mineral separates were broken initially in a steel mortar and further reduced to minus 100-120 mesh size by a silica mortar and pestle. A Frantz isodynamic separator, Haultain Superpanner, Bromoform, and Methylene Iodide were used for mineral separation. Samples were checked optically for purity and were finally cleaned by handpicking and rinsing in H_2O in an ultrasonic bath. Samples are estimated to be at least 99 percent pure.

ANALYTICAL EQUIPMENT

Major-, minor-, and trace-element annalyses were carried out on a Phillips X-ray fluorescence spectrometer, model PW 1410, equipped with a

TABLE B.5

Precision - Major and Minor Elements

	WITS P		WITS G		WITS B	
	mean	std. dev.	mean	std. dev.	mean	std. dev.
SiO_2	55.13	0.200	75.34	.341	57.71	.362
TiO_2	0.22	.001	0.29	.004	.92	.004
Al_2O_3	5.83	.027	11.98	.079	8.89	.064
Fe_2O_3	11.95	.120	3.47	0.45	9.12	.036
MnO	0.20	.007	.05	.006	.13	.005
MgO	21.80	0.121	.04	.016	10.97	.072
CaO	4.01	.025	1.51	.012	6.86	.029
Na_2O	1.12	0.40	3.09	.097	2.55	.077
K_2O	0.16	.001	4.46	0.26	.08	.002
P_2O_5	0.02	.002	.04	.003	.09	.004
H_2O^-	.06	.018	.02	.005	.21	.226

TABLE B.6

Precision - Trace Elements

	WITS B		WITS G	
	mean	std. dev.	mean	std. dev.
Cu	107	1.41	8	0.62
Ni	983	12.97	2	0.81
Zn	60	0.70	74	0.87
Rb	1	0.00	99	1.49
Sr	99	1.49	108	1.36
Y	14	1.07	80	1.22
Zr	77	0.91	354	10.61
Nb	3	0.78	24	0.49
Ba	49	6.81	2744	35.00
Ce	20	2.05	186	6.30
La	6	2.28	122	1.00

3kw generator (PW 1140). Angular settings were controlled automatically but crystal changing, collimator setting and filter placement were done manually. The data were captured on paper tape and later processed on an IBM 370 computer at the University Computer Centre.

A few Sr and Rb analyses were done on a Phillips X-ray fluorescence spectrometer, model 1520, with all settings and data readings done manually.

A sample holder of Cu was used for major and minor elements with the exception of Na, and a holder of Al for Na and for trace elements.

DATA COLLECTION AND REDUCTION

Machine operating conditions for major, minor and trace elements may be found in Tables B.7 and B.8. Instrumental drift was monitored by reading of a reference regularly, usually every three samples and no data was used when drift exceeded 5 percent.

Calibration curves used standard concentrations of Flanagan (1973).

Data reduction was done by standard programs available in the department of geology (written by T. S. McCarthy).

Fe, Mn, Ti, Ca, K, P, Si, Al, and Mg were analyzed on fused discs and Na on pressed rock pellets according to the method of Norrish and Hutton (1969). Rock powder was heated to 110° C and 1000° C to constant mass and the weights recorded after each heating to give loss on ignition and H_2O^-. Fused pellets were made with heated powder and rock pellets of unheated sample.

Trace element analyses were made on pressed rock pellets according to Norrish and Hutton (1969). Mass absorption coefficients were calculated from major element chemistry using the tables of Birks (1963).

TABLE B.7

Machine Conditions - Major and Minor Elements

Element	Fe	Mn	Ti	Ca	K	P	Si	Al	Mg	Na	Bg	Bg
Spectral Line	K	K	K	K	K	K	K	K	K	K	K	K
Crystal	LIF (220)	LIF (220)	LIF (200)	LIF (200)	PET	PET	PET	PET	ADP	RAP	RAP	RAP
Angle	85.73	95.20	86.14	113.09	50.69	89.66	109.21	145.12	136.72	54.25	54.70	58.00
Collimator (mm)	550	150	150	150	150	550	550	550	550	550	550	550
Detector	----------Flow proportional counter----------											
Counting Time	40	100	20	20	20	40	20	100	200	200	100	100
Tube Target	----------Chromium----------											
KV	----------50----------											
MA	----------50----------											
Filter	in	in	out	out	out	out	out	out	out	out	out	out
Interference	-	-	-	-	-	2nd order Ca	-	-	-	-	-	-

TABLE B.8

Instrumental Conditions

Trace Elements

Element	Bg	Nb	Bg	Zr	Bg	Y	Bg	Sr	Bg	Rb	Bg
Spectral Line	-	K_α	-	K_α	-	K_α	-	K_α	-	K_α	-
Crystal	LIF (220)										
Angle (2θ)	29.52	30.44	30.92	32.10	33.20	33.90	34.80	35.85	36.80	37.99	38.80
Collimator (mm)	150										
Detector	Scintillation counter										
Counting times	40	100	40	100	40	100	40	100	40	100	40
Tube target	Tungsten										
KV	60										
MA	40										
Filter	out										
Interference	-	$Y_{K\beta}$	-	$Sr_{K\beta}$		$Rb_{K\beta}$	-	-	-	-	-

Element	Bg	Bg	Ba	Bg	Bg	Ti	Ce	Bg	Bg	La
Spectral Line			$L_{\beta 2}$			K_β	$L_{\alpha 1}$			$L_{\alpha 1}$
Crystal	LIF (220)									
Angle	112.50	113.60	115.18	118.00	121.00	123.94	128.16	133.00	136.50	138.78
Collimator (mm)	550									
Detector	Flow									
Counting times	20	20	40	20	20	10	40	20	20	40
Tube target	Chromium									
KV	50									
MA	50									
Filter	out									
Interference			TiK_α				$BaL_{\beta 1}$			

Bg = background

TABLE B.8 (continued)

Element	Ti	Bg	V	Bg	Bg	Cr	Bg
Spectral Line	K_β		$K_{\alpha 2}$			$K_{\alpha 2}$	
Crystal	LIF (220)						
Angle	123.94	130.30	123.38	116.90	110.90	107.29	102.90
Collimator (mm)	150						
Detector	Flow						
Counting times	10	40	100	40	40	100	40
Tube target	Gold						
KV	50						
MA	50						
Filter	out	out	out	out	in	in	in
Interference	-	-	TiK_β	-	-	VK_β	-

Element	Au	Bg	Zn	Bg	Cu	Bg	Ni	Bg
Spectral Line	$L_{\alpha 1}$	-	K_α	-	K_α	-	K_α	-
Crystal	LIF (220)							
Angle (20)	53.25	56.80	60.58	62.58	65.55	69.25	71.26	75.25
Collimator (mm)	150							
Detector	Flow proportional + Scintillation							
Counting times	10	20	40	20	40	20	40	20
Tube target	Gold							
KV	50							
MA	50							
Filter	out							
Interference								

Sr-Rb

Element	Mo	Bg	Sr	Bg	Rb	Bg
Spectral Line	Compton	-	K_α	-	K_α	-
Crystal	LIF (220)					
Angle (20)	29.02	34.85	35.85	37.26	37.99	38.85
Collimator (mm)	150					
Detector	Scintillation					
Counting times	40	20	40	20	40	20
Tube target	Molybdenum					
KV	60					
MA	40					
Filter	out					
Interference						

Bg = background

Trace elements were analysed in groups of similar X-ray characteristics or with interelement interference as described below.

Ba, Ce, La

Ba, Ce, and La were measured along with the TiK_{β} peak. Two backgrounds were measured on each side of $BaL_{\beta}2$. Two spiked Ba samples containing no Ca or Ti were read to obtain the interference factor of Ba on Ce and two spiked Ti samples with no Ba, Ce, or La were measured to correct for TiK_{β} interference with the $BaL_{\beta}2$.

Two blanks were used to calculate background factors, and absorption effects were corrected from calculated primary and secondary mass absorption coefficients (primary CeK_{α}, secondary BaL_{α}). Calibration curves using standards GSP-1, W-1, BCR, and AGV-1 were used for Ba; because of the quality of standard values for Ce and La, these elements were standardized by GSP-1 alone.

Rb, Sr

Rb and Sr concentrations were calculated using background factors calculated from two blanks and absorption effects based on the intensity of the Compton peak of the molybdenum tube (Reynolds, 1967).

Standards BCR, AGV-1, and GSP-1 were used for silicate materials and two carbonate samples with Sr values measured by isotope dilution were used as standards for carbonatites.

Cu, Ni, Zn

Measurement of Cu, Ni, and Zn concentrations involved the measurement of blanks to determine the Au tube's contribution to Cu, Ni, and Zn intensities and the background factors. The molybdenum Compton peak was measured for each sample to correct for absorption.

Standards used were AGV-1, GR, BCR, and W-1.

Zr, Nb, Y

Rb, Sr, Nb, Y, and ZrK_{α} peaks were measured with a background reading between each peak. Spikes of Rb, Sr, and Y were measured to correct for interference on Y, Zr, and Nb respectively. Blanks were measured for background corrections and absorption correction was made by molybdenum Compton peak.

Standards used were GSP-1, AGV-1, and W-1. Flanagan's (1973) values were used with the exception of GSP-1 value for Zr where 562 ppm (J. P. Willis, personal communication, 1977) was used.

V

Ti, V, and Cr were measured together because of mutual interferences. Spiked Ti samples were measured to find its interference on V; likewise spiked V samples yielded V interference on Cr. Calculated mass absorption coefficients (from primary W rad., secondary V) were used and backgrounds were measured on blanks.

Acceptable Cr values could not be obtained due to massive tube interference, so were not used in this study and Ti concentrations from major element runs are used.

Standards used were BCR, PCC-1, and W-1.

APPENDIX B.4

Wet Chemical Technique

FeO

FeO determinations were made following the modified method of Wilson (Maxwell, 1968) involving cold acid decomposition. Care was taken to avoid oxidation of the sample by analyzing after 24 hours of dissolution. Blanks and standards were run with each set of dissolutions, and a sample was rerun if duplicate analyses varied more than 10%. Internal standard WITS B yielded FeO = 7.13 $\pm$0.285, as compared to WITS B, FeO = 7.23 $\pm$ 0.274 obtained by McCarthy (personal comm, 1977) using the method of Schafer (1966).

B.5 TRACE ELEMENT MODEL CALCULATIONS - SPITSKOP

Assuming rock with composition of S23R is liquid with 10% cumulus aegirine-riebeckite.

Ba	777
Rb	244
Sr	1156
Zr	559

$D_{Ba}^{hb} = 0.044$

Let B = true liquid composition of Ba

$0.1\ (.004)B + .9B = 777$

$.9044B = 777$

$B = 859$

$D_{Sr}^{hb} = 0.022$

Let A = true liquid composition of Sr

$0.1\ (.022)A + .9A = 1156$

$A = 1281$

$D_{Rb}^{hb} = 0.014$

Let C = true liquid composition of Rb

$0.1\ (.014)C + .9C = 244$

$C = 271$

$D_{Zr}^{hb} = 0.80$

Let D = true liquid composition of Zr

$0.1\ (.80)D + .9D = 559$

$D = 570$

Starting composition of liquid

Ba	859 ppm
Rb	271
Sr	1281
Zr	570

Using the equation: $D - 1 = \dfrac{\log \frac{C_L}{C_O}}{\log F}$

in which C_L = concentration in liquid remaining
C_O = concentration in initial liquid
F = proportion of liquid remaining
D = bulk distribution coefficient

Stage 1, phases crystallizing are 65% aegirine and riebeckite, 34% potassium feldspar and 1% apatite

$D_{Ba} = .65(.044) + .34(6.12) = 2.11$
$D_{Sr} = .65(.022) + .34(4.5) + .01(15) = 1.69$
$D_{Rb} = .65(.014) + .34(.34) = 0.125$
$D_{Zr} = .65(.80) = 0.52$

	C_O	C_L (F=.8)	C_L (F=.6)
Ba:	859	670	487
Sr:	1281	1098	900
Rb:	271	329	423
Zr:	570	634	728

Stage 2, phases crystallizing are 95% feldspar, 5% aegirine-riebeckite

$D_{Ba} = .95(6.12) + .05(.044) = 5.82$
$D_{Sr} = .95(4.5) + .05(.022) = 4.28$
$D_{Rb} = .95(.34) + .05(.014) = 0.324$
$D_{Zr} = .05(.80) = 0.04$

	C_O	C_L (F=.8)	C_L (F=.6)	C_L (F=.4)	C_L (F=.2)
Ba:	487	166	41.5	5.88	0.208
Sr:	900	433	168	44.6	4.59
Rb:	423	492	597	786	1250
Zr:	728	902	1190	1750	3410

Appendix C

ISOTOPIC STUDY

C.1 Sample Descriptions

C.2 Mass Spectrometry Techniques

Figure C.1 Change in spike concentrations over time

Table C.1 Rb, Sr, $^{87}Sr/^{86}Sr$ for NBS 607-K-feldspar standard

Table C.2 $^{87}Sr/^{86}Sr$ values for Eimer and Amend standard

Table C.3 Duplicate $^{87}Sr/^{86}Sr$ data for same dissolutions

Table C.4 Duplicate $^{87}Sr/^{86}Sr$ data for different dissolutions

C.3 Sample Preparation, P29P

C.4 Calculations of Radiogenic Sr Generated from Formation of Vermiculite

C.1 SAMPLE DESCRIPTIONS

For Locations, see Figures 9.2 and 9.2a

Carbonatites

P10C Fine-grained, banded with magnetite contains calcite, apatite, minor magnetite, sulphides and one large flake of mica which was removed. Bench 14 East, Sept. 1975.

P51C Coarse white calcite with occasional grains of apatite. Very minor, small flecks of mica (removed). Central part of plug, Bench 19, Dec. 1976.

P146-1368C Coarse grained, white with some apatite and magnetite. Borehole core.

Pir 64-2356C Coarse, nearly pure calcite with minor apatite. Borehole core.

P152-1430C Greyish, fine-grained sugary with one piece of magnetite. Borehole core.

P68C Medium-grained calcite and chalcopyrite. Bench 19 East, Aug. 1977.

P72C Coarse white calcite with abundant phlogopite, magnetite, chalcopyrite with large (2-6 cm) crystals of diopside. Also contains some portions of fine-grained sugary carbonate. Bench 18 East, Aug. 1977.

Clinopyroxene

P150-875P Dark green augite from micaceous pyroxenite.

F101P Part of a diopside crystal 35-40 cm in length by 20 cm wide, parting well developed, rare tremolite along parting, contains minute flakes of mica (removed) from pegmatitic micaceous pyroxenite.

P72C Pale green diopside 4 cm in diameter. Rare megacryst from carbonatite, cloudy appearance in hand specimen.

F15M Pale green diopside from massive pyroxenite with a bimodal size distribution of diopside crystals.

G12F Euhedral crystal of diopside from feldspathic pyroxenite contains pronounced oscillatory zoning from Guide Copper Mine pyroxenite pipe.

F23F Pale green diopside from feldspathic pyroxenite.

Apatite

F16P Apatite-mica rock with apatites growing through and around mica grains, from south side of Foskor Pit.

Pir 64-2356C Apatite from coarse-grained carbonatite.

F15M Apatite from massive pyroxenite with prismatic clinopyroxenes and interstitial apatite.

Mica

P1C Large crystals, no visible impurities in mica, reverse pleochroism, from Trangressive Carbonatite, Bench 12 East, Sept. 1975. PMC

P28P Contains some apatite, normal pleochroism but nearly equal in intensities of red and gold, from micaceous pyroxenite, Bench 17 South West, Sept. 1975. PMC

P29P Glimmerite contains large amounts of apatite, phlogopite has normal pleochroism of red and gold, Bench 17 South West, Sept. 1975. PMC

F16P Large book of mica with large crystals of apatite growing perpendicular through the book of mica, from near edge of Foskor Pit.

Pir 64-2395P Dark brown phlogopite from glimmerite in massive pyroxenite, borehole core.

P134-1006K Contains abundant calcite and contains veinlet of calcite with chalcopyrite and magnetite, from phoscorite, borehole core.

Vermiculite Large book of golden vermiculite from vermiculite quarry. PMC

F100P Mica from micaceous pyroxenite with inch-scale layering, west side of Foskor Pit.

F102X Dark brown phlogopite from finely-banded, micaceous pyroxenite xenolith in Foskor Pit. Xenolith is several metres in diameter.

Uranothorianite

Thor I LK135-1831 ft., banded carbonatite.

Thor II LK146-1208 m, transgressive carbonatite from borehole core.

Baddeleyite

BaddI Phoscorite, rock of carbonate, olivine, serpentine, and chondrodite.

BaddII Transgressive carbonatite, apatite rich, 238 m above mean sea level, western fringe of transgressive carbonatite.

BaddIII Phoscorite.

BaddIV Phoscorite, coarse-grained.

Appendix C.1 (continued)

COUNTRY ROCK DESCRIPTIONS
For Locations, see Figure 9.1

C1G, C2G, C3G Pink, equigranular, medium-grained granite, taken from water-pipe trenches between Kgopoeloe Hill and a small syenite pipe to northeast. Samples slightly iron-stained but in thin section look fresh although recrystallized.

C7V Fine-grained white granite, taken at intersection of waterwork road with railway line. In thin section seems fresh, highly recrystallized, contains muscovite, no obvious metasomatism.

C8V Coarse-grained muscovite pegmatite, closely interfingered with weathered fine-grained gneiss, taken from intersection of waterworks road and railway.

C9B Leucocratic, medium-grained granite with biotite and veins of feldspar and quartz, taken from large outcrop along power lines by Selati River.

C10G Pink granite with scattered aegirine, taken from area containing minor amounts of weathered biotite gneiss and some pegmatitic rocks.

C11V, C12V White muscovite pegmatite, taken north of Selati River next to road. Muscovite from this rock dated by Rb-Sr.

C13B, C14B Medium-grained, biotite granite, taken from large boulder blasted from side of road.

C15G, C16G Coarse-grained pink granite, taken from cutting along railroad tracks in area with equal proportions of pink and gneissic type rocks.

C17G-C20G Pink granite, taken from trenches showing area to consist of muscovite pegmatite and fine- and coarse-grained pink granite.

C21B Gneissic biotite from boulder containing this type and a pegmatitic pink granite.

C22G Pink granite from area containing gneissic- and pink-granite, slightly altered feldspar.

C23B, C24B Gneissic biotite granite.

C25B Dark, biotite-rich gneissic granite.

C26G-C30G Pink granite from roadside boulders.

C.2 MASS SPECTROMETRY TECHNIQUES

Sample Preparation

Whole-rock samples ranged from 10 g to about 0.5 kg depending on the grain size of the sample. Whole rocks were pulverized in a chromium-steel Siebtecnik mill.

Mineral separates were finally hand picked from rocks crushed in a steel mortar. Thorianite was concentrated using a Haultain superpanner. All separates are at least 99.9 percent pure.

Spikes

Spikes of ^{87}Rb (spike > 99.2% ^{87}Rb), ^{84}Sr (spike > 99.3% ^{87}Sr), ^{39}K (spike > 99.2% ^{39}K), ^{238}U (spike > 99% ^{238}U), and ^{206}Pb (spike > 88% ^{206}Pb) were used in determining element content. Spikes were calibrated against gravimetric standards and checked periodically.

Changes in concentration of U and Pb spikes over the time of this study are shown in Figure C.1.

Chemical Procedures

Micas. Phlogopites were washed in deionized, distilled water in an ultrasonic bath to remove intergrown material or substances adhering to surfaces, with the exception of those noted in Table 9.3. The micas were washed repeatedly and washes discarded until wash water remained clear.

Rb and Sr spikes were weighted into teflon beakers and dried, and the sample was added along with 10 ml HF and a

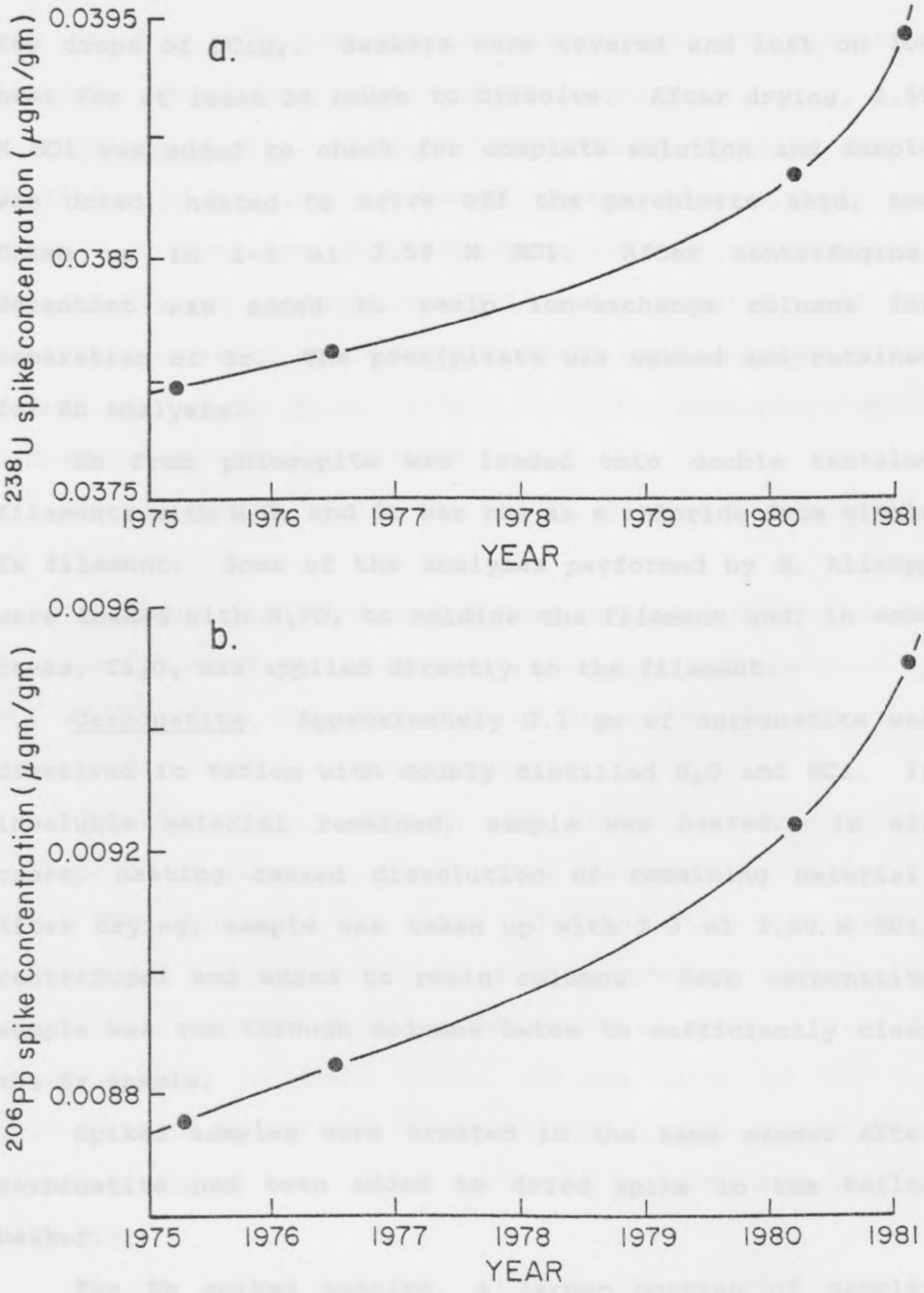


Figure C.1 a) Concentration of U spike over the period of this study, b) Concentration of Pb spike over the period of this study.

few drops of $HClO_4$. Beakers were covered and left on low heat for at least 24 hours to dissolve. After drying, 2.59 N HCl was added to check for complete solution and sample was dried, heated to drive off the perchloric acid, and taken up in 2-3 ml 2.59 N HCl. After centrifuging, decantant was added to resin ion-exchange columns for separation of Sr. The precipitate was washed and retained for Rb analysis.

Rb from phlogopite was loaded onto double tantalum filaments with H_2O, and Sr was run as a chloride from single Ta filament. Some of the analyses performed by H. Allsopp were loaded with H_3PO_4 to oxidize the filament and, in some cases, Ta_2O_5 was applied directly to the filament.

Carbonatite. Approximately 0.1 gm of carbonatite was dissolved in teflon with doubly distilled H_2O and HCl. If insoluble material remained, sample was heated. In all cases, heating caused dissolution of remaining material. After drying, sample was taken up with 2-3 ml 2.59 N HCl, centrifuged and added to resin columns. Each carbonatite sample was run through columns twice to sufficiently clean the Sr sample.

Spiked samples were treated in the same manner after carbonatite had been added to dried spike in the teflon beaker.

For Rb spiked samples, a larger portion of sample, around two grams, was added to dried spike in a teflon beaker. Doubly distilled acids were used. Ammonia solution

was added to dissolved sample, centrifuged, and decantant removed. 8M HNO_3 was added and sample dried.

Clinopyroxenes. Samples were cleaned in cold, doubly distilled 6N HCl for six hours, rinsed several times and dried. Spiking and dissolution method was identical to phlogopites but reagents were all doubly distilled. Sr was separated on resin columns and K and Rb were isolated by the method of Allsopp et al. (1969) involving precipitation of hydroxides by ammonia solution.

Sr was run on triple Re, and K, Rb were run on double Ta filaments.

Apatites. Apatites were rinsed in dilute HCl to remove tiny particles of optically visible calcite. Dissolution by HCl was complete and separation of Sr and Rb was identical to that described for clinopyroxenes.

Uranothorianite. Samples were washed in reagent-grade acetone in an ultrasonic bath, then dissolved by boiling in 2.5 N HNO_3 for about two hours. This solution was further diluted to a litre solution of 0.5 normality from which about 10 ml were added to a given amount of spike. U and Pb were isolated in small teflon columns using 6N HCl for collection of Pb and H_2O for U. Pb was further concentrated by electrodeposition. U was converted to nitrate by heating with HNO_3.

Pb was loaded with HNO_3 onto silica gel on single Re filament, dried, and then converted to phosphate.

U was loaded on triple Re filament as nitrate and then converted to an oxide by heating.

Baddeleyite. Baddeleyite samples were boiled in 1 N HNO_3 for one hour to remove traces of sulphides and then rinsed by boiling in H_2O twice for one hour each time. Sample was weighed into a teflon bomb with 3 ml doubly distilled HF and a few drops of doubly distilled HNO_3. The bomb was sealed and heated to 220°C overnight. This solution was transferred to another teflon container and dried to remove HF. This was then taken up with 10 ml of 1 N HCL for splitting and spiking. U and Pb separation followed the same method as uranothorianite.

Equipment and Running Conditions

A Micromass 12-inch, 90° solid source mass spectrometer with automatic peak switching and digital voltmeter output was used for Sr, U, and Pb measurements. Rb and K were measured on an 8-inch, 60° mass spectrometer of Bernard Price Institute construction. The bulk of Sr analyses of carbonatites were measured by X-ray fluorescence on a Philips 1540 X-ray fluorescence instrument (see Appendix B for further X-ray technique) with standards measured by mass spectrometry by isotope dilution technique (values in Table 9.7).

Strontium isotopic measurements were normalized to a $^{86}Sr/^{88}Sr$ value of 0.1194. Because normalization is not possible for Pb, K and Rb, fractionation of isotopes was minimized by running Pb at a constant temperature of 1200°C

and running at constant temperature and obtaining data for K, Rb, and U in as short a time as possible. Peaks were checked for centering between blocks of data, and data were recorded after interfering elements were burned off.

Quality of Data

Accuracy of Rb and Sr elemental concentrations by isotope dilution are gauged by replicate analyses of feldspar standard in the BPI laboratory. Table C.1 lists the results of these analyses and the values obtained at the National Bureau of Standards. The mean values and variation (2σ) in elemental concentrations are Sr = 65.645 ± 0.290 µg/g and Rb = 520.48 ± 2.48 µg/g giving an accuracy of Sr concentration of 0.44 percent and an accuracy of Rb concentration of 0.48 percent. The accuracy of $^{87}Sr/^{86}Sr$ analyzed from the NBS feldspar standard is 0.05 percent from the average of 1.20033 ± 0.0006 (Table C.2).

Accuracy of $^{87}Sr/^{86}Sr$ for carbonatites, apatites and clinopyroxenes which contain substantial amounts of Sr is measured from replicate analyses of the Eimer and Amend standard $SrCO_3$ with a BPI laboratory value of 0.70799 ± 0.00002 (2σ). Table C.2 lists laboratory measurements over the time period this work was done.

Table C.1. NBS 607 - K-feldspar standard.

NBS: Rb = 523.90 ± 1.01
Sr = 65.485 ± 0.32
$^{87}Sr/^{86}Sr$ = 1.20039 ± 0.0002

Date	Rb	±	Sr	±	$^{87}Sr/^{86}Sr$	±	Analyst
24.6.75	521.9	*	65.223				HLA
10.8.75	524.8		66.305				HLA
1.6.77	518.4		65.715	0.045	1.2011	0.0008	HLA
30.6.77	519.8		65.683	0.068	1.1999	0.0002	HLA
7.1.80	518.6		65.495		1.2005	0.0002	TPE
7.1.80	516.5		65.450		1.2005	0.0001	TPE
24.1.80	522.2		65.745	0.130	1.19939	0.00007	EB
3.3.80	520.4		65.608		1.19998	.0001	RAA
6.4.80	521.7		65.585		1.20095	.0001	HLA

Analysts: HLA H. Allsopp
EB E. Barton
RAA R. Armstrong
TPE T. Elworthy

*Where errors are missing, data were not available.

Table C.2. $^{87}Sr/^{86}Sr$ values for Eimer and Amend standard over period of this study.

Date	$^{87}Sr/^{86}Sr$	Standard Deviation
7-77	0.707909	0.00009
8-77	0.70792	0.00006
9-76	0.707981	0.00002
11-76	0.708001	0.00002
7-76	0.70802	0.00002
7-76	0.70795	0.00003
7-76	0.70804	0.00003
7-75	0.70801	0.00002
7-75	0.70794	0.00002
7-75	0.70805	0.00003

Combined mean 0.70799 $\pm$ 0.00002 (2σ).

Analysts: H. Allsopp, S. Eriksson

Table C.3. Duplicate $^{87}Sr/^{86}Sr$, K, Rb analyses of same dissolutions.

Sample	Type	A	B	% Difference
P51C	carbonatite	$^{87}Sr/^{86}Sr$ = 0.70569±8	$^{87}Sr/^{86}Sr$ = 0.70569±6	0.00
F101P	pyroxene	K/Rb=194.0	K/Rb=194.7	0.36

Table C.4. Duplicate $^{87}Sr/^{86}Sr$ analyses of different sample dissolutions.

Sample	Type	A	B	% Difference
P28P	mica	3.1987±7	3.342±5	4.30
P134-1006K	mica	3.157±3	2.709±1	16.38
P72C	carbonatite	0.70448±18	0.70425±4	0.00
PIR 64-2356C	carbonatite	0.71006±4	0.71027±6	0.02
F16M	apatite	0.71125±10	0.71039±4	0.10
F101P	pyroxene	0.71282±24	0.71229±6	0.03

C.3 NOTES ON SAMPLE PREPARATION - P29P

a(1)(SCE) No washing, flakes of phlogopite hand picked. No obvious inclusions or discrete grains of apatite or calcite. Grains 0.5 to 1 mm.

a(2)(SCE) Same as a(1).

a(3)(HLA) Same as a(1).

b(1)(SCE) Sample selected as in a(1), washed in H_2O in ultrasonic for two 15-minute periods. Sample appeared free of inclusions and were free of powder adhering to surfaces. Grains are 0.5 to 1 mm.

b(2)(SCE) Same as b(1).

b(3)(HLA) Selected as for a(3), slightly ground and cleaned in ultrasonic for several washes; selected from this material, flakes with no inclusions.

c(1)(SCE) Sample selected as for a(1); sample then ground, washed in ultrasonic for three 10-minute periods in H_2O, last wash was clear. Grains are 0.1-0.3 mm.

c(2)(SCE) Ground by hand in agate mortar at least 15 minutes, washed three 15-minute periods; H_2O was clear after third wash.

c(3)(HLA) First crushing in agate mortar on Siebtecnik mill, sieved off fines (125 μm) and cleaned in ultrasonic. Magnetite flakes removed by magnet. White mineral still present so crushed in agate mortar by hand until like powder, washed in ultrasonic.

c(4)(HLA) Same as c(3). Mica flakes were larger than white grains, so majority of white material removed by sieving at 63 μm (the material passing through 63 um sieve was analyzed on microprobe, see text p. 304, and Table 9.6 (SCE).

Appendix C-4

ALTERATION OF PHLOGOPITE AS A SOURCE OF RADIOGENIC Sr

Estimate of area containing vermiculite from Hanekom *et al.* (1965):

northern inner pegmatoid	1.00 km^2
southern pegmatoid	0.32
hydrobiotite	0.50
	1.82 km^2

Assuming this area (1.82 km^2) is pure mica weathered to a depth of 50 m with a specific gravity of 2.65 for vermiculite:

$$2.4 \times 10^8 \text{ tons of vermiculite}$$

For a vermiculite composition found in Table 9.13, having lost 110 ppm ^{87}Rb which has decayed to ^{87}Sr over 20 m.y.:

$$20 \times 10^6 \text{ yr} = 1/\lambda \ln \left(1 + \frac{^{87}Sr^*}{110}\right) \qquad \lambda = 1.42 \times 10^{-11}$$

$$^{87}Sr^* = 0.03124 \text{ ppm}$$

$$2.4 \times 10^8 \text{ tons} \times 0.03124 \text{ ppm } ^{87}Sr^* =$$

$$2.4 \times 10^8 \text{ tons} \times 0.0312 \times 10^{-6} = 0.07488 \times 10^2$$

$$= 7.488 \text{ tons } ^{87}Sr^* \text{ from decay of } ^{87}Rb.$$

3.5 ppm lost of radiogenic Sr.

$$2.4 \times 10^8 \times 3.5 \times 10^{-6} = 8.4 \times 10^2 = 840 \text{ tons } ^{87}Sr^*$$

$$840 + 7.5 = 847.5 \text{ tons } ^{87}Sr^* \text{ available from alt. of phlogopite.}$$

Case I

Clinopyroxenites cover about 9.6 km^2; if 50% is clinopyroxene = 4.8 km^2 with specific gravity of 3.4; for a depth of 0.5 km = 8.16×10^9 tons clinopyroxene.

Assuming an initial ratio of 0.704, and a Sr content of 425 ppm,

$$\frac{0.704(8.16\times10^9)(4.25\times10^{-4} \text{ tons } {}^{87}Sr) + 847.5 \text{ tons } {}^{87}Sr^*}{(8.16\times10^9)(4.25\times10^{-4} \text{ tons } {}^{87}Sr)}$$

$$= \frac{(24.415\times10^5 \text{ tons}) + 847.5 \text{ tons}}{34.68 \times 10^5}$$

$$\frac{2441500 + 847.5}{3468000} = 0.70425$$

Case II

Carbonatites cover 0.33 km^2
1/2 km depth = 0.165 km^3 with specific gravity of 2.72 = 4.49×10^8 tons carbonatite.

Average Sr = 4500 ppm

$$\frac{0.704(4.49\times10^8 \text{ tons})(.0045 \text{ tons } {}^{87}Sr) + 847.5 \text{ tons } {}^{87}Sr^*}{(4.49\times10^8)(.0045)}$$

$$= \frac{1.422 \times 10^6 + 847.5}{2.0205 \times 10^6} = 0.70421$$

Case III

Assuming clinopyroxene with an initial ratio of 0.7115, the lowest initial Sr ratio measured from the clinopyroxenites with Sr = 425 ppm.

$$\frac{0.71151(8.16 \times 10^9 \text{ tons})(4.25 \times 10^{-4}) + 847.5}{(8.16\times10^9)(4.25\times10^{-4})}$$

$$\frac{24.6055 \times 10^5 + 847.5}{34.68 \times 10^5} = 0.71176$$

REFERENCES

Abbott, M.J., 1969, Petrology of the Nadewar Volcano, N.S.W. Australia, Contrib. Mineral. Petrol. 20, 115-134.

Aldous, R., 1980, Ore genesis in copper bearing carbonatites; a geochemical fluid inclusion and mineralogical study, unpublished Ph.D. & DIC thesis, Imperial College.

Allsopp, H.L., L.O. Nicolaysen, and P. Hakn-Weinheimer, 1969, Rb/K ratios and Sr-isotopic compositions of minerals in eclogitic and peridotitic rocks, Earth Planet. Sci. Lett. 5, 231-244.

Allsopp, H.L. and J. Ferguson, 1970, Measurements relating to the genesis of the Tsumeb pipe, South West Africa, Earth Planet. Sci. Lett. 9, 448-453.

Allsopp, H.L. and D.R. Barrett, 1975, Rb-Sr age determinations on South African Kimberlite pipes, Physics and Chemistry of the Earth 9, 605-618.

Allsopp, H.L. and J. Kramers, 1977, Rb-Sr and U-Pb age determinations on southern African kimberlite pipes (abstr.), Proc. 2nd Inter. Kimb. Conf., extended abstracts.

Aoki, K., 1974, Phlogopites and potassic richterites from mica nodules in South African kimberlites, Contrib. Mineral. Petrol. 48, 1-7.

Arth, J., 1976, The behavior of trace elements during magmatic processes: A summary of theoretical models and their applications, USGS Journal of Research 4, 41-47.

Baadsgaard, H. and O. Van Breemen, 1970, Thermally-induced migration of Rb and Sr in an adamellite, Ecol. Geol. Helv. 63, 31-44.

Bachinski, S. and R.B. Scott, 1979, Rare-earth and other trace element contents and the origin of minettes (mica-lamprophyres), Geochim. Cosmochim. Acta 43, 93-100.

Bacon, C.R. and I.S.E. Carmichael, 1973, Stages in the P-T path of ascending basalt magma: An example from San Quentin, Baja California, Contrib. Mineral. Petrol. 41, 1-22.

Baertschi, P., 1957, Messung und Deutung relativer Haufigkeits-variationen von ^{18}O and ^{13}C in Karbonatgesteinen und Mineralen, Schweiz. Mineral. Petrol. Mitt. 37, 73-152.

Bailey, D.K., 1969, The stability of acmite in the presence of H_2O, Amer. Jour. Sci. 167-A, 1-16.

Bailey, D.K., 1970, Volatile flux, heating-focusing and the generation of magma, in G. Newall and N. Rast, eds., Mechanism of Igneous Intrusion, Liverpool, Gallery Press, pp. 177-186.

Bailey, D.K. and J.F. Schairer, 1964, Feldspar-liquid equilibria in peralkaline liquids - the orthoclase effect, Amer. Jour. Sci. 262, 1198-1206.

Bailey, D.K. and J.F. Schairer, 1966, The system Na_2O-Al_2O_3-Fe_2O_3-SiO_2 at 1 atms, and the petrogenesis of alkaline rocks, Jour. Petrol. 7, 114-170.

Baldock, J.W., 1973, Potassic fenitization, trachytes, and agglomerates at the Bukusu Carbonatite Complex, Uganda, Overseas Geol. Mineral. Resour. 42.

Barker, D.S., 1969, North American feldspathoidal rocks in space and time, Geol. Soc. Amer. Bull. 80, 2369-2372.

Barth, T.F. and I. Ramberg, 1966, The Fen Circular Complex, in, Tuttle and Gittins, eds., Carbonatites, John Wiley and Sons, London, pp. 225-257.

Barton, J.M., Jr., 1979, The chemical compositions, Rb-Sr isotopic systematics and tectonic setting of certain post-kinematic mafic igneous rocks, Limpopo mobile belt, southern Africa, Precambrian Res. 9, 57-80.

Barton, J.M., Jr., R.E.P. Fripp, P. Horrocks, and N. McLean, 1979, The geology, age, and tectonic setting of the Messina Layered Intrusion, Limpopo mobile belt, southern Africa, Amer. Jour. Sci. 179, 1108-1134.

Barton, J.M., D.R. Hunter, M.P. Jackson, and A.C. Wilson, 1980, Rb-Sr age and source of the Bimodal Suite of the Ancient Gneiss Complex, Swaziland, Nature 283, 756-788.

Barton, M. and D.L. Hamilton, 1978, Water-saturated melting relations to 5 kb of three Leucite Hills lavas, Contrib. Mineral. Petrol. 66, 41-49.

Barton, M. and D.L. Hamilton, 1979, The melting relationships of a madupite from the Leucite Hills, Wyoming, to 30 kb, Contrib. Mineral. Petrol. 69, 133-142.

Bass, I.T., V.A. Boronikhin, and S.M. Kraochenko, 1974, Trends in the variation of magnesium, iron, calcium and sodium concentrations in different zones of crystals of monoclinic pyroxenes and phlogopite from carbonatite complexes as criteria of their origin. Dokl. Akad. Nauk. SSSR 291, 447-450 (in Russian).

Basu, A.R. and V.R. Murthy, 1977, Ancient lithosphere lherzolite xenolith in alkali basalt from Baja, California, Earth Planet. Sci. Lett. 35, 239-246.

Bates, R.L. and J.A. Jackson, 1980, Glossary of Geology, 2nd edition, American Geological Institute, Falls Church, Virginia, p. 394.

Bell, K. and J.L. Powell, 1969, Strontium isotopic studies of alkalic rocks: The potassium-rich lavas of the Birunga and Toro-Ankole Regions, East and Central equatorial Africa, Jour. Petrol. 10, 536-572.

Bell, K. and J.L. Powell, 1970, Strontium isotopic studies of alkalic rocks: The alkalic complexes of Eastern Uganda, Geol. Soc. Amer. Bull. 81, 3481-3490.

Beswick, A.E., 1976, K and Rb relations in basalts and other mantle-derived materials: Is phlogopite the key?, Geochim. Cosmochim. Acta 40, 1167-1183.

Bhattacharji, S., 1967, Scale model experiments on flowage differentiation in sills, in, P.J. Wyllie, ed., Ultramafic and Related Rocks, pp. 69-70.

Birch, F., 1965, Speculations on the earth's thermal history, Geol. Soc. Amer. Bull. 76, 133-154.

Birks, L.S., 1963, Electron Probe Microanalysis, Interscience, New York.

Blaxland, A.B., O. Van Breenan, and A. Steenfelt, 1976, Age and origin of agpaitic magmatism at Ilimaussaq, South Greenland, Rb-Sr study, Lithos 9, 31-38.

Bloomfield, A., 1973, Economic aspects of Uganda carbonatite complexes, Overseas Geol. Min. Res. 41, 139-167.

Boctor, N.Z. and H.O.A. Meyer, 1975, Oxide and sulfide minerals in kimberlite from Green Mountain, Colorado, Proc. 2nd Int. Kimb. Conf. 1, 217-228.

Boctor, N.Z. and D.P. Svisero, 1978, Iron-titanium oxide and sulfide minerals in carbonatite from Jacqupiranga, Brazil, 876-879.

Boettcher, A.L., 1966, Vermiculite, hydrobiotite, and biotite in the Rainy Creek igneous complex near Libby, Montana, Clay Minerals 6, 283-296.

Boettcher, A.L., 1967, The Rainy Creek alkaline-ultramafic igneous complex near Libby, Montana, I: Ultramafic rocks and fenite, Jour. Geol. 75, 526-553.

Boettcher, A.L., J.R. O'Neil, K.E. Windom, D.C. Stewart, and H.G. Wilshire, 1979, Metasomatism of the upper mantle and the genesis of kimberlites and alkali basalts, Proc. 2nd Int. Kimb. Conf. 2, 173-182.

Boettcher, A.L. and J.R. O'Neil, 1980, Stable isotope chemical and petrographic studies of high-pressure amphiboles and micas: evidence for metasomatism in the mantle source regions of alkali basalts and kimberlites, Amer. Jour. Sci. 280A, 594-621.

Bolivar, S.L. and D.G. Brookins, 1979, Geophysical and Rb-Sr study of the Prairie Creek, Arkansas kimberlite, Proc. 2nd Int. Kimb. Conf. 1, 280-288.

Borley, G.D., 1967, Potash-rich volcanic rocks from southern Spain, Mineral. Mag. 36, 364-379.

Borodin, L.S., 1965, Rare elements in ultrabasites from complex massifs of ultrabasic-alkaline rocks, in Problems of Geochemistry, Nauka, Moskow, pp. 396-405.

Borodin, L.S. and A.S. Pavlenko, 1974, The role of metasomatic processes in the formation of alkaline rocks, in, H. Sorenson, ed., The Alkaline Rocks, John Wiley and Sons, London, pp. 515-534.

Bottinga, Y. and D.F. Weill, 1970, Densities of liquid silicate systems calculated from partial molar volumes of oxide components, Amer. Jour. Sci. 269, 169-182.

Bowden, P., 1974, Oversatuarted alkaline rocks, granites, pantellerites and comendites, in, H. Sorensen, ed., The Alkaline Rocks, John Wiley and Sons, London, pp. 109-123.

Bowen, N. L., 1937, Recent high-temperature research on silicates and its significance in igneous petrology, Amer. Jour. Sci. 33, 1-21.

Boyd, F.R., 1975, Ultramafic xenoliths from the Frank Smith Mine and the Kimberley area, in, Extended Abstracts, Kimberlite Symposium, Cambridge, England, pp. 9-14.

Boyd, F.R. and D. Smith, 1971, Compositional zoning in pyroxenes from Lunar Rock 12021, Carnegie Inst. Wash., Yearbook 70, 131-133.

Brandt, J.W., 1948, Die geologie van'n gebied in Noord-oos Transvaal met spesiale verwysing na die verspreiding en petrografie van die rotssoorte van die Palabora-stollings-kompleks: unpublished D.Sc. Thesis, University Stellenbosch.

Brey, G. and D.H. Green, 1977, Systematic study of liquidus phase relations in olivine meliltite + H_2O + CO_2 at high pressures and petrogenesis of an olivine melilite magma, Contrib. Mineral. Petrol. 61, 141-162.

Briden, 1976, Application of palaeomagnetism to Proterozoic tectonics, Phil. Trans. R. Soc. Lond. A. 280, 405-416.

Brink, A.B.A., 1979, Engineering Geology of Southern Africa, Building Publications, Pretoria, 319 pp.

Brooks, C. and S.R. Hart, 1978, Rb-Sr mantle isochrons and variations in the chemistry of Gondwanaland's lithosphere, Nature 271, 220-223.

Brooks, C., S.R. Hart, A.W. Hofmann, and J.D. James, 1976a, Rb-Sr mantle isochrons from oceanic regions, Earth Planet. Sci. Lett. 32, 51-61.

Brooks, C., D.E. James, and S.R. Hart, 1976b, Ancient lithosphere: its role in young continental volcanism, Science 193, 1086-1094.

Brown, G.E., 1980, Olivines and silicate spinels, in, P.H. Ribbe, ed., Orthosilicates, Mineral. Soc. Amer. Reviews in Mineralogy 5, 275-364.

Brown, G.M. and E.A. Vincent, 1963, Pyroxenes from the late stages of fractionation of the Skaergaard intrusion, East Greenland, Jour. Petrol. 4, 175-197.

Buchanan, D.L., 1976, The sulphide and oxide assemblages in the Bushveld Complex rocks of the Bethal area, Trans. Geol. Soc. S. Africa 79, 76-80.

Buchanan, D.L., 1979, A combined transmission electron microscope and electron microprobe study of Bushveld pyroxenes from the Bethal area, Jour. Petrol. 20, 327-354.

Buchanan, D.L. and J. Nolan, 1978, Solubility of sulfur and sulfide immiscibility in synthetic tholeiitic melts and their relevance to Bushveld complex rocks, Contrib. to the Symposium on Sulfide Deposits, Toronto, Oct. 1978.

Buchanan, D.L., J. Nolan, and E.A. Viljoen, 1980, Determination of silica activity in Bushveld rocks, Contrib. Mineral. Petrol. 73, 311-319.

Buddington, A.F. and D.H. Lindsley, 1964, Iron-titanium oxide minerals and synthetic equivalents, Jour. Petrol. 5, 310-357.

Burwell, A.D.M., 1975, Rb-Sr isotope geochemistry of lherzolites and their constituent minerals from Victoria, Australia, Earth Planet. Sci. Lett. 28, 69-78.

Butler, S.A., 1972, Breakdown reactions in the Humite minerals, Ph.D. dissertation, Cambridge University, Cambridge, England.

Button, A., 1976, Stratigraphy and relations of the Bushveld floor in the eastern Transvaal, Geol. Soc. S. Africa Trans. 79, 3-12.

Campbell, I.H., 1978, Some problems with the cumulus theory, Lithos 11, 311-323.

Carmichael, I.S.E., 1967, The mineralogy and petrology of the volcanic rocks from the Leucite Hills, Wyoming, Contrib. Mineral. Petrol. 15, 24-66.

Carmichael, I.S.E. and W.S. MacKenzie, 1963, Feldspar-liquid equilibria in pantellerites; an experimental study, Amer. Jour. Sci. 261, 382-396.

Carmichael, I.S.E., J. Nicholls, F.J. Spera, B.J. Woods, and S.A. Nelson, 1977, High-temperature properties of silicate liquids: Application to the equilibration and ascent of basic magma, Phil. Trans. R. Soc. Lond. A. 286, 373-431.

Carmichael, I.S.E., F.J. Turner, and J. Verhoogen, 1974, Igneous Petrology, McGraw-Hill Book Co., New York, 739 pp.

Carter, S.R., N.M. Evensen, P.J. Hamilton, and R.K. O'Nions, 1978, Neodymium and strontium isotope evidence for crustal contamination of continental volcanics, Science 202, 743-747.

Cawthorn, R.G. and K.D. Collerson, 1974, The recalculation of pyroxene end-member parameters and the estimation of ferrous and ferric iron content from electron microprobe analysis, Amer. Mineral. 59, 1203-1208.

Cohen, E., 1895, Melilithgestein and calcitfuhrender Aplit aus Sudafrika, Tscher. Mineral. Petrol. Mitt. 14, 155.

Compston, W. and J.F. Lovering, 1969, The strontium isotopic geochemistry of granulitic and eclogite inclusions from the basic pipes at Delegate, eastern Australia, Geochim. Cosmochim. Acta 33, 691-699.

Cox, K.G., J.D. Bell and R.J. Pankhurst, 1979, The Interpretation of Igneous Rocks, Allen and Unwin, London, 450 pp.

Cullers, R.L. and G. Medaris, Jr., 1977, Rare earth elements in carbonatite and cogenetic alkaline rocks: Examples from Seabrook Lake and Callander Bay, Ontario, Contrib. Mineral. Petrol. 65, 143-153.

Cundari, A., 1979, Petrogenesis of leucite-bearing lavas in the Roman volcanic region, Italy, Contrib. Mineral. Petrol. 70, 9-21.

Cundari, A. and R.W. LeMaitre, 1970, On the petrogeny of leucite-bearing rocks of the Roman regions, Jour. Petrol. 11, 33-47.

Daly, R. A., 1933, Igneous Rocks and the Depths of the Earth, McGraw-Hill, New York, 598 pp.

Daly, R.A., G.E. Manager, S.P. Clark, Jr., 1966, Density of rocks, in Handbook of Physical Constants, Geol. Soc. Amer. Mem. 97, 19-26.

Danchin, R.V., 1979, Mineral and bulk chemistry of garnet lherzolite and garnet harzburgite xenoliths from the Premier Mine, South Africa, Proc. 2nd Int. Kimb. Conf. 2, 104-126.

Dasch, E.J. and D.H. Green, 1975, Strontium isotope geochemistry of lherzolite inclusions and host basaltic rocks, Victoria, Australia, Amer. Jour. Sci. 275, 461-469.

Davidson, P.M., M. Engi, and D.H. Lindsley, 1979, The nature of clinopyroxenes (Cpx) solutions near Di($CaMgSi_2O_6$) in the system En-Wo($Mg_2Si_2O_6$-$Ca_2Si_2O_6$) II, Abstracts with Programs, Geol. Soc. Amer. meeting, 1979.

Davies, R.D., H.L. Allsopp, A.J. Erlank, and W.I. Manton, 1970, Sr-isotopic studies on various layered mafic intrusions in southern Africa, in, "Symposium on the Bushveld Igneous Complex and Other Layered Intrusions," Geol. Soc. S. Africa Spec. Publ. 1, 576-593.

Dawson, J.B., 1960, A comparative study of the geology and petrography of the kimberlites of the Basutoland province, unpublished Ph.D. thesis, University of Leeds.

Dawson, J.B., 1966, Oldoinyo Lengai, an active volcanoe with sodium carbonatite lava flows, in, Tuttle and Gittins, eds., Carbonatites, John Wiley and Sons, London, pp. 155-167.

Dawson, J.B., 1967, Geochemistry and origin of kimberlite, in, P.J. Wyllie, ed., Ultramafic and Related Rocks, John Wiley and Sons, Inc., New York, pp. 269-278.

Dawson, J.B., 1971, Advances in kimberlite geology, Earth Sci. Rev. 7, 187-214.

Dawson, J.B., 1972, Kimberlites and their relation to the mantle (with discussion), in A discussion on volcanism and the structure of the Earth, Roy. Soc. Lond., Phil. Trans. Ser. A 271, 297-311.

Dawson, J.B., 1980, Kimberlites and Their Xenoliths, Springer-Verlag, Berlin-Heidelberg, 252 pp.

Dawson, J.B. and J.V. Smith, 1973, Alkalic pyroxenite xenoliths from the Lashaine Volcano, Northern Tanzania, Jour. Petrol. 14, 113-132.

Dawson, J.B. and J.V. Smith, 1975, Chemistry and origin of phlogopite megacrysts in kimberlite, Nature 253, 336-338.

Dawson, J.B. and J.V. Smith, 1977, The MARID (mica-amphibole-rutile-ilmenite-diopside) suite of xenoliths in kimberlite, Geochim. Cosmochim. Acta 41, 309-323.

Dawson, J.B., J.V. Smith, and R.L. Hervig, 1977, Late-stage diopsides in kimberlite groundmass, 2nd Int. Kimb. Conf., extended abstracts.

Dawson, J.B. and F. Fuge, 1980, Halogen content of some African primary carbonatites, Lithos 13, 139-143.

Dawson, J.B., D.G. Powell, and A.M. Reid, 1970, Ultrabasic lavas and xenoliths from the Lashaine Volcano, Tanzania, Jour. Petrol. 11, 519-548.

Deans, T., 1966, Economic mineralogy of African carbonatites, in, Tuttle and Gittins, eds., Carbonatites, John Wiley and Sons, London, pp. 385-416.

Deans, T. and J.L. Powell, 1968, Trace elements and Sr isotopes in carbonatites, fluorites and limestones from India and Pakistan, Nature 218, 750-752.

Deans, T., N.J. Snelling, and J. Rapson, 1966, Sr isotopes and trace elements in carbonatites and limestones from Ice River, British Columbia, Nature 210, 290.

Deer, W.A., R.A. Howie, and J. Zussman, 1962, Rock Forming Minerals, Vol. 3, Sheet Silicates, John Wiley and Sons, Inc., New York, 270 pp.

Deer, W.A., R.A. Howie, and J. Zussman, 1963, Rock Forming Minerals, Vol. 4, Framework Silicates, Longmans Green and Co., London, 435 pp.

Deer, W.A., R.A. Howie, and J. Zussman, 1978, Single-Chain Silicates, John Wiley and Sons, New York, 668 pp.

Deines, P., 1970, The carbon and oxygen isotopic composition of carbonates from the Oka carbonatite complex, Quebec, Canada, Geochim. Cosmochim. Acta 34, 1199-1225.

Deines, P. and D.P. Gold, 1973, The isotopic composition of carbonatite and kimberlite carbonates and their bearing on the isotopic composition of deep-seated carbon, Geochim. Cosmochim. Acta 37, 1709-1733.

De Jager, D.H. and P.J. Fourie, 1978, A review of and some new aspects on phosphate mineralization in the Palabora Igneous Complex, South Africa, Society of Mining Engineers of AIME, preprint #78-H-24, 27 pp.

De Paolo, D.J. and G.J. Wasserburg, 1976, Nd isotopic variations and petrogenetic models, Geophys. Res. Lett. 3, 249-252.

Denaeyer, M., 1970, Rapports isotopiques O et C et conditions d'affleurement des carbonatites de l'Afrique centrale, C. R. Acad. Sc. Paris 270, 2155-2158.

Donaldson, C.H. and J.B. Dawson, 1978, Skeletal crystallization and residual glass compositions in a cellular alkalic pyroxenite nodule from Oldoinyo Lengai, Contrib. Mineral. Petrol. 67, 139-149.

Downes, J.J., 1974, Sector and oscillatory zoning in calcic augites from Mt. Etna, Sicily, Contrib. Mineral. Petrol. 47, 187-196.

Duke, J.M., 1976, Distribution of the period four transition elements among olivine, calcic clinopyroxene and mafic silicate liquid: experimental results, Jour. Petrol. 17, 499-521.

Duke, J.M. and A.J. Naldrett, 1978, A numerical model of the fractionation of olivine and molten sulfide from komatite magma, Earth Planet. Sci. Lett. 39, 255-266.

DuToit, A.L., 1931, The genesis of the pyroxenite-apatite rocks of Palabora, Eastern Transvaal, Trans. Geol. Soc. S. Africa 34, 107-127.

Eby, G.N., 1975, Abundance and distribution of the rare-earth elements and yttrium in the rocks and minerals of the Oka carbonatite complex, Quebec, Geochim. Cosmochim. Acta 39, 597-620.

Edgar, A.D., 1979, Mineral chemistry and petrogenesis of an ultrapotassic-ultramafic volcanic rock, Contrib. Mineral. Petrol. 71, 171-175.

Edgar, A.D. and J. Nolan, 1966, Phase relations in the system $NaAlSi_3O_8$ (albite)-$NaAlSiO_4$ (nepheline)-$NaFeSi_2O_6$ (acmite)-$CaMgSi_2O_6$ (diopside)-H_2O and its importance in the genesis of alkaline undersaturated rocks, Indian Mineral., I.M.A. vol., 176-181.

Edgar, A.D., D.H. Green, and W.O. Hibberson, 1976, Experimental petrology of a highly potassic magma, Jour. Petrol. 17, 339-356.

Eggler, D.H., 1975, CO_2 as a volatile component of the mantle: The system Mg_2SiO_4-SiO_2-H_2O-CO_2, Phys. Chem. Earth 9, 869-881.

Eggler, D.H., 1978, The effect of CO_2 upon partial melting of peridotite in the system Na_2O-CaO-Al_2O_3-MgO-SiO_2-CO_2 to 35 kb, with an analysis of melting of a peridotite - H_2O-CO_2 system, Amer. Jour. Sci. 278, 305-343.

Eggler, D.H. and C.W. Burnham, 1973, Crystallization and fractionation trends in the system andesite - H_2O-CO_2-O_2 at pressures to 10 kb, Geol. Soc. Amer. Bull. 84, 2517-2532.

Eggler, D.H. and M. Rosenhauer, 1978, Carbon dioxide in silicate melts and crystals: II, solubilities of CO_2 and H_2O in $CaMgSi_2O_6$ (diopside) liquids and vapors to 40 kb, Amer. Jour. Sci. 278, 64-94.

Emeleus, C.H. and J.R. Andrews, 1975, Mineralogy and petrology of a kimberlite dyke and sheet intrusions and included peridotite xenoliths from southeast Greenland, Phys. Chem. Earth 9, 179-198.

Erikson, R.L. and L.V. Blade, 1963, Geochemistry and petrology of the alkalic igneous complex at Magnet Cove, Arkansas, U. S. Geol. Surv. Prof. Paper 425.

Erlank, A.J. and R.S. Rickard, 1977, Potassic richterite-bearing peridotites from kimberlite and the evidence they provide for upper mantle metasomatism, 2nd Int. Kimb. Conf., extended abstracts.

Ernst, W.G., 1968, Amphiboles, Springer-Verlag, New York, 125 pp.

Ewart, A. and J.J. Stipp, 1968, Petrogenesis of the volcanic rocks of the Central North Iceland, New Zealand, as indicated by a study of $^{87}Sr/^{86}Sr$ ratios, and Sr, Rb, K, U and Th abundances, Geochim. Cosmochim. Acta 32, 699-735.

Faure, G. and P.M. Hurley, 1963, The isotopic composition of strontium in oceanic and continental basalts: Application to the origin of igneous rocks, Jour. Petrol. 4, 31-50.

Faye, G.H. and D.D. Hogarth, 1969, On the origin of "reverse pleochroism" of a phlogopite, Canadian Mineral. 10, 25-34.

Ferguson, A.K., 1978, The crystallization of pyroxenes and amphiboles in some alkaline rocks and the presence of a pyroxene compositional gap, Contrib. Mineral. Petrol. 67, 11-15.

Ferguson, J. and Currie, 1972, The alkaline and carbonatite complex of Callandar Bay, Ontario, Geol. Surv. Canada Bull. 217, 1-103.

Fesq, H.W., E.J.D. Kable, and J.J. Gurney, 1975, Aspects of the geochemistry of kimberlites from the Premier Mine, and other selected South African occurrences with particular reference to the rare earth elements, Phys. Chem. Earth 9, 687-707.

Finnerty, A.A. and F.R. Boyd, 1978, Pressure-dependent solubility of calcium in forsterite coexisting with diopside and enstatite, Carnegie Inst. Wash. Yearbook 77, 713-717.

Flanagan, F.J., 1973, 1972 values for international geochemical reference samples, Geochim. Cosmochim. Acta 37, 1189-1200.

Flower, M.F.J., H.U. Schmincke, and R.N. Thompson, 1975, Phlogopite stability and the $^{87}Sr/^{86}Sr$ step in basalts along the Reykjanes Ridge, Nature 254, 404-406.

Foland, K.A. and I. Friedman, 1977, Application of Sr and O isotope relations to the petrogenesis of the alkaline rocks of the Red Hill complex, New Hampshire, U.S.A., Contrib. Mineral. Petrol. 65, 213-225.

Forster, I.F., 1958, Paragenetical ore mineralogy of the Loolekop-Phalaborwa carbonatite complex, Eastern Transvaal, Trans. Geol. Soc. S. Africa 61, 359-365.

Frey, F.A., B.W. Chappell, and S.D. Roy, 1978, Fractionation of rare-earth elements in the Tuolumne Intrusive Series, Sierra Nevada Batholith, California, Geology 6, 239-242.

Frey, F.A., J. Ferguson, and B.W. Chappell, 1977, Petrogenesis of South African and Australian kimberlitic suites, extended abstract, Second International Kimberlite Conference, Santa Fe.

Frick, C., 1975, The Phalaborwa syenite intrusion, Trans. Geol. Soc. South Africa 78, 201-214.

Gast, P.W., 1960, Limitations on the composition of the upper mantle, Jour. Geophys. Res. 65, 1287-1297.

Gast, P.W., G.R. Tilton, and C. Hedge, 1964, Isotopic composition of lead and strontium from Ascension and Gough islands, Science 145, 1181-1185.

Gerasimovsky, V.I., 1963, Geochemical features of agpaitic nepheline syenites, in, A.P. Vinogradov, ed., Chemistry of the Earth's Crust, I, pp. 104-118.

Gevers, T.W., 1948, Vemiculite at Loolekop, Palabora, N.E. Tvl., Trans. Geol. Soc. S. Africa 51, 133-178.

Gibb, F.G.F., 1973, The zoned clinopyroxenes on the Shiant Isles Sill, Scotland, Jour. Petrol. 14, 201-230.

Gittins, J., 1979, Problems inherent in the application of calcite-dolomite geothermometry to carbonatites, Contrib. Mineral. Petrol. 69, 1-4.

Gittins, J., H.R. Hewins, and A.F. Laurin, 1975, Kimberlitic-carbonatitic dikes of the Saguenay River Valley, Quebec, Canada, Phys. Chem. Earth 9, 137-148.

Goldsmith, J.R. and R.C. Newton, 1969, P-T-X relations in the system $CaCO_3$-$MgCO_3$ at high temperatures and pressures, Amer. Jour. Sci. 267-A, 169-190.

Gomes, G., S.L. Moro, and C.V. Dutra, 1970, Pyroxenes from the alkaline rocks of Itapirapua, Sao Paolo, Brazil, Amer. Mineral. 55, 224-230.

Green, D.H. and A.E. Ringwood, 1967, The genesis of basaltic magmas, Conrtrib. Mineral. Petrol. 15, 103-190.

Griffin, W.L. and P.N. Taylor, 1975, The Fen damkjeinite: Petrology of a "central-complex kimberlite," in, L.H. Ahrens, J.B. Dawson, A.R. Duncan, and A.J. Erlank, eds., Physics and Chemistry of the Earth, Pergamon, Oxford, pp. 163-177.

Haggerty, S.E., 1976, Opaque mineral oxides in terrestrial igneous rocks, in, Oxide Minerals, Mineral. Soc. Amer. Short Course Notes 3, pp. 101-175.

Hall, A.L., 1912a, The Palabora plutonic complex of the low country and its relationship to the pegmatites of the Leydsdorp mica-fields, Trans. Geol. Soc. S. Africa 15, 4-17.

Hall, A.L., 1912b, The crystalline metamorphic limestone of Lulukop and its relationship to the Palabora Plutonic Complex, Trans. Geol. Soc. S. Africa 15, 18-25.

Hamilton, D.L. and W.S. MacKenzie, 1965, Phase equilibrium studies in the system $NaAlSiO_4$ (nepheline)-$KAlSiO_4$ (kalsilite)-SiO_2-H_2O, Mineral. Mag. 34, 214-231.

Hamilton, E.I. and T. Deans, 1963, Isotopic composition of strontium in some African carbonatites and limestones and in strontium minerals, Nature 198, 776-777.

Hamilton, J., 1977, Sr isotope and trace element studies of the Great Dyke and Bushveld mafic phase and their relation to early proterozoic magma genesis in Southern Africa, Jour. Petrol. 18, 24-52.

Hanekom, H.J., C.M. van Staden, P.J. Smit, and D.R. Pike, 1965, The geology of the Palabora Igneous Complex, S. Africa Geol. Surv., Memoir 54, 179 pp.

Harris, P.G., R. Hutchison, and D.K. Paul, 1972, Plutonic xenoliths and their relation to the upper mantle, Phil. Trans. R. Soc. Lond., Ser. A 271, 313-.

Hart, R., 1978, A study of the isotopic and geochemical gradients in the old granite of the Vredefort structure, with implications for continental heat flow, unpublished Ph.D. thesis, Univ. Witwatersrand.

Hart, S.R. and K.E. Davis, 1978, Nickel partitioning between olivine and silicate melt, Earth Planet. Sci. Lett. 40, 203-219.

Haughton, D.R., P.L. Roeder, and B.J. Skinner, 1974, Solubility of sulfur in mafic magmas, Econ. Geol. 69, 451-467.

Hawkesworth, C.J., S. Moorbath, R.K. O'Nions, and J.F. Wilson, 1975, Age relationships between greenstone belts and "granites" in the Rhodesian Archaean Craton, Earth Planet. Sci. Lett. 25, 251-262.

Hedge, C.E. and F.G. Walthall, 1963, Radiogenic strontium-87 as an index of geologic processes, Science 40, 1214-1217.

Heier, K.S., 1964, Rubidium/strontium and Sr^{87}/Sr^{86} ratios in deep crustal material, Nature 202, 477-478.

Heier, K.S., 1973a, Geochemistry of granulite facies rocks and problems of their origin, Phil. Trans. R. Soc. London, A273, 429-442.

Heier, K.S., 1973b, A model for the composition of the deep continental crust, Fortschr. Mineral. 50, 174-187.

Heier, K.S. and J.A. Adams, 1965, Radioactive elements in the continental crust, Nature 208, 479-480.

Heinrich, E.W. and D.G. Moore, 1970, Metasomatic potash feldspar rocks associated with igneous alkalic complexes, Canadian Mineral. 10, 571-584.

Helz, G.R. and P.J. Wyllie, 1979, Liquidus relationships in the system $CaCO_3$-$Ca(OH)_2$-CaS and the solubility of sulfur in carbonatite magmas, Geochim. Cosmochim. Acta 43, 259-265.

Hennig-Michaeli, C., 1968, Mikroskopische untersuchungen an hanstucken der kupfererzlagerstatte am Loolekop im Phalaborwa Komplex, NE-Transvaal, Sudafrikanische Union, Mineralogishe Diplomarbeit Institut fur Mineralogie und Lagerstattenlehre der RW and H AAchen.

Hess, H.H., 1949, Chemical composition and optical properties of common clinopyroxenes, Part I, Amer. Mineral. 34, 621-666.

Hess, H.H., 1960, Stillwater igneous complex, Montana: A quantitative mineralogical study, Mem. Geol. Soc. Amer. 80, 230 pp.

Hess, H.H. and A. Polderwaart, 1967, Basalts, vol. 1, Interscience, New York, 482 pp.

Hiemstra, S.A., 1955, Baddeleyite from Phalaborwa, Eastern Transvaal, Amer. Mineral. 40, 275-282.

Higazy, R.A., 1954, Trace elements of volcanic ultrabasic rocks of southwestern Uganda and adjorning part of the Belgian Congo, Bull. Geol. Soc. Amer. 65, 39-70.

Hofmann, A.W. and S.R. Hart, 1978, An assessment of local and regional isotopic equilibrium in the mantle, Earth Planet. Sci. Lett. 38, 44-62.

Hogarth, D.D., 1964, Normal and reverse pleochroism in biotite (abstr.), Canadian Mineral. 8, 136.

Holmes, A., 1950, Petrogenesis of katungite and its associates, Amer. Mineral. 35, 772-792.

Holmes, A. and L. Cahen, 1956, Geochronologie Africiane, Academie royale der Sciences coloniales, Mem -8', TV, fosc. I.

Huang, W.L. and P.J. Wyllie, 1974, Eutectic between wollanstonite II and calcite contrasted with thermal barrier in MgO-SiO_2-CO_2 at 30 kb, with applications to kimberlite-carbonatite petrogenesis, Earth Planet. Sci. Lett. 24, 305-310.

Huang, W.L. and P.J. Wyllie, 1976, Melting relationships in the systems $CaO-CO_2$ and $MgO-CO_2$ to 33 kb, Geochim. Cosmochim. Acta 40, 129-132.

Hurley, P.M., H. Hughes, G. Faure, H. Fairbairn, and W. Pinson, 1962, Radiogenic strontium-87 model for continent formation. Jour. Geophys. Res. 67, 5315-5334.

Hutchison, R. and J.B. Dawson, 1970, Rb, Sr and $^{87}Sr/^{86}Sr$ in ultrabasic xenoliths and host rocks, Lashaine Volcano, Tanzania, Earth Planet. Sci. Lett. 9, 87-92.

Irvine, T.N., 1974, Petrology of the Duke Island ultramafic complex, Southeastern Alaska, Mem. Geol. Soc. Amer. 138, 240 pp.

Irving, A.J., 1978, A review of experimental studies of crystal/liquid trace element partitioning, Geochim. Cosmochim. Acta 42, 743-770.

Jacobson, R.R.E., W.N. MacLeod, and R. Black, 1958, Ring-complexes in the younger granite province of northern Nigeria, Mem. Geol. Soc. 1.

Jaeger, J.C., 1957, The temperature in the neighborhood of a cooling intrusive sheet, Amer. Jour. Sci. 255, 306-318.

Jennings, D.S. and R.H. Mitchell, 1969, An estimate of the temperature of intrusion of carbonatite at the Fen complex, S. Norway, Lithos 2, 167-169.

Kay, R.W. and P.W. Gast, 1973, The rare earth content and origin of alkali-rich basalts, Jour. Geol. 81, 653-682.

Kerr, P.F., 1959, Optical Mineralogy, McGraw-Hill, New York, 442 pp.

King, B.C. and D.S. Sutherland, 1966, The carbonatite complexes of Eastern Uganda, in, O.F. Tuttle and J. Gittins, eds., Carbonatites, John Wiley and Sons, Ltd., London, pp. 73-126.

Kobelski, B.J., D.P. Gold and P. Deines, 1979, Variations in stable isotope compositions for carbon and oxygen in some South African and Lesothan kimberlites, Proc. 2nd Int. Kimb. Conf. 1, 252-271.

Kogarko, L.N., 1978, Strontium fractionation during the formation of apatite deposits, Ann. Meeting GSA-GSAC, Program with Abstracts, p. 436.

Koster Van Groos, A.F., 1975, The distribution of strontium between coexisting silicate and carbonate liquids at elevated pressures and temperatures, Geochim. Cosmochim. Acta 39, 27-34.

Koster Van Groos, A.F. and P.J. Wyllie, 1966, Liquid immiscibility in the system Na_2O-Al_2O_3-SiO_2-CO_2 at pressures to 1 kb, Amer. Jour. Sci. 264, 234-255.

Koster Van Groos, A.F. and P.J. Wyllie, 1973, Liquid immiscibility in the join $NaAlSi_3O_8$-$CaAl_2Si_2O_8$-Na_2CO_3-H_2O, Amer. Jour. Sci. 273, 465-487.

Kostyuk, V. P., L.I. Panina, and E.C. Guletskaya, 1970, The mineralogy of high potassic alkaline rocks of Synnirskii pluton (northern Near-Baikal), in, N.L. Dobretsov, ed., Problems of Petrology and Genetic Mineralogy, Publ. House Nauka, Moscow, pp. 181-197 (in Russian), reported in Deer et al. (1978).

Kramers, J.D., 1977, Lead and strontium isotopes in Cretaceous kimberlites and mantle-derived xenoliths from southern Africa, Earth Planet. Sci. Lett. 34, 419-431.

Kudo, A.M., D.G. Brookins, and A.W. Laughlin, 1972, Sr isotopic disequilibrium in lherzolites from the Pureco Necks, New Mexico, Earth Planet. Sci. Lett. 15, 291-295.

Kulp, J.L., 1967, Concordance and discordance between K-Ar and Rb-Sr isotopic ages from micas, in, A.P. Vinogradov, ed., Chemistry of the Earth, V. 2, Israel Program for Scientific Translations Ltd., pp. 592-606.

Kushiro, I., 1960, Si-Al relation in clinopyroxenes from igneous rocks, Amer. Jour. Sci. 258, 548-554.

Kushiro, I., 1964, The system diopside-forsterite-enstatite at 20 kilobars, Carnegie Inst. Washington, Ann. Rept., Dir. Geophys. Lab., 1963-64, 101-108.

Kushiro, I., 1975, On the nature of silicate melt and its significance in magma genesis: regularities in the shift of liquidous boundaries involving olivine, pyroxene and silica minerals, Amer. Jour. Sci. 275, 411-431.

Lancelot, J.R. and C.J. Allegre, 1974, Origin of carbonatitic magma in the light of the Pb-U-Th isotope system, Earth Planet. Sci. Lett. 22, 233-238.

Larsen, L.M., 1976, Clinopyroxenes and coexisting mafic minerals from the alkaline Ilimaussaq intrusion, South Greenland, Jour. Petrol. 17, 258-290.

Le Bas, M.J., 1962, The role of Al in igneous clinopyroxenes with relation to their parentage, Amer. Jour. Sci. 260, 267-288.

Le Bas, M.J., 1977, Carbonatite-nephelinite Volcanism: An African Case History, Wiley, London, 347 pp.

Le Bas, M.J., A.A. Mills, and A.H. Rankin, 1972, Preliminary evidence on the nature and composition of carbonatite magma, Nature 239, 215.

Le Maitre, R.W., 1962, Petrology of volcanic rocks, Gough Island, South Atlantic, Bull. Geol. Soc. Amer. 73, 1309-1342.

Lee, C.A., 1973, Petrochemistry of the Katete, Shawa, and Dorowa carbonatites, unpublished Ph.D. thesis, University of London.

Lindstrom, D.J., 1976, Experimental study of the partitioning of the transition metals between clinopyroxene and coexisting silicate liquids, Ph.D. thesis, University of Oregon, 188 pp.

Lindstrom, D.J. and D.F. Weill, 1978, Partitioning of transition metals between diopside and coexisting silicate liquids. I. Nickel, cobalt and manganese, Geochim. Cosmochim. Acta 42, 817-831.

Lloyd, F.E. and D.K. Bailey, 1975, Light element metasomatism of the continental mantle: the evidence and the consequences, Phys. Chem. Earth 9, 389-416.

Lombaard, A.F., N.M. Ward-Able, and R.W. Bruce, 1964, The exploration and main geological features of the copper deposit in carbonatite at Loolekop, Palabora Complex, in, S.H. Haughton, ed., The geology of some ore deposits in Southern Africa, Geol. Soc. S. Africa, Johannesburg, 315-337.

Long, P.E., 1978, Experimental determination of partition coefficients for Rb, Sr, and Ba between alkali feldspar and silicate liquid, Geochim. Cosmochim. Acta 42, 833-846.

Loubet, M., M. Bernat, M. Javoy, and C.L. Allegre, 1972, Rare earth contents in carbonatites, Earth Planet. Sci. Lett. 14, 226-232.

Luth, W.C., 1967, Studies in the system $KAlSiO_4$-Mg_2SiO_4-SiO_2-H_2O: 1. Inferred phase relations and petrologic applications, Jour. Petrol. 8, 372-416.

MacGregor, I.D., 1970, An hypothesis for the origin of kimberlite, Mineral. Soc. America Spec. Paper 3, 51-62.

Martineau, M.P. and R. Lambert, 1974, The Big Spruce Lake Nepheline - syenite/carbonatite-complex, N.W.T., Abstracts with Programs, Geol. Assoc. Canada, 59.

Maxwell, J.A., 1968, Visual titration, following the modified cold acid dcomposition method of Wilson, in Rock and Mineral Analysis, Interscience, pp. 419-422.

McBirney, 1979, Effects of assimilation, in, H.S. Yoder, Jr., ed., The Evolution of the Igneous Rocks, Princeton Univ. Press, Princeton, 588 pp.

McCarthy, T.S. and R.G. Cawthorn, 1980, Changes in initial $^{87}Sr/^{86}Sr$ ratio during protracted fractionation in igneous complex, Jour. Petrol. 21, 245-264.

McIver, J.R. and J. Ferguson, 1979, Kimberlitic, melilititic, trachytic and carbonatite eruptives at Saltpetre Kop, Sutherland, South Africa, Proc. 2nd Int. Kimb. Conf. 1, 111-128.

McKie, D., 1966, Fenitization, in, O.F. Tuttle and J. Gittins, eds., Carbonatites, John Wiley and Sons, Ltd., London, pp. 261-294.

McNutt, R.H., 1964, Variations in isotopic abundances of Sr, Ca, and Ar and related topics, Extracts from the thesis of Robert H. McNutt, "A Study of the Strontium redistribution under controlled condition of T and P. from M.I.T. - 1381-12, 12th Annual Progress Report for 1964, pp. 125-158.

Melcher, G.C., 1966, The carbonatites of Jacupiranga, Sao Paulo, Brazil, in, Tuttle and Gittins, eds., Carbonatites, John Wiley and Sons, New York, pp. 169-182.

Mellor, E.J., 1906, The geology of the district about Haenertsburg, Leydsdorp, and the Murchison Range, Annual Report Geol. Surv., Trans., pp. 21-52.

Menzies, M. and V.R. Murthy, 1980, Mantle metasomatism as a precursor to the genesis of alkaline magmas - isotopic evidence, Amer. Jour. Sci. 280-A, 622-638.

Meyer, H.O.A. and F.R. Boyd, 1972, Composition and origin of crystalline inclusions in natural diamonds, Geochim. Cosmochim. Acta 36, 1255-1273.

Mitchell, R.H. and K. Bell, 1976, Rare earth element geochemistry of potassic lavas from the Birunga and Toro-Ankole regions of Uganda, Africa, Contrib. Mineral. Petrol. 58, 293-304.

Mitchell, R.H. and A.O. Brunfelt, 1974, Scandium, cobalt, and iron geochemistry of the Fen Alkaline Complex, Southern Norway, Earth Planet. Sci. Lett. 23, 189-192.

Mitchell, R.H. and J.H. Crockett, 1972, Isotopic composition of strontium in rocks of the Fen Alkaline Complex, South Norway, Jour. Petrol. 13, 83-97.

Mitchell, R.H. and H.R. Krouse, 1975, Sulfur isotope geochemistry of carbonatites, Geochim. Cosmochim. Acta 39, 1505-1515.

Modreski, P.J. and A.L. Boettcher, 1973, Phase relationships of phlogopite in the system K_2O-MgO-CaO-Al_2O_3-SiO_2-H_2O to 35 kilobars: A better model for micas in the interior of the earth, Amer. Jour. Sci. 273, 385-414.

Moorbath, S., 1975, Constraints for the evolution of Precambrian crust from strontium isotopic evidence, Nature 254, 395-398.

Moorbath, S., 1976, Age and isotope constraints for the evolution of Archaean Crust, in, B. Windley, ed., The Early History of the Earth, John Wiley and Sons, London, pp. 351-360.

Morse, S.A., 1969, The Kiglapait Layered Intrusion, Labrador, Mem. Geol. Soc. Amer. 112, 146 pp.

Mysen, B.O., 1977, Distribution of trace elements among phases during partial melting of a multiphase system, Carnegie Inst. Wash., Yearbook 76, 541-545.

Mysen, B.O., 1978, Limits of solution of trace elements in minerals according to Henry's Law: Review of experimental data, Geochim. Cosmochim. Acta 42, 871-885.

Mysen, B.O. and A.L. Boettcher, 1975, Melting of a hydrous mantle, I. Phase relations of natural peridotite at high pressures and temperatures with controlled activities of water, carbon dioxide, and hydrogen, Jour. Petrol. 16, 520-548.

Nagasawa, H. and C.C. Schnetzler, 1971, Partitioning of rare earth, alkali and alkaline earth elements between phenocrysts and acidic igneous magma, Geochim. Cosmochim. Acta 35, 953-968.

Nash, W.P., 1972, Mineralogy and petrology of the Iron Hill carbonatite complex, Colorado, Geol. Soc. Am. Bull. 83, 1361-1382.

Nash, W.P. and J.F.G. Wilkinson, 1970, Shonkin Sag Laccolith, Montana, pt. I, Mafic minerals and estimates of temperature, pressure, oxygen fugacity and silica activity, Contrib. Mineral. Petrol. 25, 241-269.

Nicholls, J., 1976, The activities of components in natural silicate melts, in, D.G. Fraser, ed., Thermodynamics in Geology, Reidel Publ. Co., Dordrecht, pp. 327-348.

Nicholls, J. and I.S.E. Carmichael, 1969, Peralkaline acid liquids: A petrological study, Contrib. Mineral. Petrol. 20, 268-294.

Nicholls, J. and I.S.E. Carmichael, 1972, The equilibriation temperature and pressure of various lava types with spinel and garnet peridotite, Amer. Mineral. 57, 941-959.

Nicholls, J. and I.S.E. Carmichael, and J.C. Stormer, Jr., 1971, Silica activity and P total in igneous rocks, Contrib. Mineral. Petrol. 33, 1-20.

Noble, D.C. and J. Haffty, 1969, Minor-element and revised major-element contents of some Mediterranean pantellerites and comendites, Jour. Petrol. 10, 502-509.

Nolan, J., 1966, Melting relations in the system $NaAlSi_3O_8$-$NaAlSiO_4$-$NaFeSi_3O_6$-H_2O and their bearing on the genesis of alkaline undersaturated rocks, Quar. Jour. Geol. Soc. London 122, 119-157.

Norrish, K. and B.W. Chappell, 1967, in, J. Zussman, ed., Physical Methods in Determinative Mineralogy, Academic Press, New York, pp. 161-214.

Norrish, K. and J.T. Hutton, 1969, An accurate X-ray spectrographic method for the analysis of a wide range of geological samples, Geochim. Cosmochim. Acta 33, 431-453.

O'Hara, M.J., 1965, Primary magmas and the origin of basalts, Scot. Jour. Geol. 1, 19-40.

O'Hara, M.J., 1973, Non-primary magmas and dubious mantle plume beneath Iceland, Nature 243, 507-511.

O'Hara, M.J., 1975, Is there an Icelandic mantle plume?, Nature 253, 708-710.

O'Hara, M.J. and H.S. Yoder, 1967, Formation and fractionation of basic magmas at high pressures, Scot. Jour. Geol. 3, 67-117.

O'Nions, R.K. and R.J. Pankhurst, 1974, Petrogenetic significance of isotope and trace element variation in volcanic rocks from the Mid-Atlantic, Jour. Petrol. 15, 603-634.

O'Nions, R.K. and R. Powell, 1976, The thermodynamics of trace element distribution, in, D.G. Fraser, ed., Thermodynamics in Geology, Reidel Publ. Co., Dordrecht, pp. 349-362.

Orville, P.M., 1963, Alkali ion exchange between vapor and feldspar phases, Amer. Jour. Sci. 261, 201-237.

Palabora Mining Company Limited Mine Geological and Mineralogical Staff, 1976, The geology and the economic deposits of copper, iron, and vermiculite in the Palabora Igneous Complex: A brief review, Econ. Geol. 71, 177-192.

Pankhurst, R.J., 1969, Strontium isotope studies related to petrogenesis in the Caledonian Basic Igneous Province of N.E. Scotland, Jour. Petrol. 10, 115-143.

Partridge, T.C., 1973, Geomorphological dating of cave openings at Makapanogat, Sterkfontein, Sworthians and Taung, Nature 246, 75-79.

Paul, D.K., 1971, Isotopic composition of strontium in Indian kimberlites, Geochim. Cosmochim. Acta 43, 389-394.

Pearce, J.A. and M.J. Norry, 1979, Petrogenetic implications of Ti, Zr, Y, and Nb variations in volcanic rocks, Contrib. Mineral. Petrol. 69, 33-47.

Pecora, W.T., 1956, Carbonatites: a review, Geol. Soc. Amer. Bull. 67, 1537-1556.

Peterman, Z.E., I.S.E. Carmichael, and A.L. Smith, 1970, Strontium isotopes in quaternary basalts of southwestern California, Earth Planet. Sci. Lett. 7, 381-384.

Philpotts, A.R., 1967, Origin of certain iron-titanium oxide and apatite rocks, Econ. Geol. 62, 303-315.

Pierozynski, W.J. and C.M.B. Henderson, 1978, Distribution of Sr, Ba, and Rb between alkali feldspar and silicate melt, Progress in Experimental Petrology, the Natural Environment Research Council, Publ. Series D. No. 11, pp. 40-46.

Pineau, F. and M. Javoy, 1969, Determination des rapports isotopiques $^{18}O/^{16}O$ et $^{13}C/^{12}C$ dans diverses carbonatites, implications genetiques, C. R. Acad. Sci. Paris 269, 1930-1933.

Pineau, F. and C. Allegre, 1972, Etude et signification des rapports isotopiques $^{87}Sr/^{86}Sr$ dans les carbonatites, C. R. Acad. Sci. Paris 274, 2620-2623.

Pineau, F., M. Javoy, and C.J. Allegre, 1973, Etude systematique des isotopes de l'oxygene, du carbons et du strontium dans les carbonatites, Geochim. Cosmochim. Acta 37, 2363-2377.

Platt, R.G. and A.D. Edgar, 1972, The system nepheline-diopside-sanidine and its significance to the genesis of melilite- and olivine-bearing alkaline rocks, Jour. Geol. 80, 224-236.

Powell, J.L., P.M. Hurley, and H.W. Fairbairn, 1966, The strontium isotopic composition and origin of carbonatites, in, O.F. Tuttle and J. Gittins, eds., Carbonatites, John Wiley and Sons, Ltd., London, pp. 365-378.

Powell, J.L. and K. Bell, 1970, Strontium isotopic studies of alkalic rocks: Localities from Australia, Spain and western United States, Contrib. Mineral. Petrol. 27, 1-10.

Powell, M. and R. Powell, 1974, An olivine-clinopyroxene geothermometer, Contrib. Mineral. Petrol. 48, 249-263.

Presnall, D.R., 1966, The join forsterite-diopside-iron oxide and its bearing on the crystallization of basaltic and ultramafic magmas, Amer. Jour. Sci. 264, 753-809.

Prinz, M., D.V. Manson, P.F. Hlava, and K. Keil, 1975, Inclusions in diamonds: Garnet lherzolite and eclogite assemblages, Phys. Chem. Earth 9, 797-815.

Rajamani, V. and A.J. Naldrett, 1978, Partitioning of Fe, Co, Ni, and Cu between sulfide liquid and basaltic melts and the composition of Ni-Cu sulfide deposits, Econ. Geol. 73, 82-93.

Rankin, A.H., 1975, Fluid inclusion studies in apatite from carbonatites of the Wasaki area of Western Kenya, Lithos 8, 123-136.

Rankin, A.H. and M.J. Le Bas, 1974, Nahcolite ($NaHCO_3$) in inclusions in apatites from some E. African ijolites and carbonatites, Mineral. Mag. 39, 564-570.

Ribbe, P.H., 1979, The structure of a strained association with twinned plagioclase, Amer. Mineral. 64, 402-408.

Ribbe, P.H., 1980, Orthosilicates, Mineral. Soc. Amer., Reviews in Mineralogy 5, 381 pp.

Rimsaite, J., 1969, Evolution of zoned micas and associated silicates in the Oka carbonatite, Contrib. Mineral. Petrol. 23, 340-360.

Rock, N., 1976, The comparative strontium isotopic composition of alkalic rocks: New data from Southern Portugal and East Africa, Contrib. Mineral. Petrol. 56, 205-228.

Rollinson, H.R., 1979, Ilmenite-magnetite geothermometry in trondhjemites from the Scourian complex of N.W. Scotland, Mineral. Mag. 43, 165-170.

Russell, H.D., S.A. Hiemstra, and D. Groeneveld, 1954, The mineralogy and petrology of the carbonatite at Loolekop, Eastern Transvaal, Trans. Geol. Soc. S. Africa 57, 197-108.

Sabine, P.A., 1950, The optical properties and composition of acmitic pyroxenes, Mineral. Mag. 29, 113-125.

Sahama, T.G., 1974, Potassium-rich alkaline rocks, in, H. Sorenson, ed., The Alkaline Rocks, Wiley, London, pp. 76-109.

Schafer, H.N.S., 1966, The determination of iron (II) oxide in silicate and refractory materials. Part I. A review. Analyst 91, 755-762.

Schreiber, H.D., 1976, The experimental determination of redox states, properties, and distribution of chromium in synthetic silicate phases and application to basalt petrogenesis, unpublished Ph.D. thesis, University of Wisconsin, 222 pp.

Scott, B.H., 1977, Petrogenesis of kimberlites and associated potassic lamprophyres from Central West Greenland, unpublished Ph.D. thesis, University of Edinburgh.

Shand, S.J., 1931, The granite-syenite-limestone complex of Palabora, Eastern Transvaal, and the associated apatite deposits, Trans. Geol. Soc. S. Africa 34, 81-105.

Shaw, H.R., 1972, Viscosities of magmatic silicate liquids: An empirical method of prediction, Amer. Jour. Sci. 272, 870-893.

Sheppard, S. and S. Epstein, 1970, D/H and $^{18}O/^{16}O$ ratios of minerals of possible mantle or lower crustal origin, Earth Planet. Sci. Lett. 9, 232-239.

Sheppard, S.M.F. and J.B. Dawson, 1973, $^{13}C/^{12}C$ and D/H isotope variations in "primary igneous carbonatites," Fortsch. Mineral. 50, 128-129.

Shima, H. and A.J. Naldrett, 1975, Solubility of sulfur in an ultramafic melt and the relevance of the system Fe-S-O, Econ. Geol. 70, 960-967.

Shimizu, N., 1975, Geochemistry of ultramafic inclusions from Salt Lake Crater, Hawaii, and from Southern African kimberlites, Phys. Chem. Earth 9, 655-669.

Simkin, T. and J.V. Smith, 1970, Minor element distribution in olivine, Jour. Geol. 78, 304-325.

Smith, A.L. and I.S.E. Carmichael, 1969, Quaternary trachybasalts from S. E. California, Amer. Mineral. 54, 909-923.

Smith, D. and D.H. Lindsley, 1971, Chemical variations in pyroxene and olivine from Picture George basalt, Carnegie Inst. Wash. Yearbook 69, 269-274.

Smith, J.V., 1974, Feldspar Minerals, 2: Chemical and Textural Properties, Springer-Verlag, New York, 690 pp.

Smith, J.V., R. Brennesholtz, and J.B. Dawson, 1978, Chemistry of micas from kimberlites and xenoliths -- I, Micaceous kimberlites, Geochim. Cosmochim. Acta 42, 959-971.

Sood, M.K. and A.D. Edgar, 1972, The system diopside-forsterite-nepheline-albite-leucite and its implication to the genesis of alkaline rocks, 24th Int'l Geol. Congr. Montreal 14, 68-74.

Sorensen, H., 1969, Rhythmic igneous layering in peralkaline intrusions. An essay review on Ilimaussaq (Greenland) and Lovozero (Kola, USSR), Lithos 2, 261-283.

Spooner, C.M. and H.W. Fairbairn, 1970, Strontium 87/strontium 86 initial ratios in pyroxenite granulite terranes, Jour. Geophys. Res. 75, 6706-6713.

Stacy, J.S. and J.D. Kramers, 1975, Approximation of terrestrial lead isotope evolution by a two-stage model, Earth Planet. Sci. Lett. 26, 207-221.

Steiger, R.H. and E. Jager, 1977, Subcommission on geochronology: Convention on the use of decay constants in geo- and cosmochronology, Earth Planet. Sci. Lett. 36, 359-362.

Stephenson, D., 1972, Alkali clinopyroxenes from nepheline syenites of the South Toroq Centre, South Greenland, Lithos 5, 187-201.

Stormer, J.C. and I.S.E. Carmichael, 1971, Fluorine-hydroxyl exchange in apatite and biotite: A potential igneous geothermometer, Contrib. Mineral. Petrol. 31, 121-131.

Strauss, C.A. and F.A. Truter, 1950, The alkali complex at Spitzkop, Sekukuniland, Eastern Transvaal, Trans. Geol. Soc. S. Africa 53, 81-125.

Streckeisen, A., 1967, Classification and nomenclature of igneous rocks, Neues Jb. Mineral. Abh. 107, 144-240.

Stueber, A.M. and V.R. Murthy, 1966, Strontium isotope and alkali element abundances in ultramafic rocks, Geochim. Cosmochim. Acta 30, 1243-1259.

Sun, C.-O., R.J. Williams, and S.-S. Sun, 1974, Distribution coefficients of Eu and Sr for plagioclase-liquid and clinopyroxene-liquid equilibria in ocean ridge basalt: an experimental study, Geochim. Cosmochim. Acta 38, 1415-1433.

Sun, S.S. and G.N. Hanson, 1975, Evolution of the mantle: Geochemical evidence from alkali basalt, Geology 3, 297-302.

Suwa, K. and K. Aoki, 1975, Reverse pleochroism of phlogopites in kimberlites and their related rocks from South Africa, 1st Prelim. Rept. African Studies, Nagoya Univ., pp. 60-64.

Suwa, Kaneomori, OANNA Shinya, Hideki, WADA, and Susumu OSAKI, 1975, Isotope geochemistry and petrology of African carbonatites (abstr.), 1st Prelim. Rep. African Studies, Nagoya Univ., pp. 81-84.

Taljaard, M.S., 1936, South African melilite basalts and their relations, Trans. Geol. Soc. S. Africa 39, 281-316.

Tatsumoto, M., 1966, Genetic relations of oceanic basalts as indicated by lead isotopes, Science 153, 1094-1101.

Taylor, H.P., 1968, The oxygen isotope geochemistry of igneous rocks, Contrib. Mineral. Petrol. 19, 1-71.

Taylor, H.P., Jr., J. Frechen, and E.T. Degens, 1967, Oxygen and carbon isotope studies of carbonatites from the Laacher See District, West Germany and the Alno District, Sweden, Geochim. Cosmochim. Acta 31, 407-430.

Taylor, S.R. and M.P. Gorton, 1977, Geochemical application of spark source mass spectrography; III, Element sensitivitiy, precision, and accuracy, Geochim. Cosmochim. Acta 41, 1375-1380.

Thornton, C.P. and O.F. Tuttle, 1960, Chemistry of igneous rocks, I. Differentiation index, Amer. Jour. Sci. 258, 664-684.

Troger, W.E., 1952, Tabellen zur optischen Bestimmung der gesteinbaldenden Minerale, Schweizerbartasche Verlag, Stuttgart, reported in Deer et al. (1978).

Truter, F.C., 1955, Modern concepts of the Bushveld, C.C.T.A. Southern Regional Committee for Geology, 1st Meeting, Salisbury, pp. 77-92.

Tuttle, O.F. and J. Gittins, 1966, Carbonatites, John Wiley and Sons, New York, 591 pp.

Tyler, R.C. and B.C. King, 1967, The pyroxenes of the alkaline igneous complexes of Eastern Uganda, Mineral. Mag. 280, 5-22.

Upton, B.G.J., 1960, The alkaline igneous complex of Kungnat fjeld, South Greenland, Meddr. Gronland 123, 1-145.

Upton, B.G.J., 1964, The geology of Tugtutoq and neighboring islands, South Greenland. Part II. Nordmarkitic syenites and related alkaline rocks, Meddr. Gronland 169, 1-62.

Upton, B.G.J., 1967, Alkaline pyroxenites, in, P.J. Wyllie, ed., Ultramafic and Related Rocks, Interscience, pp. 281-288.

Upton, B.G.J. and J.E. Thomas, 1973, Precambrian potassic ultramafic rocks: South Greenland, Jour. Petrol. 14, 509-534.

Van der Molen, I. and M.S. Paterson, 1979, Experimental deformation of partially-melted granite, Contrib. Mineral. Petrol. 70, 299-318.

Van Rensburg, W.C., 1965, Copper mineralization in the carbonate members and phoscorite, Phalaborwa, South Africa, unpublished Ph.D. thesis, University of Wisconsin.

Varet, J., 1969, Les pyroxenes des phonalites du Cantal (Auvergne, France), Neues Jb. Mineral. Mh. 4, 174-184.

Verhoogen, J., 1962, Distribution of titanium between silicates and oxides in igneous rocks, Amer. Jour. Sci. 260, 211-220.

Verwoerd, W.J., 1966, Fenitization of basic igneous rocks, in, Tuttle and Gittins, eds., Carbonatites, John Wiley and Sons, London, pp. 295-310.

Verwoerd, W.J., 1967, The carbonatites of South Africa and South West Africa, S. Africa Geol. Surv. Handbook 6.

Vlasov, K.A., M.Z. Kuz'menko, and E.M. Es'kova, 1966, in, Oliver and Boyd, eds., The Lovozero Alkali Massif, Edinburgh.

Von Gehlen, K., 1976, Sulphur isotopes from the sulphide-bearing carbonatite of Palabora, South Africa (abstr.), Trans. Inst. Min. Metal. 76, B223.

Wager, L.R., 1963, The mechanism of adcumulus growth in the layered series of the Skaergaard Intrusion, Min. Soc. Am. Spec. Paper 1, 1-9.

Wager, L.R. and G.M. Brown, 1967, Layered Igneous Rocks, W.H. Freeman and Co., San Francisco, 588 pp.

Wager, L.R., G.M. Brown, and W.J. Wadsworth, 1960, Types of igneous cumulates, Jour. Petrol. 1, 73-83.

Washington, H.S. and H.E. Merwin, 1927, The acmitic pyroxenes, Amer. Mineral. 12, 233-252.

Wasserburg, G.J., 1963, Diffusion processes in lead-uranium systems, Jour. Geophys. Res. 68, 4823-4846.

Watkinson, D.H., 1970, Experimental studies bearing on the origin of the alkali rock-carbonatite complex and niobium mineralization at Oka, Quebec, Canadian Mineral. 10, 350-361.

Watson, E.B. and T.H. Green, 1981, Apatite/liquid partition coefficients for the rare earth elements and strontium, Earth Planet. Sci. Lett. 56, 405-421.

Weill, D.F., R.A. Grieve, I.S. McCallum, and Y. Bottinga, 1971, Mineralogy-petrology of the lunar samples, microprobe studies on samples 12021 and 12022, Proc. Second Lunar Sci. Conf. 1, 413-430.

Wendlandt, R.F., 1977, The system K_2O-MgO-Al_2O_3-SiO_2-H_2O-CO_2: phase relations of the joins Ph-H_2O-CO_2 and Ph-En-Mg at high temperatures and high pressures and applications to the genesis of alkalic magmas, 2nd Int. Kimb. Conf., extended abstracts.

Wendlandt, R.F. and D.H. Eggler, 1980a, The origins of potassic magmas: 1. Melting relations in the systems $KAlSiO_4$-$MgSiO_2$ and $KAlSiO_4$-MgO-SiO_2-CO_2 to 30 kb, Amer. Jour. Sci. 280, 385-420.

Wendlandt, R.F. and D.H. Eggler, 1980b, The origins of potassic magmas: 2. Stability of phlogopite in natural spinel lherzolite and in the system $KAlSiO_4$-MgO-SiO_2-H_2O-CO_2 at high pressures and high temperatures, Amer. Jour. Sci. 280, 421-458.

Wendlandt, R.F. and W.J. Harrison, 1979, Rare earth partitioning between immiscible carbonate and silicate liquid and CO_2 vapor: Results and implications for the formation of light rare earth-enriched rocks, Contrib. Mineral. Petrol. 69, 409-419.

Wetherill, G.W., 1963, Discordant uranium-lead ages, Part 2, Discordant ages resulting from diffusion of lead and uranium, Jour. Geophys. Res. 68, 2957-2965.

Wilkinson, J.F.G., 1966, Clinopyroxenes from the Square Top intrusion, Nundle, New South Wales, Mineral. Mag. 35, 1061-1070.

Wones, D.R. and H.P. Eugster, 1965, Stability of biotite: Experiment, theory, and application, Amer. Mineral. 50, 1228-1272.

Wood, B.J., 1976, An olivine-clinopyroxene geotherometer (a discussion), Contrib. Mineral. Petrol. 56, 297-303.

Wyllie, P.J., 1971, Experimental limits for melting in the Earth's crust and upper mantle (with discussion): in The Structure and Physical Properties of the Earth's Crust, Amer. Geophys. Union, Geophys. Monogr. No. 14, 279-301.

Wyllie, P.J., 1977a, Peridotite-CO_2-H_2O and carbonatitic liquids in the upper asthenosphere, Nature 266, 45-57.

Wyllie, P.J., 1977b, Crustal anatexis; an experimental review, Tectonophysics 43, 41-71.

Wyllie, P.J., 1978, Mantle fluid compositions buffered in peridotite-CO_2-H_2O by carbonates, amphibole, and phlogopite, Jour. Geol. 86, 687-713.

Wyllie, P.J., 1979, Kimberlite magmas from the system peridotite-CO_2-H_2O, 2nd Int. Kimb. Conf. Proc. 1, 319-329.

Wyllie, P.J. and W.L. Huang, 1975a, Influence of mantle CO_2 in the generation of carbonatites and kimberlites, Nature 257, 297-299.

Wyllie, P.J. and W.L. Huang, 1975b, Peridotite, kimberlite, and carbonatite explained in the system CaO-MgO-SiO_2-CO_2, Geology 3, 621-624.

Wyllie, P.J. and W.L. Huang, 1976, Carbonation and melting reactions in the system CaO-MgO-SiO_2-CO_2 at mantle pressures with geophysical and petrological applications, Contrib. Mineral. Petrol. 54, 79-107.

Wyllie, P.J. and O.F. Tuttle, 1959, Melting of calcite in the presence of water, Amer. Mineral. 44, 453-459.

Yagi, K. and K. Onuma, 1969, An experimental study on the role of Ti in alkalic basalts in light of the system diopside-akermanite-nepheline-$CaTiAl_2O_6$, Amer. Jour. Sci. 267-A, 509-549.

Yoder, H.S., Jr. and I. Kushiro, 1969, Melting of a hydrous phase: Phlogopite, Amer. Jour. Sci. 267-A, 558-582.

Yoder, H.S., Jr. and C.E. Tilley, 1962, Origin of basalt magmas: An experimental study of natural and synthetic rock systems, Jour. Petrol. 3, 342-532.

York, D., 1966, Least squares fitting of a straight line with correlated errors, Earth Planet. Sci. Lett. 5, 320-324.

Zartman, R.E. and G.J. Wasserburg, 1969, The isotopic composition of lead in potassium feldspars from some 1.0-b.y.-old North American igneous rocks, Geochim. Cosmochim. Acta 33, 901-942.